UNIVERSITY OF CALIFORNIA SAN DIEGO

Lateral-Spreading Effects on Pile Foundations: Large-scale Testing and Analysis

A dissertation submitted in partial satisfaction of the
requirements for the degree of Doctor of Philosophy

in

Structural Engineering

by

Ahmed Amr Ebeido

Committee in charge:

Professor Ahmed Elgamal, Chair
Professor John S McCartney
Professor Gilberto Mosqueda
Professor Peter Shearer
Professor Pui-Shum Shing

2019

The Dissertation of Ahmed Amr Ebeido is approved, and it is acceptable in quality and form for publication on microfilm and electronically:

Chair

University of California San Diego

2019

Dedication

To my parents, Amr Ebeido and Perihan Kandil,

Epigraph

"When utilizing past experience in the design of a new structure we proceed by analogy and no conclusion by analogy can be considered valid unless all the vital factors involved in the cases subject to comparison are practically identical. Experience does not tell us anything about the nature of these factors and many engineers who are proud of their experience do not even suspect the conditions required for the validity of their mental operations. Hence our practical experience can be very misleading unless it combines with it a fairly accurate conception of the mechanics of the phenomena under consideration."

Karl Terzaghi

Table of Contents

List of Symbols

r_u	Excess pore pressure ratio
u_e	Excess pore pressure
σ_{vo}'	Initial effective vertical stress
D_{50}	Diameter that passes 50% of the soil sample
D_{10}	Diameter that passes 10% of the soil sample
F_c	Fines content for sand
C_u	Uniformity coefficient for soils
CPT	Cone penetration test
qt	Tip resistance for CPT corrected for pore pressure
Rf	Friction ratio for CPT
SPT	Standard penetration test
N_{60}	SPT blow count corrected for hammer efficiency
$N_{1,60}$	SPT blow count corrected for overburden pressure
D_r	Soil relative density
p	Lateral soil force per unit length acting on the pile
y	Relative soil-pile displacement
y_p	Pile displacement
y_s	Soil free field displacement
γ	Unit weight of soils
Φ	Friction angle
S_r	Residual strength
c	Cohesion
D	Pile diameter

z	Depth
Cu	Degradation factor for *p-y* curves based on excess pore pressure build-up
E	Elastic modulus
I	Section Inertia
q_{n1}	Lateral load per unit area (kPa) due to a non-liquefied layer
q_1	Lateral load per unit area (kPa) due to a liquefied layer
h	Depth (m) from ground surface
K_p	Passive soil pressure coefficient of the non-liquefied soil layer
γ_{n1}	Total unit weight of the non-liquefied soil layer
H_{n1}	Thickness of the non-liquefied soil layer
c_{n1}	Factor (0-1) depending on the liquefaction resistance of the soil layer
γ_1	Total unit weight of the liquefied soil layer
k_y	Slope yield acceleration
M	Earthquake magnitude
PGA	Peak ground acceleration
PGV	Peak ground velocity

List of Figures

List of Tables

Acknowledgments

I would like to thank Professor Ahmed Elgamal, for his support, guidance and encouragement throughout this work.

My deepest gratitude also to my fellow graduate students: Muhammed Zayed, Ismaail Ghaaowd, Abdullah Elmutairi, Kyungtae Kim, Jinchi Lu and Athul Prabhakaran, to name a few. I will always be grateful for their guidance and friendship throughout the years.

Thanks to the Powell lab staff: Dr. Chris Latham, Darren McKay, Michael Sanders, Edward Stovin, Noah Aldrich, Andrew Sander and Abdullah Hamid for their invaluable help and advice during the experimental part of this work.

I would like to thank the Englekirk Structural Engineering Research Center staff, Alex Sherman, Jeremy Fitcher and Robert Beckley for going above and beyond during the large-scale testing at the outdoor shake table.

I am grateful to Professor Geoffrey R. Martin of USC for proving valuable suggestions and insights. I would also like to express my gratitude to the California Department of Transportation (Caltrans) for providing the funding for this research.

Finally, I want to thank the members of my committee for the time they dedicated and their valuable contribution to define the objectives for this dissertation.

This thesis contains a mix of a journal paper accepted for publication and new content being prepared for publication. A summary of the work in this thesis is given below.

Chapter 4, in full, has been submitted for publication of the material as it may appear in the following journal publication (The dissertation author was the primary investigator and author of this paper):

Ebeido, A., Elgamal, A., Tokimatsu, K. and Abe, A. (Manuscript accepted, 2019). "Pile and pile-group response to liquefaction induced lateral spreading in four large scale shake-table experiments." Journal of Geotechnical and Geoenvironmental Engineering.

Chapter 5, in part, is currently being prepared for submission for publication of the material as it may appear in the following journal publication (The dissertation author was the primary investigator and author of this paper):

Ebeido, A. and Elgamal, A., "Pile behavior trends in fully saturated laterally spreading soils".

Chapter 6, in part, is currently being prepared for submission for publication of the material as it may appear in the following journal publication (The dissertation author was the primary investigator and author of this paper):

Ebeido, A. and Elgamal, A., "Pile behavior trends in fully saturated laterally spreading soils".

Chapter 7, in part, is currently has been submitted for publication of the material as it may appear in the following conference publication (The dissertation author was the primary investigator and author of this paper):

Ebeido, A. and Elgamal, A., (Manuscript accepted, 2019). "Assessment of Seismic Behavior of Deep Foundations from Large‐Scale Liquefaction Shake Table Experiments". Proc. of the 7 ICEGE, International conference on earthquake geotechnical engineering. Rome, Italy. 17-20 June.

Chapter 7, in part, is a reprint of material as it appears in the following conference publications (The dissertation author was the primary investigator and author of this paper):

Ebeido, A., Elgamal, A., and Zayed, M., (2018). "Pile response during liquefaction-induced lateral spreading: 1-g shake table tests with different ground inclination". Proc. 9th international conference on Physical Modelling in Geotechnics. City, University of London. 17-20 July.

Ebeido, A., Elgamal, A., and Zayed, M. (2019). "Large Scale liquefaction-induced lateral spreading shake table testing at the University of California San Diego". Proc. of the 8th International Conference on Case Histories in Geotechnical Engineering. Philadelphia, Pennsylvania. 24-27 March.

Chapter 8, in full, is currently being prepared for submission for publication of the material as it may appear in the following journal publication (The dissertation author was the primary investigator and author of this paper):

Ebeido, A., Elgamal, A. and Zayed, M., "Pile Response during Liquefaction-Induced Lateral Spreading: 1-g Shake Table Tests with Different Pile Stiffness".

Chapter 8, in part, is currently has been submitted for publication of the material as it may appear in the following conference publication (The dissertation author was the primary investigator and author of this paper):

Ebeido, A. and Elgamal, A., (Manuscript submitted, 2019). "Experimental investigation of a single pile during liquefaction-induced lateral spreading". Proc. of the 16th Panamerican Conference on Soil Mechanics and Geotechnical Engineering. Cancun, Mexico. 17-20 November.

Chapter 9, in full, is currently being prepared for submission for publication of the material as it may appear in the following journal publication (The dissertation author was the primary investigator and author of this paper):

Ebeido, A. and Elgamal, A., "Response of Reinforced Concrete Pile in Multi-layer Lateral Spreading Liquefaction Shake Table Test".

Chapter 9, in part, is a reprint of material as it appears in the following conference publication (The dissertation author was the primary investigator and author of this paper):

Ebeido, A., Zayed, M., Kim, K., Wilson, P., and Elgamal, A., (2018). Large Scale Geotechnical Shake Table Testing at the University of California San Diego. Proc. of the 2nd GeoMEast International Congress and Exhibition on Sustainable Civil Infrastructures. Cairo, Egypt. 24-28 November.

Chapter 10, in full, is currently being prepared for submission for publication of the material as it may appear in the following journal publication (The dissertation author was the primary investigator and author of this paper):

Ebeido, A. and Elgamal, A., "Restraint Single Pile Response in Large Scale Laterally Spreading Experiment".

Chapter 11, in full, is currently being prepared for submission for publication of the material as it may appear in the following journal publication (The dissertation author was the primary investigator and author of this paper):

Ebeido, A. and Elgamal, A., "Prestressed Concrete Pile Response in Large Scale Laterally Spreading Experiment".

Vita

2012	Bachelor of Engineering in Civil Engineering
	Alexandria University, Egypt.
2012 –2013	Project Engineer
	Ebeido Consultants, Alexandria, Egypt.
2013 –2014	Project Engineer
	Geotechnics Consultants, Alexandria, Egypt.
2012 –2014	Teaching Assistant, Structural Engineering Department
	Alexandria, Egypt.
07/2014	Master of Science in Structural Engineering
	Alexandria, Egypt.
2014-2019	Graduate Student Researcher
	University of California San Diego.
2019	Doctor of Philosophy in Structural Engineering
	University of California San Diego.

Publications

Ebeido, A., Elgamal, A., Tokimatsu, K. and Abe, A. (2019). "Pile and pile-group response to liquefaction induced lateral spreading in four large scale shake-table experiments." Journal of Geotechnical and Geoenvironmental Engineering.

Zayed, M., **Ebeido, A.**, Prabhakaran, A. Qiu, Z., and Elgamal, A. (Manuscript Submitted). "Asymmetric input motion for accumulation of ground deformation in laminar container shake table testing." Canadian Geotechnical Journal.

Ebeido, A. and Elgamal, A., (Manuscript submitted, 2019). "Experimental investigation of a single pile during liquefaction-induced lateral spreading". Proc. of the 16th Panamerican Conference on Soil Mechanics and Geotechnical Engineering. Cancun, Mexico. 17-20 November.

Ebeido, A. and Elgamal, A., (Manuscript accepted, 2019). "Assessment of Seismic Behavior of Deep Foundations from Large - Scale Liquefaction Shake Table Experiments". Proc. of the 7 ICEGE, International conference on earthquake geotechnical engineering. Rome, Italy. 17-20 June.

Qiu, Z., **Ebeido, A.**, Almutairi, A., Lu, J., Elgamal, A. and Martin, G., (Manuscript accepted, 2019). "Bridge-ground seismic response and liquefaction-induced deformations". Proc. of the 7 ICEGE, International conference on earthquake geotechnical engineering. Rome, Italy. 17-20 June.

Ebeido, A., Elgamal, A., and Zayed, M. (2019). Large Scale liquefaction-induced lateral spreading: 1-g Shake Table Testing at the University of California San Diego. Proc. of the 8th International Conference on Case Histories in Geotechnical Engineering. Philadelphia, Pennsylvania. 24-27 March.

Ebeido, A., Zayed, M., Kim, K., Wilson, P., and Elgamal, A., (2018). Large Scale Geotechnical Shake Table Testing at the University of California San Diego. Proc. of the 2nd GeoMEast International Congress and Exhibition on Sustainable Civil Infrastructures. Cairo, Egypt. 24-28 November.

Ebeido, A., Elgamal, A., and Zayed, M., (2018). Pile response during liquefaction-induced lateral spreading: 1-g shake table tests with different ground inclination. Proc. 9th international conference on Physical Modelling in Geotechnics. City, University of London. 17-20 July.

Abouseeda, H. M., Elwakil, A. Z., and **Ebeido, A.** (2014). Effect of pile spacing on group behavior. Proc. of the 8th Alexandria international conference on Structural and Geotechnical Engineering. Department of Structural Engineering, Faculty of Engineering, Alexandria University, Egypt. 14-16 April.

Abstract of the Dissertation

Lateral-Spreading Effects on Pile Foundations: Large-scale Testing and Analysis

by

Ahmed Amr Ebeido

Doctor of Philosophy in Structural Engineering

University of California San Diego, 2019

Professor Ahmed Elgamal, Chair

Current techniques for assessing the effects of liquefaction-induced lateral spreading on pile foundations are based on simplified analytical methods that potentially lead to estimates that vary within a wide range. This might lead to potential excessive design demands, with high expenses for pre-event mitigation. Conversely, underestimated design demands might lead to costly post-event damage remediation.

The conducted study is directed towards enhancements to the assessment of liquefaction induced lateral spreading effects on bridge foundation systems. Current simplified analysis techniques have been only been developed recently in preliminary form. In addition, quantitative data sets from large-scale experimentation are needed concerning the response of such ground-foundation scenarios.

An effort was undertaken to address the simplified method areas of applicability and potential for enhancements. Challenges in implementing the methodology are presented within a comparative scope contrasting results of a California bridge site from different studies. On this basis, insights are derived for improvement of the currently employed simplified analysis guidelines.

Furthermore, large scale shake table testing was performed on pile foundation-ground systems, under conditions of liquefaction-induced lateral spreading. A total of 7 different experiments were conducted with varying heights, ground inclination, soil profiles, pile material and cross-section. The tested models were densely instrumented, including strain gauges, total pressure and excess pore-pressure sensors, accelerometers and displacement pots. In addition, data from 4 different experiments conducted in the NIED Japan shake table facility, including single piles and pile groups and varying soil profiles were utilized to provide additional insights and characteristics.

In these tests, the laminar soil container was placed in a mildly-inclined configuration to allow for accumulation of the liquefaction-induced lateral deformations. Detailed instrumentation and data interpretation procedures enable measurement of the fundamental soil-pile interaction behavior. The loading mechanisms have large cyclic components that may act in-phase or out-of-phase along the pile embedded length.

The conducted heavily instrumented tests resulted in a wealth of quantitative response data sets, to be used for: i) drawing insights and recommendations of practical significance based directly on the observed response, ii) calibration of simplified and more elaborate computational analysis tools, and iii) enhancement of our design guidelines and practical assessment procedures. Monotonic pushover analysis based on newly derived *p-y* curves in this study is found to provide useful design estimates in good agreement with the observed experimental results.

Chapter 1 Introduction

1.1. Overview

Liquefaction occurs during seismic excitation of saturated cohesionless soils due to the passing of seismic shear waves. The rapid excitation results in a pore-pressure build up mechanism with a corresponding reduction in effective stresses. As such, large settlements or structural damage might be expected.

Liquefaction by itself may not be hazardous, and only when coupled with some form of ground movement or failure; may be destructive. There are several main forms of damage, such as: i) Flow failures, ii) Lateral spreading, iii) Ground oscillation and iv) Loss of bearing strength. Liquefaction is often coupled with lateral spreading as it induces downslope deformations in sloping ground most commonly towards a free face such as a river.

Depending on the ground motion characteristics, and number of cycles that mobilize the soil strength, ground displacements range from minor to large (Kramer 1996). Displacements as large as 10 m were recorded in the Shinano River region during the 1964 Niigata earthquake (Hamada *et al.* 1986). Lateral spreading of sloping ground has caused severe damage to pile foundations and pile-supported structures (Hamada 1992; Hamada and O'Rourke 1992; Ishihara 1997; Tokimatsu and Asaka 1998; Berrill *et al.* 2001). Earth structures are also subjected to damage during earthquakes due to liquefaction of the embankment or foundation soils (Seed 1968; Krinitzsky and Hynes 2002).

Although significant advances have been made in the past 50 years, this subject is still of interest to both researchers and practitioners (Finn 2015) as liquefied soils continues to challenge designers and result in extensive damage to superstructures and the underlying pile foundation. For example, the recent Maule earthquake in Chile caused severe foundation and superstructure

damage due to liquefaction of the surrounding soils (GEER 2010a).

1.2. Liquefaction Potential Evaluation

The first method of evaluating liquefaction potential in soils was the simplified procedure proposed by Seed and Idriss (1971). The method relied on several factors, such as: i) Soil type, ii) Relative density, iii) Initial confining pressure, iv) Intensity of ground shaking, and v) Duration of ground shaking. The procedure entailed comparing a cyclic stress ratio derived from the ground motion parameters to a cyclic resistance ratio from the soil properties as shown in Figure 1-1.

Based on this work, several methods were developed to increase accuracy and reliability (Youd *et al.* 2001). The modern methods utilize standard in-situ testing such as SPT and CPT. The recent and most widely used procedures are those by Youd *et al.* (2001) and Idriss and Boulanger (2008). CPT data is usually more reliable and repeatable and is being more widely adopted in modern in-situ testing.

1.3. Case History Investigations for Pile Foundation Damage due to Liquefaction-Induced Lateral Spreading

Over the past 100 years, case histories of damage of pile foundations and their supported structures have been documented for a number of earthquakes. Representative cases are presented below.

The 1906 San Francisco earthquake caused lateral spreading towards the Salinas River at Moss Landing. As a result, large displacements were induced in the timber pile foundation of a railroad bridge causing bridge collapse (Figure 1-2, Wood 1908).

During the 1964 Alaskan earthquake, lateral spreading was the primary cause of damage to over 250 bridges (Bartlett and Youd 1992, 1995). Recorded damage varied in bridge foundation, abutments, piers and superstructures. Figure 1-3 shows a collapsed bridge due to liquefaction and

lateral spreading.

Lateral spreading during the 1964 Niigata earthquake, resulted in large displacements and failure of reinforced pile foundations supporting a variety of structures (Hamada and O'Rourke 1992, Meymand 1998). Figure 1-4 shows the Showa Bridge collapse. The multiple span bridge was simply supported, and the collapse was a result of substantial lateral movement of the underlying pile foundation (Figure 1-5, Bhattacharya *et al.* 2014). Figure 1-6 presents the shear damage to the pile foundation under the NHK building caused by about 2 m of ground movement. A sketch of the soil profile (Figure 1-7) illustrates the loose layer and pile damage locations. A double plastic hinge was formed at both interfaces of the liquefiable layer. Similar damage occurred in the NFCH building pile foundation (Figure 1-8) as shown by the soil profile and damage sketch. In the case study, lateral flow took place as a result of liquefaction exerting substantial load on the reinforced concrete foundation supporting the three-story building. Water table was 1-1.5m deep. Investigations found the movement of the ground was about 1 m (Yoshida and Hamada 1991) and a 10 m ground excavation was performed. Cracks on the piles show that large bending moments were developed during lateral flow (Ishihara and Cubrinovski 1998a). Pile 2 was found broken off at 2m below pile head (Figure 1-8). In foundation, a number of slabs have been connected by horizontal beams about 1m height and 0.8m width. This connection has produced some constraint on movement of surface soil deposit.

The Magsayay Bridge collapsed during the 1990 Luzon earthquake, Philippines (Hall and Scott 1995). The four simply supported spans collapse was induced by approximately 2 m of lateral ground movement (Figure 1-9). During that same earthquake, six of the thirteen spans of the Carmen Bridge also collapsed due to significant lateral movement resulting from liquefaction, lateral spreading and loss of bearing capacity (Schiff 1991, Meymand 1998).

One of the most prominent earthquakes was the 1995 Kobe earthquake resulting in major pile foundation damage (Hamada *et al.* 1996, Matsui and Oda 1996). Figure 1-10 shows the complete shear failure of a pile supporting a warehouse on Port Island near Kobe City caused by about 1.5 m of lateral spreading. The piles were designed primarily for carrying vertical load and could not sustain the moments and shears due to strong shaking and lateral spreading.

Another case study from 1995 Kobe Earthquake showing performance of pile foundations in liquefied deposits undergoing lateral spreading. An oil storage tank (Ishihara and Cubrinovski 2004) was supported on 69 precast concrete piles, 23 m long and 45 cm diameter. Piles were embedded in a 0.5m thick slab. Piles were found to suffer most damage at interface between the liquefiable layer and underlying non-liquefiable one. Sand compaction piles had been installed around perimeter of the tank to 15m depth. The tank had 4 m wide belt of improved soil around its foundation. During the earthquake, the fill deposit surrounding foundation developed liquefaction. A quay wall located 20m west of the tank moved seawards causing lateral spreading. Soil profile fill deposit of 13.6m and underlying silty soil 10m thick, water level is at 2.5-3m depth. Original fill deposit has a very low SPT of about 5 or 6 blow count throughout the depth, silty soil had 20-35 blow count and 50 for deep gravel. Permanent deformation of the tank was between 55 and 35 cm. Investigations of piles 2 and 9 (Figure 1-11) as a camera was lowered through the interior of cylinder showing multiple cracks and the largest damage occurring at a depth of 8 to 14 m corresponding to the depth of the interface zone.

Tokimatsu *et al.* (1996) reported that many quay walls in the reclaimed land areas between Kobe and Amagasaki moved several meters towards the ocean. Mizuno *et al.* (1996) surveyed more than 30 cases of foundation damage in the form of shear and flexural cracks, as well as excessive rotation of the pile heads. The damaged foundations included pre-cast concrete, cast-in-

place concrete and steel pipe piles. Lateral spreading was found to be a major cause of the damage.

The 1999 Chi-Chi Taiwan earthquake (Idriss and Abrahamson 2000) again illustrates the expensive and significant damage that may result from lateral spreading. Figure 1-12 shows the collapse of a highway bridge. The unseated deck is due to the significant pier movement resulting from lateral spreading.

Koyamada *et al.* (2006) investigated pile damage during the 2003 Tokachi-Oki earthquake in Japan of magnitude 8. The site observations were verified by earthquake response analysis and piles extracted from ground. Piles were pre-stressed high-strength concrete (PHC) pile with a diameter of 40 cm and length of 28.5 m. Surface soil above 30m depth comprises of very soft layers of peat, clay and sandy silt underlain by dense gravel. Superstructure suffered a maximum roof horizontal displacement of 56mm and tilt angle 1/220. Maximum settlement of first floor was 110 mm and slope angle 1/160. Piles were damaged by compression failure with flexure cracks at pile head. Compression failure at pile head induced differential settlements of the superstructure. Moments were calculated by means of a soil spring model and dynamic simulation. Ultimate bending moment is 130 kN-m and Figure 1-13 shows that excessive deformations were incurred. Figure 1-14 shows the damage occurred at pile head and near the depth of 20 m.

During the 2010 Maule earthquake in Chile, numerous foundation and supported superstructures were damaged due to liquefaction and lateral spreading (GEER 2010a). Lateral spreading caused unseating of a bridge deck as shown in Figure 1-15. In other locations, cracks in the ground were observed as the pushed the embedded foundation towards the river while the superstructure restrained the top of the pile. This large relative displacement imposed significant inelastic flexural strains on the column-pile shaft extension resulting in large cracking and unseating of the column from the foundation (Figure 1-16). Similar failures and damage were also

observed during the 2010 El Mayor-Cucapah earthquake (GEER 2010b) as illustrated in Figure 1-17 of the unseating of a railway bridge.

The examples of case histories mentioned illustrate how destructive damage caused by liquefaction-induced lateral spreading can be. Extensive damage to pile foundations of buildings, bridges and marine structures is caused by the large lateral pile displacements during the mechanism. The superstructure is hence affected and can suffer severe damage or collapse. While the case histories have provided insights and increased our understanding of the phenomenon, the problem still exists with as much damage and expense. As such, it is vital to improve the lateral performance of piles during strong motions and enhance the design methodology. Physical modelling emerged as an essential tool to study the mechanism. Experiments are needed as the observed response is scarce and ongoing research is needed to help reduce conservatism and uncertainty in State of Practice.

1.4. Physical Modelling of Piles in Liquefaction-Induced Lateral Spreading Scenarios

Loads exerted by lateral spreading are complex, involving large cyclic ground deformations, inertial effects and soil-pile-superstructure interaction. All occur in the presence of rapidly changing soil properties. The available case histories are limited and only provide after the fact data. This includes a great level of uncertainty.

Physical modelling emerged as a main tool to study the lateral spreading phenomenon over the past 25 years (Kutter 1984, Taboada 1995). Mainly, centrifuge experiments studying the effect of lateral spreading on pile foundations (Wilson *et al.* 2000, Abdoun and Dobry 2002, Haigh and Madabushi 2002, Abdoun *et al*. 2003, Dobry *et al.* 2003, Brandenberg *et al.* 2005, 2007a). Centrifuge modelling became a vital and cost-effective tool. It is widely used and provided much needed insights and increased understandings. Larger scale tests are needed to complement

centrifuge experiments (Ubilla *et al.* 2011). Continued physical research using rigid box 1-g shake table tests (Tokida *et al.* 1993, Hamada 2000), full scale blasting (Ashford *et al.* 2000, Ashford *et al.* 2004, Weaver *et al.* 2005) and laminar box 1-g shake table tests (Tokimatsu and Suzuki 2004, He 2005, Cubrinovski *et al.* 2006, He *et al.* 2009, Motamed *et al.* 2013 and Chang and Hutchinson 2013) derive more insight and help improve pile design methodology. All these studies and others contributed to calibrating models, verifying design procedures and unclouding the complexity of the loading mechanism.

1.4.1 Centrifuge Experiments

Centrifuge tests allow the use of small size models to simulate prototype field stress conditions. A small model is built at a 1/N scale of the prototype. It is then placed on a shake table mounted inside a centrifuge. The centrifuge basket containing the model is then spun at an acceleration N times gravity. This allows the simulation of the prototype stress state and the response of the embedded piles (Kutter 1984, Taboada 1995, Haigh 2002). Centrifuge facilities have different basket sizes, arm lengths and maximum attainable acceleration. The larger the facility, the larger the prototype it can simulate.

Abdoun (1997), Abdoun and Dobry (2002), Abdoun *et al.* (2003) and Dobry *et al.* (2003) reported modelling of single piles and pile groups subjected to lateral spreading in different configurations, geometries and soil conditions. They studied 8 different centrifuge models of single piles and pile groups. Experiments were performed in a mildly inclined container at 2°. Prototype layer thickness was estimated to be 6.0 m built using Nevada sand at a 40% relative density. Effective prototype pile diameter was 0.6 m. Models varied from a single loose layer to a 2 layered profile (dry layer on top). All models had a cemented layer at the base. Piles simulated both end-bearing and floating models. Figure 1-18 illustrates a single pile model tested at that 2°

inclined configuration. During shaking as the ground surface accumulated displacements (Figure 1-19), pile head displacement and base bending moment reached a peak early in the shaking phase at small ground displacements. As the shaking continued, pile started to rebound residing at a much lower value. Other models in the study (Figure 1-20 and others not shown herein) showed the same peak response at the start of ground movement during shaking and pile rebounding afterwards. Results of pile response (5a) from the second model (Model 5) holding a 2-pile configuration with separate pile caps (Figure 1-20) are compared to the first model in Figure 1-21. General results show the peak bending moment occurred at the interface between the loose and the underlying dense layer. These studies recommended a 10.3 kPa uniform pressure acting on the pile for design purposes.

Wilson *et al.* (2000) conducted a series of centrifuge tests for pile supported structures as shown in Figure 1-22. Models consisted of 2 layers, a dense base layer about 80% relative density anchoring the pile underlying a loose liquefiable layer. The loose layer was varied between the models. To be able to scale permeability, a pore fluid was used (Stewart *et al.* 1998) having 10 times the viscosity of water. Back figured *p-y* curves from the generated data during shaking are presented in Figure 1-23 showing sample subgrade reaction, *p* against relative soil-pile displacement, *y*. The produced curves verify the softening behavior of the liquefied soil and is shown by the stiffness slope decreasing with each cycle.

Singh *et al.* (2000) and Brandenberg *et al.* (2004) performed a series of centrifuge experiments to study pile behavior under lateral spreading (Figure 1-24). Prototype steel pipe piles were modeled using aluminum tubing of different diameters of 3.8 cm, 1.9 cm, and 0.95 cm. The soil strata were built with a 2.5 cm high coarse sand layer, overlying a 7.5 cm high deposit of over-consolidated clay over a 12.5 cm high loose (Dr = 22%) sand layer and a base underlying dense

sand (Dr = 90%). All the layers were inclined at 3°. A “river” channel was cut through the surface deposit across the short dimension of the model container at the south end of the container. The riverbank was built at a slope of 25°. The model layout is shown in Figure 1-24. Brandenberg *et al.* (2004) found that the liquefiable sand provided a large upslope resistance (400 kN/m) instead of exerting a load on the pile during critical loading cycles. This can be attributed to the non-liquefiable crust behavior mechanism and an out-of-phase response.

Haigh (2002) and Haigh and Madabhushi (2002) used silicon oil saturated soils (Dr = 40% and $\phi = 32°$) in their testing models to study pile response in lateral spreading soils (Figure 1-25). Their findings showed the acting lateral soil pressure is about 3 times that recommended by the JRA (2002). Bending moment analysis shows that the level of moment corresponds to a uniform pressure profile that is 60% higher than that recommended by Abdoun (1997) and Dobry *et al.* (2003).

Other centrifuge tests by Bhattacharya (2003) studied buckling effects during liquefaction. His findings suggested that buckling could be a significant failure mechanism. His conclusions were confirmed by analyzing data from 15 case histories of pile foundation behavior during seismic shaking.

Brandenberg *et al.* (2005, 2007a) conducted their centrifuge testing on models with single piles and pile groups that penetrated a sloping ground (Figure 1-26). Models had an overlying crust and an underlying dense sand and were shaken by a series of realistic earthquake motions. Several factors were studied, effect of crust strength, pile diameter and pile cap dimensions. They provided new insights regarding the applied lateral loads from the crust and the loose liquefiable layer. Brandenberg *et al.* (2007a) found that the backbone relationship for the non-liquefiable crust is about an order of magnitude softer than static loading relations. This can be beneficial for sites

where displacements are not large enough to fully mobilize the passive pressures.

All the above-mentioned tests and others were extremely valuable; however, their limitations must be considered when studying complex problems. The centrifuge scaling limitation does not only affect the model dimensions but extends to particle size, permeability, scaling of the pore fluid viscosity and the few numbers of sensors installed because of the small size (Ubilla *et al.* 2011). To obtain an accurate loading profile, dense instrumentation is required although not possible to achieve in the centrifuge scale. Gravity effects on displacement measurements and liquefied soil flow must be considered (Arulanandan and Scott 1993).

As such, it is essential to consider large scale testing, 1-g shake table and full scale to get a better understanding of the problem. Centrifuge testing is still needed to refine the scope of research and narrow the large configurations needed due to the large associated cost and time. Furthermore, scaling down of large prototypes configurations is much more feasible in centrifuge environment.

1.4.2 One-g Shake Table Tests

Large scale 1-g shake table testing is popular in Japan to study the effects of liquefaction and the induced lateral spreading on pile foundations (Hamada *et al.* 1992, Hamada 2000). Hamada *et al.* (1992) was among the first to conclude that pressures exerted by liquefied soil are equal to a liquid pressure of similar specific gravity. Thus, the forces from lateral displacements are based on flow velocity not magnitude of shaking. Hamada (2000) investigated pile behavior using a rigid soil box (3 m long, 1 m wide, 0.6 m high) on a 1-g shake table. The box was inclined to induce downward ground deformation. The main conclusion from this study is that, forces from lateral spreading can be estimated as a drag force against a cylindrical object subject to flow of a viscous fluid.

Cubrinovski *et al.* (1999) conducted large laminar box shake table experiments (Figure 1-27) with dimensions of 12 m length, 3.5 m width and 6 m height. Three independent pile foundation groups were installed aligned in the direction of shaking. Each group consisted of 4 piles, two groups were of pre-stressed high strength concrete (PHC) and the third was steel. Analysis was done only on the PHC piles which were 5m long and 20cm in diameter. Two sinusoidal shaking events were performed with the main shaking event of 0.21 g in peak amplitude. Results show liquefaction of entire soil even in the small shaking event of 0.084 g peak amplitude. Naturally, the larger shaking amplitude liquefied the soil faster. The piles in first group had a pinned head connection and recorded maximum moment of 19 kN-m with maximum displacement around 8 cm. While, the piles in second group had a fixed head connection and reached 26 kN-m maximum moment at displacement of 6cm with the corresponding ground displacement being 9 cm. The difference between the small and large shaking events is how fast the soil liquefied and the amount of ground movement affecting the moment developed.

Cubrinovski *et al.* (2006) used the same laminar box to conduct another test where 2 single piles fixed at the base were embedded 4.8 m in a saturated soil deposit and 1 m of upper crust. The experiment (Figure 1-28) was performed in 2 phases, first was a dynamic excitation with base input motion of 0.217 g amplitude and 2 Hz frequency. After liquefaction was induced during a 30 second shaking duration, a frame was attached to the laminar box and the liquefied portion was subjected to a forced motion of 4.1cm/s at the top of the layer. Forced movement was initiated 6s after shaking until reaching a max displacement of 84 cm. PWP measurements show that soil below 1.4 m depth has liquefied while soil from 0.8 to 1.4 m only shows partial buildup of pore water pressure and no pore water pressure recorded at 0.5 m depth (within the crust). The PHC pile reached maximum moment at 9 cm lateral displacement and failed right away. The steel pile

showed that moment gradually increased until reaching 5 cm displacement in the first 6s and then remained constant. Maximum bending moment was about 60% of yield moment in the steel pile while the PHC pile failed. Lateral pressure recorded on the steel pile was about 18 times the vertical stress and was reached at 20 cm relative displacement between pile and ground, this pressure is roughly 4.5 times the Rankine passive pressure. On the other hand, the PHC pile only recorded about 1.5 times the Rankine passive pressure at 5 cm relative displacement between ground and pile, this is because the concrete pile failed and exhibited even more displacement than the ground. This response is typical for a flexible brittle pile. Bending moment on the steel pile measured was about 500 kN-m at 45 cm ground displacement which corresponds to the 4 cm pile displacement, and since the steel pile didn't move much and moment stayed constant, the 500 kN-m corresponds to about 0.6 M_y (yield value). Steel pile exhibits stiff pile behavior and its response is mainly controlled by the lateral load from the crust, so maximum pile response was achieved when maximum pressure was mobilized in the crust.

Suzuki and Tokimatsu (2003) conducted a large shake table test on a closely spaced pile group in liquefiable soil (Figure 1-29). Focus was placed on pore water pressure measurement and one main conclusion is that excess pore pressure is more significant on extension side rather than compression side. Although there were different pore pressures recorded around each pile, subgrade reaction is almost same within the pile group. This happens because horizontal subgrade reaction on each pile is induced by this pore pressure difference on both sides of pile which is almost the same within the pile group. Suzuki *et al.* (2006) continues to discuss the test showing subgrade and displacement oscillations around zero with no residual pressures after the shaking stopped.

Motamed and Towhata (2009) studied a 1-g shaking table model of a 3x3 pile group behind a quay wall. The testing model is presented in Figure 1-30 showing the pile group embedded in liquefiable ground with a thin dry layer on top. The configuration employed a quay wall to trigger large deformations. Ten tests were performed in this study with the same configuration and varying liquefiable layer heights. Pile group spacing was 2.80D with diameter of 3.20 cm. Sample results from the shown configuration are presented in Figure 1-31. Soil deformations keep accumulating with shaking with no added displacements after shaking stopped. Although deformations continue, peak bending moments were noted early during shaking. That maximum moment occurred with small soil displacements despite the larger values at the end. After peak bending moment, the pile group starts rebounding gradually reaching near zero values by the end of shaking.

Experiments by Motamed *et al.* (2013) tested a 2x3 pile group behind a quay wall (Figure 1-32, Figure 1-33). The container was 16m x 5m x 4m. The Takatori station during 1995 Kobe earthquake motion was employed, with peaks of 5.96 m/s^2 horizontal and 1.71 m/s^2 vertical. Piles had a yield bending moment of 7.1 kN-m and 10.5 kN-m under 37 kN axial load. Excess pore pressure values that are larger than the initial effective vertical stress were recorded because the sensors sunk into the ground during liquefaction. Large ground deformation of 2.2 m was observed. Top of wall moved 2.2 m towards sea.

As such, large scale 1-g testing is a useful tool to study the liquefaction- induced lateral spreading mechanism. One drawback of the models is that they are limited in depth and might not realistically simulate the stress state in the field (Arulanandan and Scott 1993). Other limitations include, shorter drainage paths and effect of the rigid container boundary on the soil behavior. Employing a laminar box eliminates the rigid wall effect by simulating a periodic boundary. Pile sizes are limited to reduce the boundary effects. Large pile groups are seen to influence the soil

response within the container and affect the system behavior. Consequently, soils might behave differently in models than in a corresponding free field prototype scenario.

1.5. Numerical Modelling of Piles in Laterally Spreading Soils

There are two approaches to model pile foundations in liquefaction-induced lateral spreading ground: the Winkler model or more commonly known as *p-y* curve method and the Finite Element Method (FEM). Both allow for estimation of pile bending moments, shear and displacements with time. The FEM is more sophisticated and with proper calibration can lead to better estimates of pile response and deformation of the surrounding ground. This method is more time consuming and requires time, effort and expertise for implementation. On the other hand, the *p-y* method is faster and less time consuming.

1.5.1 *P-y* Curves for Modelling Soil Structure Interaction in Liquefiable Soils

The current numerical methods for modelling soil-structure interaction are based on the Beam on Elastic Foundation approach (Hetényi 1946). This approach is based on the assumption that the reaction forces exerted by the foundation are proportional at every point to the deformation of the pile at that same point and independent of deflections produced elsewhere. The *p-y* application of this method is an equivalent design procedure as the soil is replaced by a series of springs. Given the assumption that the pile moves relative to a stationary mass of the soil, the governing equation is given by Reese *et al.* (1974):

$$EI \frac{d^4 y_p}{dz^4} - p\, y_p = 0 \qquad (1.1)$$

where EI is the bending stiffness of the pile, z is the depth, *p* is the soil pressure on the pile and y_p is the pile displacement.

In the case where liquefaction induces lateral spreading, the soil mass itself moves causing the pile to deform. In such case, the displacements of the soil and pile are different and must be accounted for. The relative movement between the soil and pile is then considered in evaluating the pile response. The governing equation according to Tokimatsu and Asaka (1998) becomes:

$$EI \frac{d^4 y_p}{dz^4} - p\,(y_p - y_s) = 0 \qquad (1.2)$$

where p is the soil resistance as a function of the relative displacement between the free field soil y_s and the pile displacement y_p. The free field soil displacement must be known in advance to solve the problem.

One of the earlier attempts to develop *p-y* curves for laterally loaded piles in liquefied soils is presented by Dobry *et al.* (1995). The proposed methodology consists of multiplying the conventional *p-y* curves for sandy soils by a degradation factor Cu that is referred to as the *p-multiplier*. As shown on Figure 1-34, the degradation factor decreases with the increase in excess pore pressure ratio, reaching a value of 0.1 at full liquefaction. Other studies recommended different degradation factors ranging from 1/80 to 1/30 (Cubrinovski *et al.* 2006) or as a function of blow counts obtained from SPT (Brandenberg *et al.* 2007b, AIJ 2001). The variances between the different approaches can be attributed to uncertainties associated with back calculating the degradation factor. A detailed overview of the *p-multiplier* approach can be found in Finn (2005).

Another method for modelling pile foundation in laterally spreading soils is based on the soil behaving as soft clay as recommended by the American Petroleum Institute (2000) but replacing the undrained shear strength with the liquefiable layer residual strength (Goh and O'Rourke 1999, Seed and Harder 1990).

Ashford *et al.* (2004) conducted a full-scale foundation test by using controlled blast to induce liquefaction. Lateral loads were applied to the pile using actuator at the pile head. Ashford

and Rollins (2002) and Rollins *et al.* (2005) back-calculated *p-y* curves and found the shape of the curves is greatly different than the traditional curves (Figure 1-35), however similar to the ones from centrifuge testing (Wilson *et al.* 2000). Ashford and Rollins (2002) and Rollins *et al.* (2005) also investigated pile group behavior. Their study concluded that group interaction effects were insignificant in liquefied soil for level sites, thus group reduction factors can be neglected.

1.5.2 Finite Element Analysis

FEM is the most sophisticated analysis tool as it has the capability of capturing detailed soil and pile response. It can compute the contractive and dilative tendency of liquefiable soils, accurately model the interaction between the soil, pile and pore pressure build up and find the pile response on an element level as well as the ground profile movement. This type of analysis is dynamic with real ground motion input opposite to the *p-y* curve approximate ground movement or pile pushover. The FEM is cost effective and enable the exploration of configurations that cannot be mimicked in a test as well as extensive parametric studies to identify the effect of key variables. However, the solution depends on accuracy and calibration of the employed soil constitutive model, thus an adequate constitutive soil model for this type of analyses must be developed and calibrated with experimental data. As such, physical modelling is still needed as a baseline study. An additional challenge is that considerable effort is required to build and run the numerical model for soil-pile-structure interaction during liquefaction induced lateral spreading.

FEM is mainly used for research as an added effort and required skill obstructs using it in day to day design and practice. Examples of using the FEM tool are by Fujii *et al.* (1998) for two-dimensional (2D) modelling to examine pile damage due to liquefaction. Tazoh *et al.* (2000) employed three-dimensional numerical analysis to investigate pile damage of a bridge during the 1995 Kobe earthquake. He (2005) used a FEM model to calibrate s soil constitutive model based

on large scale testing. He *et al.* (2017) continued the use of the model for parametric studies on the effect of permeability among other considerations.

The recent addition of liquefaction constitutive soil models in OpenSees, the Open System for Earthquake Engineering Simulation (http://opensees.berkeley.edu/), enables the simulation of piles in liquefaction-induced lateral spreading situations. This software can consider complex 3D aspects of soil-structure interaction, the mechanism of liquefaction, and the associated soil contraction/dilation.

1.6. Current Approaches for Evaluating Pile Loads under Lateral Spreading

Over the years, different recommendations have been proposed for piles subjected to liquefaction-induced lateral spreading (JRA 2002, Abdoun 1997, Dobry *et al.* 2003, NCHRP-12-49 1998, ATC and MCEER 2001, Martin *et al.* 2002). Some of these methods are summarized in this section.

1.6.1 Japanese Road Association Approach

The Japanese Road Association recommended a limit equilibrium approach (JRA 2002). This methodology assumes that all involved layers of the soil profile apply lateral loads in the direction of the lateral spread (Figure 1-36). For pile foundations within 0.50 m of the water front, the load is given by a triangular form:

$$q_{n1} = c_{n1} K_p \gamma_{n1} h \tag{1.3}$$

$$q_1 = 0.3[\gamma_{nl} H_{n1} + \gamma_1 (h + H_{n1})] \tag{1.4}$$

where

q_{n1} is the lateral load per unit area (kPa) due to a non-liquefied layer,

q_1 is the lateral load per unit area (kPa) due to a liquefied layer,

h is the depth (m) from ground surface,

c_{n1} is a factor (0-1) depending on the liquefaction resistance of the soil layer,

K_p is the passive soil pressure coefficient of the non-liquefied soil layer,

γ_{n1} is the total unit weight of the non-liquefied soil layer,

H_{n1} is the thickness of the non-liquefied soil layer,

γ_1 is the total unit weight of the liquefied soil layer.

The above equations were derived based on case history data from the 1995 Kobe earthquake and needs to be assessed for other cases.

The design code advises practicing engineers to consider two different loading conditions: (i) kinematic load exerted by the lateral pressure of the liquefied layer and/or any non-liquefied crust resting on the top of the liquefied deposit; (ii) inertial load because of the oscillation of the superstructure. The code also recommends checking against bending failure because of kinematic and inertia loads, separately.

1.6.2 Dobry *et al.* (2003) Approach

Based on centrifuge experimentation, Dobry *et al.* (2003) proposed a limit equilibrium approach. Two cases were suggested: i) Surface soil layer liquefaction and ii) liquefied soil underlying a non-liquefied crust.

1.6.2.1 Soil Surface Liquefaction Case

In this case (Figure 1-37a), the liquefied layer overlies a non-liquefiable base layer. This is an end bearing pile scenario. Calibration was based on earlier tests (Abdoun 1997, Abdoun and Dobry 2002, Abdoun *et al.* 2003). The maximum moment is defined at the base of the liquefiable

layer. During liquefaction, the soil flows around the pile exerting flow pressure against the pile. This pressure value is assumed to be uniform along the pile length in the liquefied layer and calibrated to be 10.3 kPa based on the earlier testing.

1.6.2.2 Liquefied Layer Underlying a Non-Liquefiable Crust Case

This scenario entails an upper non-liquefiable crust on top of the liquefiable layer. Centrifuge testing by Abdoun (1997), Abdoun and Dobry (2002) and Abdoun *et al.* (2003) noted that lateral pressures from the liquefied soil can be neglected in this case (Figure 1-37b). The maximum moment is found to occur at the boundary of the liquefiable layer (top and bottom). By combining static equilibrium and kinematic considerations involving displacements and rotations of pile and soil, the maximum bending moment $(M_A)_{max}$ is defined as:

$$3\left[1+\frac{2}{\frac{L}{h}}\right] = 1 - 2[\,0.5 - \frac{2}{L/h}\left\{\frac{(M_A)_{max}}{p_0 h^3}\right\}]^{1.5} \tag{1.5}$$

and for L/h ≥ 2

$$(M_A)_{max} = \frac{p_0 h^3}{[10.23 + \frac{6}{L/h}]} \tag{1.6}$$

where

h is the thickness of the top non-liquefied soil layer,

p_0 is the slope of the ultimate soil force per unit length on the pile,

M_A is the bending moment at boundary A, and

L is the pile length embedded in liquefied soil layer.

Other centrifuge experiments (Haigh 2002, Haigh and Madabhushi 2002, Gonzalez *et al.* 2005) have found lateral loads to be much higher than those of Dobry *et al.* (2003). Both the JRA (2002) and Dobry *et al.* (2003) approaches do not address pile displacements which are important for the purposes of performance-based design.

1.6.3 Displacement Controlled Iterative Approach

This methodology provides a displacement controlled iterative procedure for piles subjected to steep slope deformation due to liquefaction-induced lateral spreading (NCHRP-12-49 1998, ATC and MCEER 2001, Martin *et al.* 2002). It involves four steps as follows:

1. Slope stability analysis conducted to determine yield acceleration, k_y. This method employs the residual strength of the liquefied layer and degraded strength for others with partial pore pressure build up. The analysis includes the additional shear resistance of the pile supporting the slope.

2. Displacements of the soil-pile system are estimated from a Newmark time history analysis or simplified Newmark charts.

3. If soil flow around the pile is indicated, the pile is then designed for passive pressures due to the flow. Otherwise, plastic mechanisms may develop in the pile and substructure, that must be evaluated to check the pile ability to sustain the displacement and bending demands.

4. If the pile is not able to sustain the demands, then it is re-designed, or ground improvement can be implemented, and the above steps are repeated.

This method is an integrated framework for the design and analysis of piles under lateral spreading conditions. This framework incorporates knowledge of slope stability analysis, liquefaction analysis, plastic structure analysis, and soil-structure interaction analysis into an iterative procedure. It considers the reinforcement effects (“pile pinning’) of the pile on the ground. It allows inelastic behavior of pile foundations under lateral spreading load. One drawback is the assumption that the slope failure plane does not change throughout the analysis (with or without piles), which is not the actual case.

1.6.4 Other Methodologies in Design Codes

Eurocode 8 (1998) advises engineers to design piles against bending because of inertia and kinematic loads arising from the deformation of the surrounding soil. In the event of liquefaction, however, it recommends ignoring the side resistance of soil layers that are susceptible to liquefaction or may be subjected to substantial strength degradation.

Recent studies (Knappett and Mababhushi 2009, Bhattacharya *et al.* 2009) suggest a possible alternative failure mechanism, where end-bearing piles act as unsupported long slender columns due to loss of stiffness and strength of the surrounding liquefied layer. As a result, piles may become unstable and buckle under the action of large axial loads imposed by the superstructure. Accordingly, piles would be better modelled as beam-column elements carrying both lateral and axial loads rather than laterally loaded beams, as adopted in current routine practice.

1.7. Research Scope and Objectives

The current available methodology for pile design and analysis in laterally spreading grounds remains with large uncertainty. Case histories continue to observe damage to pile foundations and the failure or collapse of the supported superstructure.

On this basis, an extensive study is performed on the pile design methodology according to current practice. Uncertainties and weak points were identified and recommendations for improvements were made. Furthermore, a case study using this approach was undertaken with the results compared with that of an earlier study. Based on study results, the need for further research and experimentation was identified. A large scale 1-g testing program was undertaken to highlight key issues. A total of 7 tests were conducted in the series covering a wide range of configurations

and scenarios. In addition, data sets from earlier experimentation was employed to provide more insight and understanding.

The experimentation program is discussed in the following chapters, each with its own findings and conclusions. New *p-y* curves were derived from the test results and loading patterns were identified. Finally, recommendations for pile design procedures are made and improvements to the current design methodology are suggested.

1.8. Outline

The dissertation consists of 12 chapters as follows,

- *Chapter 1: Introduction.* Presents a brief overview of the motivation behind the research program, a summary of the previous experimental work available with some of its findings. This chapter discussed an overview of the current design methodologies and approaches currently available and implemented.
- *Chapter 2: Simplified Method Analysis.* This chapter discusses a current simplified method of analysis and design with an implemented example and various parametric studies on key factors. Recommendations for improvements and updates are presented.
- *Chapter 3: Simplified Analysis Applied to a Bridge Structure.* This chapter analyzes an existing California bridge using the Simplified Analysis Method and compares the result with that of an earlier study. Key differences are identified and reasons for the variability are presented along with recommendations for future updates to make the methodology more consistent.
- *Chapter 4: Pile and Pile-Group Response to Liquefaction Induced Lateral Spreading in Four Large Scale Shake-Table Experiments.* This chapter summarizes observations and results from 4 different mildly inclined 1-g shaking table experiments conducted at the

Japan NIED facility. Different configurations are compared, and conclusions are drawn based on the difference in results.

- *Chapter 5: Pile Behavior Trends in Liquefied Lateral Spreading Ground and Pushover P-Y Curve Response.* The chapter focuses on one of the tests discussed in Chapter 4 as it identified salient characteristics affecting the response. A general response trend is highlighted contrasting earlier work by other researchers. A new pushover *p-y* curve for liquefied soil is derived based on the experimental results.
- *Chapter 6: Effect of an Upper Crust on Pile Behavior under Liquefaction-Induced Lateral Spreading.* This chapter present a second test from the Japan NIED series briefly discussed in Chapter 4, similar to the experiment in Chapter 5 but with an added upper crust on top. The effect of the crust is presented and *p-y* curve modifications for non-liquefied soil overlying a liquefied stratum are suggested based on the experimental results.
- *Chapter 7: Pile Response to Liquefaction-Induced Lateral Spreading and Influence of Ground Inclination.* This chapter discusses three experiments conducted at the UCSD Powell Laboratory Shake Table. The 3 tests are compared to highlight the effect of the overlying crust and the difference in sloping ground inclination on the response. The *p-y* curves in the previous chapters are compared to the experimental response during shaking.
- *Chapter 8: Effect of Linear and Nonlinear Pile Behavior on System Response.* Two experiments conducted at the UCSD Powell Laboratory Shake Table. The tests are compared to present the difference in response of piles with different material behavior and stiffness.
- *Chapter 9: Inertial and Kinematic Effects during 1-g Shake Table Testing.* The chapter focuses on the response of a single reinforced concrete pile with an inertial mass. The

inertial and kinematic effects are discussed, and the non-linear behavior of the pile is presented.

- *Chapter 10: Effect of Pile Head Restraint on the Soil-Pile Response in Large Shake Table Testing.* This chapter describes in detail a 5 m high shake table test performed on a pile with a restrained head. Results of the effect of the restraint on the pile and the entire soil-box system are presented.
- *Chapter 11: Prestressed Concrete Pile During Liquefaction-Induced Lateral Spreading.* The chapter focuses on a unique one of a kind test, where a Caltrans Alternative X Pile Class 90 is tested during liquefaction induced lateral spreading shake table tests. The response of the pile is discussed in detail.
- *Chapter 12: Summary and Conclusions.* This chapter summarizes the main findings from the experimental investigation with recommendations for updating design procedures.

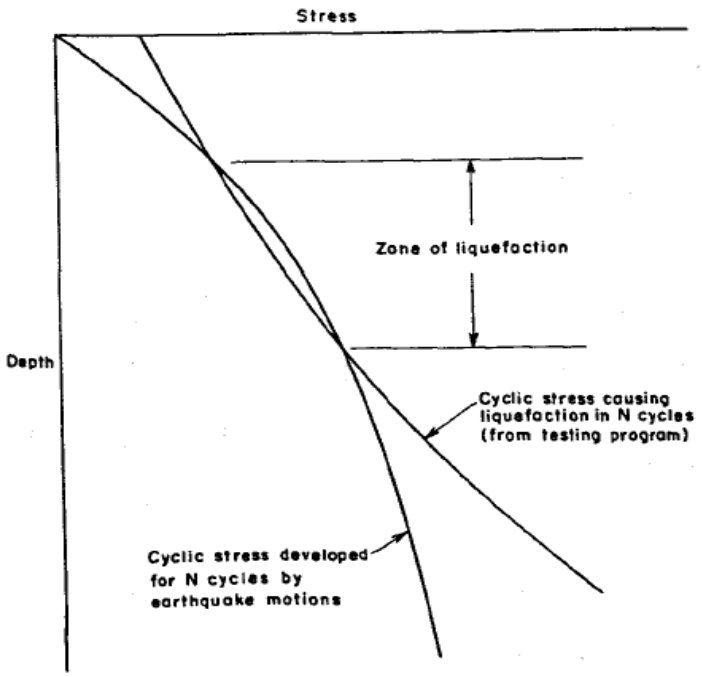

Figure 1-1. Simplified procedure for evaluating liquefaction potential (after Seed and Idriss 1967)

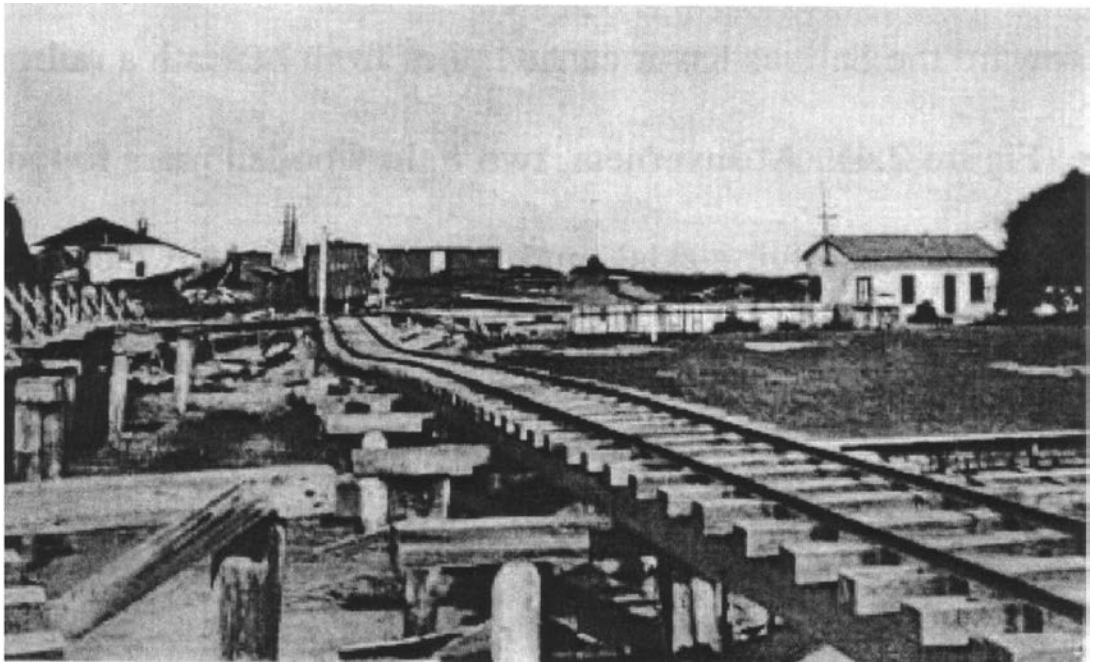

Figure 1-2. Collapsed bridge at Moss Landing due to large displacements of timber pile due to lateral spreading during the 1906 San Francisco Earthquake (after Wood 1998)

Figure 1-3. Collapsed bridge due to liquefaction-induced lateral spreading during the 1964 Alaska Earthquake (after Bartlett and Youd 1992)

Figure 1-4. Collapse of the Showa Bridge due to unseating resulting from large lateral displacement of its pile foundations during lateral spreading induced by the 1964 Niigata earthquake (after NISEE)

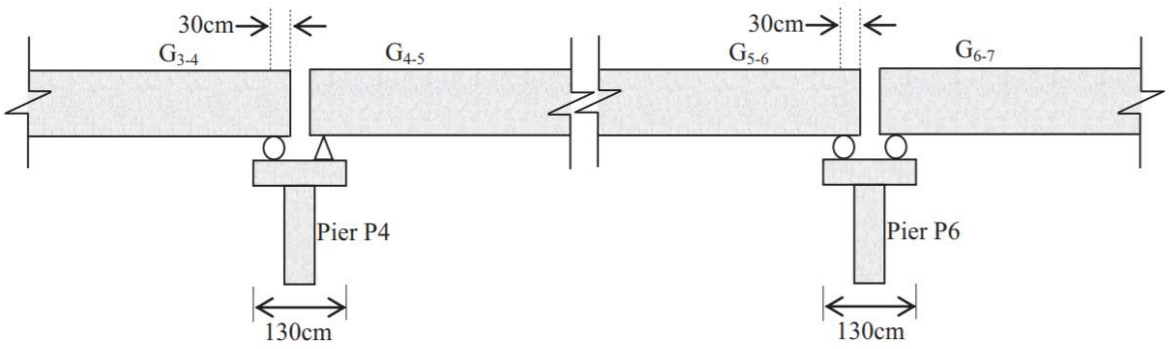

Figure 1-5. Support mechanism illustration for the Showa bridge piers (after Bhattacharya *et al.* 2014)

Figure 1-6. Piles supporting the NHK building sheared by lateral spreading during the 1964 Niigata earthquake (after Hamada 1991)

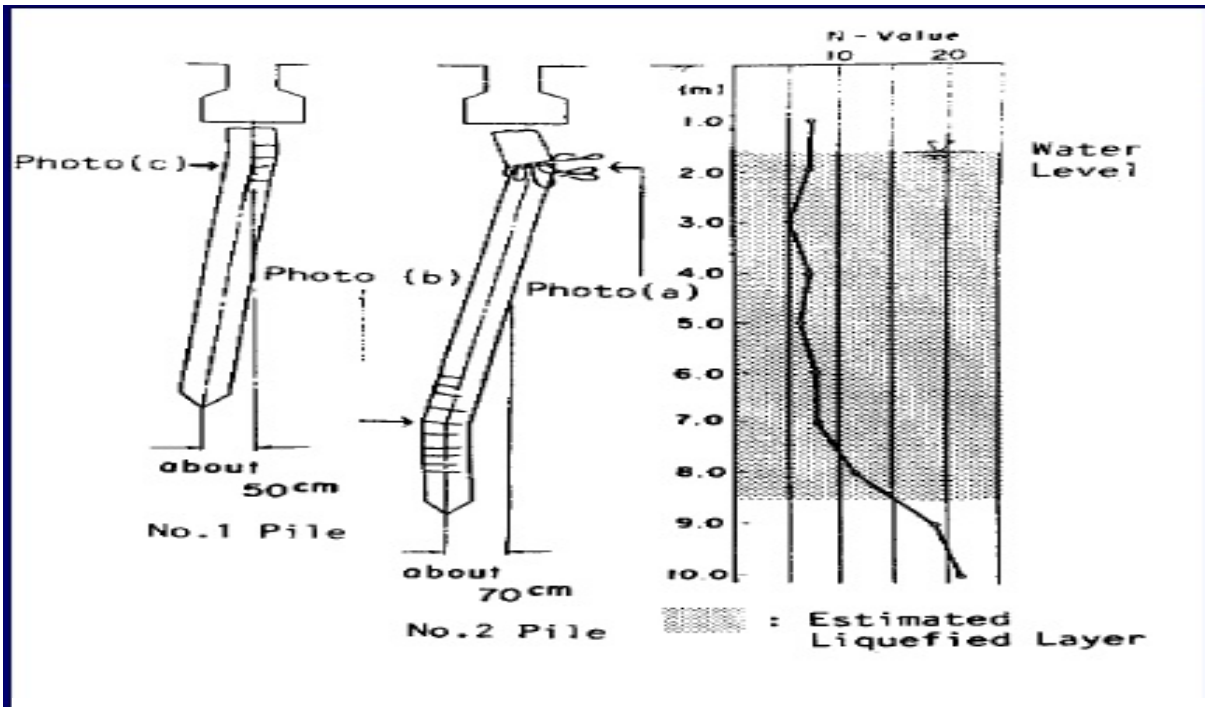

Figure 1-7. Illustration of the soil profile and damage to the NHK building pile foundation due to the 1964 Niigata earthquake (after Doi and Hamada 1992)

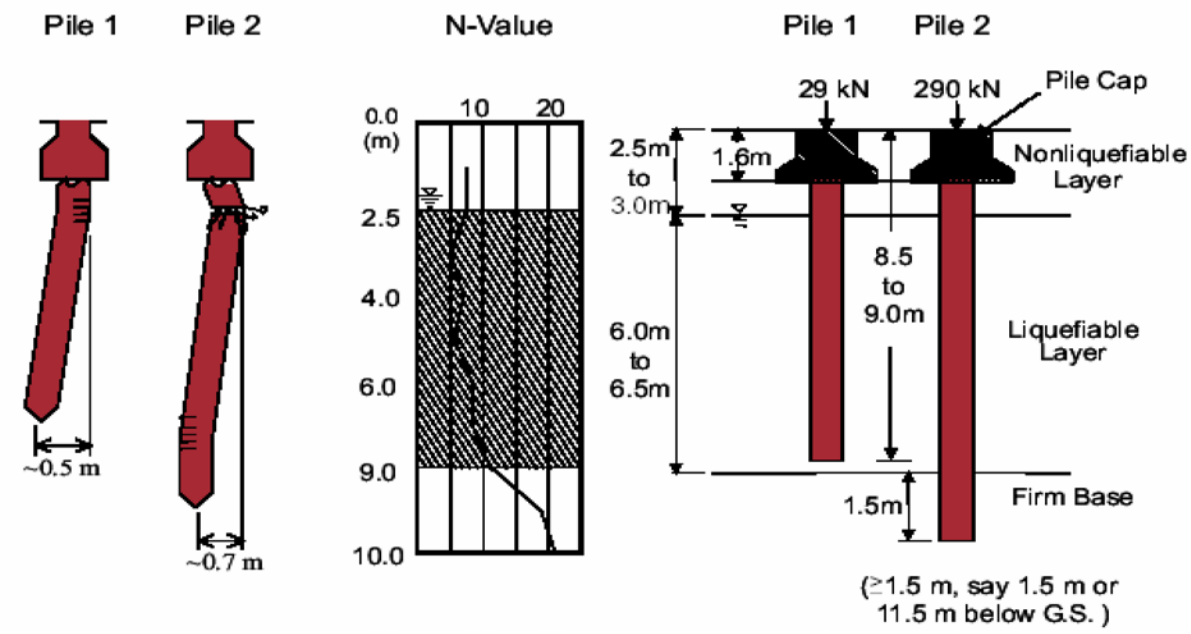

Figure 1-8. Damage to the NFCH building pile foundations as a result of lateral spreading during the 1964 Niigata earthquake (after Hamada 1992)

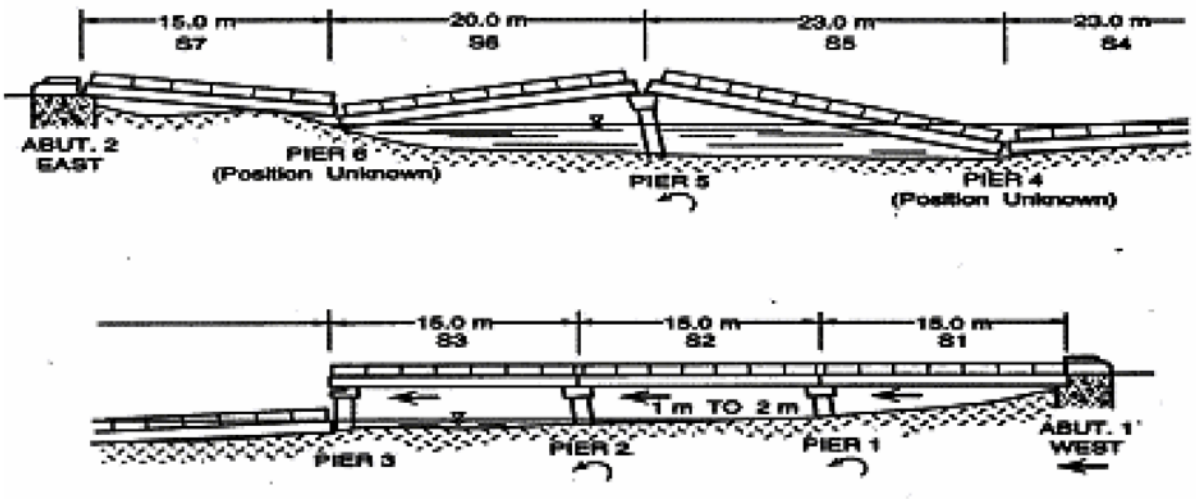

Figure 1-9. Magsayay Bridge sketch illustrating lateral spread damage during the 1990 Luzon earthquake (after Hall and Scott 1995)

Figure 1-10. Pile shear failure during the 1995 Kobe earthquake (after Finn and Fujita 2002)

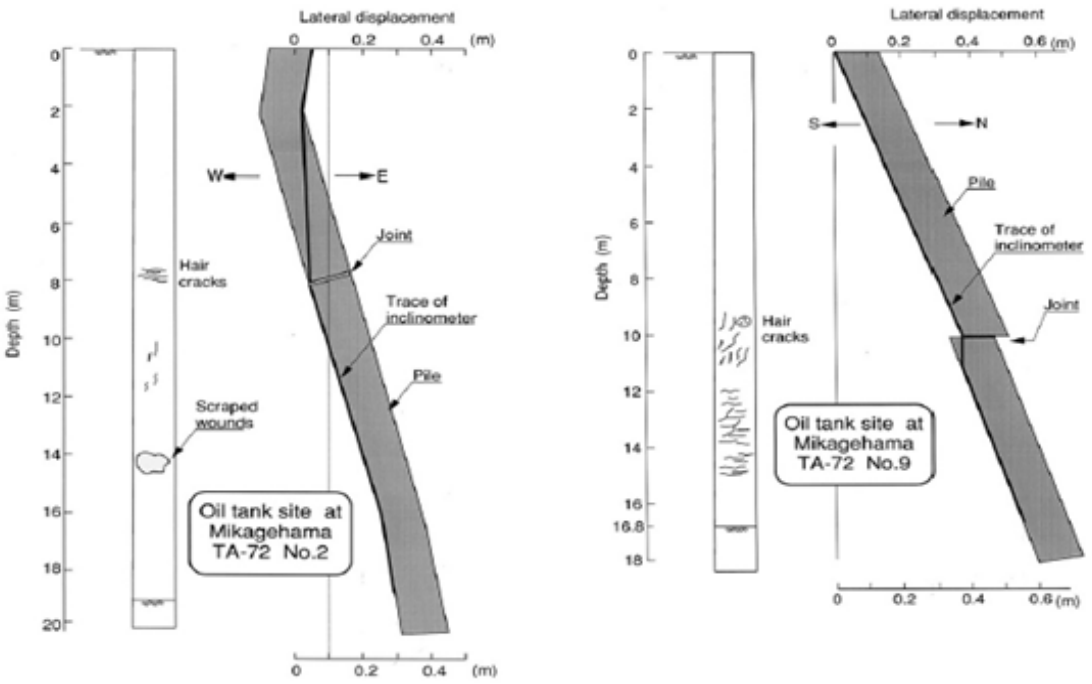

Figure 1-11. Lateral displacement and observed cracks for an oil tank foundation during the 1995 Kobe earthquake (after Ishihara and Cubrinovski 2004)

Figure 1-12. Collapse of a bridge by excessive lateral movement during the 1999 Chi-Chi Taiwan earthquake (after Moehle and Eberhard 2000)

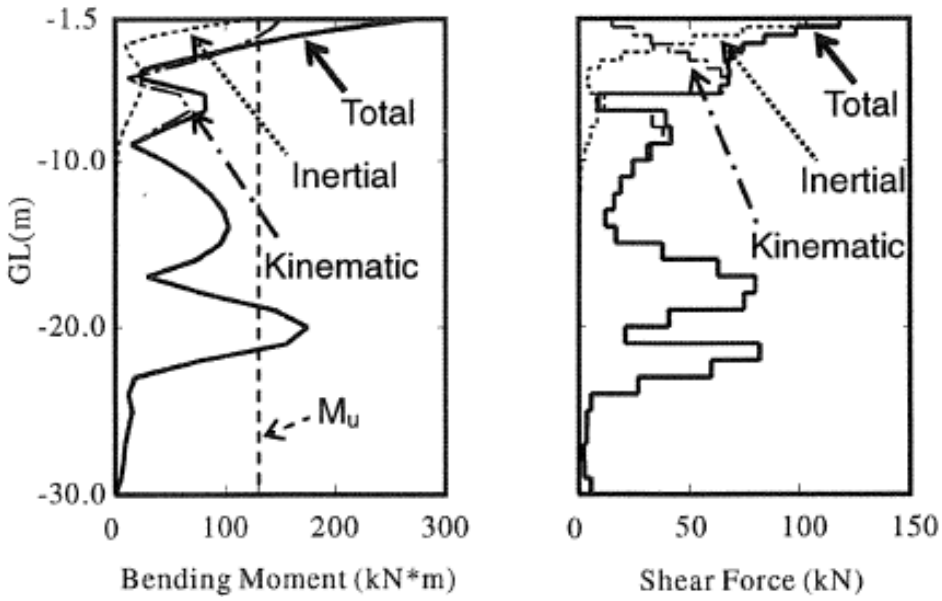

Figure 1-13. Maximum bending moments and shear forces for the concrete pile exceeding the ultimate capacity during the 2003 Tokachi-Oki Earthquake (after Koyamada *et al.* 2006)

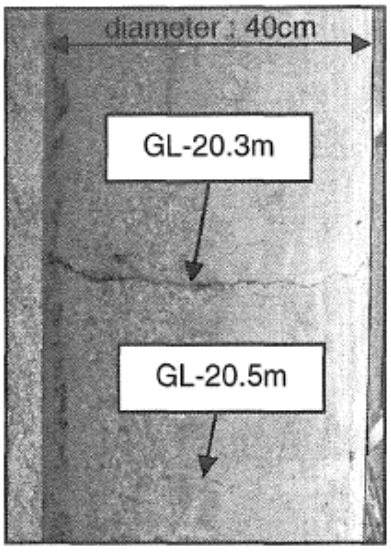

Photo 5 : Discovered cracks of pile near the depth of 20m

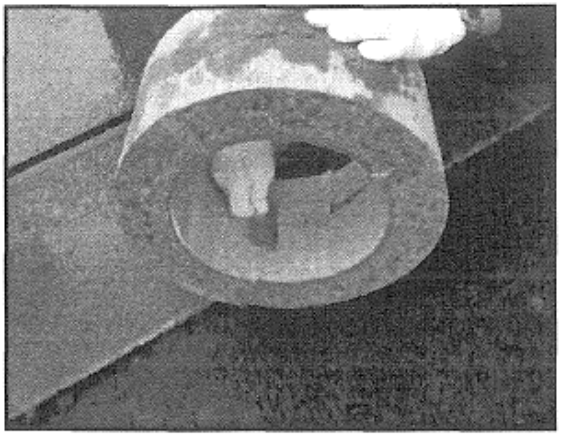

Photo 6 : Investigation of the inner side for the PHC pile by cutting out the area of the largest crack

Figure 1-14. Photos showing the discovered cracks in piles at the location of flexural failure and cutting out pile portions from investigations (after Koyamada *et al.* 2006)

Figure 1-15. Collapsed decks caused by lateral spreading, Photo by Scott Brandenburg (GEER Association Maule Chile 2010a)

Figure 1-16. Unseated pier caused by lateral spreading, Photo by Scott Brandenburg (GEER Association Maule Chile 2010a)

Figure 1-17. Unseated pier caused by lateral spreading, Photo by Scott Brandenburg (GEER Association Baja California 2010b)

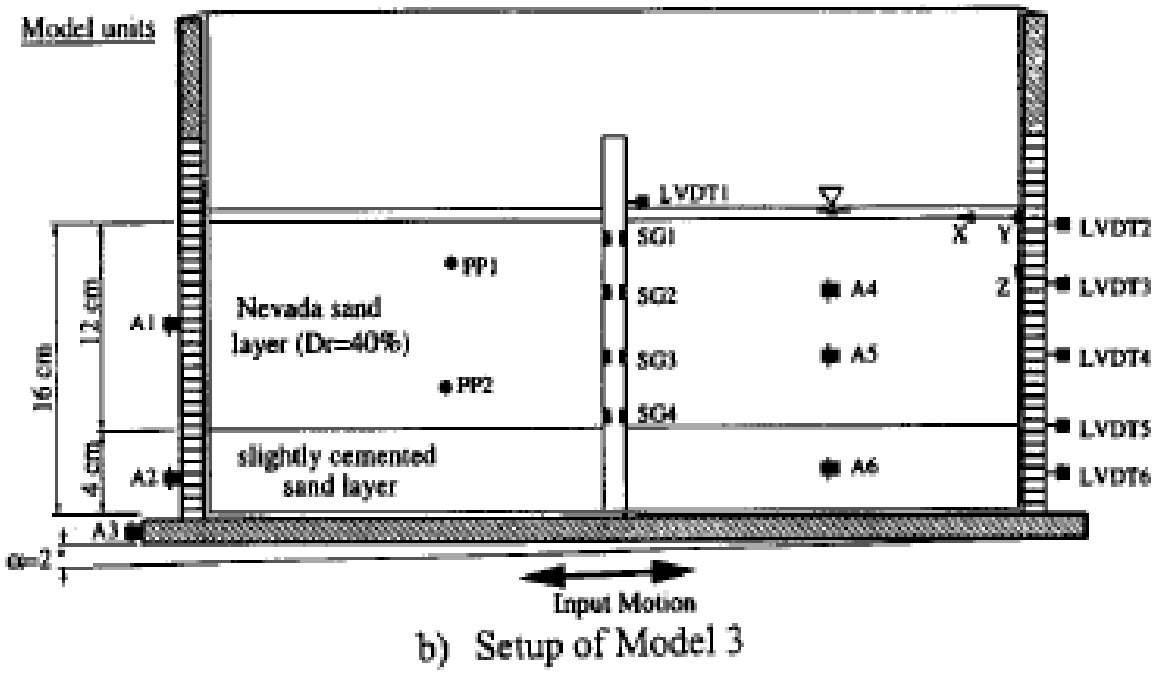

Figure 1-18. Centrifuge Model 3 (after Abdoun *et al.* 2003)

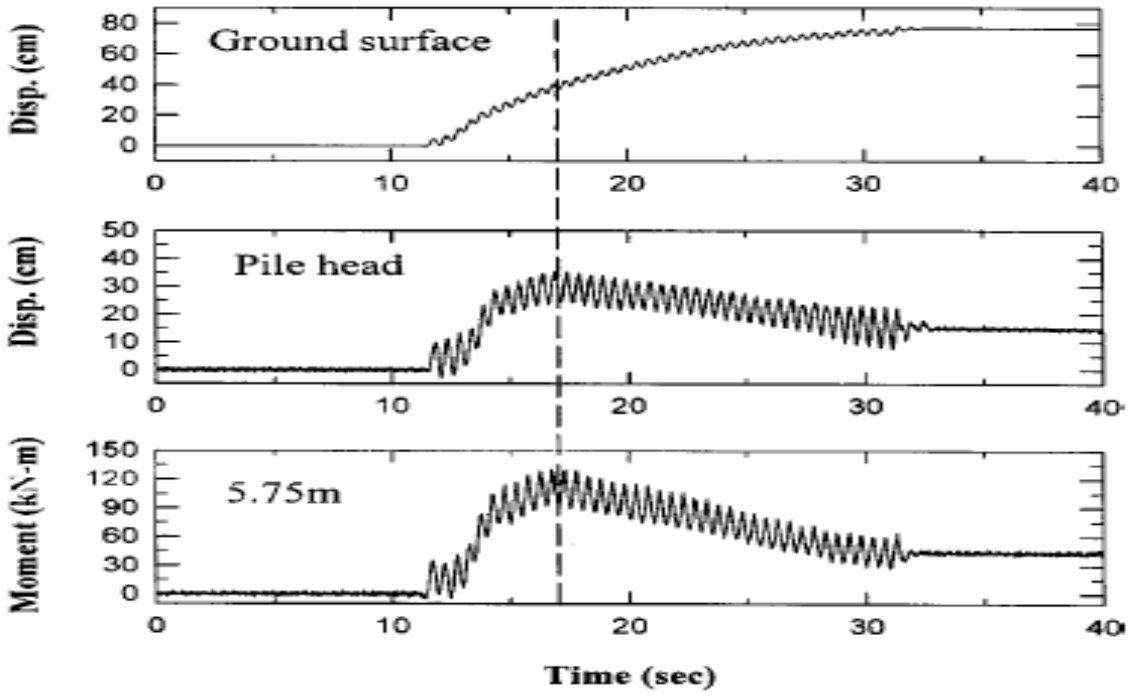

Figure 1-19. Centrifuge Model 3 selected results (after Abdoun *et al.* 2003)

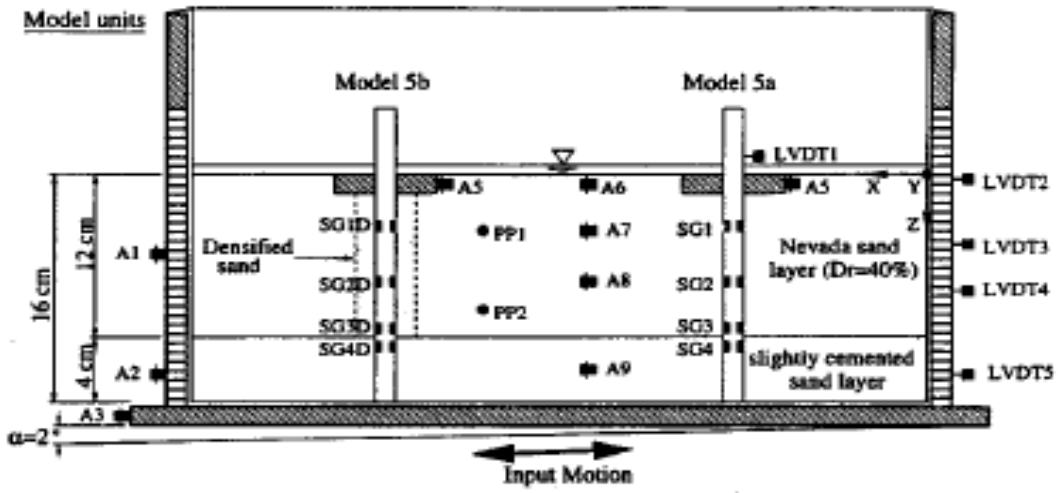

Figure 1-20. Centrifuge Model 5 (after Abdoun *et al.* 2003)

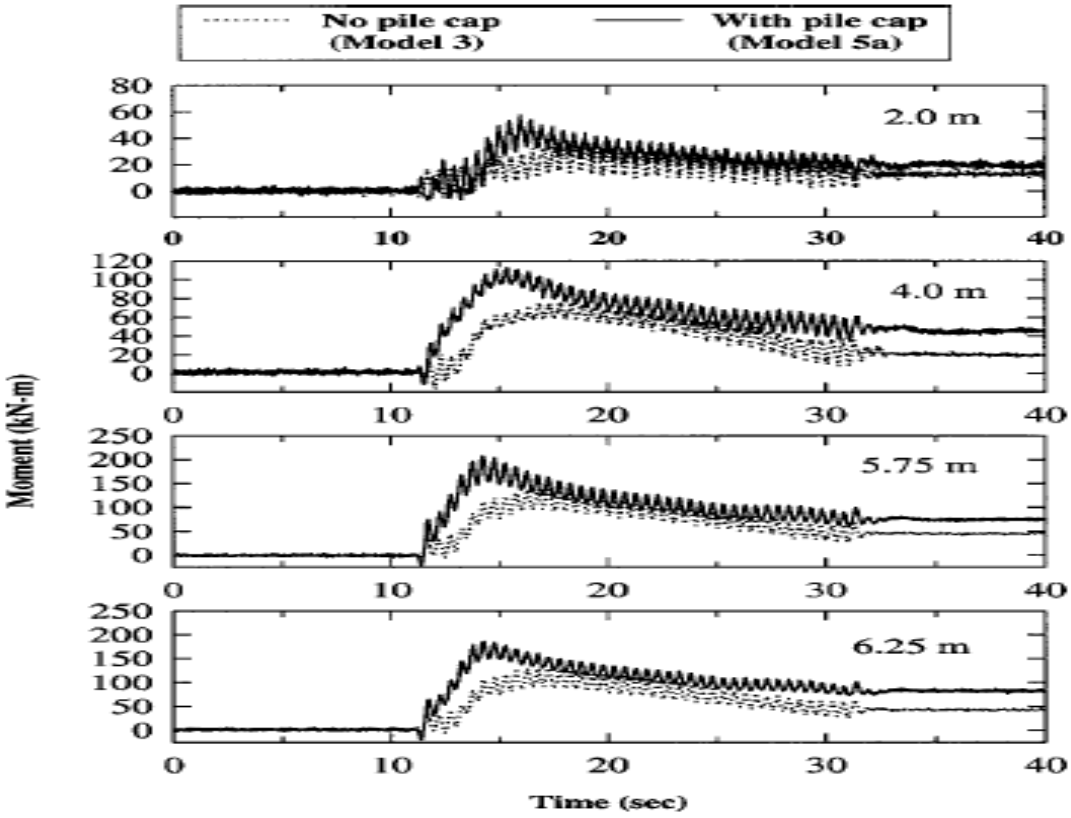

Figure 1-21. Comparison between centrifuge Model 3 and 5a selected results (after Abdoun *et al.* 2003)

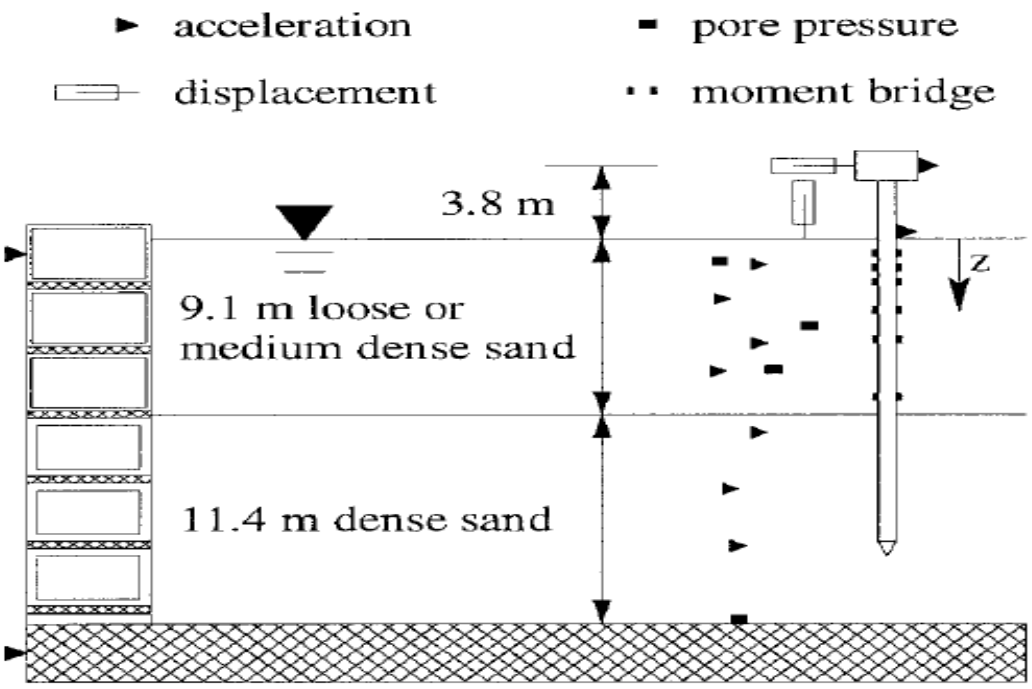

Figure 1-22. Schematic of layout and instrumentation for Centrifuge test model (after Wilson *et al.* 2000)

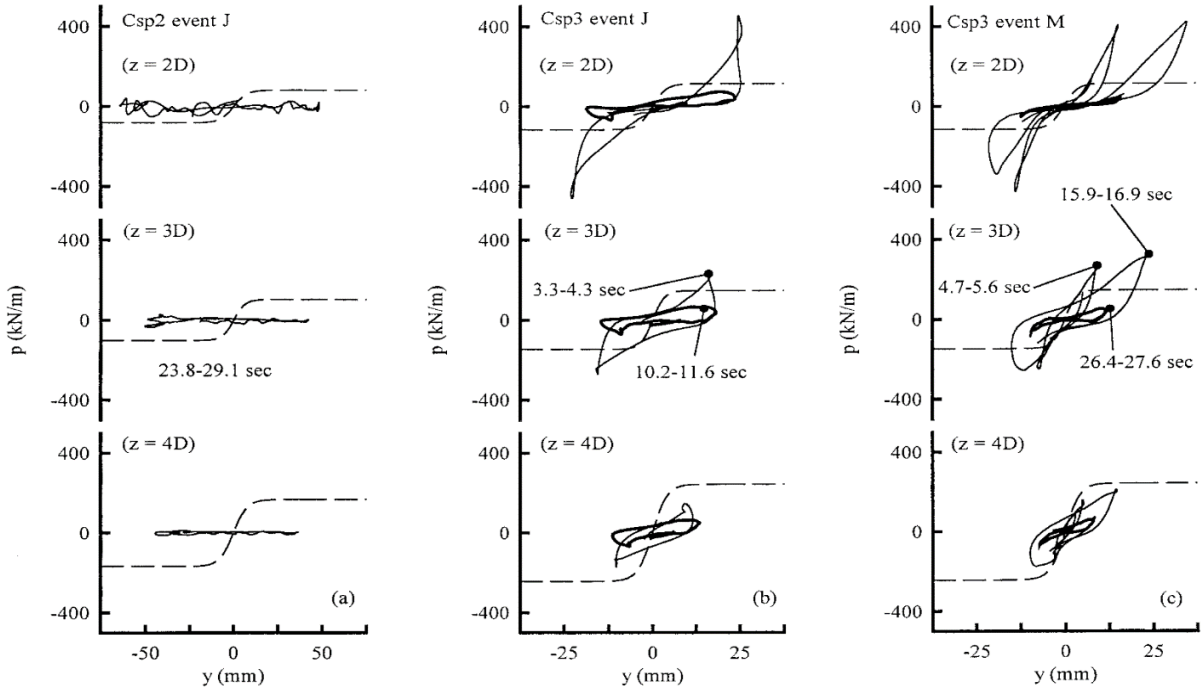

Figure 1-23. Back calculated *p-y* curves from physical testing data (after Wilson *et al.* 2000)

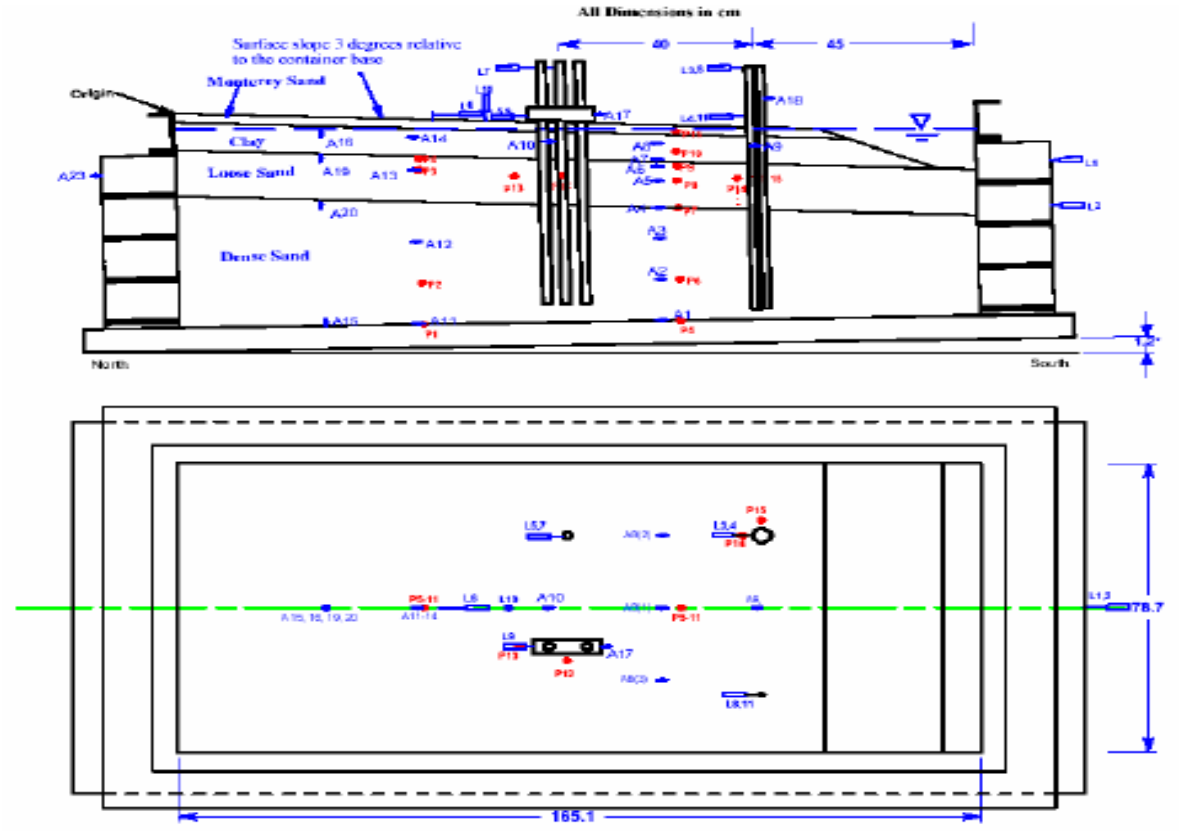

Figure 1-24. Centrifuge testing model of a pile group (after Singh *et al.* 2000)

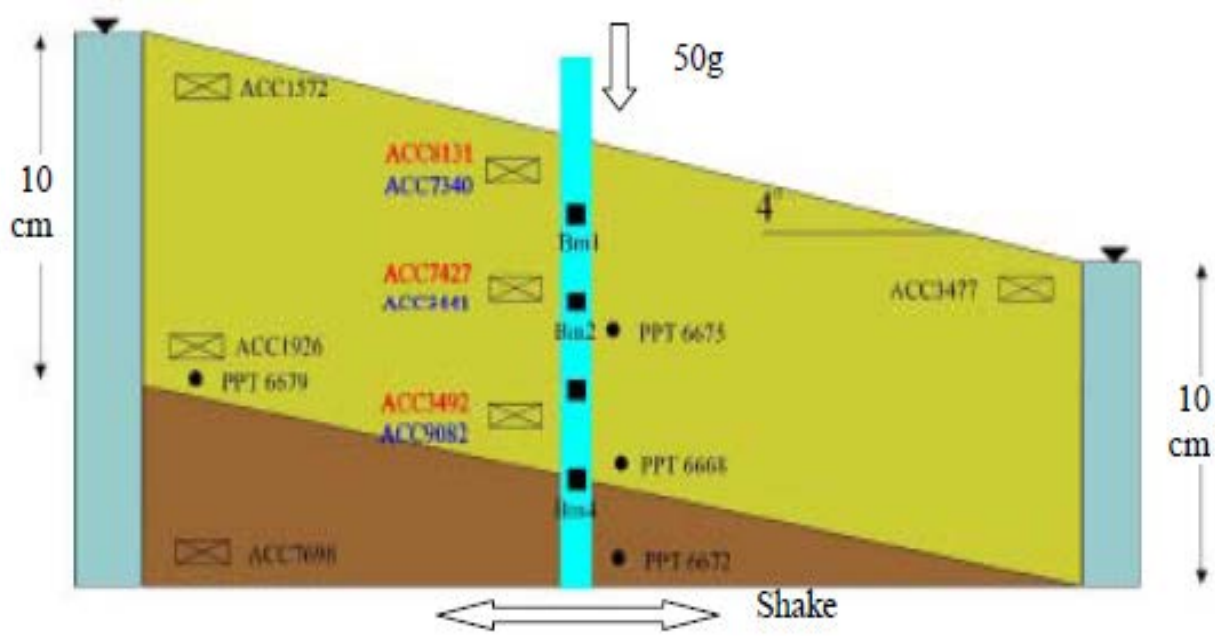

Figure 1-25. Centrifuge testing of a single pile in lateral spreading (after Haigh 2002)

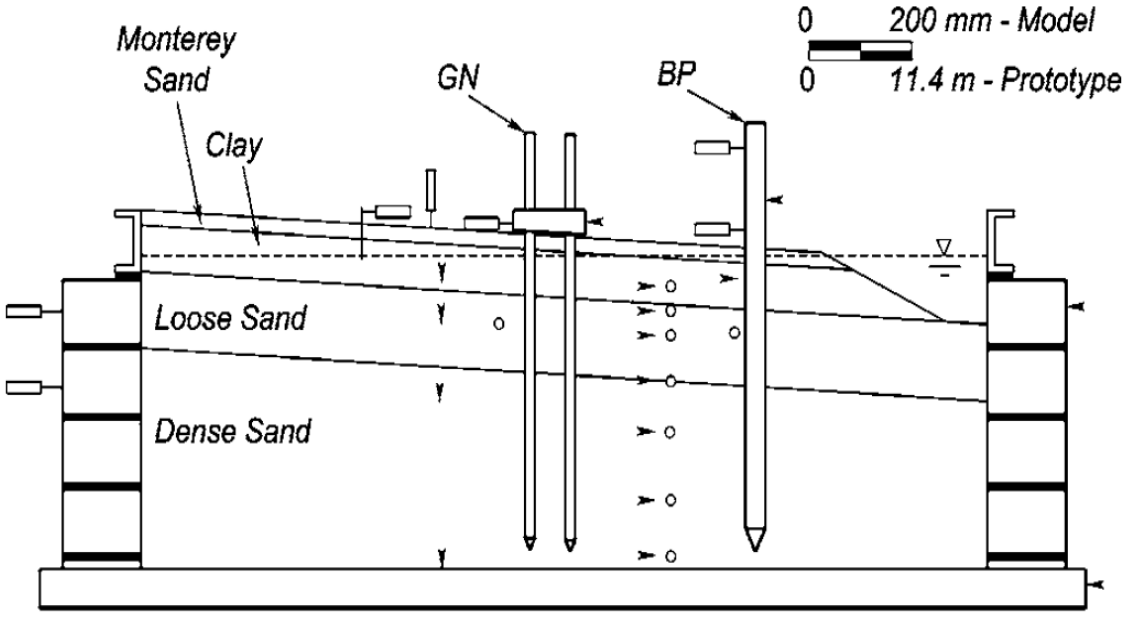

Figure 1-26. Centrifuge Model for single pile and pile group in lateral spreading (after Brandenberg *et al.* 2005)

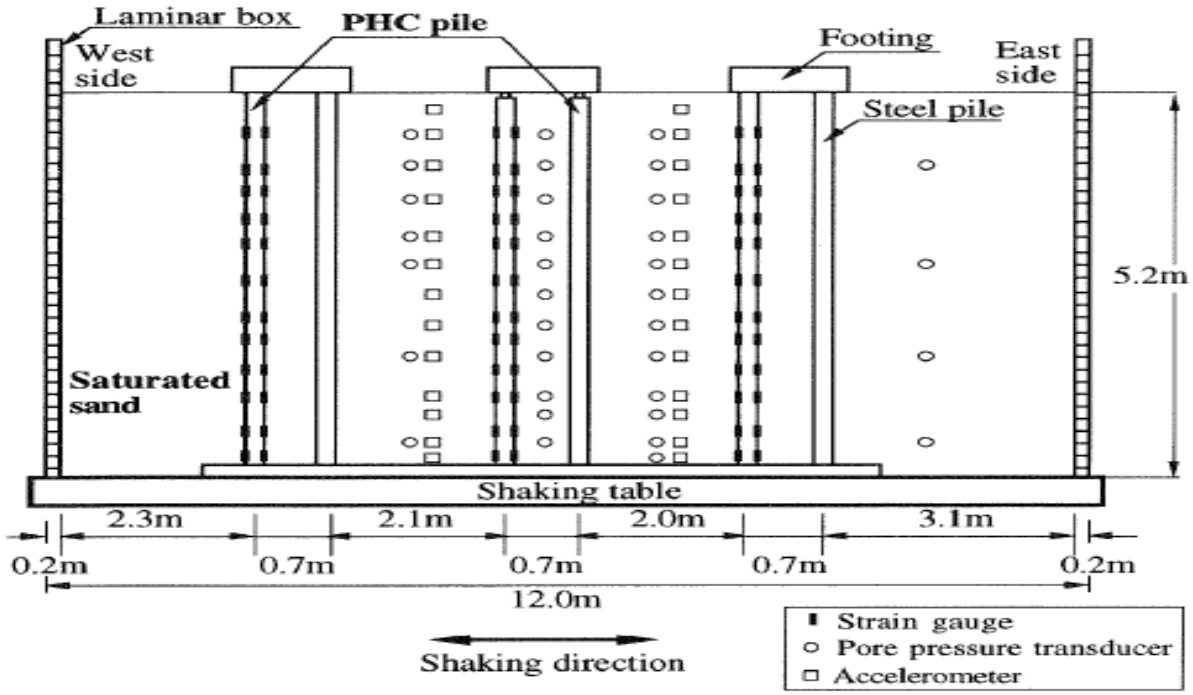

Figure 1-27. Cross-section view of the employed model (after Cubrinovski *et al.* 1999)

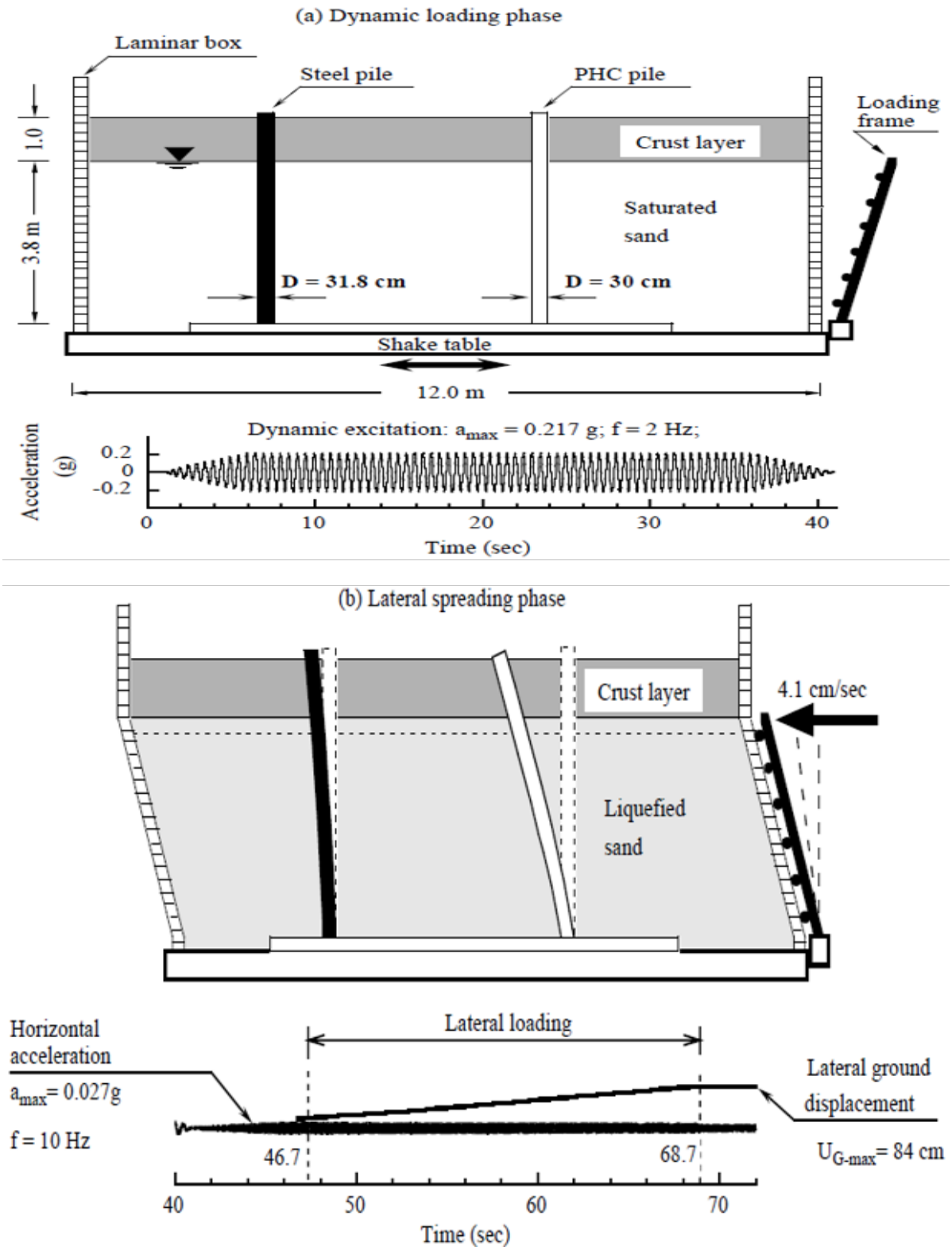

Figure 1-28. View of the conducted shake table test, a) shaking phase, b) pushover phase (after Cubrinovski *et al.* 2006)

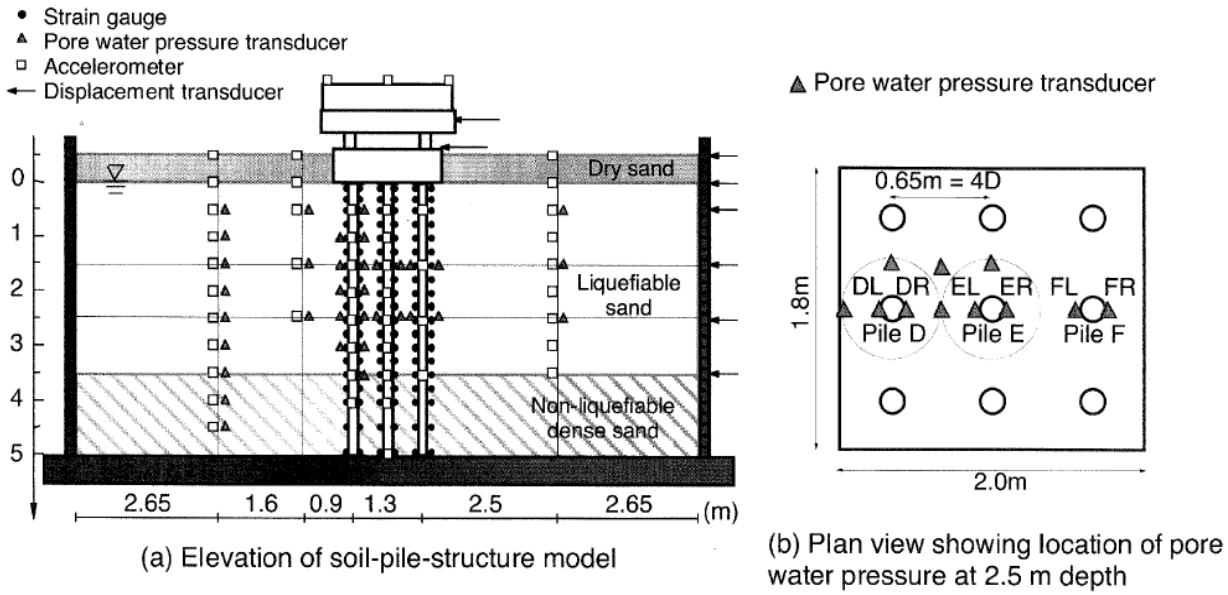

Fig. 1 Soil-pile-structure system

Figure 1-29. Shake table testing model (after Suzuki and Tokimatsu 2003)

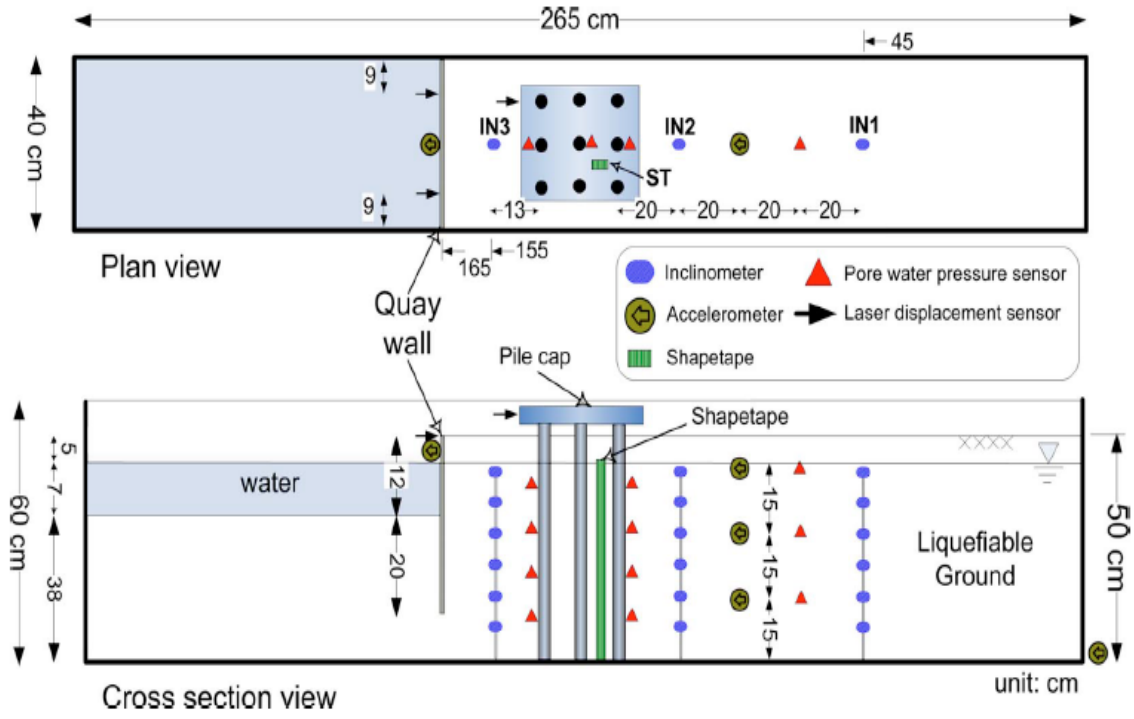

Figure 1-30. Pile group model behind a quay wall setup (after Motamed and Towhata 2009)

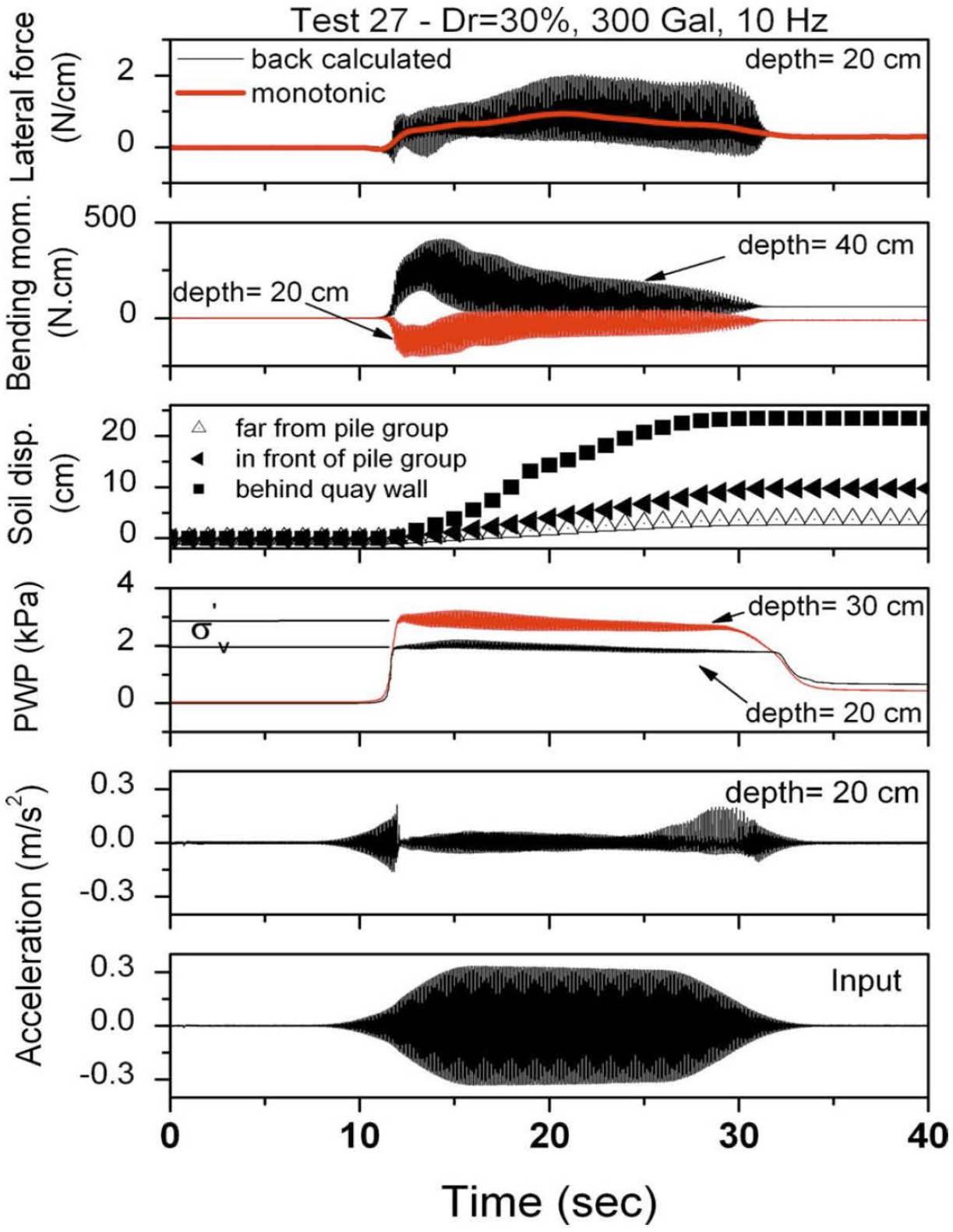

Figure 1-31. Selected results from pile group configuration (after Motamed and Towhata 2009)

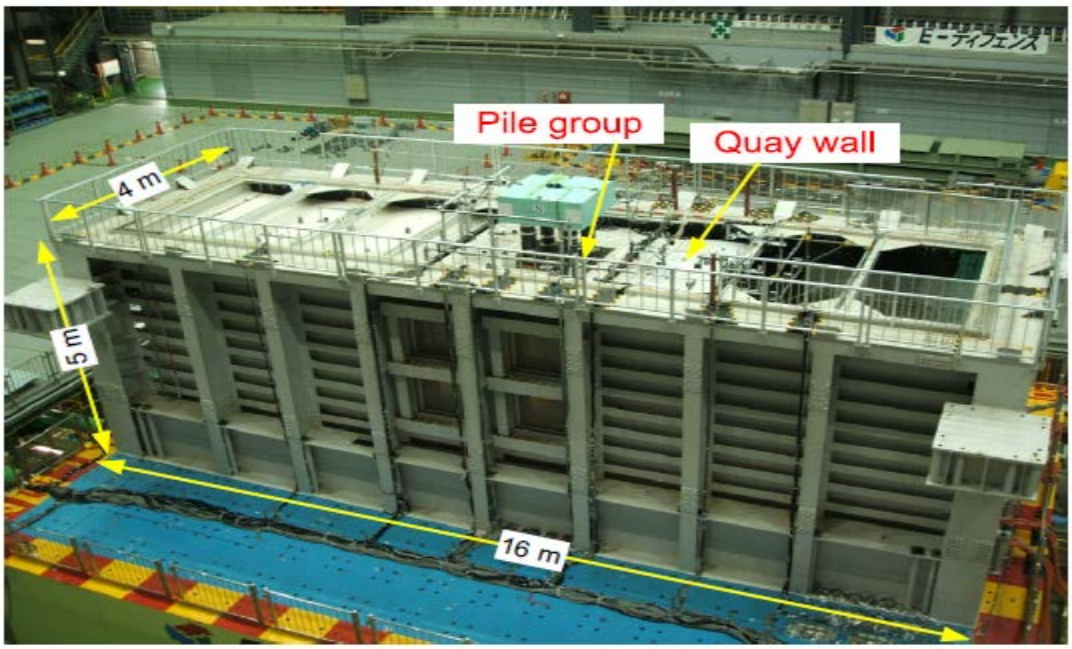

Figure 1-32. Large scale testing of pile group and quay wall at the E-Defence (after Motamed *et al.* 2013)

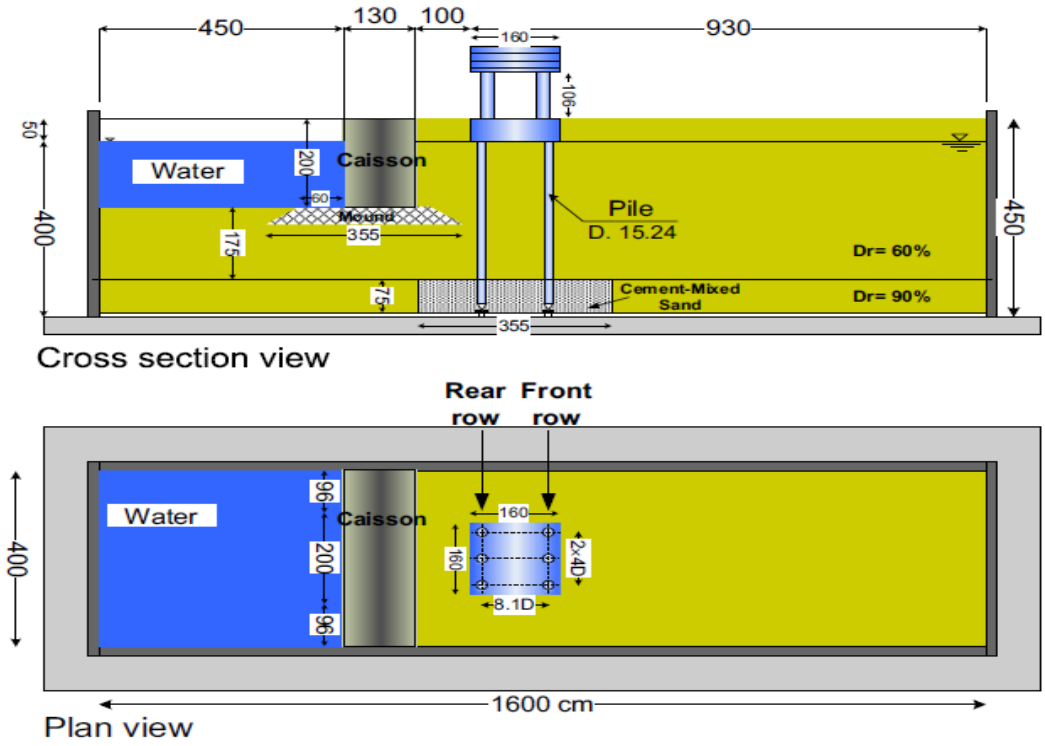

Figure 1-33. Schematic illustration of the test layout in E-Defense (after Motamed *et al.* 2013)

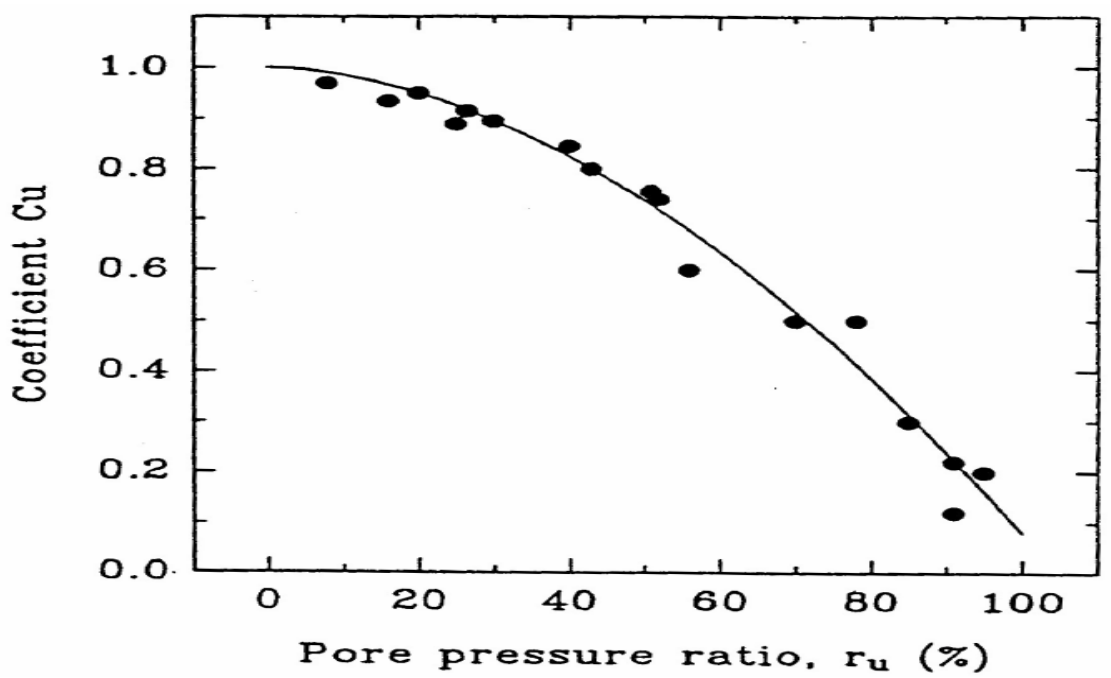

Figure 1-34. Degradation coefficient against excess pore pressure ratio (after Liu and Dobry 1995)

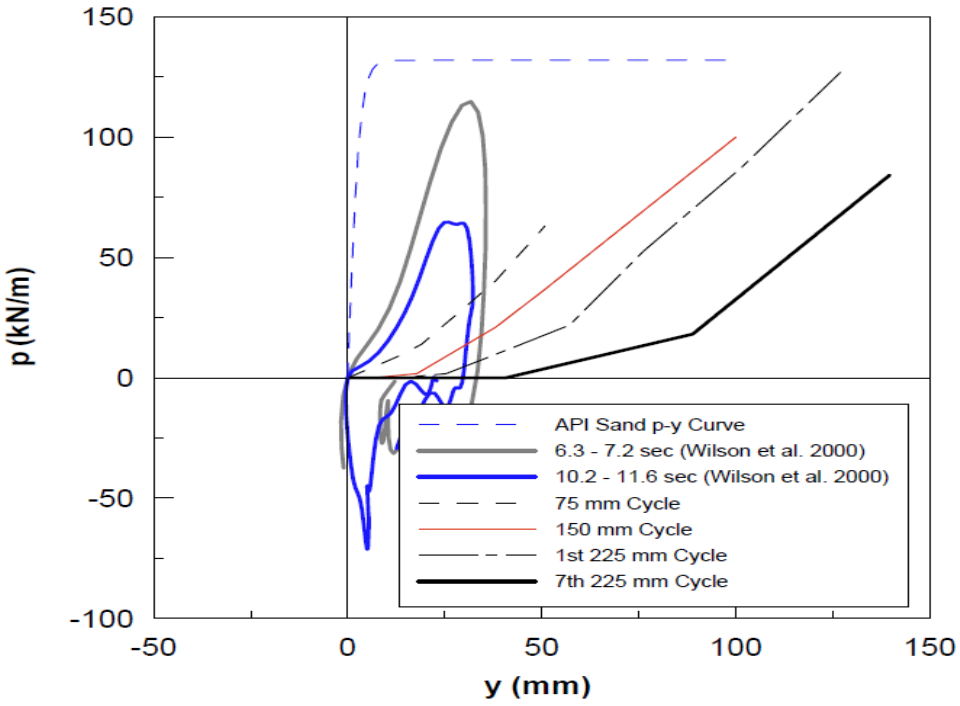

Figure 1-35. Comparison of Treasure Island *p-y* curves to API curves and back-calculated ones from centrifuge tests (after Ashford and Rollins 2002)

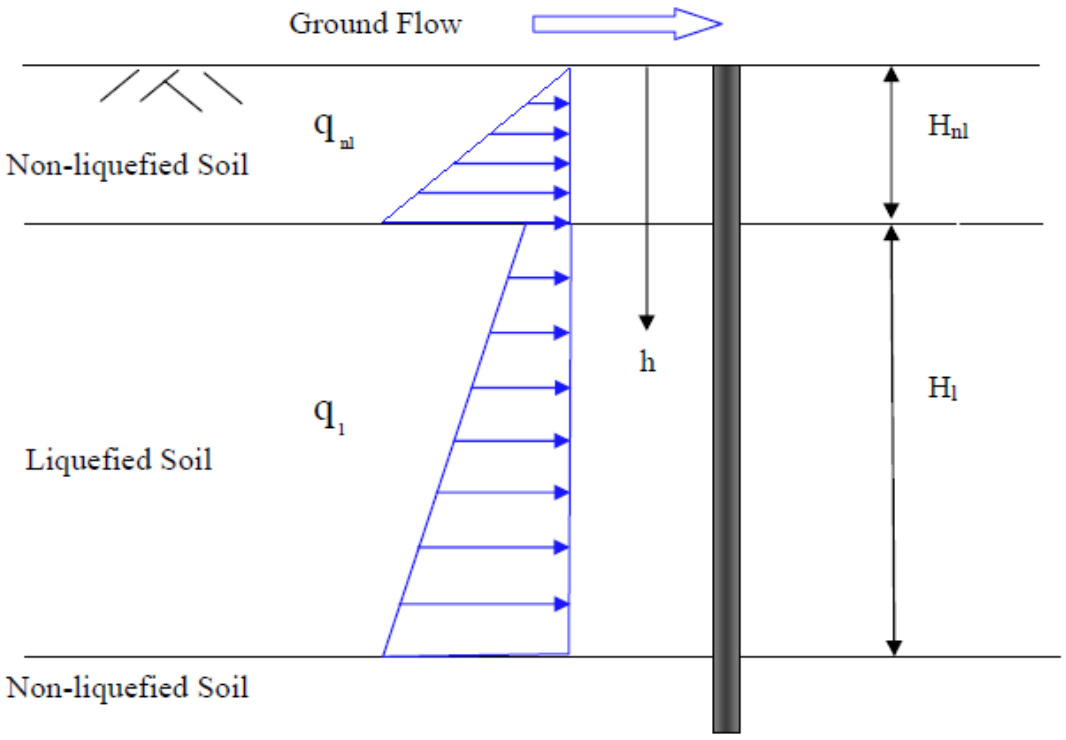

Figure 1-36. Illustration of lateral pressures on piles in lateral spreading (after JRA 2002)

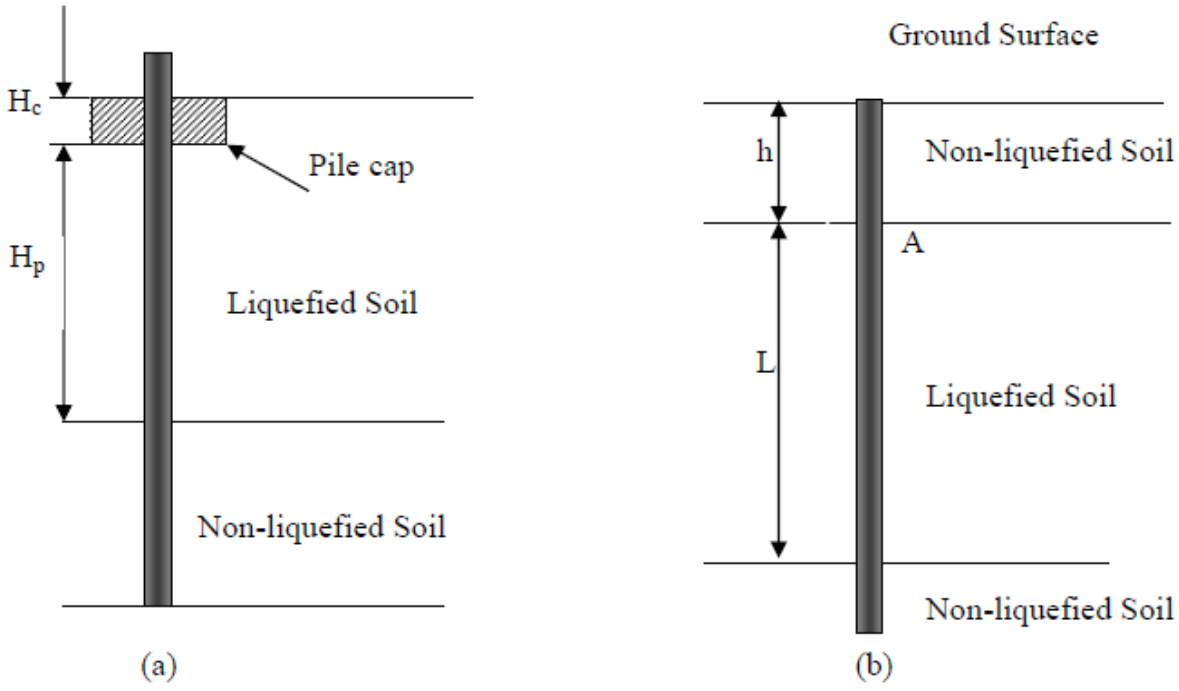

Figure 1-37. Pile foundation scenarios calibrated by Dobry *et al.* (2003)

Chapter 2 Simplified Method Analysis

2.1. Lateral Spreading Analysis for Bridge Foundations

2.1.1 Background

This chapter presents an example setup (Shantz 2013) used to evaluate the MTD 20-15 (2017) simplified procedure. It begins by describing the example including pile group configuration and pile and soil properties with a quick overview of the procedure followed. Next, the results of the implemented simplified method are presented, mainly in terms of bending moment, shear and displacement profiles, with comparison to those in the MTD 20-15 (2017) guidelines. After that, ambiguities in the procedure are discussed. Finally, recommendations and additional insights are given.

2.1.2 Example Problem Statement

Following the example from the Shantz (2013) guidelines document is addressed herein (Figure 2-1). The example is concerned with a bridge abutment with a two-row pile group in a multi-layered soil profile. The abutment is at the top of a slope with piles passing through a liquefiable layer to the dense one. The considered abutment is evaluated against lateral spreading and liquefaction. Figure 2-2 shows the pile group configuration and pile properties.

2.2. Simplified Method Procedure

This section presents the results of this study following the simplified MTD 20-15 (2017) procedure. The method uses slope stability analysis (step 1) to evaluate the soil lateral movement and imposes this ground displacement on a super pile via *p-y* curves (step 2) to evaluate the response. The super pile is an equivalent single pile with the combined pile group stiffness maintaining the diameter of the single pile. The combination of the two steps produces the design displacement and forces acting on the pile foundation. For slope stability analysis, Spencer's

method is employed. However, Bishop's and Janbu's methods were used for comparison and differences are discussed in the following sections. The computer code Slide 7 (rocscience.com) with Spencer's method was used as recommended by SCEC (2002).

2.2.1 Evaluating Liquefaction Potential

Following the methods of Youd (2001) and Idriss and Boulanger (2008), the liquefaction potential of the soil profile was evaluated (Figure 2-1). The results are shown in Table 2-1, which determine that only the loose sand layer is susceptible to liquefaction. For analysis purposes, the loose sand layer is modelled as a soft clay layer with residual strength S_r. All other layers will retain their original properties during the analysis.

After identifying the third layer as a liquefiable layer, the residual strength for the layer is calculated by using the equation by Kramer and Wang (2007) below:

$$S_r = 2116.\exp\left(-8.444 + 0.109(N_1)_{60} + 5.379\left(\frac{\sigma'_v}{2116}\right)^{0.1}\right) \tag{2.1}$$

Since the residual strength is dependent on the vertical stress in the layer, the residual strength values were evaluated at 3 depths for the loose layer to account for the inclination of the slope. One location beneath the top (beginning) of the slope, second location beneath the middle (center) of the slope, and third location beneath the bottom (end) of the slope, depending on the soil height above the loose layer. Residual strength values are shown below in Table 2-2.

2.2.2 Finding the Critical Failure Surface

After establishing the soil profile and properties to be used in the analysis. We now proceed to finding the failure wedge by defining a critical failure surface in the centerline of the loose layer. We will proceed to use properties from Figure 2-1 (Table 2-3) and preform a slope stability analysis using Slide 7. We specify a block type failure in the analysis to achieve a non-circular

surface or a wedge failure. The failure wedge and the resulting critical yield acceleration are shown in Figure 2-3. The figure illustrates 24 ft of fill, followed by 6 ft of soft clay, 13 ft of liquefied soil and dense sand at the bottom.

Before getting into the pseudo static calculations, a static run is performed to make sure the slope is stable under static conditions and liquefiable properties. If slope is stable, we proceed with the pseudo-static analysis, otherwise, the guidelines (MTD 20-15 2017) suggests flow failure. For this profile, static factor of safety is greater than 1, meaning a stable slope. The critical failure surface yield acceleration is 0.138g for an unrestraint slope using Spencer's method for slope stability analysis. Spencer's method was chosen for analysis based on recommendations from SCEC (2002).

This critical yield acceleration can be substituted into Bray and Travasarou (2007) equation to estimate the free field displacement based on the expected earthquake's PGA and Magnitude as shown below:

$$D(cm) = Exp[-0.22 - 2.83Ln(k_y) - 0.333Ln(k_y)^2 + 0.566Ln(k_y)Ln(PGA) + 3.04Ln(PGA) - 0.244Ln(PGA)^2 + 0.278(M_w - 7)] \quad (2.2)$$

The free field displacement calculated from this analysis is 2.80 inches.

2.2.3 Modeling the Super Pile

The simplified procedure depends on modelling the pile group as an equivalent super pile. This super pile has the equivalent stiffness of all piles in the group but retains the single pile width. Each pile was a 24-in diameter Cast-In-Steel Shell with 0.5-in steel shell thickness and 7 x #10 bars. There were 12 piles in the group. To convert the group into an equivalent super pile with the necessary input parameters for LPILE, the Moment-Curvature curve for the single pile needs to be

scaled accordingly and the rotational stiffness of the group is calculated based on geometry and axial stiffness.

The Moment-Curvature response can be calculated using LPILE by plugging in the single pile cross section (Figure 2-2) as shown in Figure 2-4. Properties of the pile materials are listed in Table 2-4. For super pile calculations, we multiply the Moment values by the number of piles (12 in this case). In LPILE, the super pile is defined with the diameter of the single pile along with the super pile Moment-Curvature.

This Moment-Curvature applies for most of the pile length, however certain considerations must be taken when modeling the pile cap part or the connected portion of the pile to the pile cap. The Shantz (2013) guidelines suggest that the first 2 feet of the pile, be modelled also as a super pile with the same properties but with half the steel shell thickness. Due to this modification, a second Moment-Curvature is developed for the first 2 feet and then scaled up by the number of piles. The outer diameter of the pile is still 24 in. The Moment Curvature for the reduced section is shown in Figure 2-5.

The pile cap is modelled also with the same width as the super pile (same as single pile, 24 in). The only difference is that the pile cap is modelled as elastic non-yielding section with a much larger stiffness. For super pile stiffness of the pile cap portion, the stiffness of the single pile is multiplied by the number of piles in the group multiplied by a factor of 100.

$$EI_{cap} = 100\ n\ EI \tag{2.3}$$

$$K_{ax} = 0.75*2*200/0.25 = 1200 \text{ kips/in} \tag{2.4}$$

$$K_{rot} = 144*\ K_{ax}\ \text{sum}\ (n_i*x_i^2) = 5.2x10^{10} \text{ lb-in} \tag{2.5}$$

Where n is the number of piles in i^{th} row and x is the row center distance from group centerline.

2.2.4 *P-y* curves for Super Pile

This section is divided into 2 parts. The first is calculating the *p-y* curves for the pile cap according to Shantz (2013) and the second is using the *p-y* curve models existing in LPILE to model the soil strata surrounding the pile.

2.2.4.1 *P-y* curves for the Crust Soil

This part is concerned with finding the maximum forces acting on the pile cap from the crust, upper portion of the piles still in the crust and the side friction between the pile cap and the crust. All required equations are present in Shantz (2013), to calculate the ultimate crust force and the maximum displacement then used to develop a tri-linear *p-y* curve for the crust portion of the super pile. The tri-linear plot is shown in Figure 2-6. This *p-y* curve is applied to the pile cap and the portion of the pile in the crust. Therefore, it is applied to the super pile in the 18 feet of fill and 6 feet of soft clay for this study. Since the tri-linear curve is calculated on a pile group basis, the number of piles and group reduction factor is already included in the relevant part of the calculations.

2.2.4.2 *P-y* curves for the Liquefied Soil

For the liquefied soil, the residual strength previously calculated for the loose sand is used as shown in Table 2-2 for *p-y* calculation. The calculations are done based on the Matlock (1974) soft clay model. For the dense sand beneath the liquefied soil, the Reese *et al.* (1975) sand model is used for *p-y* calculation. These models for soft clay and sand are developed based on soil strength and pile diameter, thus it is essential to multiply *p* by a factor. This factor includes the number of piles (12 in this case) and a reduction factor (m_p), referred to as group reduction factor, GRF.

For the liquefied zone, there is no reduction factor and the employed *p-y* is multiplied by the number of piles. On the other hand, for the dense sand, a group reduction factor is used, and it is higher near the liquefied boundary. The reduction factor is obtained according to Mokwa (2000), depending on the row position as shown in Figure 2-7.

To summarize, after accounting for the liquefied boundary effect in the dense sand, we get the reduction factors shown in Table 2-5. Figure 2-8 shows the *p-y* curves for the soil models constructed by LPILE for modeling the liquefied layer as soft clay.

2.2.5 LPILE Model

The LPILE model is employed to impose a range of displacements on the super pile up to 24 in and plot the restraining (shear) force at the critical surface against the soil surface displacement. The soil displacements are applied in 4 in increments until we reach 24 inches. The critical surface is in the center of the liquefied layer, at 31 feet depth, hence this is where the restraining force is calculated and then the average of the restraining force is obtained by dividing the restraining forces obtained by 2 or a running average can be calculated instead. Results are shown in Table 2-6 and plotted in Figure 2-9.

2.2.6 Slope Stability Analysis

A range of restraining forces are applied in the slope stability model to calculate the corresponding critical accelerations, k_y. Furthermore, additional restraining action is applied from the superstructure acting at the lower 1/3 of the abutment backwall. This point force should be less than the passive resistance of the abutment divided by a factor of 2 to reflect the average resistance. Both restraining forces should be divided by the effective abutment width as the slope stability slide model is per unit width.

2.2.7 Effective Abutment Width

The effective abutment width is calculated based on the following equation:

$$W_e = W + \frac{m}{2}.H \tag{2.6}$$

Where, W is the width of the embankment (44 ft)

H is the height (24 ft)

m is the slope (2:1)

Therefore, the effective width W_e = 68 ft.

2.2.8 Superstructure Restraining Force

The restraining force is calculated in the same manner the force on the pile cap is calculated using the log-spiral method. The result is a restraining force of 464 kips.

Therefore, the restraining force applied in the slope stability analysis is F=464/68=6.8 kip/ft. This force is to be applied in the lower 1/3 of the abutment wall (lower 6 ft of the 18 ft).

2.2.9 Slope Stability Slide Model

The restraining force of the super structure and a range for the pile restraining forces are applied to the slope model as shown in Figure 2-10. After running the Slide model and obtaining a range of critical accelerations from the analysis, we substitute the k_y obtained along with the design earthquake of magnitude 7.5 and 0.5g PGA into equation (2.2) by Bray and Travasarou (2007) for displacement (Table 2-7).

2.2.10 Design Displacement

After the Slide analysis is complete, results from Slide are plotted against the results from LPILE already obtained and shown in Figure 2-9. The main slope stability analysis method used

to complete the analysis is Spencer's method, however Bishop's and Janbu's methods are also plotted in Figure 2-11 to compare the effect of the analysis method on the results. The intersection of the restraining force against displacement curve from Slide with the restraining average curve from LPILE analysis is the design displacement as shown in Figure 2-11. This design displacement is applied to the LPILE model to compute the final reaction forces on the super pile. An approximate 11% difference between the resulting design displacements is observed from the different methods.

Design displacement = 2.8 in using Spencer's Method.

Design displacement = 2.9 in using Janbu's Method.

Design displacement = 3.1 in using Bishop's Method.

By applying those design displacements to the *p-y* curve LPILE model, the outcome of each analysis is then compared. Figure 2-12 shows the different pile deflections that result from applying the design displacements mentioned above. Figure 2-13a presents the bending moments for the different analysis methods and Figure 2-13b shows the shear forces. For the analyzed soil profile, the difference in design displacement was approximately 11% between the 3 cases. However, the displacement values are small so the resulting difference in pile deflection, bending moment and shear force were minimal. For a soil profile where the design displacement is substantial, difference in results would be significant.

2.2.11 Simplified Method Results Summary

The final design displacement is 2.80 in, obtained by following the procedure described in the earlier sections. The calculated 2.80 in (0.071m) design displacement profile is applied by pushing the entire crust layer by this design displacement and linearly decreasing the displacement in the liquefiable layer reaching zero at the bottom of the liquefied layer (Figure 2-14). This

displacement profile is applied to the LPILE *p-y* curve model and the resulting displacement, bending moment and shear are shown in Figure 2-14 and Figure 2-15 (results referred to as UCSD). On the same figures, the results obtained from Shantz (2013) as a reference are presented for comparison.

Figure 2-14 shows the imposed soil displacement on the super pile and the resulting pile displacement. The imposed displacement was 2.80 in and the pile head displacement was 2.35 in (0.06 m). This compares to an imposed soil displacement of 4.6 in giving a pile head displacement of 3.9 in for the Shantz (2013) model.

Figure 2-15a shows the bending moment profile on the super pile with the maximum moment of 96,700 kip-in occurring in the liquefied layer. The bending moment calculated resembles the shape of the one from Shantz (2013). However, due to the lower imposed displacement and resulting reduced pile head displacement, the bending moment from the UCSD model is much lower than that of the Shantz (2013) guidelines, which reached a value of 151,000 kip-in at maximum.

Figure 2-15b shows the shear profile with a maximum shear force of 1,306 kips. The shear force diagram also has the same shape for both UCSD and Shantz (2013) model, but the Shantz result is higher due to the higher design displacement applied. Maximum shear value from the Shantz model was 2000 kips.

Table 2-8 summarizes the difference between maximum values recorded for the two models. Finally, Table 2-9 summarizes the moment capacity and demand for the different pile sections. As described in Shantz (2013), the top section, between the pile cap and the rest of the

super pile is modeled with steel shell thickness, half that of the normal pile. The second bottom section assumes the full super pile properties.

From Table 2-9 , we conclude that the demand on the pile group is less than the allowable capacity. Therefore, the pile group is safe against loading imposed by liquefaction and lateral spreading.

2.2.12 Main Difference between the Results

The UCSD implementation of the simplified method resulted in 60% of the displacements and bending moments resulting from the Shantz (2013) implementation. This difference is a result of several factors and ambiguities that will be discussed below. Therefore, implementation by designers is subjected to interpretations and variations.

The main cause for the difference between the results is the slope stability analysis procedure. The LPILE *p-y* analysis part of the procedure has been verified against Shantz (2013) results and the verification is shown in the following sections. In the UCSD model, slope stability analysis was performed using Rocscience Slide 7 employing Spencer's method. The software and method of analysis for the Shantz (2013) solution were not stated.

2.2.13 Previous Studies

Several studies were conducted to examine design parameters that account for this incompatibility in displacements between pile foundation restraining forces and abutment displacement, and some of those studies are presented here. Boulanger *et al*. (2006) highlighted four issues that need to be considered: i) the equivalent constant restraining forces is smaller than pile force at the end of shaking, ii) critical sliding mass increases as pile pinning forces increase, iii) tributary slide mass width is greater than abutment crest width, and iv) deformations in the

abutment can reduce pile fixity above the liquefied layer. Turner *et al.* (2016) highlighted the importance of considering superstructure inertial demands while considering the full bridge contribution to the restraint. Turner *et al.* (2015) discussed the importance of having high quality boring logs to generate an accurate high-resolution soil profile.

Numerical studies by Turner *et al.* (2014) show that moment demand does not increase significantly for lateral spreading displacements in excess of 2 feet as full passive pressure has been mobilized. Their field observations point to non-yielding of the sections as columns did not undergo rotations or displacements indicative of that. Other numerical assessments demonstrate the accuracy gained by using 3D FEA (McGann and Arduino 2014). They show the effect of changing the bridge gap and slope stability method on the system response.

2.3. Verification of LPILE Model Against Shantz (2013) Example

The purpose of this section is just to compare results of UCSD LPILE model with the LPILE model used in Shantz (2013) guidelines. Therefore, both models impose a 4.6 in displacement profile as the guidelines example prescribes, and compare the results, mainly moment, shear and displacement. Figure 2-16 and Figure 2-17 show those comparisons respectively and while the numbers are not exactly the same, the results are very close.

Table 2-10 compares the maximum values for displacement, bending moment and shear between the 2 models. A slight difference in results can be attributed to different LPILE versions used. The new LPILE version has automatic spring reduction factors in regions near the liquefied zone, i.e. top 2 or 3 feet of the dense sand layer. These newly introduced reductions add to the reduction factors already calculated manually.

2.4. Simplified Method with Different Liquefied Layer Properties

The purpose of this section is to study the effect of weakening the liquefied layer strength. The liquefied layer had an original blow count of 14 giving a residual strength of 587 psf at the top of the slope. This section compares different strengths of the soft clay model by changing the blow count of the liquefied layer. Blow counts of 14, 8 and 4 are compared each of those giving a different residual strength. Table 2-11 shows the residual strength of the original model (Model 1) and Model 2 with 8 blow counts and Model 3 with 4 blow counts.

Figure 2-18 shows the different *p-y* curves for the different residual strength, showing that as the strength decreases, the soil spring stiffness and strength decreases. Figure 2-19 and Figure 2-20 show the design displacements for Model 2 and 3 respectively. Design displacement was 6.65 in and 10.7 in for Models 2 and 3 respectively. For model 3, increasing the restraining force stopped providing additional resistance after a certain limit and did not affect the design displacement afterwards.

2.4.1 Comparison of the results

The design displacement for the 3 models are then applied to the LPILE model to calculate the actual pile displacement, bending moments and shear force. Figure 2-21 and Figure 2-22 presents the results of the comparison showing deflection profiles, bending moment and shear force profiles for the three models studied. As the liquefied soil model weakens, it causes more displacement and results in more loads acting on the pile. It is observed that by decreasing the blow count from 14 to 8, the displacements, bending moments and shear forces increase by more than double. Further decrease in blow count from 8 to 4 also results in increased displacements by almost 1.5 times but with a much lesser increase in bending moments and shear forces.

2.5. Simplified Method with Varying Failure Surface Location

In this section, focus is placed on the location of the failure surface and its effect on the results. As the critical failure surface changes from the center of the liquefiable layer to the bottom of the layer, the contribution of the liquefiable layer changes affecting the results. Spencer's method is also used for this part.

2.5.1 Free Field Analysis

Referring to section 2.1.4 for the original location in the center of the layer arriving to a critical acceleration coefficient of 0.138 and a displacement of 4.05 inches, when restraining forces are zero mimicking free field state. Figure 2-23 illustrates the failure wedge when the location of the critical failure surface is changed to the bottom of liquefiable layer. The critical yield acceleration decreased to 0.074 resulting in a displacement of 10.15 inches.

2.5.2 Design Displacement Calculations

The design displacement is then incrementally applied in the LPILE model discussed previously. The resulting restraining forces are recorded in Table 2-12 and plotted in Figure 2-24 showing the average and running average as well.

The restraining forces in the slope stability model are then varied to find the soil displacement for each restraining force used as shown in Table 2-13. Results are plotted to intersect with values from Table 2-12 in order to find the design displacement as shown in Figure 2-25. Final design displacement is found to be 4.00 inches. This design displacement has increased compared to the 2.80 inches found when the failure surface was in the center of the layer.

2.5.3 Comparison of the Results

Figure 2-26 and Figure 2-27 present the comparison for deflection, bending moment and shear profiles respectively for the 2 cases with different critical surface locations. When changing the location of the critical failure surface from the middle of the liquefiable layer to the bottom of the layer, the displacements and forces acting on the piles increase significantly as the critical yield acceleration decreases. Table 2-14 presents the comparison between the two cases for maximum values calculated.

2.6. Use of Different Sliding Block Displacement Equations

In this section, two sliding block displacement equations and their effect on the resulting design displacement are compared. The first equation was proposed by Bray and Travasarou (2007) as mentioned before and is shown below:

$$D(cm) = Exp[-0.22 - 2.83Ln(k_y) - 0.333Ln(k_y)^2 + 0.566Ln(k_y)Ln(PGA) + 3.04Ln(PGA) - 0.244Ln(PGA)^2 + 0.278(M_w - 7)] \quad (2.7)$$

The second equation is the one by Martin and Qiu (1994) and depends mostly on the peak ground velocity, in addition to the peak ground acceleration. The second equation is shown below:

$$D(in) = 6.82\ (\frac{k_y}{k_{max}})^{-0.55}\ (1 - (\frac{k_y}{k_{max}}))^{5.08}\ A^{-0.86}\ V^{1.66} \quad (2.8)$$

The analysis procedure shown in this chapter is repeated using both displacement equations and the comparison for restraining force against displacement is presented in Figure 2-28. The figure shows the comparison between both equations. Based on available ground motion data with an average peak ground velocity of 36.6 in/s for 14 motions, having a maximum of maximum 45.8 and minimum of maximum values 25.9 in/s. Furthermore, this document uses the average peak

ground velocity of 36.6 in/s to compare with Bray's equation while also showing the minimum and maximum cases. The average peak ground velocity produced a design displacement of 5.45 inches compared to 2.8 inches from the first equation. The minimum and maximum envelopes of the peak ground velocity gave a design displacement of 3.4 in and 7.4 in respectively. The minimum displacement value is still higher than the displacement from the first equation used.

Pile head displacement, bending moments and shear forces are compared using the average peak ground velocity for Martin and Qiu's (1994) equation (2.8) and only using peak ground acceleration for Bray and Travasarou's (2007) equation (2.7). Equation (2.8) produces greater displacement than Equation (2.7) and thus greater pile displacement profile and lateral forces. Figure 2-29 and Figure 2-30 compare the results of pile displacement profiles, bending moments and shear forces respectively for the two cases. We can deduce that velocity is a contributing factor in the results.

2.7. Pile Stabilized Slope Analysis

This section compares results of the regular slope analysis methodology previously discussed in this document with results from a new feature introduced in Slide 7 (2017). The new feature allows modelling of a pile to support the slope instead of the resisting force usually applied in the middle of the liquefiable layer. This feature allows to more accurately model the pile-soil system for more reasonable results without the need to vary the restraining force in the liquefiable layer and find the intersection between the slope stability model in Slide and the *p-y* displacement push model in LPILE.

The super-pile previously computed was modeled in Slide using an elastic plastic model with modulus of elasticity of $6.79*10^7$ lbs/in^2 ($5.8*10^8$ kPa) and yield stress of $5.0*10^4$ lbs/in^2 ($3.45*10^5$ kPa).

Slope analysis (Figure 2-31) resulted in a critical yield acceleration k_y=0.187 which corresponds to a design displacement of 2.36 inch. The resulting displacement is 84% of the displacement from the original method (2.80 inch).

2.8. Summary and Conclusions

This chapter addresses the implementation of the MTD 20-15 (2017) simplified method and its implementation for design and analysis of pile foundation under liquefaction and lateral spreading. Furthermore, the UCSD implementation of the simplified method was compared to the Caltrans (Shantz 2013) implementation and a number of factors contributing to the outcome were compared.

2.8.1 Findings from Implementation of the Simplified Method Including Some Encountered Ambiguities

- The UCSD implementation of the simplified method resulted in 60% of the displacements and bending moments based on the Caltrans implementation. This difference is due to several factors and ambiguities that will be discussed below. Therefore, implementation by designers is subject to interpretations and variability.
- The analysis does not specify a slope stability analysis software or model dimensions which have an effect on the outcome.
- Pile head condition modelled as rotational stiffness at the top (fixation) for one pile group is different than stiffness calculated when engaging the full bridge.
- The displacement equation by Bray and Travasarou (2007) may not provide accurate representation of the slope displacement and if this method is to be used, a more rigorous earthquake displacement analysis should be considered as PGA and Magnitude may not be sufficient for adequately accurate results.

- The *p-y* analysis may not be a sufficient tool for lateral response due to the cyclic nature of loading.
- Super pile analysis may not be a good representation of the pile group as pile response varies between different rows and locations in the pile group.
- *p-y* reduction factors for transition between liquefied layer and layer below needs to be carefully looked at.

2.8.2 Conclusions and Limitations for the Simplified Method

- Pile group effect and contributions from the bridge super-structure reduce the pile displacement demands. Shadowing and shielding effects of the bents should be considered.
- Current analysis takes into account the abutment effect on top of the pile group but does not consider the full resistance of the bridge. As the bridge becomes stiffer with added foundation resistance, the total displacement incurred by the abutment foundation decreases.
- Method limitations in applicability should be clearly defined. For instance, slopes in narrow canyons will interact and behave differently from the postulated simplified method assumptions.
- Axial forces developed during shaking (particularly for pile groups) might have a significant effect on the pile resistance and pile lateral response should be adjusted accordingly.
- The simplified procedure should be evaluated against physical data.
- The displacements being applied are cumulative and result in a permanent displacement at the end, thus equivalent restraining force should be compatible to the loading condition.

- Analysis assumes restraining force in piles is constant throughout shaking. The actual restraining force changes during shaking according to the displacement.
- Analysis of the slope in the free field case without the presence of piles then modifying the acquired results by representing piles as forces at the failure surface is not accurate. Procedure is likely to over predict displacements.
- Fixing the location of the failure surface in the middle of the loose layer neglects the effects of the contribution of the entire layer. This procedure neglects the higher displacement that could have been calculated.
- Fixing the location of the failure surface fixes the resulting failure wedge. Analysis also neglects that failure sliding wedge is greater than the abutment width.
- The critical sliding wedge changes as it displaces and pushes on the pile foundation. The critical wedge size increases with increasing displacements and as pile restraining forces increase. The analysis procedure does not account for that. This was also identified by Boulanger *et. al.* (2006).
- Boulanger *et. al.* (2006) concluded that deformations within the abutment can reduce pile fixity above the liquefied layer resulting in reduced shear resistance of piles.
- Modelling of the pile cap and abutment in LPILE does not provide accurate representation of the deck fixation and structure interaction.
- Soil rigid plastic behavior and discrete sliding surfaces are a crude approximation of the soil behavior. Thus, the assumption that deformations only occur in the liquefied layer can overestimate the pile resistance.
- The procedure underestimates the residual strength of the liquefied soil and thus over predicting the soil displacement which might involve significant uncertainty.

- A more accurate soil property representation might be considered, by evaluating the shear stress-strain response.
- Method neglects effects of the bridge contribution to the pile response.
- Full bridge model analysis allows the modelling of more comprehensive soil profile properties, as well as better representation of pile restraining effects and full bridge contribution conditions.
- Results from the full bridge model analysis show significantly lower bending moments and pile forces.
- When the liquefaction-induced permanent displacement is applied to the full-bridge with all of its components engaged, lower displacement response is obtained compared to the case of the abutment foundation on its own.
- The bridge deck integrates its structural response and should be considered in the analysis.

2.8.3 Recommendations for the Simplified Method

- Clearly define the slope stability analysis methodology to be used. The author recommends Spencer's method of analysis.
- Different slope stability package result in varying factors of safety and critical yield acceleration. This issue needs to be verified and the final slope stability results should be confirmed by a hand calculation procedure.
- Slope stability software with the capability to model the embankment in three dimensions with better pile resistance representation are now available and are likely to produce more accurate results where applicable.

- Modelling should transition towards modelling the pile within the slope to calculate the design displacement without the need for varying forces and displacement to get the abutment displacement curve and pile restraining force curve intersections.
- Slope stability mechanics should be further investigated under lateral spreading loading mechanism. The slope will reshape itself to become more stable when subjected to high displacements. This reshaping will result in less cumulative displacement.
- Clear definition of model dimensions, for both slope stability and p-y model. Slope stability model should be long enough to avoid boundary issues.
- The failure surface location in the analysis is fixed and does not change with increasing displacements or loading which is not the case as the failure surface is affected by the pile foundation presence and resistance of the foundation to lateral spreading and imposed displacement.
- Values of restraining force used to obtain design displacement is average value not total. The lateral spreading load is not an alternating dynamic load so the full shear force in piles should be used.
- Different loose sand layer strength based mainly on blow count or friction angle has a significant effect on the results. Choosing a very low blow count will result in obtaining almost double the lateral forces and triple the displacement.
- Rethink the reduction factors for p-multipliers on the interface between the liquefied layer and layers above and below. LPILE already has a built-in reduction factor so that this issue needs to be reconsidered.

- Developing conversion factors to obtain bending moment and shear forces for each single pile from the super pile results. Some piles will be affected more than others.
- Consider modeling the pile cap and abutment as a fixed condition for the pile head with an added shear force. This way, we obtain a more realistic bending moment and shear force profile for the piles.
- Clarify pile head conditions whether fixed or pinned and how to include in the analysis.
- Conducting sliding block displacement analysis under specific design earthquake motions. Alternatively, an equation dependent on peak velocity and peak acceleration might provide better outcomes.
- Looking into LPILE enforcing zero shear force at the end of the pile.

2.8.4 Additional General Considerations

- Site stratification, and particularly presence of loose/soft strata at depth might result in lower than assumed peak ground accelerations at the site (and lower demand from the liquefaction triggering point of view).
- Highly recommended to rely on Cone Penetration Test (CPT) data, rather than SPT-type data.
- The applied displacement profile might be modified to account for potential weakening and deformations in an underlying dense sand stratum, due to liquefaction of the overlying loose stratum.

- A softening spring for liquefied soil response (shape more like that of stiff clay rather than soft clay) might result in more realistic outcomes, particularly for scenarios of large soil deformation. More details are further discussed in later sections of this document.

.

Table 2-1. Soil profile liquefaction evaluation

Layer	Soil Type	FS_{liq}	Notes
1	Fill	>2	Non-liquefiable
2	Soft Clay	>2	Use residual strength method for analysis
3	Loose Sand	0.46	Non-liquefiable
4	Dense Sand	1.35	Non-liquefiable

Table 2-2. Liquefied layer properties

Liquefied Layer	S_r [psf]
Top of slope	587
Middle of slope	444
Bottom of slope	251

Table 2-3. Soil profile properties

Layer	Soil Type	Layer Height [ft]	γ [pcf]	Φ	S_r [psf]
1	Fill	24	114	36	-
2	Soft Clay	6	102	-	835
3	Loose Sand	13	127	-	Table 2-2
4	Dense Sand	20+	130	38	-

Table 2-4. Pile properties

Pile Property	Assigned Value
Steel casing yield stress [lbs/in^2]	48,000
Steel casing elastic modulus [lbs/in^2]	2.9x10^7
Rebar yield stress [lbs/in^2]	48,000
Rebar elastic modulus [lbs/in^2]	2.9x10^7
Concrete compressive strength [lbs/in^3]	10,000

Table 2-5. *p-y* group reduction factors (GRF)

Depth [ft]	GRF
0-24	1
24-37	12
37-38	4.1
38-39	7
39-57	10

Table 2-6. Restraining forces resulting from soil displacement

Soil Surface Displacement [in]	Restraining Force [kips]	Restraining Force [kips]	Restraining Force Average [kips]
2	603	302	302
4	1,046	523	550
8	1,629	815	820
12	1,843	921	1,024
16	1,956	978	1,179
20	2,026	1,013	1,300
24	2,074	1,037	1,397

Table 2-7. Slide results

Restraining Force [kips]	Restraining Force per unit width [kips/ft]	Spencer's Method k_y	Spencer's Method Displacements [in]
0	0	0.159	3.17
136	2	0.164	3.00
272	4	0.168	2.87
374	5.5	0.171	2.78
408	6	0.172	2.75
544	8	0.175	2.67
680	10	0.179	2.56
816	12	0.182	2.48
952	14	0.187	2.36

Table 2-8. Comparison summary for different implementations

Model	Imposed Displacement [in]	Pile Head Displacement [in]	Bending Moment [kip-in]	Shear Force [kips]
UCSD	2.80	2.35	96,700	1306
Shantz (2013)	4.60	3.90	151,000	2000

Table 2-9. Moment demand and allowable moment on super pile (Shantz 2013)

Pile Section	Location	Allowable Moment [kip-in]	Moment Demand [kip-in]
Top reduced zone	0-2 ft depth	167,000	72,700
Main zone	>2 ft depth	239,000	96,700

Table 2-10. Result comparison for LPILE model verification

Results	Pile Head Displacement [in]	Max Bending Moment [kip-in]	Max Shear Force [kips]
UCSD	3.80	148,000	2010
Shantz (2013)	3.90	151,000	2100

Table 2-11. Liquefied layer properties

Liquefied Layer Properties	Model 1 S_r [psf]	Model 2 S_r [psf]	Model 3 S_r [psf]
Top of slope	587	306	198
Middle of slope	444	231	149
Bottom of slope	251	130	84.4

Table 2-12. Restraining forces resulting from soil displacements

Soil Surface Displacement [in]	Restraining Force [lbs]	Restraining Force Average [lbs]	Restraining Force Running Average [lbs]
0	0	0	0
2.00	631,391	315,695	315,695
4.00	1,059,093	529,546	563,494
8.00	1,620,623	810,311	827,776
12.00	1,791,127	895,563	1,020,447

Table 2-13. Slide results for bottom failure surface

Restraining Force [kips]	Restraining Force per unit width [kips/ft]	Spencer's Method k_y	Spencer's Method Displacements [in]
0	0	0.093	7.465
136	2	0.107	6.079
272	4	0.119	5.157
374	5.5	0.129	4.529
408	6	0.130	4.472
544	8	0.139	4.000
680	10	0.142	3.858
816	12	0.147	3.636
952	14	0.150	3.512
1,088	16	0.156	3.279

Table 2-14. Result comparison for different slope failure surface location

Location of Failure Surface	Soil Displacement [in]	Pile Head Displacement [in]	Max Bending Moment [kip-in]	Max Shear Force [kips]
Centerline	2.80	2.35	96,700	1306
Bottom of layer	4.00	3.34	132,000	1781

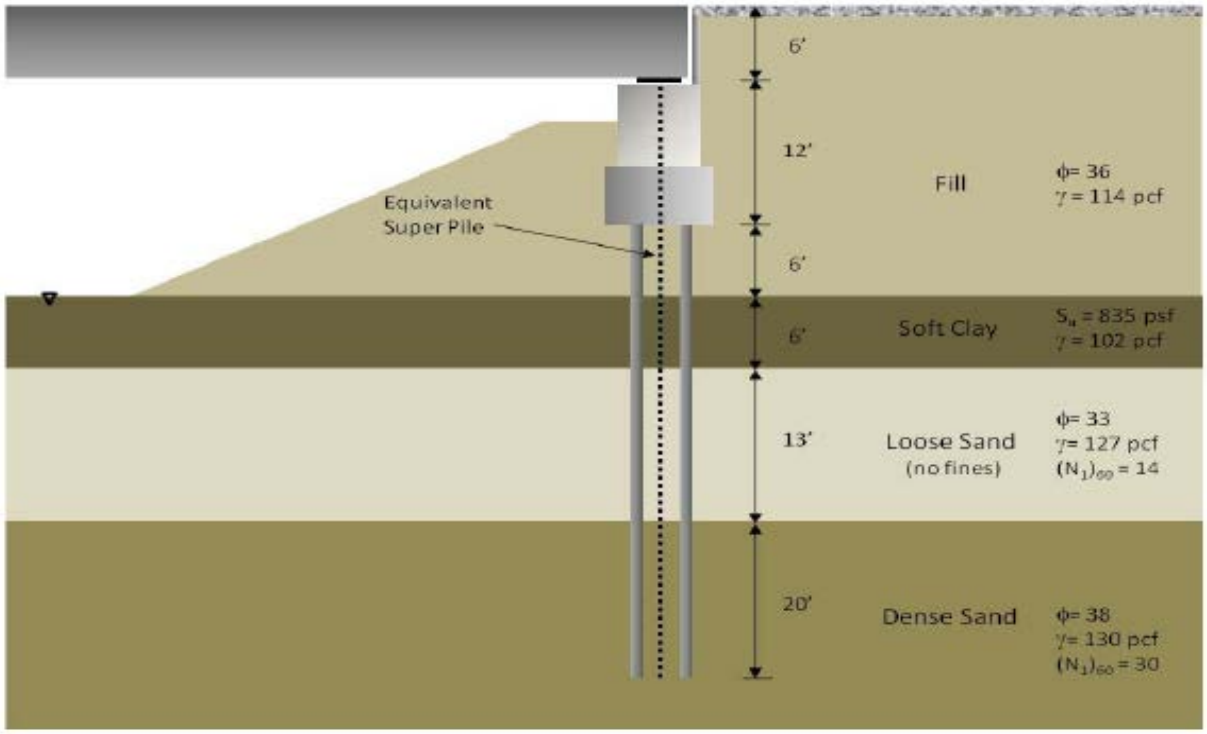

Figure 2-1. Example used to evaluate the simplified method (after Shantz 2013)

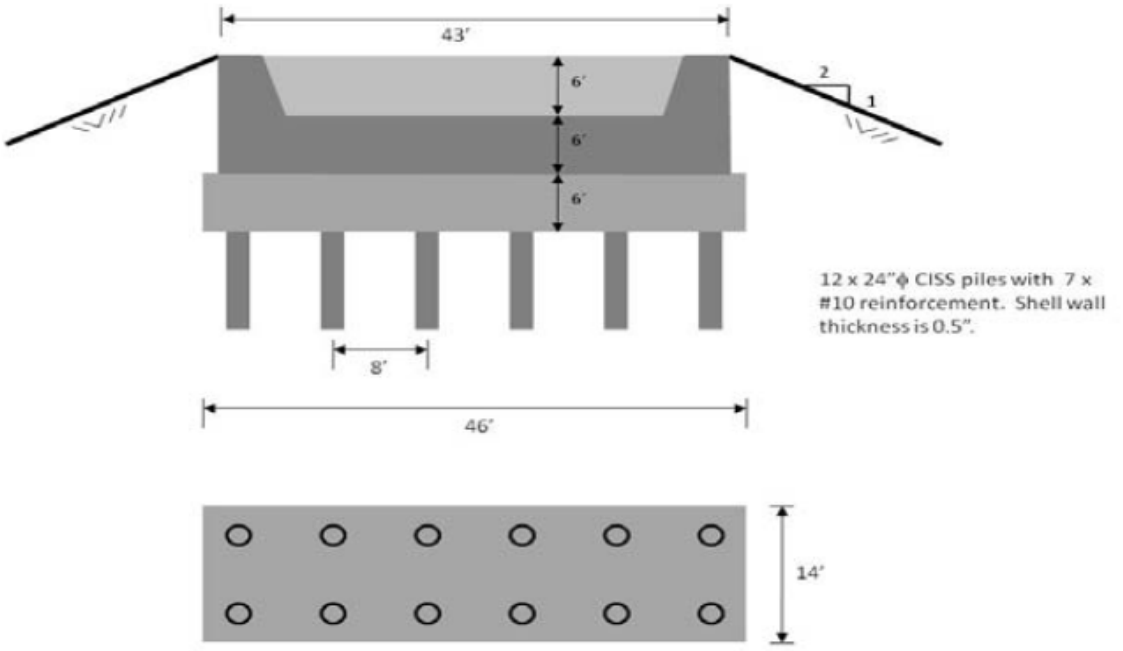

Figure 2-2. Abutment pile foundation arrangement with 8-foot pile spacing (side view & plan, after Shantz 2013)

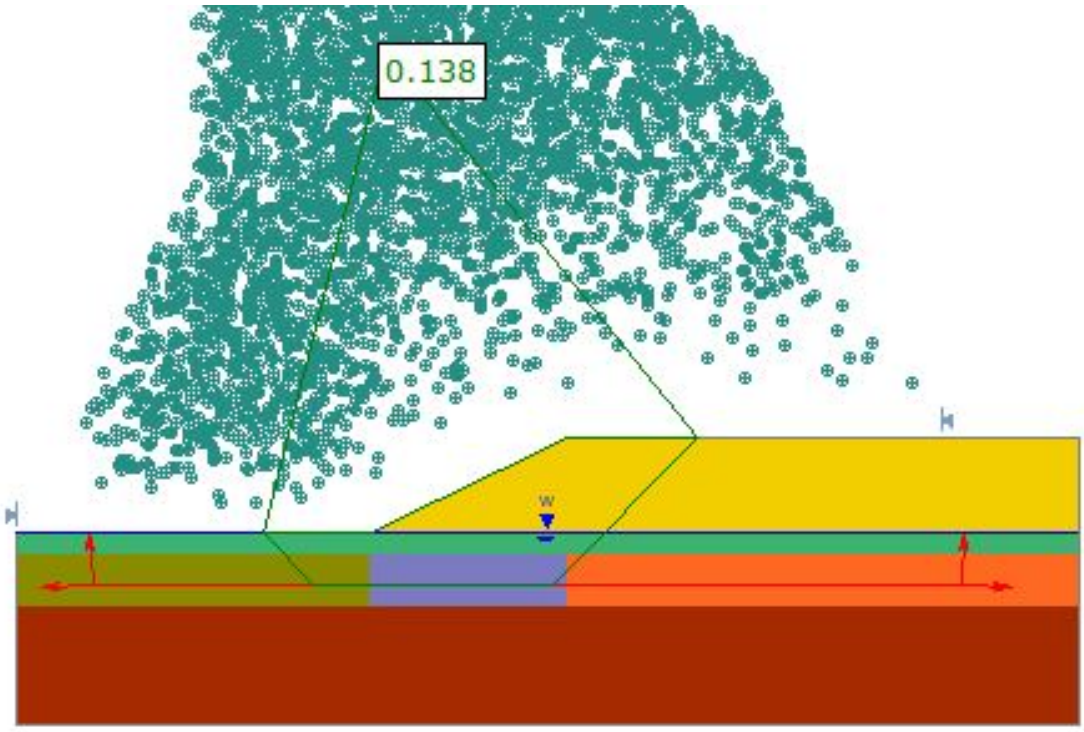

Figure 2-3. Critical Failure Surface from Slide analysis ($k_{y\ Spencer}$ = 0.138)

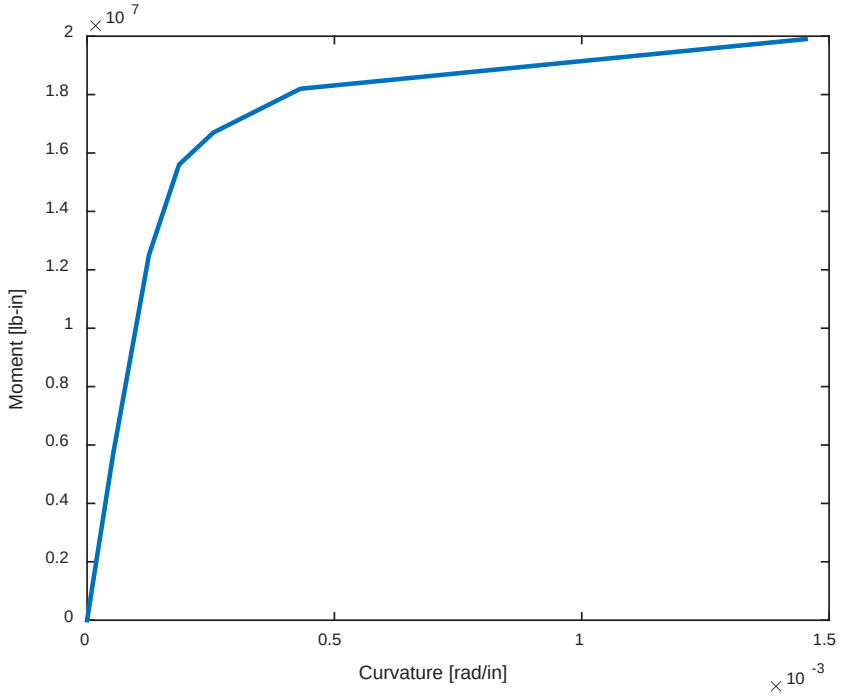

Figure 2-4. Moment-Curvature for single pile (derived from LPILE)

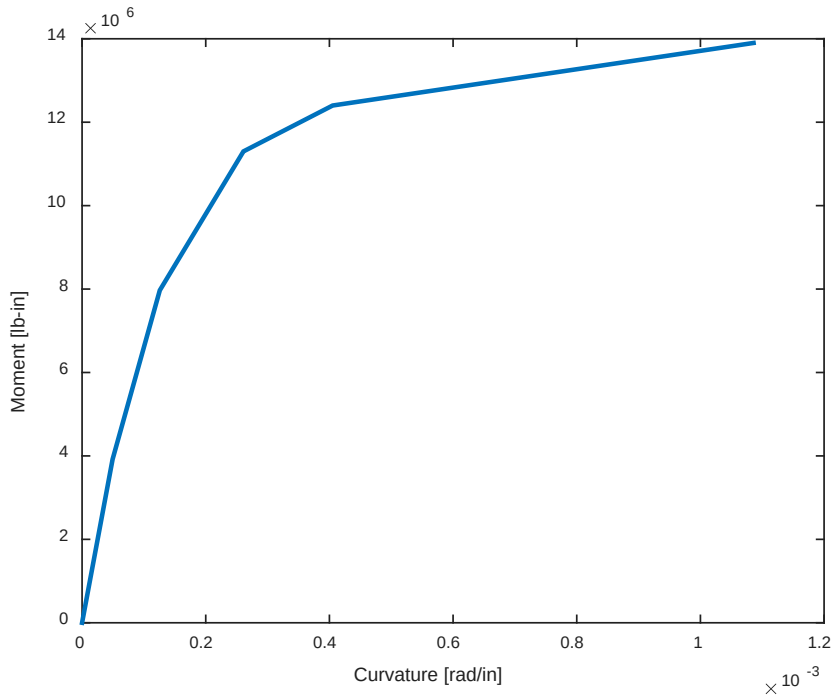

Figure 2-5. Moment-Curvature for single pile with reduced shell thickness

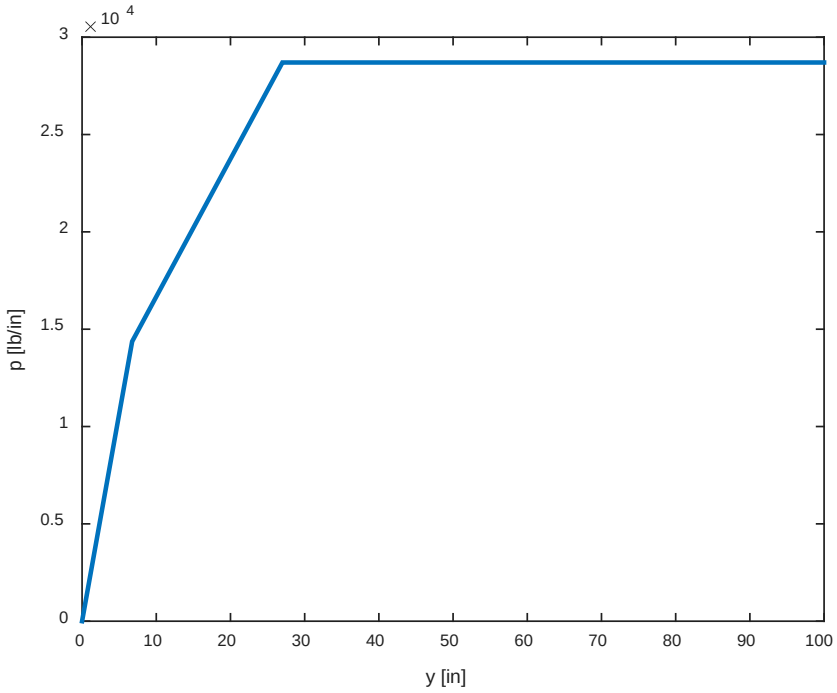

Figure 2-6. Generated *p-y* curve for pile cap

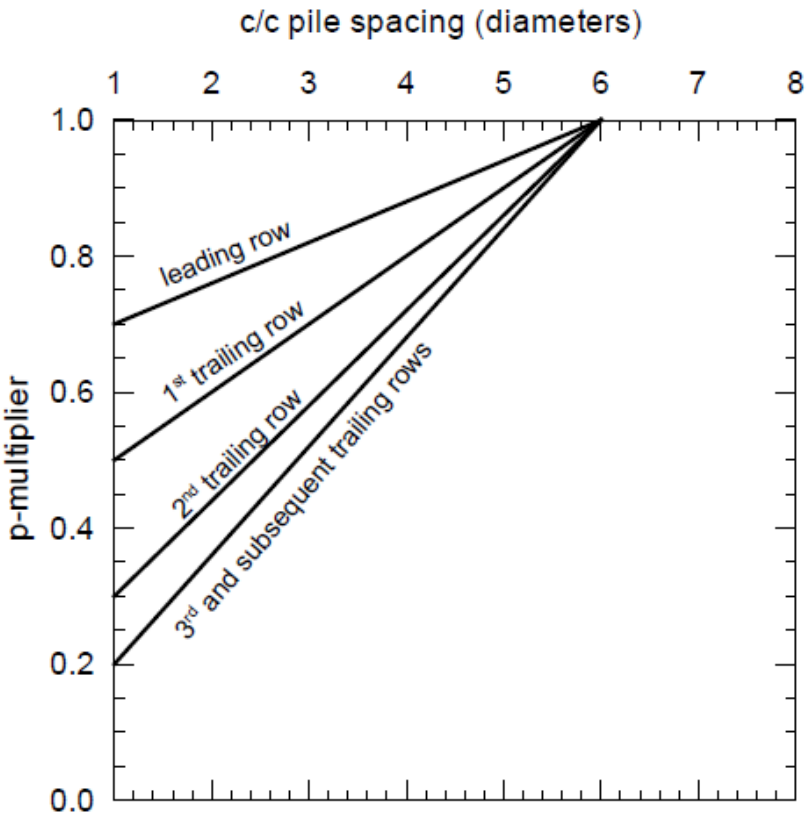

Figure 2-7. *p*-multiplier for group effect (after Mokwa 2000)

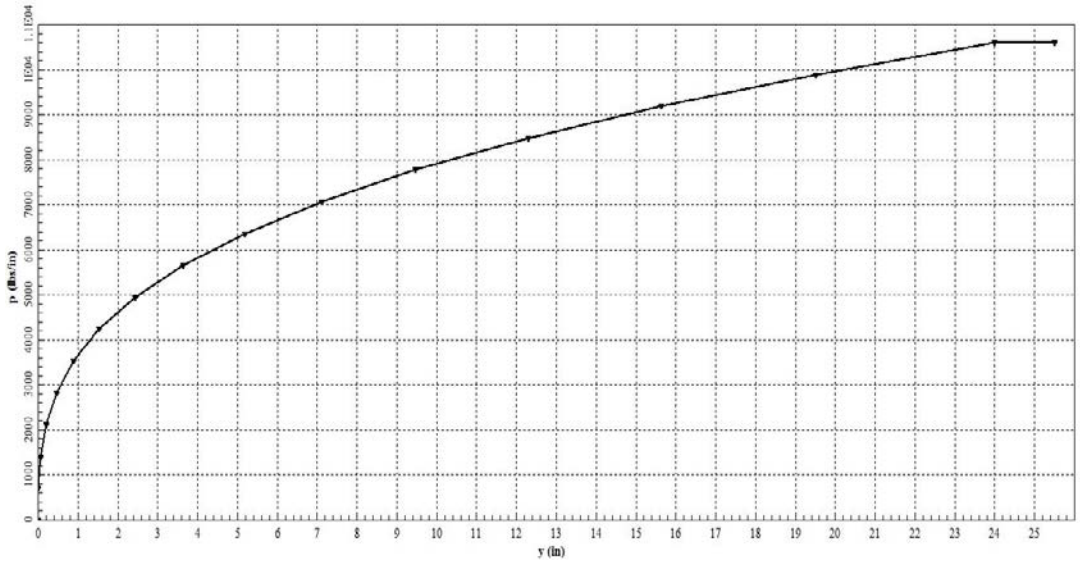

Figure 2-8. Generated *p*-*y* curve for liquefied layer

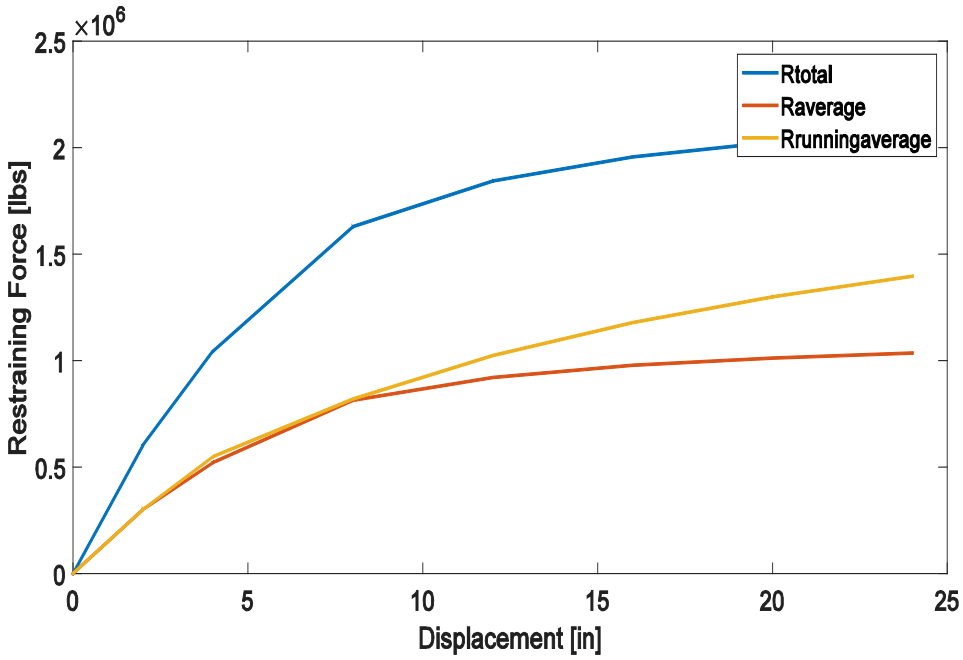

Figure 2-9. Restraining force (R) verses pile displacement from LPILE model

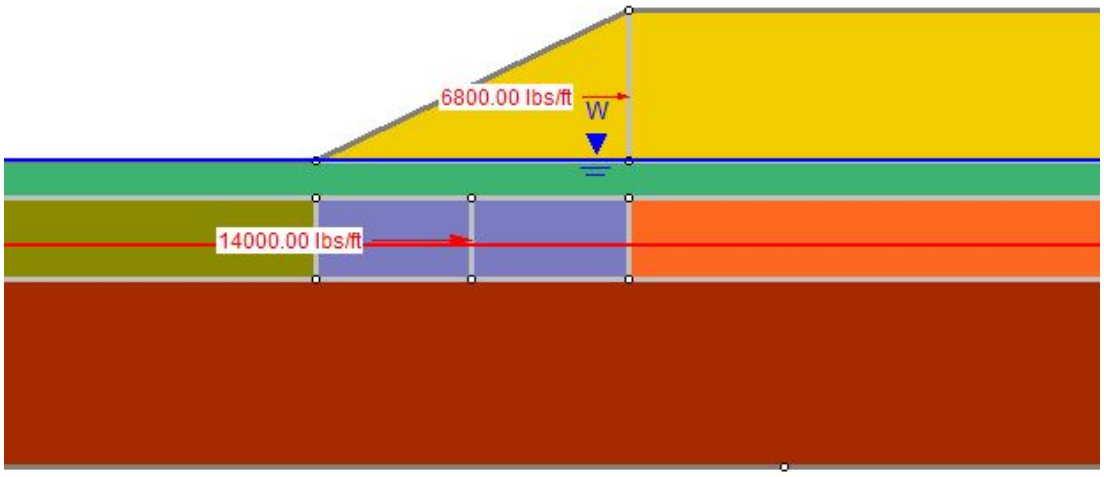

Figure 2-10. Slide model with restraining forces

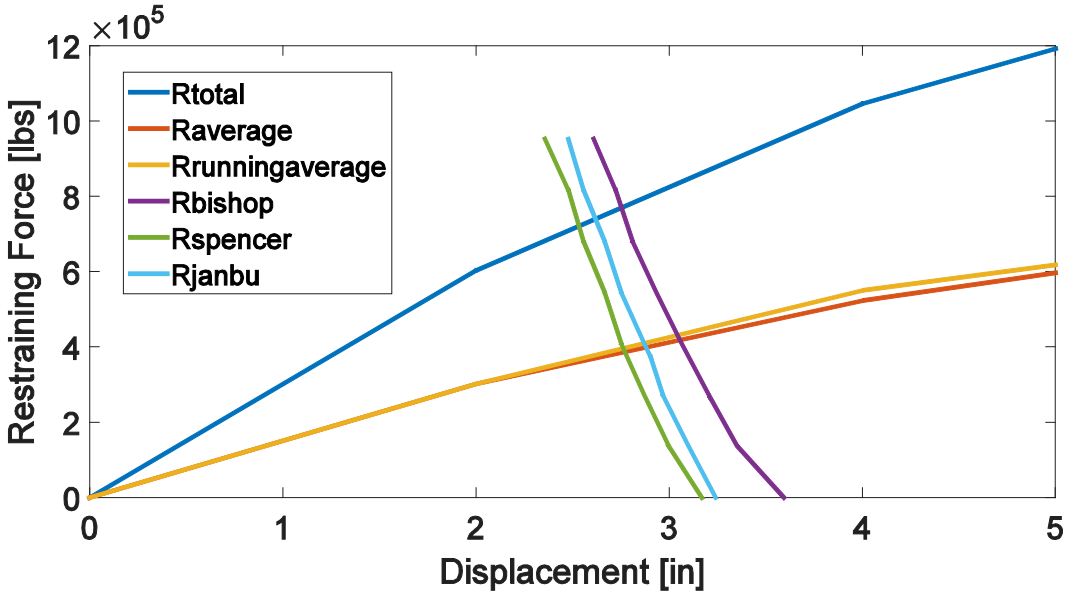

Figure 2-11. Design Displacement calculation

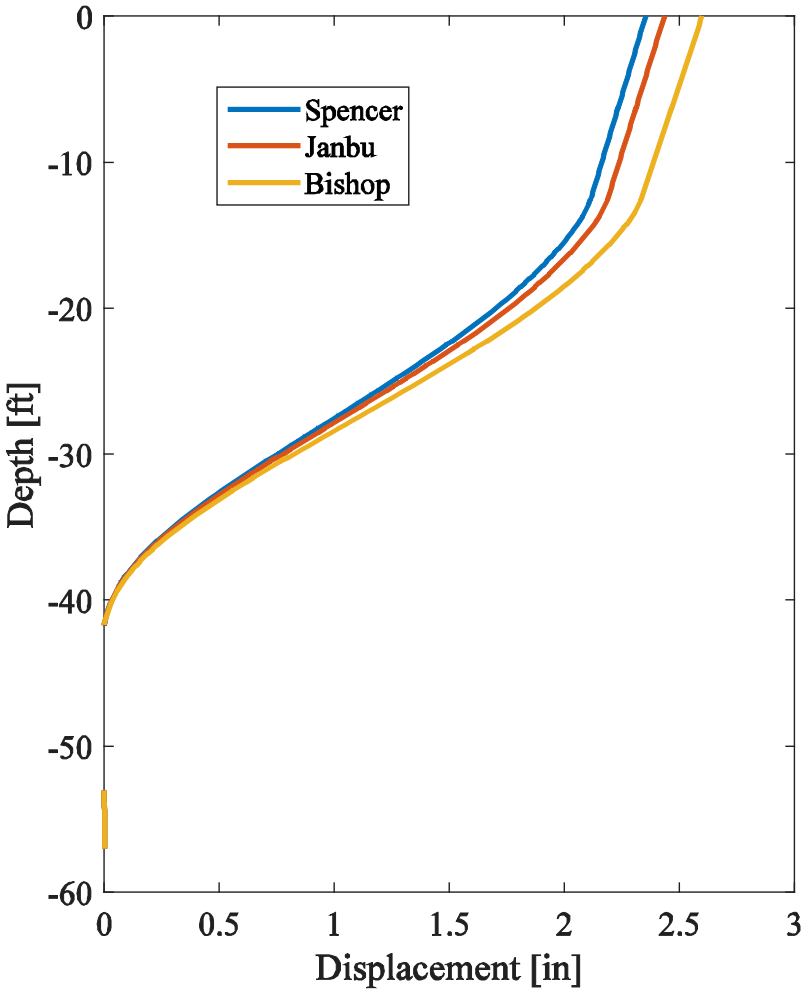

Figure 2-12. Super pile deflection profile for different analysis methods

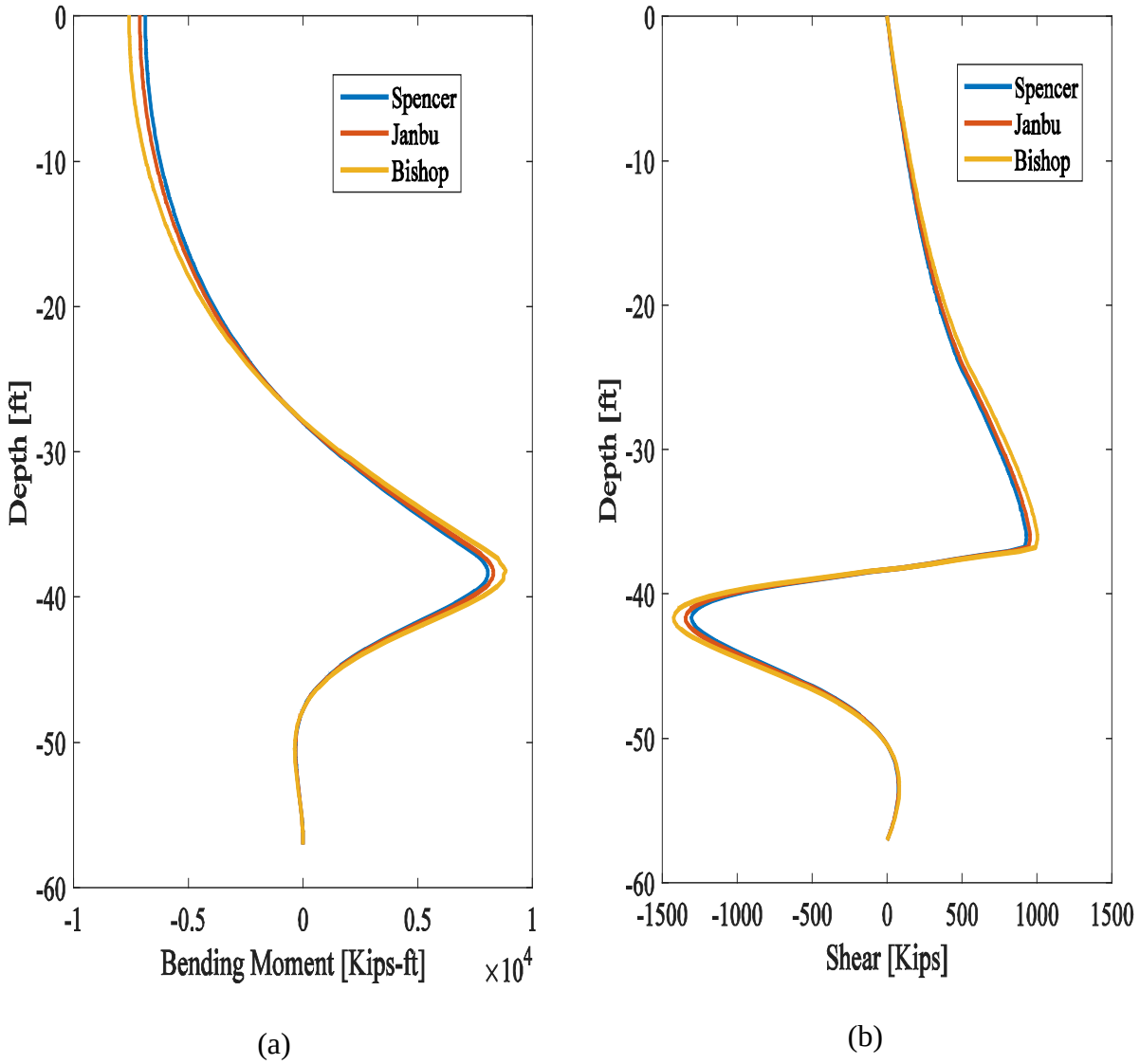

Figure 2-13. Super pile bending moment and shear force for different analysis methods

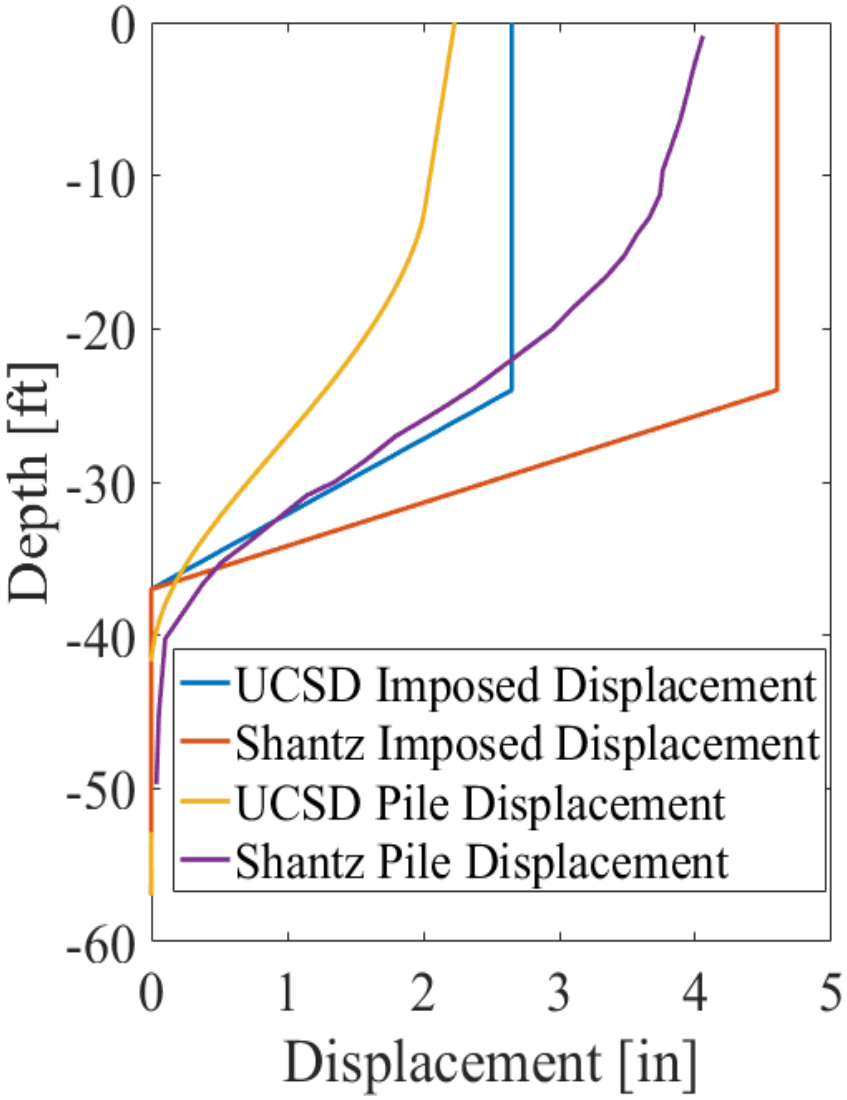

Figure 2-14. Super pile deflection profile

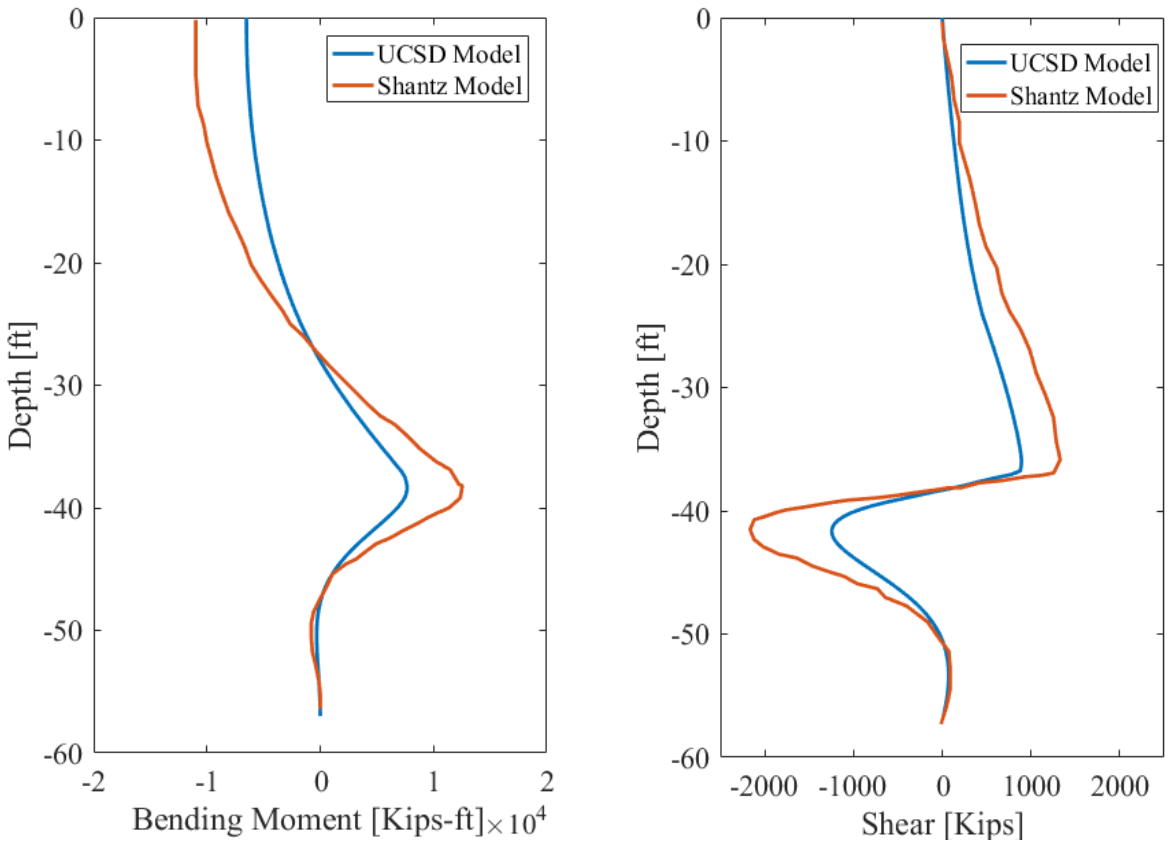

(a) (b)

Figure 2-15. Super pile bending moment and shear force profiles

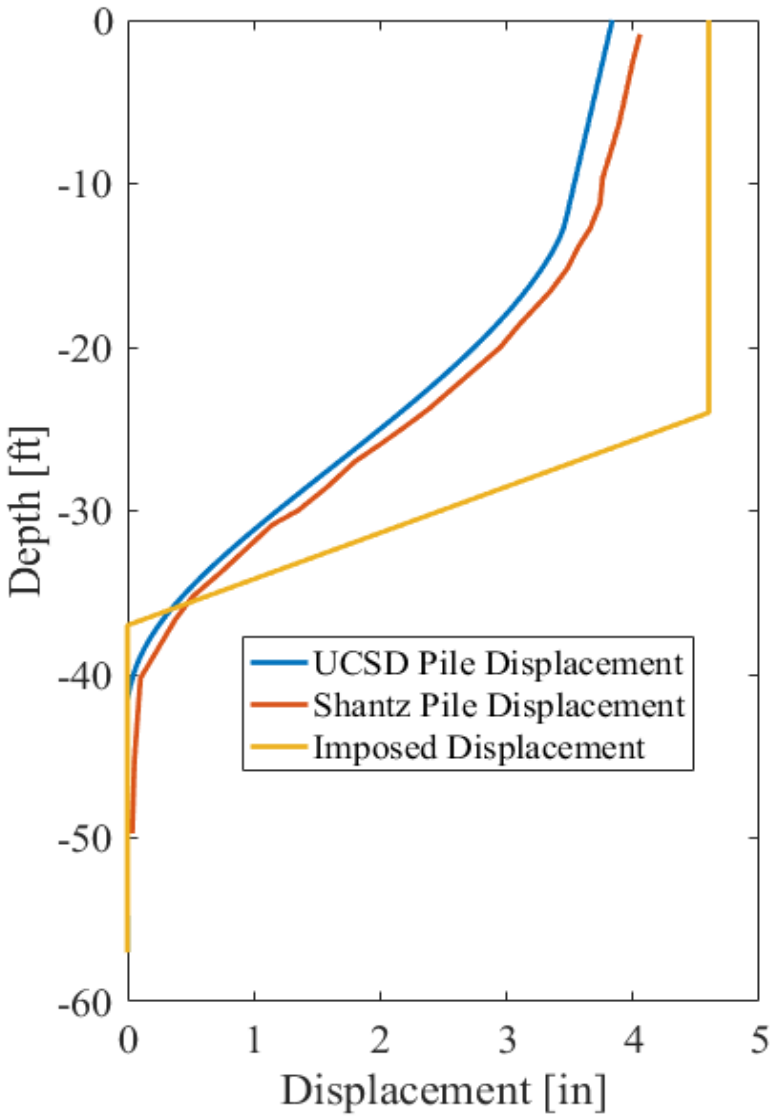

Figure 2-16. LPILE model displacement push comparison

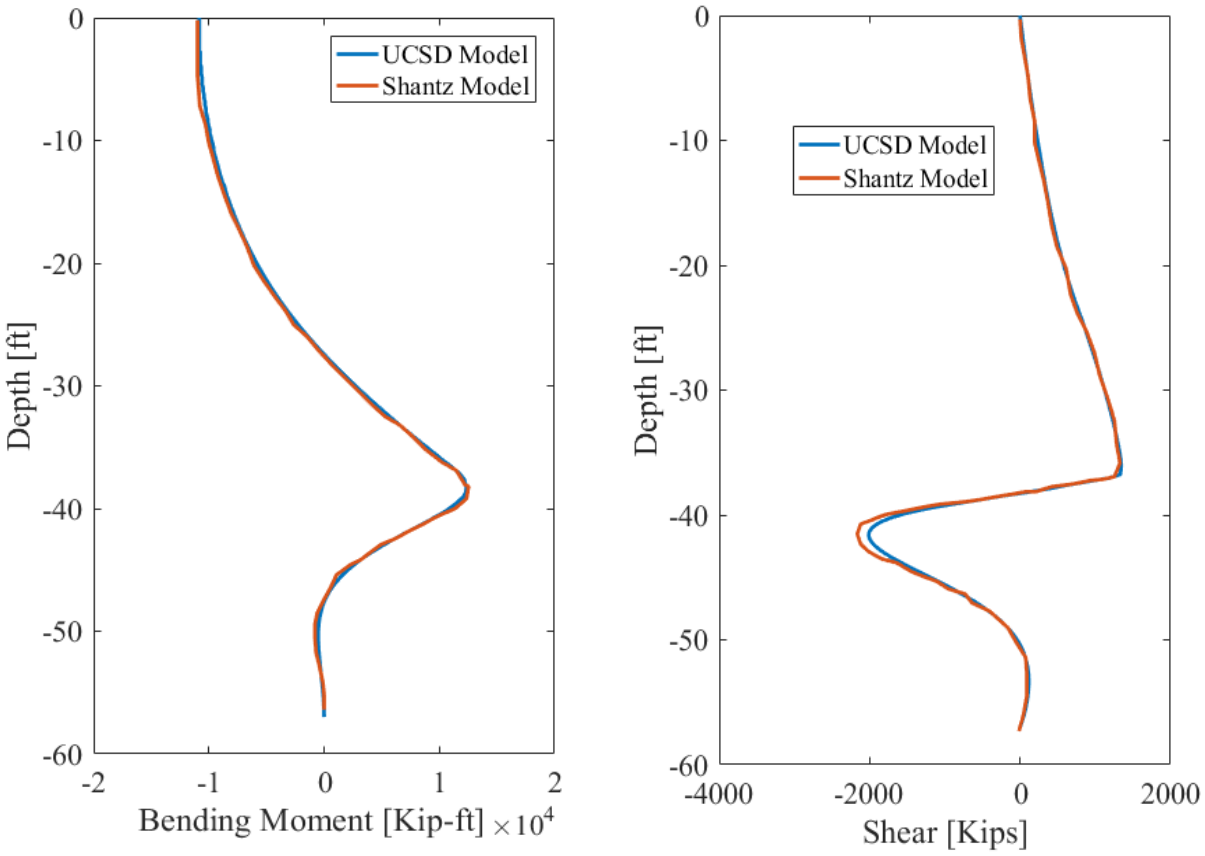

(a) (b)

Figure 2-17. LPILE model bending moment and shear force comparison

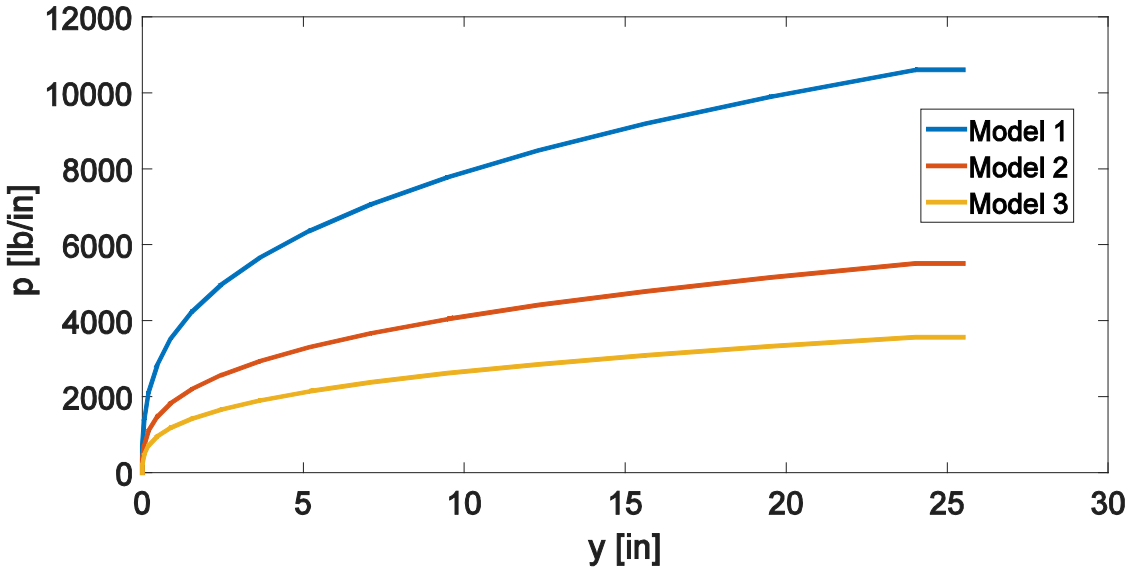

Figure 2-18. *P-y* curves for different liquefied soil strengths

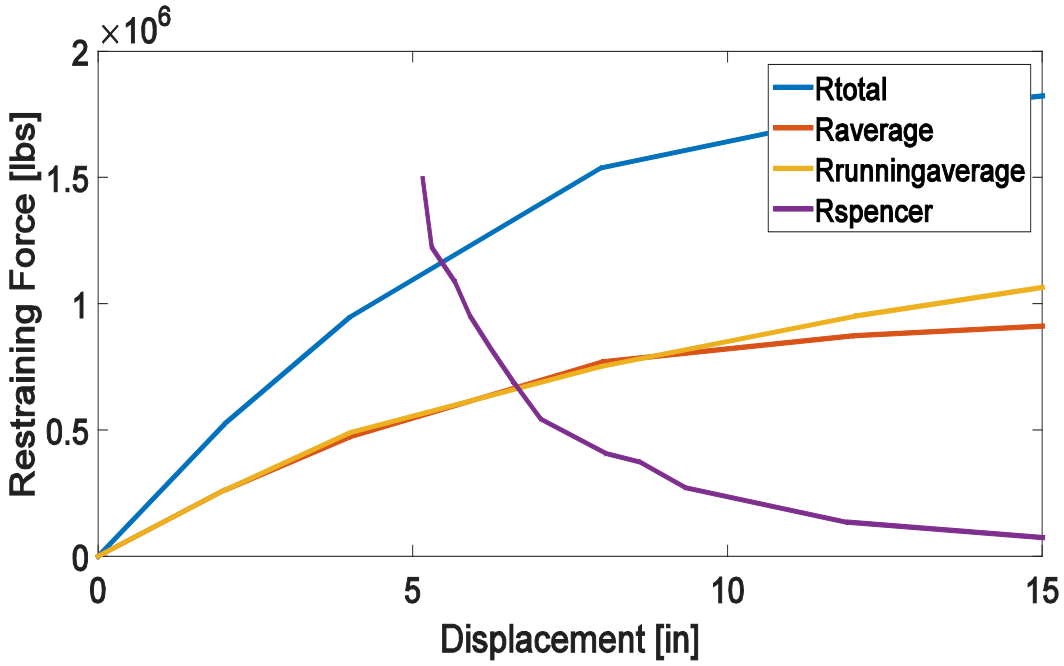

Figure 2-19. Design Displacement for Model 2

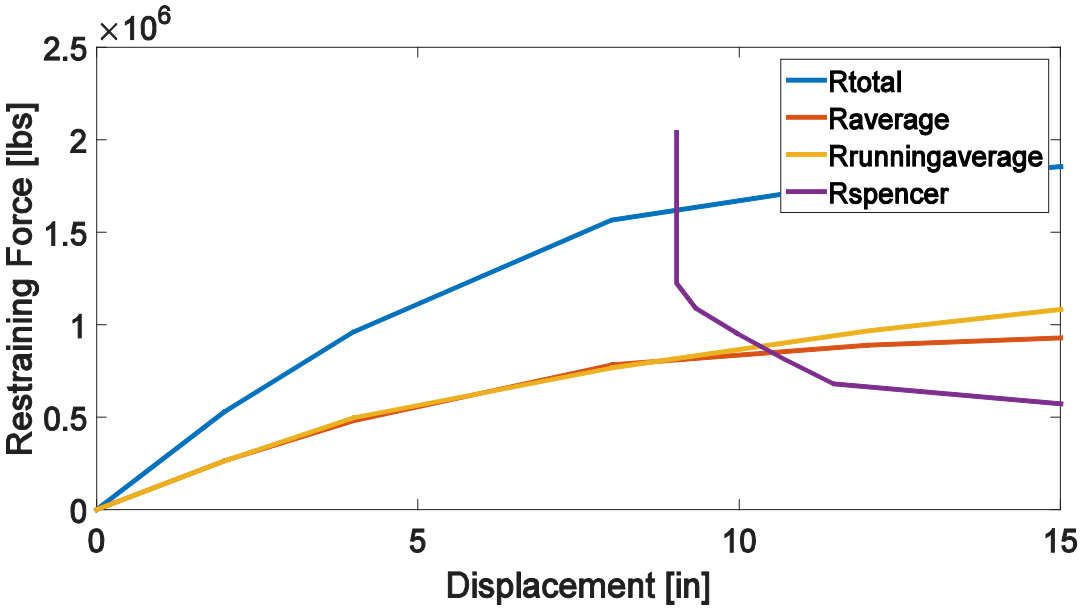

Figure 2-20. Design Displacements for Model 3

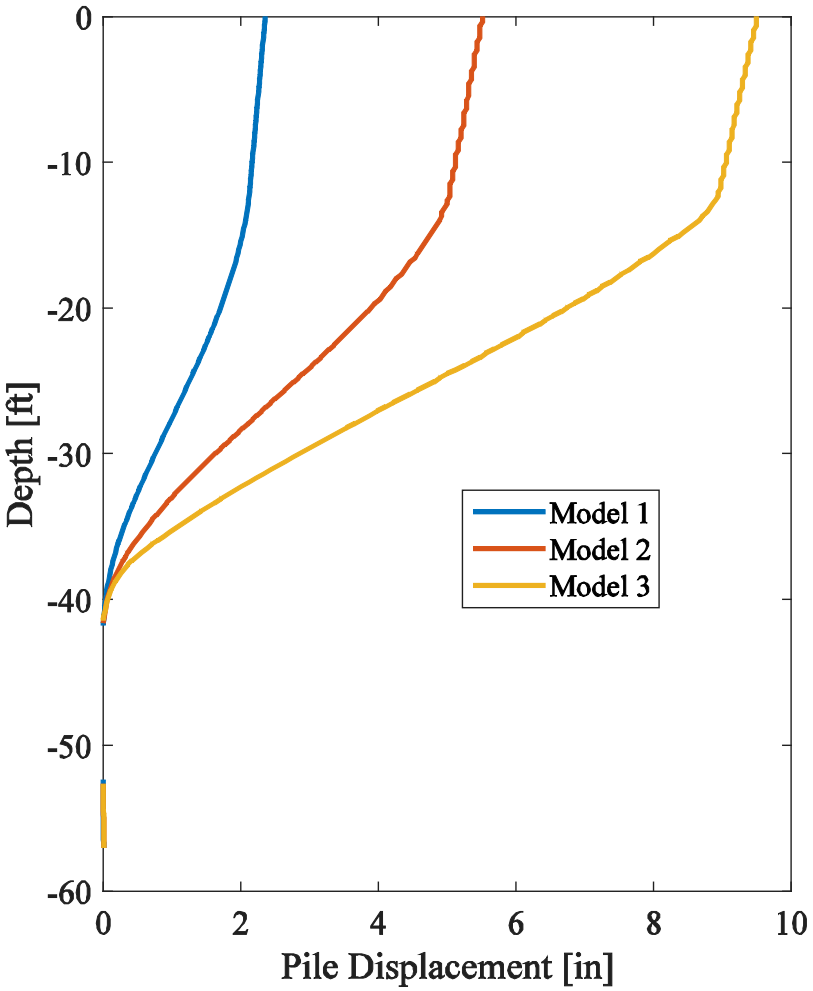

Figure 2-21. Super pile deflection profile for the 3 models

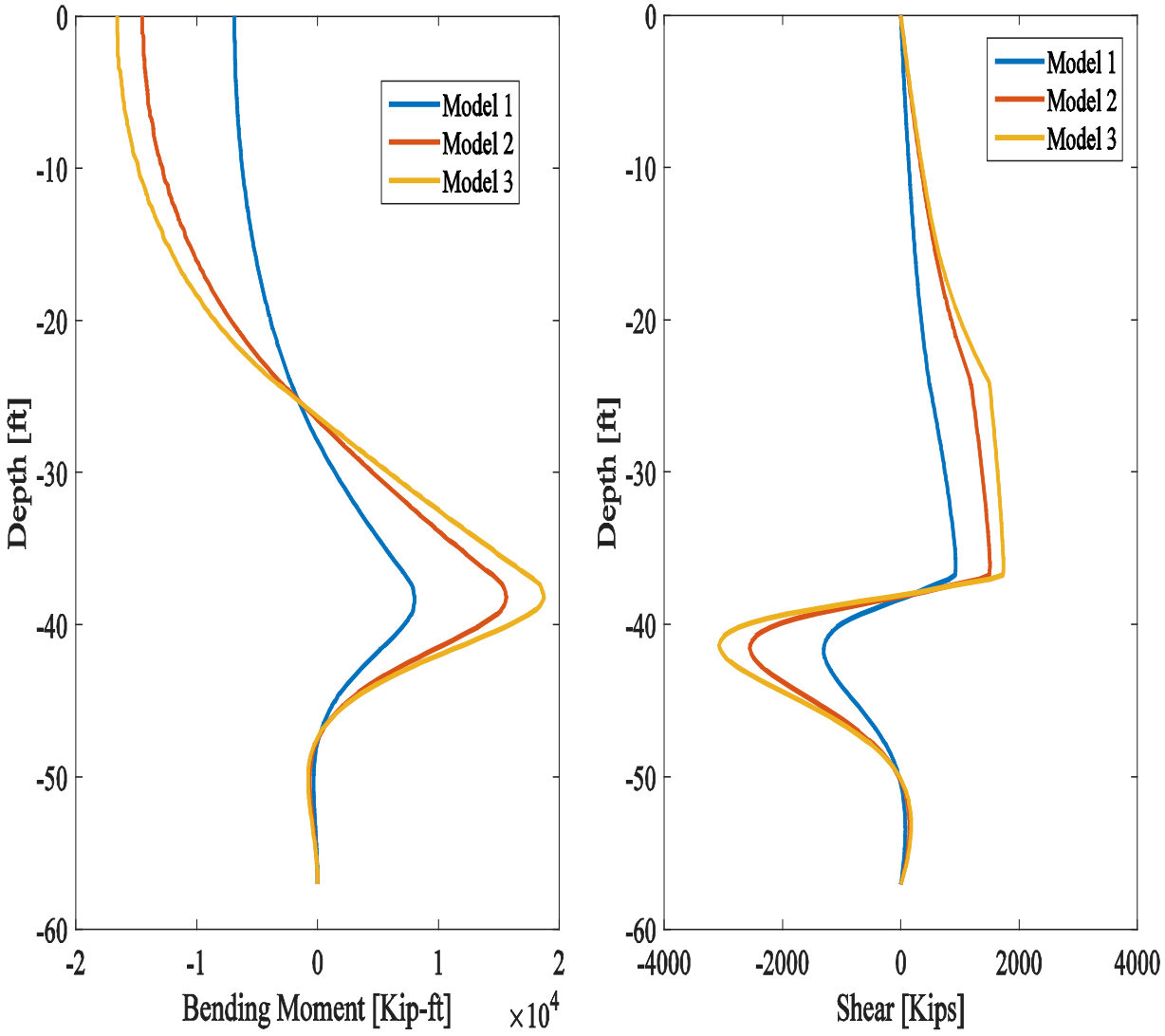

(a) (b)

Figure 2-22. Super pile bending moment and shear force comparison for the 3 models

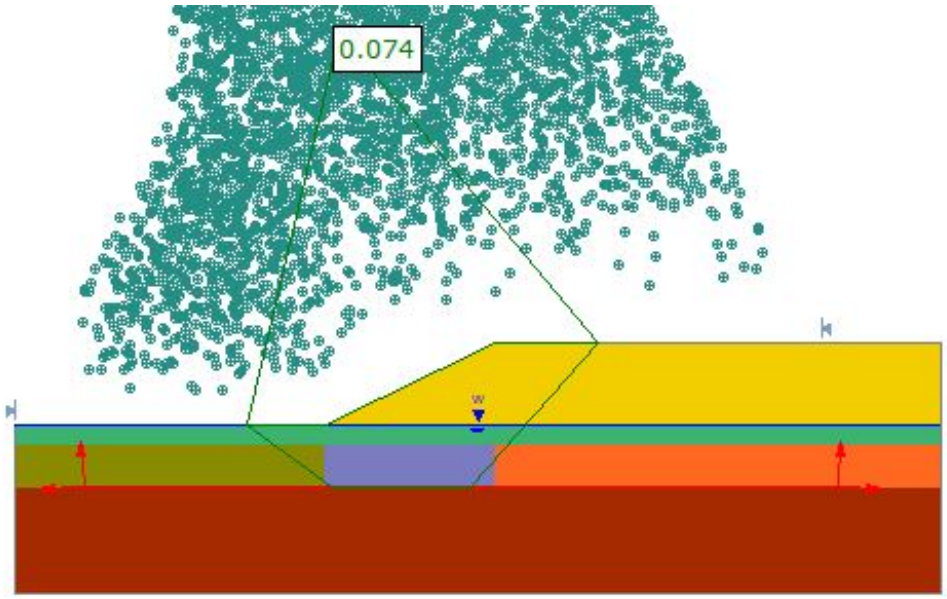

Figure 2-23. Failure wedge for bottom critical surface position

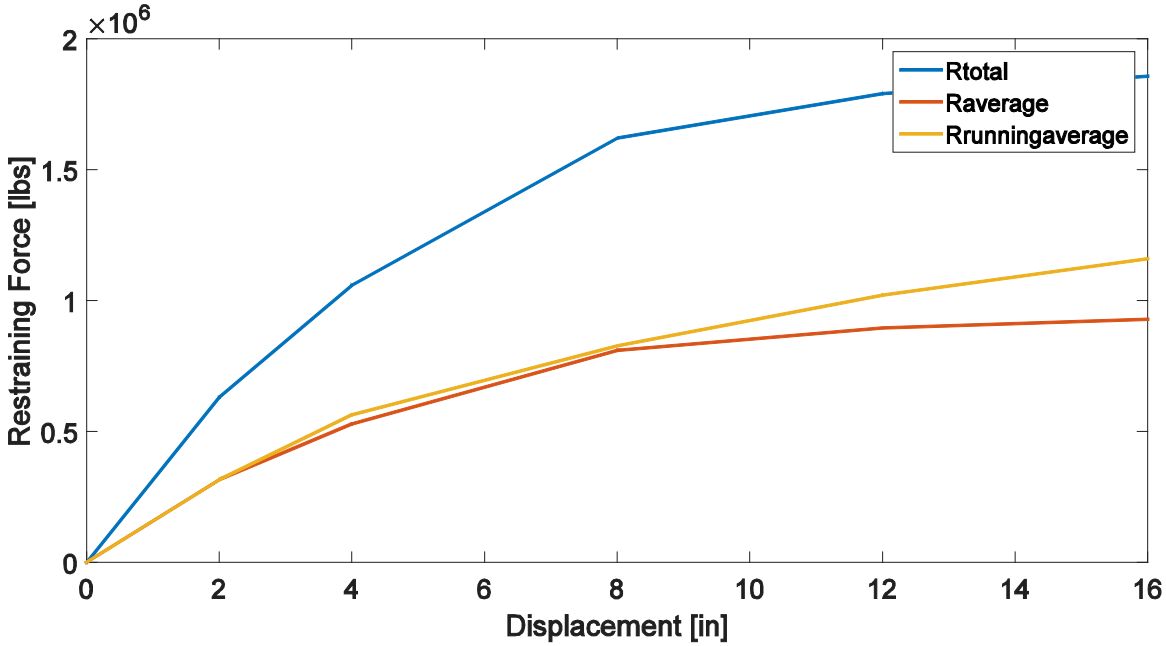

Figure 2-24. Restraining forces versus imposed displacement from LPILE for bottom critical surface position

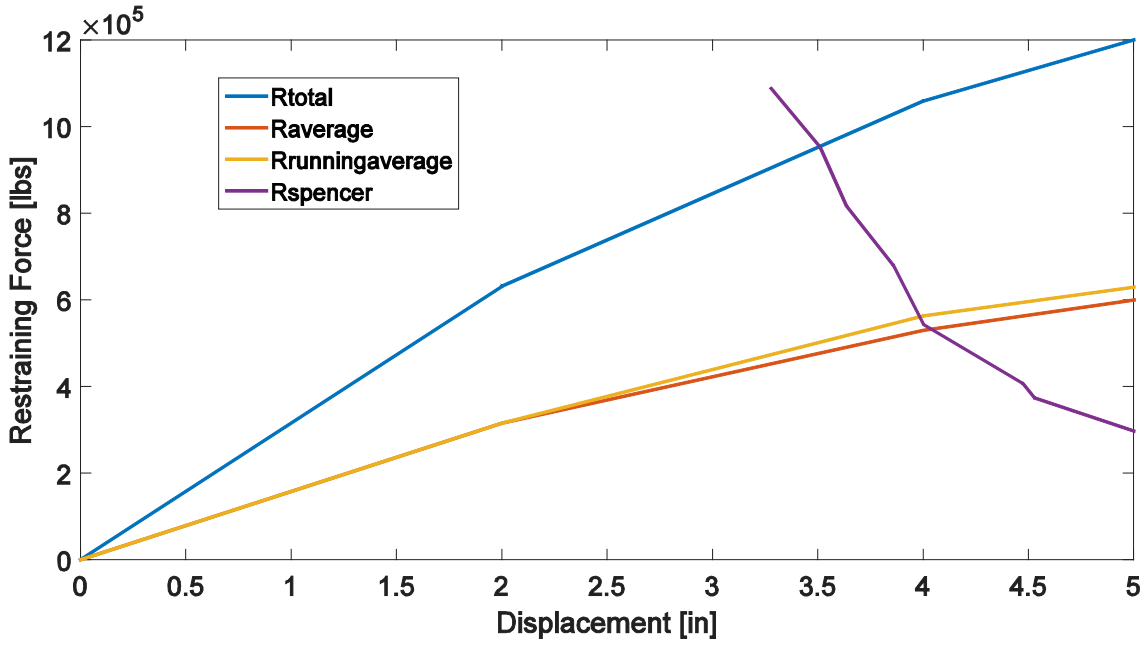

Figure 2-25. Restraining forces versus displacement for design displacement for bottom critical surface position

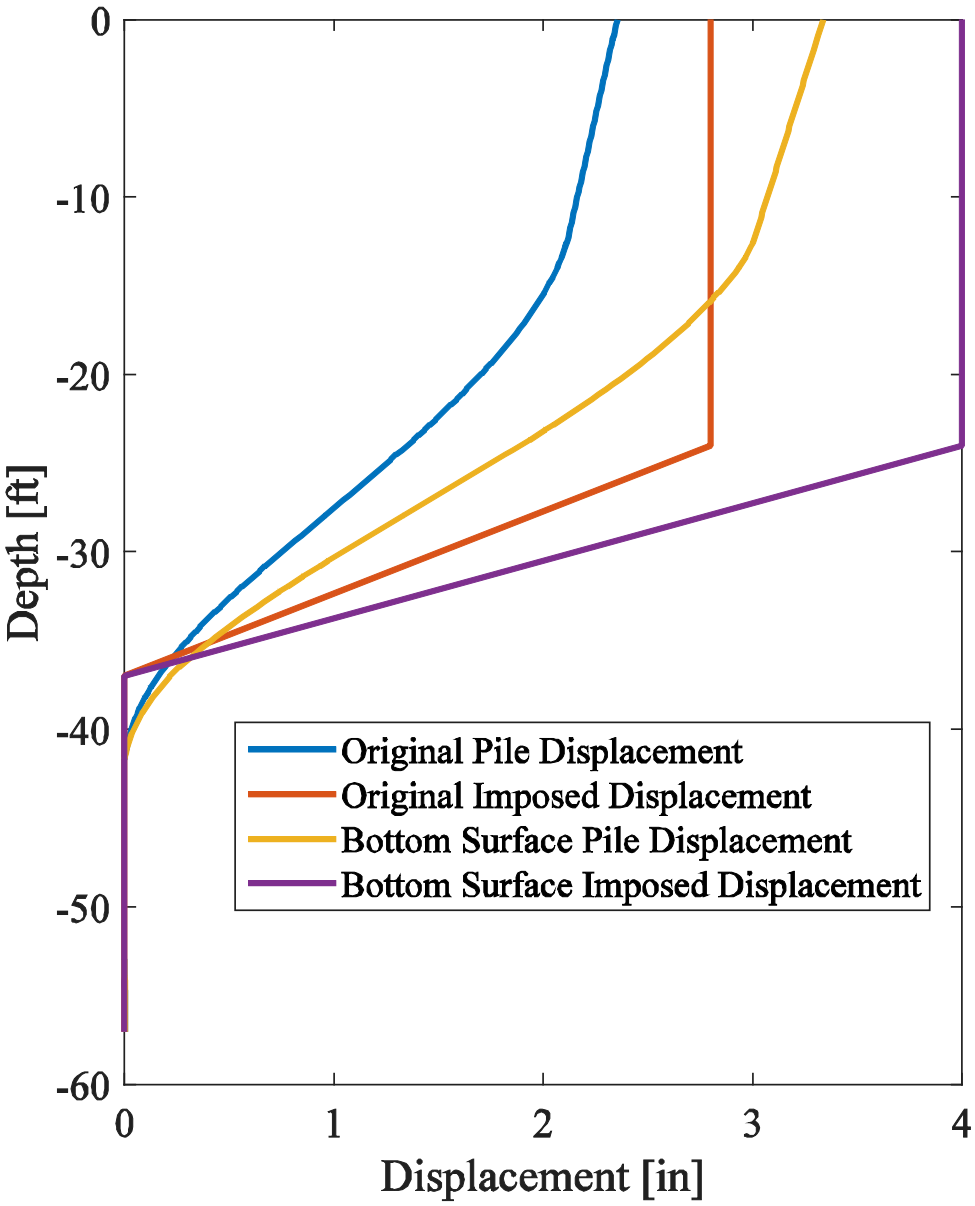

Figure 2-26. Super pile deflection profiles for different failure surface locations

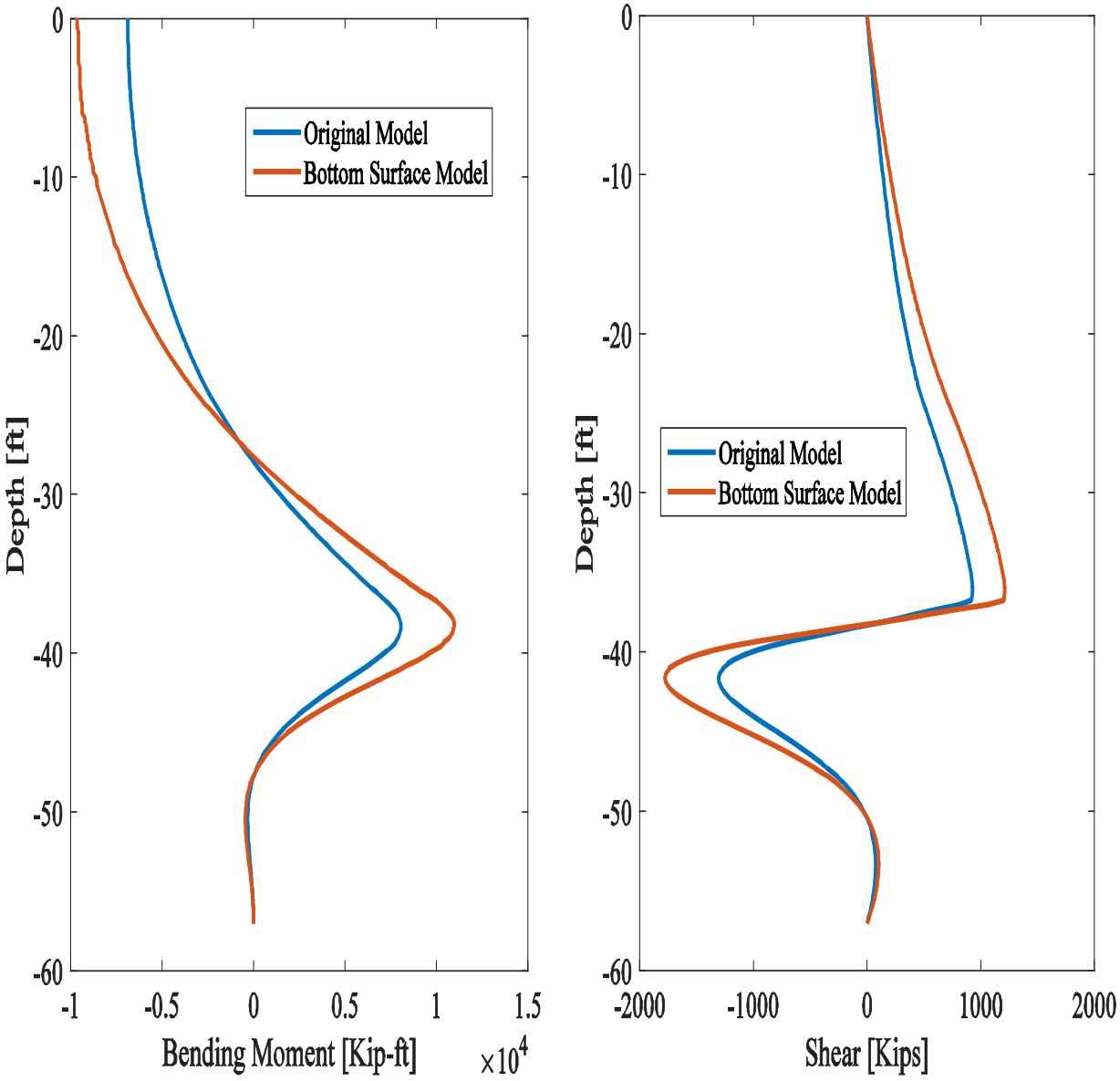

(a) (b)

Figure 2-27. Super pile bending moment and shear force profiles for different failure surface locations

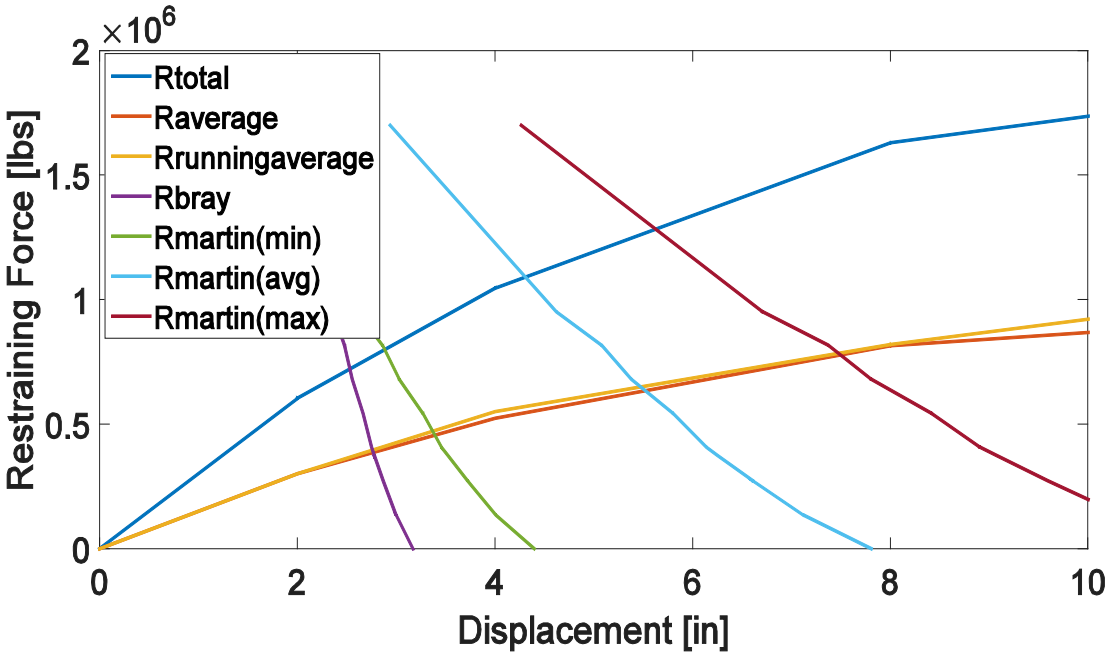

Figure 2-28. Design displacement comparison for different sliding block equations

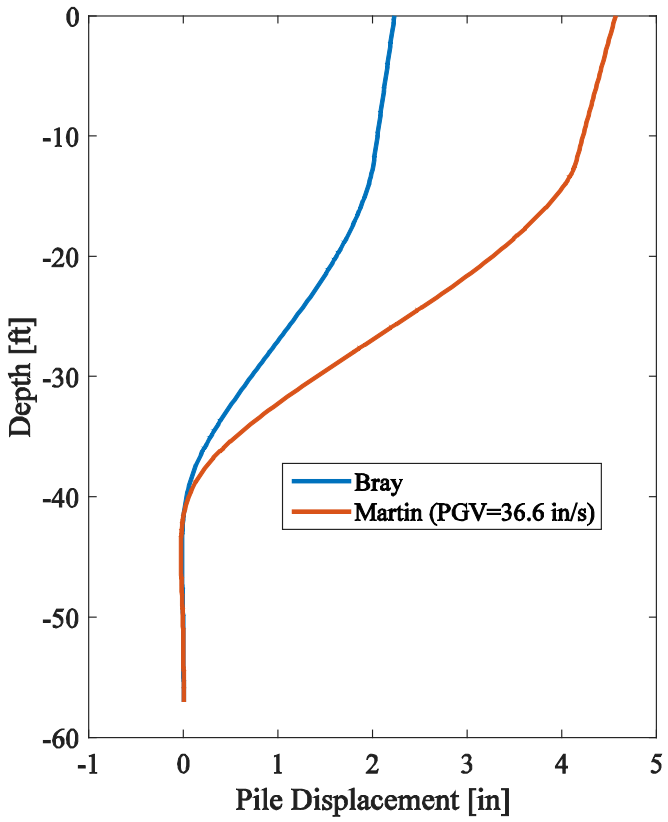

Figure 2-29. Pile displacement profile comparison for different sliding block equations

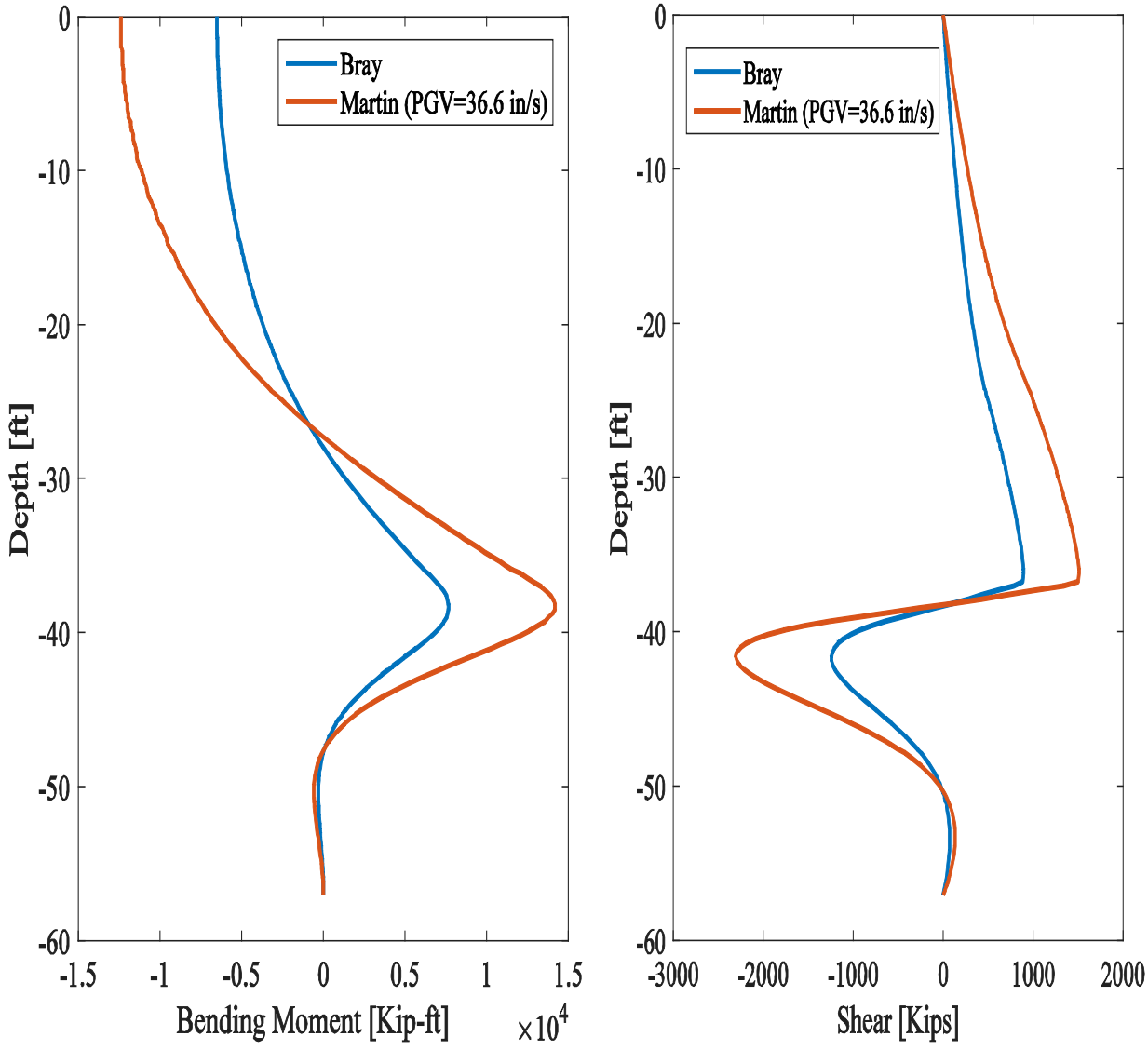

Figure 2-30. Pile bending moment and shear force profiles for different sliding block equations

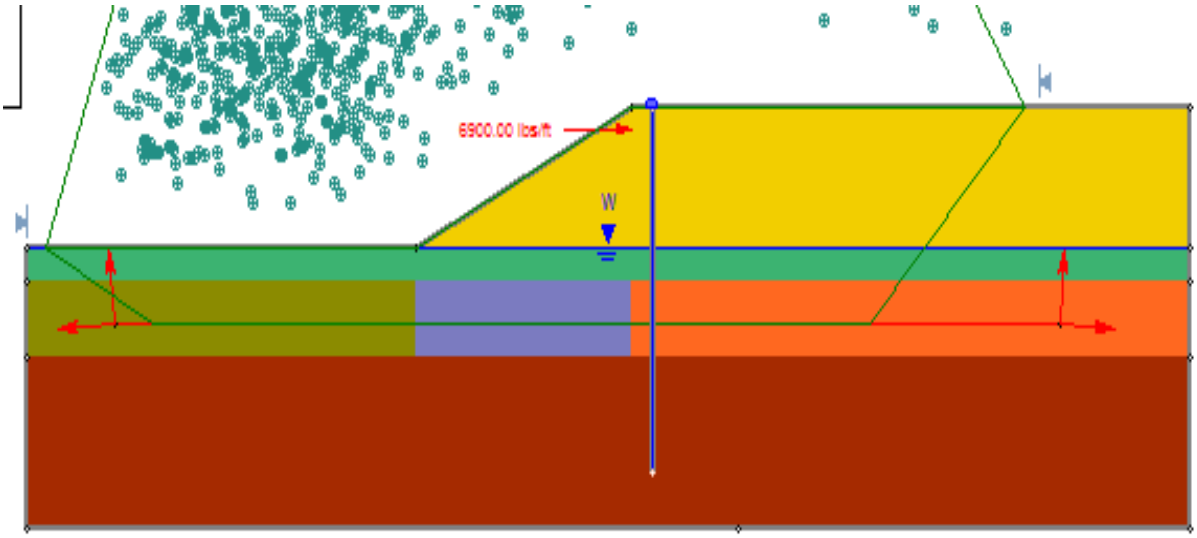

Figure 2-31. Modified slope stability model with pile support (k_y=0.187)

Chapter 3 Simplified Analysis Applied to a Bridge Structure

3.1. Introduction

This chapter presents a study of liquefaction induced lateral spreading effects on the pile foundation system of a Bridge Structure. The outcomes are presented within the scope of a comparative analysis contrasting results of this study referred to as UCSD to that reported by an earlier consultant study (Caltrans 2016).

The chapter is composed of eight sections. Section 3.2 presents the bridge description. Section 3.3 discusses the Caltrans simplified method and the "pile-pinning effect". Section 3.4 presents the results obtained by UCSD in contrast with those reported by the consultant. On this basis, the main differences between the results and possible sources of discrepancies are presented in Section 3.5. The pile analysis by UCSD and comparison summary are presented in Section 3.6 and 3.7, respectively. Section 3.8 discusses the challenges in implementing the simplified method. Finally, Section 3.9 presents the recommended modifications to the methodology.

3.2. Bridge Structure

The Bridge is a reinforced concrete structure with 18 spans. Dimensions are 647-foot long and 32.5 feet wide, consisting of T-Beams for main span supporting a concrete slab. The bridge structure is supported by pier walls and 2 end reinforced concrete open-end diagraph abutments. The piers and abutments are supported by pile foundations in the ground.

3.3. Simplified Method

Liquefaction-induced displacements can cause a severe damage to an engineered structure. Therefore, a number of ground improvement techniques have been developed and enhanced to bring the ground deformations to an acceptable level. However, the mitigation cost can be reduced if the foundation piles are designed to "pin" the layers above and below the liquefied layer and as

a result would stabilize the slope. This technique is known as “pile-pinning” effect (Figure 3-1) where the piles are locked into both non-liquefiable soil layers above and below the liquefiable soil layer.

The simplified method (MTD 20-15 2017) analysis is conducted in 2 steps in order to calculate the design displacement and forces acting on the pile foundation. The first step is performing the slope stability analysis to evaluate the soil lateral movement. After that, a ground displacement profile is imposed on the pile foundation via *p-y* curves. The intersection of the 2 curves is the design displacement (Figure 3-1).

Displacements from slope stability analysis are determined using Newmark’s sliding block (Equation 3.1) by Bray and Travasarou (2007). In the analysis, liquefiable soil is modelled as soft clay having a residual undrained shear strength calculated using equation 3.2 by Kramer and Wang (2015). The slope stability analysis was performed with and without the pile supported bridge effect (restrained and unrestrained). The calculated design displacement is applied to the *p-y* curve super pile model to evaluate the response (bending moment and shear force).

$$\begin{aligned} \mathrm{D(cm)} = \mathrm{Exp}[&-0.22 - 2.83\mathrm{Ln}(\mathrm{k_y}) - 0.333\mathrm{Ln}(\mathrm{k_y})^2 + 0.566\mathrm{Ln}(\mathrm{k_y})\mathrm{Ln(PGA)} \\ &+ 3.04\mathrm{Ln(PGA)} - 0.244\mathrm{Ln(PGA)}^2 + 0.278(\mathrm{M_w} - 7)] \end{aligned} \tag{3.1}$$

where,

k_y is the horizontal acceleration required to achieve a factor of safety of unity

PGA is the peak ground acceleration

Mw is the magnitude of the design event

$$\mathrm{S_r} = 2116.\exp[-8.444 + 0.109(\mathrm{N_1})_{60} + 5.379\left(\frac{\sigma_v'}{2116}\right)^{0.1}] \tag{3.2}$$

where,

Sr is the residual strength in units of psf

$(N_1)_{60}$ is the SPT blow count

σ_v' is the effective vertical stress in units of psf

3.4. Implementation of Simplified Method

This study compares the Bridge slope stability analyses performed by UCSD to those of an earlier study (Caltrans 2016). Regarding the UCSD analysis, the computer code *Slide7* was used with both Spencer's method as recommended by SCEC (2002) and Bishop's method. On the other hand, the earlier study performed the slope stability analysis using the software *Slope/W*.

3.4.1 Slope Stability Analysis by Earlier Study

Figure 3-2 presents a general layout of the bridge, as modelled by the earlier study and divided into 3 zones. The first zone referred to as the East Embankment (left side) which considers Abutment 1 to Pier 6. A second middle zone referred to as the Channel Area which includes Piers 7 and 8 then a third zone referred to as the West Embankment (right side) containing Pier 9 to Abutment 19. The earthquake properties used for analysis are site specific. In this case, a magnitude of 6.6 and PGA of 0.36g.

The East Embankment is studied once with no piles present in the slope then another including the piles resisting the deformation. Table 3-1 shows the soil profile and parameters used. The slope was studied using the software *Slope/W*. Figure 3-2 highlights the failure wedge (green color) showing a global failure affecting the locations of Abutment 1 through Pier 6. Caltrans (2016) reports a post-earthquake factor of safety of 0.7 using the Spencer's method without the pile pinning effect. As the slope is statically unstable which leads to the prediction of excessive

movement (flow failure). However, after adding the pile pinning effect to the slope stability model, Caltrans (2016) reported slope displacements reduced to 72 inches using equation 3.3 by Faris *et al.* (2006). Equation 3.3 is only used for the unstable post-earthquake factor of safety case instead of equation 3.1 by Bray and Travasarou (2007).

$$\mathrm{H(m)} = [\int_{layer}^{liq.} \gamma_{max}\, dz]^{1.07} \tag{3.3}$$

where,

where, H is deformation in meters and γ_{max} is the limiting shear strain

The West Embankment is analyzed same as the East Embankment with and without the pile pinning effect. Table 3-2 shows the soil profile and parameters used in the Slope/W model. Figure 3-3 presents the studied slope with the failure wedge highlighted in green. The analysis is concerned with the global failure of the embankment which affects Pier 9 through Abutment 19. The static factor of safety generated was 1.2 using the Spencer's method. This points to a statically stable slope. Caltrans (2016) reports an unrestrained yield acceleration (k_y) of 0.019g that yields 12 inches of displacement. When adding the pile pinning effect, displacement is reduced to 2 inches.

The last part of the analyses is performed on the Channel Area (middle section) which contains Piers 7 and 8. The soil surface is relatively horizontal and away from both embankment failure wedges. Therefore, no lateral spread loading is considered to act on the piles, and the pile drift is not considered critical. Table 3-3 shows the summary of Caltrans (2016) results.

3.4.2 Slope Stability Analysis by UCSD

UCSD (this study) performed its' own slope stability analysis to verify the results. Similarly, the bridge was divided into 3 zones for the analyses (East Embankment, West Embankment and Channel Area). Slope stability analysis for the East Embankment (Abutment 1 through Pier 6) is shown in Figure 3-4 using the same soil profile mentioned in the previous section (Table 3-1). Embankment was modelled using the computer code *Slide7*. The failure wedge is illustrated on the figure with the location of the piles (shown as forces in the soil). Analysis results without considering pile pinning, found unrestrained yield acceleration (k_y) of 0.096g that yielded 5 inches of displacement. However, after adding the pile pinning effect, in terms of the forces shown in the slope, the displacement was reduced to 3 inches. Post-earthquake static stability shows a factor of safety of 1.45 using Spencer's method (1.50 using Bishop's). This factor is much larger than the 0.7 of Caltrans (2016) and points to a stable slope.

Analysis of the West Embankment (Figure 3-5) showed unrestrained yield acceleration (k_y) of 0.13g that yields 3 inches of displacement. When including the pile pinning effect, the displacement is reduced to 2 inches. Soil profile used was the same as the previous section (Table 3-2) modelled using *Slide7*. Figure 3-5 highlights the global failure wedge affecting Pier 9 through Abutment 19.

The Channel Area (Middle section) containing Piers 7 and 8 is on a relatively level ground far from the effects of both embankments. Thus, no lateral spread loading load is considered to act on the piles, and pile drift is not considered critical. Furthermore, Table 3-4 shows the summary of UCSD results.

3.5. Main Difference between Results

Result comparison show a significant difference between both studies. The main difference is in the results of the East Embankment. It is observed that Caltrans (2016) reported a post-earthquake factor of safety of 0.7 using the Spencer's method, leading to this suggested excessive movement (flow failure). On the other hand, the UCSD *Slide7* model resulted in a factor of safety of 1.45 using Spencer's method of slices (FS=1.50 using Bishop's). This factor is much larger than the 0.7 and points to a stable slope.

In an attempt to identify the source of discrepancy, UCSD performed an analytical hand calculation study using Bishop's method of slices. This study resulted in a factor of safety of 1.3 (close to the 1.5 value calculated by *Slide7*). All UCSD calculations were focused on the reported global failure mode and pointed to a post-earthquake stable slope with relatively little seismic induced displacement.

UCSD noted the presence of a second local slope (Figure 3-6) in the East Embankment between bent 3 and 4 having a much steeper inclination angle than the global model. By checking the local failure of this slope, it was found to have a low post-earthquake factor of safety of 0.85 using Bishop's method of slices (1.06 using Spencer's method). This low factor of safety points to a statically unstable slope leading to much higher displacements than previously calculated when studying the global model. It is important to note that the low factor of safety is locally confined to the second slope affecting only bent 4. While high displacements are expected in this location, it will not have a significant effect on the global embankment stability. In addition, the low factor of safety does not consider pile pinning effects. When adding a restraining force to the local model to account for pile pinning effect, the slope was found to be stable.

Focusing only on the stability of the local steep slope, the analysis using Spencer's method led to 4.5 inches of displacement considering the pile pinning effect (and 8 inches using Bishop). Table 3-5 shows the summary of results for the local slope using Spencer's and Bishop's methods.

3.6. Pile Analysis by UCSD

The global analysis performed on the bridge by UCSD using Spencer's Method yielded a 3-inch design displacement. A super pile was used combining the moment curvatures of all piles from Abutment 1 till Bent 6. The pile model varied slightly between bents. One pile model existed from Abutment 1 till Bent 4 shown in Figure 3-7 (modelled in LPILE) while another model for bent 5 and 6. Both piles were similar in cross section. In order to simplify the analysis and add all piles from the 6 foundation locations, a 6 ft slice was taken in the bridge. The 6 ft slice included one pile from Abutment 1 till Bent 4 and 2 piles at each of bent 5 and 6. The moment curvature of all those 8 piles was added. As such, at any given curvature, the super pile had the combined moment capacity of all 8 piles while having the same diameter as a single pile. The UCSD analysis accounted for the smear zone (2 feet) above and below the liquefiable layer by reduction in the *p-y* curves accordingly.

Given that the abutment and bents had different soil profiles, different pile lengths and embedment lengths, the worst case was chosen for study purposes. The worse scenario is using the abutment profile as it provides the largest displacement push profile. Since each pile carries a different load and as the liquefiable layer is not constant, the varied displacements distributed over varied layer heights can result in very different bending moment profiles. Therefore, it is virtually impossible to make a good super pile that can accurately mimic the response.

Other difficulties include modelling the rotational stiffness of the pile head. The simplified method calculates the pile head rotational stiffness using the number of rows in the pile group and

group spacing. In this case, with only one pile per bent and large distances between bents, a pinned connection at the pile head location is considered. The method underestimates the rotational value of the pile head specially with the presence of some rotational stiffness from the pile-bridge connection.

Since the bridge piles were combined into 1 super pile for the analysis, the resulting bending moment and shear force is the combined effect of all piles considered. There is no accurate methodology to distribute the reactions calculated over the number of piles as dividing by the number of piles does not account for pile location and other varied parameters. The bending moment, shear force and displacement for each single pile after dividing by the number of piles is presented in Figure 3-8.

A proposed solution to the super pile challenge is to build separate models for each foundation element, one model for the abutment and a model for each bent. Then apply the displacement profile according to each pile length and soil profile. For the purpose of finding the design displacement, each pile is incrementally pushed and the resulting shear forces at the mid liquefiable layer location are added. The liquefiable layer may vary across the different profiles and different models; however, some approximations might be needed to standardize the mid liquefiable layer locations. After calculating the design displacement, the displacement is applied in each of the models to get the bending moment and shear force profiles in each pile separately.

3.7. Summary of Result Comparison between UCSD and the Earlier Study

The comparison between UCSD and Caltrans (2016) analyses show some differences in the results with significant influence on the final displacement demands on the bridge, among the main conclusions of this study are:

1. By comparing the East Embankment results without pile pinning effect, Caltrans (2016)

reports unlimited displacement (flow failure), while the UCSD study suggests 5 inches of displacement.

2. Adding the pile pinning effect, the Caltrans (2016) reported displacement being reduced to 72 inches, while the UCSD analysis yielded 3 inches.
3. Further investigating this difference between both models, it is noted that Caltrans (2016) reports a post-earthquake factor of safety of 0.7 using the Spencer's method, leading to this suggested excessive movement. However, by investigating the post- earthquake factor of safety, the UCSD *Slide7* model resulted in a factor of safety of 1.45 also using Spencer's method. This factor is much larger than the 0.7 and points to a stable slope.
4. UCSD noted that there is a local slope between bent 3 and 4 which is much steeper than usual. As such, by checking local failure, it was found to have a low post-earthquake factor of safety equals to 0.85 using Bishop's method (1.06 for Spencer's). In addition, the low factor of safety does not consider pile pinning effects. The slope becomes stable when considering presence of the bridge.
5. By comparing the West Embankment results without pile pinning effect, Caltrans (2016) reports 12 inches of displacement, while the UCSD study gives 3 inches of displacement.
6. When adding the pile pinning effect, Caltrans (2016) reported displacement being reduced to 2 inches, with the UCSD analysis yielding the same 2 inches.
7. By further investigating the discrepancies between both outcomes, it is noted that Caltrans (2016) were using the equation by Bray and Travasarou per the 2012 Caltrans lateral spreading guidelines which contains a typo in the equation. This will have a significant effect on the results.

3.8. Challenges in Applying the Simplified Method

The UCSD implementation of the simplified method included some challenges that have a significant influence on the results, among the main challenges are:

- Different soil profile in the zones, the ground model consists of three zones (i.e. East Embankment, Channel Area, and West Embankment) each with different soil profile. The effect of liquefaction occurs across the bridge in varied liquefiable layer heights and properties which makes it difficult to perform simplified analysis.
- Varied soil profiles specifically liquefiable layer thickness between the zones imposes a challenge. The displacement profile depends on the height of the liquefiable layer. As such, the profile decreases linearly along the liquefiable layer to reach zero at the bottom of the layer. This can cause very different bending moment profiles and maximum bending moment and shear force locations.
- The change in soil profiles specially with sloping ground gives different pile lengths and different pile head to bridge deck distance. Same as mentioned before, displacements distributed over varied heights causes varied bending moment. UCSD used the abutment pile height in modeling the super pile.
- Piles affected by the slope movements do not have the same cross-sections. UCSD used an average cross-section to model the super pile.
- The pile head connection is assumed to be pinned with no rotational stiffness due to the pile spacing using the Simplified Method. This assumption would affect the bending moment, shear force and displacement for each single pile.
- A super pile was modeled by combining the moment curvatures of all piles affected by the slope, and then the loads are divided equally to each pile. While, each pile should carry

different loads. However, going back from super pile to single pile is challenging as a simple division by the number of piles is not adequate.

- A proposed solution to the super pile challenge is to build separate models for each foundation element, one model for the abutment and a model for each bent. Then apply displacement profile according to each pile length and soil profile. For the purpose of finding the design displacement, each pile is incrementally pushed and the shear forces at the mid liquefiable layer location are added. After calculating the design displacement, then apply the displacement in each of the models to get the bending moment and shear force profiles in each pile separately.
- For this case, it was challenging to simulate pile-pinning effect since the pile embedment length in the non-liquefiable layer below the liquefiable one is very small.

3.9. Recommended Modifications for the Simplified Method

The simplified method is widely used to estimate the displacement demands and the resulting pile foundation behavior and response. In light of the challenges and discrepancies discussed in this chapter, some recommended modifications are made in order to achieve more accurate results.

- Vary displacement push profile from abutment to far end of sliding zone. Due to the change in soil profile, pile lengths and cross sections. Displacement push profile need to reflect that, thus each pile bent is pushed with the corresponding profile.
- Use different displacement values, which can vary linearly from abutment to the far end of the sliding zone. Slope movement at the abutment location is more likely higher than down the slope failure wedge.
- Local slope failures must be considered in the overall profile. Analysis must account for

the stability of small slopes included in the overall failure wedge and their effect on the overall lurch.

- Revise the vertical displacement distribution. Vertical profile should start from the upper crust through the liquefiable layer and into the underlying layer as affected by the liquefaction process. The smear zone of the underlying layer might need to be included.
- For cases similar to this Bridge when more than 1 bent is included in the analysis. separate analysis for each bent should be conducted depending on the underlying soil configuration then combining the shear resistance of all bents. That is instead of creating a super pile out of different bents.
- This multi-bent analysis will optimize the calculation of the rotational stiffness of the pile head and also allow for including the connectivity effect of the bridge deck. This connectivity is vital for the pile head stiffness and specifically important in similar cases where each bent has only 1 row of piles.
- Each pile should be modelled as accurately as possible. Most piles have different cross-sections with depth. Pipe piles maybe be empty, filled with sand, filled with concrete or contain rebar. The variation of the pile cross-section will affect the locations of maximum moment and shear force.
- The procedure underestimates the residual strength of the liquefied soil and thus over predicting the soil displacement which is done with great uncertainty. Correlations need to be carefully selected and studied. A more accurate soil property representation could be done by evaluating the shear stress-strain response.
- Residual strength modelled by soft clay *p-y* analysis is not a sufficient tool for lateral response of liquefied soil. Another type of *p-y* curves might be a better representation

particularly with the gradual loss of soil strength with the cyclic loading.

- Use site specific earthquakes in rigorous block displacement analysis or at least an equation dependent on peak velocity and peak acceleration instead of Newmark's sliding block analysis that is only PGA dependent.
- Model entire canyon with both side slopes in slope stability models. In cases where canyons are narrow enough, failure surfaces from both sides are likely to interact.

Table 3-1. Soil properties of East Embankment used by Caltrans (2016) in *Slope/W*

Depth (ft)	Soil Type	Unit Weight [pcf]	Friction Angle [°]	Cohesion [psf]	Residual Undrained Shear Strength [psf]
0-13 (0-4m)	Stiff Clay	130 (20.4 kN/m^3)	-	2000 (95.8 kPa)	-
13-18 (4-5.5m)	Soft Clay	129 (20.3 kN/m^3)	-	500 (23.9 kPa)	-
18-24 (5.5-7.3m)	Medium Sand	120 (18.9 kN/m^3)	31	-	-
24-39 (7.3-11.9m)	Loose Sand*	120 (18.9 kN/m^3)	29	-	350 (16.6 kPa)
39-54 (11.9-16.5m)	Medium Sand*	120 (18.9 kN/m^3)	31	-	650 (31.1 kPa)
54-69 (16.5-21m)	Dense Sand	130 (20.4 kN/m^3)	34	-	-
69-99 (21-30m)	Dense Sand	130 (20.4 kN/m^3)	36	-	-
99-124(30-37.8m)	Very Dense Sand	130 (20.4 kN/m^3)	40	-	-

* Liquefied Layers

Table 3-2. Soil properties of East Embankment used by Caltrans (2016) in *Slope/W*

Depth (ft)	Soil Type	Unit Weight [pcf]	Friction Angle [°]	Cohesion [psf]	Residual Undrained Shear Strength [psf]
0-12 (0-3.7m)	Stiff Clay	130 (20.4 kN/m^3)	-	2000 (95.8 kPa)	-
12-15 (3.7-4.6m)	Stiff Clay	120 (18.9 kN/m^3)	-	1000 (47.9 kPa)	-
15-24 (4.6-7.3m)	Medium Sand	120 (18.9 kN/m^3)	33	-	-
24-54 (7.3-16.5m)	Loose Sand*	120 (18.9 kN/m^3)	31	-	500 (23.9 kPa)
54-99 (16.5-30m)	Dense Sand	130 (20.4 kN/m^3)	38	-	-
99-124(30-37.8m)	Very Dense Sand	130 (20.4 kN/m^3)	40	-	-

* Liquefied Layers

Table 3-3. Summary of results by Caltrans (2016)

Location	Bridge Supports	Post-Earthquake Slope Stability Factor of Safety	Yield Acceleration (k_y)	Displacement [inch]	
				Unrestrained	Restrained
East Embankment	Abutment 1 through Pier 6	0.7	N/A	Unlimited	72 (183 cm)
Channel Area	Pier 7 and 8	-	-	-	-
West Embankment	Pier 9 through Abutment 19	1.2	0.019	12 (30.5 cm)	2 (5.1 cm)

Table 3-4. Summary of results by UCSD

Location	Bridge Supports	Post-Earthquake Slope Stability Factor of Safety	Yield Acceleration (k_y)	Displacement [inch]	
				Unrestrained	Restrained
East Embankment	Abutment 1 through Pier 6	1.5	0.096	5 (12.7 cm)	3 (7.6 cm)
Channel Area	Pier 7 and 8	-	-	-	-
West Embankment	Pier 9 through Abutment 19	1.3	0.13	3 (7.6 cm)	2 (5.1 cm)

Table 3-5. Summary of local slope results by UCSD

Location	Bridge Supports	Post-Earthquake Slope Stability Factor of Safety		Yield Acceleration (k_y)		Displacement [inch]	
		Spencer's	Bishop's	Spencer's	Bishop's	Spencer's	Bishop's
East Embankment (local slope)	Bent 4	1.06	0.85	0.1	N/A	4.5 (11.4 cm)	8 (20.3 cm)

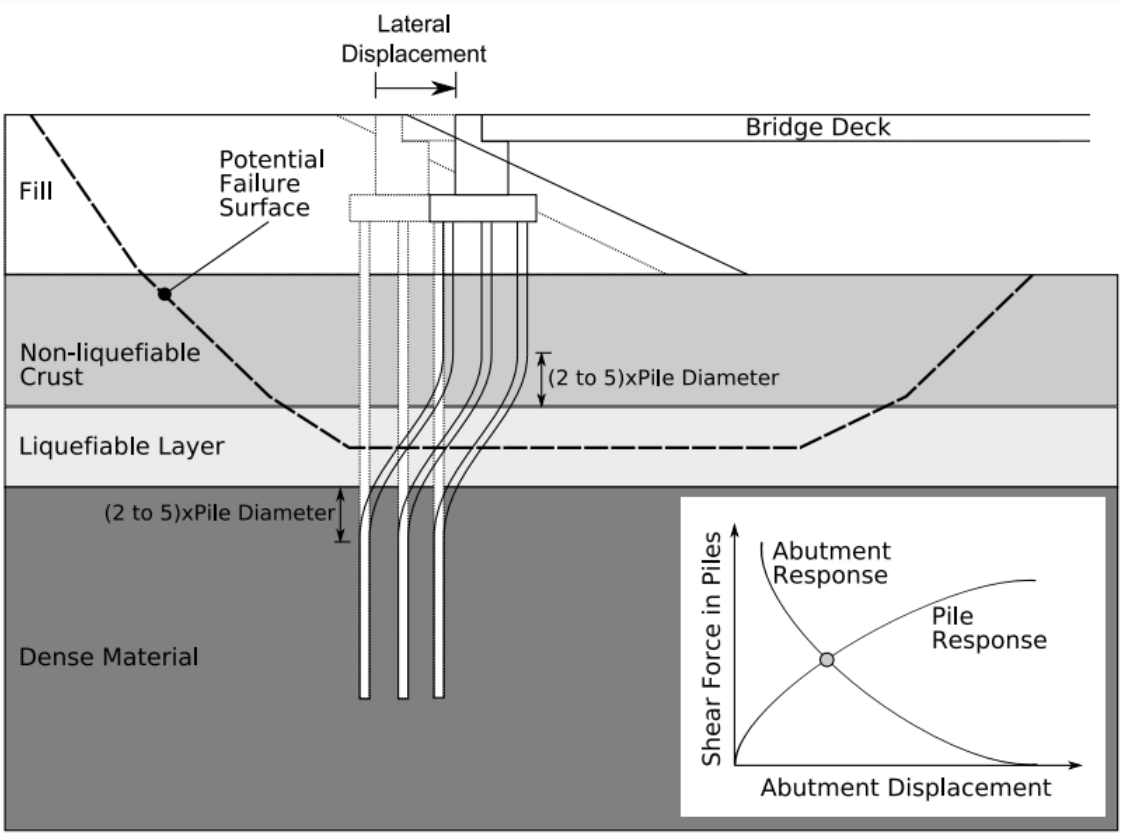

Figure 3-1. Illustration of pile-pinning effect (after Bray and Ledezma 2007)

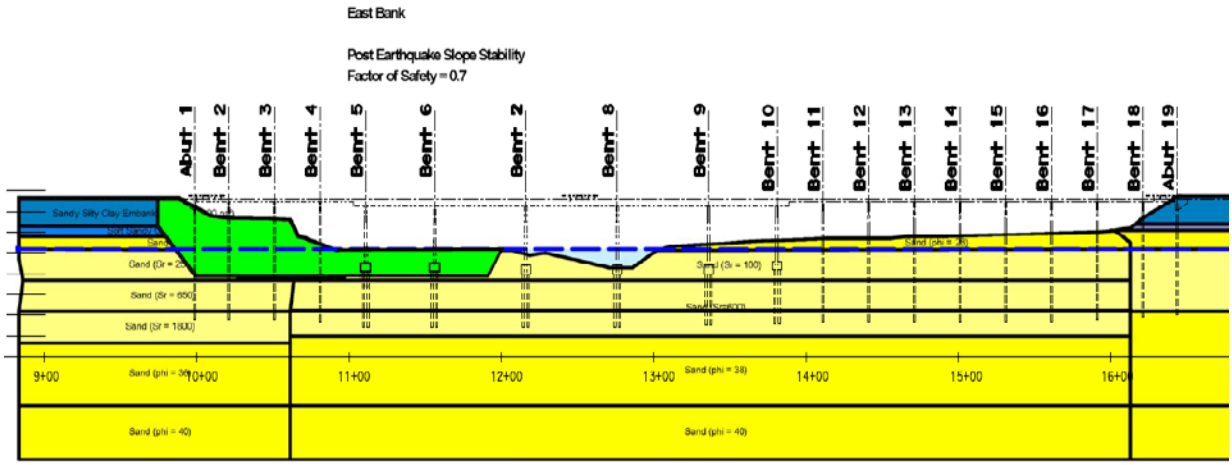

Figure 3-2. Caltrans (2016), *SlopeW* model for the East Embankment

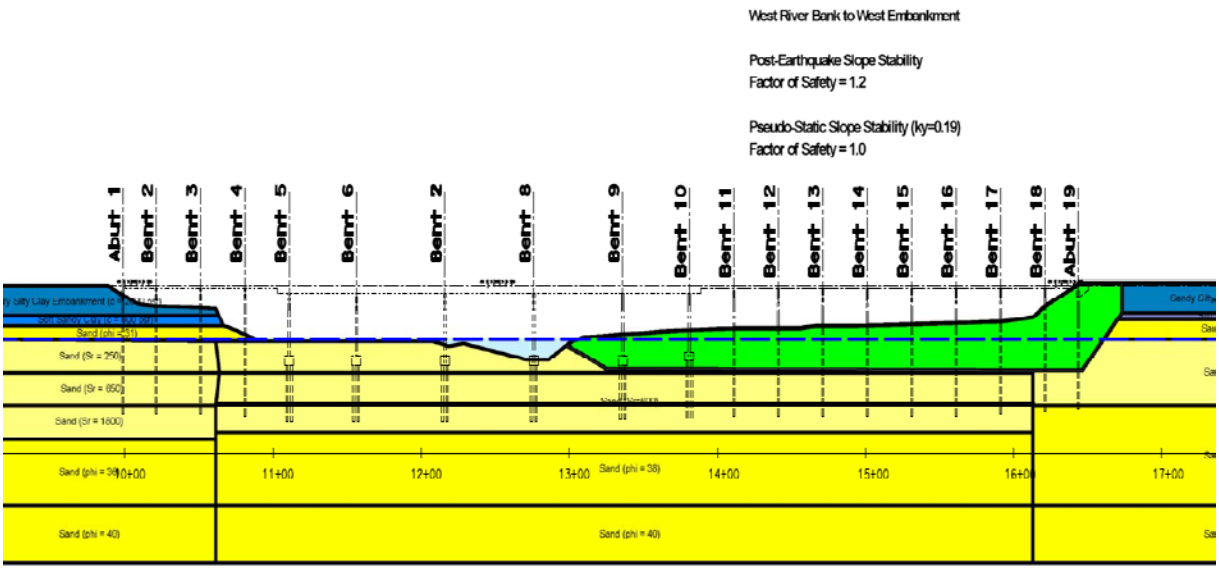

Figure 3-3. Caltrans (2016), *SlopeW* model for the West Embankment

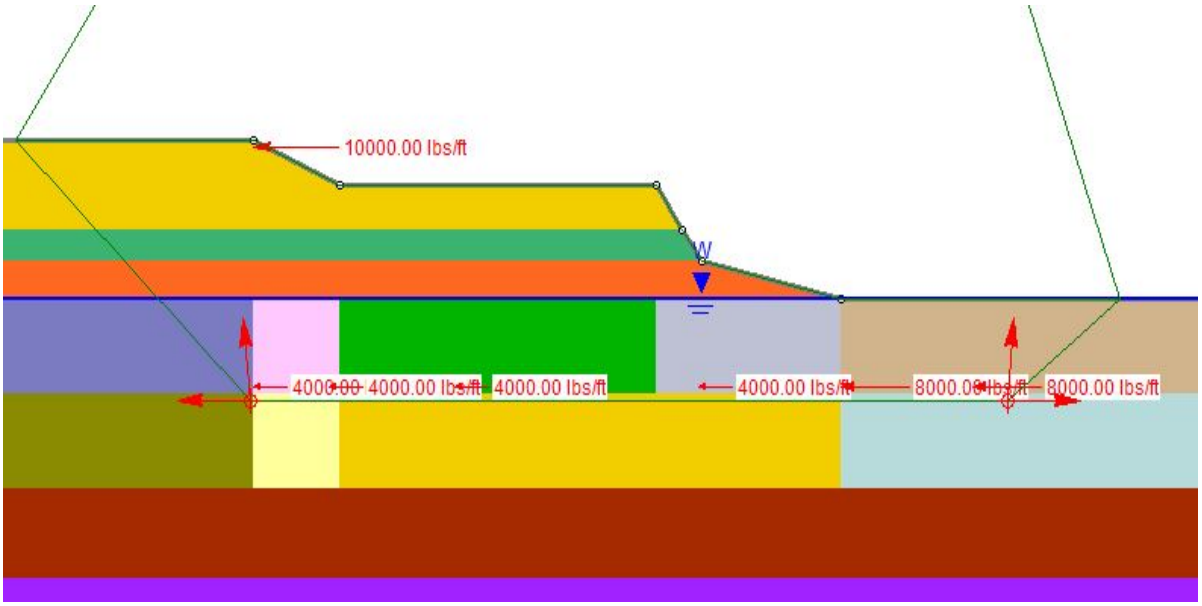

Figure 3-4. UCSD *Slide7* model for the East embankment

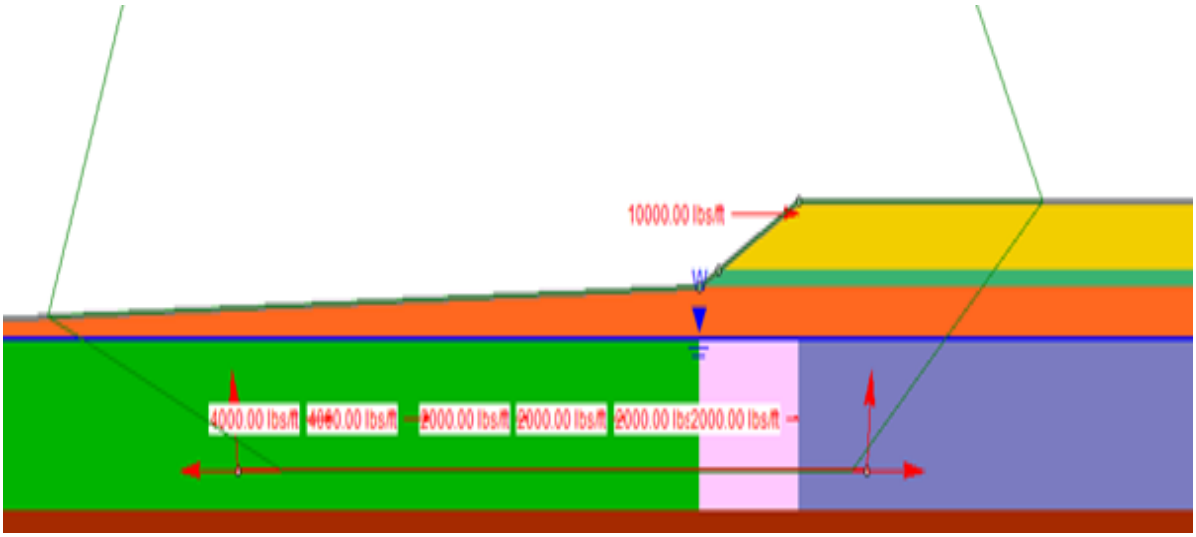

Figure 3-5. UCSD *Slide7* model for the West embankment

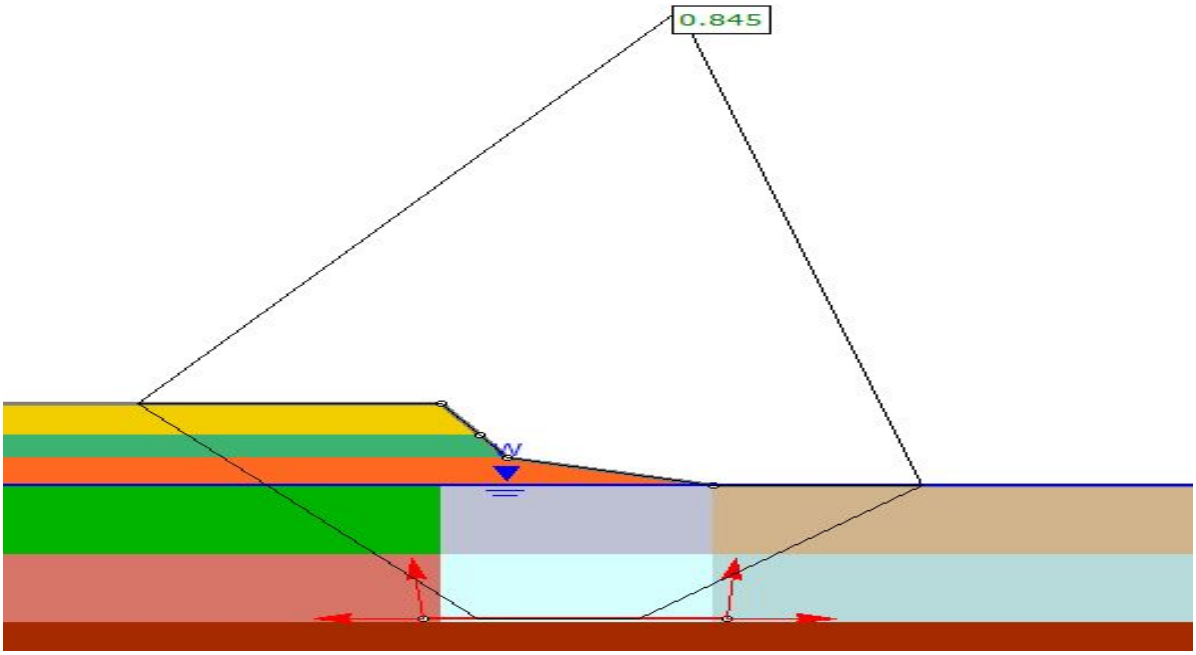

Figure 3-6. Local failure of second slope in the East Embankment (Static factor of safety using Bishops Method, FS=0.845)

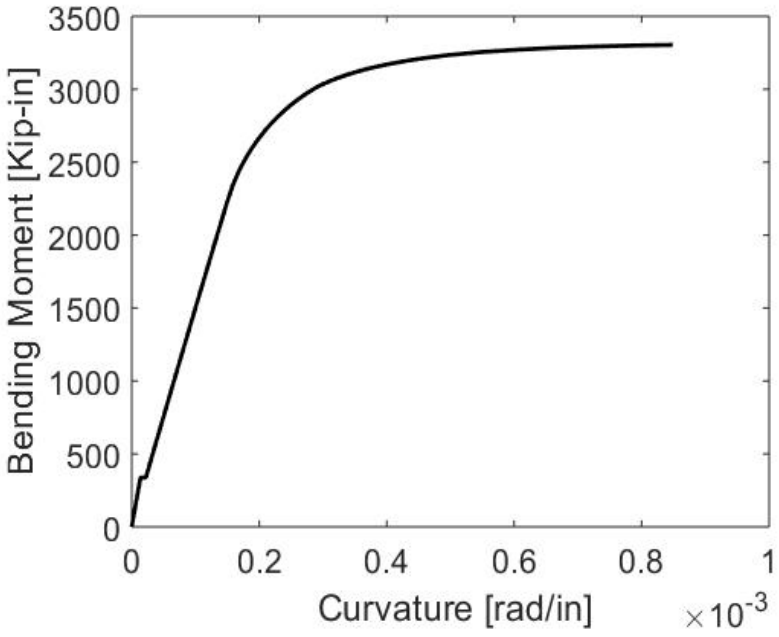

Figure 3-7. Moment Curvature for Single Pile Section Model existing from Abutment 1 till Bent 4 (modelled by LPILE) 1 Kip-in = 0.113 kN-m

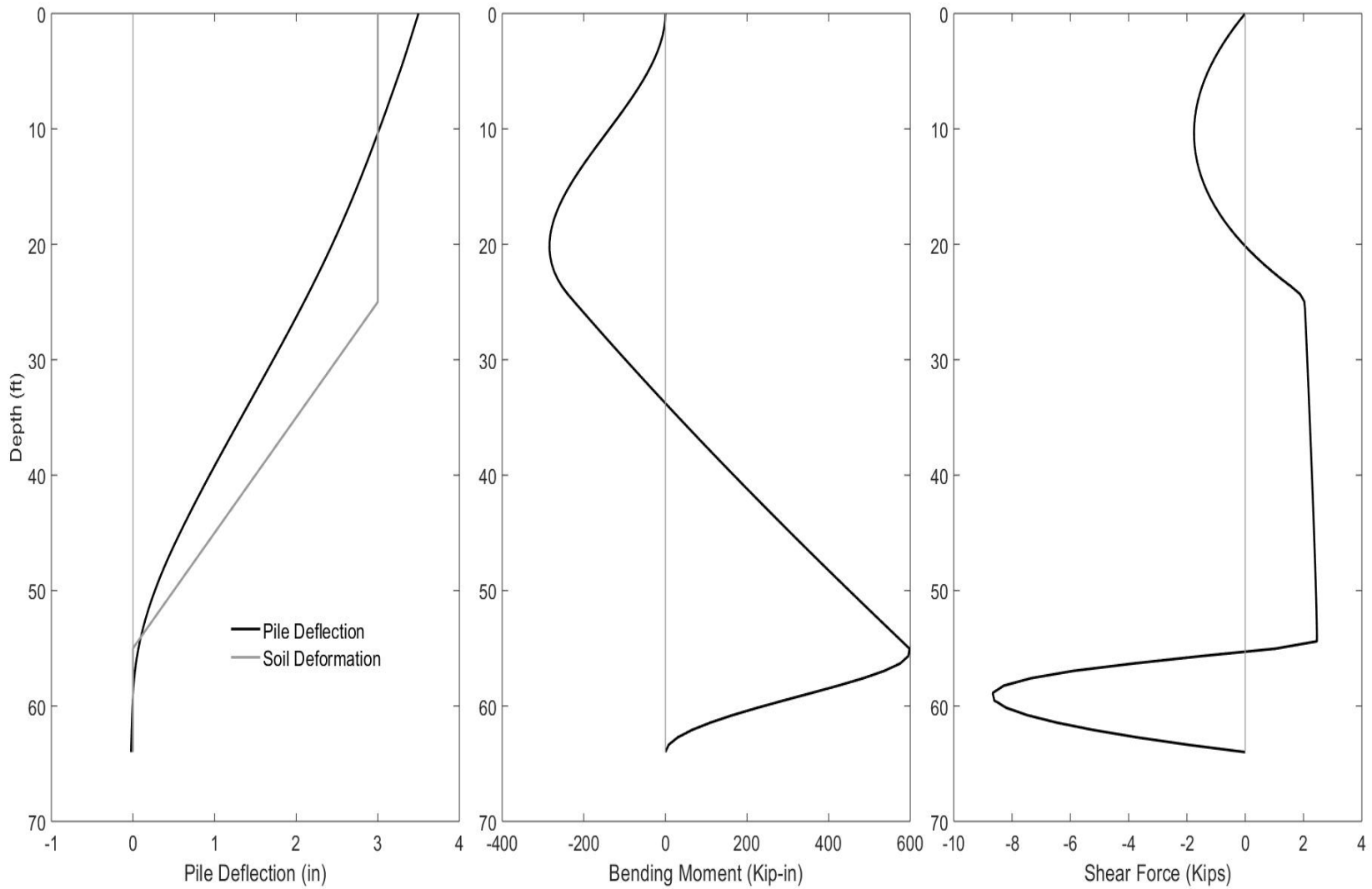

Figure 3-8. Pile Response from the design restraint displacement push for single pile (after division by number of piles), 1 Kip-in = 0.113 kN-m & 1 Kips = 4.45 kN

Chapter 4 Pile and Pile-Group Response to Liquefaction Induced Lateral Spreading in Four Large Scale Shake-Table Experiments

4.1. Abstract

Four large laminar-box shaking table experiments are conducted to document pile response due to the mechanism of liquefaction-induced lateral spreading. Single pile and pile group configurations are tested in a mildly inclined ground configuration. Two ground profiles of about 5 m in height are investigated, one with a liquefiable saturated sand stratum and the second with an added upper crust. The recorded data sets from this series of experiments are analyzed collectively to document and track the evolution of lateral loading on the deployed pile and pile-group configurations. Ground and pile lateral displacement as well as excess pore pressure are discussed. In this series of tests, it is observed that some of the highest pile lateral loads occur at the initial stages of lateral deformation, as the excess pore pressures approach the level of liquefaction. Thereafter, lateral load might decrease with further shear strength reduction and deformation in the liquefied stratum. For such soil profiles, lateral ground deformation that continues to accumulate due to the shaking process may not always result in significantly larger loads on the embedded pile foundation.

4.2. Introduction

Lateral spreading due to earthquake excitation presents a complex loading situation on piles and pile group systems (Boulanger and Tokimatsu 2005, Finn 2015). The underlying pile-ground interaction mechanisms take place as the soil undergoes significant change in its dynamic properties.

Case history investigations document a wide range of damage to structures and underlying pile foundations during liquefaction and lateral spreading (Hamada 1992, Hamada and O'Rourke

1992, Ishihara 1997, Tokimatsu and Asaka 1998, Berrill *et al.* 2001). The observed damage and deformations were analyzed in order to improve our understanding of the involved response mechanisms (Ishihara and Cubrinovski 1998, Ishihara and Cubrinovski 2004, Koyamada *et al.* 2006). As such, field studies have been of much value, further refining the scope of related research (Ishihara and Cubrinovski 2004, Koyamada *et al.* 2006).

Other efforts have derived insights from numerical investigations. For instance, Martin and Chen (2005) show that the relative stiffness between soil and pile is important in predicting the failure mode. They conclude that for stiff piles, lateral load can be high with the soil eventually flowing around the pile. On the other hand, a relatively flexible pile might experience lower lateral load as it undergoes large deflections.

Experiments play an important role as well, since the observed quantitative response remains scarce. To this end, centrifuge experiments were conducted to study liquefaction, lateral spreading and their effect on pile foundations (Abdoun 1997, Haigh 2002, Bhattacharya *et al.* 2004, Brandenberg *et al.* 2004, Kagawa *et al.* 2004, Towhata *et al.* 2006, Motamed *et al*. 2008, Motamed and Towhata 2010). Brandenberg *et al.* (2005) show that the instantaneous direction of lateral loads from the varying soil layers depends on the incremental and total relative displacement between the pile and soil. Brandenberg *et al.* (2007) discuss the load transfer mechanism of an upper non-liquefiable layer (crust) and the softening of this mechanism relates to the passive mode of failure. Other centrifuge tests (Abdoun and Dobry 2002, Abdoun *et al.* 2003, and Dobry *et al.* 2003) showed that the largest free head pile bending moment was at the boundary between the liquefied and non-liquefied strata.

In addition to the above, large scale one-g shake table experiments were performed (Tokida *et al.* 1993, Hamada, 2000, Meneses *et al.* 2002, Tokimatsu and Suzuki 2004, Cubrinovski *et al.*

2006, He *et al.* 2009, Motamed *et al.* 2013 and Chang and Hutchinson 2013). Suzuki *et al.* (2006) document stiffer piles having larger relative cyclic displacement but smaller permanent counterpart as compared to flexible piles.

The above-mentioned studies have provided insight and increased our understanding of the pile response mechanisms during liquefaction and lateral spreading. However, this challenging area remains a subject of research interest (Finn, 2015), with further efforts needed towards more accurate quantification of the outcomes.

Following in the footsteps of these earlier efforts, this paper investigates lateral spreading effects on pile foundations. The experiments were configured after the mildly inclined ground layout used in earlier centrifuge studies (e.g., Taboada *et al.* 1996, Abdoun *et al.* 2003). In this layout, lateral shaking is dominant, with no input vertical excitation involved.

Testing included 5 m long single piles and pile groups, with and without an upper crust soil stratum. As such, this set of four large laminar-box shake table tests is unique, currently being the only one-g series with a mild downslope lateral spreading configuration. As indicated by Ubilla *et al.* (2011), such one-g tests are needed as a complement to centrifuge studies where challenges remain in fully deciphering all consequences of the involved scaling laws.

In the following sections, the 4-test experimentation program is outlined. Recorded response time histories such as bending moments, displacements, and excess pore water pressures are discussed. Data from this test program are employed to document and elucidate the observed salient response characteristics. Finally, conclusions are drawn, and recommendations are presented.

4.3. Experimental Program

Using the large laminar box (Figure 4-1) at the National Research Institute for Earth Science and Disaster Prevention in Japan (NIED), response of piles subjected to liquefaction-induced lateral spreading was explored. Figure 4-2 and Figure 4-3 show schematic layouts of the four shake-table experiments. In this testing configuration, the soil box (Figure 4-1,Figure 4-2,Figure 4-3) was 11.6 m long, 5.5 m high and 3.5 m wide (inner dimensions) and was inclined at 2° to the horizontal. This inclination corresponds to an infinite slope of about 3º in the field upon accounting for the laminate weight (about 10% of tributary contained soil) and water table corrections (Ramirez 2009) following the procedure of Taboada (1995). As noted by Law and Lam (2001), the laminar box outer frames essentially simulate a form periodic boundary condition. Input motions for the experiments were in the form of sinusoidal acceleration with a 2 Hz frequency and amplitudes ranging from 0.2-0.3 g (Table 4-1).

The soil stratum was constructed by sand deposition in water. Kasumigaura sand (Kagawa *et al.* 2004) was used with the following grain size characteristics: D_{50} = 0.31 mm, fines content F_c = 3%, and uniformity coefficient C_u = 3. Soil relative density was estimated to be in the range of 40-50 % and saturated density was about 1940 kg/m3.

For the configuration of Figure 4-2, the model consisted of a 5.5 m sand layer with a single pile and a 2x2 pile group. The configuration of Figure 4-3 consisted of a 5.0 m sand layer and two single piles of different stiffness. In these configurations (Figure 4-2,Figure 4-3), water table was near ground surface in one, and lower than that in the other.

As such, each of those experiments contained two foundation elements, with either the water covering the whole soil or the stratum having a crust layer on top. We will refer to the fully saturated setups with water covering the soil by the letter “W” and to the setups with a crust layer

by the letter “C”. In addition, the letter “G” will represent tests with the 2x2 pile group (Figure 4-2), and the letter “P” will represent tests with single piles (Figure 4-3). For example, GW refers to the configuration of Figure 4-2a, and GC refers to that of Figure 4-2b, and so forth.

Table 4-2 shows characteristics of the soil stratum and pile foundations. Steel pipe piles of 0.318 m (1 ft) diameter were employed in all four experiments, with either a 6 mm (stiff pile) or 3 mm (flexible pile) wall thickness (denoted thereafter as the Stiff “S” and Flexible “F” piles respectively). Plastic moment capacity (Geschwindner 2011) is estimated to be 180 kN-m for the stiff pile and 93 kN-m for the flexible pile (Mild steel with ultimate strength of 400 MPa and bending moment equal to strength multiplied by section modulus). At the base of the box, the piles were welded with the intent of mimicking fixity in an assumed underlying firm soil stratum. As such, preliminary static pushover tests were performed on the piles before adding the sand to estimate the pile base rotational stiffness (Table 4-2), via a force-displacement bending beam calculation.

Each model was instrumented with a large number of accelerometers, pore pressure sensors, total pressure transducers, strain gauges and LVDTs (Figure 4-2, Figure 4-3). Instrumentation was placed along the pile shaft and along the profile of the ground stratum. Pore pressure transducers were placed on the piles in addition to being embedded in free field soil. Strain gauges were densely deployed along the pile shaft to aid in back-calculation of bending moment during shaking. Displacement transducers were mounted on the laminar box exterior wall to measure lateral motion, and on the soil surface to measure horizontal and vertical deformation. Furthermore, the piles were instrumented with transducers to measure head displacement above the ground surface.

4.4. Analysis Protocol

Focus is placed on system response mainly in terms of excess pore water pressure, ground deformation, and pile behavior. Bending moment in the piles was calculated based on the measured strain assuming linear behavior using the traditional Euler-Bernoulli beam theory (Wilson *et al.* 2000); and is an indicator of the acting pressure profile.

From the calculated bending moment time histories, the instant of maximum moment is identified. Table 4-3 shows an overview summary of the results, showing the attained maximum bending moment in each pile, along with pile head and soil displacement at both the maximum instant and at the end of shaking.

4.5. Results and Interpretation

4.5.1 Test GW

In this test illustrated in Figure 4-2a and Table 4-2, liquefaction occurred early in the shaking phase as evident from the reduction in acceleration (unfiltered) at shallower depths (Figure 4-4a) and the recorded excess pore pressure ratio r_u (Figure 4-4b), where $r_u = u_e / \sigma_{vo}'$ in which u_e = excess pore pressure and σ_{vo}' = initial effective vertical stress. The vertical line in these figures denotes attainment of maximum pile bending moment (Figure 4-5) at about 3.5 seconds and is included on all time history plots for ease of tracking. Bending moment profiles at this maximum instant are presented in Figure 4-6.

We observe that at the instant of peak bending moment, excess pore-pressure ratio (r_u) was somewhat lower than 1.0 (Figure 4-4b), and liquefaction (r_u =1.0) occurred shortly thereafter. Shear stress strain loops (Figure 4-7) calculated from the accelerations (Zeghal and Elgamal 1994) of the center array at 3.75, 4.25 and 4.75 m depths qualitatively denote the corresponding gradual loss of soil stiffness and strength.

From the presented response, it can be seen that:

i) The minor oscillations in pore water pressure after liquefaction (Figure 4-4b) suggest the lack of significant shear-induced dilative tendency (Zeghal and Elgamal, 1994) in this relatively loose liquefied soil stratum.

ii) Around the onset of liquefaction, it may be interest to note the clear phase-shift in acceleration between the upper and lower locations of the soil profile (Figure 4-4a), indicating a degree of dynamic motion incoherency along the liquefied soil profile.

iii) Ground displacement continued to accumulate in the downslope direction throughout the shaking phase (Figure 4-5a) with no additional bending demands on the piles after the first few cycles, where the peak was reached.

iv) Early in the shaking phase, as the stratum progressed towards liquefaction (r_u = 1), the single pile moments (peak of about 90 kN-m near the base) are seen to approach their highest values. Thereafter, with the progress of liquefaction and related decrease in soil stiffness and strength (Figure 4-4 and Figure 4-7), the pile gradually rebounded to about 50% of its peak deformed configuration, with a corresponding reduction in its moments (approximately 100 mm at peak vs 50 mm at end).

v) The pile group peak bending moment was observed at the pile-cap interface (Figure 4-5c), reaching values of 55 kN-m and 45 kN-m for the downslope and upslope piles respectively. With the highest soil displacements at ground surface, bending moments recorded at the base were about 90% and 50% of the top maximum values for the downslope and upslope piles respectively (Figure 4-6). With the aforementioned progress of liquefaction and related decrease in soil stiffness and strength (Figure 4-4 and Figure 4-7), bending moment gradually decreased and residual values were approximately 50% of peak values.

vi) The downslope pile was subjected to higher moments than the upslope pile by approximately 20%, highlighting the complex lateral soil pressure mechanism within and around the perimeter of the pile group.

vii) The plateau in bending moment with increasing pile cap displacement (Figure 4-5) might be associated with soil around the pile group becoming gradually weaker at greater depths (Figure 4-7). This mechanism would possibly permit for the observed slight additional cap displacement with little impact on the moment (due to the increase in effective free pile length).

4.5.1.1 GW System Response

The aim of this section is to touch on the system response as dictated by testing of a pile and a pile group simultaneously, within the soil box. As seen in Figure 4-5, the box boundaries eventually experienced about 270 mm of accumulated displacements with the pile and pile group responses being significantly lower. The displacements of Figure 4-5 (at maximum pile response and at end of shaking) can be displayed as shown in Figure 4-8 in the form of average axial longitudinal strains (strictly portraying the response along the box longitudinal centerline). For each zone along the length, these strains are calculated simply based on the difference in recorded displacements at the boundaries. In the vicinity of the single pile, it can be seen that:

1. At the maximum instant, the pile head (due to the pile's cantilever bending beam configuration): i) moved slightly farther than the upslope soil and ii) caused some compression in the immediate downslope soil.

2. By the end of shaking, the soil box was moving much more than the single pile, the upslope ground pushing on the pile, while the downslope ground moving away. This resulted in an upslope compression zone and a downslope extension zone.

In the vicinity of the pile group, it can be seen throughout that the immediate upslope soil is compressed, with an extension in the downslope ground. Lateral load on the pile group is thus clearly influenced by the increase in upslope and decrease in downslope lateral soil pressure. It is also noted that the upslope compression zone was interrupted by presence of the upslope single pile, providing a sort of shadowing effect mechanism for the pile group.

4.5.2 Test GC

Compared to the earlier GW experiment above, water table was at a depth of about 0.5 m (Figure 4-2b and Table 4-2). Similar to the above GW scenario, acceleration and excess pore pressure displayed the characteristics of Figure 4-4, and bending moments reached their peak value just before soil liquefaction (r_u = 1). With a relatively stiff non-liquefiable crust stratum at the top, firmly engaging and sustaining contact with the deployed pile foundations, observations include (Figure 4-9):

i) A crust binding mechanism was in effect, closely tying ground deformations to those of the embedded foundations. Compared to the GW response (Figure 4-5), a) pile displacements and moments were higher by approximately 40 % (Table 4-3), b) the embedded single pile and pile group underwent similar levels of deformation, and c) the box and center soil displacements were quite similar, d) more constrained by resistance of the foundation to crust movement, overall soil displacement was significantly lower.

ii) At the maximum instant (Figure 4-10), ground surface axial strains were quite low near the pile group. Higher strains are seen in the vicinity of the more flexible cantilever single pile.

iii) At end of shaking (Figure 4-10), the highest strains were in the middle of the box, away from the upslope and downslope boundaries.

iv) In the downslope vicinity of the pile foundations, video monitoring of the crust soil surface (Figure 4-11) displays the actual cracking and gap formation characteristics in the axial extension zones of Figure 4-10. It may be seen that there is no gap formation downslope of pile elements prior to the maximum instant (3.60 sec) confirming the measured small compressive strains. Thereafter, the ground keeps deforming downslope with no further pile movement. Thus, the gap and extension lines visible downslope confirm the large measured axial extension strains.

4.5.3 Test PW

Figure 4-3a and Table 4-2 show the second tested configuration with a fully saturated loose layer and 2 single piles. Essentially, the stiff pile group (Figure 4-2a) has been replaced by a single flexible pile (Figure 4-3a). As such, a much more compliant overall soil-pile system is being studied.

Similar to above, minimal oscillations in pore water pressure during liquefaction (Figure 4-12) suggest the lack of a significant dilative tendency in the liquefied soil response (Zeghal and Elgamal 1994). Compared to the results of Test GW (Figure 4-5) where the pile group was providing significant lateral stiffness, the response in Figure 4-12 shows that:

i) Potentially influenced by the added system compliance, liquefaction occurred more rapidly (about one cycle earlier).

ii) Displacement of the box and soil surface where much higher. For instance, at about 15 s, box permanent downslope deformation was about 0.5 m versus 0.25 m in the GW test. Thereafter, soil and box displacements continued to accumulate, reaching as much as 1.00 m (more than 3 pile diameters).

iii) Peak response of the stiff pile occurred right after liquefaction. Due to soil deformation during build-up of excess pore pressure, the stiff pile experienced increased lateral pressures.

However, upon liquefaction and further lateral deformation, the soil was not exerting additional pressure, presumably just flowing around the pile. With the gradual loss in soil strength, the pile, still in its elastic state (Figure 4-13), fully rebounded back to its initial position.

iv) Bending moment response mimics the observed displacement of this stiff pile as it rebounded to its initial position. Maximum attained bending moment was about 132 kN-m at the base.

v) Alternatively, the flexible pile shows signs of material failure and geometric non-linearity that caused excessive deformation and erratic bending moment response. The shown peak moment, calculated on the basis of measured axial strain, exceeds to pile's bending capacity (Table 4-3), indicating large localized plastic strains and significant plastic yielding near the pile's base. Upon yielding (buckling) of this flexible pile (Figure 4-13), moment in the stiff pile further downslope (Figure 4-3a) may be seen to experience a slight bump during the 5s-7s time window (Figure 4-12).

vi) The ground surface average axial strain between recording stations (Figure 4-14) denotes: 1) the observed upslope compression and downslope extension for each pile, and 2) at end of shaking, some boundary axial strains appear (about 19 %), compressive on the upslope side and tensile on the downslope side, partially due to the relatively heavier border laminates moving a bit further downslope as compared to the nearby liquefied soil inside the box.

4.5.4 Test PC

Compared to the above PW experiment above, this test (Figure 4-3b and Table 4-2) included an upper non-liquefiable crust. As mentioned earlier, this relatively stiff crust stratum firmly engages and sustains contact with the deployed pile foundations, with the following main observations (Figure 4-15):

i) Early in the shaking phase, right after liquefaction (r_u = 1), moments are seen to approach their peak values.

ii) Similar to the GW-GC scenario, lateral resistance of the piles, exerted on the engaged upper crust, resulted in PC displacements being significantly lower than PW (about 40% decrease at the end of shaking).

iii) With absence of the GC pile group, the stiff pile underwent the highest displacements and moments of all tests, reaching about 1.25 times those of the PW case.

iv) The stiff pile, remaining in its elastic state, gradually rebounded to 40 % of peak value, while the soil and box permanent displacements continued to steadily increase. As opposed to PW, the pile did not fully rebound to its initial position due to pressure from the upper non-liquefied crust stratum.

v) Similar to PW above, the flexible pile was yielded near its base, with analogous response characteristics. Due to this yielding, no rebound was observed.

vi) Longitudinal axial strains shown in Figure 4-16 follow the general trend set in GW and GC. The pile heads moved more than the soil at the maximum instant. Thereafter, the soil kept displacing, creating increasing pile upslope compression and downslope extension zones. This response is depicted in the still frames of Figure 4-17, where the extension zones are manifested in the form of large gaps as the soil moves farther and farther away from the pile.

4.6. Summary and Conclusions

Four lateral spreading experiments were conducted in a large laminar box, with different pile and soil stratum configurations. From this test series, a number of salient response characteristics were documented in this study. The presented data was compared, with a focus on

documenting and tracking the evolution of soil displacements, pile bending moments, and the involved ground-pile system response. Among the main observations and findings are:

1. Maximum moment occurred during the first few cycles of shaking, around the onset of liquefaction. Further accumulated lateral soil deformation thereafter was generally associated with reduction in pile moment and rebound towards its initial starting position. In view of this mechanism:

1.1. In seismic assessments, uncoupling the effects of lateral spreading (kinematic) and superstructure (inertial) loads has been a topic of discussion (e.g., Ramos 1999, Miwa *et al.* 2006, Ashford *et al.* 2011). While presence of the superstructure might result in a more complex pattern of response, consideration should be given to the potential for high inertial and kinematic loads occurring simultaneously during the early strong shaking phase of the earthquake.

1.2. Permanent pile displacements as documented from a post-earthquake reconnaissance effort, may be significantly lower than peak values due to potential partial pile rebound. In addition, peak pile moments might have occurred at ground deformation levels that are significantly lower than the final observed values.

2. The tested configurations vividly showed that the observed lateral response was driven by the overall pile-ground system interaction. Along the longitudinal axis of the box, local average axial strains varied considerably, driven by geometric configuration of the deployed pile foundations. Most obvious was the influence of the relatively stiff pile group in reducing lateral moment on the neighboring single pile. In general, the test results must be interpreted in this light, with the further understanding that the soil box is a form of periodic boundary as opposed to a surrounding free-field half-space.

3. Due to liquefaction, acceleration peaks along the stratum profile were significantly out of phase. As such, lateral forces due to the liquefied soil inertia may not be fully in-phase along the stratum's thickness.

4. Presence of a non-liquefied upper crust resulted in, a) larger bending moments due to the associated relatively high lateral pressure exerted by this stratum, as highlighted in earlier studies (e.g., Brandenberg *et al.* 2007), and b) lower overall soil displacements.

5. The downslope pile in the group experienced somewhat higher bending moments than its upslope counterpart in agreement with the observations of Motamed *et al.* (2013). Closer examination of this mechanism is suggested.

4.7. Acknowledgements

Chapter 4, in full, has been submitted for publication of the material as it may appear in the following journal publication (The dissertation author was the primary investigator and author of this paper):

Ebeido, A., Elgamal, A., Tokimatsu, K. and Abe, A. (2019). "Pile and pile-group response to liquefaction induced lateral spreading in four large scale shake-table experiments." Journal of Geotechnical and Geoenvironmental Engineering.

Table 4-1. Shake Table input harmonic motion for the experiments

Test	Input Motion		
	Frequency [Hz]	Amplitude [g]	Duration [s]
GW (Figure 4-2a)	2	0.2	14
GC (Figure 4-2b)	2	0.3	14
PW (Figure 4-3a)	2	0.2	44
PC (Figure 4-3b)	2	0.2	44

Table 4-2. Characteristics of Soil stratum and Pile foundations (Figures 4-2, 4-3)

Test	Soil Profile		Pile Properties					
	Height [m]	Water Table	Embedded length [m]	Diameter [cm]	Wall thickness [cm]	Bending stiffness [kN.m^2]	Base rotational stiffness [kN.m/rad]	Yield bending moment [kN.m]
GW	5.5	Covers entire soil	5.5	31.8	0.6	14320	18500	180
GC		1m below downslope soil						
PW	5.0	Covers entire soil	5.0	31.8	0.6*	14320	18500	180
					0.3**	7360	8500	93
PC		0.50m below downslope soil			0.6*	14320	18500	180
					0.3**	7360	8500	93

* Denoted in text as stiff pile (S)

** Denoted in text as flexible pile (F)

Table 4-3. Summary of experimental results (Figures 4-2, 4-3)

Test	Pile Configuration		At maximum pile response				At enf of shaking		
				Relative Displacement [mm]			Relative Displacement [mm]		
			M_{max} [kN-m]	Pile Head	Center Array @ Ground Surface	Box Surface (Top Frame)	Pile Head	Center Array @ Ground Surface	Box Surface (Top Frame)
GW	Single Pile		92	110	82	75	59	155	275
	Pile Group	Downslope	55	61			62		
		Upslope	45						
GC	Single Pile		119	126	92	76	75	173	149
	Pile Group	Downslope	77	84			66		
		Upslope	65						
PW	Stiff		132	110	160	142	0	710	980
	Flexible		93**	187			N/A		
PC	Stiff		166	138	103	170	61	480	588
	Flexible		93**	158			166		

* At about 14 s for GW and GC, and 44 s for PW and PC

** Denotes yielding of pile cross-section, with estimated value being limited by this yielding mechanism

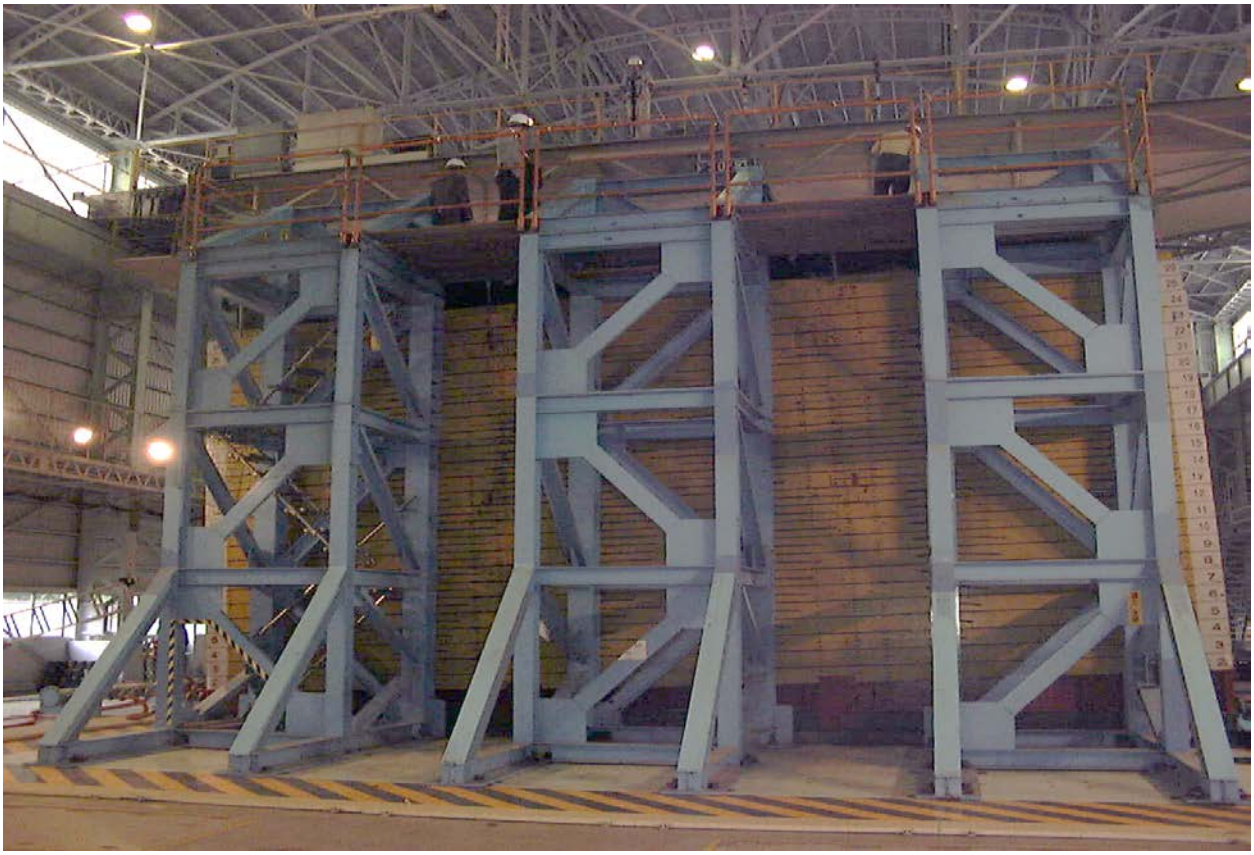

Figure 4-1. Mildly inclined large laminar box on shake table

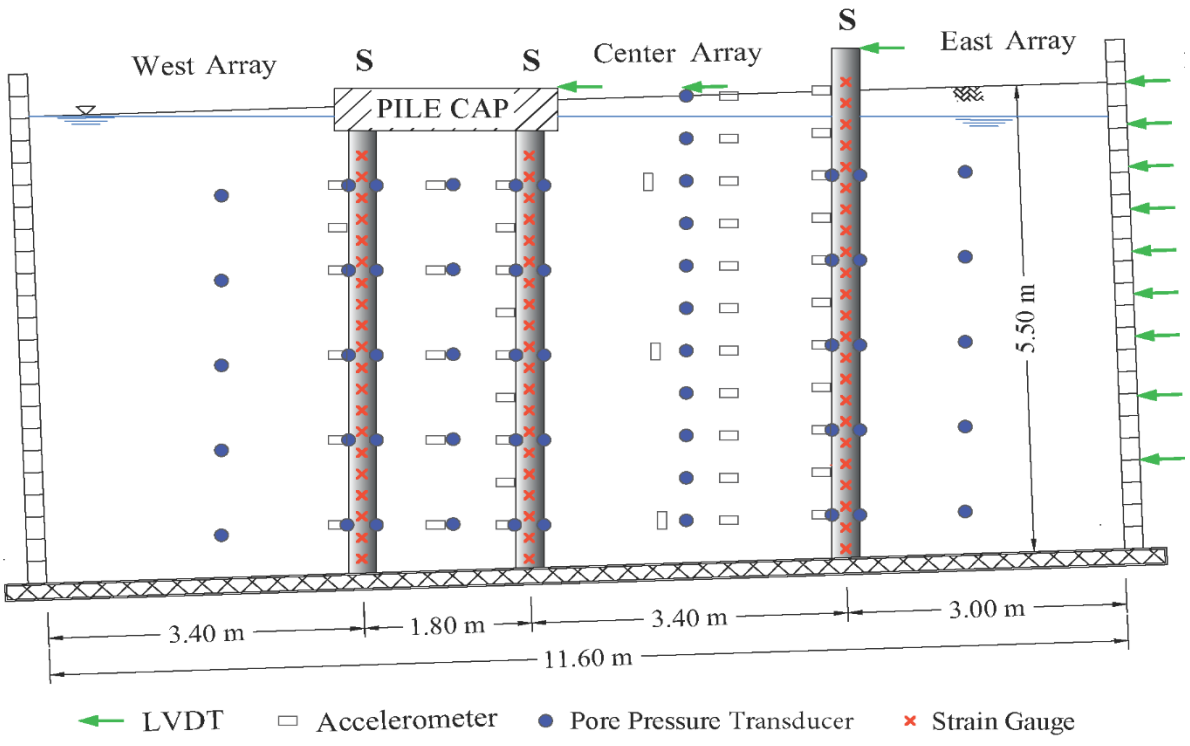

(a)

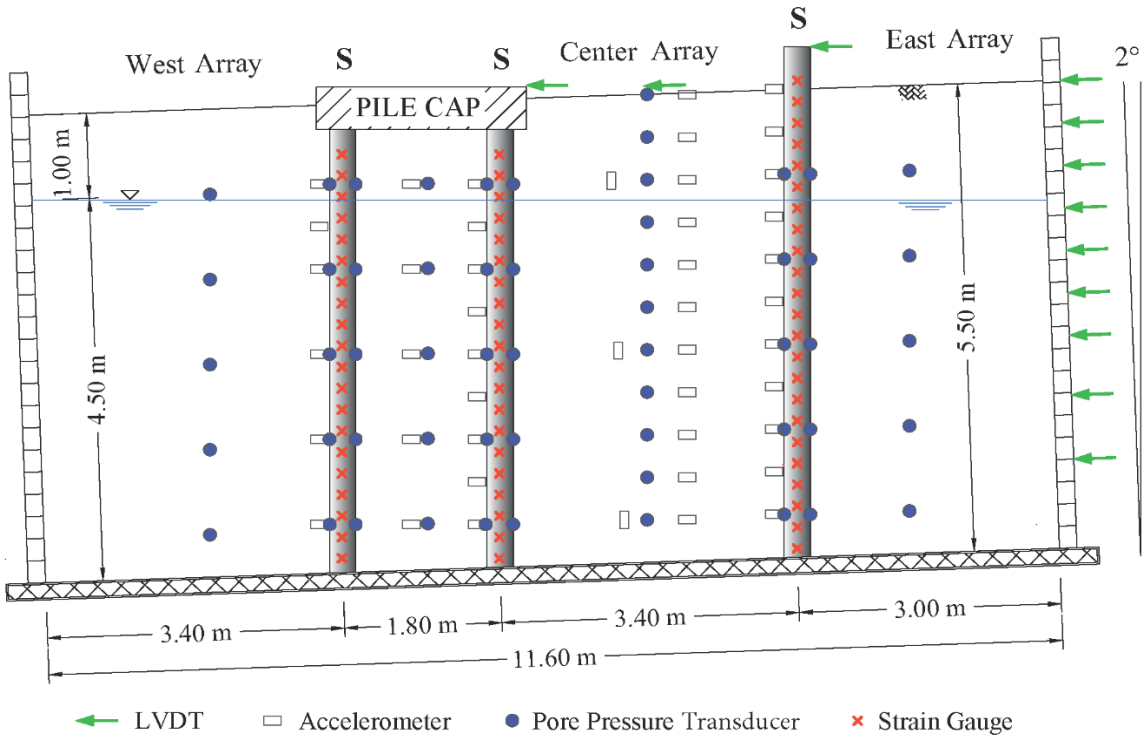

(b)

Figure 4-2. Testing Configurations: a) GW, and b) GC (S denotes stiff pile)

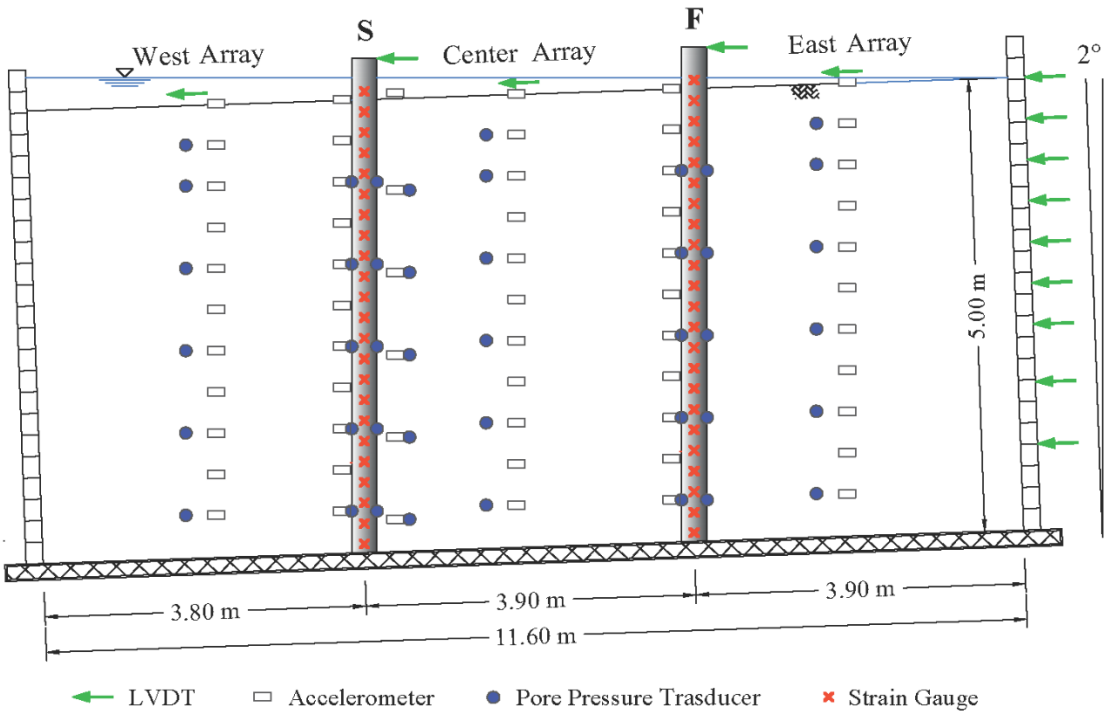

(a)

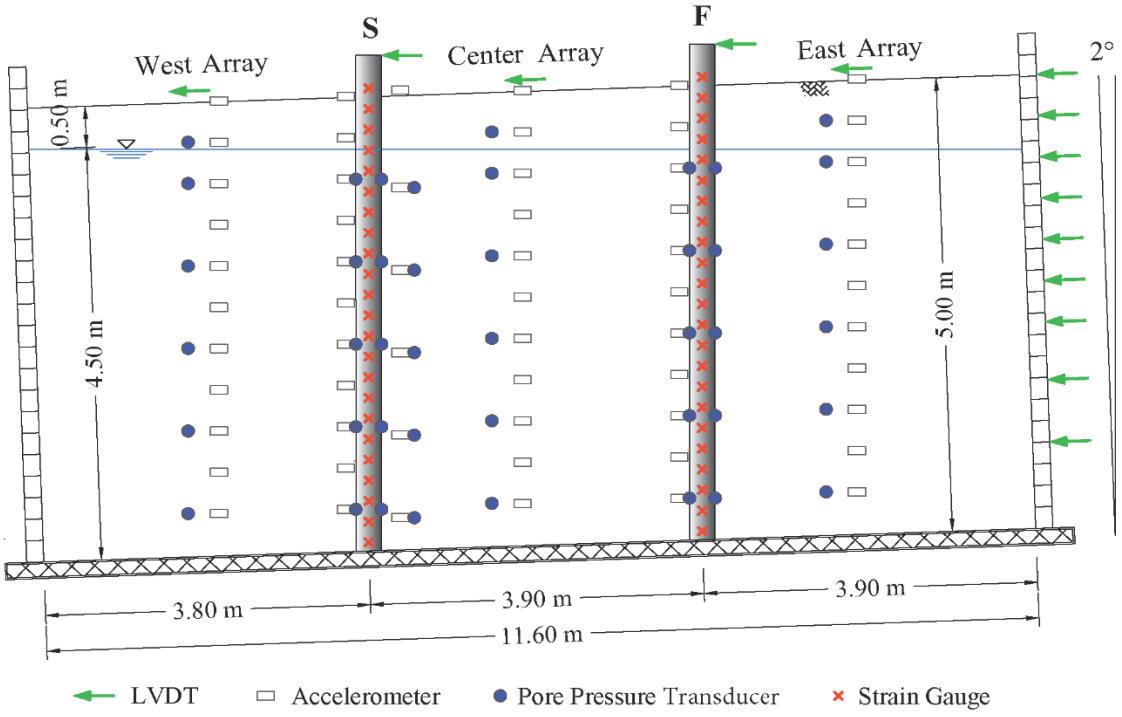

(b)

Figure 4-3. Testing configurations: a) PW, and b) PC (S denotes stiff and F denotes flexible pile)

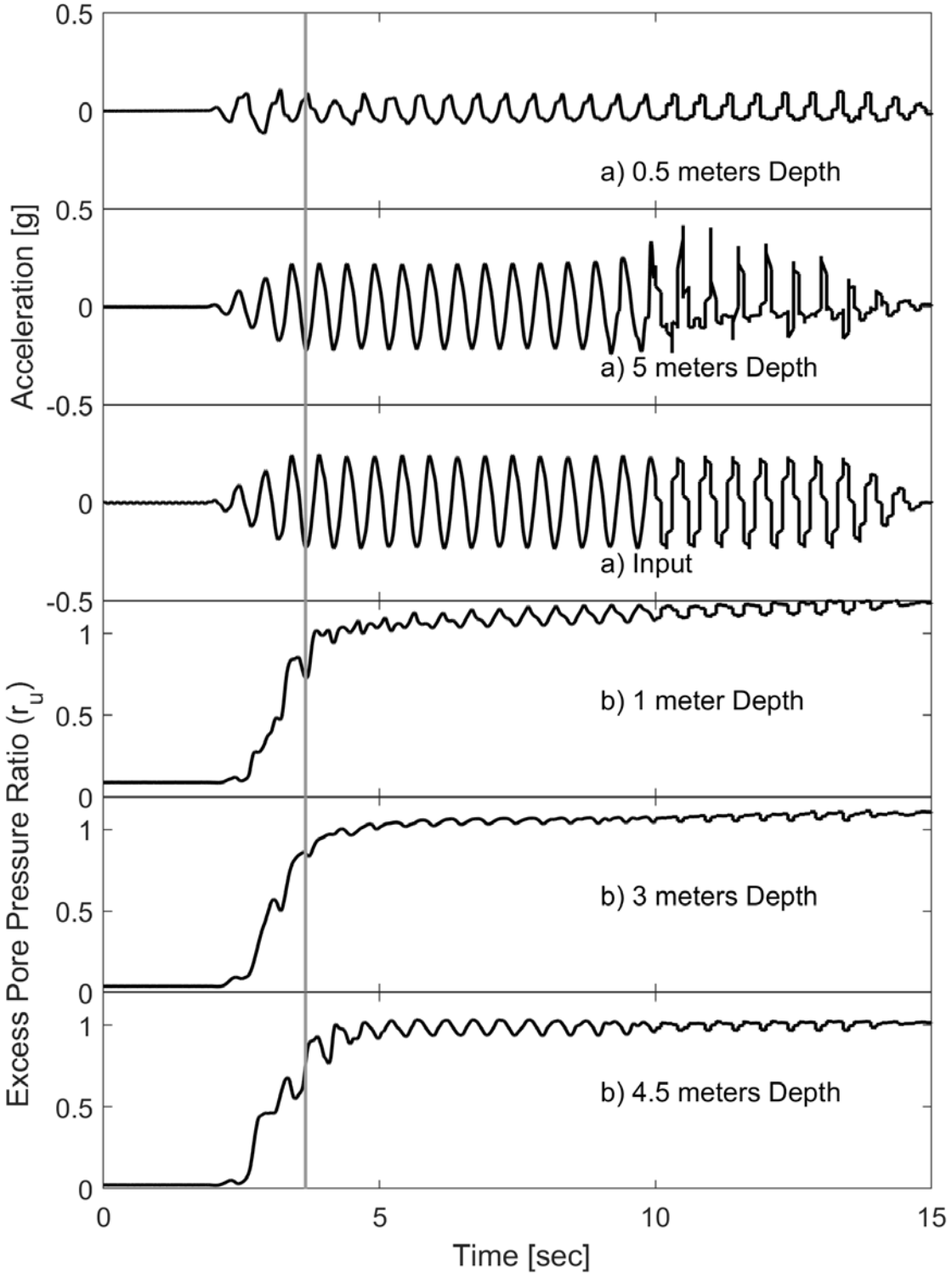

Figure 4-4. GW test: a) soil center array acceleration time history and input motion, and b) center array excess pore-pressure (vertical line denotes instant of maximum bending moment)

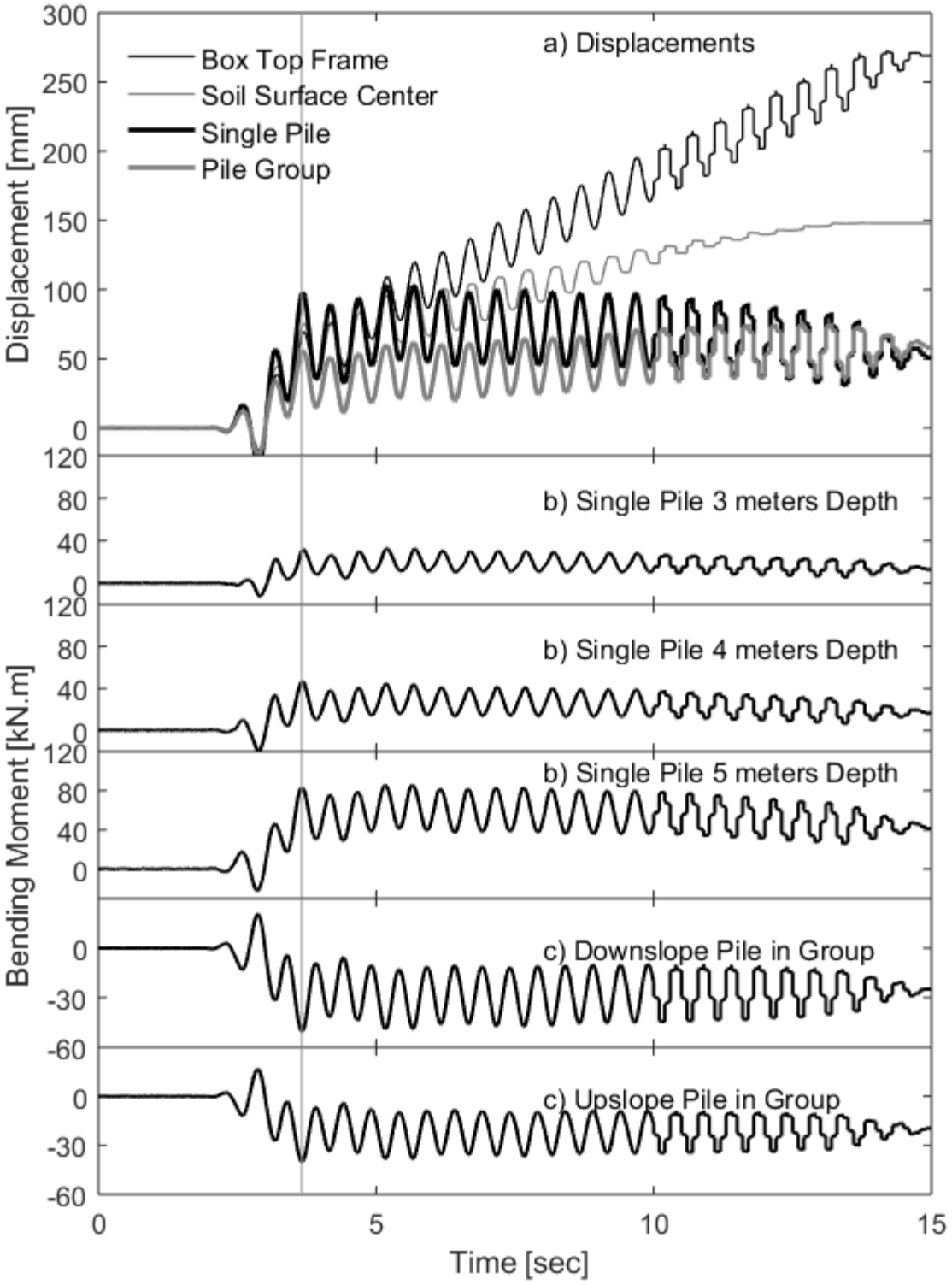

Figure 4-5. GW Test: a) displacement time history, b) single pile bending moment, c) pile group head bending moment

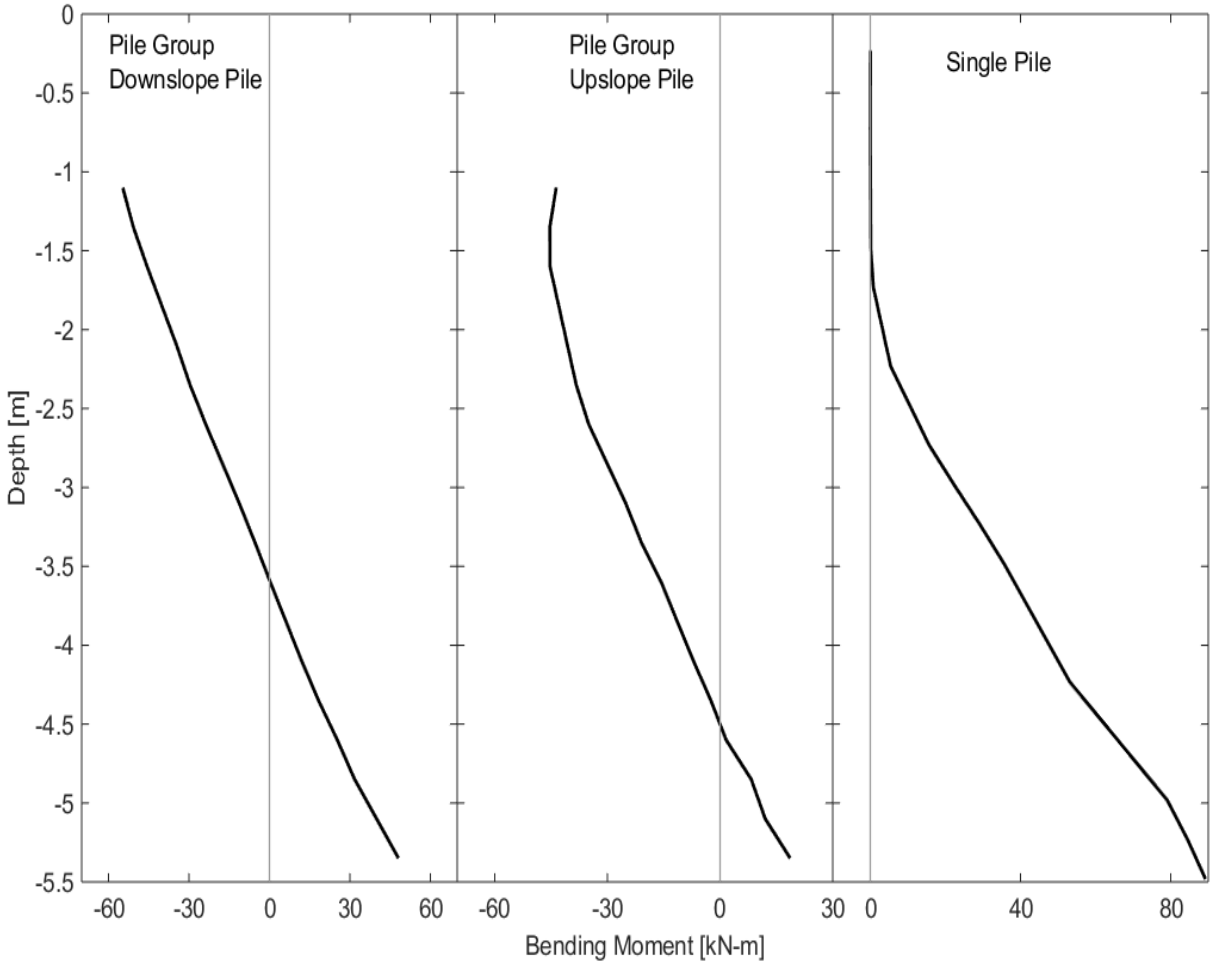

Figure 4-6. GW Test bending moment profiles at the maximum time instant for pile group downslope and upslope, and single pile

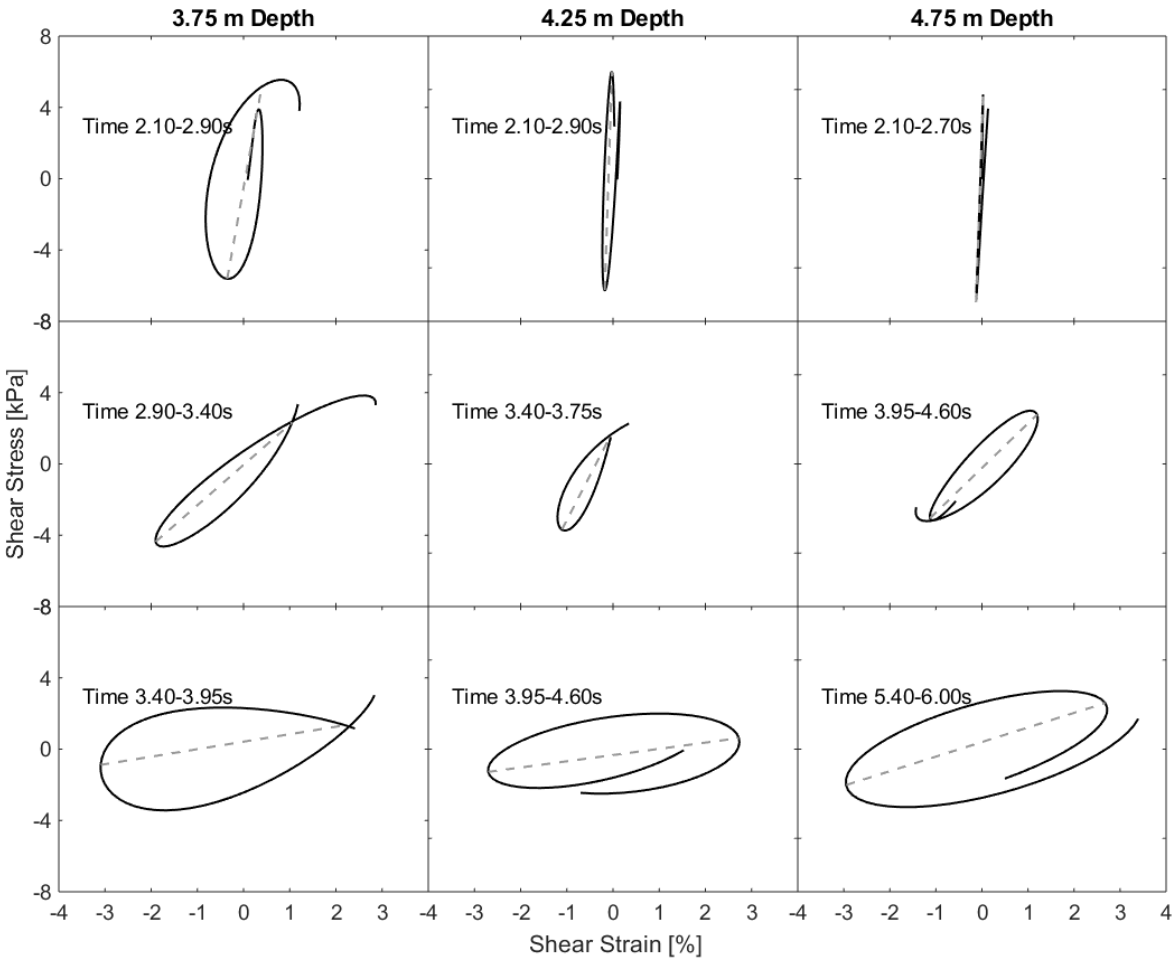

Figure 4-7. GW shear stress-strain soil response (center array at 3.75, 4.25 and 4.75 m depth)

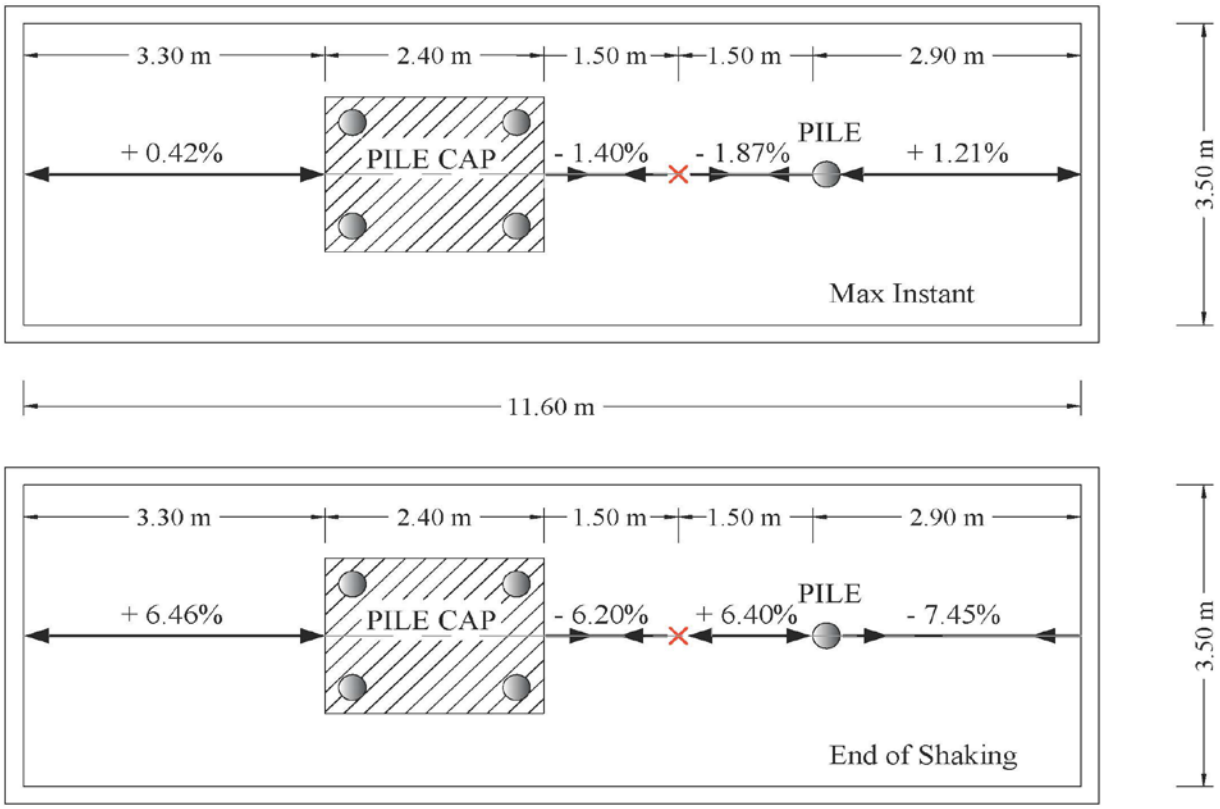

Figure 4-8. GW plan view displaying average axial strain between recording locations along the ground surface (positive values refer to tensile strains while negative values are compressive)

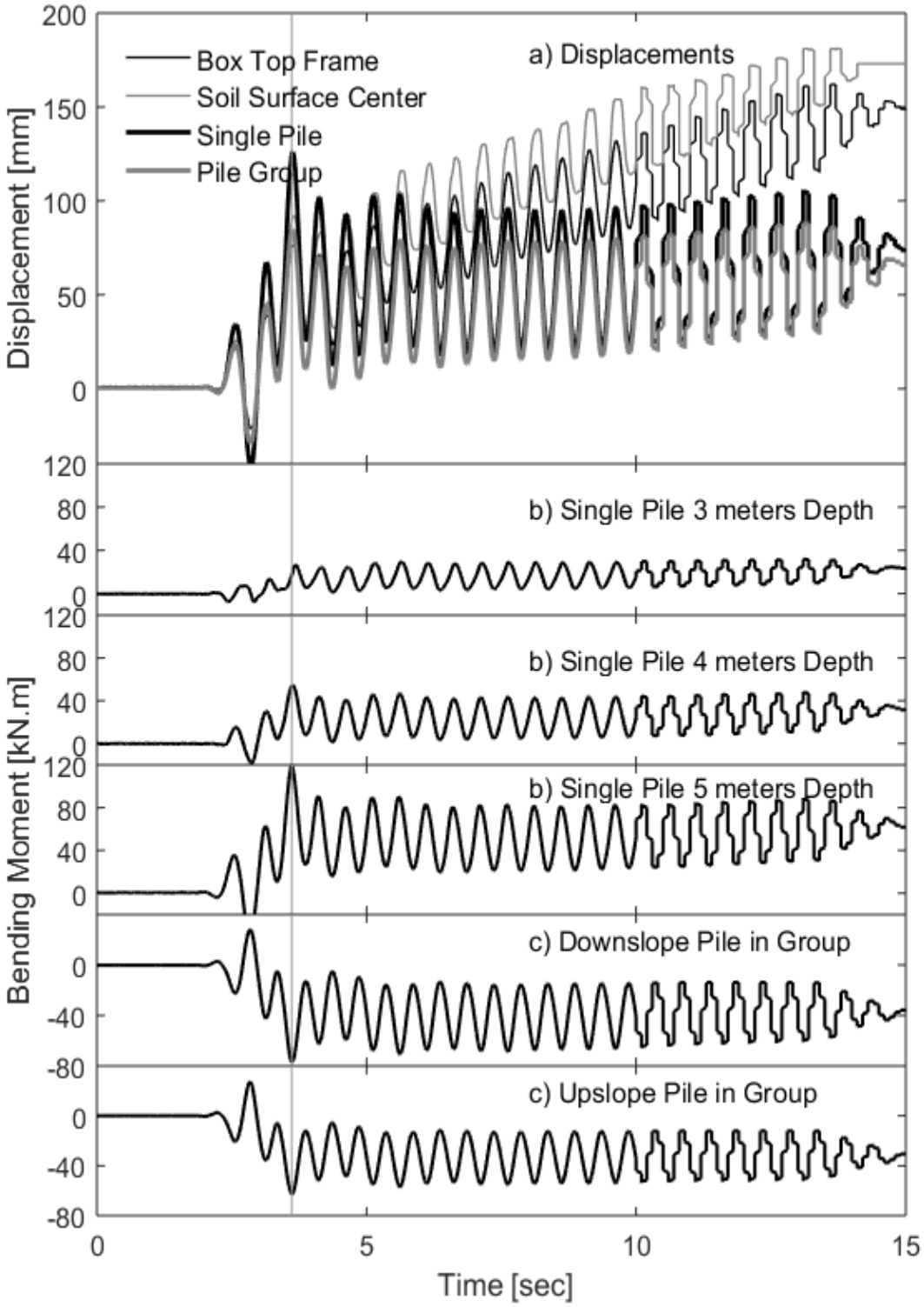

Figure 4-9. GC Test: a) displacement time histories (vertical line denotes instance of maximum bending moment, b) single pile bending moment, c) pile group head bending moment

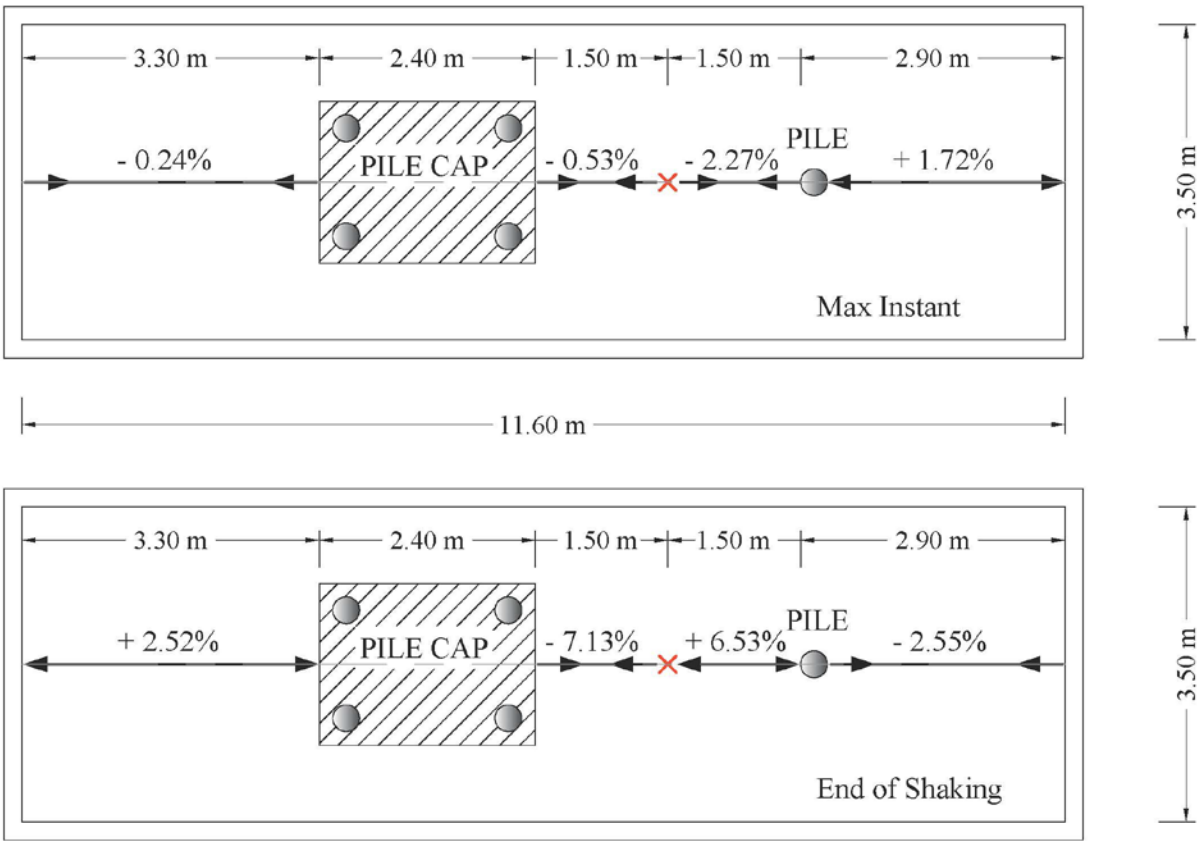

Figure 4-10. GC plan view displaying average axial strain between recording locations along the ground surface (positive values refer to tensile strains while negative values are compressive)

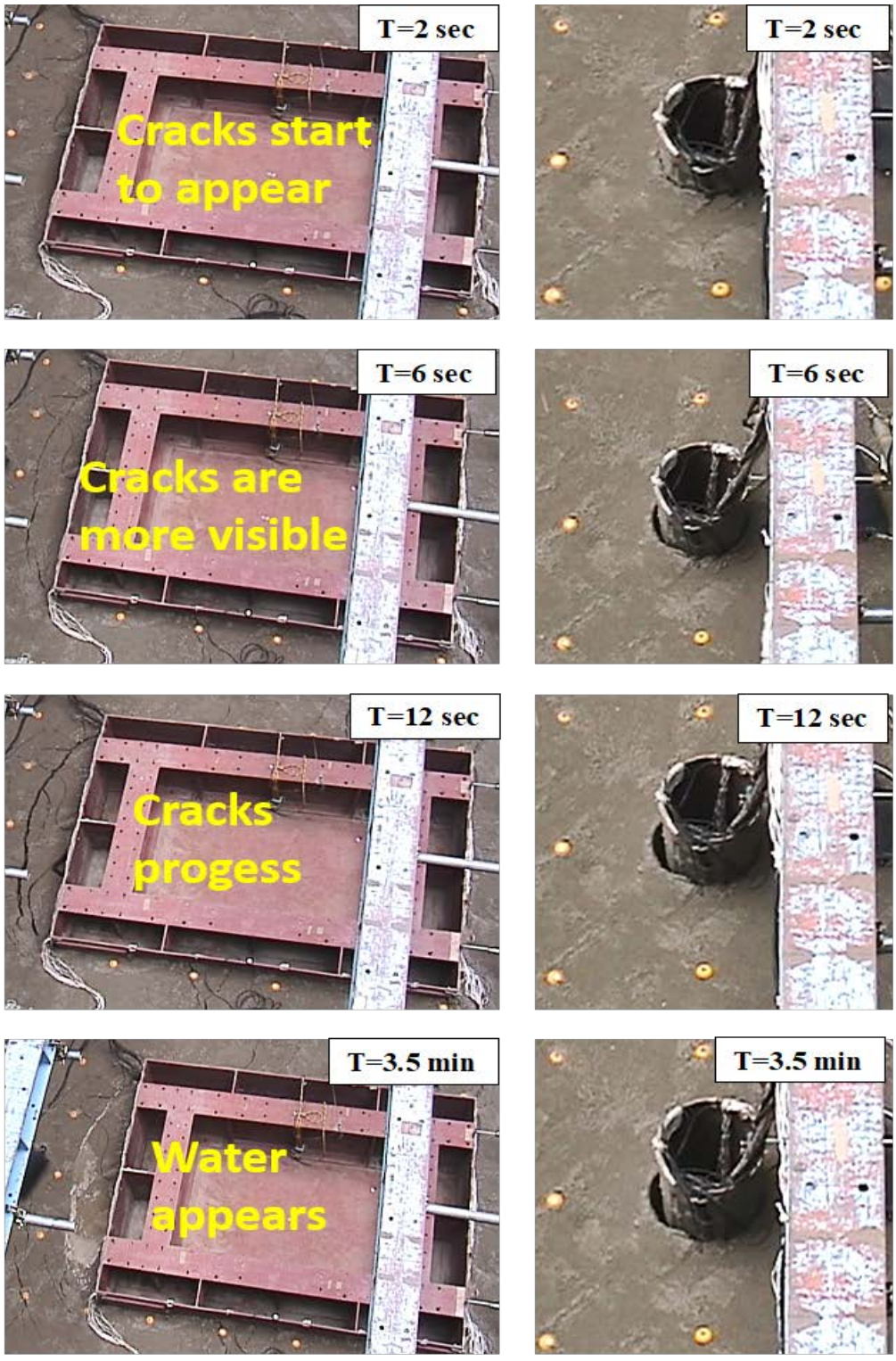

Figure 4-11. GC Test pile-ground deformation: a) pile group, and b) stiff pile

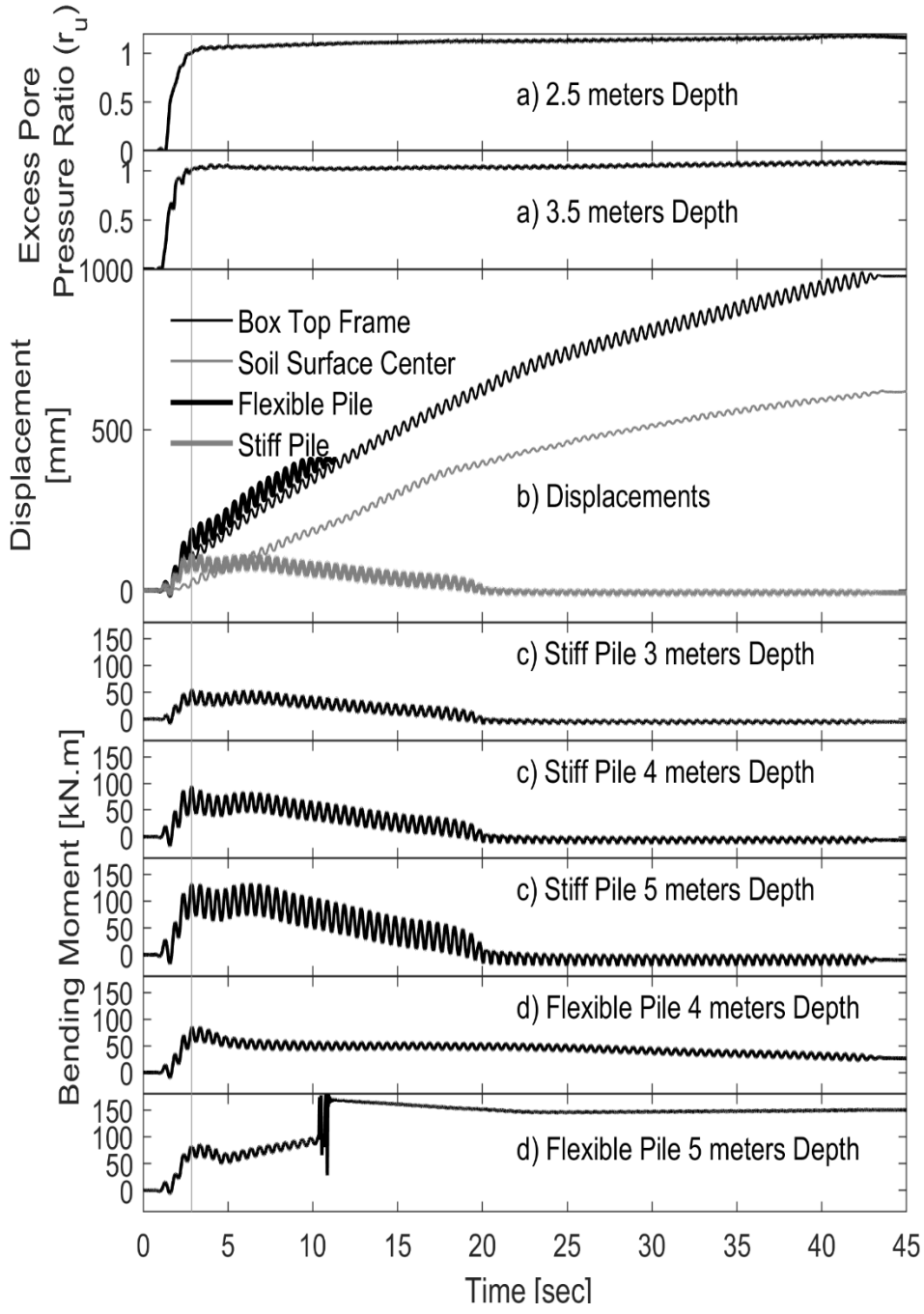

Figure 4-12. PW Test: a) center array excess pore-pressure (vertical line denotes instance of maximum bending moment), b) displacement time history results, c) stiff pile bending moment, d) flexible pile bending moment

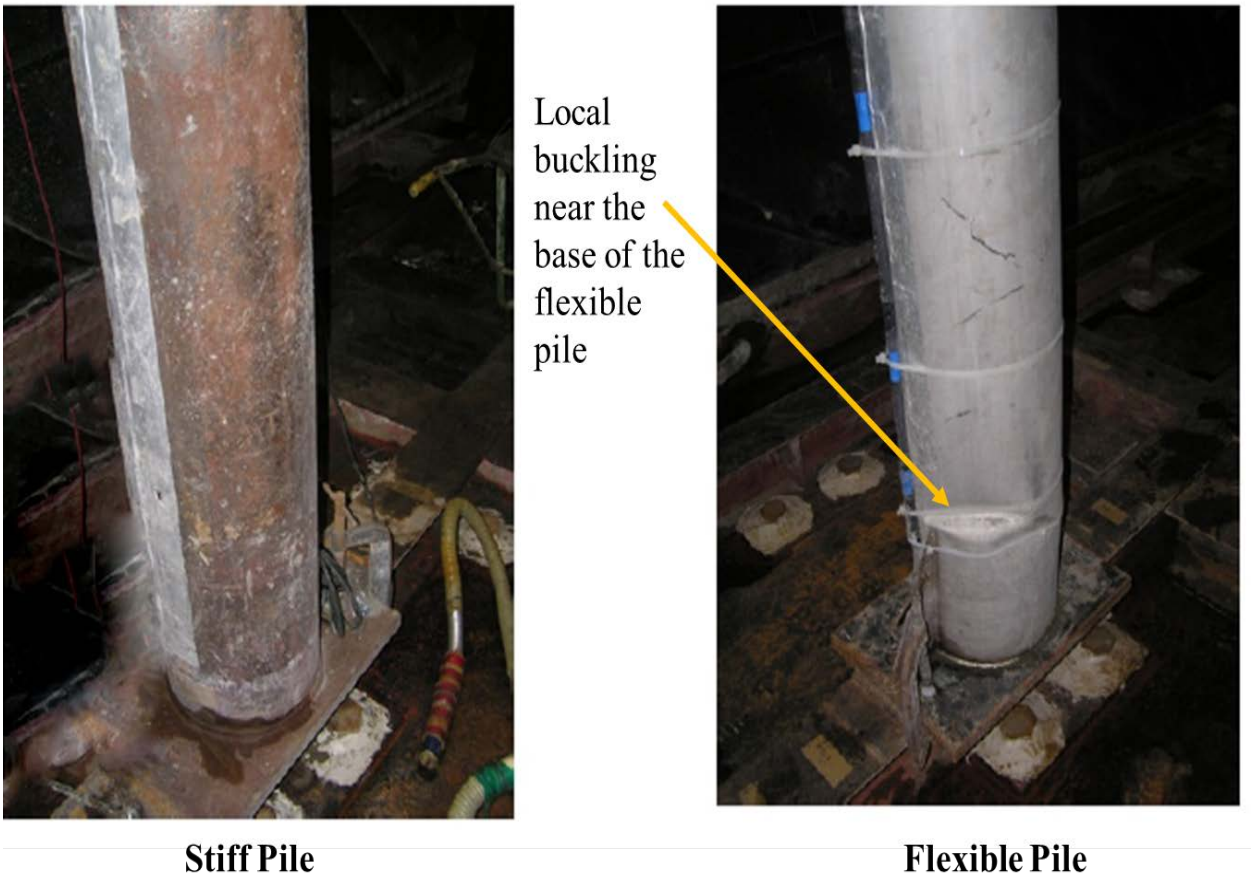

Figure 4-13. PW piles at base after testing

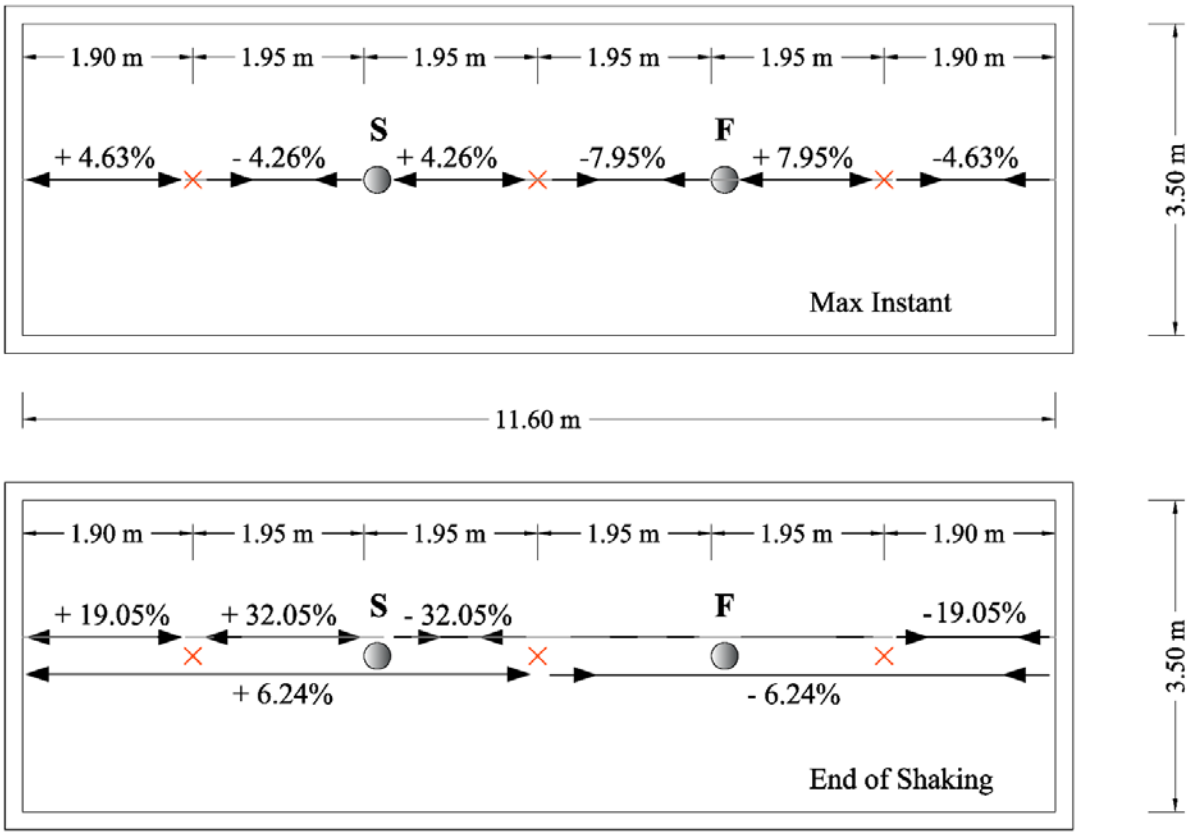

Figure 4-14. PW plan view displaying average axial strain between recording locations along the ground surface (positive values refer to tensile strains while negative values are compressive, and final displacement not available for flexible pile)

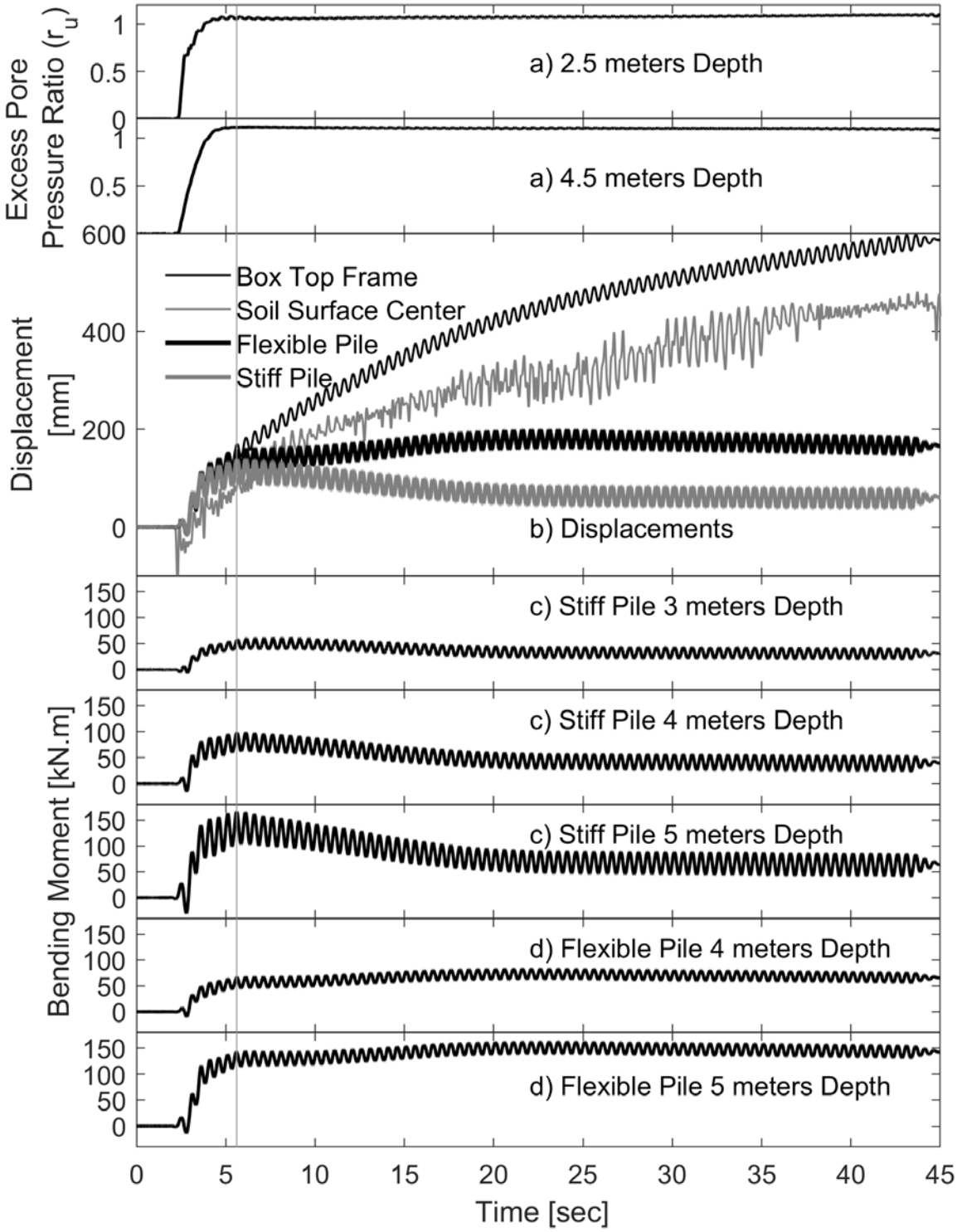

Figure 4-15. PC Test: a) center array excess pore pressure (vertical line denotes instant of maximum bending moment), b) displacement time histories, c) stiff pile bending moment, d) flexible pile bending moment

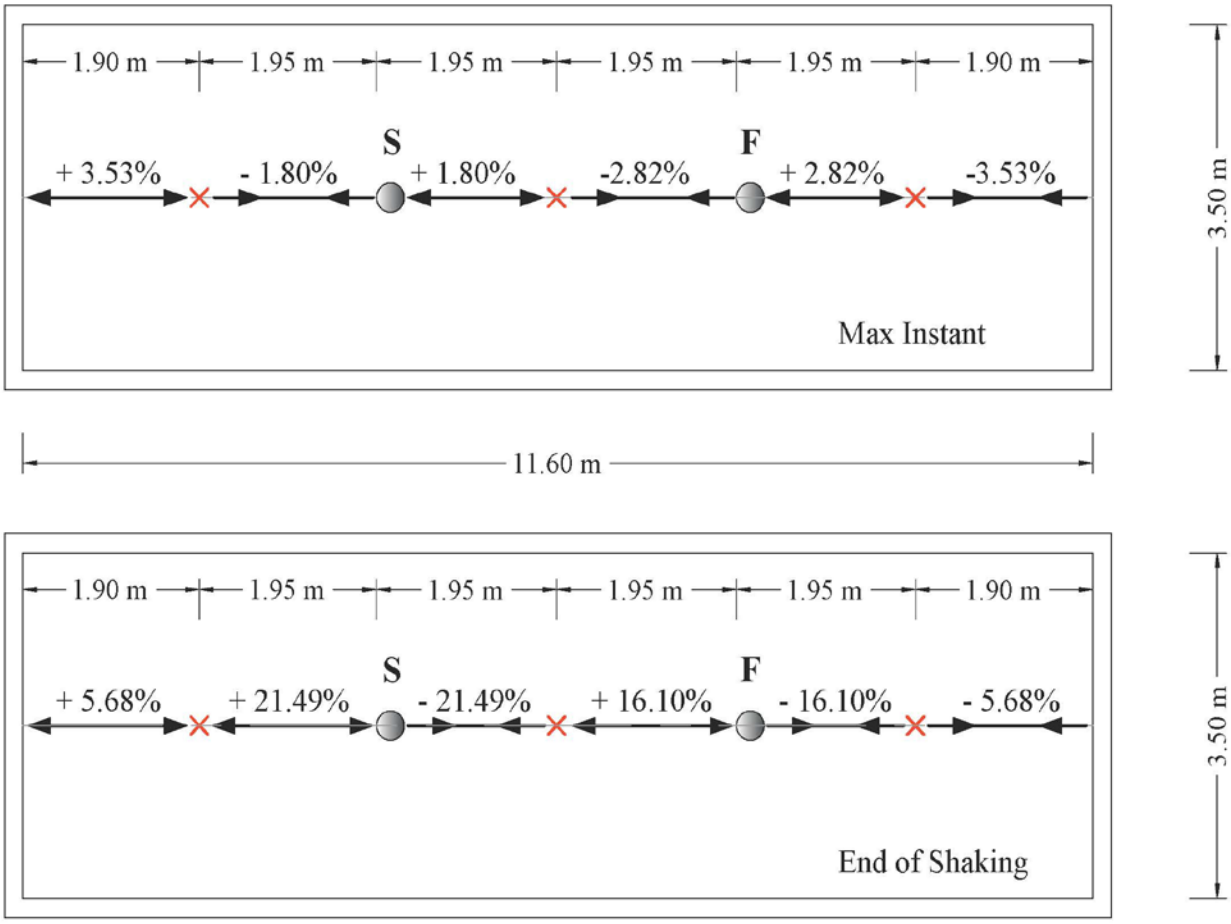

Figure 4-16. PC plan view displaying average axial strain between recording locations along the ground surface (positive values refer to tensile strains while negative values are compressive)

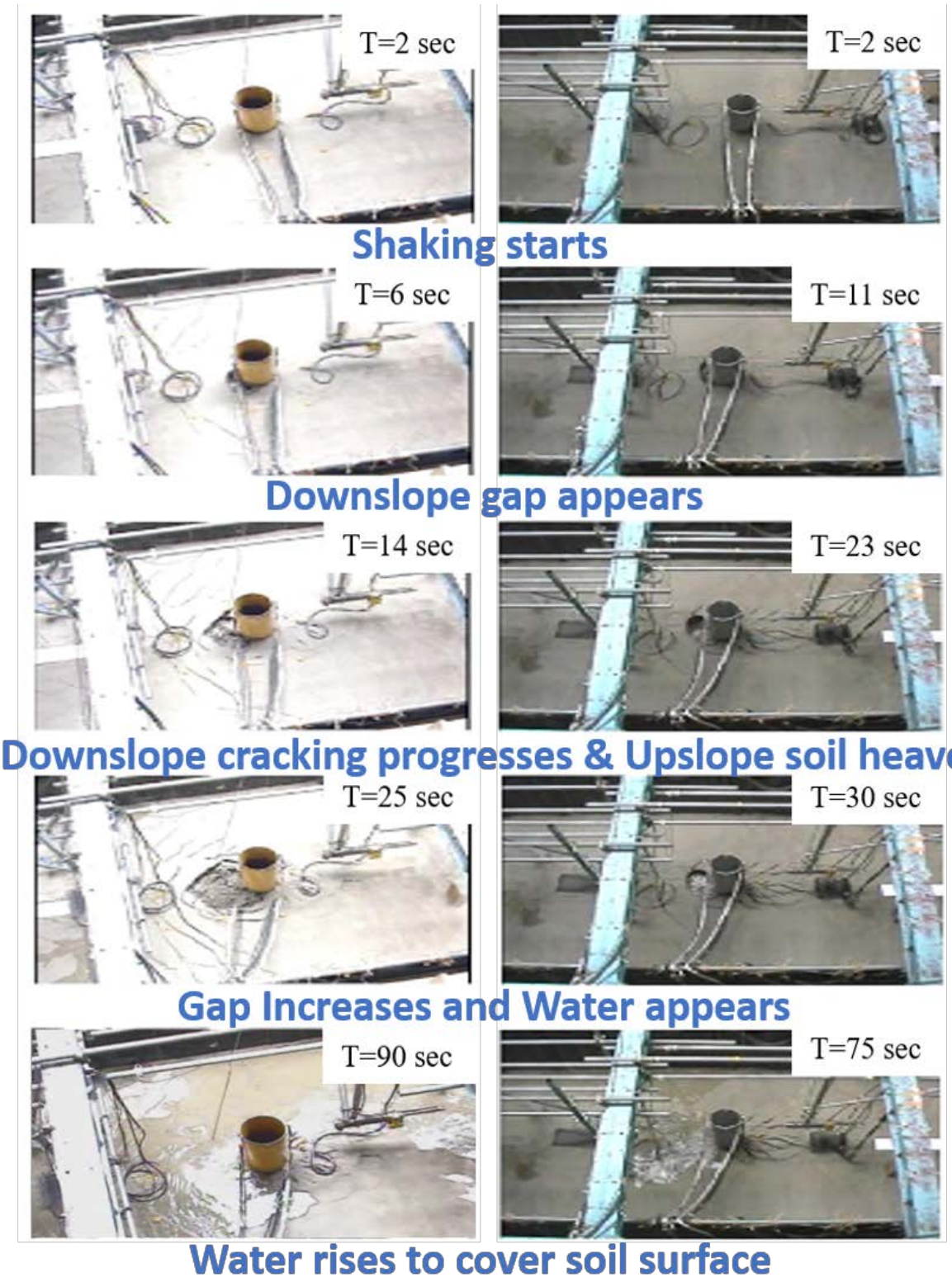

(a) (b)

Figure 4-17. PC Test pile-ground deformation: a) stiff pile, and b) flexible pile

Chapter 5 Pile Behavior Trends in Liquefied Lateral Spreading Ground and Pushover *P-Y* Curve Response

5.1. Abstract

Data sets from a large-scale laminar container shaking table experiment was employed to investigate pile response, due to the mechanism of liquefaction-induced lateral spreading. A configuration of 2 single piles of different stiffnesses was tested in a mildly inclined single stratum loose sand profile. The recorded data sets from this experiment were analyzed to document and track the evolution of lateral loading on the deployed single piles. In this test, it is observed that some of the highest pile lateral loads occur at the initial stages of lateral deformation, as observed from the calculated bending moment. Thereafter, as the soil liquefies, further shear strength reduction might permit the soil to more easily flow around the piles. As such, lateral ground deformation that continues to accumulate during the shaking process may not always result in significantly larger lateral pile loads. Evidence from previous studies is presented where similar response was observed. Such a pile-ground interaction mechanism is of consequence for analyses that correlate pile moments to the accumulated lateral soil deformation as in the conventional soil spring approach. A new strain softening *p-y* curve is derived from the studied data and resulting response is compared with the experimental counterpart.

5.2. Introduction

The scenario of lateral spreading during earthquake excitation presents a complex loading situation on piles and pile group. Recently, performance-based design in geotechnical engineering is receiving a great deal of attention, and many design codes initiated applying its concepts. As a

result, the estimation of deformation of structures subjected to intense loadings, such as earthquakes, is becoming more important.

The 1-g shaking table model test is one of the most common and efficient tools in the field of experimental geotechnical engineering. However, limitations of the model size decreases its efficiency. To overcome this disadvantage, large shaking table tests were initiated mainly in Japan in which a similar stress level as the prototype is reproduced (Cubrinovski *et al.* 2006; Orense *et al.* 2000; among others). Tokimatsu and Suzuki (2004); Tokimatsu *et al.* (2001); Tokimatsu *et al.* (2005) reported several large-scale shaking table tests on pile groups and investigated in particular the cyclic behavior of the soil-pile-structure model.

Mechanisms of interaction between piles and liquefied, spreading soils have become better understood in recent years through evaluation of case histories, centrifuge model studies, 1g model tests, full-scale field tests, and analytical studies (Boulanger and Tokimatsu 2005). These physical observations and research findings also provide the basis for evaluating the accuracy and limitations of analytical models and design guidelines.

A review of physical model studies and lessons from case histories showed a need for characterization of soil–pile interaction in liquefiable ground in which lateral spreading occurred. Pile damage in cases associated with liquefaction and lateral spreading is linked to ground deformation either permanent or cyclic. In order to clarify the kinematic loading on pile foundation, *p-y* curve behavior has been studied extensively using large-scale shaking table tests and centrifuge models (Tokimatsu *et al.* 2001 and Wilson *et al.* 2000). These studies and many others identified and helped improve our understanding of the response mechanisms.

The objective of this study is to investigate 2 single pile responses of different stiffnesses in a large-scale shake table test during the mechanism of liquefaction induced lateral spreading.

Focus is placed on pile response such as displacements and bending moments, as total soil and excess pore-water pressure develop with shaking. A new *p-y* curve is derived from the physical data and pile response resulting from this *p-y* curve is compared with experimental observations.

5.3. Large Scale Test

Using the large laminar box (Figure 5-1) at the National Research Institute for Earth Science and Disaster Prevention in Japan (NIED), response of piles subjected to liquefaction-induced lateral spreading was explored (Chapter 4). Figure 5-2 shows schematic layout of the 2 single piles of different stiffnesses in a 5.0 m single loose sand stratum. Water table was above the ground surface in the model. In this testing configuration, the soil container (Figure 5-1 and Figure 5-2) was 11.6 m long, 5.5 m high and 3.5 m wide (inner dimensions) and was inclined at 2° to the horizontal. This test is part of an experiment series, fully described in Chapter 4. This inclination corresponds to an infinite slope of about 3º in the field upon accounting for the laminate weight and water table corrections (Ramirez 2009) following the procedure of Taboada (1995). As noted by Law and Lam (2001), the laminar configuration simulates that of a periodic boundary condition. Input motion for the experiment was in the form of sinusoidal acceleration with a 2 Hz frequency and amplitude of 0.2 g for a 44 second duration (Table 5-1).

5.4. Soil Properties

The soil stratum was constructed by sand deposition in water. Kasumigaura sand (Kagawa *et al.* 2004) was used with the following grain size characteristics: D_{50} = 0.31 mm, fines content F_c = 3%, and uniformity coefficient C_u = 3. Soil relative density was estimated to be in the range of 40-50 % and saturated density was about 1940 kg/m^3.

5.5. Pile Properties

Table 5-2 shows characteristics of the soil stratum and pile foundation. Steel pipe piles of 0.318 m diameter were employed in the experiment, with both a 6 mm (stiff pile) and a 3 mm (flexible pile) wall thickness (denoted thereafter as the Stiff "S" and Flexible "F" piles respectively). Plastic moment capacity (Geschwindner 2011) is estimated to be 180 kN-m for the stiff pile and 93 kN-m for the flexible pile (Mild steel with ultimate strength of 400 MPa; and bending moment equal to strength multiplied by section modulus). At the container base, the piles were welded with the intent of mimicking fixity in an assumed underlying firm soil stratum. As such, preliminary static pushover tests were performed on the piles before adding the sand to estimate the attained pile base rotational stiffness values (Table 5-2).

5.6. Instrumentation

The model was instrumented with a large number of accelerometers, pore pressure sensors, total pressure transducers, strain gauges and LVDTs (Table 5-2). Instrumentation was placed along the pile shaft and along the profile of the ground stratum. Pore pressure transducers were placed on the piles in addition to being embedded in free field soil. Total soil pressure transducers were also placed along the pile shaft on both sides. Strain gauges were densely deployed along the pile shaft to aid in back-calculation of bending moment during shaking. Displacement transducers were mounted on the laminar box exterior wall to measure lateral motion, and on the soil surface to measure horizontal and vertical deformation. Furthermore, the piles were instrumented with transducers to measure pile head displacements above the ground surface.

5.7. Test Results

Focus is placed on pile response mainly in terms of bending moment on the piles, displacements and lateral loading. Analysis will concentrate on the salient characteristics where

(i) the soil liquefies, (ii) maximum pressures and bending moments are recorded, (iii) pile exhibits softening behavior and (iv) the flexible pile yielding. Table 5-3 shows an overview summary of the results, showing the attained maximum bending moment in each pile, along with pile head and soil displacement at both the maximum instant and at the end of shaking.

The recorded response (Chapter 4) illustrates the following trends:

1. Liquefaction occurred rapidly as evident from acceleration attenuation between base input and soil surface and the recorded excess pore pressure ratio shown in Figure 5-3. Evidence of acceleration reduction is also observed along the pile shafts.

2. A phase shift of approximately 180° is observed from the soil acceleration record as it propagates upwards. The stiff pile is oscillating in-phase with the input motion. However, the flexible pile starts in-phase and with yielding and excessive deformation, moves slightly out of phase.

3. Minimal oscillations in pore water pressure during liquefaction (Figure 5-3) suggest the lack of a significant shear-induced dilative tendency in the liquefied soil response (Zeghal and Elgamal 1994).

4. Soil and box displacement start to accumulate and continue throughout the shaking phase as shown in Figure 5-4. The stiff pile experienced peak response (2.26 s) during the fourth shaking cycle then gradually rebounds as liquefied soil flows around the pile without exerting additional pressures till complete unloading. Bending moments presented in Figure 5-5 support that observation.

5. Alternatively, the flexible pile continues to displace excessively throughout the shaking phase showing evidence of yielding and non-linearity. Bending moment plots (Figure 5-5) confirm that the capacity has been reached around the forth shaking cycle. Development of these large

localized plastic strains and significant plastic yielding near the pile base, might have contributed to some extent to a higher demand on the stiff pile located further downslope (Figure 5-2). This increased demand can be observed in the slight rise of bending moments (Figure 5-5) prior to rebounding at around 4-6 seconds.

6. The laminar box continues to displace throughout shaking accumulating as much as 1 m while the stiff pile rebounds to its starting position. Flexible pile displacement is presented till the instant of yielding as it displayed excessive deformations out of the transducer's stroke.

5.8. Stiff Pile Response

The main discussion is about the stiff pile response denoted by "S" (Figure 5-2). Liquefaction occurs just before the instant of peak response. Figure 5-6 shows the evolution of the pile response as the box accumulates displacements. Maximum bending moment is recorded at 2.26 seconds at the lowest location following a cantilever like behavior (Figure 5-6). For the first few seconds up until peak response (2.26 s), the lower portion of the pile is observed to deform more than the soil around it suggesting resistance to the pile movement. Afterwards, with the entire stratum liquefied, box and soil displace much more than the pile. A second peak (Figure 5-5;Figure 5-6) forming after a slight reduction is evidence of the stiff pile, as it is subjected to more load while the flexible pile yields. Bending moment and pile displacement profiles are still high and close to the maximum. The post peak behavior shows a gradual decrease in pile bending moments and displacements as the soil continues to flow. The rebound response is also observed in Figure 5-4 and Figure 5-5, and continues till the complete unloading of the pile as discussed in Chapter 4. The top 1 m of the soil is exerting negligible pressures on the pile as seen from the bending moment histories and profiles. By 20 seconds, the pile was not being subjected to lateral loads as the bending moments and displacements rebounded to zero.

Similar to the calculation of bending moment from strain gauge data, soil resistance, *p* is shown for the stiff pile against relative displacement between soil and pile, *y* in Figure 5-7. Observations confirm earlier discussions as the soil exerts pressures on the pile early during shaking with gradual pressure reduction afterwards. Soil pressure increase after the first peak at the 1 m depth location and the sustained pressures at the shallower depths coincide with the flexible pile yielding. As the flexible pile failed, the stiff pile was subjected to abruptly higher pressures before the soil smoothly started flowing around the pile. The deeper locations did not record the same behavior. In a case where the flexible pile was still intact, the stiff pile might have been subjected to somewhat lower pressures.

The small resistance to the pile movement at the lower profile portion at the start of shaking is exhibited by the initial minor negative soil resistance. This is a consequence of larger deflections near the pile top resulting in the pile moving more than the soil at the lower depths.

5.9. Pushover *P-y* Curve for Liquefied Laterally-Spreading Soils

Based on the discussed response observed and the generated physical data, this section discusses the development of a *p-y* curve to be used with liquefied laterally spreading soil and calibrated based on the 2 piles in the study. The Winkler model (*p-y*) is one of the most common analysis methodologies and is shown in Figure 5-8 where the actual recorded displacement profiles from the discussed experiment are going to be used in a lateral pushover analysis. Figure 5-9 presents the current curves used in practice in an effort to track maximum response such as Soft Clay (Matlock 1970), Liquefied Sand (Rollins *et al.* 2005) and Hybrid Liquefied Sand (Franke and Rollins 2013). However, none account for the degradation in the response. The soft clay model is applied using residual strength as a substitute for the cohesion and Figure 5-9 presents 2 soft clay models with different strengths. The hybrid model depends on either the SPT blow count or the

residual strength and it is shown with 2 different blow count input. Liquefied sand (Rollins *et al.* 2005) only requires the effective unit weight as an input and does not depend on the stratum strength.

The proposed *p-y* curve herein was modelled after Reese *et al.* (1975) including the modifications for cyclic loading made by Long (1984). The original spring (Reese *et al.* 1975) was developed for Stiff Clay in the presence of Free Water then modified (Long 1984) to account for the erosion and the hydraulic action of the free water flushing from the annular gap around the pile as the pile moved back and forth during cyclic loading. The derived *p-y* curve is modelled by 2 parts and is presented in Figure 5-10. It is noted that a softening spring model was previously proposed by Goh and O'Rourke (2008) where their model showed an early peak response with a softening response to a residual value that was calibrated based on centrifuge tests by Abdoun *et al.* (2003). A comparison of their proposed *p-y* model with the one presented in this study is shown in Figure 5-10.

The proposed *p-y* curve is based on residual strength (with a calibration multiplier) of the liquefied soil that can be calculated based on SPT blow counts. The $N_{1,60}$ corresponding to the 40-50% relative density present in the experiment is approximately 9.3 blows. The estimated residual strength for this experiment is 6.20 kPa to be used as cohesion input in the steps and equations described below (Figure 5-10):

1. Obtain values of residual shear strength S_r and pile diameter D.

2. Compute the soil resistance per unit length of pile, p_c, using the following equation.

$$p_c = 9\ (IF\ \ S_r)D \tag{5.1}$$

where IF is an inclination factor to account for lateral spreading (a value of IF = 2.22 fits this mildly inclined experiment)

3. Compute A_c as a function of depth over the pile diameter (z/D) using the following equation.

$$A_c = 0.2 + 0.1 \tanh 1.5\ z/D \tag{5.2}$$

Note that A_c is fairly constant at a value of 0.30 for depths greater than one pile diameter

4. Compute the deflection at one half the ultimate soil resistance (y_{50}) as follows (with ε_{50}=0.028, see Reese *et al*. 1975).

$$y_{50} = 2.5\ \varepsilon_{50}\ D \tag{5.3}$$

5. Compute y_p using

$$y_p = 4.1\ A_c\ y_{50} \tag{5.4}$$

6. Establish the first (parabolic) portion of the *p-y* curve,

$$p = A_c\ p_c[1.15 - |\frac{y - 0.45y_p}{0.45y_p}|^4\ ] \tag{5.5}$$

This equation defines the portion of the curve from the start to where y is equal to 0.60 y_p.

7. Establish the last portion of the curve, a straight-line portion

$$p = 1.138\ A_c p_c - \frac{0.018}{y_{50}}\ p_c(y - 0.6y_p) \tag{5.6}$$

This equation should define the portion of the *p-y* curve from the point where y is equal to 0.60y_p to the point where *p* is equal to zero (y = 16.16 y_p). The resulting *p-y* curve peaks at 0.04 D then exhibits strain softening till the soil resistance acting on the pile reach zero at about 1.4 D (Figure 5-10).

In the next section, the actual box deformation profiles from the experiment (Figure 5-6) were used to push the pile model in an OpenSees lateral *p-y* analysis. The piles were modelled with their stiffness and base rotational springs (Table 5-2).

5.10. *P-y* Curve Verification

The stiff pile was chosen to calibrate and verify the *p-y* curve response as it remained elastic and fully rebounded while the flexible pile yielded and experienced excessive deformations (soil spring spacing was 0.25 m). Vital aspects of the calibration process are to match peak response at the same box displacement and to simulate soil flowing around the pile. Experimental and *p-y* developed responses where compared in terms of base bending moment against box displacement (Figure 5-11) and pile head deformation against box displacement (Figure 5-12). Both curves present a good match between results with respect to peak response at the required displacement and similar peak bending moment values. The pile head displacement was under-estimated by the *p-y* curve; however, it is still within an acceptable range. More importantly, the proposed curve is able to capture both the initial slope of the curves and the rebound response.

Figure 5-13 compares peak profiles for the experiment and the *p-y* model. The comparison shows almost an exact match for the bending moment profile and very similar deformed pile configurations from the imposed box displacement. The box displacement was applied in a pushover analysis and the time history for the top box location (soil surface) is presented in Figure 5-14. Figure 5-15 and Figure 5-16 show the individual spring responses for various depths along the height. The progression of the forces applied on the pile by the spring against time step (Figure 5-15) show that each spring reaches its peak value at a different point in time then softens resulting in a lower maximum bending moment than the current conventional models. Figure 5-16 shows the individual spring response in terms of force against relative displacement at that location.

The developed *p-y* curve was applied to the flexible pile model as well. Figure 5-17 presents comparison between experimental and soil spring results for bending moment against box displacement. The peak bending moment value was similar. The match is acceptable due to the

non-linearity and erratic strain readings at the base location. Pile head displacement against box displacement shown in Figure 5-18 was under-estimated by the soil spring due to the excessive deformations associated with the complex pile yielding mechanism (that cannot be captured by the numerical model), however, the initial slope suggests a good match.

A simple parametric study was conducted to test the effect of varying the residual strength and the pile diameter on the resulting soil spring model. Figure 5-19a shows that for the same pile diameter (0.32 m), the peak strength increases with the increase in SPT blow counts, $N_{1,60}$. The strength increases by a ratio lower than the blow count increase. For the same blow count, $N_{1,60}$ (9.3) and varying the pile diameter, Figure 5-19b shows that both the peak strength and the softening behavior are affected. The model is more sensitive to pile diameter changes than the surrounding soil strength.

5.11. Documented Pile Liquefaction-Induced Lateral Spreading Behavior

The observed pile behavior in the previous sections, mainly rebound during shaking has been observed in different previous testing configurations by several researchers. The response mechanism was observed in similar large-scale testing on embedded pile foundations (Ebeido *et al.* 2018, Ebeido *et al.* 2019), pile groups behind a quay wall (Motamed and Towhata 2009) and centrifuge tests (Abdoun *et al.* 2003, González *et al.* 2009). The common behavior noted in all those studies is that soil deformations keep accumulating with shaking with no added detrimental effects after the first few seconds and soil liquefaction. Peak bending moments were noted early during shaking. That maximum moment occurred with small soil displacements despite the larger values at the end. After peak bending moment, piles start rebounding gradually reaching near zero values by the end of shaking. This mechanism suggests the need to develop a softening *p-y* curve to accurately capture the observed pile rebound mechanism.

Figure 5-20 presents a large-scale test having the same configuration of the test described herein with an upper non-liquefiable crust. The experiment is part of the same series and is discussed in full in Chapter 4. The same response mechanism described earlier is observed were peak pile response occurs in the first few seconds of shaking despite the continued accumulation of soil deformations. Pile rebound response is observed, but the upper crust prevented the pile from fully rebounding. The flexible pile is this test yielded as well. Photographic evidence (Figure 5-21) is presented for this test where it can be seen that: i) soil and pile start moving downslope together with the start of shaking, ii) soil then starts to displace much more than the pile creating a downslope gap, iii) pile rebounds as the soil continues to deform increasing the downslope gap between them.

Figure 5-22 presents additional photographic evidence from a third test in the same series (Chapter 4) where a stiff single pile was tested with a pile group. Similar observations are noted as the soil and pile move downslope with the soil starting to deform much more than the pile. Afterwards, the pile rebounds and the soil kept accumulating displacements.

A pile group tested behind a quay wall by Motamed and Towhata (2009) is presented in Figure 5-23. The model was subjected to seismic shaking and as the soil profile accrued displacements, bending moments (Figure 5-23) of the piles in the group exhibited a maximum response early with gradual reduction afterwards.

A series of centrifuge experiments were conducted by Abdoun *et al.* (2003) at RPI with one of their models presented in Figure 5-24. Similar pile response was recorded with the ground surface continuing to deform and the pile rebounding. Comparison of the illustrated Model 3 with another Model 5a (Figure 5-24) that included a pile cap exhibited the same response as well.

5.12. Discussion

General observations that can apply to both piles are:

1. Piles experienced maximum bending moments and displacements early during shaking.

2. Stiffer piles have larger relative cyclic displacement. On the other hand, flexible piles have lower relative cyclic displacements.

3. Looking closely at Figure 5-3, besides observing the reduction in acceleration amplitude at shallower depths indicative of liquefaction, there is a clear 180° phase shift observed in the acceleration record along the soil height. The phase shift is an indicative of soil pressure direction acting on the pile.

4. The guidelines and design methods depending on post-earthquake inspection do not provide a full picture of the liquefaction process. Full rebound of the stiff pile illustrates that residual post-shaking values are not a full indication of the pile response.

5. The continued excessive lateral spreading cause no additional loading as evident from the stiff pile, as pressures decrease after the first few cycles of shaking.

6. Developed *p-y* curve calibrates well with the experiment in terms of peak response, ground movement needed to mobilize the peak response and degradation patterns.

5.13. Summary and Conclusions

Data sets from a large scale laterally spreading test with 2 piles of different stiffness in a single loose liquefiable layer configuration was utilized. From this test, pile response was studied in detail with focus placed on developing soil pressures. The presented data was employed, with a purpose of deriving a lateral pushover *p-y* curve from the observed pile-ground interaction. Among the main observations and findings are:

1. High bending can occur early as soil starts moving and possibly before liquefaction of the entire strata.
2. The region of the pressure profile causing the bending moment changes with soil movement. Regions that cause high pressure at the start of shaking could result in zero added forces on the pile just a few seconds later.
3. Observed reduction in soil resistance suggests that with continued shaking, soil flows around the pile without exerting pressures.
4. Post shaking deformed configurations might not account for the peak pile bending moment and displacement.
5. The developed *p-y* curve mode with resistance degradation model shows a good match with the experimental results, in terms of peak bending moment and corresponding ground displacement. Pile head displacement is in an acceptable range compared to the observed counterpart.
6. The proposed *p-y* curve is recommended for use in liquefiable soils with further modifications needed to include other variables (such as soil permeability and acting shear stress for instance) contributing to the response.

5.14. Acknowledgements

Chapter 5, in part, is currently being prepared for submission for publication of the material as it may appear in the following journal publication (The dissertation author was the primary investigator and author of this paper):

Ebeido, A. and Elgamal, A., "Pile behavior trends in fully saturated laterally spreading soils".

Table 5-1. Shake Table input harmonic motion for the experiment

Input Motion		
Frequency [Hz]	Amplitude [g]	Duration [s]
2	0.2	44

Table 5-2. Characteristics of Soil stratum and Pile foundations

Soil Profile		Pile Properties					
Height [m]	Water Table	Embedded Length [m]	Diameter [cm]	Wall Thickness [cm]	Bending Stiffness [kN-m^2]	Base Rotational Stiffness [kN-m/rad]	Yield Bending Moment [kN-m]
5.0	Covers entire soil	5.0	31.8	0.6*	14320	18500	190
				0.3**	7360	8500	93

* Denoted in text as stiff pile (S)

** Denoted in text as flexible pile (F)

Table 5-3. Summary of experimental results

Pile Configuration	At maximum response				At end of shaking (44 s)		
	M_{max} [kN-m]	Relative Displacement [mm]			Relative Displacement [mm]		
		Pile Head	Center Array @ ground surface	Container Top Frame	Pile Head	Center Array @ ground surface	Container Top Frame
Stiff	132	110	160	142	0	710	980
Flexible	93**	206			N/A		

* Denotes yielding of pile cross-section; with estimated value being limited by this yielding mechanism

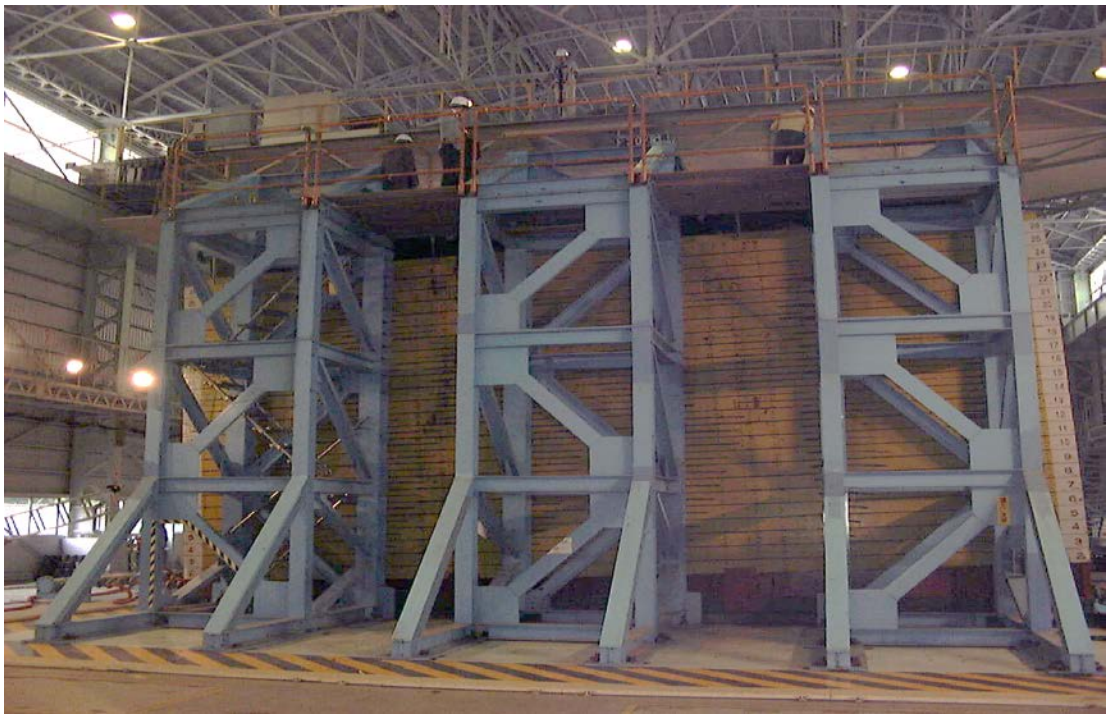

Figure 5-1. Mildly inclined large laminar container on shake table

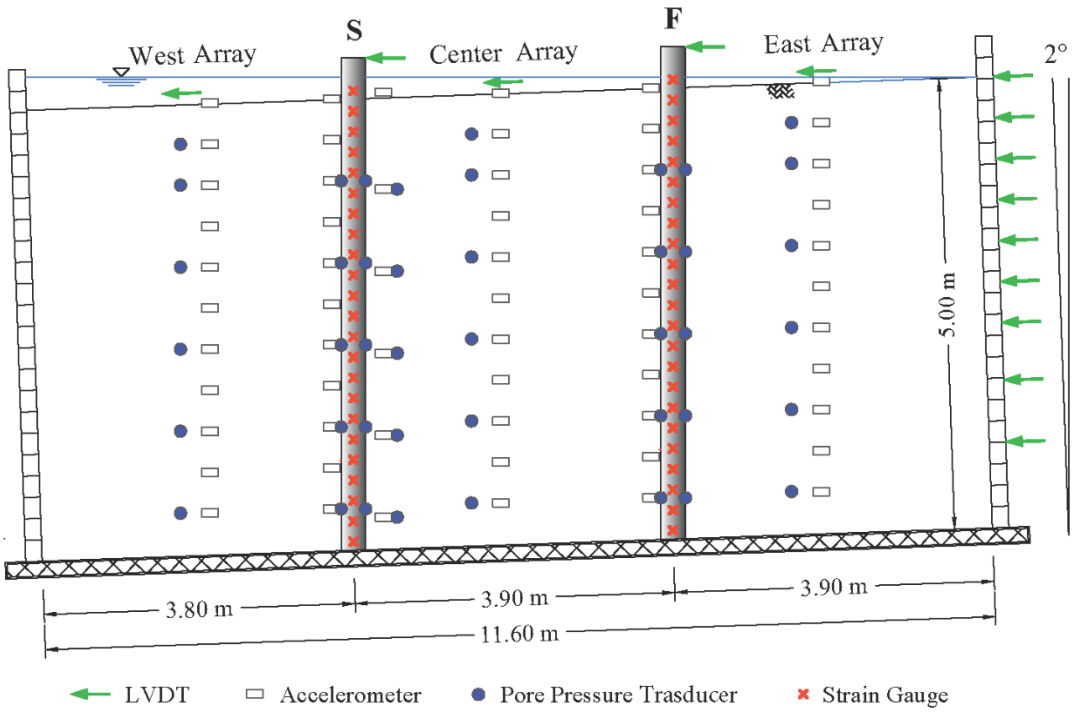

Figure 5-2. Experimental Configuration

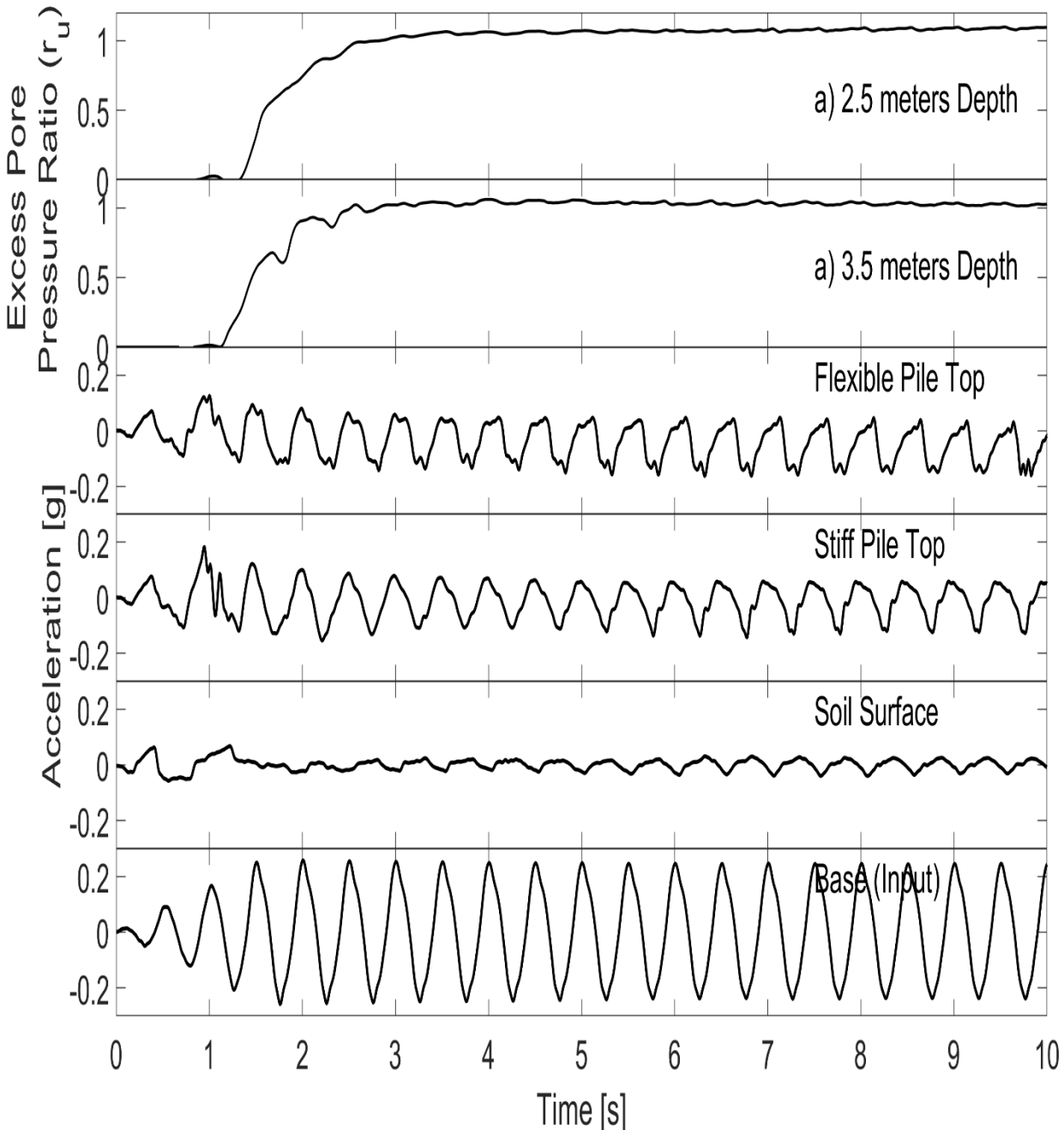

Figure 5-3. Acceleration time histories

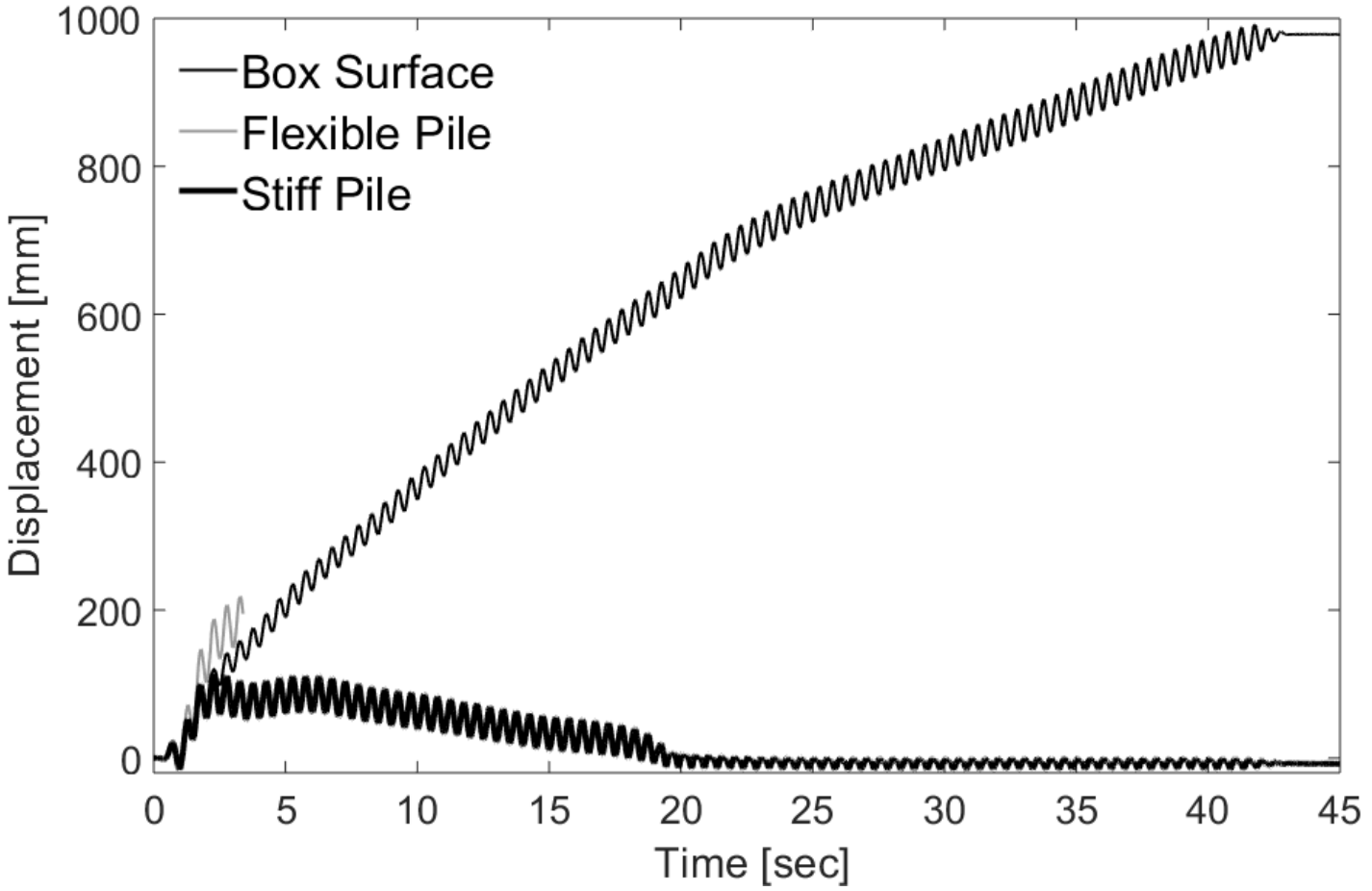

Figure 5-4. Displacement time histories (Flexible pile displacement stopped at bending moment failure at 3 s)

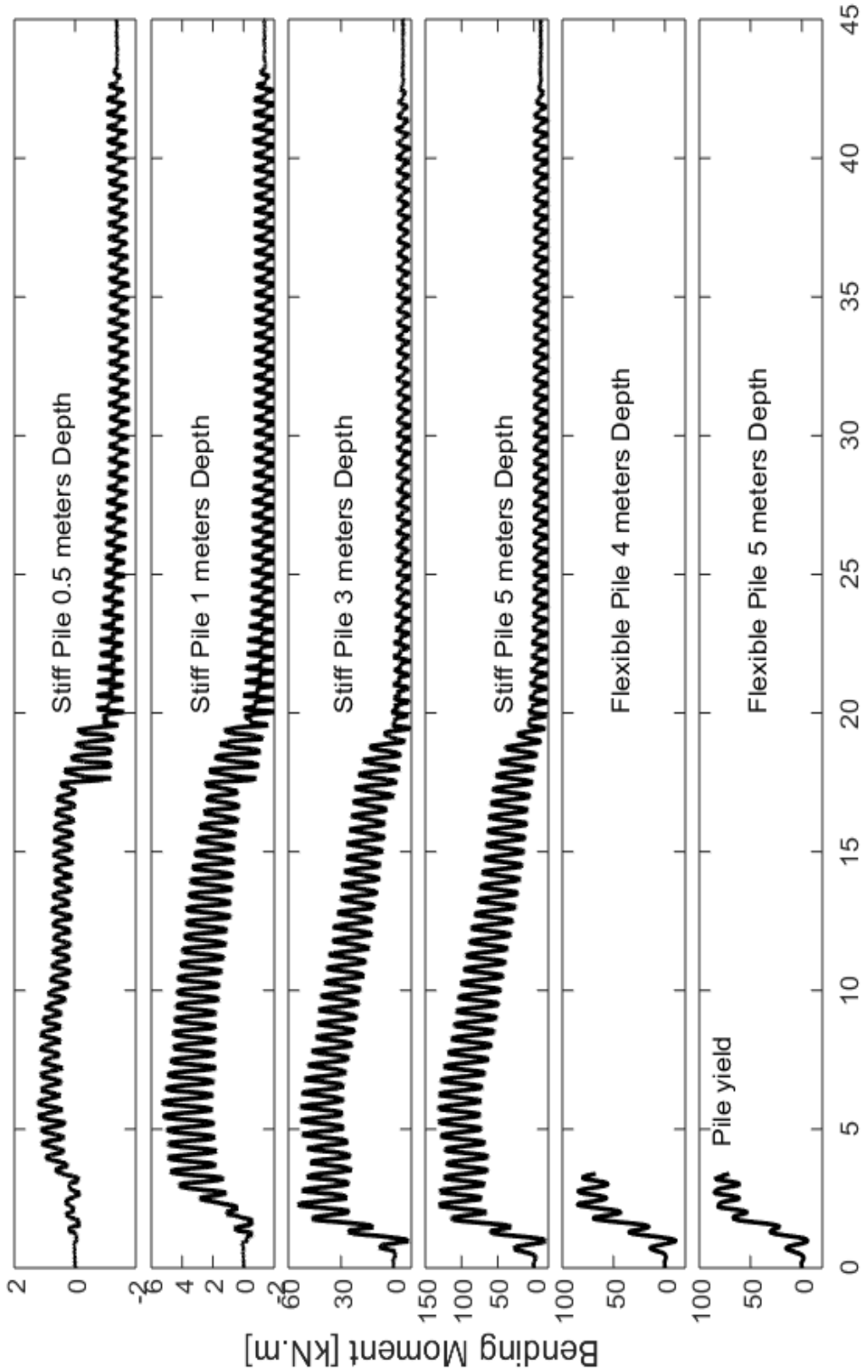

Figure 5-5. Bending moment histories for both stiff and flexible piles

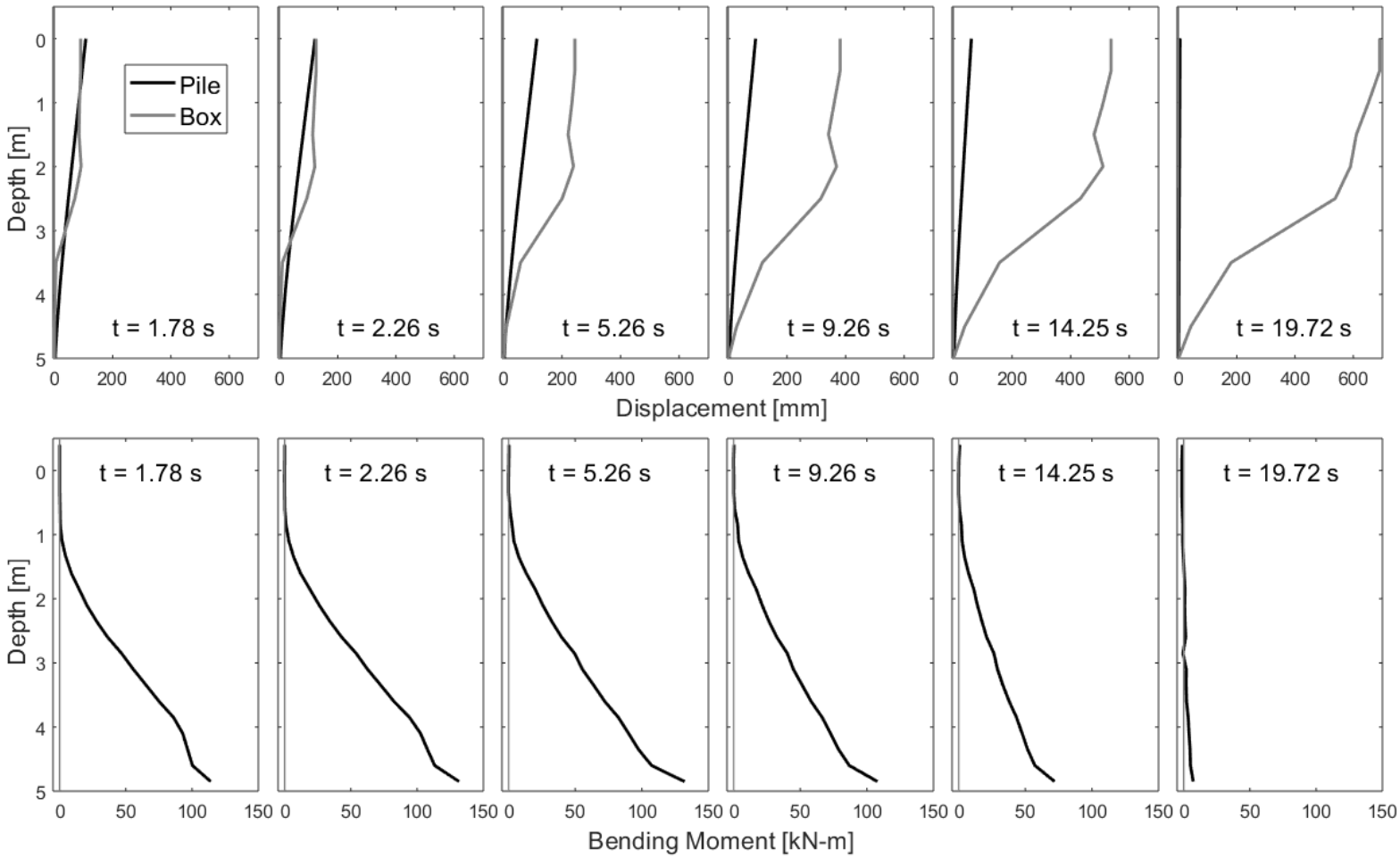

Figure 5-6. Progression of displacement and bending moment profiles with shaking for stiff pile

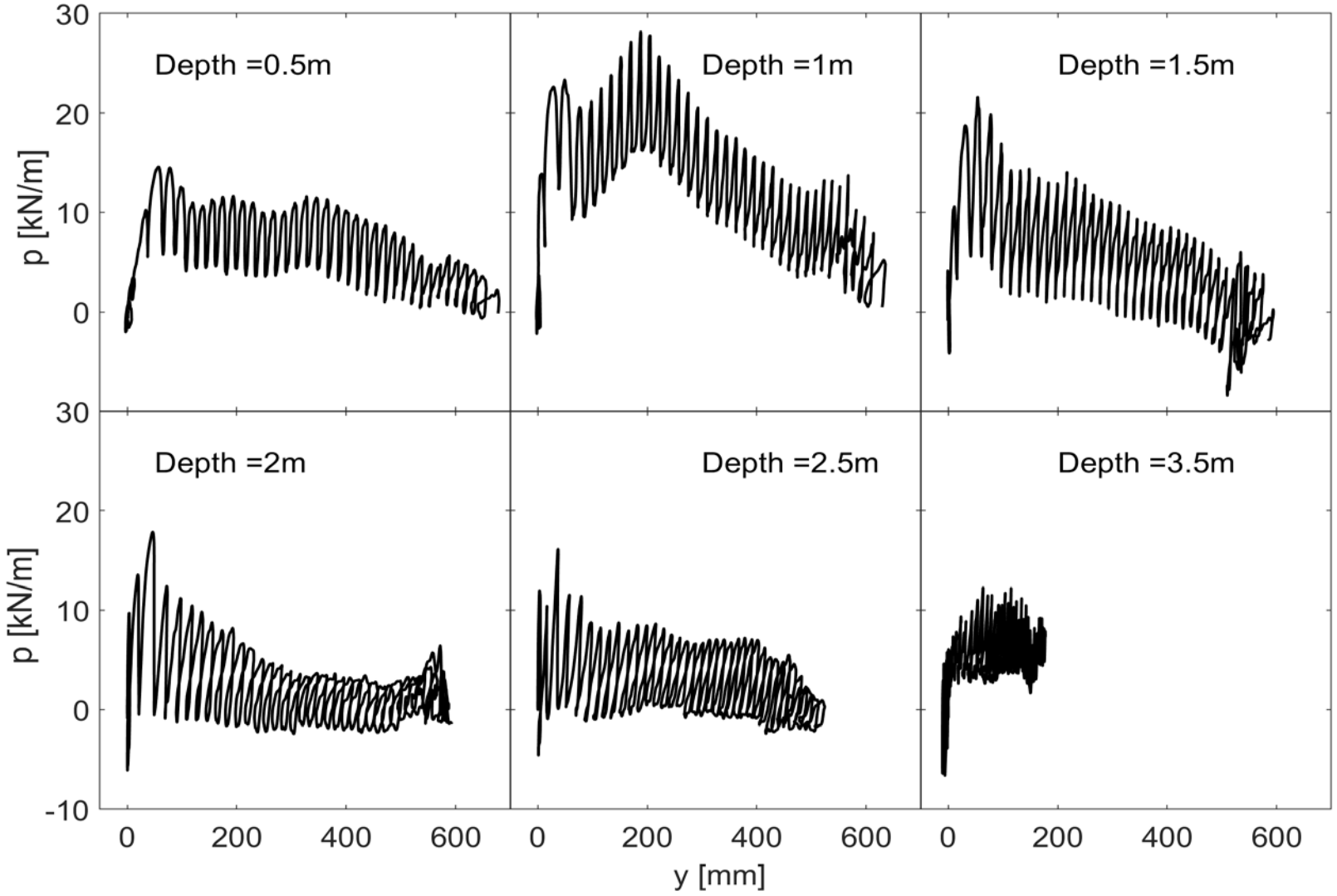

Figure 5-7. Back calculated *p-y* response for stiff pile

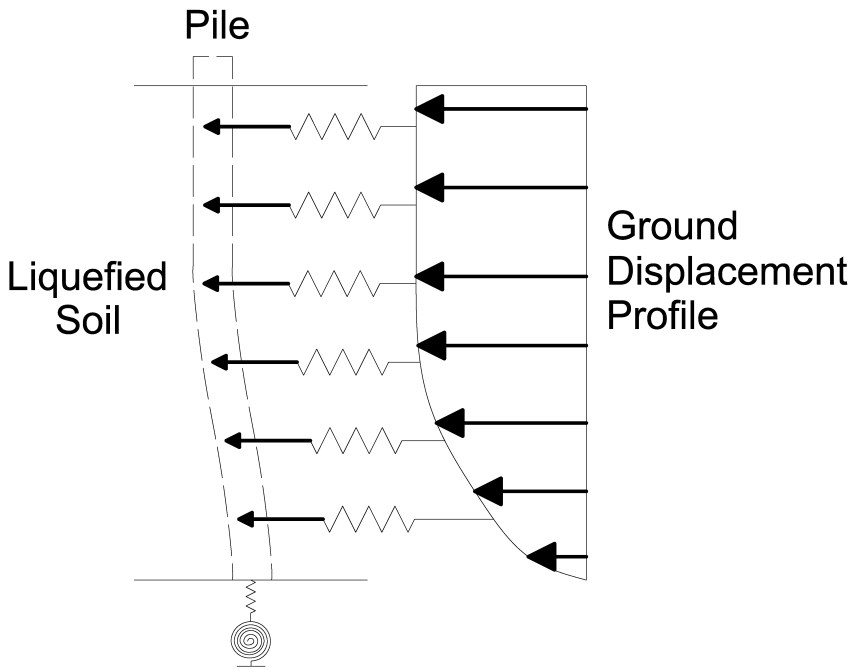

Figure 5-8. Soil displacement profile *p-y* lateral analysis of pile in liquefied soil

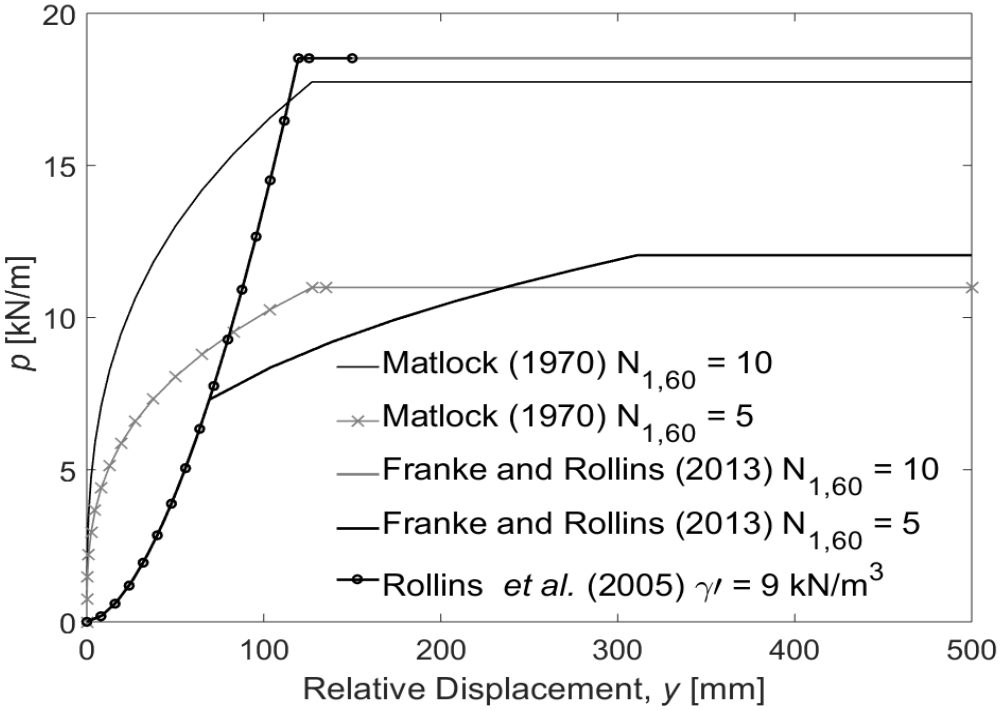

Figure 5-9. Current available *p-y* curve models used in practice

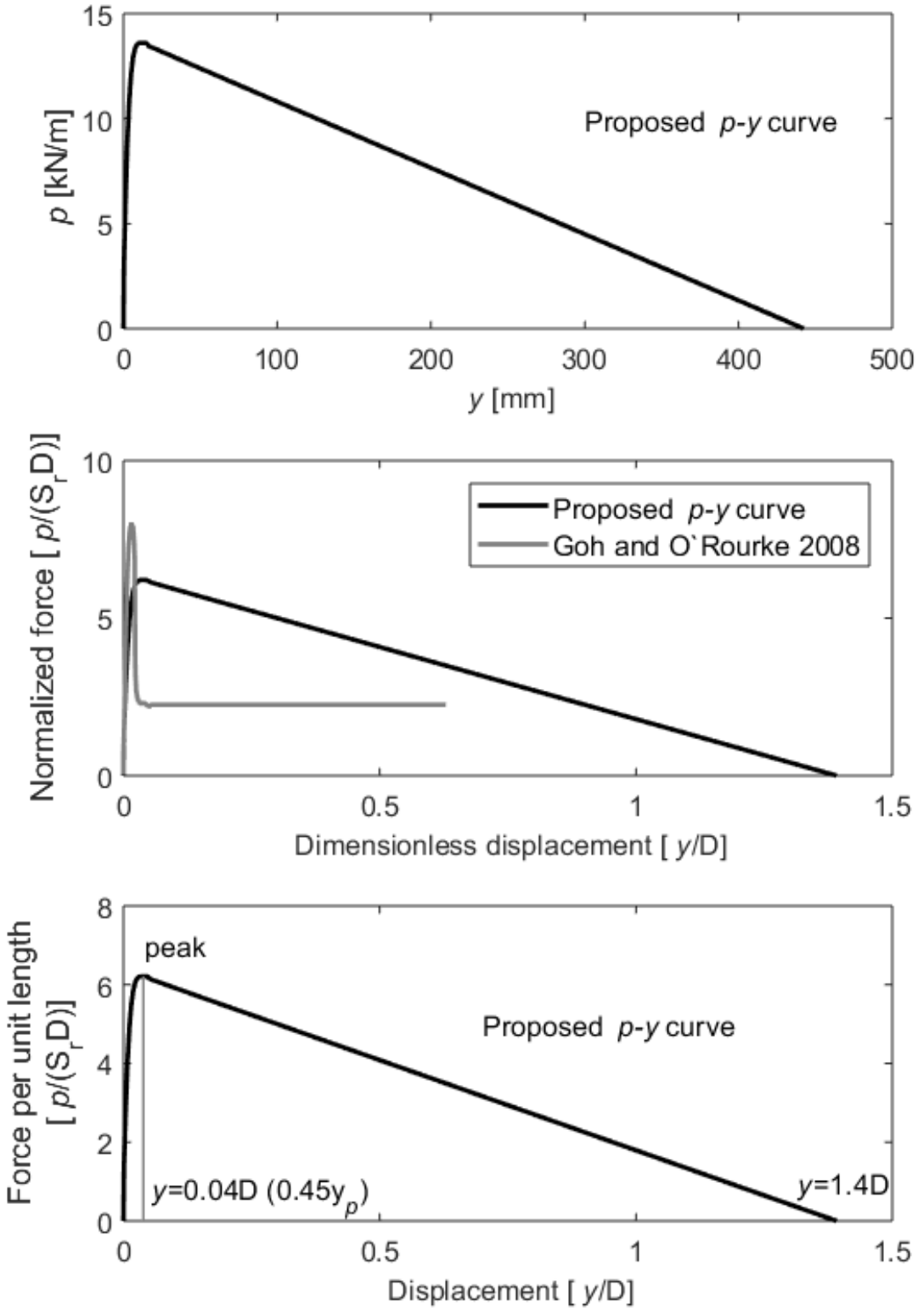

Figure 5-10. New proposed softening *p-y* curve for liquefiable soil

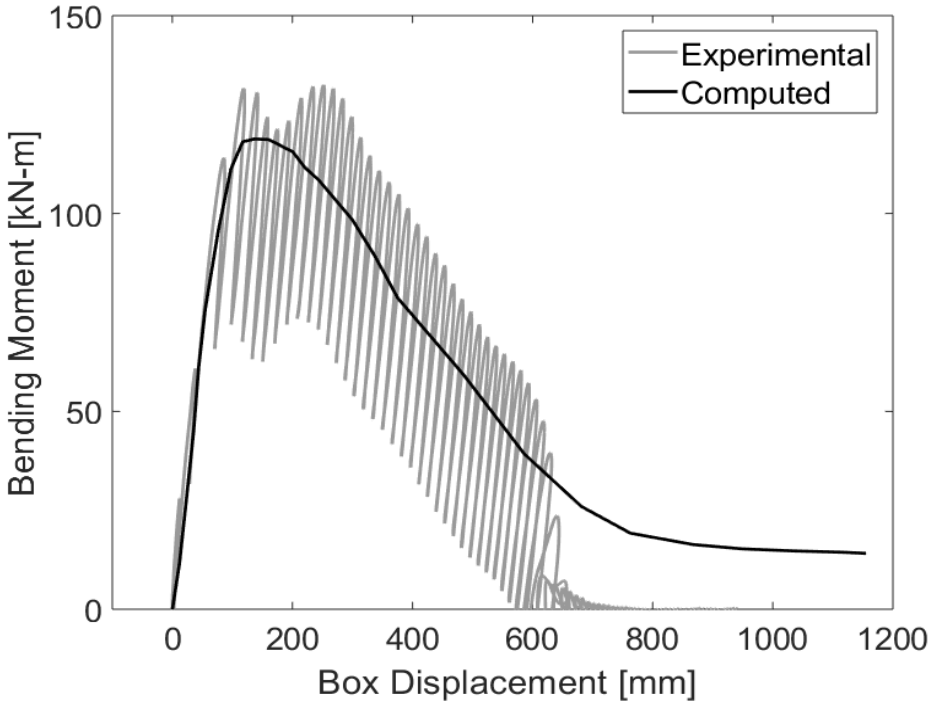

Figure 5-11. Comparison of stiff pile experimental and soil spring bending moment against box displacement curve

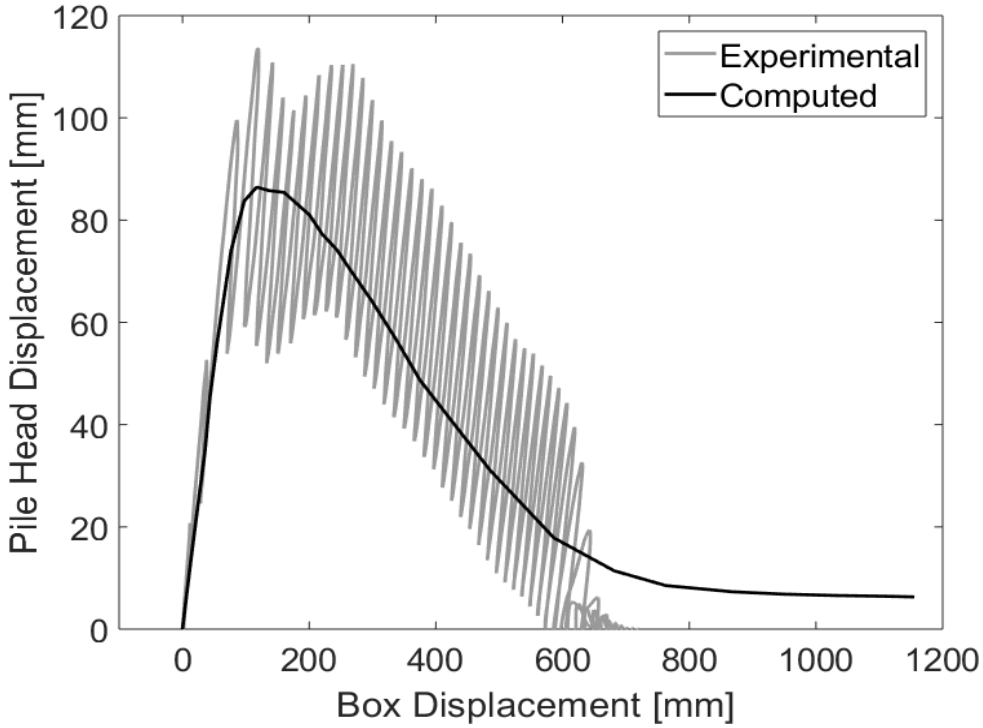

Figure 5-12. Comparison of stiff pile experimental and soil spring pile displacement against box displacement curve

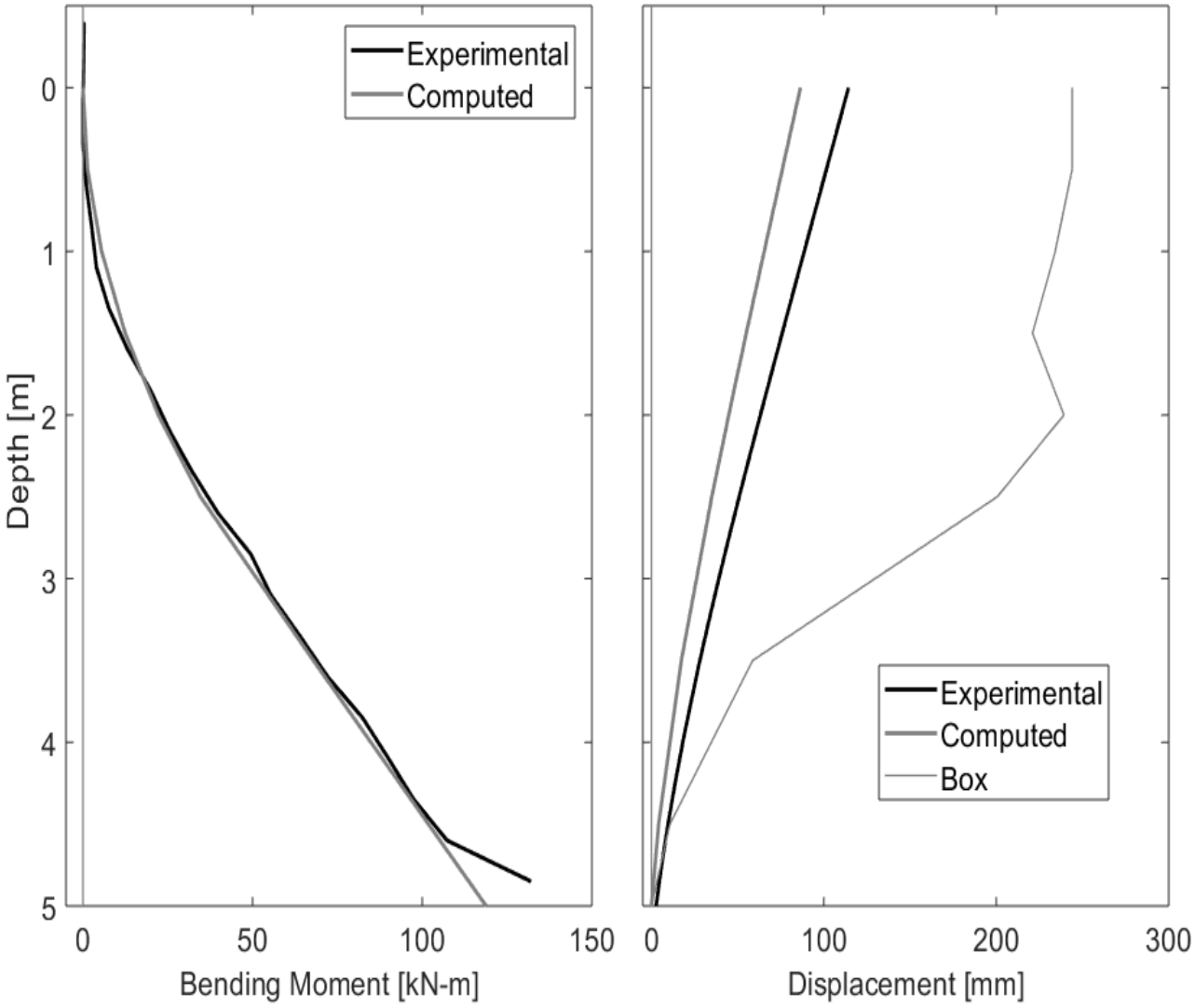

Figure 5-13. Comparison of stiff pile experimental and soil spring pile bending moment and displacement profiles at maximum response

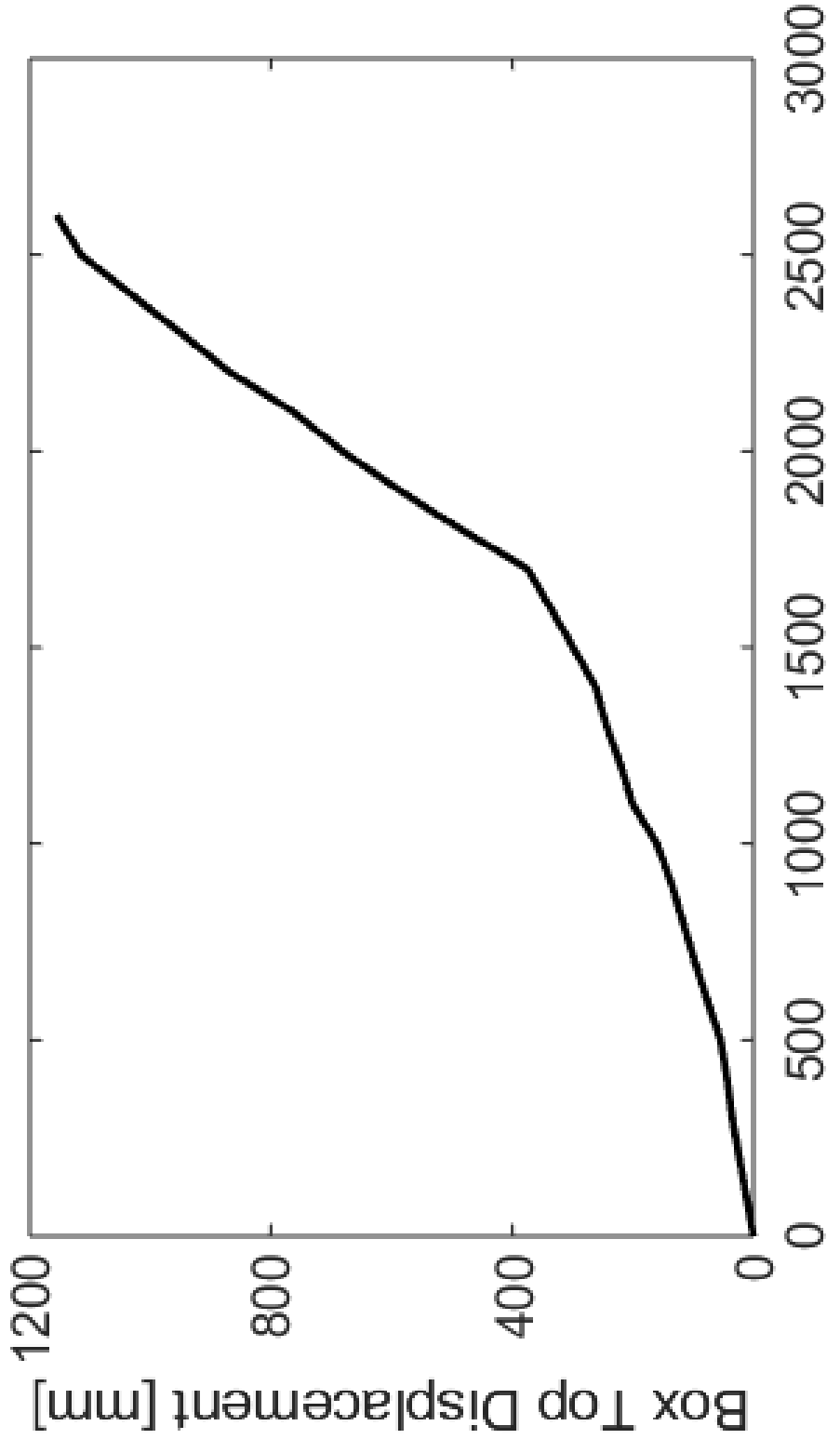

Figure 5-14. Imposed box top displacement history for the stiff pile *p-y* curve model

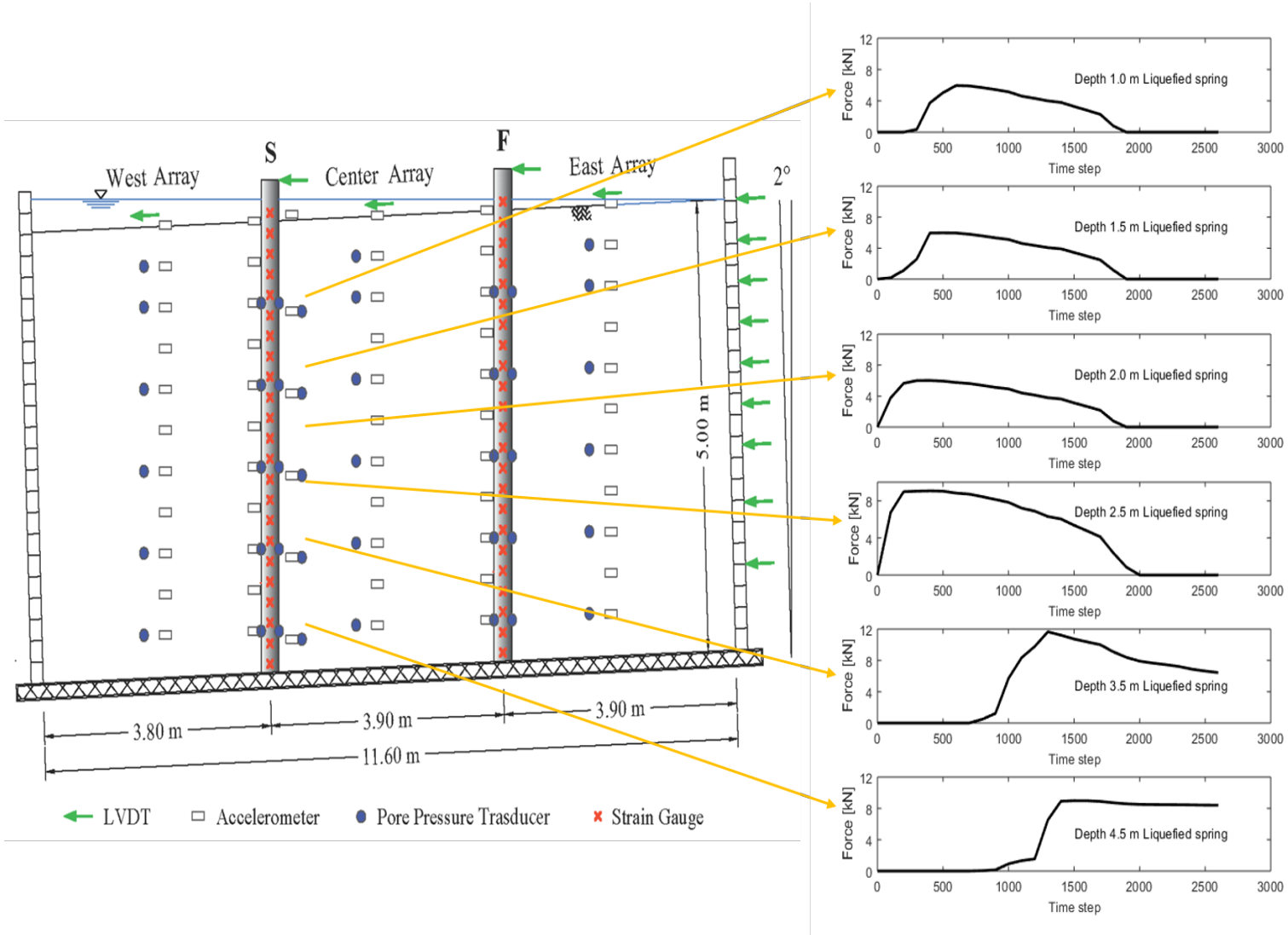

Figure 5-15. Resulting force time histories applied on the stiff pile from the *p-y* lateral analysis

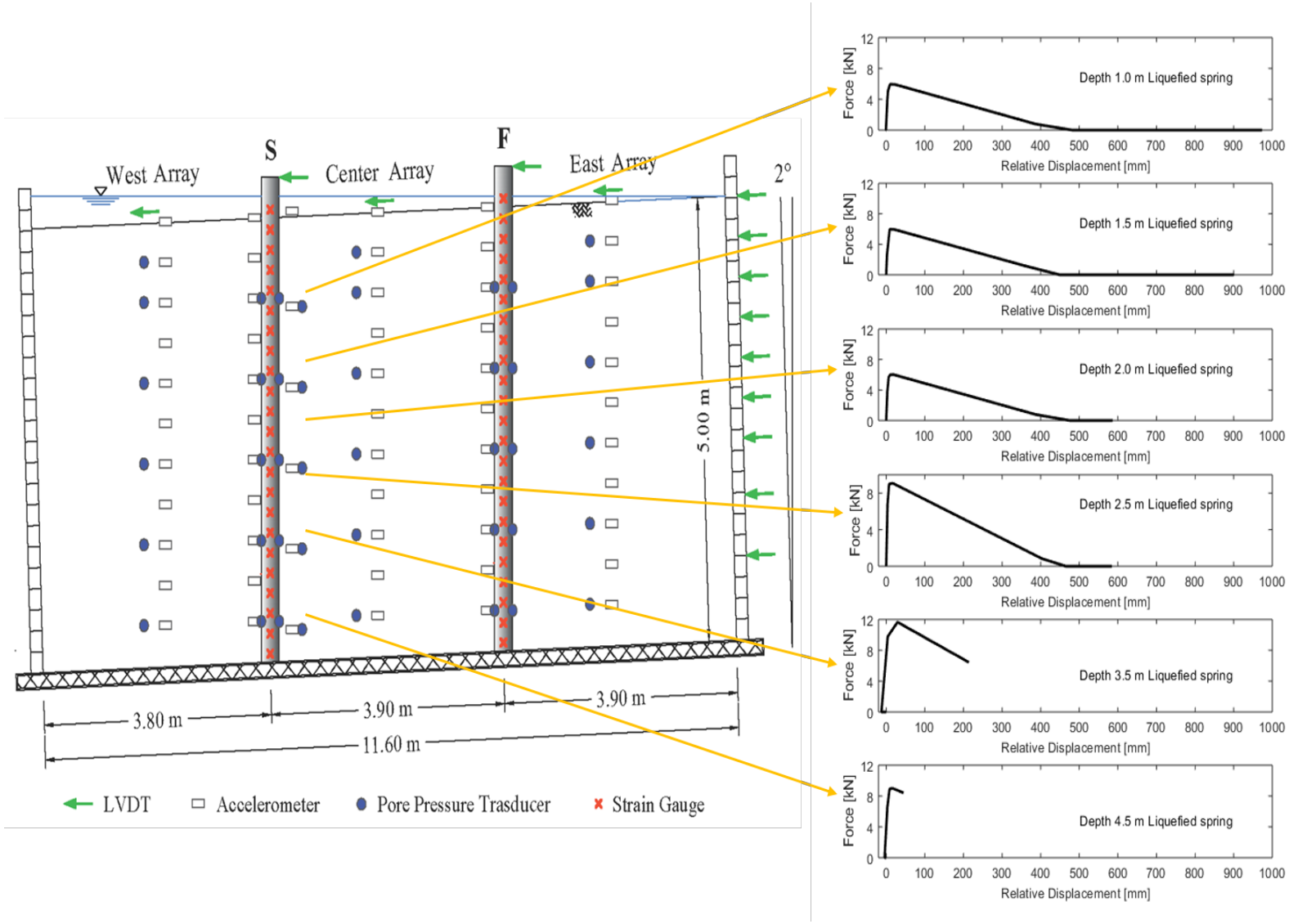

Figure 5-16. Resulting force-displacement response of the soil springs

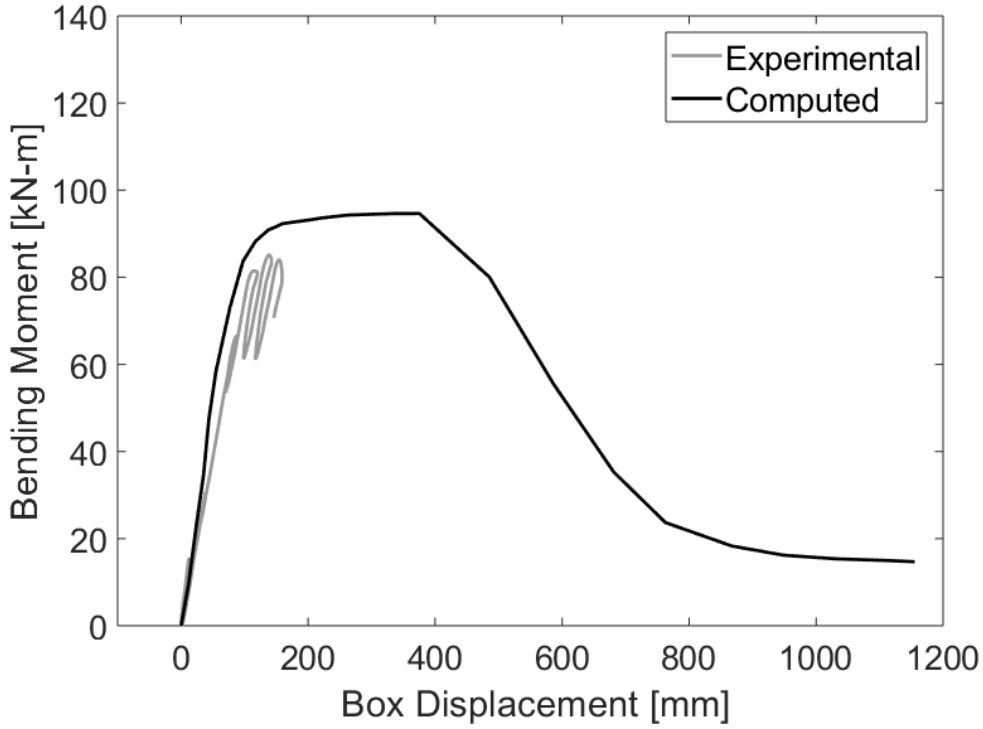

Figure 5-17. Comparison of flexible pile experimental and soil spring bending moment against box displacement curve

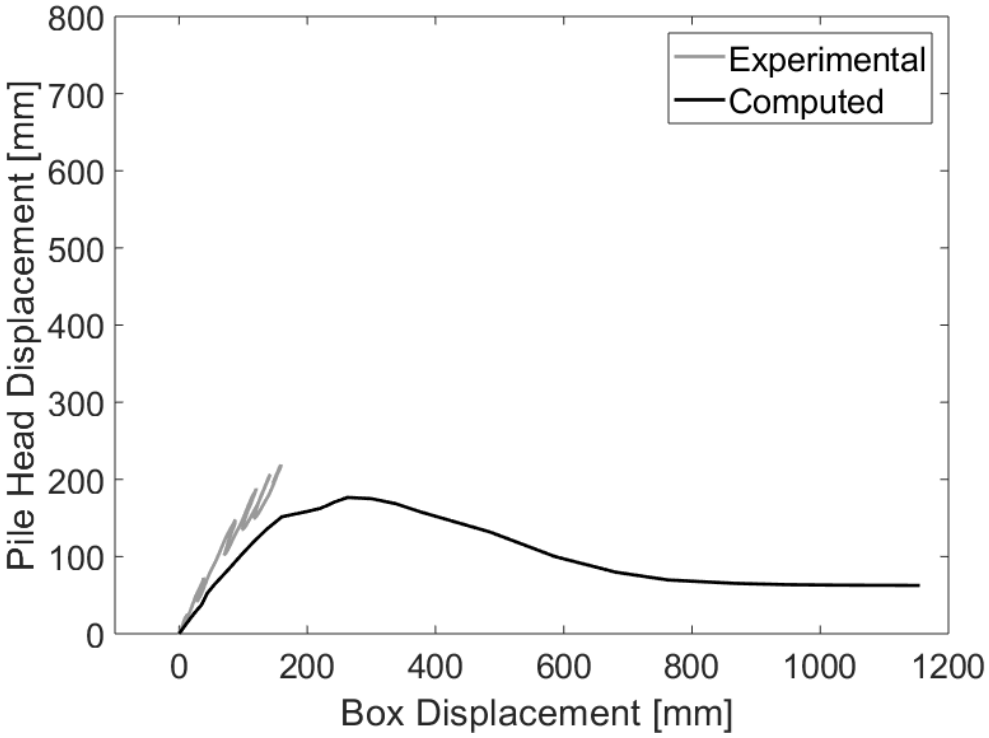

Figure 5-18. Comparison of flexible pile experimental and soil spring pile displacement against box displacement curve

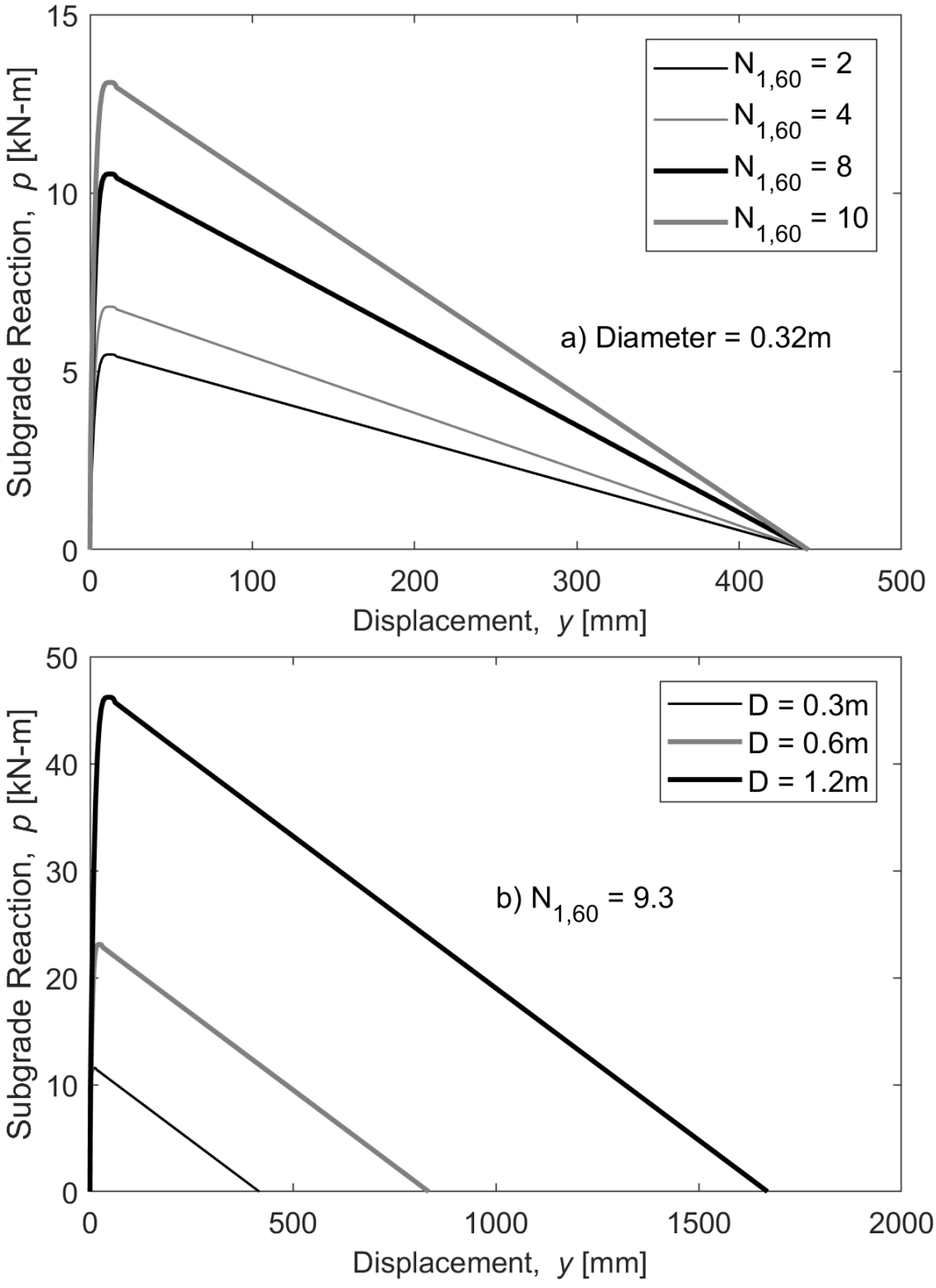

Figure 5-19. Parametric study on the proposed spring, a) varying soil strength and b) pile diameter

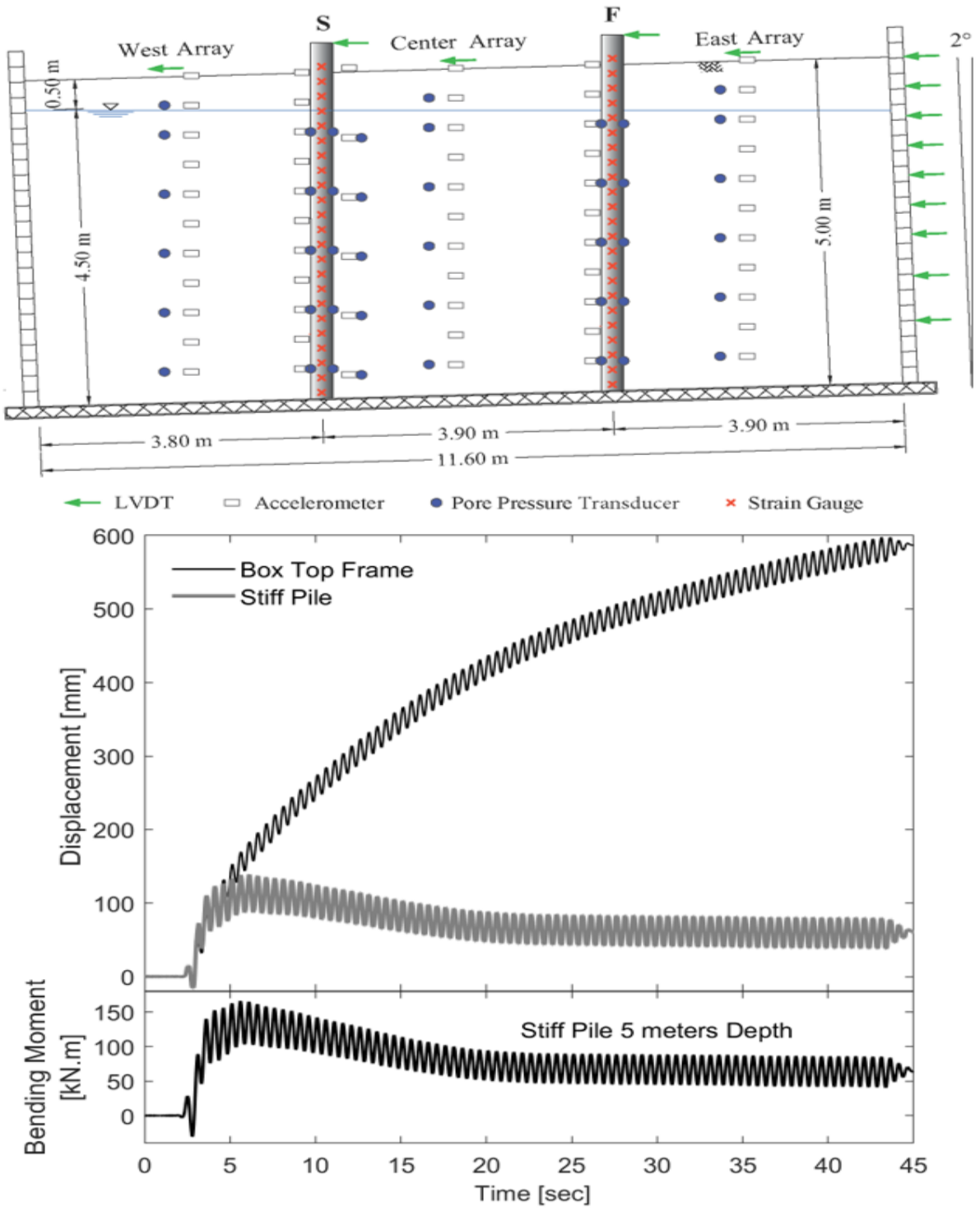

Figure 5-20. Experimental configuration of second test in series with non-liquefiable layer on top (S denotes stiff and F denotes flexible pile, after Ebeido *et al.* 2019b)

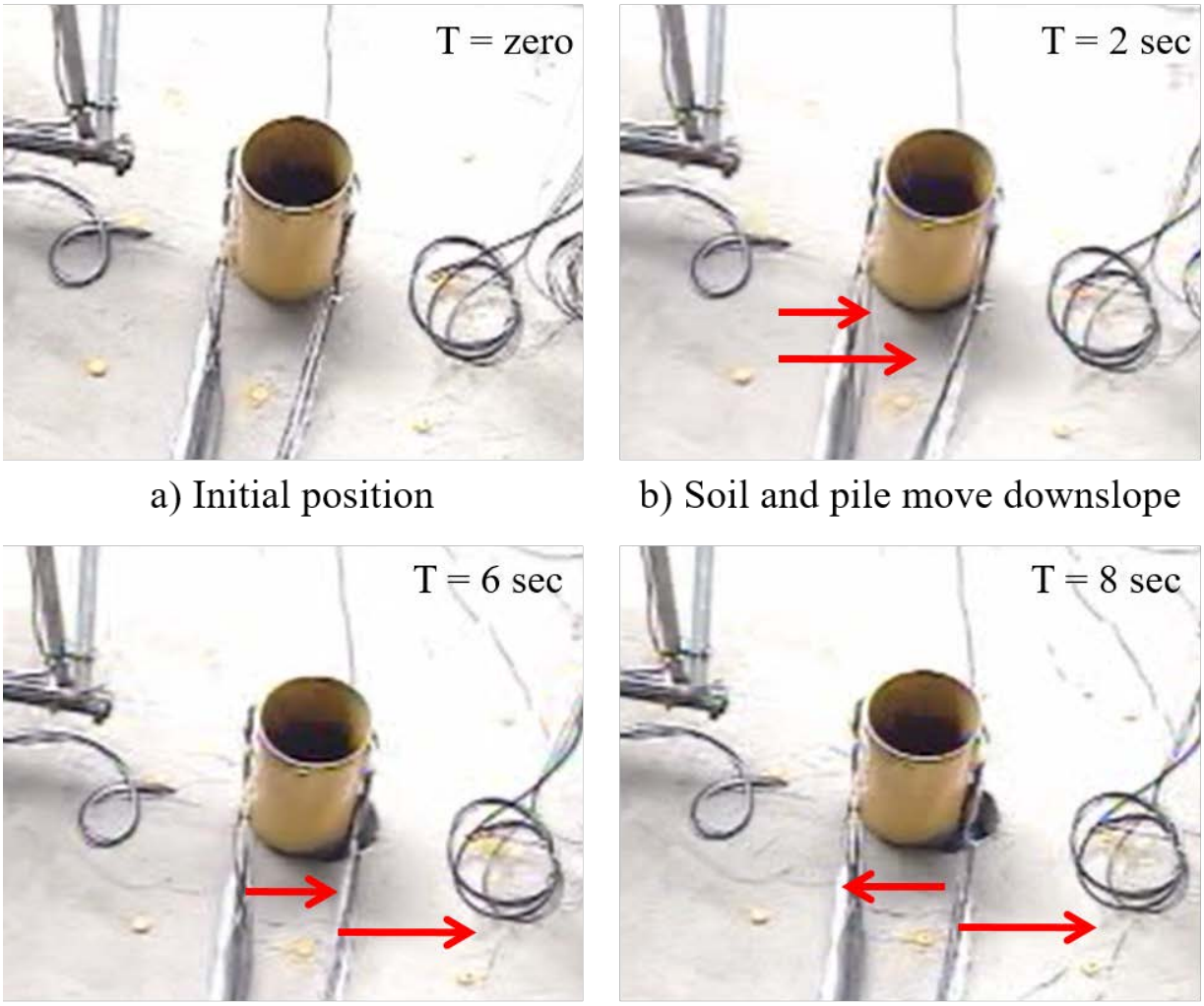

Figure 5-21. Stiff pile movement relative to the surrounding ground in the crust experiment (after Ebeido *et al.* 2019b)

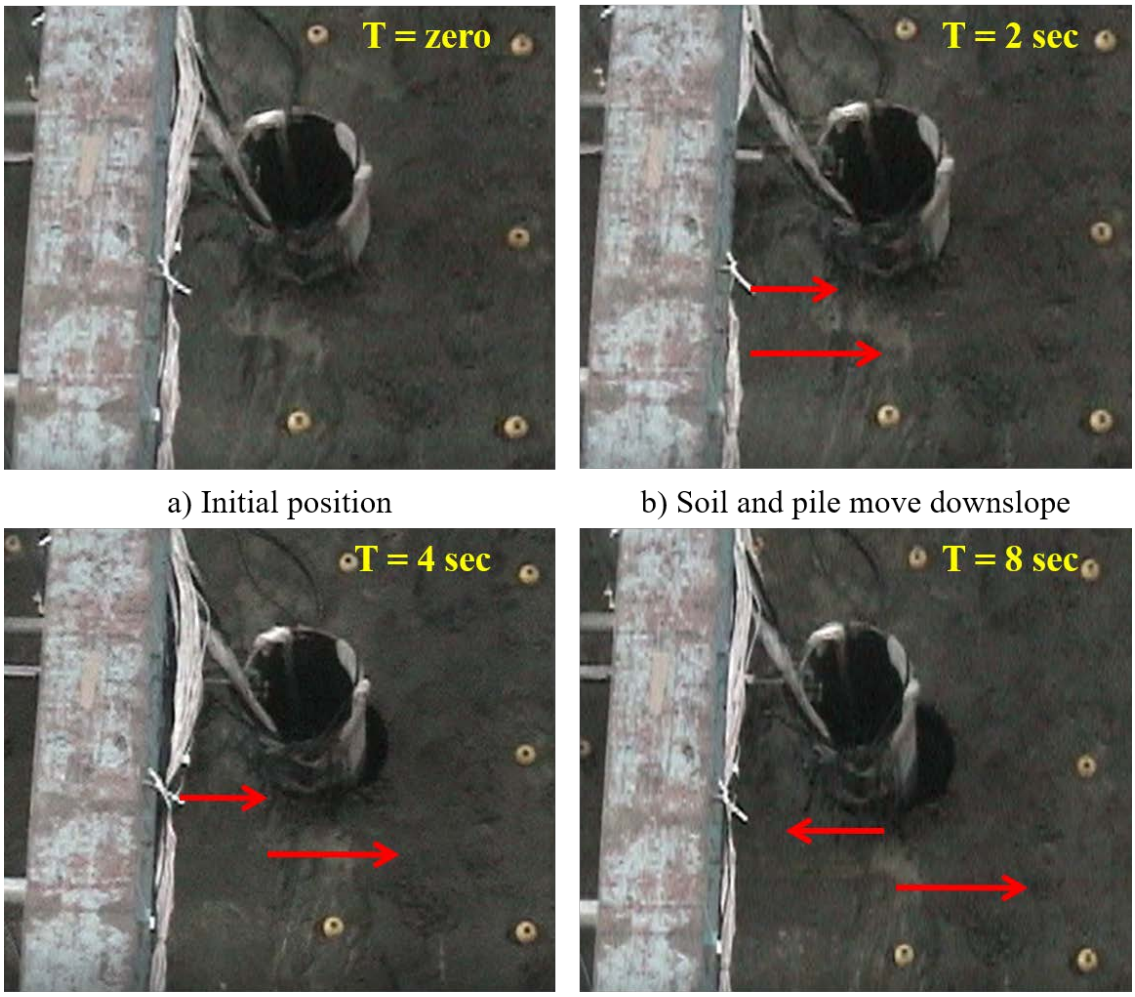

a) Initial position

b) Soil and pile move downslope

c) Soil moves more than pile

d) Pile rebounds

Figure 5-22. Stiff pile movement relative to the surrounding ground in the similar experiment with a pile group (after Ebeido *et al.* 2019b)

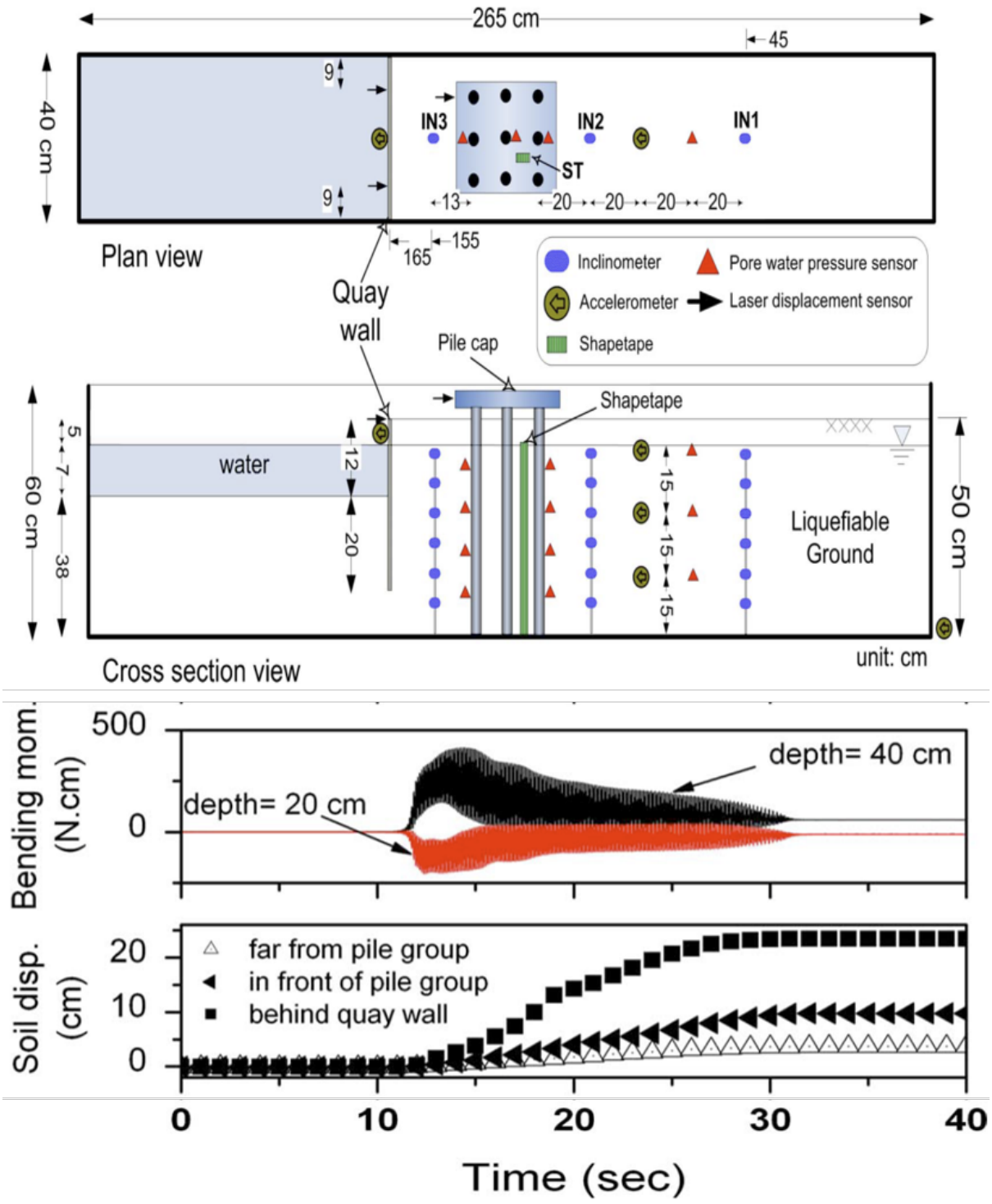

Figure 5-23. Pile group behind a quay wall model showing bending moment (mom.) and displacement (after Motamed and Towhata 2009)

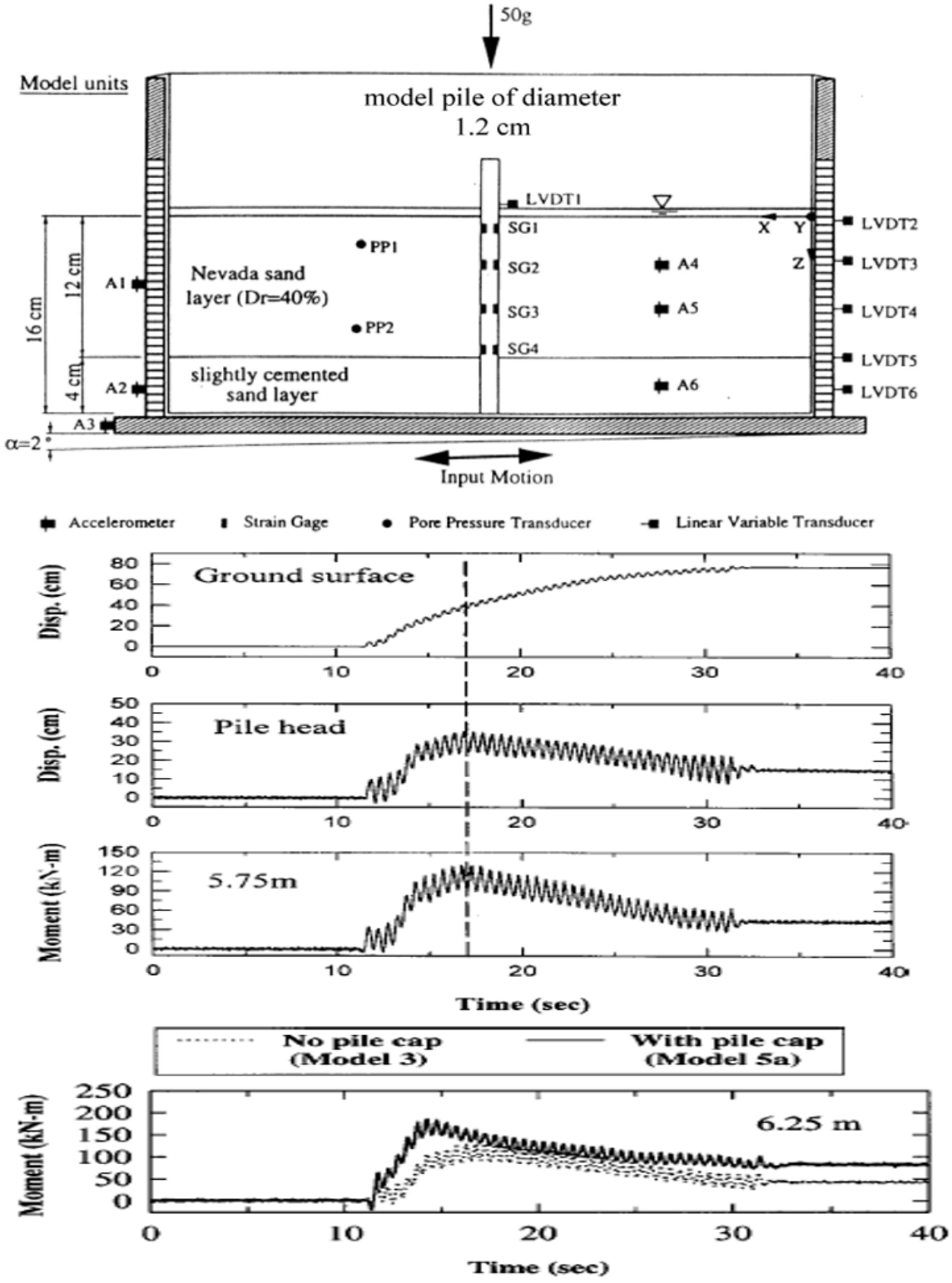

Figure 5-24. RPI centrifuge model 3 (after Abdoun *et al.* 2003)

Chapter 6 Effect of an Upper Crust on Pile Behavior under Liquefaction-Induced Lateral Spreading

6.1. Abstract

Data sets from a large-scale laminar box shaking table experiment was employed to investigate pressure development on pile foundation, due to the mechanism of liquefaction-induced lateral spreading. A mildly inclined configuration with 2 single piles of different stiffness in a 2-layered profile was employed. Ground and pile lateral displacement as well as excess pore pressures are discussed. In this test, it is observed that some of the highest pile lateral loads occur at the initial stages of lateral deformation, as observed from the recorded soil pressures and calculated bending moment. Non- liquefied crusts on top of liquefied sand can exert large pressures on pile foundation during the process of liquefaction-induced lateral spreading. The dynamic lateral load verses relative displacement between the soil and the pile from the tested configuration is employed to examine the load transfer behavior. A softer load transfer mechanism is documented as much larger displacements are needed for the non-liquefied crust to develop full passive pressures on the embedded foundation. Consequently, findings are employed in a BNWF (Beam on Non-linear Winkler Foundation) model to compare experimental results with existing *p-y* curves used in practice. Finally, recommendations are made for minor suggested modifications of existing curves.

6.2. Introduction

Liquefaction-induced lateral spreading is one of the major causes of damage of bridges and port structures during seismic shaking resulting in detrimental effects on pile foundations (Mizuno 1987; Dobry and Abdoun 2001; Ishihara 2003; Tokimatsu *et al.* 2005). Such damage can have drastic economic consequences. Documented cases of bridge failures due to deep foundation

damage by liquefaction and lateral spreading has been summarized by Dobry and Abdoun (2001) and Boulanger *et al.* (2003). These cases show permanent lateral and vertical displacement of piles, cracking and foundation failure at shallow and deep elevations and ruptured connections with corresponding effects on the superstructures.

Berrill *et al.* (1997) showed that if a stiff shallow non-liquefiable crust exists on top of the liquefied soil, the soil pressures affecting the piles can be reasonably related to the passive failure and hence the shear strength of the soil. Model studies have identified that loads from non-liquefied crust layers are often the critical loads that control the response of a pile foundations. Centrifuge tests by Dobry *et al.* (2003) found that the strength of the non-liquefied crust significantly influenced pile bending moments, while loads from the liquefied layer had negligible effects on the outcome. However, great uncertainty still exists when estimating pressures applied by liquefied soil and the significance of soil permeability (He *et al.* 2017). Current design methods still need to be updated for important parameters affecting the response from recent large scale and centrifuge tests (Dungca *et al.* 2004; Hwang *et al.* 2004; Suzuki et al. 2005; Ubilla 2007; Gonzalez *et al.* 2009).

In general, lateral spreading represents a complex loading mechanism as it involves large cyclic and permanent ground deformations, both inertial and kinematic effects and superstructure effect on the soil-foundation interaction, all occur simultaneously in the presence of rapid changes in soil properties. As such, physical modelling is a vital tool for studying the involved mechanism. Centrifuge tests (Abdoun 1997; Wilson *et al.* 2000; Haigh 2002; Bhattacharya *et al.* 2004; Brandenberg *et al.* 2004; Kagawa *et al.* 2004, Towhata *et al.* 2006; Motamed *et al.* 2008; Motamed and Towhata 2010) and large scale 1-g shake table experiments (Cubrinovski *et al.* 2006; Tokimatsu and Suzuki 2004; Tokimatsu *et al.* 2001; Tokimatsu *et al.* 2005; Orense *et al.* 2000; He

2005) have recently provided much of useful data and information. Outcomes from the tests can be employed to quantify the interacting parameters and calibrate analytical procedures and numerical models.

Pressures on pile foundations from non-liquefied crust layers (Brandenberg *et al.* (2005; 2007) are commonly represented as a function of the relative displacement between the pile foundation and the "free-field" ground (the ground displacement that would occur without any influence from the embedded foundation). Loading conditions for upper crusts during lateral spreading cannot be modelled by static load tests in the non-liquefied ground. Brandenberg *et al.* (2005; 2007) used the terminology "load transfer" to refer to crust load on piles as a function of the relative displacement between the foundation and the ground. Their centrifuge tests showed that load transfer behavior during lateral spreading was about an order of magnitude softer than load transfer relations from static field tests. The difference was attributed to the effect of liquefaction on the stress distribution within the crust layer and on cyclic degradation and cracking in the crust materials.

The objective of this study is to investigate the response of a single stiff pile in a large-scale shake table test during the mechanism of liquefaction induced lateral spreading. Focus is placed on lateral pile response as total pressures and bending moments against developed soil and box displacements. Attention is given to the upper non-liquefied crust and the load transfer mechanism on the pile. A softer load transfer mechanism is observed confirming earlier observations by Brandenberg *et al.* (2007). A softening factor is proposed to available *p-y* curves in practice and results are compared with experimental observations.

6.3. Large Scale Test

A large 1-g shake-table experiment (Figure 6-1, Figure 6-2) was conducted under a US-Japan Cooperative Research Program. The experiment was performed on piles subjected to liquefaction-induced lateral spreading using a mildly inclined large laminar box at the National Research Institute for Earth Science and Disaster Prevention in Japan (NIED). The entire testing series is discussed in Chapter 4. Input motion for the experiment was sinusoidal accelerations with a 2 Hz frequency and amplitude of 0.2 g.

The laminar box used was 11.6 m long, 5 m high and 3.5 m wide. The box was inclined at 2° to the horizontal which stimulated an infinite slope of about 3° in the field (Taboada 1995). According to Law and Lam (2001), this configuration presents a periodic boundary condition. Two single piles of different stiffness were employed in a 5 m stratum. Water table was 0.5 m below the downslope ground surface.

6.4. Soil Properties

The soil stratum was constructed by sand deposition in water. Kasumigaura sand was used with the following grain size characteristics (Kagawa *et al.* 2004): D_{50} = 0.31 mm, fines content F_c = 3%, and uniformity coefficient C_u = 3. Soil relative density was estimated to be in the range of 40-50 % and saturated density was about 1940 kg/m^3.

6.5. Pile Properties

Figure 6-2 shows the soil stratum and pile foundations. Steel pipe piles of 0.318 m (1 ft) diameter were employed, with a 6 mm (stiff pile) and a 3 mm (flexible pile) wall thickness. All piles were installed with a mechanism intended to mimic a fixed base connection. A preliminary static pushover test was performed on the piles before adding the sand to obtain the bending stiffness and base fixity rotational stiffness values presented in Table 6-1.

6.6. Instrumentation

The model was instrumented with a large number of accelerometers, pore pressure sensors, pressure transducers, strain gauges and displacement transducers (Figure 6-2). Sensors were placed along the pile shaft and along the depth of the free field soil. Strain gauges were densely instrumented along the pile shaft to aid in back calculation of the bending moment during shaking. Displacement transducers were mounted on the laminar box exterior wall to measure box lateral displacements as well as being placed on the soil surface to measure ground surface displacement. Piles were also instrumented with transducers to measure pile head displacements above the ground surface.

6.7. Test Results

Focus is placed on pile response mainly in terms of soil pressure development on the piles, relation between pressures and ground displacement and difference between pressures on both sides of the pile. Key values for pile bending moments and displacements are presented in Table 6-2. Variation between total and effective pressures are discussed, as well as how pressures relate to bending moment. Analysis will concentrate on the first 10 seconds where (i) the soil liquefies, (ii) maximum pressures and bending moments are recorded, (iii) the flexible pile yields, and (iv) rebound response of stiff pile.

The recorded response (Chapter 4) illustrates the following trends:

1. Liquefaction occurred quickly as evident from acceleration attenuation between base input and soil surface shown in Figure 6-3. Evidence of acceleration reduction is also observed along the pile shaft. A phase shift of approximately 180° is observed from the soil acceleration record.

2. Soil and box displacement start to accumulate with shaking and continue with shaking as shown in Figure 6-4. The stiff pile experienced peak response during the seventh shaking cycle then gradually rebounds as liquefied soil flows around the pile without exerting additional pressures. Bending moments presented in Figure 6-5 support that observation.

3. Alternatively, the flexible pile (not shown here) passes its yield point in the first few cycles and shows evidence of failure and non-linearity (Chapter 4).

Only the stiff pile will be discussed as the pressures are presented with their development with time and displacement. Total pressures exerted by the soil are also related to the bending moments recorded. Finally, the collective results are used to study the load transfer mechanism and a minor modification factor for the currently available crust *p-y* curve is proposed.

6.8. Displacement Profile of Liquefied Layer

Maximum pile response was observed in the seventh shaking cycle, precisely at 4.01 seconds. Figure 6-6 shows the soil box and pile deformed shape at that instant. The soil moved much more than the pile and the box displaced configuration is noted to be curved (parabolic or cosine wave like) in shape.

The curved deformed shape has been previously observed by other researchers (Elgamal *et al.* 1996; Okamura *et al.* 2001; Dobry and Abdoun 2001; Abdoun *et al.* 2005; Goh and O'Rourke 2008; Thevanayagam *et al.* 2009; Dobry *et al.* 2010). Figure 6-7 shows the testing configuration used in the large scale 1-g testing at the University of Buffalo with the resulting displaced configuration. The curved shape of displacement shows highest shear strains at the bottom and very low strains at the top.

6.9. Total Pressures on the Stiff Pile

In order to directly measure the lateral pressure of the liquefied soil on the pile, total earth pressure transducers were installed on the piles as shown in Figure 6-2. These sensors were placed at different depths along the pile height at 0.64 m, 1.56 m, 2.56 m and 3.56 m to measure the development of pressures. Earth pressures were recorded at the upslope and downslope of each pile. Figure 6-8 shows the evolution of the pressure profiles on both sides of the pile as well as the resultant. Time instants for the profiles were chosen in the first 5 seconds where the peak values are recorded. The following deductions can be made, i) resultant pressures are a combination of upslope pushing on pile and downslope moving away, ii) high pressures are exerted by the liquefied layer at the beginning, iii) as shaking continues, crust pressures start to increase and become prominent, and iv) at maximum instant, the high pressures are coming from both the crust and the upper portion of the liquefied layer.

The lower portion of the liquefied layer starts by resisting the pile movement and with shaking, no pressures are exerted by this part of the layer.

Figure 6-9 shows the development of resultant pressures with time. The pressure from the crust layer keeps increasing with time showing that even the excessive displacements were not enough to mobilize the full pressures coming from that layer. Pressure transducers with in the liquefied layer show pressure development during the first few cycles of shaking but decreasing afterwards. The highest initial pressures are being exerted at the 1.56 m depth. From Figure 6-8 and Figure 6-9, we can observe that the pressures are out of phase. Peak pressure in a particular time history at a certain depth does not correspond to peak pressures in all time histories.

Figure 6-10 relates resultant pressure at 0.64 m and 2.56 m depth with ground movement while Figure 6-11 separates time histories for the upslope, downslope and resultant pressures. It is

observed that pressures for the crust took much more displacements to develop than the lower portions. The 0.64 m location was still increasing for the first 10 seconds. Early peaks in the 2.56 m resultant history correspond to both upslope push and negative downslope peaks (soil moving away from pile). The 2.56 m location got to its peak earlier then quickly decreased and started oscillation around a lower value. Figure 6-12 highlights that the total pressures at 2.56 m are a result of both pore pressure build up and effective stress forces from the inclined ground movement. The downslope total pressure is mainly caused by the pore pressure development and its dilation trends. The pore pressure in dominant and is the main component of the total pressures. Resulting effective pressures are seen to oscillate around zero with dilative peaks corresponding to the pore pressure dips.

6.10. Pile Response

More focus is placed on the pile response in terms of acting soil pressures. Figure 6-13 presents the soil resistance over the period of shaking. In general, the soil resistance agrees with the recorded total pressures. Mainly in terms of, i) high soil pressures are exerted by the liquefied layer early during shaking, ii) as shaking progress, the crust applies more pressure on the pile and requires more mobilized displacements, and iii) eventually, the liquefied soil pressures disappear, and the crust pressure stays constant driving the pile response.

Bending moment and shear profiles (Figure 6-14 - Figure 6-17) confirm the observations made and show the rebound response of the pile, acting as a cantilever.

6.11. Previous Studies

The observed pile behavior in the previous sections, mainly rebounding during shaking has been observed in different previous testing configurations by several researchers. The response mechanism was observed in similar large-scale testing on embedded pile foundations (Ebeido *et*

al. 2018; Ebeido *et al.* 2019), pile groups behind a quay wall (Motamed and Towhata 2009) and centrifuge tests (Abdoun *et al.* 2003). The common behavior noted in all those studies is that soil deformations keep accumulating with shaking. Although deformations continue, peak bending moments occurred early during the shaking phase. That maximum moment occurred with small soil displacements despite the larger values at the end. After peak bending moment, the pile starts rebounding gradually.

The observed mechanism suggests the need for the development of the degrading liquefaction *p-y* curve already presented in Chapter 5 and a crust *p-y* curve that can represent the overlying non-liquefied layer.

6.12. *P-y* Curves for Non-Liquefied Crust

Based on the described experiment and the generated physical data, this section discusses the development of a *p-y* curve to be used with non-liquefied crust on top of a liquefiable layer. Figure 6-18 presents the derived *p-y* response based on the strain gauge data of the stiff pile. Response shows the degradation of strength in the liquefied layer and the softer load transfer of the crust layer. Much higher displacements are needed to mobilize the full crust pressures compared to the static scenario. Brandenberg *et al.* (2007) suggest a reduction of an order of magnitude in stiffness for the crust *p-y* curves. Applying the *p-y* lateral analysis for the stiff pile as shown in Figure 6-19 and using the actual soil box deformation profiles such as the one shown in Figure 6-6, an effort was undertaken to match the crust response in the analysis. The analysis accounts for the base rotational spring of the test presented in Table 6-1.

The API (2010) sand *p-y* curve, one of the most widely used in practice, was employed with a reduction factor and is shown in Figure 6-20 for a friction angle of 30° matching the experimental soil parameters. The curve is shown to peak at 0.032D then stay constant. A factor

of 20 is proposed to reduce the initial modulus of subgrade reaction used in computing the curve allowing for the effect of the generated high pore pressures in the liquefied layer below. The modified curve allows for a softer load transfer mechanism. The proposed modification reaches peak response at 0.63D, at 20 times more mobilized displacement than the original curve. The proposed modified curve compares well with the experimentally derived response matching the slope and the peak strength value (Figure 6-20). Both the proposed modified crust *p-y* curve and the liquefied *p-y* curve (Chapter 5) are shown in Figure 6-20. The liquefied soil spring peaks at very small displacements then degrades with the progress of ground displacements. The crust springs takes longer to reach peak strength then stays constant at the passive pressure value.

6.13. *P-y* Curve Verification

The stiff pile was chosen to verify the crust *p-y* curve response as it remained elastic and rebounded with increased displacements. Vital aspects of the calibration process are to match peak response at the same box displacement and to simulate liquefied *p-y* curve degradation and softer loading of the crust. Soil spring spacing used was 0.20 m for the crust and 0.25 m for the liquefied layer. Experimental and *p-y* developed responses where compared in terms of base bending moment against box displacement and pile head deformation against box displacement (Figure 6-21). Both curves present a good match between results with respect to peak response at the corresponding displacement and similar peak bending moment values. The pile head displacement was under-estimated; however, it is still within an acceptable range. The rebound response is well simulated and residual values are similar.

The box displacement was applied as a pushover analysis and the time history for the top box location (soil surface) is presented in Figure 6-22. Figure 6-23 and Figure 6-24 show the individual spring responses for various depths along the height. The progression of the forces

applied on the pile by the spring against time step (Figure 6-23) show that each spring reaches its peak value at a different point in time then rebounds resulting in a lower maximum bending moment than what would be predicted by conventional models. However, the crust spring peaks much later in time and stays constant. Figure 6-24 shows the individual spring responses in terms of force against relative displacement.

To separate the contribution of the crust and the liquefied layer soil springs, a comparison was undertaken between the full model described above with both springs and another with only employing the crust spring and no soil resistance in the liquefied layer. Results displayed in Figure 6-25 suggest that the initial slope and the peak response is dictated by both liquefied and non-liquefied layers. This confirms earlier discussions were contribution of pressures from both layers is needed for peak bending moment. The residual value is a function of the crust layer ultimate strength. Noting that the residual value for the 2 models are close, with continued application of displacement increments, the full model response will decay to the residual value of the crust only response (as the liquefied layer soil springs at the lower region of the model fully soften).

6.14. Discussion

General observations that can apply to both piles are:

1. Piles experience maximum bending moments and displacements early during shaking.

2. Post-earthquake inspection does not provide a full picture of the liquefaction process. Rebound of the stiff pile demonstrates that the residual post-shaking configuration might not fully capture the peak response of the pile.

3. The continued excessive lateral spreading might cause no additional loading as evident from the stiff pile, as pressures decrease after the first few cycles of shaking.

4. As shaking starts, an upslope gap forms and the downslope soil starts moving away at the upper part. For the lower regions, upslope soil pushes on the pile and downslope resists the movement (downslope pattern of upper soil moving away, bottom soil resisting is evident in all presented time frames).

5. The part of the pressure profile causing the bending moment changes with soil movement. Regions that cause high pressure at the start of shaking could result in zero added forces on the pile just a few seconds later.

6. Crust pressures need higher displacements to fully mobilize and continued applying pressures on the pile throughout the shaking phase.

7. Developed *p-y* curves matched well with the experiment in terms of peak response, ground movement needed to mobilize the peak response and pile rebound pattern.

8. The reduction of the initial subgrade reaction with a factor of 20 to be used for non-liquefied soils on top of the liquefied stratum ones provides a reasonable estimate accounting for the influence of cyclic degradation, cracking and high developed pore pressures in the liquefied layer. The proposed reduction value compares well with the one proposed earlier by Brandenberg *et al*. (2007).

9. Displacement shape shows crust moving relatively as a rigid body, with a curved shape within the loose liquefied layer.

6.15. Summary and Conclusions

Pile response was studied in detail with focus placed on developing soil pressures. The experimental data was employed, with the purpose of deriving a crust stratum pushover *p-y* curve from the observed pile-ground interaction. Among the main observations and findings are:

1. High bending moment can occur early as soil starts moving and possibly before liquefaction of the entire loose stratum.

2. For the soil crust scenario, applied pressures along the pile profile are not necessarily in phase. Upper locations can peak while lower ones drop.

3. Crust pressure continued to increase with the accumulation of ground deformation while pressure from the liquefied soil was decreasing,

4. Reduction in downslope side pressure contributed significantly to overall lateral pressure in the early part of the response. Eventually upslope side pressures became dominant including pressure from crust.

5. Bottom portion of the loose layer was supporting the pile during the early phase of shaking.

6. Liquefied layer total pressures are directly related to pore pressures in the layer with minimal contributions from the effective pressures.

7. Downslope suction is observed from pore pressure trends as soil pulls away from pile. Soil dilative tendencies is evident from the corresponding dips in pore pressure.

8. Developed *p-y* curves show good matching with the experimental results, in terms of peak bending moment, corresponding ground displacement and residual value. Pile head displacement is in an acceptable range.

6.16. Acknowledgements

Chapter 6, in part, is currently being prepared for submission for publication of the material as it may appear in the following journal publication (The dissertation author was the primary investigator and author of this paper):

Ebeido, A. and Elgamal, A., "Pile behavior trends in fully saturated laterally spreading soils".

Table 6-1. Characteristics of Soil stratum and Pile foundations

Soil Profile		Pile Properties					
Height [m]	Water Table	Embedded Length [m]	Diameter [cm]	Wall Thickness [cm]	Bending Stiffness [kN-m^2]	Base Rotational Stiffness [kN-m/rad]	Yield Bending Moment [kN-m]
5.0	0.5 m below downslope soil	5.0	31.8	0.6*	14320	18500	190
				0.3**	7360	8500	93

* Denoted in text as stiff pile (S)

** Denoted in text as flexible pile (F)

Table 6-2. Summary of experimental results

Pile Configuration	At maximum response				At end of shaking (44 s)		
	M_{max} [kN-m]	Relative Displacement [mm]			Relative Displacement [mm]		
		Pile Head	Center Array @ ground surface	Container Top Frame	Pile Head	Center Array @ ground surface	Container Top Frame
Stiff	166	138	103	170	61	480	588
Flexible	93**	158			166		

* Denotes yielding of pile cross-section; with estimated value being limited by this yielding mechanism

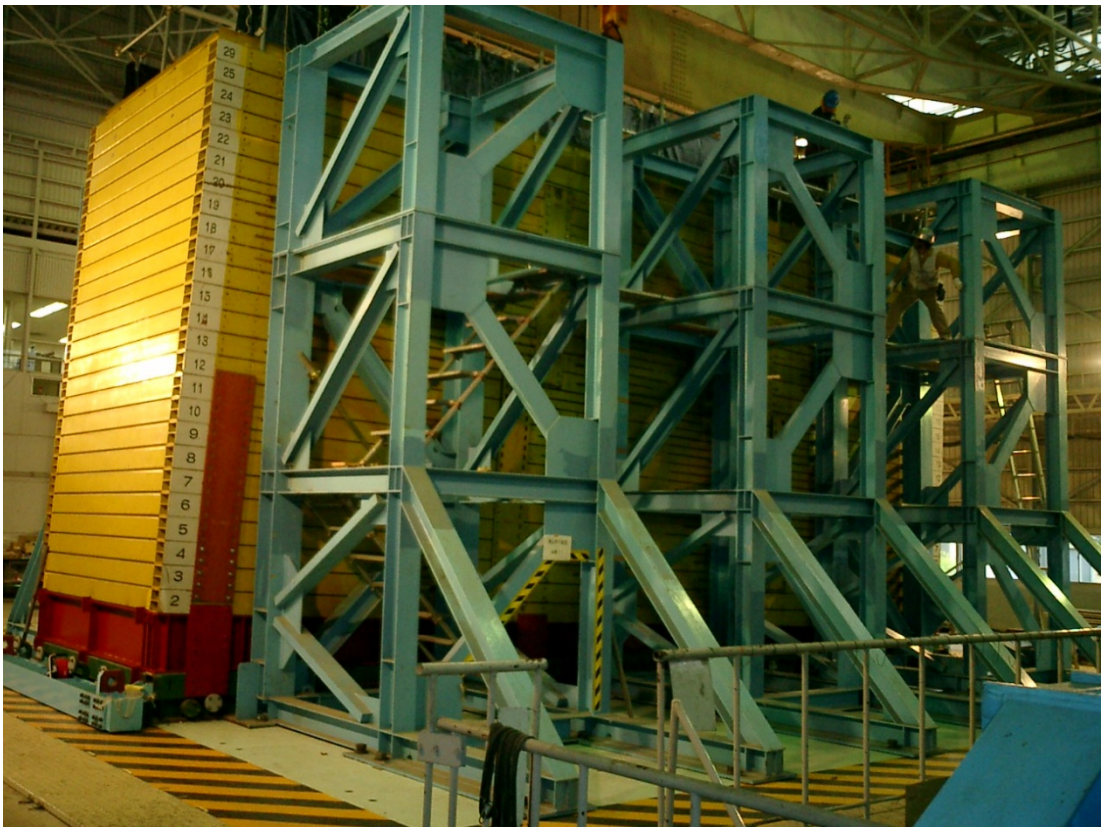

Figure 6-1. Mildly inclined large laminar box on shake table

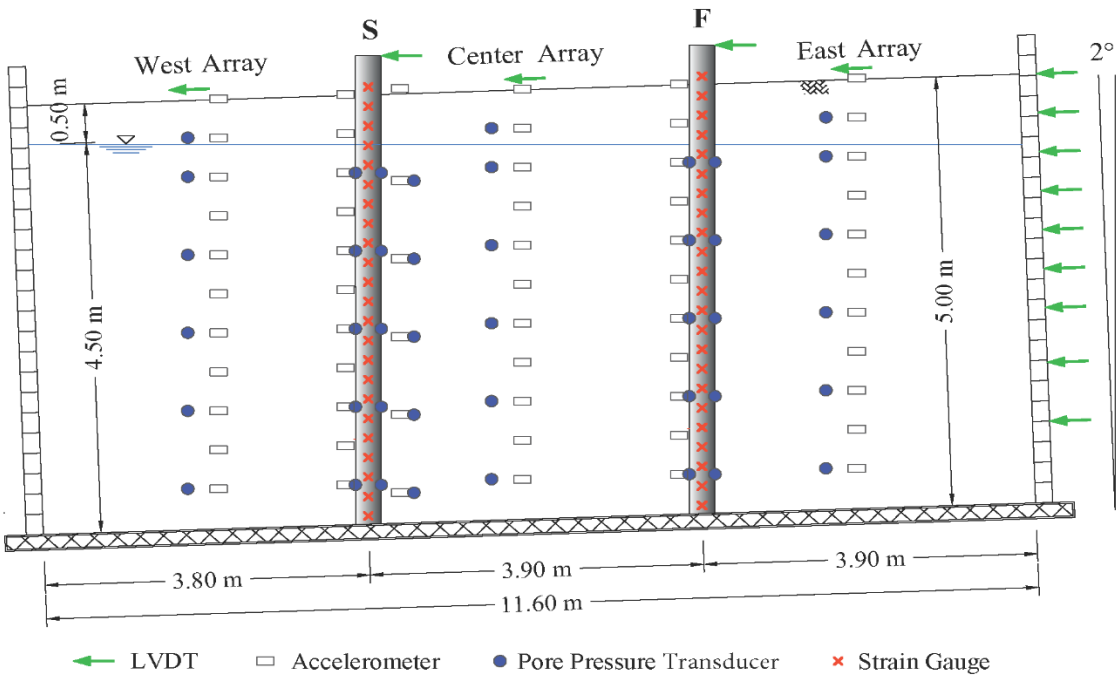

Figure 6-2. Experiment Configuration (S denotes stiff and F denotes flexible pile)

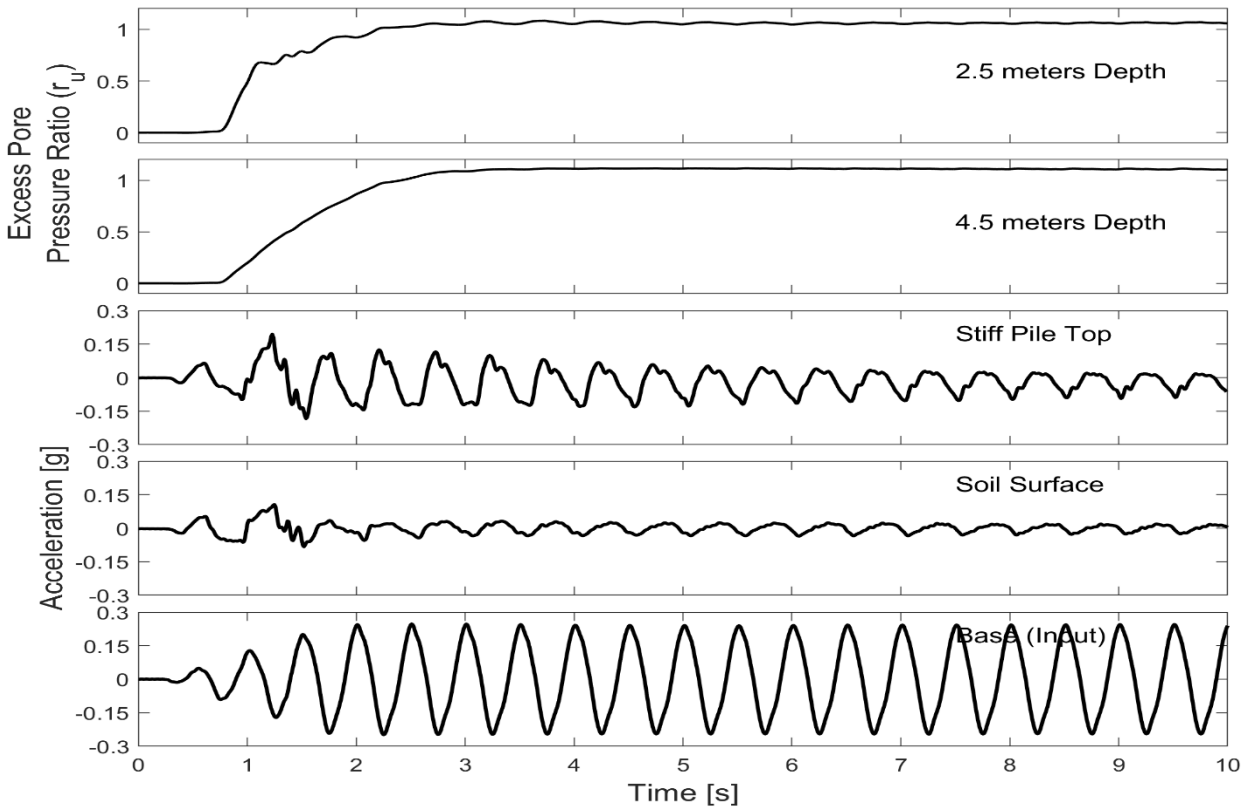

Figure 6-3. Acceleration and excess pore pressure time histories

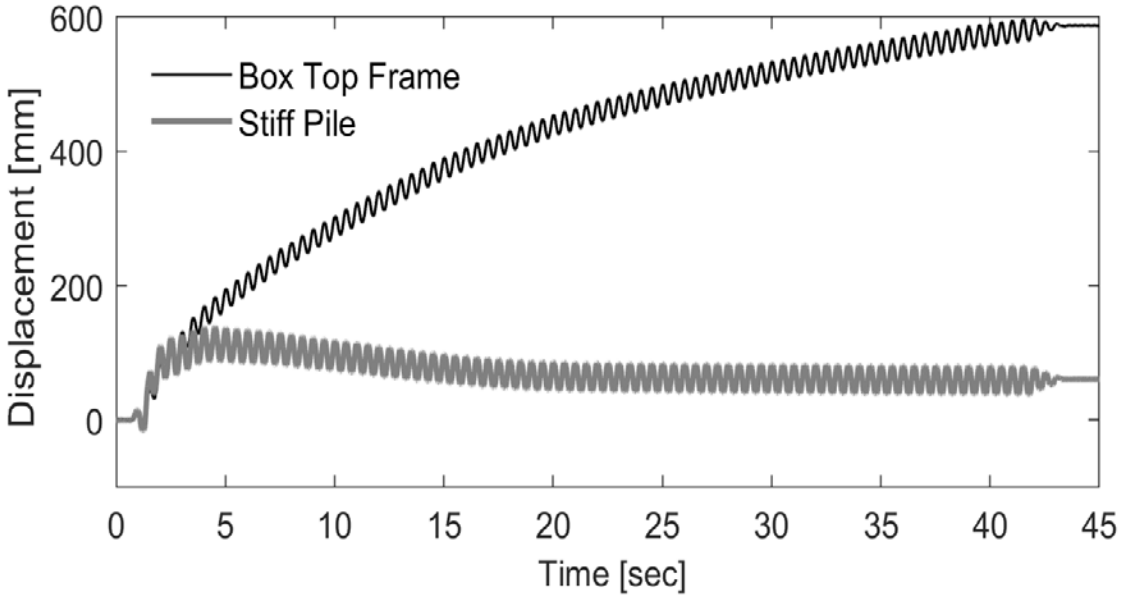

Figure 6-4. Displacement time history results

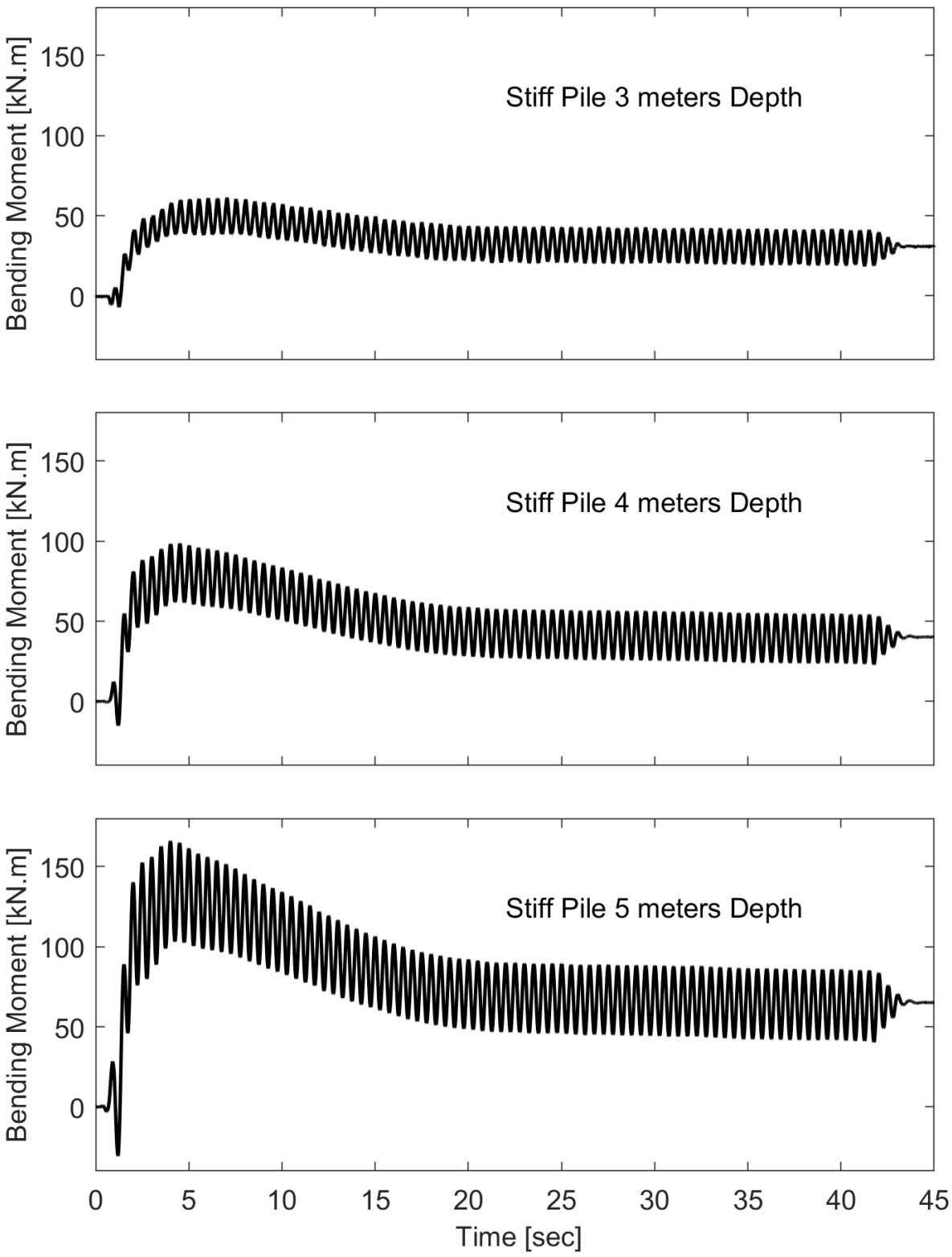

Figure 6-5. Bending time histories

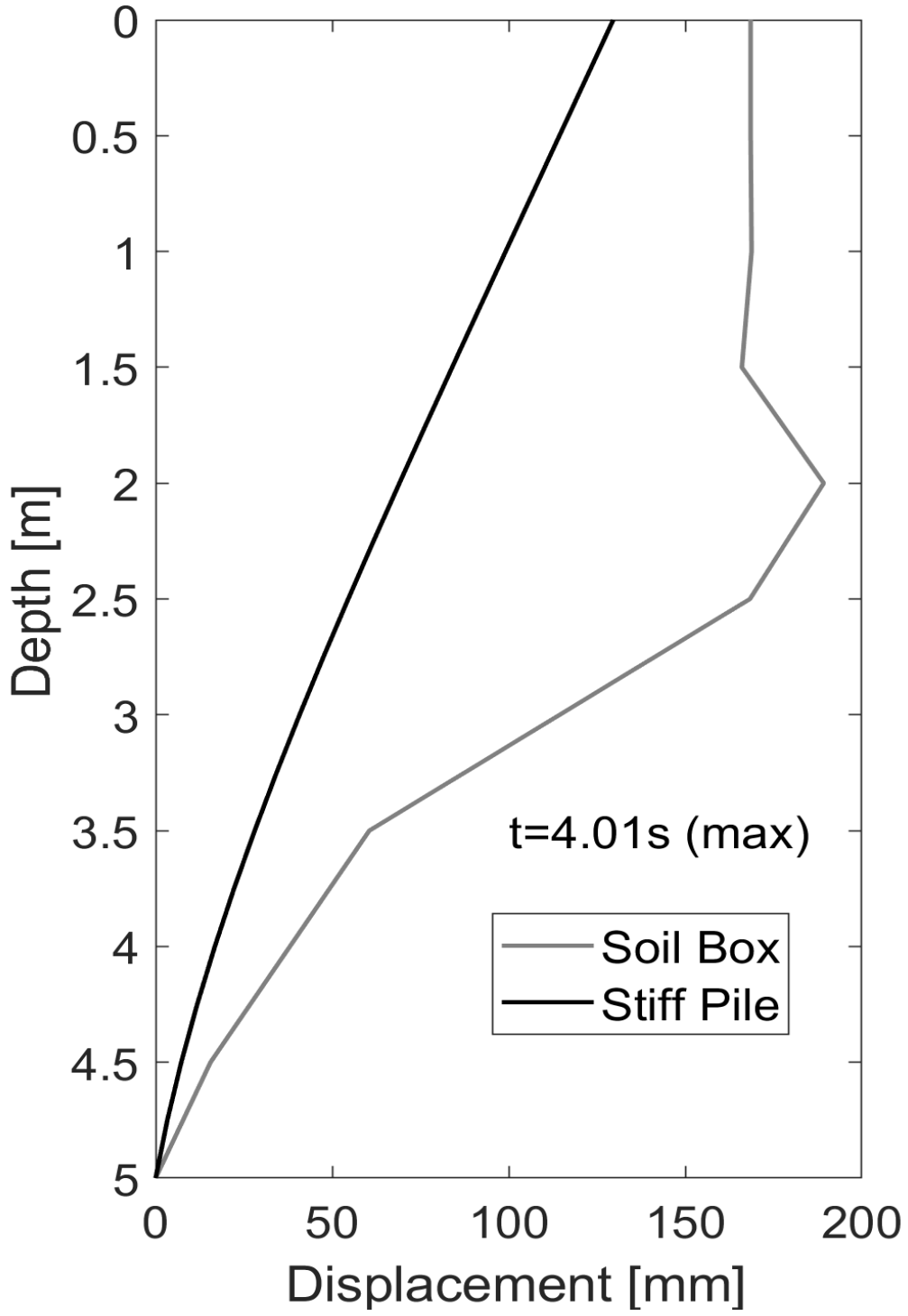

Figure 6-6. Stiff pile and box displacement profile at maximum bending moment time instant

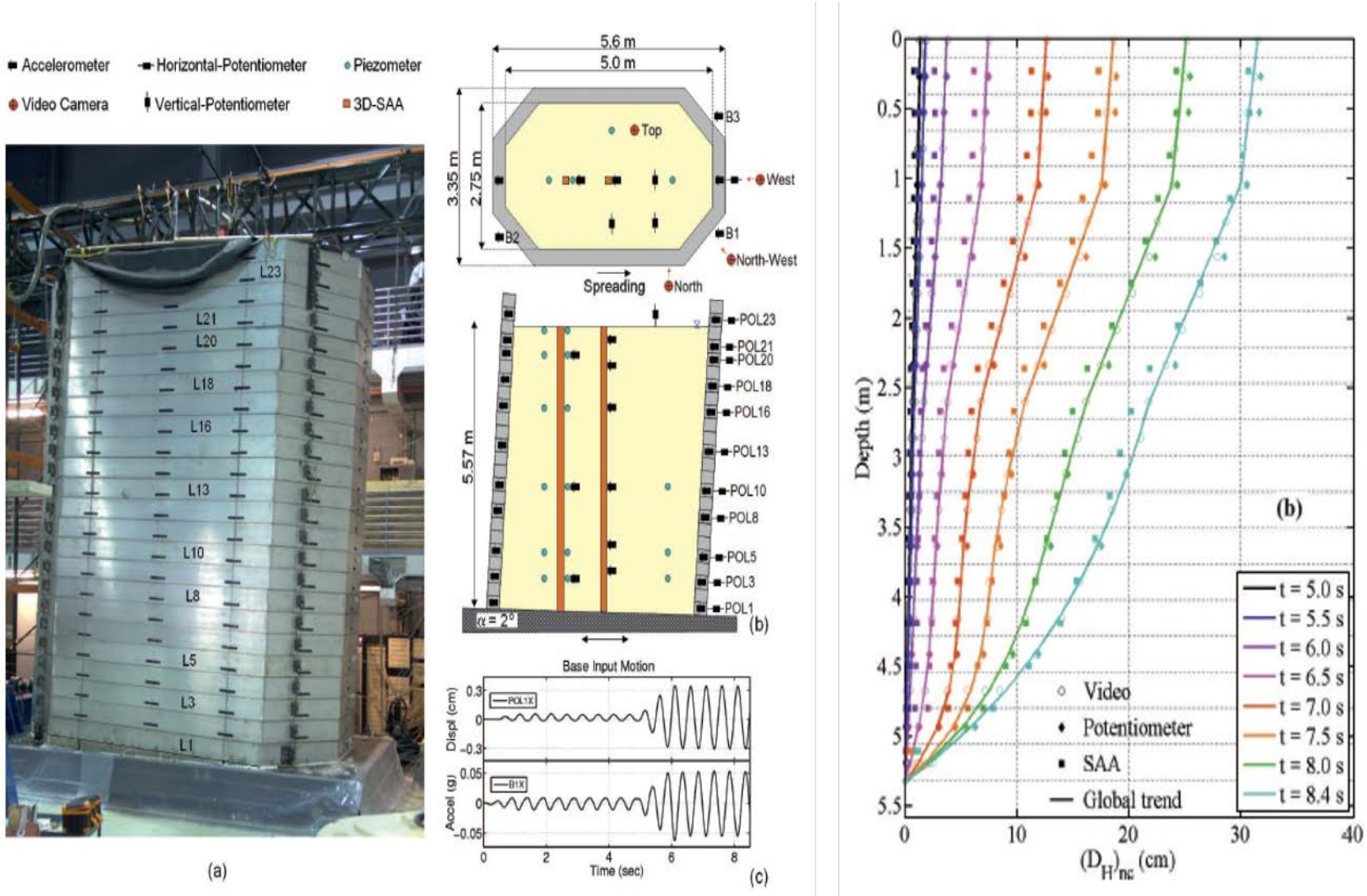

Figure 6-7. Large scale 1-g shake table test at University of Buffalo (after Dobry *et al.* 2010)

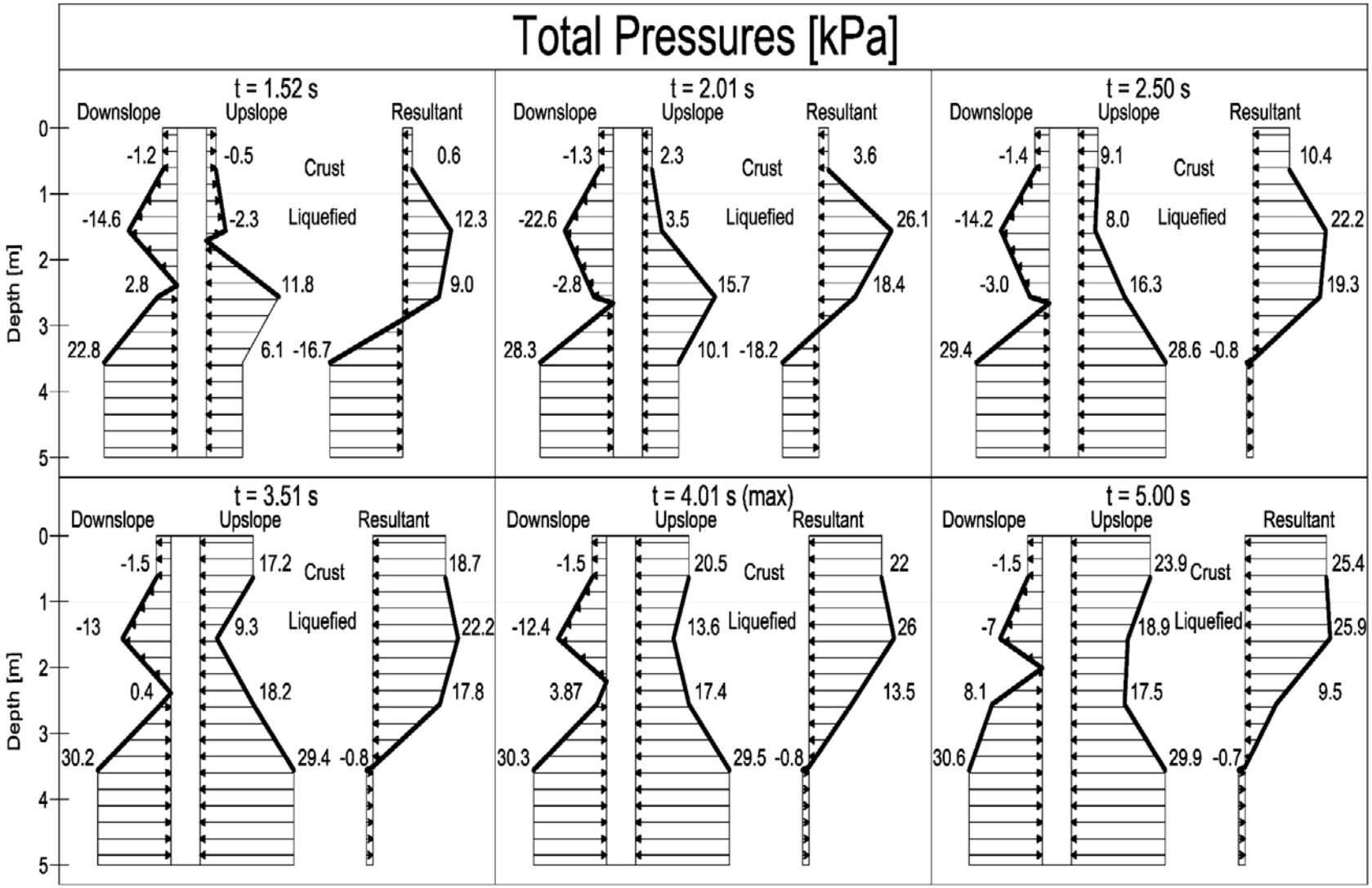

Figure 6-8. Evolution of pressure profile on stiff pile

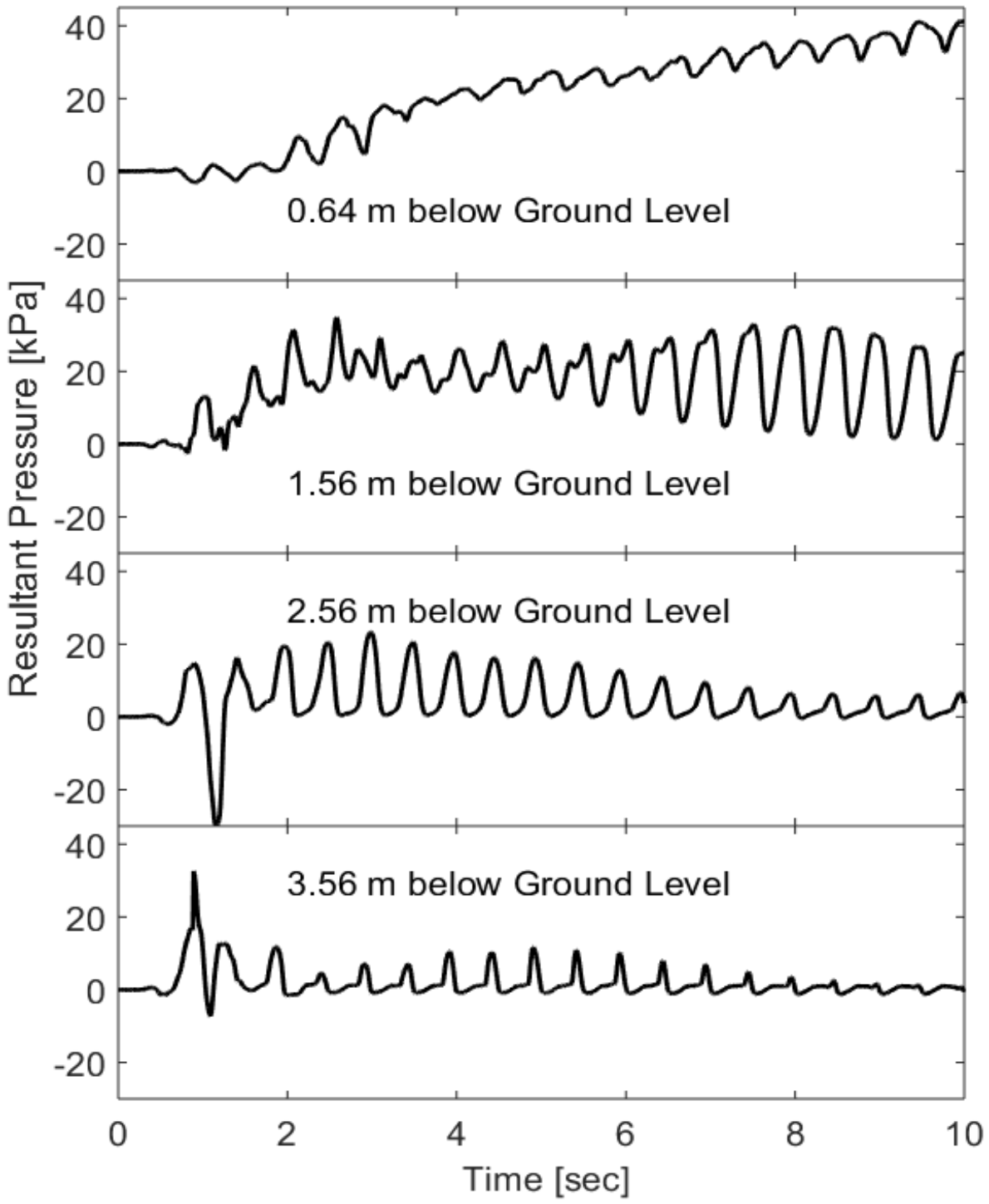

Figure 6-9. Resultant pressure time history for stiff pile

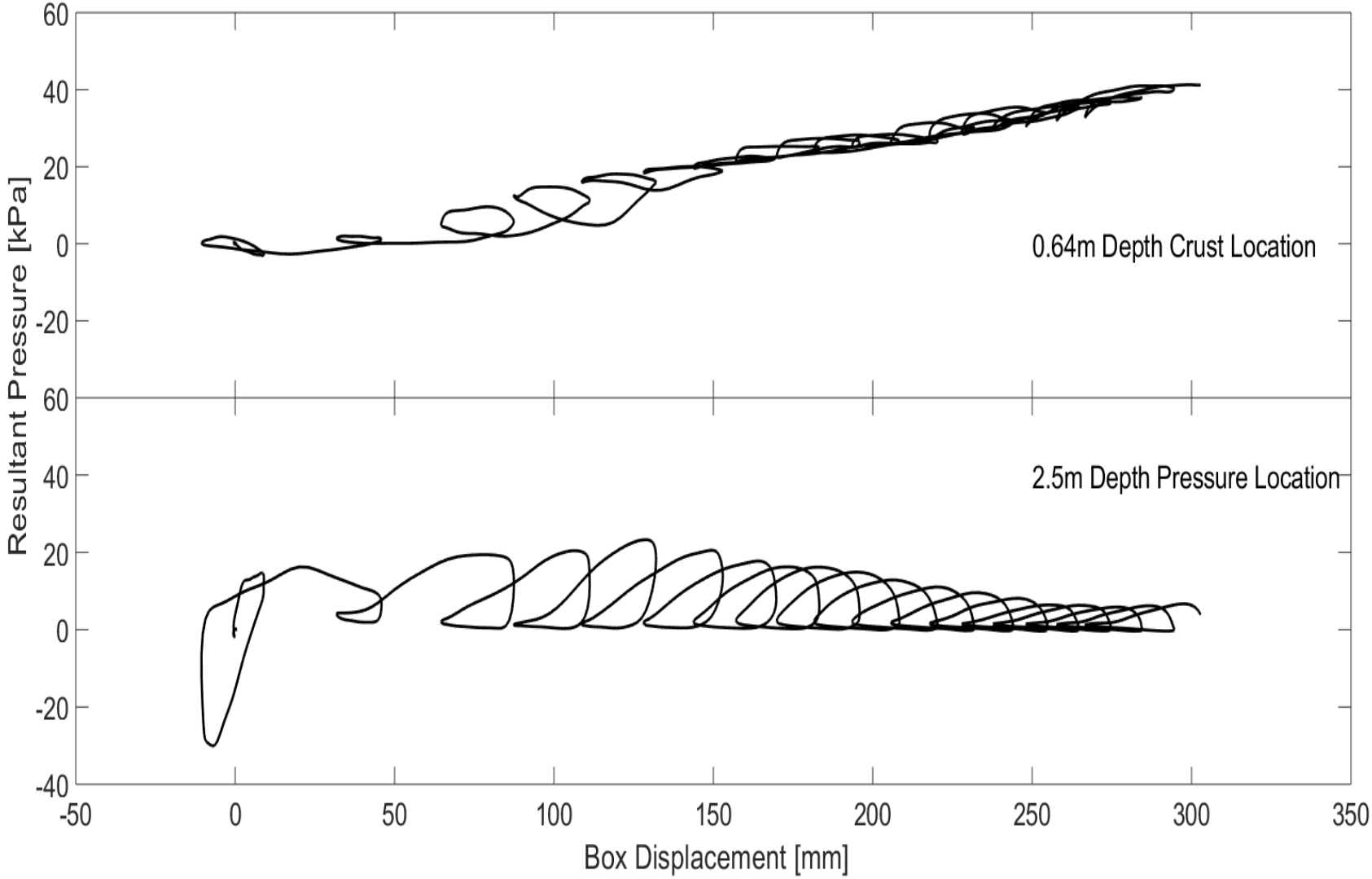

Figure 6-10. Resultant pressures against box displacement for stiff pile

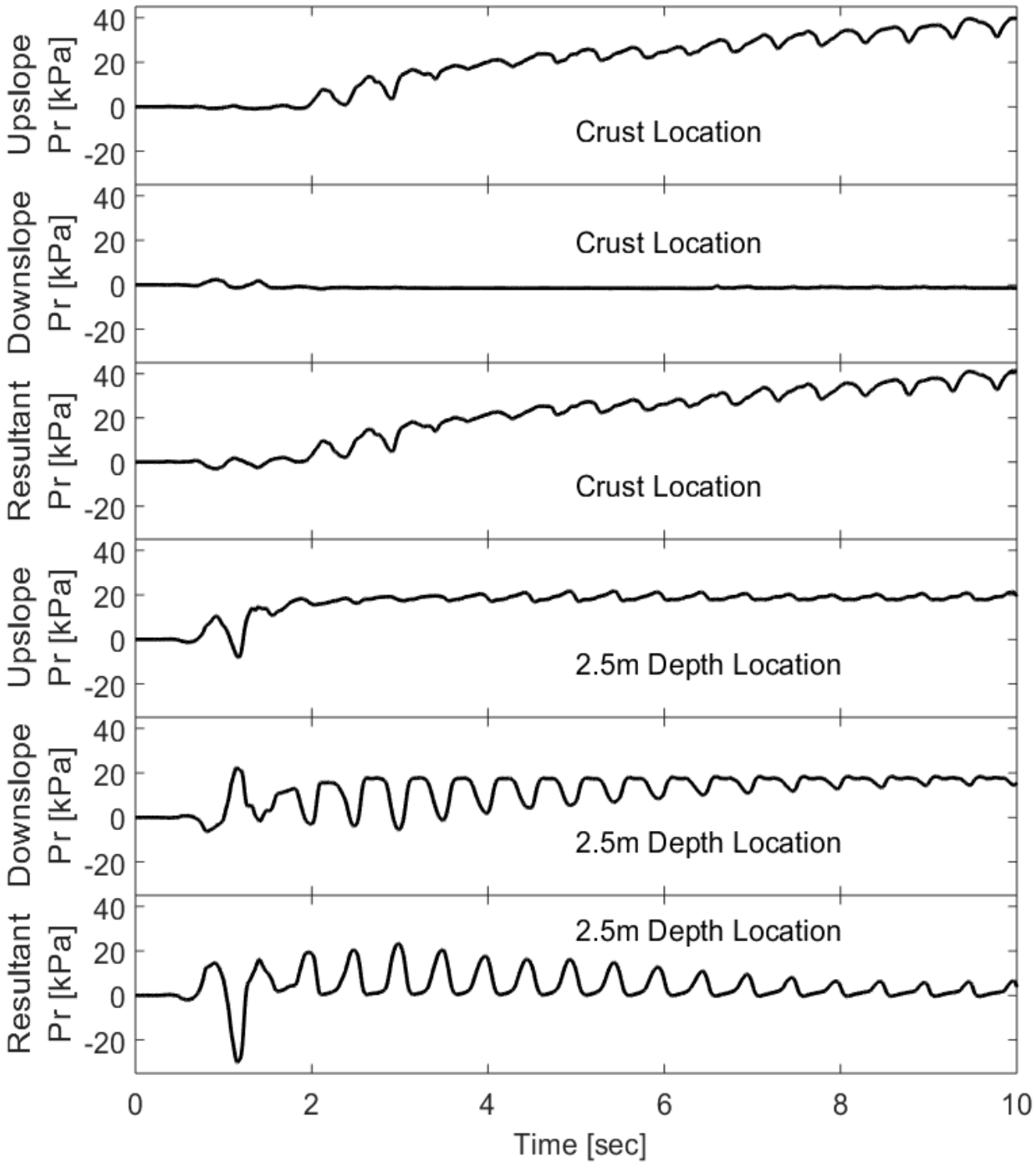

Figure 6-11. Difference of pressures between the 2 sides of the stiff pile

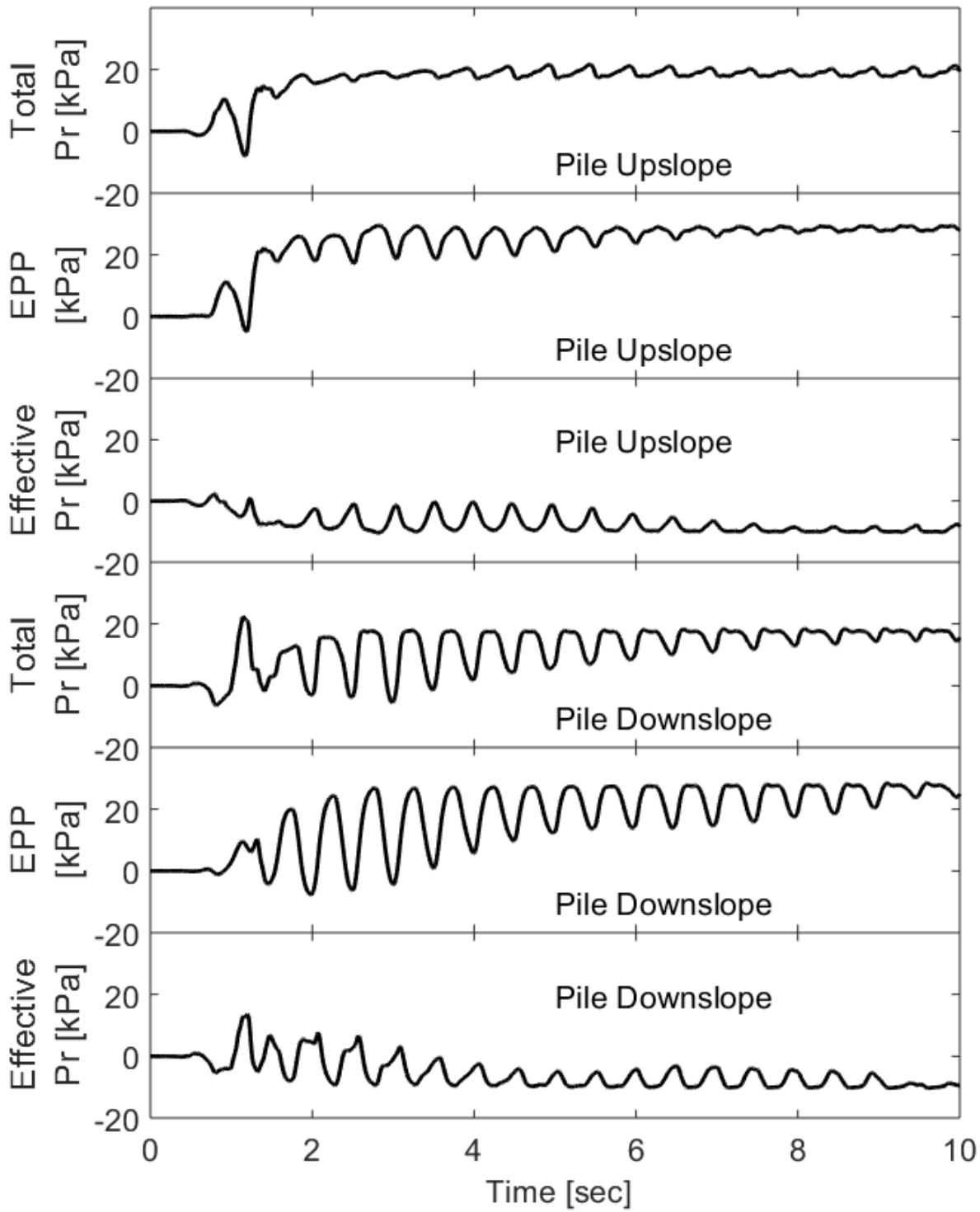

Figure 6-12. Total and effective pressures acting on the stiff pile at 2.56 m depth

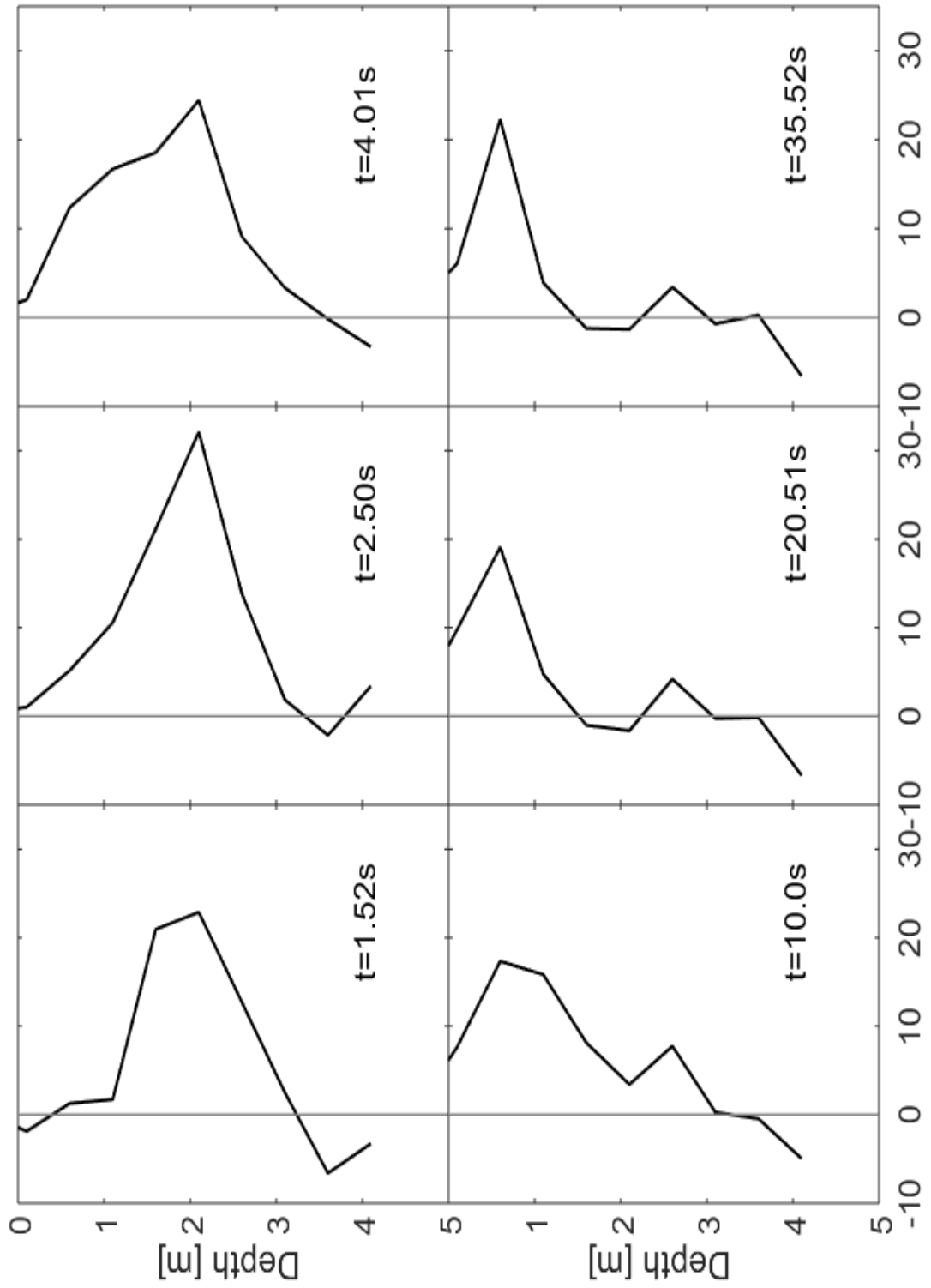

Figure 6-13. Evolution of soil resistance profiles on stiff pile during shaking

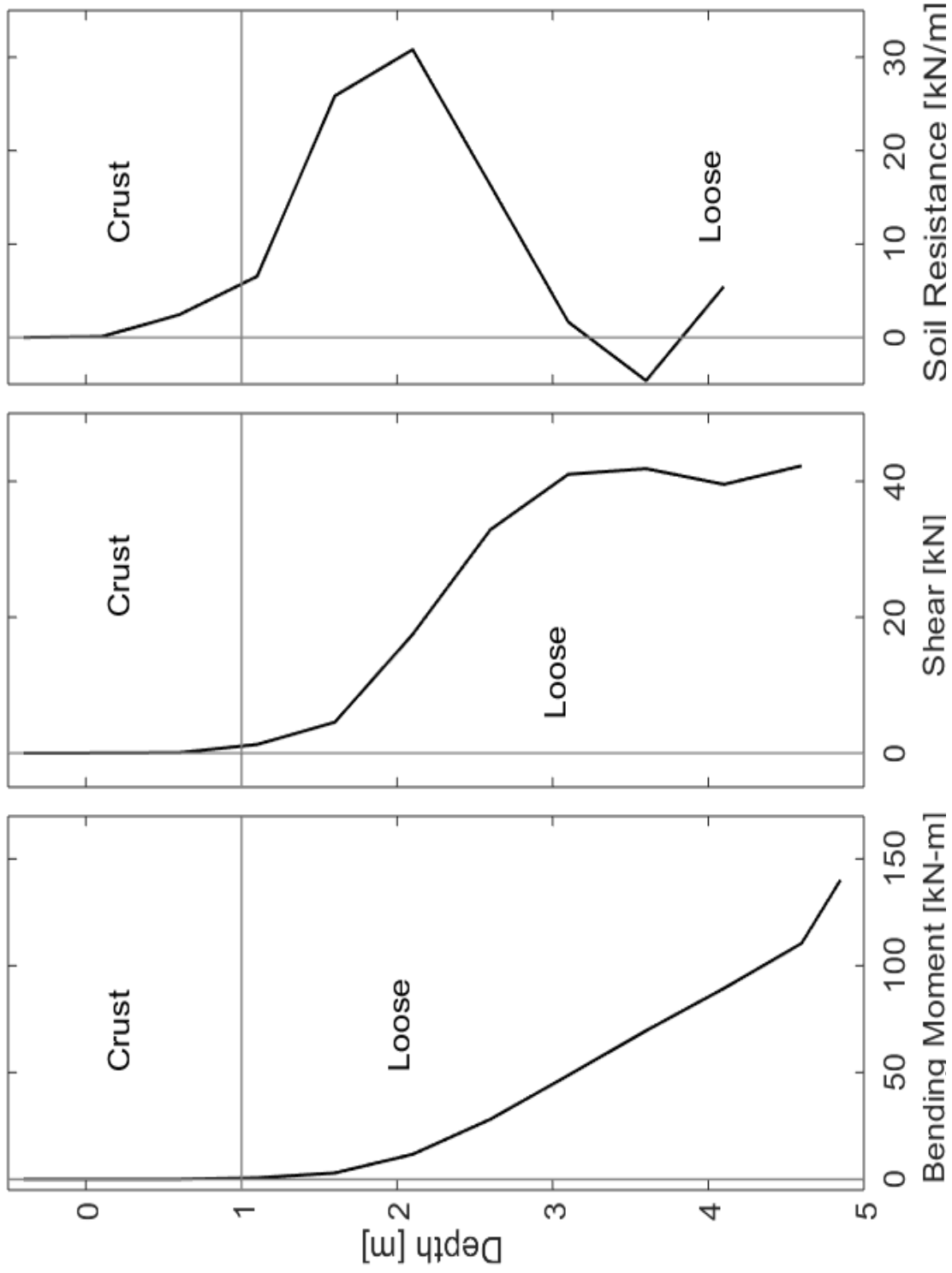

Figure 6-14. Stiff pile response profiles at 2.01 seconds

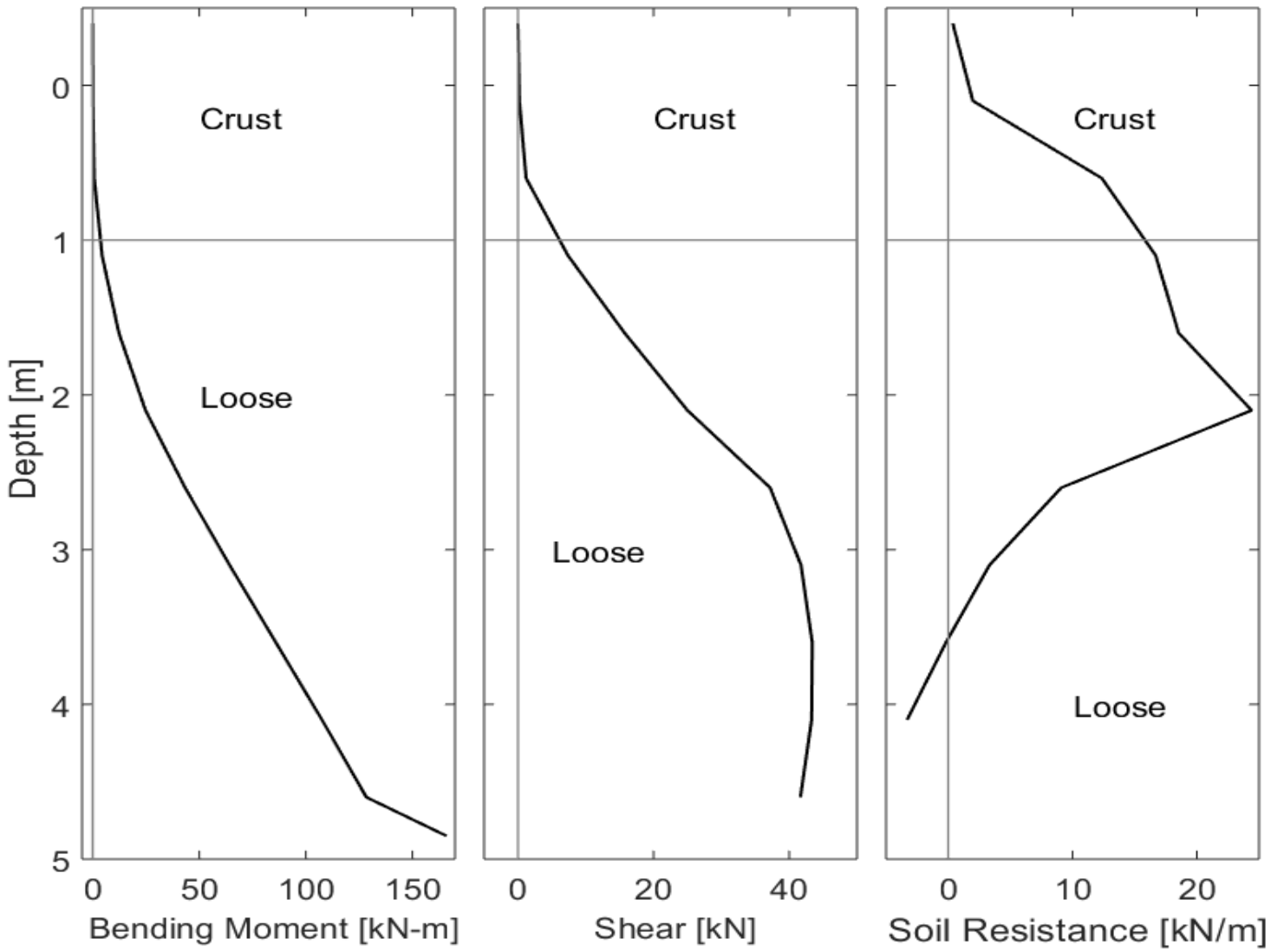

Figure 6-15. Stiff pile response profiles at 4.01 seconds (maximum time instant)

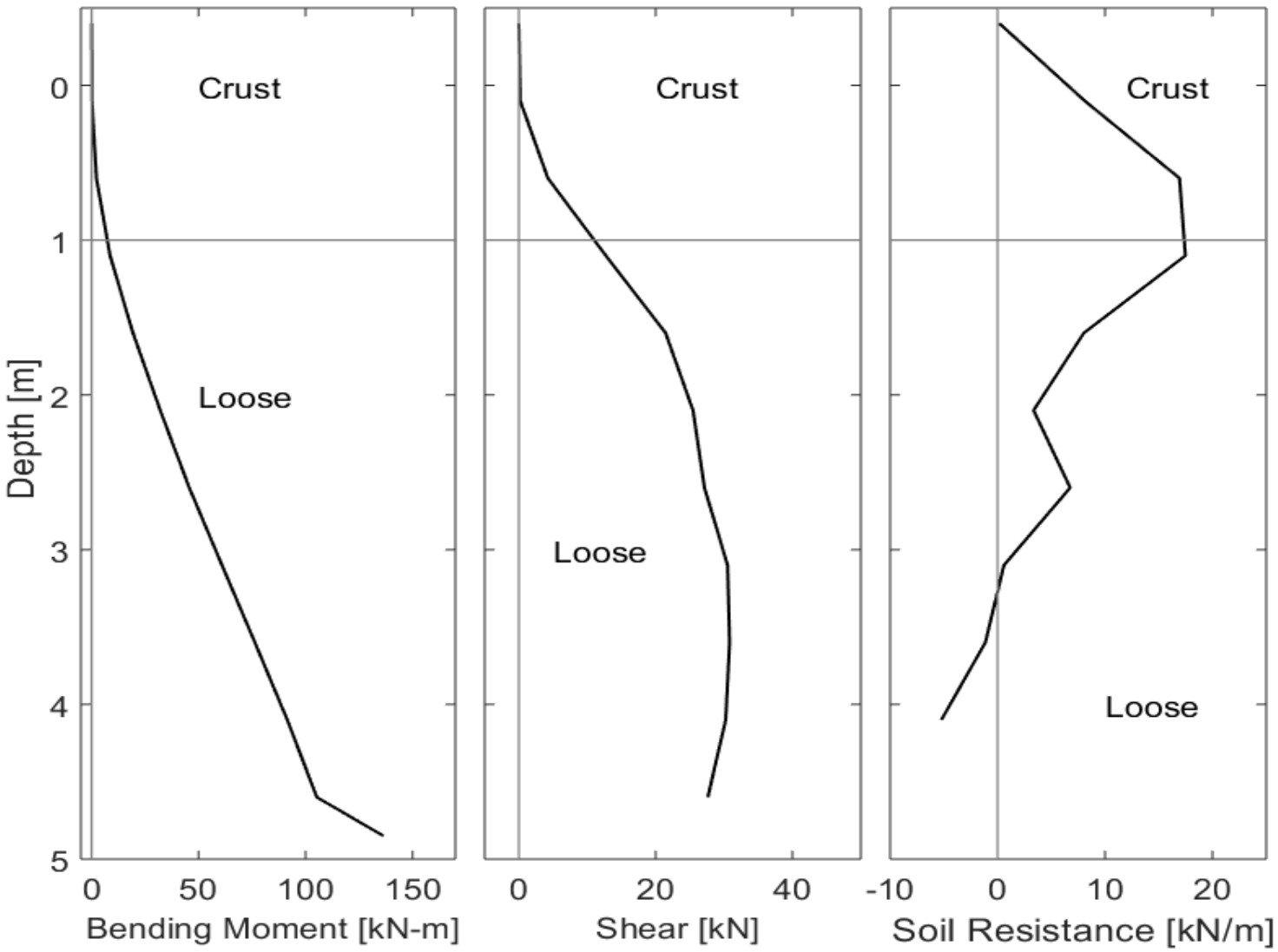

Figure 6-16. Stiff pile response profiles at 9.50 seconds

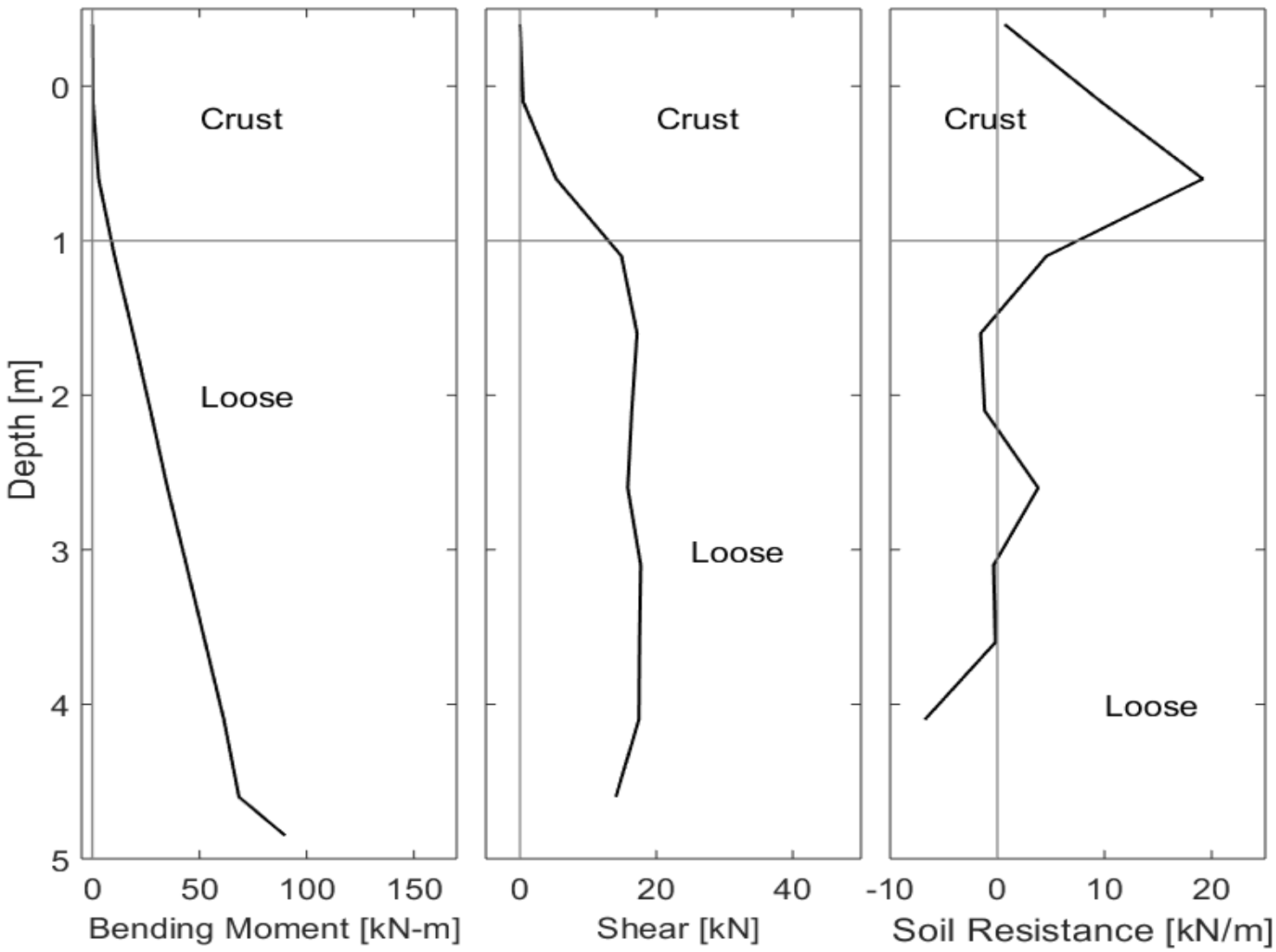

Figure 6-17. Stiff pile response profiles at 21.51 seconds

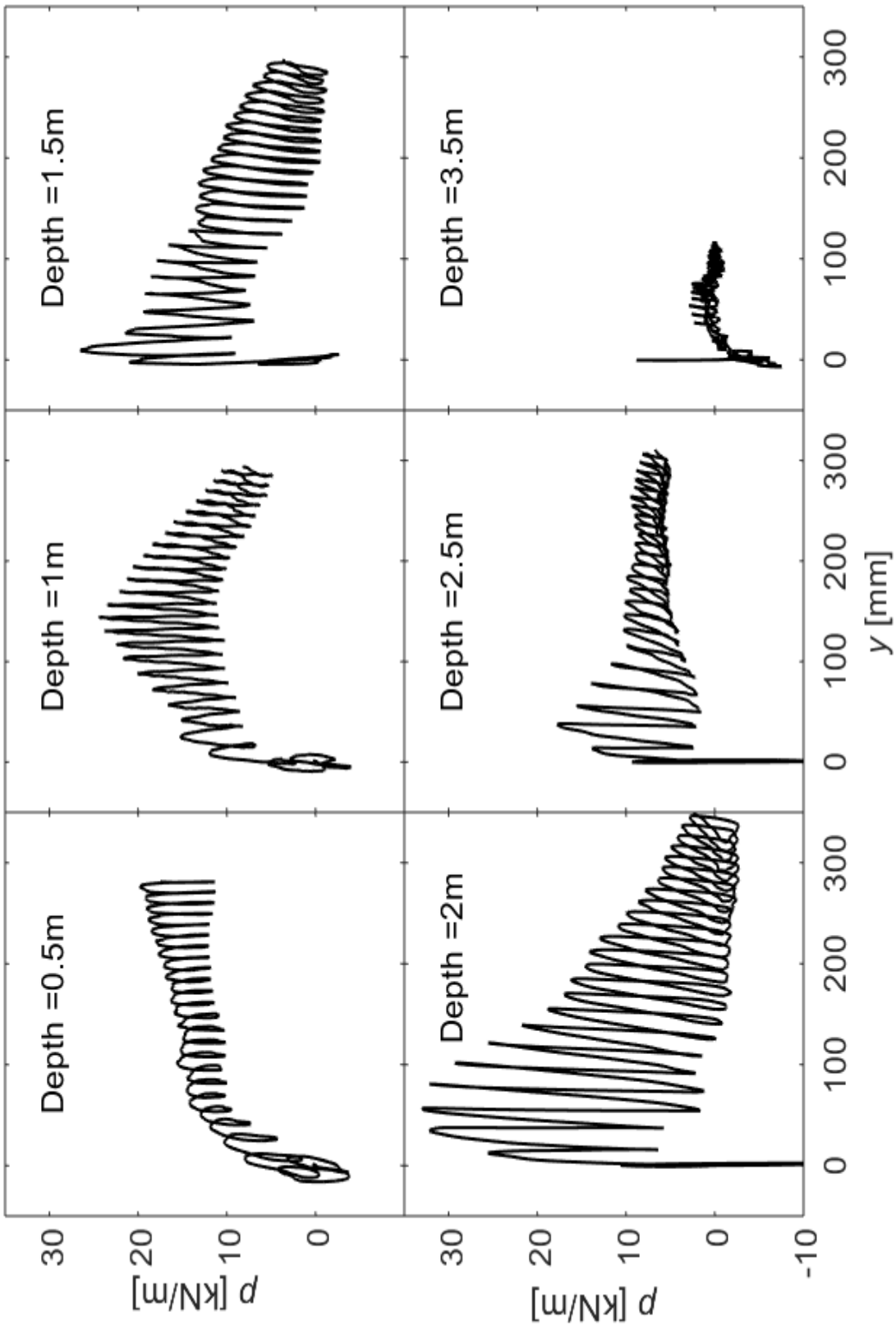

Figure 6-18. Experimental *p-y* curve response of the stiff pile

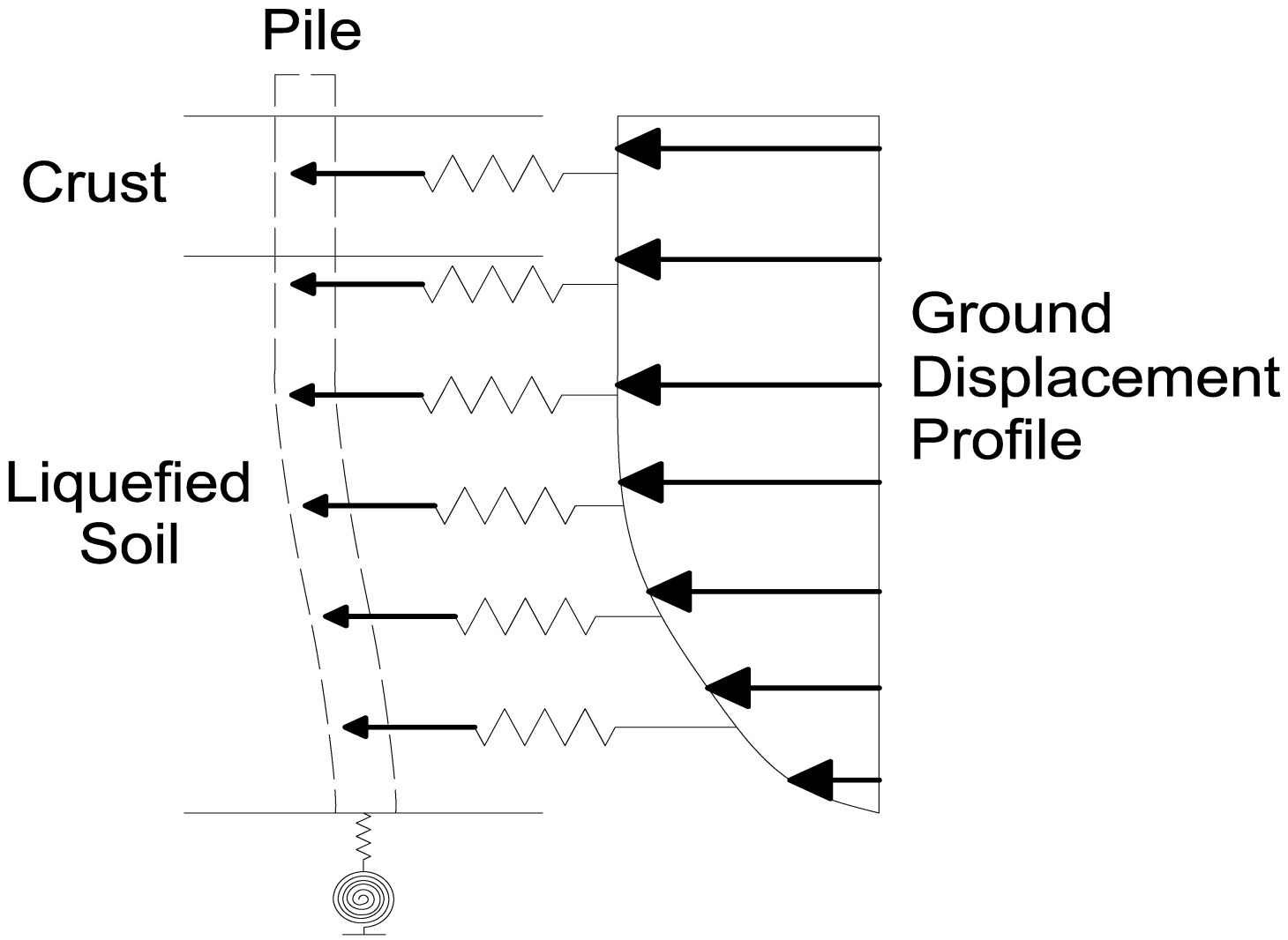

Figure 6-19. *p-y* lateral analysis mechanism of pile in the soil profile

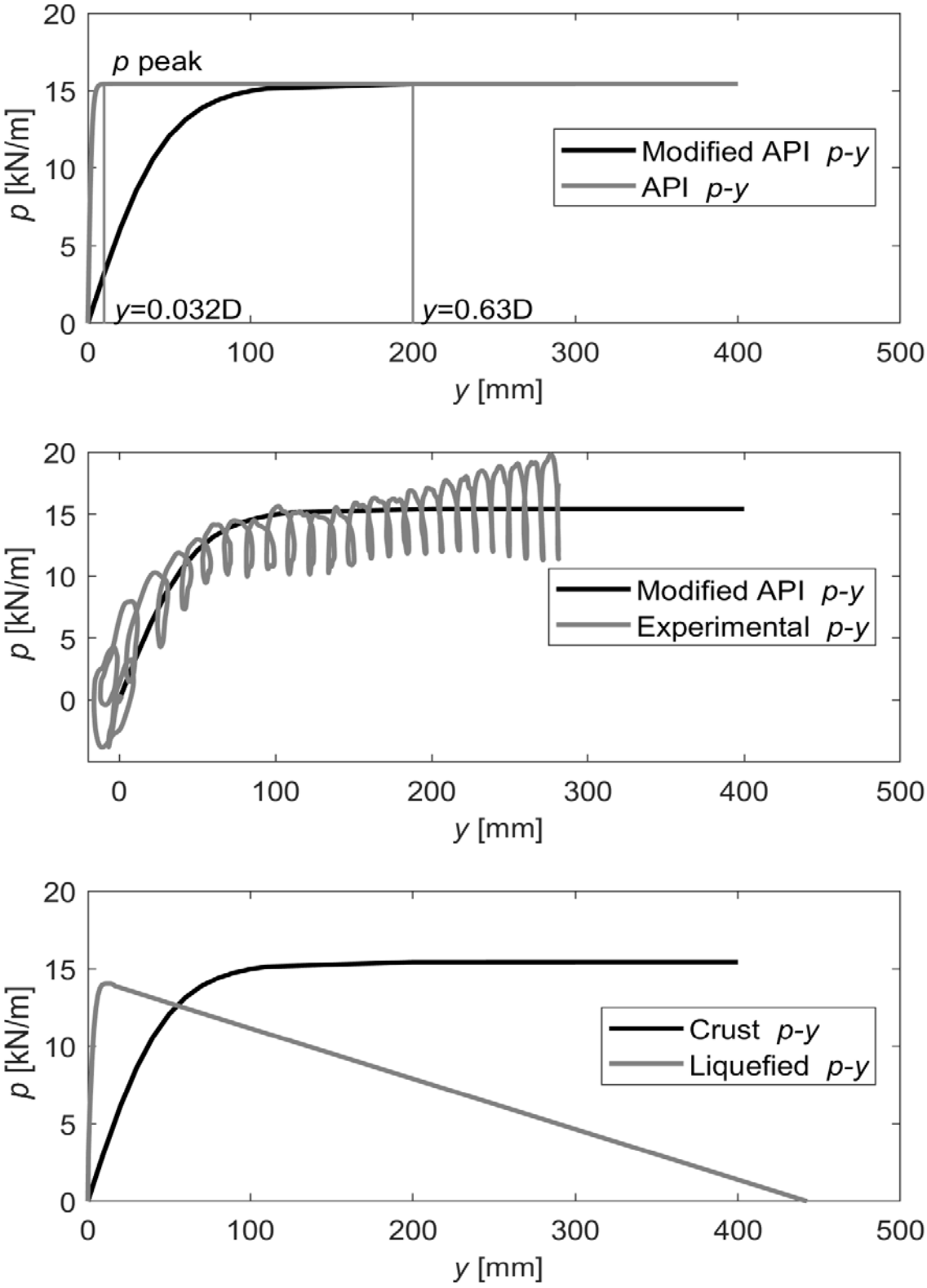

Figure 6-20. New proposed modified *p-y* curve for crust above liquefiable soil

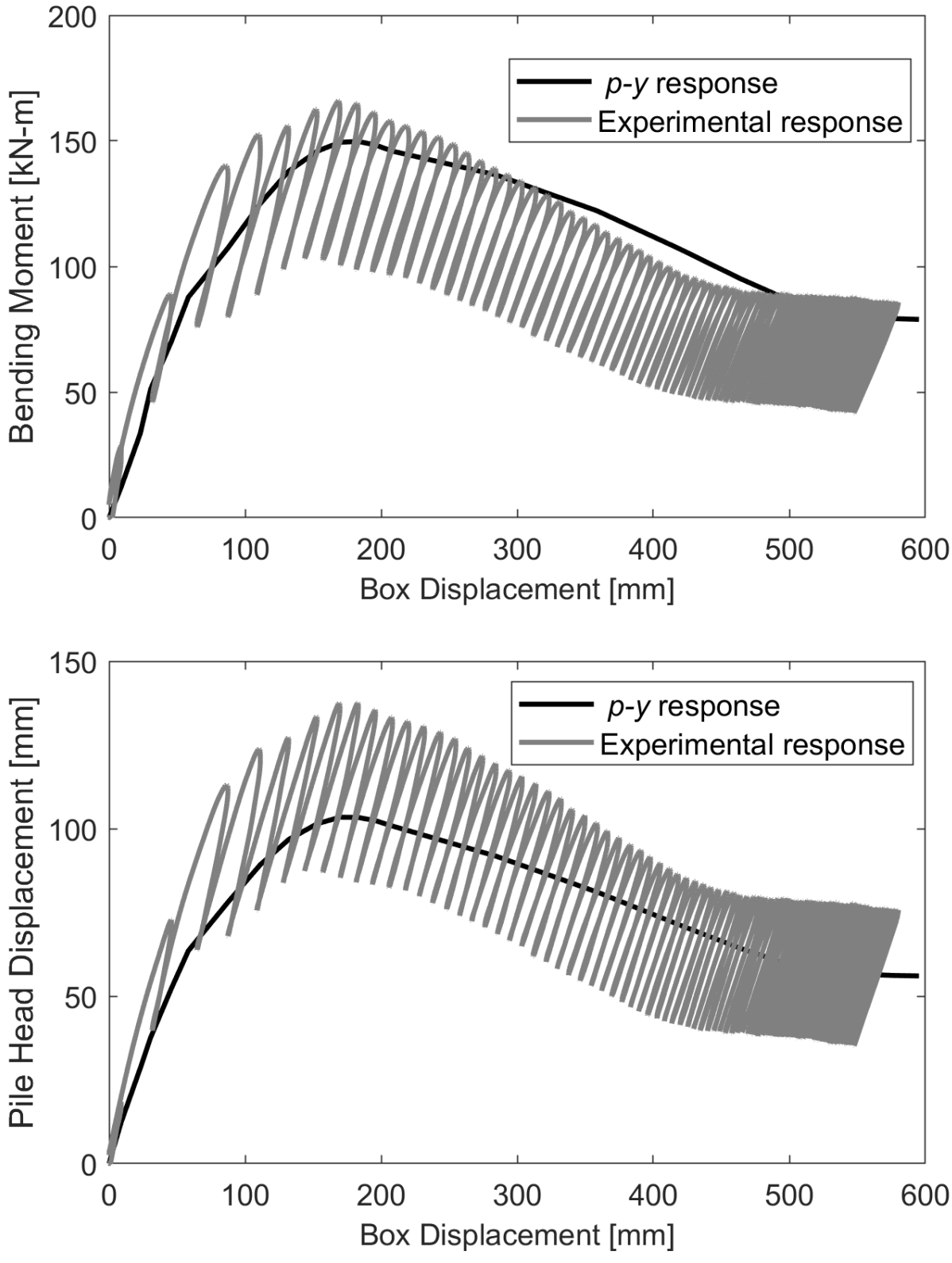

Figure 6-21. Comparison of stiff pile experimental and *p-y* curve response

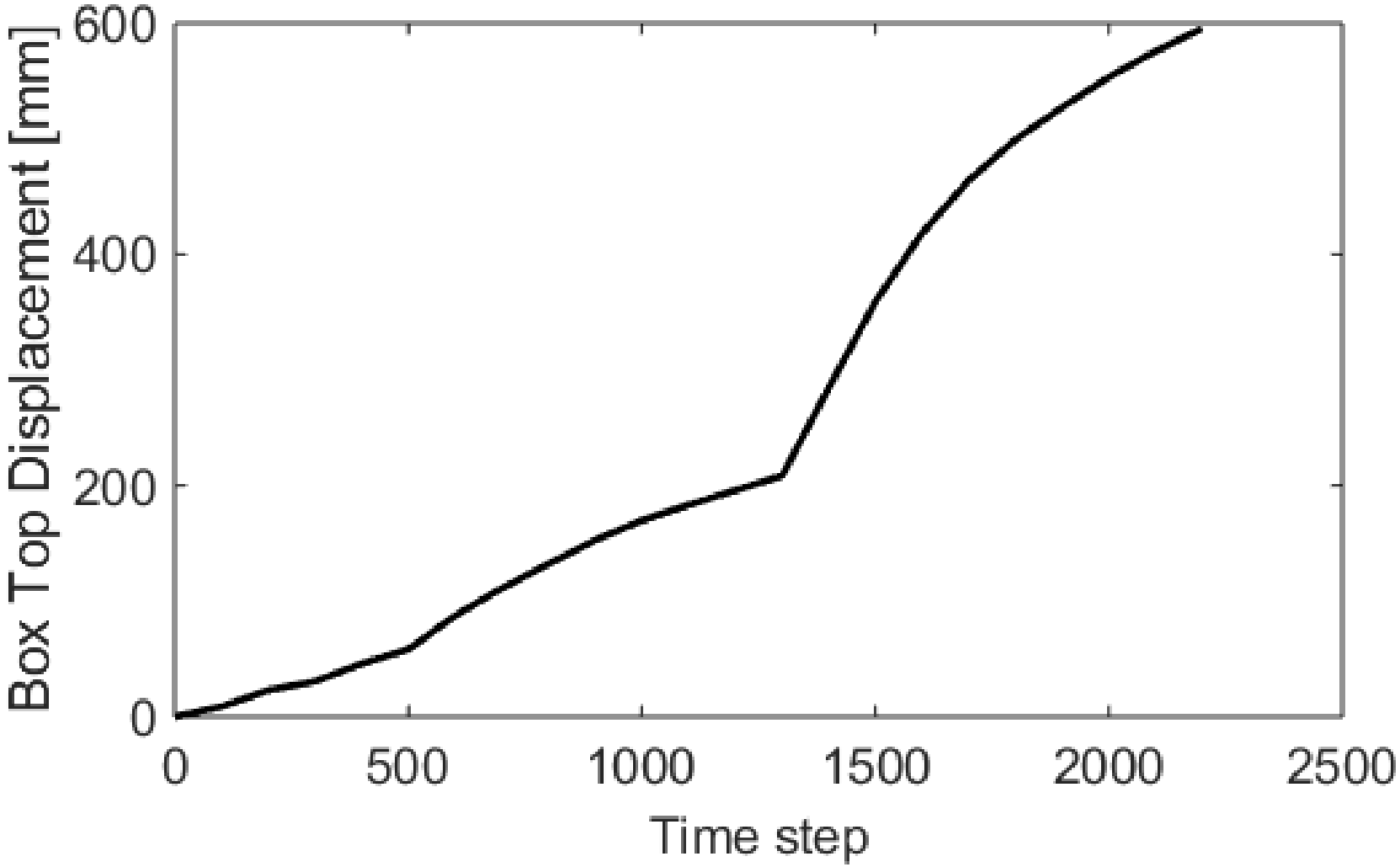

Figure 6-22. Imposed box top displacement time history in the *p-y* lateral model

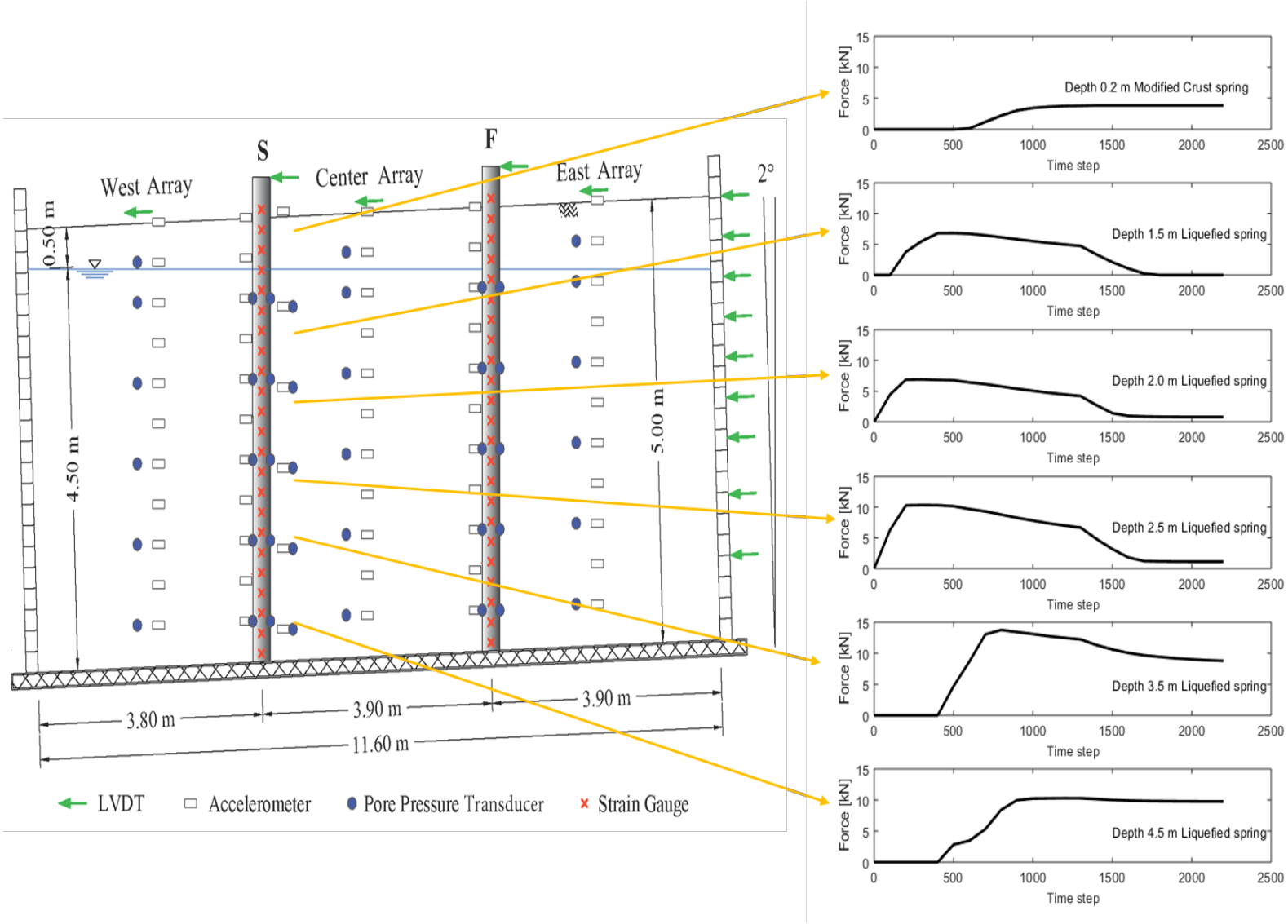

Figure 6-23. Resulting force time histories applied on the stiff pile from the *p-y* lateral analysis

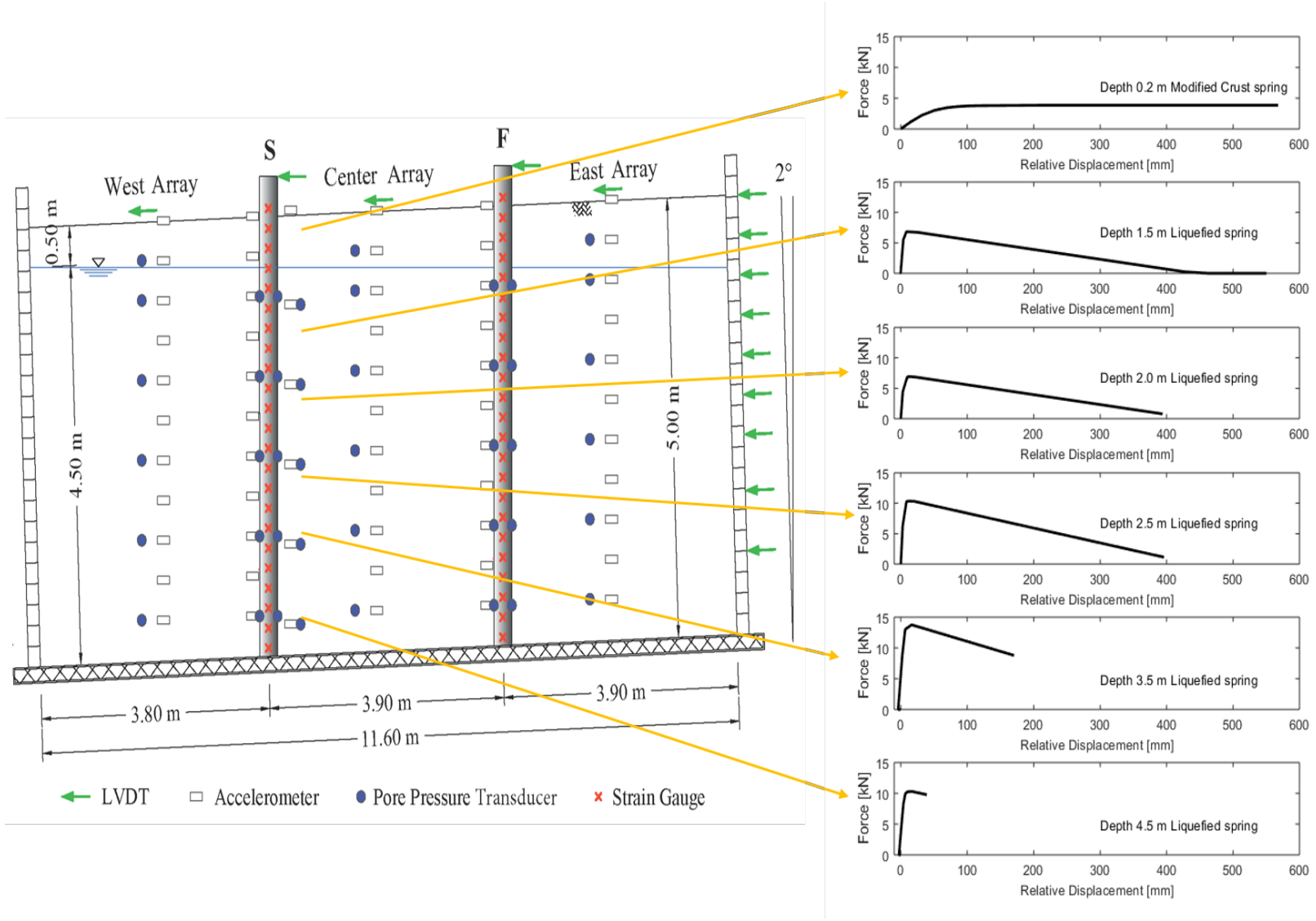

Figure 6-24. Resulting force-displacement response of the *p-y* curves

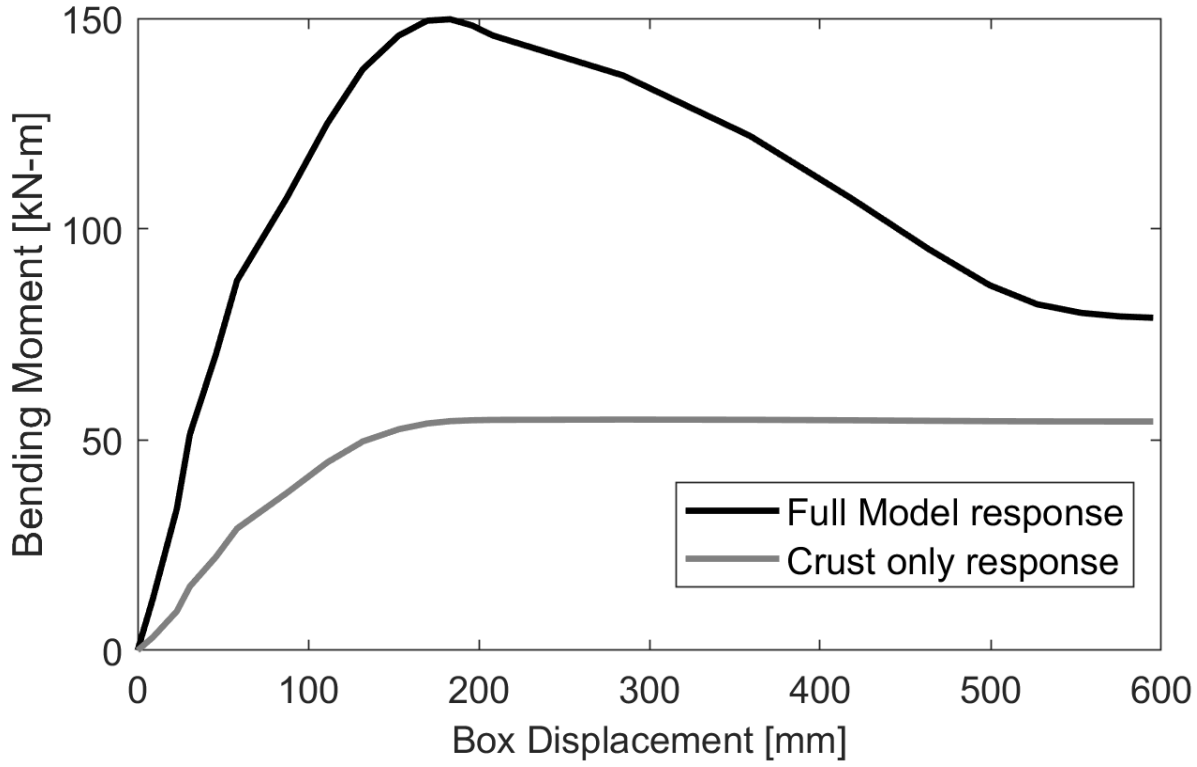

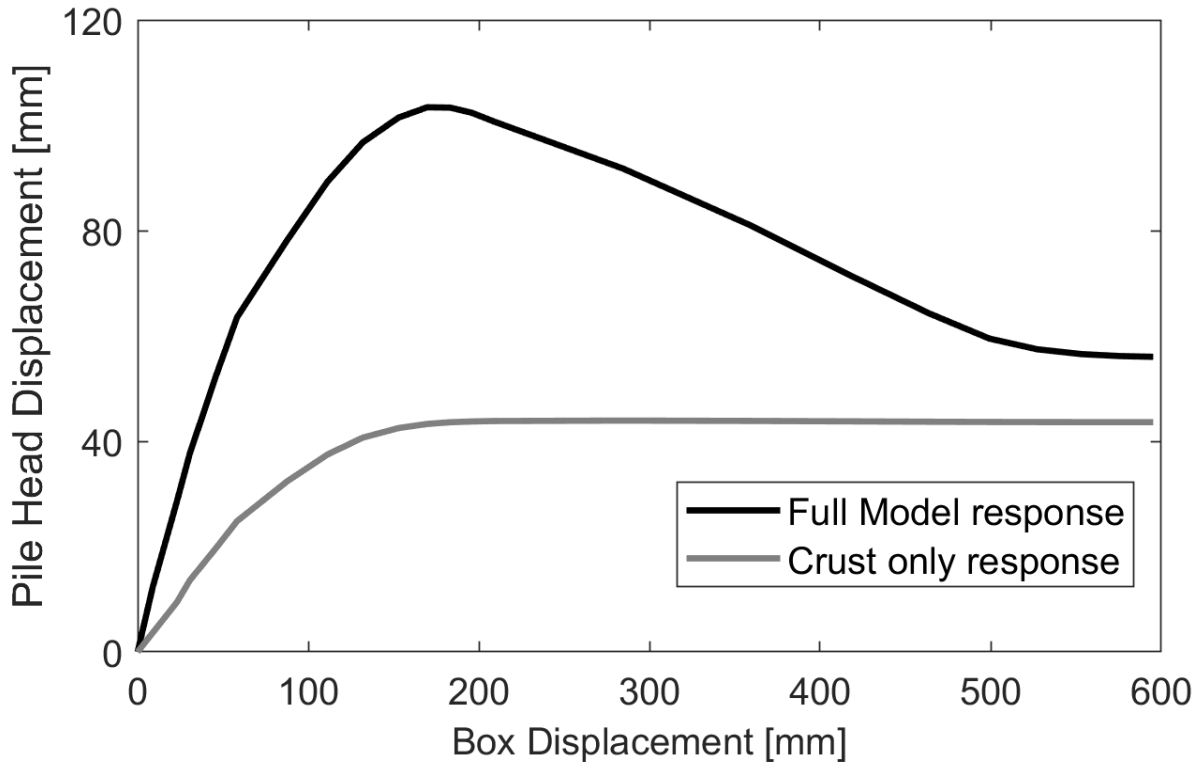

Figure 6-25. Comparison of stiff pile *p-y* curve response for the full model and crust only model without the liquefied soil

Chapter 7 Pile Response to Liquefaction-Induced Lateral Spreading and Influence of Ground Inclination

7.1. Abstract

Three large laminar-box 1-g shaking table experiments are conducted to document pile response, due to the mechanism of liquefaction-induced lateral spreading. A single steel pipe pile of 25 cm in diameter is tested in 2 different mildly inclined ground configurations. Two profiles of about 1.80 m in height are investigated, one with a liquefiable saturated sand stratum and the second with an added upper crust. The experimental setup, test procedures and test results are described in detail. The recorded data sets are analyzed collectively to document and track the evolution of lateral loading on the deployed configurations. Ground and pile lateral displacement as well as excess pore pressure are discussed. In this series, it is observed that lateral pressures from liquefiable soils might decrease with further shear strength reduction and deformation in the liquefied stratum. For each inclination, data is employed to compare and assess peak pile response and soil behavior pre- and post-liquefaction. Such a pile-ground interaction mechanism is of consequence for analyses that correlate pile bending moments to the accumulated lateral soil deformation.

Note: The second shaking for Tests 2 and 3 was the same and is used in this chapter to compare both tests.

7.2. Introduction

Pile response in laterally spreading ground is a subject of high interest among both practicing engineers and researchers (Finn 2015). A large number of foundation failures or damage were reported following each strong earthquake, as recently as Chile 2010 (Ramon

2012) and Christchurch 2011 (Cubrinovski *et al.* 2011). The observed damage patterns have been driving research to further clarify the mechanisms and update the design guidelines for embedded pile foundation systems.

Other case history investigations also document a wide range of damage to structures and underlying pile foundations during liquefaction and lateral spreading (Hamada 1992; Hamada and O'Rourke 1992; Ishihara 1997; Tokimatsu and Asaka 1998; Berrill *et al.* 2001). The observed damage and deformations were analyzed in order to enhance our understanding of the involved response mechanisms (Ishihara and Cubrinovski 1998; Ishihara and Cubrinovski 2004; Koyamada *et al.* 2006). Other investigators show that the relative stiffness between the pile and soil is important in predicting the failure modes (Martin and Chen 2005). They conclude that for stiff piles, the soil might eventually flow around the pile, while a more flexible pile might experience a reduced lateral load as it undergoes relatively large deformations. Field examinations have provided valuable insights that continue to refine the scope of necessary research (Ishihara and Cubrinovski 2004; Koyamada *et al.* 2006).

In recent years, physical modelling has emerged as a vital tool to study the laterally spreading mechanisms and its effect on pile foundation. Experimental studies were conducted by centrifuge tests (Dobry *et al.* 2003; Abdoun *et al.* 2003; Bhattacharya 2003; Brandenberg *et al.* 2005; 2007; Gonzalez *et al.* 2009; Knappett and Madabhushi 2009), large scale shake table experiments (Tokimatsu and Suzuki 2004; He 2005; Cubrinovski *et al.* 2006; Suzuki *et al.* 2008; Tokimatsu *et al.* 2007; Motamed *et al.* 2009; 2013; Ebeido *et al.* 2019) and full-scale controlled blast tests (Rollins *et al.* 2005; Ashford *et al.* 2006). Collectively, these studies have been the basis of enhancing our understanding of the mechanism and developing useful tools for calibration and load assessment.

Following up on the above efforts, a 1.80 m steel pile is employed in a 3-test experimentation series conducted at the University of California, San Diego. Recorded response time histories such as bending moments, displacements, and excess pore water pressures are discussed. Data from this test program are employed to assess the salient response of a fully saturated layer and the configuration with an added upper crust. Furthermore, a comparison is drawn between 2 different inclined models (at 2 and at 4 degrees). Finally, conclusions are drawn, and recommendations are presented.

7.3. Experimental Program

Figure 7-1 presents a schematic layout of the test series and laminar box located at the Powell Laboratory Shake table located at the University of California, San Diego. The response of a single steel pipe pile subjected to liquefaction-induced lateral spreading is explored. The laminar container composed of 28 stacked steel frames (Ashford and Jakrapiyanun 2001) with 16 cold steel rollers supporting each frame allowing for lateral movement and designed to give minimal boundary effects, simulates a 1D shear beam. The box was 3.90 m long, 1.80 m high and 1.80 m wide (inner dimensions) and was inclined at 2 and 4° to the horizontal in the different test setups (Table 7-1). A picture of the box including a top view after construction is shown in Figure 7-1. As noted by (Law and Lam 2001), this laminar configuration essentially simulates a periodic boundary condition. The container was lined with an Ethylene Propylene Diene Monomer (EPDM) rubber liner which was placed to hold soil and water in place.

7.4. Test 1 Soil Properties

A single layer soil profile (1.80 m high) shown in Figure 7-1a and Table 7-1 was constructed using Ottawa F-65 sand (Bastidas 2016) with the following grain size characteristics: D_{60} = 0.24 mm, fines content F_c = 0.25%, and uniformity coefficient C_u = 1.56. As such, this Sand

is poorly graded. The stratum was pluviated through soil meshes at a constant rate falling from a uniform height passing through water before settling. This ensures a relatively uniform loose deposit with the water breaking down clumped soil particles to release trapped air. The soil passed through about 40 cm of water before deposition. The dry soil was weighed before pluviation and the box volume was calculated. On this basis, estimated soil relative density for this layer was 20 % and saturated density was about 1900 kg/m^3 (Equivalent dry density is 1500 kg/m^3). The water table was set at the downslope ground surface (Figure 7-1a).

7.5. Test 2 and 3 Soil Properties

The soil profiles (1.80 m high) were 2-layered (Figure 7-1b and Table 7-1) constructed of the same soil. These tests included an upper non-liquefiable crust (0.70 m high). The bottom loose layer (1.10 m) was pluviated similar to the previous test, however with a reduced falling height and passing through 20 cm of water before deposition. Estimated soil relative density for this layer was 55 % and saturated density was about 1590 kg/m^3 (Equivalent dry density was 1950 kg/m^3). Next, the top 0.70 m layer referred to as crust was placed in 0.25 m lifts and compacted by a plate compactor. Achieved relative density was 85 % and bulk density was about 1817 kg/m^3 (Dry density before saturation was 1700 kg/m^3). Water table was 0.70 m below the ground surface at the pile location (box centerline).

7.6. Pile Properties

The circular steel pipe pile (Table 7-2) was 0.25 m in diameter and 3 mm in thickness. The pile was welded to a steel plate at the base then bolted to the box floor. Rotational and translational fixity were preferred for the base, however the connection flexibility allowed minimal rotation at the pile base. As such, this connection was tested and characterized to have a rotational flexibility of 670 kN-m/rad. Pile material is mild steel with 455 MPa yield strength and 2.1x10^5 MPa elastic

modulus. The theoretical yield moment is calculated based on yield stress and section modulus, estimated to be 66 kN-m. Moment curvature for the section was identified using the software OpenSees (Mazzoni *et al.* 2006). The yield curvature was identified as 0.016 rad/m. The pile remained elastic throughout the duration of the 3 tests in the series.

7.7. Instrumentation

The models were instrumented with a large number of accelerometers, pore pressure sensors, soil pressure transducers, strain gauges and LVDTs (Figure 7-1). Instrumentation was placed along the pile shaft and along the depth of the ground stratum. Strain gauges were densely deployed along the pile height to aid in back-calculation of the bending moment during shaking. The gauges, 40 in all, were placed on both sides of the pile at 10 cm spacing. A total of 9 displacement transducers were mounted on the laminar box exterior wall to measure lateral displacements, 2 on the soil surface to measure horizontal, and 2 to measure vertical displacements. The pile was also instrumented with transducers to measure pile head displacement above the ground surface. In addition, a total of 25 pore pressure transducers and 29 accelerometers were also placed in the model.

Figure 7-1 presents the distribution of these sensors along the pile and soil. In general, locations chosen for monitoring soil response were in the middle between the pile and box boundary in an effort to reduce the influence of boundary effects on the readings. For the upslope-downslope shaking direction, instrumentation was placed approximately 1 m away from the pile. In addition, in the perpendicular direction, instrumentation was 0.45 m away from the pile.

7.8. Analysis Protocol

Focus is placed on system response mainly discussing excess pore-water pressure, displacements and pile bending moments. Thus, representative time histories were chosen to

display this response. Bending moment was calculated based on strain gauge readings placed on the pile wall (Wilson *et al.* 2000). As such, bending moment is an indicator of lateral pressures acting on the pile. For ease of analysis, the time corresponding to the peak bending moment was identified and represented as a dashed line on all time history plots.

As the box was mildly inclined, the soil started moving downslope due to liquefaction of the loose saturated layer. In all tests, only the soil exhibited permanent displacements, while the pile head had no detectable residual displacements.

In the following sections, the single loose stratum test is discussed with the salient response characteristics highlighted. The test is then compared with its counterpart with the added crust, to characterize the effect of the non-liquefiable layer. Finally, the 2 tests with different inclinations are compared to assess the effect of the increased slope.

7.9. Test 1 Results

Input motion for Test 1 (2°) shown in Figure 7-2 was in the form of a sinusoidal acceleration with a 2 Hz frequency and 0.15g peak amplitude. Duration of motion was 24 cycles with constant amplitude. Due to the imparted base excitation, asymmetric accelerations with amplitude reduction (Figure 7-2) are observed along the height. Excess pore pressure ratio (r_u) presented in Figure 7-2 shows a representative trend of the response in both the upslope and downslope arrays on either side of the pile. Response shows rapid pore pressure build up reaching liquefaction ($r_u = 1$) in 1 shaking cycle. Liquefaction appears to occur simultaneously along the layer height. Dips in the excess pore pressure for the upslope array are seen to be somewhat larger than the downslope array. This can be attributed to soil attempting to dilate as it flows around the pile. The vertical line in this figure denotes the time corresponding to the instant of maximum pile bending moment as will be shown below (Figure 7-3), occurring at about 1.5 seconds (about 2

shaking cycles). Maximum moment occurred 1 cycle after liquefaction near the base of the container.

Figure 7-3 shows the downslope deformation of the soil box top frame and single pile head for Test 1. Results show an increase of ground surface displacement with shaking and a resulting accumulated permanent value. Deformations started with shaking and stopped thereafter. Maximum pile head displacement was 11 mm occurring at the same instant as the peak bending moment (Figure 7-3). Soil surface displacement at peak instant was 66 mm with the soil surface continuing to accumulate displacement throughout the shaking event. Permanent soil deformation was about 306 mm, as the box continued to displace downslope, the pile head rebounded with small oscillations around the original position. There was no permanent pile head displacement at the end of shaking. Evolution of soil profile deformation is presented in Figure 7-4. The deformed pattern is parabolic in shape as previously discussed (Chapter 6) and indicates higher shear strains near the layer base.

As mentioned earlier, peak bending moment was observed early during the shaking phase, right after soil liquefaction (Figure 7-3). Maximum bending moment recorded was 4.4 kN-m occurring in the second shaking cycle. Bending moment recorded in the first peak was close to the maximum (4 kN-m). After maximum moment, gradually decreasing oscillations of the recorded values are observed. At the end of shaking, pile rebounded to a zero-displacement position with a very low residual bending moment (1 kN-m). Peaks in bending moment are seen to correspond to the excess pore pressure transient drops, denoting coincidence with the cyclic large shear strain excursions (Zeghal and Elgamal 1994).

Recorded vertical settlements are presented in Figure 7-5 at both upslope and downslope locations. Settlements started with shaking with high rates and continued throughout at reduced

rates. Upslope readings reached about 60 mm and were much higher compared to those of the downslope. The downslope sensor even recorded the start of soil heaving halfway through shaking. The difference between readings at the end of shaking represents a 2-degree slope correction, thus making a horizontal surface post shaking. Figure 7-6 presents the displaced box shape after shaking with the parabolic deformed shape shown and a picture of the soil surface after it settled, and water rose to cover the entire ground.

7.10. Test 1 *p-y* Analysis

The *p-y* curve recommended in Chapter 5 for liquefied soil is employed. The curve was constructed based on the suggested formulation (Figure 7-7). It shows high initial stiffness followed by a post peak softening as liquefaction and downslope deformation continues. The *p-y* curve was employed in a pile lateral analysis model using OpenSees accounting for the pile properties and base rotational stiffness. Figure 7-8 compares the experimental and *p-y* results for the bending moment and pile head displacement against the box displacement. Results show general agreement and satisfactory performance. The *p-y* curve matched the initial experimental slope, peak values and degradation. Experimental results show a second peak followed by a somewhat sudden drop that the spring was not able to match.

7.11. Results for Test 2 and 3

Input motion (Figure 7-9) was a 17 second 2 Hz sinusoidal wave with gradual increase and decrease in amplitude for Test 2 and 15 seconds for Test 3. Liquefaction occurred early on, approximately 5.25 seconds into the shaking phase. Representative time history of excess pore pressure ratio (Figure 7-9) clearly displays this mechanism. The vertical line in these figures denotes the time corresponding to the instant of maximum pile bending moment as will be shown below, occurring at about 5.11 seconds for Test 2 (2°) and 3.12 seconds for Test 3 (4°) and is

included on all time histories for ease of tracking. Maximum moment occurred before liquefaction for both tests at an excess pore pressure ratio of about r_u= 0.95 for Test 2 and r_u= 0.70 for Test 3.

The general trend of the pore pressure data displays rapid pore pressure build up with instantaneous reductions for both downslope and upslope readings. There is some dilative tendency in the liquefied soil response. Dips in excess pore pressure for Test 3 are seen to be somewhat larger than those of Test 2 (Figure 7-9). This can be attributed to influence of the increased static driving shear stress in the 4° Test 3, compared to those of the 2° Test 2.

Figure 7-10 shows downslope deformation for the soil box, and single pile for Tests 2 and 3 respectively. Both tests show an increase of ground surface displacement with shaking and a resulting accumulated permanent value. Deformations started with shaking and stopped thereafter.

In light of the acting initial driving shear stress, it is seen that Test 3 incurred a significantly higher level of deformation earlier during the shaking phase (Figure 7-10). Of interest as well is that the instant of peak pile moment coincided approximately with the same level of ground deformation in both experiments (about 30 mm).

As shaking started, the pile began to oscillate back and forth recording its highest value at the time of maximum bending moment. Values close to maximum displacement were reached before liquefaction, oscillating thereafter around a constant but slightly lower value. Pile head displacement gradually decreased with the ramping down of the input acceleration reaching essentially zero at the end of the shaking event.

Maximum pile head displacement was 16.6 mm and 29.2 mm for Tests 2 and 3 respectively. This shows a 76 % increase in pile head displacement as the inclination changed from 2 to 4 degrees. On the other hand, accumulated ground surface displacement was 19.1 mm and 30.1 mm for Tests 2 and 3 displaying an increase of about 60 %. The final ground deformation

was not the maximum incurred as shown by the displacement profiles presented in Figure 7-11. Peak surface deformation was about 45 mm in both tests. The end of shaking accumulated displacement showed a reduction of 55 % and 33 % for Tests 2 and 3 respectively. Deformation profile is parabolic in shape similar to Test 1 and shows negligible strains in the upper crust.

Figure 7-10 shows representative time histories of bending moment along the pile shaft. The location chosen was at the base of the pile where the maximum values were recorded. Peaks in bending moment are seen to correspond to the excess pore pressure transient drops, denoting coincidence with the cyclic large shear strain excursions (Zeghal and Elgamal 1994).

As mentioned earlier, peak bending moment was observed early during the shaking phase, before soil liquefaction (Figure 7-9). After maximum moment was reached, both tests show oscillation around a constant slightly lower value, gradually decreasing as the shaking was ramped down (Figure 7-10). At the end of shaking, both piles rebounded to an almost zero position. As such, pile response was linear elastic.

Figure 7-10 demonstrates that soil keeps on moving, after maximum pile response, with no appreciable further pile load as the ground displacement continues to accumulate. As such, there is no correlation between the final accumulated ground deformation and the observed peak load on the pile. Brandenberg *et al.* (2005, 2007) provide further details about the involved dry crust lateral loading mechanism.

Maximum bending moment recorded for Test 2 was 8 kN-m and 13 kN-m for Test 3 as shown in Figure 7-10. Therefore, the difference in inclination caused the pile to incur an additional bending moment of about 60 %. Furthermore, maximum response occurred much earlier in the higher 4° inclination test (at 3.12 s) rather than at 5.11 s for the 2° experiment. This suggests that the higher inclination caused earlier mobilization of soil movement, just due to driving static shear

stress increase, but well before the onset of liquefaction.

Total pressure time histories measured by transducers on both sides of the pile for Test 2 are presented in Figure 7-12 (magnitude of peak values might be affected by impacts between soil and pile during cyclic deformation). Soil pressures from the upper crust are as high as 75 kPa on the upslope side while the downslope shows little resistance (20 kPa) due to the soil moving away from the pile. The interface region between the crust and the underlying liquefying soil recorded the highest upslope pressure (about 100 kPa) with some resistance to the pile movement on the downslope side. The liquified soil experienced similar values on both sides (15 kPa) giving a negligible resultant pressure value. The dashed line on the figure corresponds to the maximum bending moment instant for this test right before liquefaction. The highest pressures are observed to occur before the soil liquefied.

Settlement time histories for both tests are presented in Figure 7-13. The upslope side of the box experienced more vertical deformation than the downslope, due to the slope correction. Differential settlement was not enough to level the slope as in Test 1. The 4° test resulted in about 50% lower settlement than the 2° test. For completeness, it is important to note that the settlement results might have some discrepancies and closer examination is suggested. Cracking of the upslope soil heaving behind the pile and a gap forming downslope was observed after shaking (Figure 7-13).

7.12. Effect of the Upper Non-Liquefied Crust

The upper crust had a detrimental effect on the embedded pile, inducing 60% of additional bending moment at the pile base. The observed total pressures for Test 2 (Figure 7-12) at the upper non-liquefied locations were much higher than those for the liquefied stratum.

A crust binding mechanism was in effect, closely tying ground deformations to those of the embedded pile. Comparing Tests 1 and 2, a) pile displacements and moments were higher by approximately 60 %, b) more constrained by resistance of the foundation to crust movement, overall soil displacement was significantly lower, c) final accumulated soil deformation for tests containing a crust were lower than the observed maximum values during shaking.

7.13. Conclusions

A large scale 1-g shaking table test series was performed at University of California, San Diego to study pile foundation response during liquefaction-induced lateral spreading. Tests had different inclinations and soil profiles. The models built are described along with the dense instrumentation used, and the construction methodology is discussed. Sinusoidal input motions were chosen for the testing program.

General observations include:

- The pile displayed stiff behavior as evident from the large cyclic response then settling at zero displacement at the end. This indicates the soil flowing around the pile.
- Large recorded settlements in all tests.
- Test 1 with lower relative density liquefied much faster than the other.
- The general deformed shape for the liquefied layer is curved (parabolic) with highest strains near the base.
- Total pressure values where about double the passive pressure in the crust layer.

Some select findings from the results of Test 1:

- Liquefaction occurred rather early in the shaking phase (in 1 shaking cycle).
- Peak bending moments were noted quite early in the shaking phase (2 cycles) near container base. Accumulation of lateral spreading due to downslope deformation showed

decrease in pile displacement and bending moment. The pile shows a stiff behavior as evident from the large cyclic response then settling at zero displacement at the end. This indicates the soil flowing around the pile with no acting pressures.

- Maximum bending moment value (4.4 kN-m) is much lower than expected from conventional soil spring analyses. Maximum value occurred at 66 mm of soil surface displacement with pile head displacement at 11 mm (17% of soil deformation). Soil surface deformation continued to reach approximately 5 times the recorded value at peak instant.
- The employed *p-y* curve models the test results well and manages to capture the initial loading slope, peak values and softening response.

Some select findings from the results of Test 2 and 3:

- Values approaching peak bending moment were noted quite early in the shaking phase before liquefaction. Increased lateral spreading due to the continued soil downslope deformation, did not result in appreciable increase in pile displacements or moments.
- As the driving static shear stress increases (with increased inclination), it is likely that peak moment will be higher and occur earlier, with excess pore pressures that might be well below those corresponding to the onset of liquefaction.

7.14. Acknowledgements

Chapter 7, in part, is currently has been submitted for publication of the material as it may appear in the following conference publication (The dissertation author was the primary investigator and author of this paper):

Ebeido, A. and Elgamal, A., (Manuscript accepted, 2019). "Assessment of Seismic Behavior of Deep Foundations from Large‐Scale Liquefaction Shake Table Experiments". Proc. of the 7

ICEGE, International conference on earthquake geotechnical engineering. Rome, Italy. 17-20 June.

Chapter 7, in part, is a reprint of material as it appears in the following conference publication (The dissertation author was the primary investigator and author of this paper):

Ebeido, A., Elgamal, A., and Zayed, M., (2018). "Pile response during liquefaction-induced lateral spreading: 1-g shake table tests with different ground inclination". Proc. 9th international conference on Physical Modelling in Geotechnics. City, University of London. 17-20 July.

Chapter 7, in part, is a reprint of material as it appears in the following conference publication (The dissertation author was the primary investigator and author of this paper):

Ebeido, A., Elgamal, A., and Zayed, M. (2019). "Large Scale liquefaction-induced lateral spreading shake table testing at the University of California San Diego". Proc. of the 8th International Conference on Case Histories in Geotechnical Engineering. Philadelphia, Pennsylvania. 24-27 March.

Table 7-1. Soil Profile Properties

Property	Test 1 (2°)	Test 2 (2°) & Test 3 (4°)	
Water/soil condition	Fully saturated single layer	Fully saturated bottom layer	Relatively dry top layer
Thickness (m)	1.80	1.10	0.70
γ_{bulk} (kg/m^3)	1900	1950	1817
γ_{dry} (kg/m^3)	1500	1590	1730
Relative density (%)	20	55	85

Table 7-2. Steel Pile Properties

Steel Grade	A53B
Pipe Outer Diameter (m)	0.254
Pipe Thickness (mm)	3.05
Elastic Modulus (kPa)	2.0×10^8
Yield Strength (kPa)	4.55×10^5

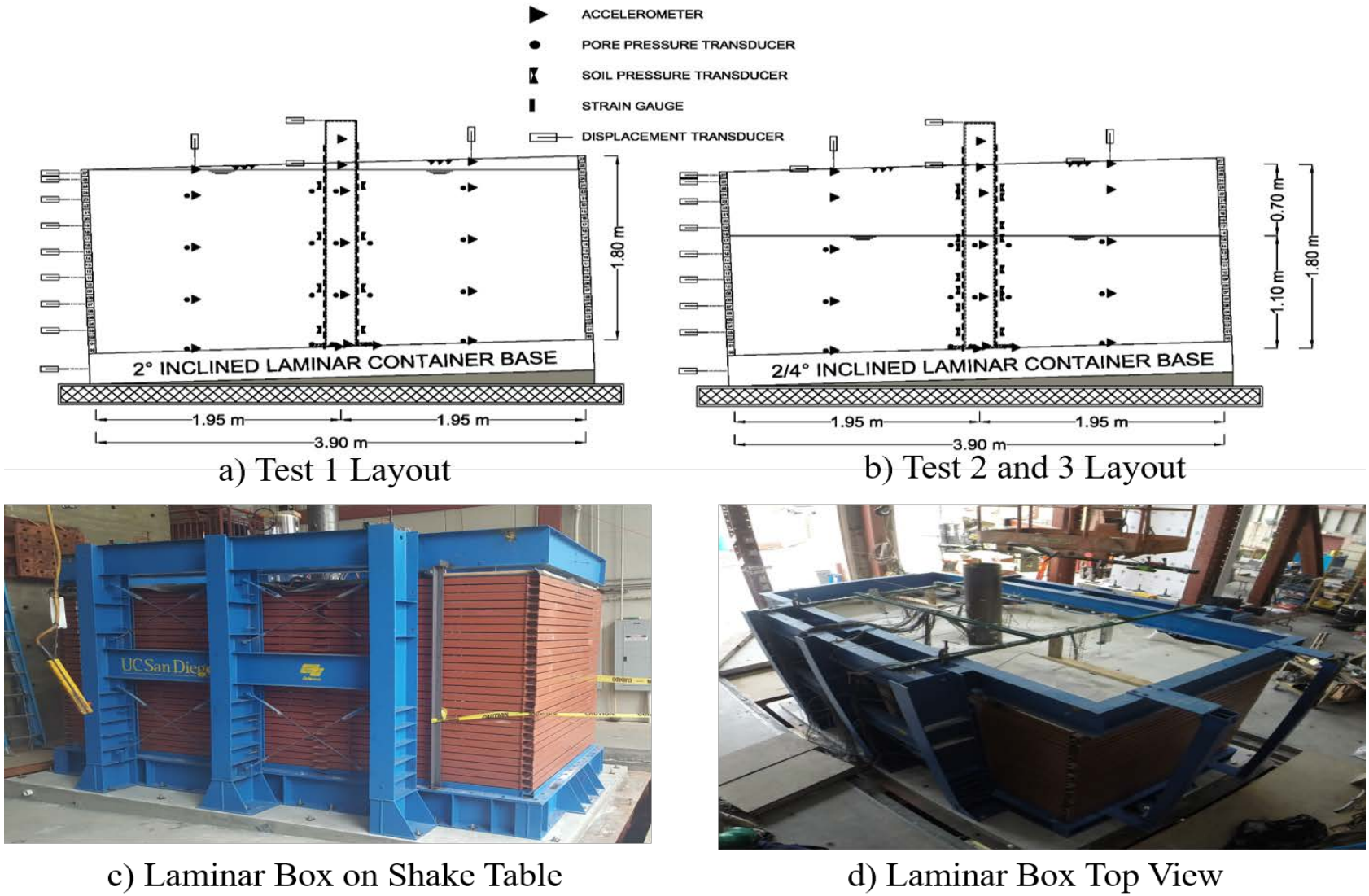

Figure 7-1. Schematic test layouts and model setup before shaking

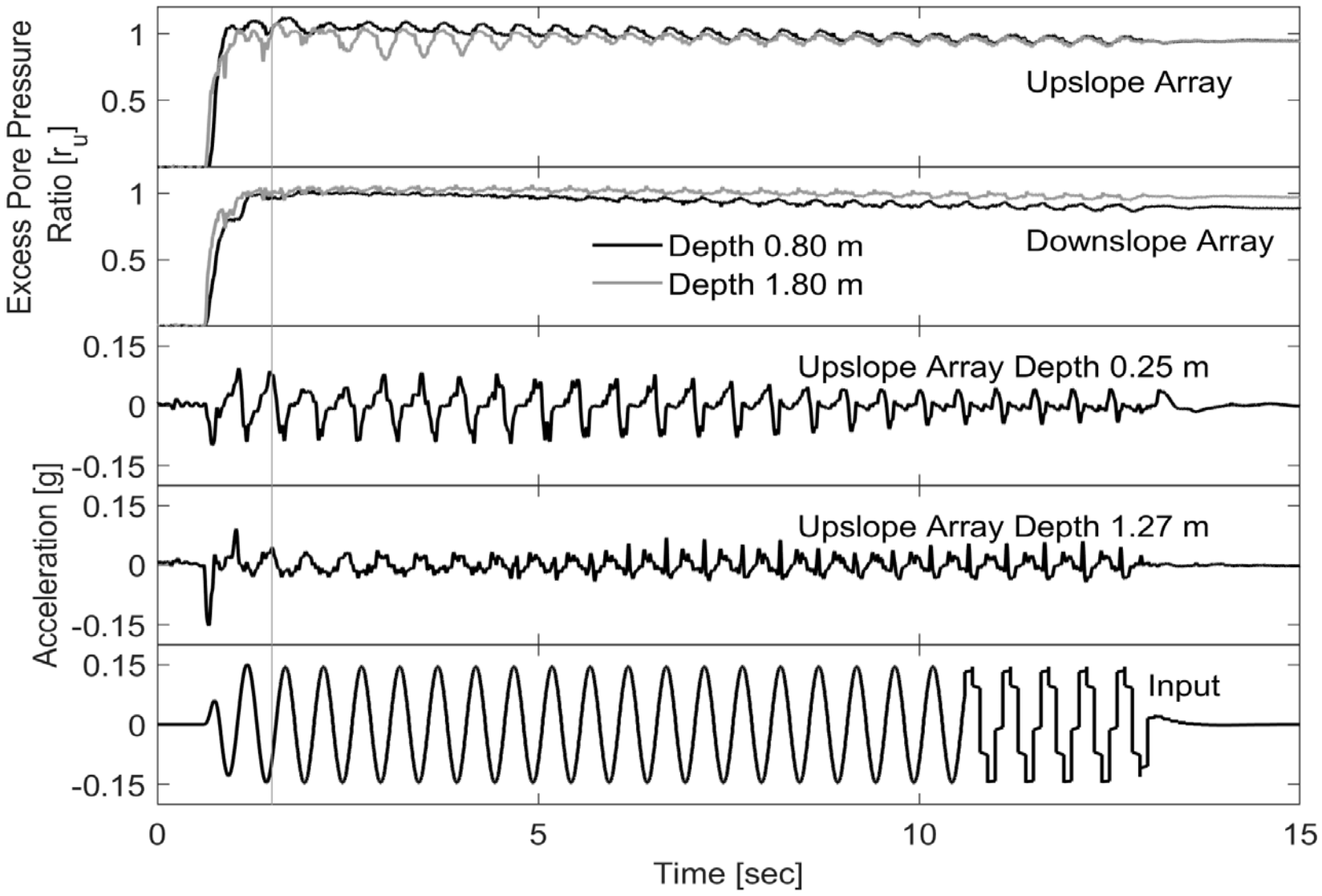

Figure 7-2. Test 1 acceleration and excess pore water pressure time histories

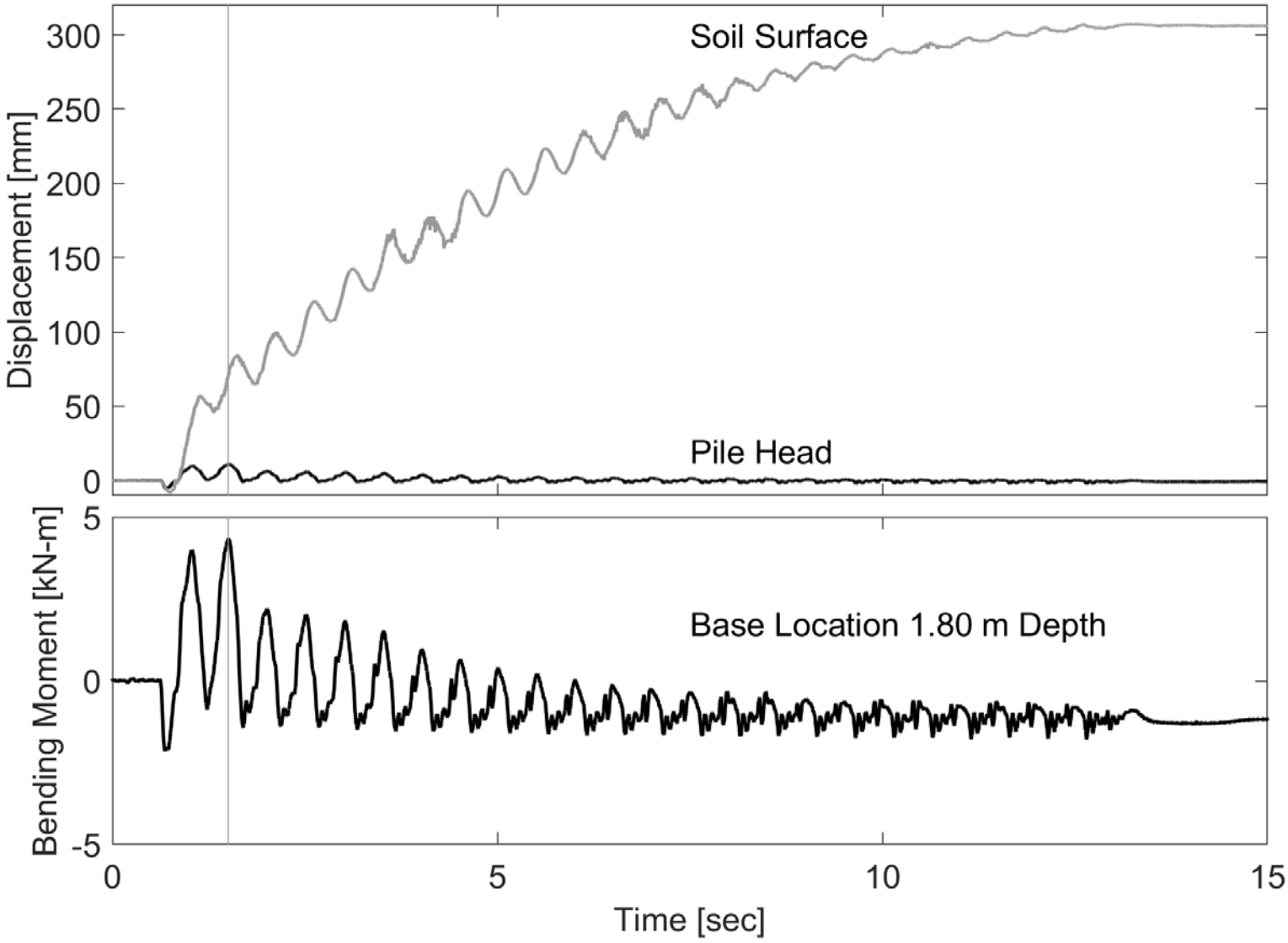

Figure 7-3. Displacement and base bending moment time histories for Test 1

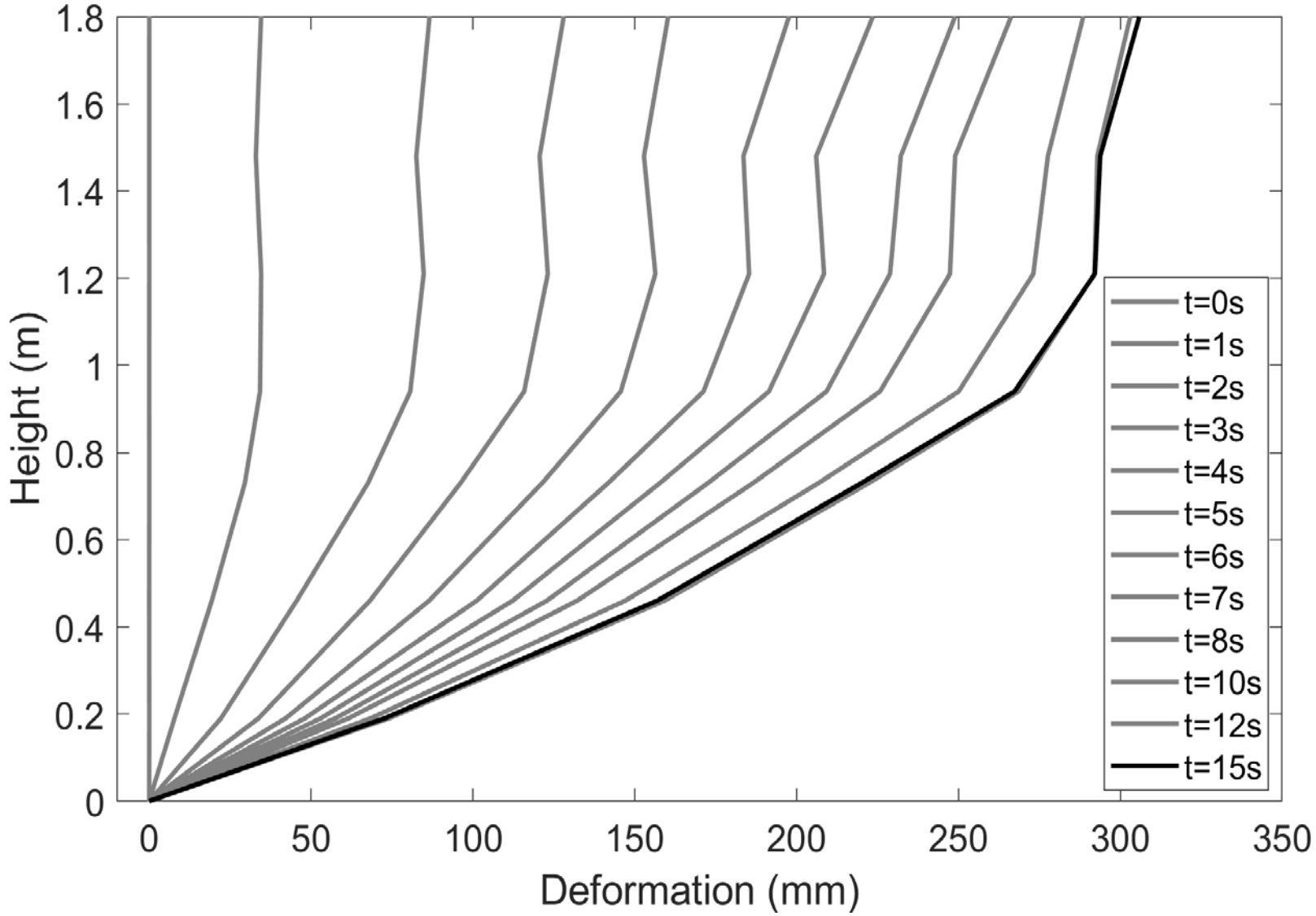

Figure 7-4. Test 1 evolution of deformation profile with shaking

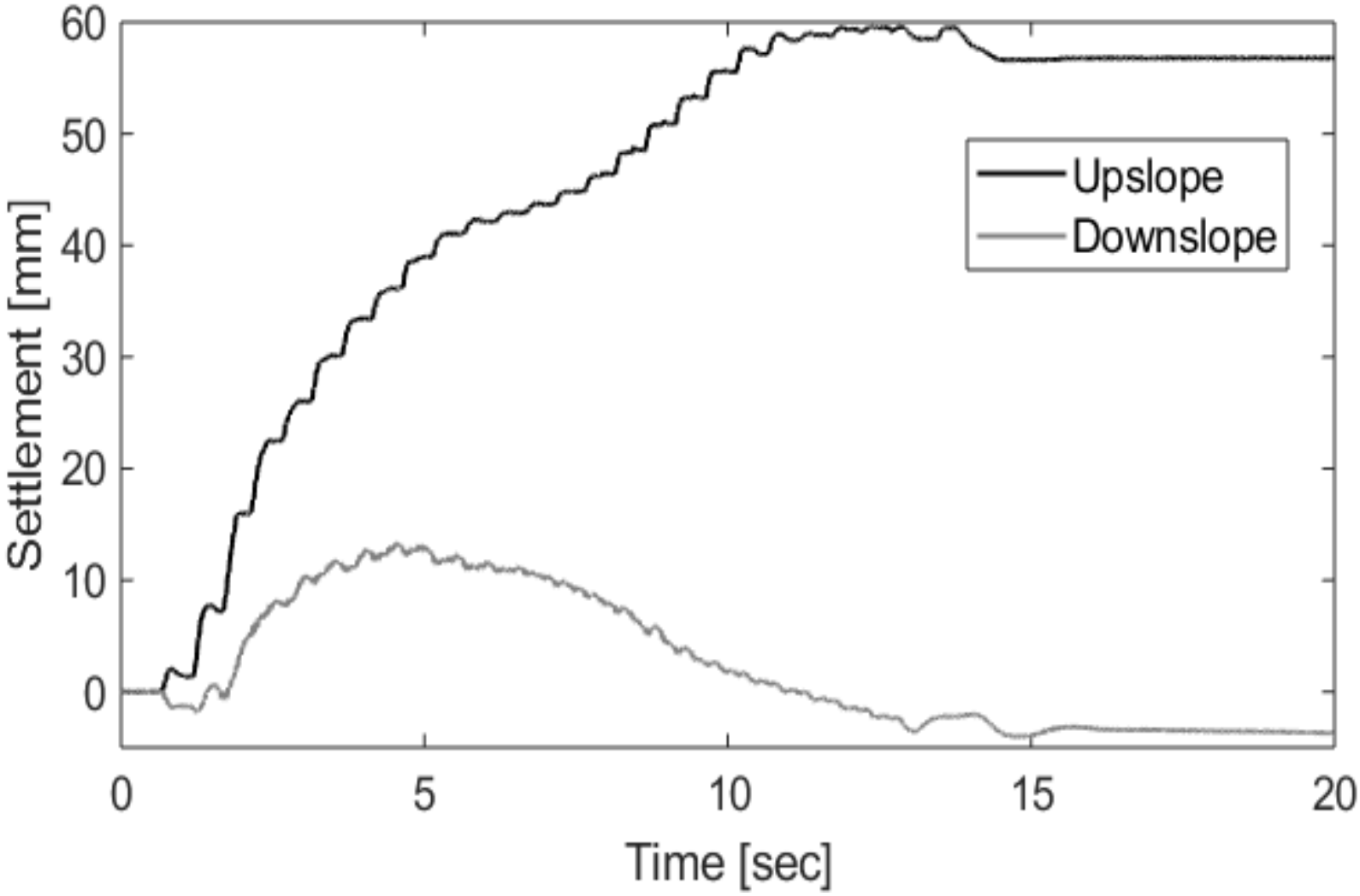

Figure 7-5. Surface settlement time history for Test 1

Figure 7-6. Soil box deformed shape and soil surface after shaking in Test 1

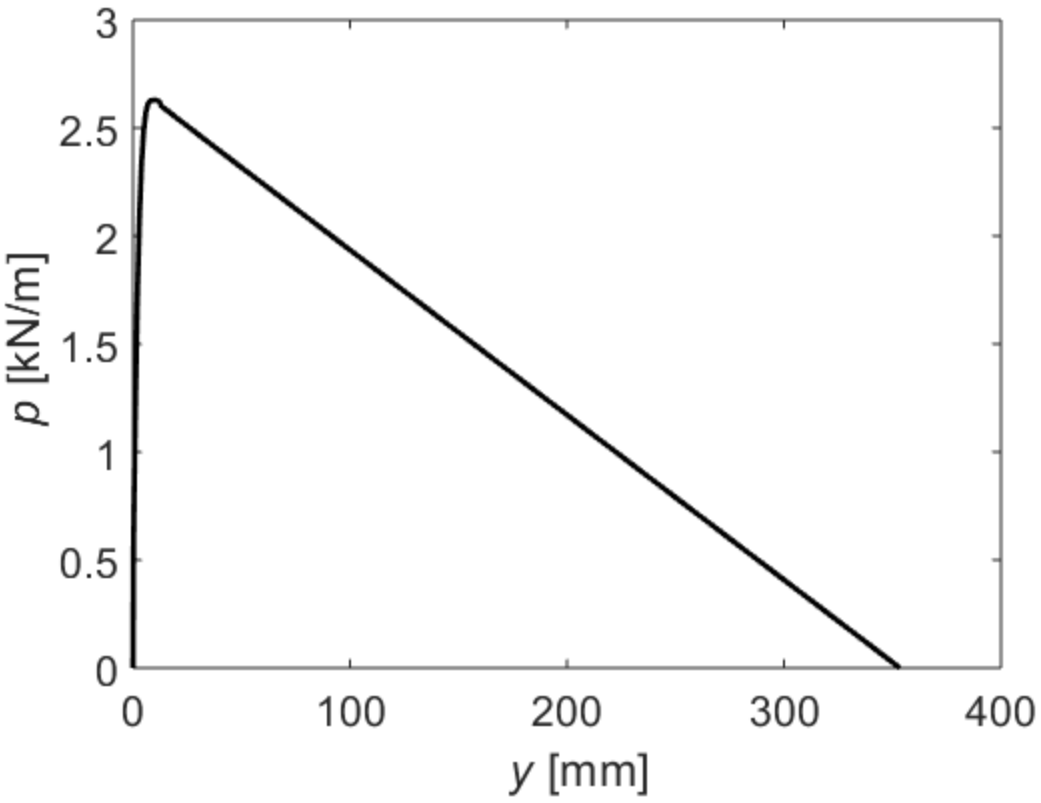

Figure 7-7. Suggested *p-y* curve for liquefiable soil (Chapter 5)

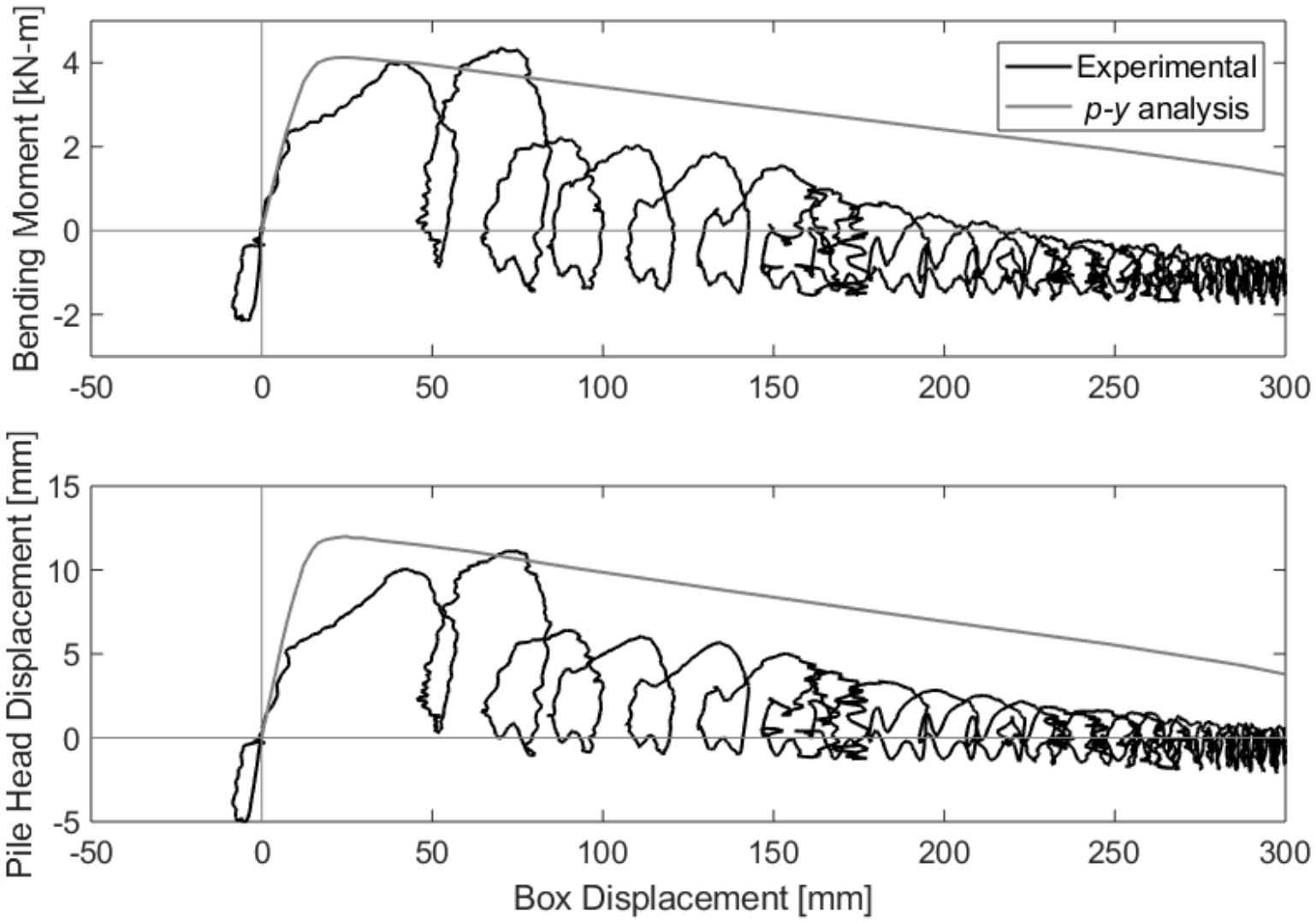

Figure 7-8. Comparison of experimental and *p-y* analysis for Test 1 using the Chapter 5 liquefied soil spring

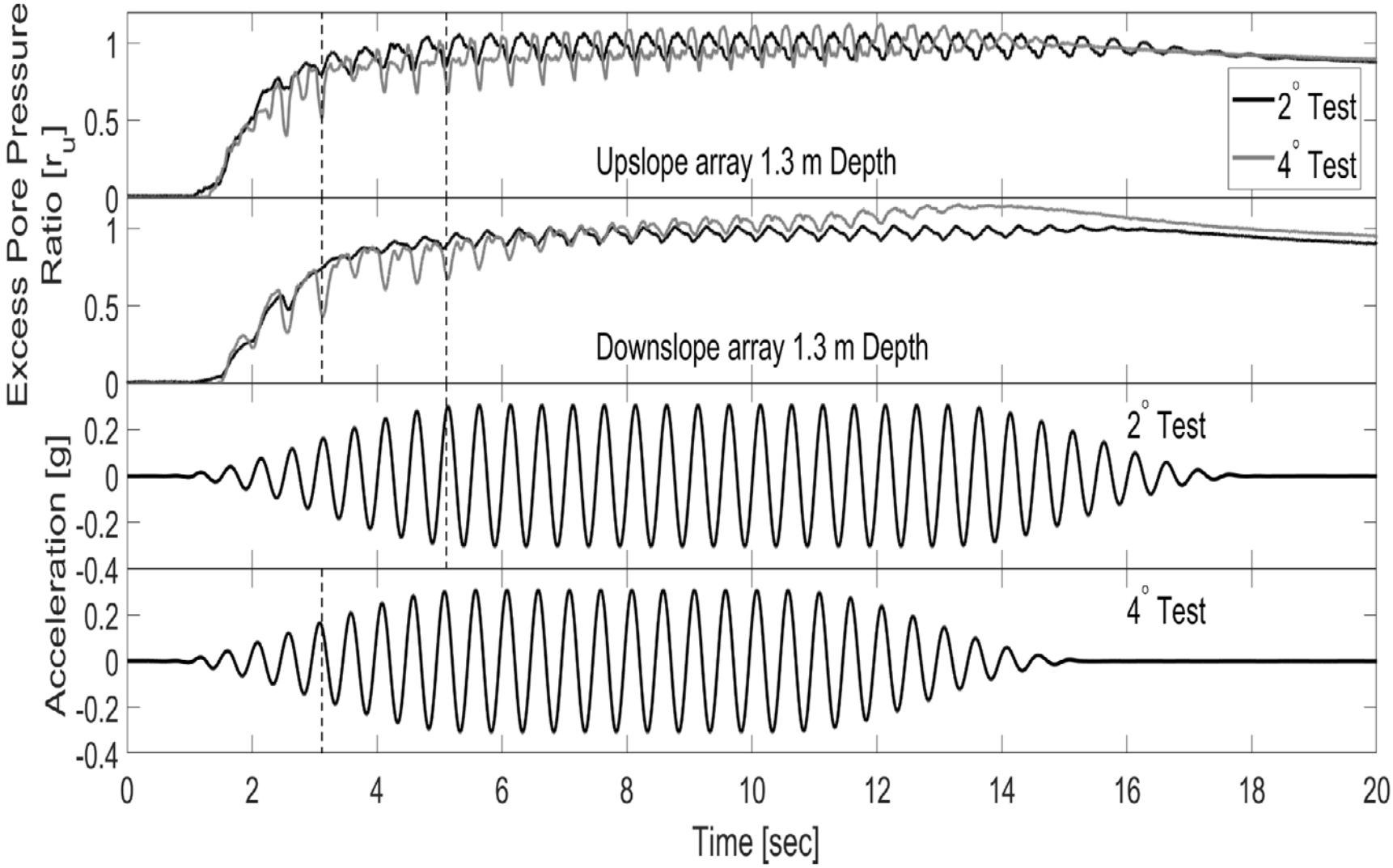

Figure 7-9. Acceleration and excess pore pressure time histories for Tests 2 (2°) and 3 (4°)

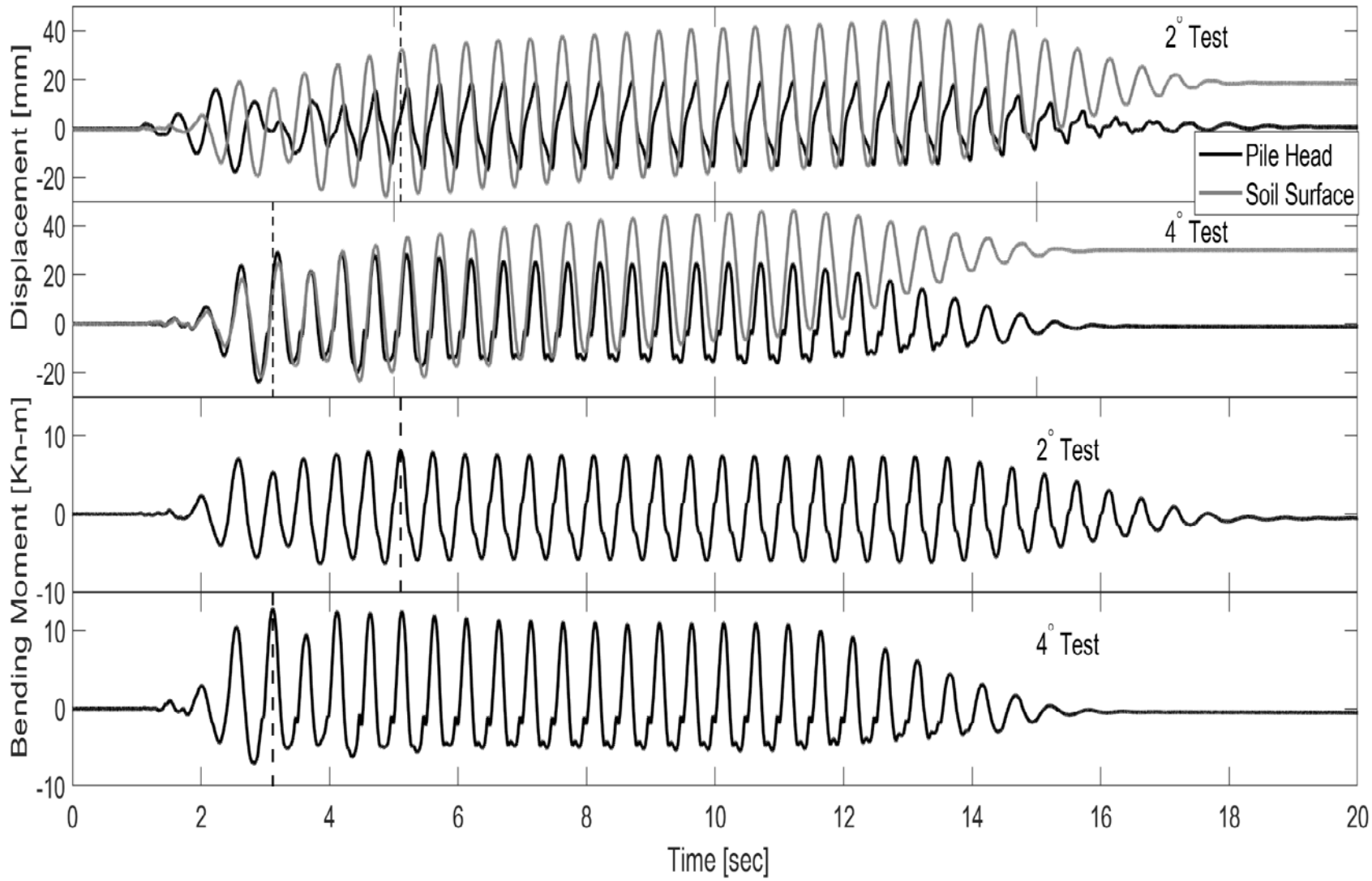

Figure 7-10. Displacement and bending moment (at base) time histories for Tests 2 (2°) and 3 (4°)

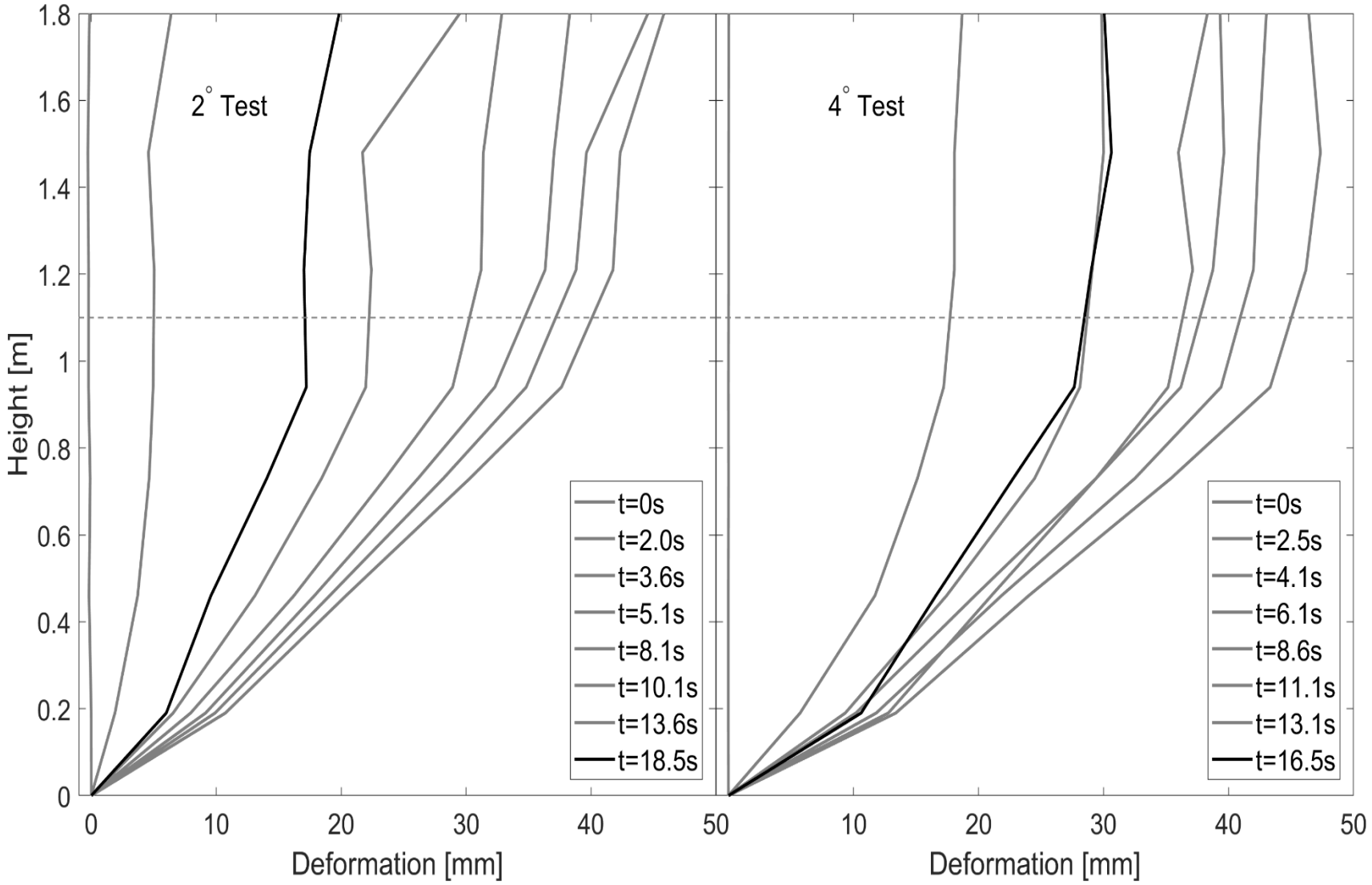

Figure 7-11. Displacement profile evolution for Tests 2 (2°) and 3 (4°)

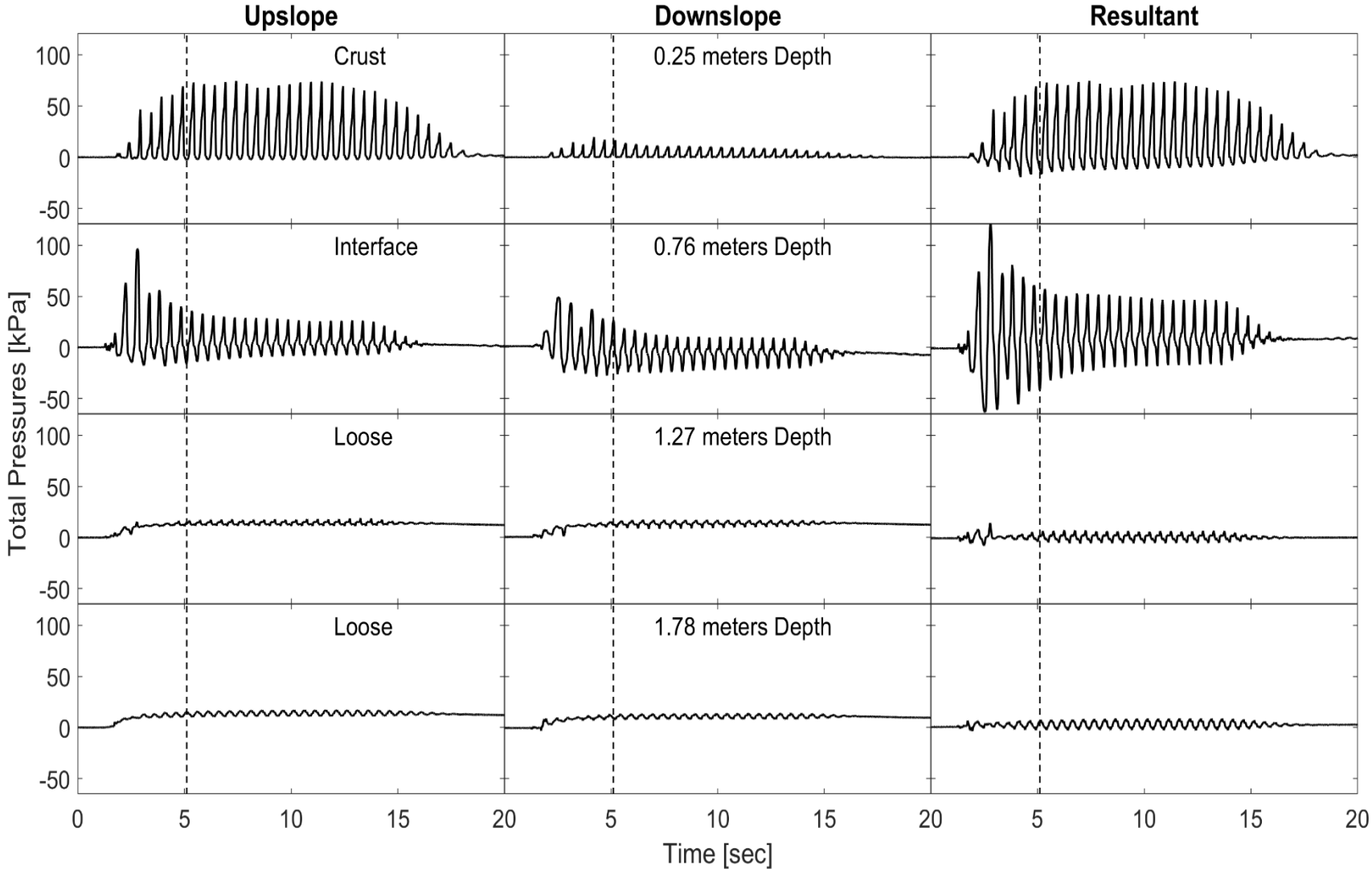

Figure 7-12. Total soil pressure time histories for Test 2 (2°)

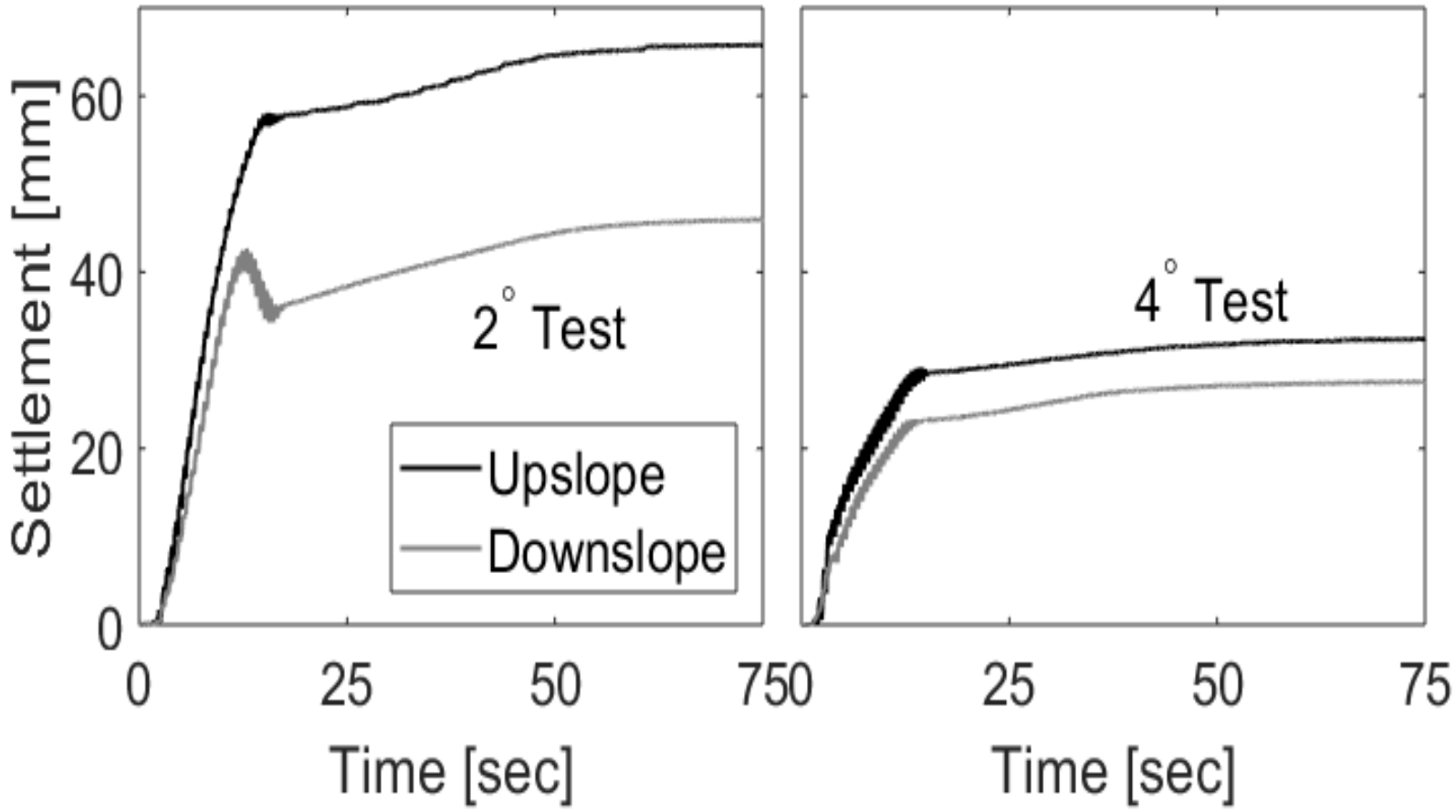

Figure 7-13. Settlement time histories for Tests 2 (2°) and 3 (4°)

Figure 7-14. Upslope cracking and downslope gap formation in the crust post-shaking (Pictures from Test 3)

Chapter 8 Effect of Linear and Nonlinear Pile Behavior on System Response

8.1. Abstract

A 1-g shake-table series of experiments was conducted to investigate the effects of liquefaction-induced lateral spreading on pile foundations in mildly inclined ground. Two piles of the same diameter (25 cm) and different stiffness/strength, steel and reinforced concrete were tested under earthquake excitation in a mildly inclined soil profile of 4 degrees. The ground stratum was built of sand at about 1.8 m in height with a 1.1 m base saturated layer and an upper 0.7 m crust. For each pile, data is employed to compare and assess peak pile response and soil behavior pre- and post-liquefaction. Soil and pile lateral displacement as well as excess pore pressure are discussed. In this series, it is observed that the stiffer pile would restrict the entire soil system response much more than the flexible one. The presence of a crust boosts the restraining effect by distributing the pile stiffness throughout the ground domain. Such a pile-ground interaction mechanism is of consequence for analyses that correlate pile bending moments to the accumulated lateral soil deformation.

Note: Difference in the reported responses below (particularly when small) might be a consequence of unavoidable experimental variability.

8.2. Introduction

Case histories describe a wide range of damage to structures and embedded foundation in soils that are susceptible to liquefaction and lateral spreading (Yasuda and Berrill 2000). Recent strong earthquakes, such as the 2010 Maule earthquake in Chile and the 2010 El-Mayor Cucapah earthquake in Mexico continue to describe cases of bridge and building damage due to the movement and failure of piles extending through liquefiable soils (GEER 2010a; b). The complex

loading mechanism from liquefaction and lateral spreading is still a subject of high interest (Finn 2015) to both researchers and practitioners.

Over the recent years, physical modelling emerged as an efficient tool to study the loading patterns and pile behavior. Centrifuge tests conducted on pile and pile group configurations (Wilson *et al.* 2000; Abdoun *et al.* 2002; Abdoun *et al.* 2003; Dobry *et al.* 2003; Kagawa *et al.* 2004; Brandenberg *et al.* 2005; Brandenberg *et al.* 2007) provided useful insights towards advancing our understanding. Other large scale 1-g experiments (Tokimatsu *et al.* 2005; He 2005; He *at al.* 2006; Motamed *et al.* 2013) complement the earlier testing efforts by reducing the scaling effects. Large scale tests on concrete piles (Chang and Hutchinson 2013) provided useful information on the inelastic behavior of concrete material that cannot be easily scaled in centrifuge tests.

Other studies have derived insights from numerical investigations. For example, Martin and Chen (2005) show that the relative stiffness between soil and pile is important in predicting the failure mode. They concluded that for stiff piles, lateral loads can be high with the soil eventually flowing around the pile, while a relatively flexible pile might experience much lower lateral loads as it undergoes larger deflections. He *et al.* (2017) identified the soil permeability as an important design consideration as higher sand permeability might weaken the dilative tendency, increase free field displacements while reducing the pile lateral loads and bending moments.

In the following sections, an experimental program is outlined to investigate the results of 2 single piles (steel and reinforced concrete) embedded in a 1.80 m high soil profile. The laminar box was mildly inclined at 4 degrees at the University of California, San Diego. The response is analyzed to compare ground and pile displacements, excess pore water pressures and pile bending moments. Finally, conclusions are drawn, and recommendations are presented.

8.3. Experimental Program

The conducted experimental series employed the same testing layout (Figure 8-1a), soil profile and instrumentation plan. The piles had the same diameter, and the only variable was the material (Figure 8-1b) and cross section. Figure 8-1c, d show pictures of the testing model using the medium size laminar box at the University of California, San Diego.

Box inside dimensions were 3.9 m long, 1.8 m wide and 1.8 m high with 28 laminates. The box was inclined at 4° to the horizontal using an external reinforced concrete ramp (Figure 8-1c). The container had an EPDM rubber liner placed to hold the soil and water. The liner allows for large deformations without tearing making it suitable to use in such testing. This laminar box configuration essentially simulates a periodic boundary condition (Law and Lam 2001).

8.4. Soil Properties

A two layered soil profile (Table 8-1) was constructed using Ottawa F-65 sand (Bastidas 2016) with the following grain size characteristics: D_{60} = 0.24 mm, fines content F_c = 0.25%, and uniformity coefficient C_u = 1.56. As such the employed soil was poorly graded in the medium to fine range (mostly fine). Each layer had a target density, and this was achieved by monitoring the dry weight of sand used to occupy the volume of each layer. Quality control using sand cone tests verified the estimated densities.

The base loose layer of 1.10 m was pluviated through soil meshes falling at a constant rate from a fixed height passing through water before settling. This ensures a relatively uniform loose deposit with the water breaking down clumped soil particles to release trapped air. Estimated soil relative density for this layer is 55 % and saturated density was about 1950 kg/m^3.

The top layer (crust) of 0.70 m height was built dry with some compaction to achieve a soil relative density of 85 % and a bulk density of 1817 kg/m^3. Water table was 0.70 m below the ground surface at the pile location (box centerline).

8.5. Steel Pile Properties

In this model (Test 1), a steel pipe pile (Figure 8-1b, Table 8-2) of 0.25 m (10 in) outer diameter and 3 mm (0.12 in) thickness was employed. Pile steel grade was A53B with properties summarized in Table 8-2. The pile was welded to a 2.5 cm thick steel plate and bolted to the box base. A 4° inclined wedge was employed below the pile to counteract the box inclination and enable the pile to stand vertically. A preliminary static pushover test was performed on the pile before adding the sand to obtain the bending stiffness and base fixity rotational stiffness values. Pile base connection was characterized to have a base rotational stiffness of 670 kN-m/rad emulating embedment in an assumed underlying dense soil stratum. The pile remained linear elastic during shaking.

8.6. Reinforced Concrete Pile Properties

For the second model (Test 2), a circular reinforced concrete pile (Figure 8-1b, Figure 8-2, Table 8-3) was constructed of regular strength concrete with 6-Grade 60 #4 US longitudinal reinforcement and #4 spiral reinforcement spaced at 10 cm (Figure 8-2a). The #4 rebar corresponds to a 12.7 mm rebar diameter. The pile was cast with a base pedestal, which was then bolted to the base of the container. Rotational and translational fixity were preferred for the base, however the connection flexibility allowed for some rotation of the pile. This connection was tested and characterized similar to the steel pile and found to have a rotational flexibility of 1500 kN-m/rad. Unconfined compression strength of the concrete was tested at 28 days and was found to be 24.1 MPa. The pile was 2.2 m long of which 1.80 m was embedded with 25.4 cm diameter and 2.54 cm

(1 inch) cover. Concrete compressive strength and steel reinforcement stress-strain properties were used to calculate the moment curvature for the section (Figure 8-2b). The theoretical first yield values were determined using the software OpenSees (fiber section model). The yield moment and curvature were 22 kN-m and 0.02 rad/m respectively.

The initial stiffness (Table 8-2, Table 8-3) was 3784 and 4704 kN-m^2 for the steel and concrete piles respectively. While the concrete pile appears to have a higher initial stiffness, it quickly degrades with shaking. On the other hand, the steel pile preserves its stiffness and remains linear elastic throughout the shaking. For example, at the maximum recorded curvature for the concrete pile, the stiffness was reduced to 25% of the initial value, making the steel pile 3.2 times stiffer. While the concrete pile did not yield, the response did deviate from linearity the curvature limit for cracking was surpassed. However, none were clearly visible in the after-test inspection, with cracks occurring during shaking.

8.7. Instrumentation

Both models were instrumented with a large number of accelerometers, pore pressure sensors, total pressure transducers, strain gauges and LVDTs (Figure 8-1a). Instrumentation was placed along the pile shaft and along the depth of the ground stratum at the locations shown. Strain gauges were densely deployed along the pile longitudinal reinforcement for the concrete pile and along the pile outer diameter for the steel pile to aid in back-calculation of the bending moment during shaking. Strain gauges were placed on both sides of the pile with a 10 cm spacing reaching a a total number of 40. Displacement transducers were mounted on the laminar box exterior wall to measure lateral displacements approximately every other laminate. Piles were also instrumented with transducers to measure pile head displacements above the ground surface. A total of 25 pore

pressure transducers and 25 accelerometers were placed on the piles in addition to being embedded in the surrounding soil.

8.8. Analysis Protocol

Focus is placed on system response mainly discussing excess pore-water pressure, displacements and pile bending moments. Thus, representative time histories were chosen to identify that response along with the peak bending moment. Bending moment was calculated based on strain gauge readings placed on the pile reinforcement (concrete) or outer surface (steel). Bending moment is an indicator of pressures acting on the pile.

As the box was mildly inclined at 4°, the soil started moving downslope when the shaking begun, even before the onset of liquefaction. Excess pore pressure evolution in the saturated layer are compared for both tests. Soil box and pile head exhibited permanent displacements in both tests. Cracking and settlement of the crust layer was also observed. A large gap formed between the pile and the downslope ground. The pile behavior and accumulated loads are highlighted and the effect of varying the pile stiffness is discussed.

8.9. Soil Response

Input motion was a 14 second 2 Hz sinusoidal wave with a 4 second gradual increase and 4 second decrease in amplitude for both tests. The actual input of the shake table was recorded (Figure 8-3) displaying a maximum amplitude of 0.25 g. Liquefaction occurred, approximately 4.25 seconds into the shaking phase for the steel pile and 6 seconds for the concrete (Figure 8-3). Around the onset of liquefaction, representative acceleration records (Figure 8-3) show the asymmetric response in the loose liquefiable layer and de-amplification of the shaking in the crust. The asymmetric response is a sign of the layer deforming in the downslope direction during shaking.

The general trend of the pore pressure data presented by records in the loose layer at a depth of 1.30 m displays gradual pore pressure build up with instantaneous reductions. The upslope pore pressure locations show higher dilative tendency as the soil liquefies, compared to the downslope locations for the steel pile and vice versa for the concrete pile. On the other hand, after liquefaction, only the concrete pile test showed pore pressure dipping (downslope higher than upslope). This shows some dilative tendency in the liquefied soil response (Zeghal and Elgamal 1994). The response above might be attributed to the steel pile movement before liquefaction, while resisting the soil as it flows around it after liquefaction. The concrete pile continues to deform with the soil flowing away from it. Displacement time histories shown in Figure 8-4 support that. maximum bending moment for both tests occurred before the soil liquefied.

Figure 8-4 and Figure 8-5 shows the downslope deformation for the soil box, and single pile for the 2 Tests. Both tests show an increase of ground surface displacement with shaking and a resulting accumulated permanent value. Deformations started with shaking and stopped thereafter.

In light of the difference in pile stiffness, it is seen that the concrete pile test incurred a higher level of deformation (15%). Of interest as well is that the instant of peak moment (Figure 8-6) on the pile coincided approximately with the same level of ground deformation in both experiments (about 4 cm).

As shaking started, the pile began to oscillate back and forth recording its highest value at the time of maximum bending moment. Values of maximum displacement were reached before liquefaction, oscillating thereafter around a constant but lower value. Pile head displacement gradually decreased with the ramping down of the input acceleration reaching a smaller value at the end of the shaking event.

Maximum pile head displacement was 3.70 cm and 3.90 cm for the steel and concrete tests respectively. This shows a 5 % increase in pile head displacement with the reduction of pile stiffness. On the other hand, accumulated ground surface displacement was 6.50 cm and 7.50 mm for Tests 1 (steel) and 2 (concrete) displaying an increase of about 15 %. The final ground deformation was not the maximum incurred as shown by the displacement profiles presented in Figure 8-5. Peak surface deformation was about 4 cm in both tests. The end of shaking accumulated displacement showed a reduction of 15 % and 9 % for Tests 1 and 2 respectively.

Pile residual displacements were 1.0 cm and 1.45 cm for the steel and concrete tests respectively. The cyclic behavior of the piles (Figure 8-4) agrees with the dilative pore pressure trends previously mentioned and confirms earlier observations by Martin and Chen (2005) and Suzuki et al. (2006), that for stiffer piles, a higher cyclic behavior is expected with lesser permanent deformation while more flexible piles with incur a larger permanent displacement with a lower cyclic component.

Deformation profile is parabolic in shape according to previous observations in Chapter 6 with the highest shear strains near the bottom of the loose layer and shows negligible strains in the upper crust. Displacement profiles and time histories indicate that most of the deformation was incurred before soil liquefaction.

8.10. Pile Response

Overall the pile response was similar. The objective of testing was for the steel pile to remain elastic while the reinforced concrete pile undergoes nonlinear response.

As mentioned earlier, peak bending moments were observed early during the shaking phase, before soil liquefaction (Figure 8-6). After maximum moment was reached, both tests show oscillation around a constant slightly lower value, gradually decreasing as the shaking was ramped

down (Figure 8-6, Figure 8-7). At the end of shaking, both piles rebounded to a lesser residual value. Both, piles did nor yield. The steel pile was linear elastic while the concrete pile passed the cracking curvature limit.

Figure 8-5 demonstrates that soil continues to accumulate displacement, after maximum pile response, with no appreciable further loading. As such, the final accumulated ground deformation is independent of the observed peak loading on the pile.

Maximum bending moment recorded for Test 1 (steel) was 26 kN-m and 17 kN-m for Test 2 (concrete) as shown in Figure 8-6 and Figure 8-7. Therefore, the stiffness reduction caused the pile to incur a lower bending moment of about 35 %. Furthermore, maximum response occurred around the same time instant, at 3.70 s for the steel test and 3.95 s for the concrete experiment before liquefaction. Bending moment is shown to decrease as liquefaction occurs. Residual values were 3.8 kN-m and 7.4 kN-m for Test 1 and 2 respectively showing a decrease of 85% and 55%.

Bending moment time histories (Figure 8-6) and profiles (Figure 8-7) show the maximum location to be at a 1.60 m depth with the bending moment decreasing near the base. Observations are in line with previous studies by Lam *et al.* (2009) who noted that the maximum bending moment occurs in a range of 1D to 4D beneath the upper crust.

8.11. Lateral Soil Pressures

Total pressure transducers were placed on both sides of the piles to measure the lateral thrust of the soil. Selected time histories were chosen to elucidate the response, Figure 8-8 for the steel test and Figure 8-9 for the concrete test. From the presented data, it is seen that the highest pressures occur before the onset of liquefaction. Lateral pressures on the upslope side, keep increasing till the soil liquefies, and after that a noted drop is observed as the sand flows around

the piles. For the downslope side, upper locations record drop in pressures as the soil moves away while lower location record increase in total pressure then a reduction as the sand loses strength.

Total pressures on the steel pile (Figure 8-8) show the crust following the observed trend of the upslope pushing while the downslope soil moving away. Pressures in the loose soil increase with shaking before liquefaction and decrease significantly with liquefaction. Post liquefaction pressures for the loose soil are lower with the increase in depth indicating that the upper portions of the layer are under the effect of the overlying non-liquefiable crust.

Figure 8-9 presents lateral pressures on the concrete pile, with the upslope crust applying a much larger pressure, which can be attributed to the higher ground deformations. The transducers at the crust-loose interface follows the crust behavior with the pressures increasing with shaking till the onset of liquefaction. Afterwards, due to the loss of strength in the loose layer, lateral forces gradually decrease with shaking. This is a result of the high pore pressures penetrating the crust and reducing its stiffness as well. Pressures in the loose layer follow the above-mentioned trend, increasing before liquefaction and almost disappearing after.

The higher pressures exerted from the liquefiable layer on the steel pile compared to the concrete is a result of the higher stiffness. The lower deformations in the stiffer pile allows for larger resistance while soil experiences less resistance around the more flexible pile. In general, total pressures exerted by the non-liquefiable layer during cyclic loading is in the range of double the passive values (might be due to impacts between pile and soil affecting accuracy of measured values).

8.12. Soil Settlement

General trends (Figure 8-10) show the settlement starting with shaking. Settlement rate at the beginning was much higher with the rate decreasing. Settlement continued to 1 minute after

the shaking stopped. Upslope and downslope records for both tests show an additional 4 mm of settlement occurring after shaking.

Differential ground settlement for the steel pile test was of the order of 3 mm which results in almost no inclination change and is very small compared to the 26 mm and 23 mm for the upslope and downslope locations respectively. The downslope settlement in the concrete pile test was about 18 mm in close range to that of the steel pile. However, the upslope location recorded 37 mm which is much larger than the others indicating the presence of a weak zone.

8.13. Post Test Physical Observations

Care was taken to document any physical observations before and during demolition. Figure 8-11 presents the box configuration after shaking for the concrete test, which was similar to the steel pile test. Soil was heaving upslope of the pile with some cracking and a downslope gap was observed in both tests. The gap depth was 0.43 m which is about 60% of the crust thickness. Although curvature and bending moments of the concrete pile indicate cracking, none was clearly observed during the after shaking inspection. Instantaneous micro cracks might have occurred during the cyclic motion.

8.14. Summary and Conclusions

A 1-g shaking table test series was performed separately on 2 piles of different stiffness, cross section, and material. A single steel pipe and a reinforced concrete pile embedded in a 2-layer soil profile were employed. The models were tested in a sloped soil profile at 4°, to investigate the liquefaction-induced-lateral spreading response. Shaking was conducted using a 2 Hz sine wave with 0.25g peak amplitude. General observations include:

- Rebounding of piles after shaking show pressure relief although soil displacement is higher. Thus, post-earthquake reconnaissance will not account for possible peak behavior of pile foundation but will show the residual values at the time of inspection.
- Maximum bending moment occurred before the onset of liquefaction when the soil had reduced strength.
- Maximum bending moment was recorded about 3.5 D below the crust layer with values decreasing near the base.
- Excess pore pressures from the liquefied layer penetrate the crust reducing its stiffness as the shaking continues.
- Stiffer piles are likely to carry higher lateral loads with reduced displacements as soil flows around it. A more flexible pile would deform much more with the ground and carry a lesser load as noted by Martin and Chen (2005).
- The cyclic component of the stiff pile is much higher than the flexible pile while the residual value is lower.
- The increased stiffness of the steel pile exerted additional restrain on the box and soil system resulting in a lower overall box movement.

8.15. Acknowledgements

Chapter 8, in full, is currently being prepared for submission for publication of the material as it may appear in the following journal publication (The dissertation author was the primary investigator and author of this paper):

Ebeido, A., Elgamal, A. and Zayed, M. "Pile Response during Liquefaction-Induced Lateral Spreading: 1-g Shake Table Tests with Different Pile Stiffness".

Chapter 8, in part, is currently has been submitted for publication of the material as it may appear in the following conference publication (The dissertation author was the primary investigator and author of this paper):

Ebeido, A. and Elgamal, A., (Manuscript accepted, 2019). "Experimental investigation of a single pile during liquefaction-induced lateral spreading". Proc. of the 16th Panamerican Conference on Soil Mechanics and Geotechnical Engineering. Cancun, Mexico. 17-20 November.

Table 8-1. Soil Profile Properties

Property	Base Loose Layer	Top Crust
Water/soil condition	Fully saturated bottom layer	Relatively dry top layer
Thickness (m)	1.10	0.70
γ_{bulk} (kg/m^3)	1950	1817
γ_{dry} (kg/m^3)	1590	1730
Relative density (%)	55	85

Table 8-2. Steel Pile Properties

Steel Grade	A53B
Pipe Outer Diameter (m)	0.254
Pipe Thickness (mm)	3.05
Elastic Modulus (kPa)	2.0×10^8
Yield Strength (kPa)	4.55×10^5
Stiffness (kN-m^2)	3784

Table 8-3. Reinforced Concrete Pile Properties

Compressive Strength (MPa)	24.1
Pipe Diameter (m)	0.254
Pipe Thickness (mm)	Solid
Elastic Modulus (kPa)	2.3×10^7
Yield Curvature (1/m)	0.02
Initial uncracked Stiffness (kN-m^2)	4704

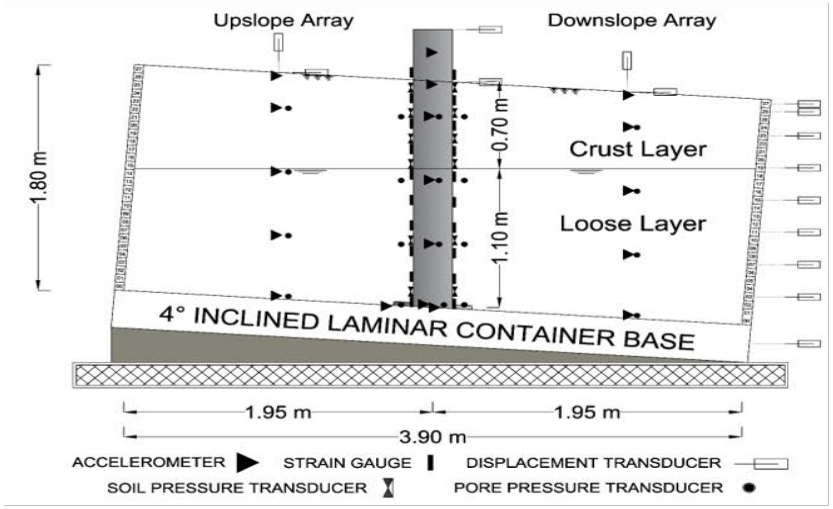

a) Test Layout

b) Steel and Concrete Piles

c) Inclined Box on Shake Table

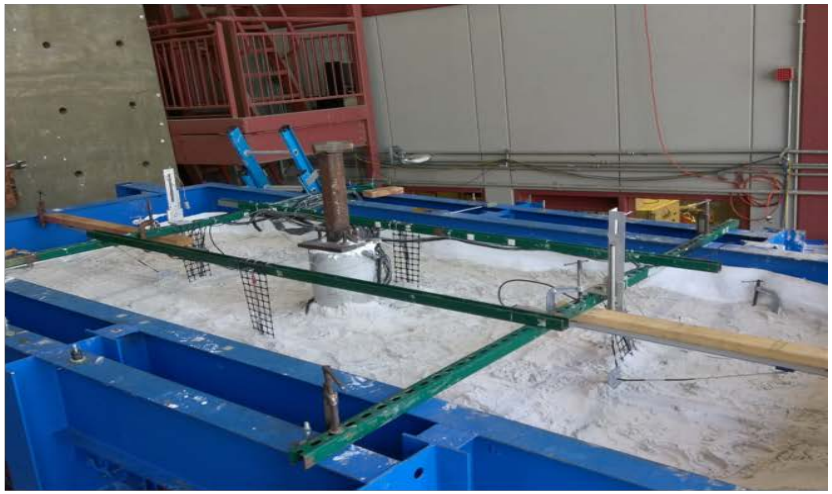

d) Laminar Box Top View

Figure 8-1. Testing layout employed piles and model setup before shaking

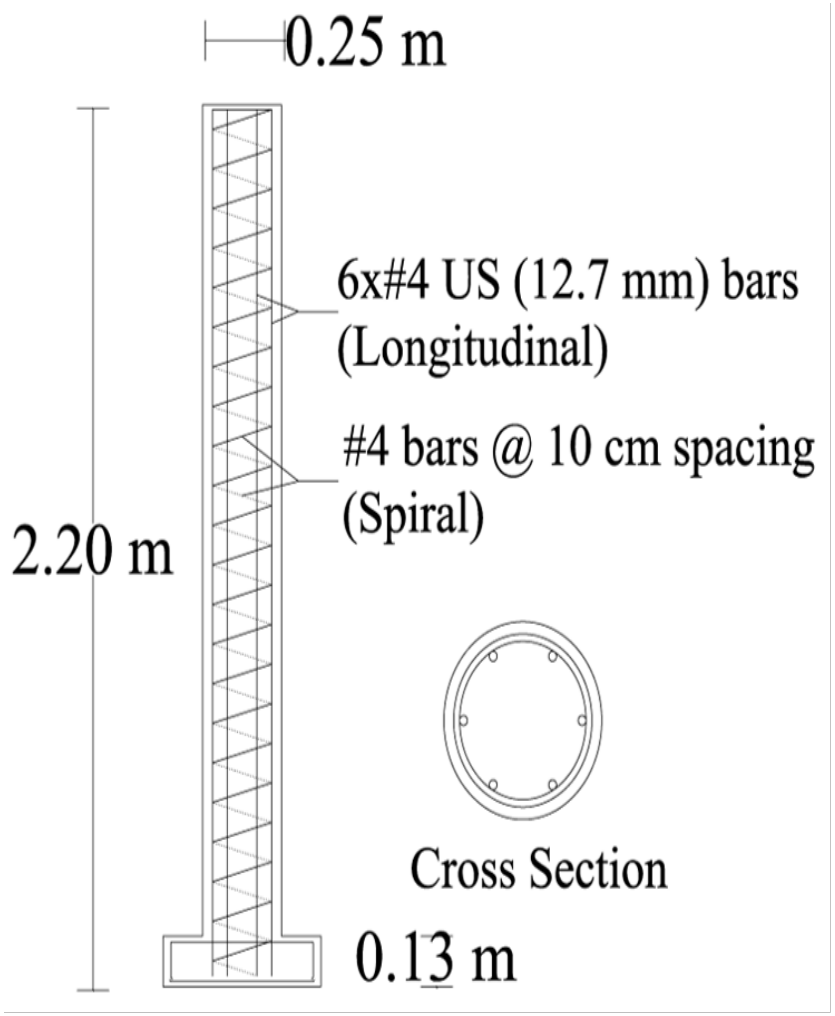

a) Reinforced Concrete Pile Details

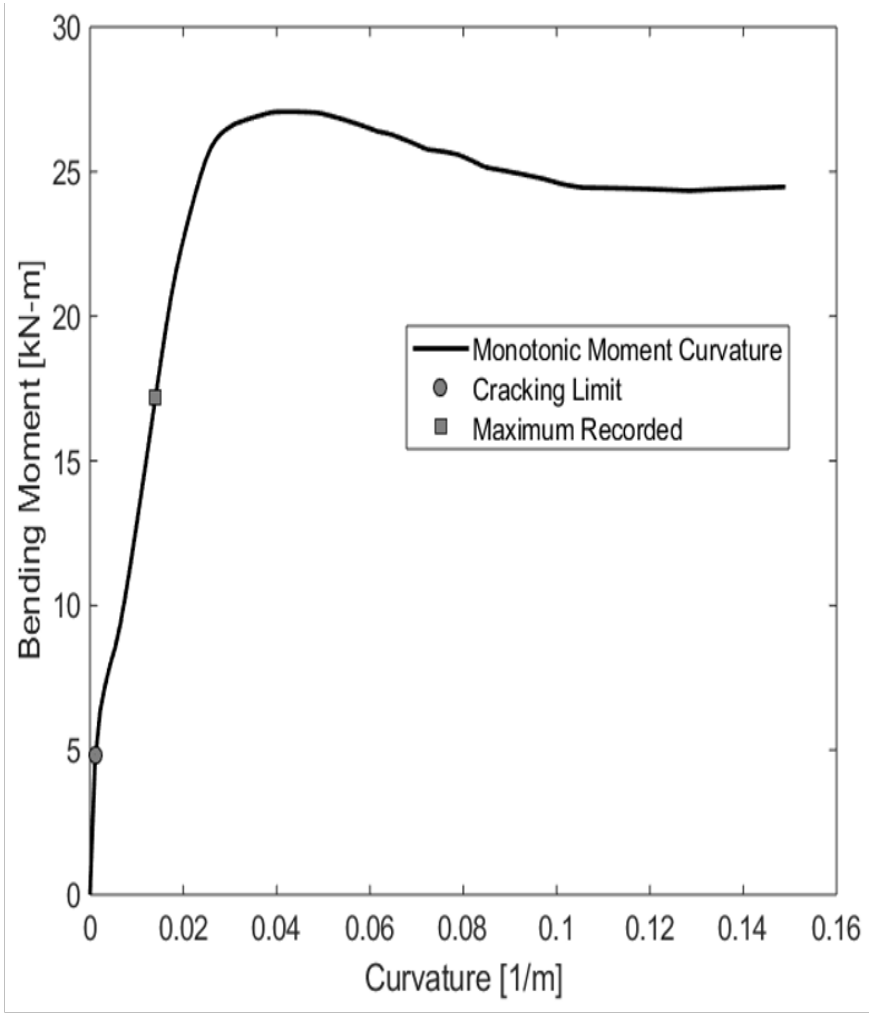

b) Reinforced Concrete Moment-Curvature

Figure 8-2. Reinforced Concrete pile properties

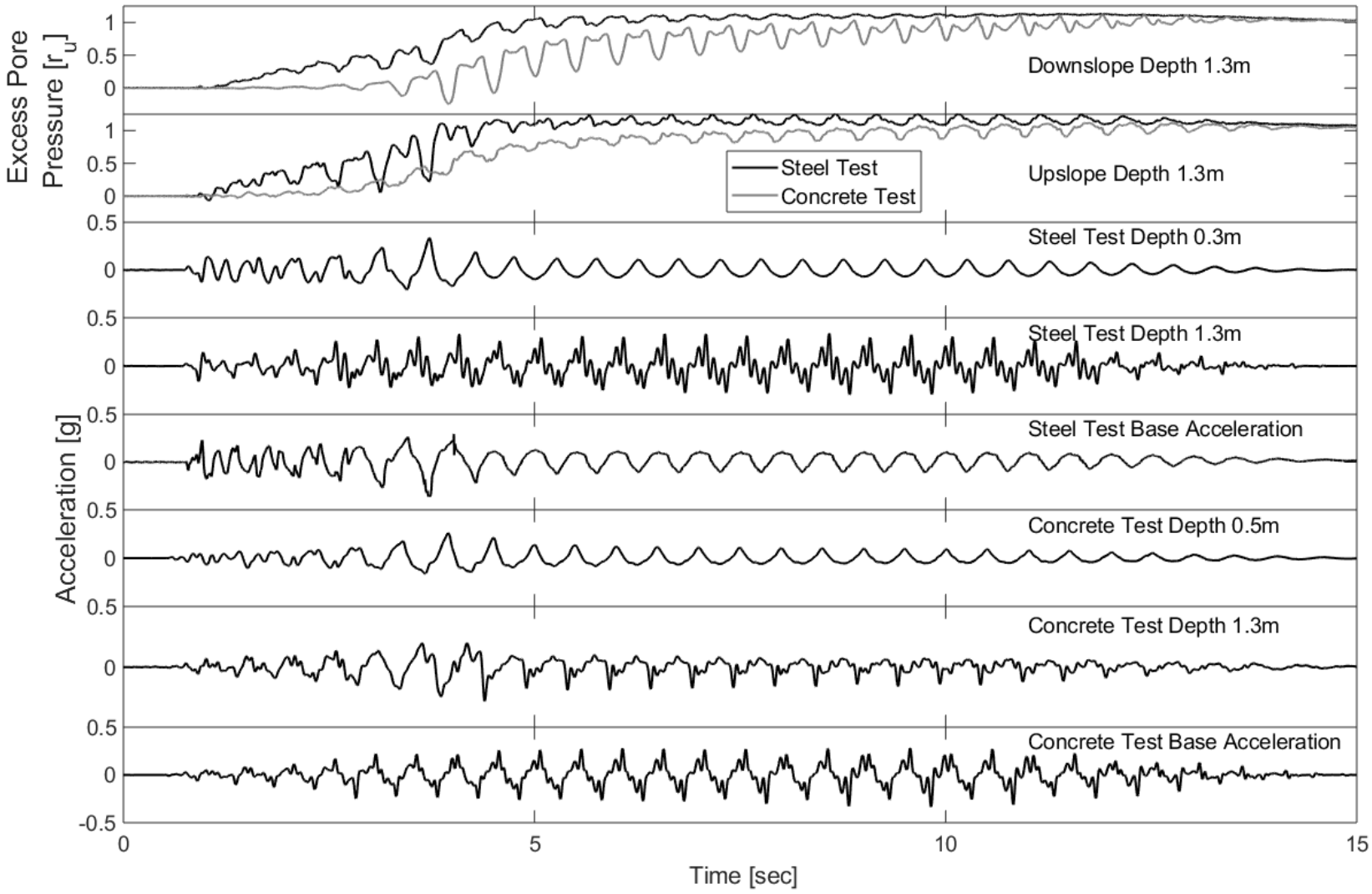

Figure 8-3. Acceleration and excess pore water pressure time histories for both tests

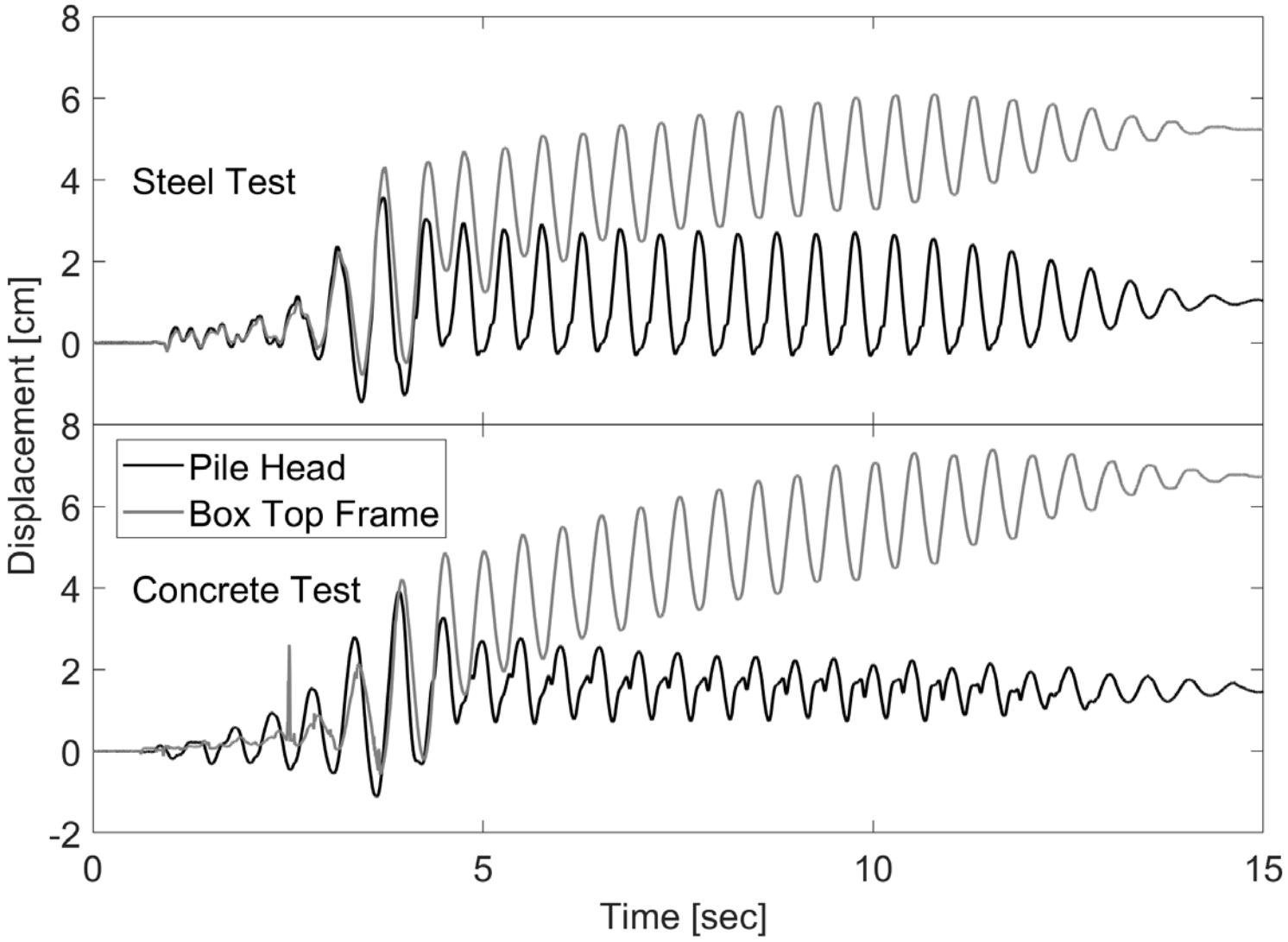

Figure 8-4. Box top and pile head displacement time histories for both tests

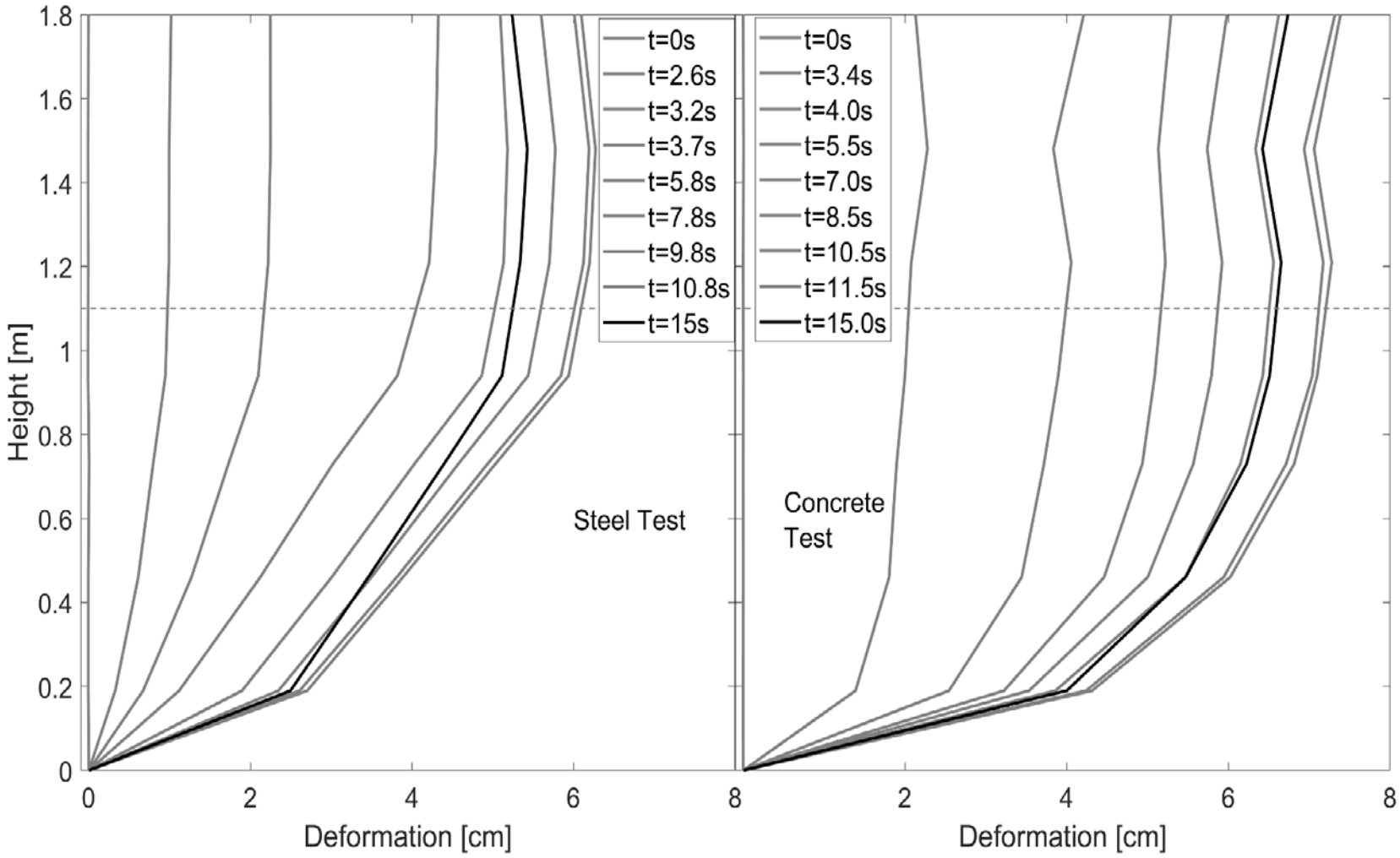

Figure 8-5. Displacement profile evolution for both tests

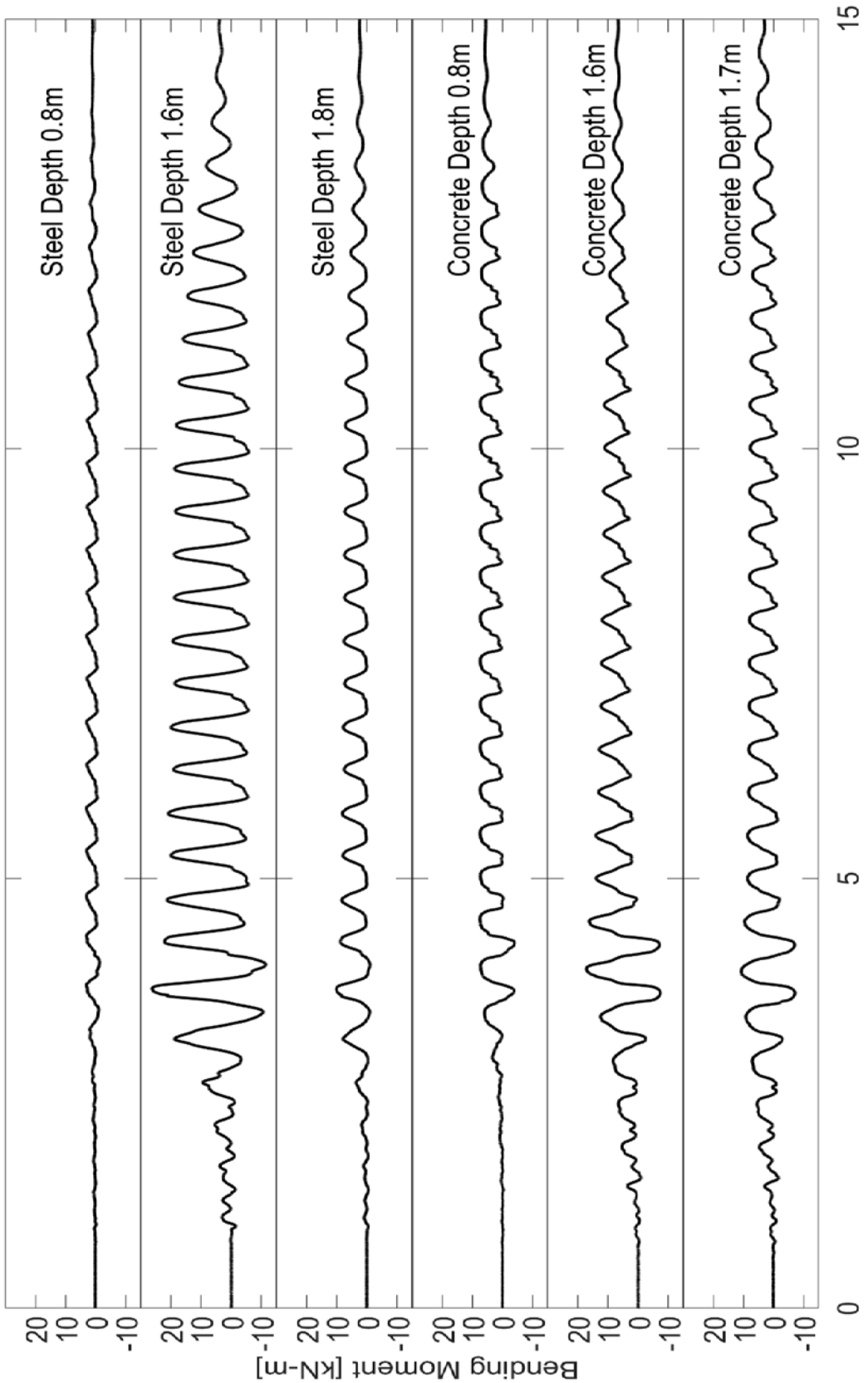

Figure 8-6. Bending moment time histories for both tests

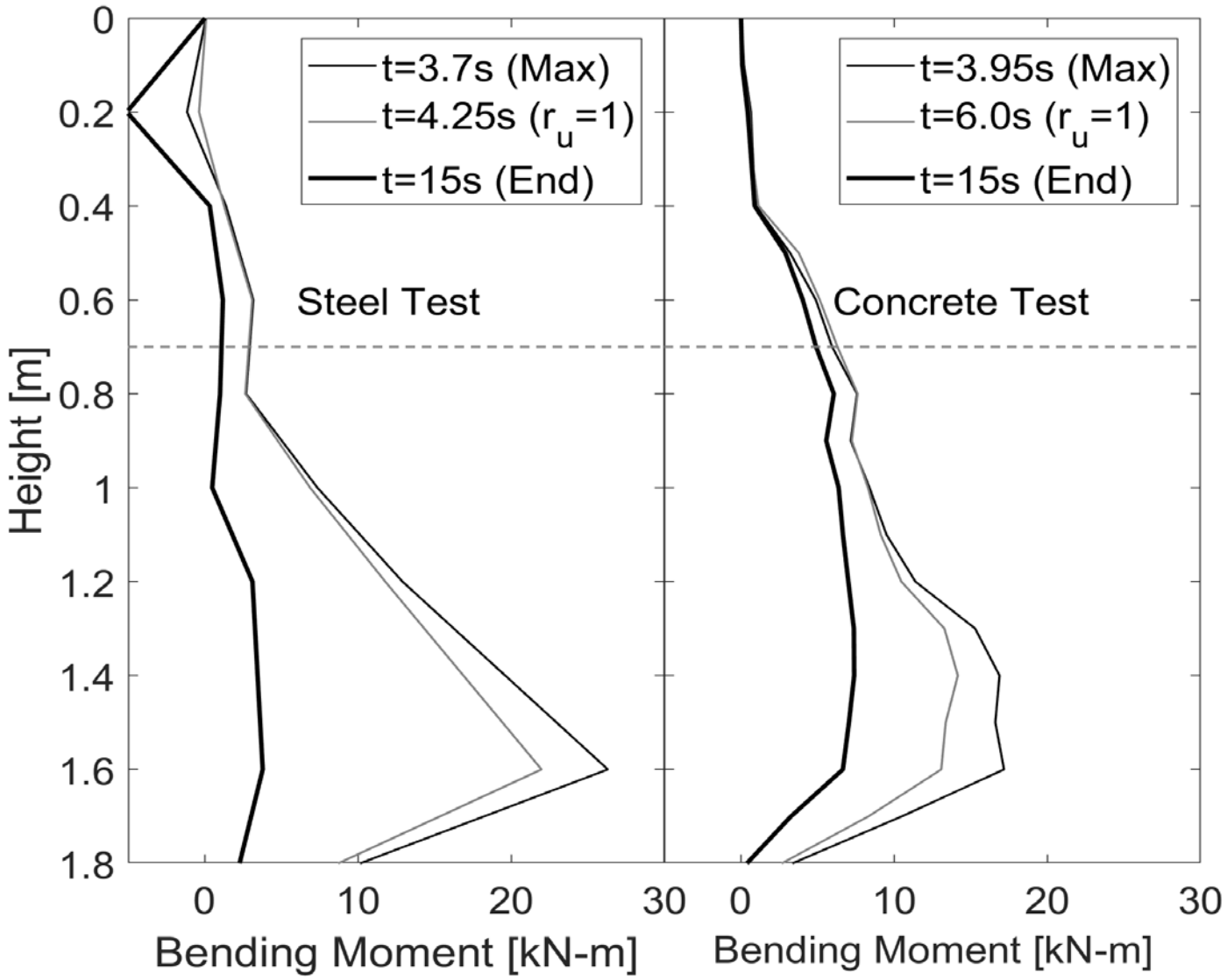

Figure 8-7. Bending Moment Profiles at select instances for both piles

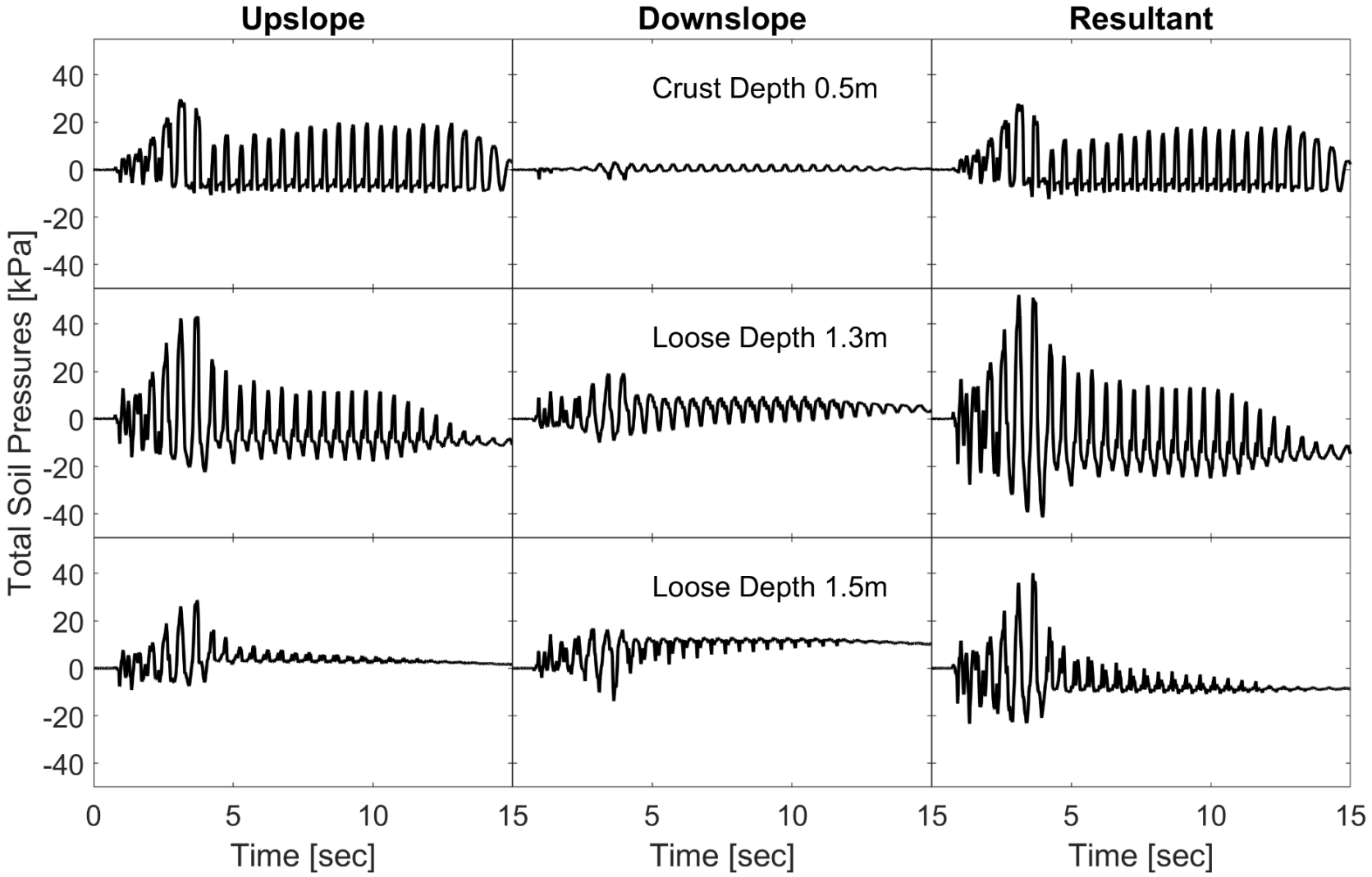

Figure 8-8. Total pressure time histories for Steel pile test

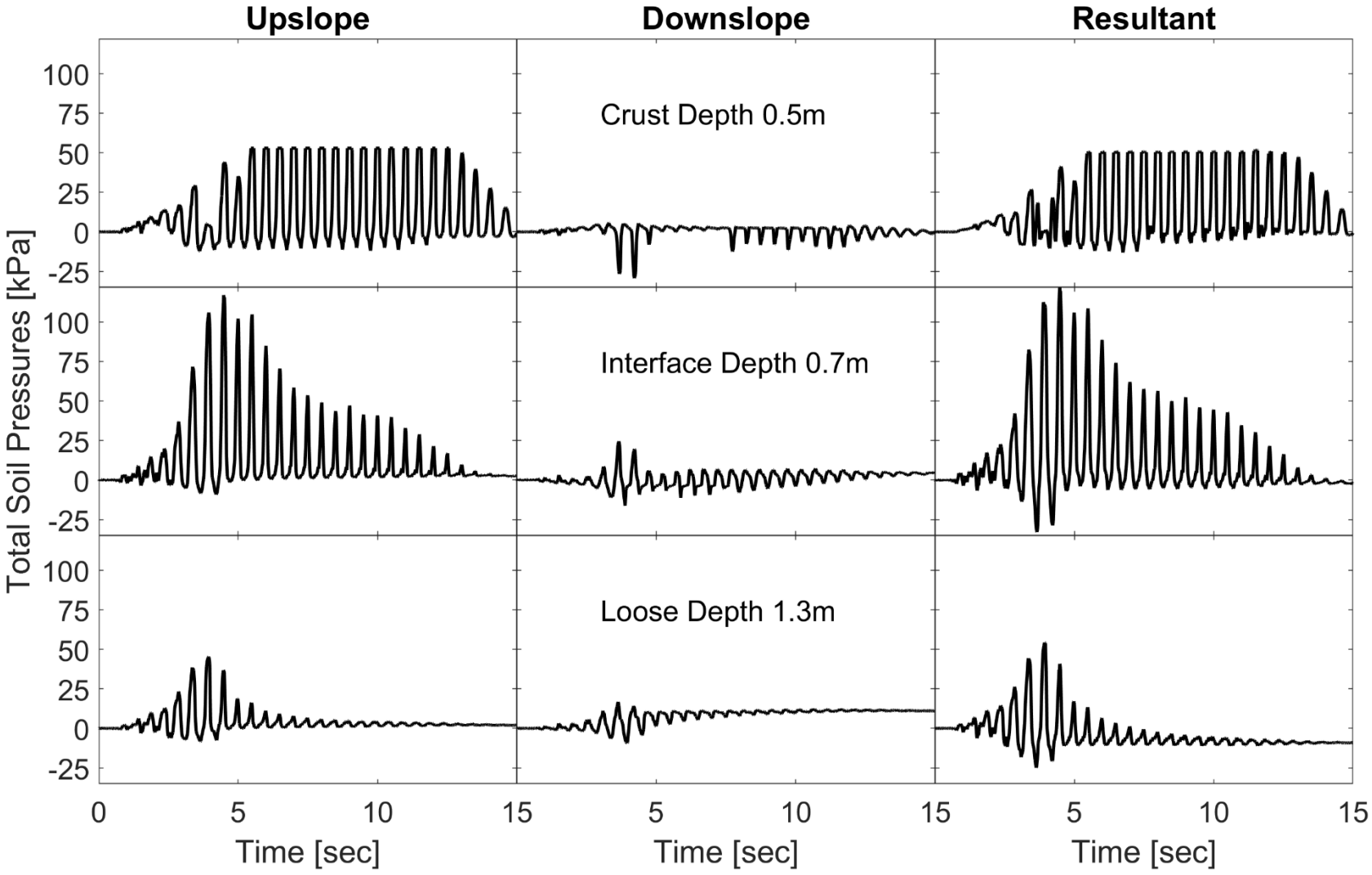

Figure 8-9. Total pressure time histories for Reinforced concrete pile test

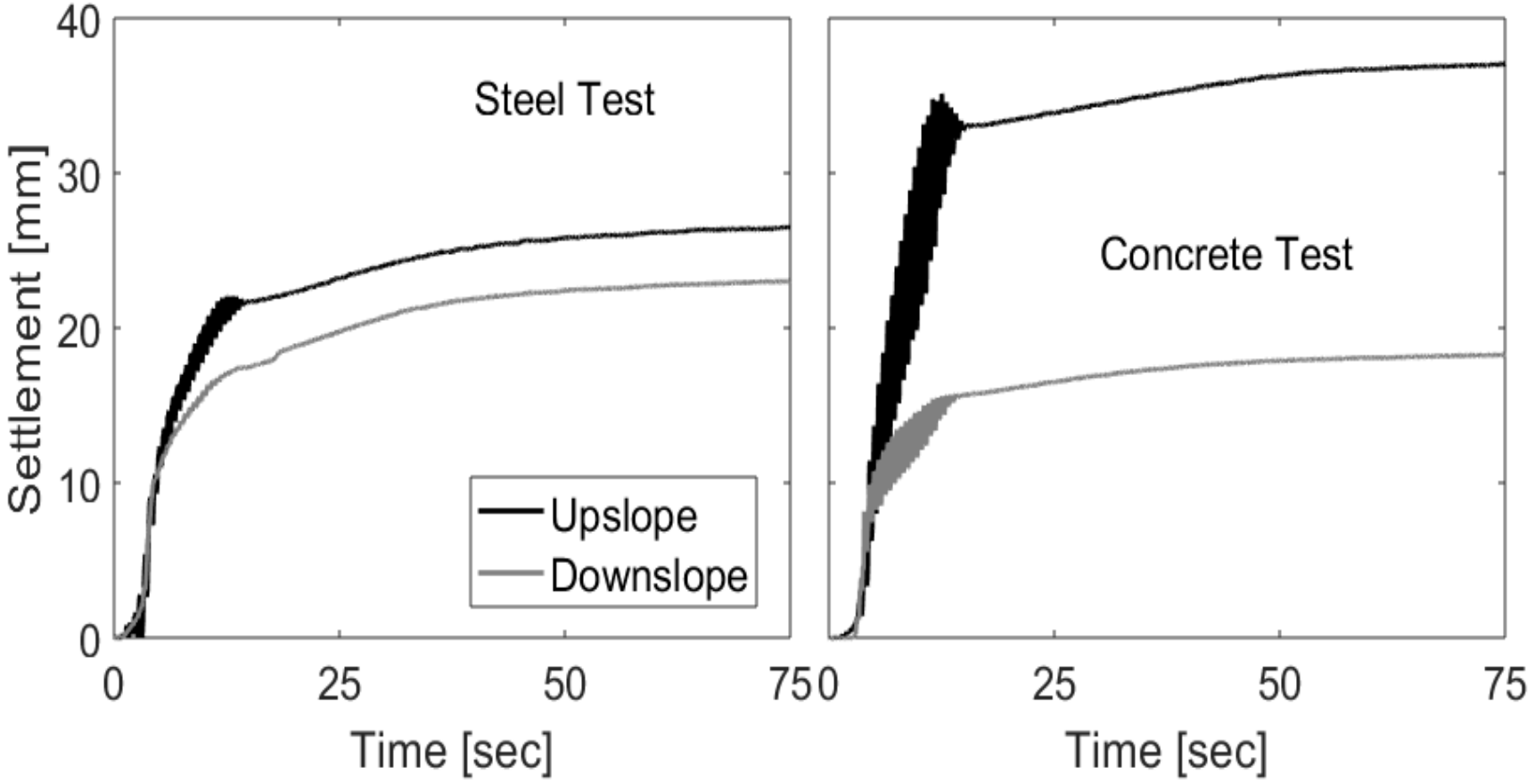

Figure 8-10. Settlement time histories for both tests

Figure 8-11. Deformed box shape and soil surface after shaking (Upslope cracking and downslope gap formation in the crust)

Chapter 9 Inertial and Kinematic Effects during 1-g Shake Table Testing

9.1. Abstract

A 2.90 m high laminar box was employed to evaluate the mechanism of liquefaction induced lateral spreading on a 0.25 m circular concrete pile in a multi-layered soil profile. The test is conducted in a 4 degrees mildly inclined ground configuration. A 1.84 ton mass was placed on top of the pile with the mass center 1.00 m above the ground surface. The profile was subjected to 1-dimesional (1D) shaking to document the pile behavior and system response. The experimental setup, test procedures and test results are described in detail. The recorded data sets are analyzed to document and track the evolution of lateral loading on the pile. Ground and pile lateral displacement as well as excess pore pressure are discussed. In this test, it is observed that both inertial and kinematic loads contributed to the stresses acting on the pile. Pile response is analyzed to document the non-linearity and formation of a plastic hinge. Thereafter, as the shaking continued, cracking appeared on the pile with final failure at the pile base. The employed multi-layered soil profile played an important role in dictating the outcomes.

9.2. Introduction

Lateral spreading induced by liquefaction may cause excessive movement and possible failure of pile foundations (e.g., Yasuda and Berrill 2000). This presents a complex loading situation as the soil undergoes a significant change in its dynamic properties (Finn 2015).

Case history investigations discuss a wide range of damage to structures and their pile foundations (Tokimatsu and Asaka 1998). In the Kobe region, the 1995 Hyogoken-Nambu earthquake was responsible for the damage of numerous pile foundation supported structures. The observed damage indicated the contribution of both inertial and kinematic forces. Tokimatsu and

Asaka (1998) describe a specific waterfront structure with deformed piles due to lateral spreading. Horizontal pile cracks appeared at the interface between the liquefiable layer and the underlying non-liquefiable ground. This cracking points to local plastic demands on the piles due to the significant change in soil properties at the interface between these layers.

Other investigators show the dependence of the failure mode on the relative stiffness between pile and soil (Martin and Chen 2005). They conclude that soil might eventually flow around stiffer piles whereas more flexible pile experience lower lateral loads while undergoing larger deflections. Many other field investigations have provided valuable insight and helped define the scope of necessary research (e.g., Tokimatsu *et al.* 2005, Ishihara and Cubrinovski 2004, Koyamada *et al.* 2006).

Physical modelling is a valuable resource to complement field investigations. Centrifuge experiments were conducted to study pile kinematic effects during liquefaction and lateral spreading in mildly inclined ground. Studies by Abdoun *et al.* (2003) and Dobry *et al.* (2003) in a laminar box with multi-layered soil profiles found the largest bending moment at the interface between liquefied and underlying non-liquefied soil layers. Conclusions from tests by Brandenberg *et al.* (2005) show that lateral load imposed by the different soil layers depends on the incremental and total relative displacement between pile and soil. Brandenberg *et al.* (2007) further discuss the softening of crust layer load transfer mechanisms during the associated passive soil failure.

In addition to the above, large scale one-g shake table experiments were performed. He (2005), He *et al.* (2006) and He *et al.* (2009) discuss four experiments in a mildly inclined laminar box with different single pile and pile group configurations. These experiments address the

evolution of pore-water pressures, total pressures and displacements on steel pipe piles along with pile foundation response to such loading.

Chang and Hutchinson (2013) tested a reinforced concrete pile in a medium size inclined laminar box and their analysis focused on local plastic demands on the pile and the failure mechanism. They discuss a 0.25 m reinforced concrete pile embedded in a 3-layer soil stratum. Box dimensions was 3.9 m length, 1.8 m width and 1.8 m height. Their main objective was to study the inelastic demands on the pile and correlate to the pattern of soil response. Under a sequence of scaled ground motions, liquefaction and lateral spreading was observed with nearly 100% reduction in shear modulus (most of the softening tied to the liquefiable loose layer). The reinforced concrete pile behaved linearly at first, but plastic behavior was observed mainly at the interface between crust and underlying loose layer. The plastic region calculated, spread over 1.5 times the pile diameter, larger than assumed in column capacity design. Inelastic strains and thus plastic behavior were observed at the loose layer and crust interface.

Building on such earlier work, this study analyzes a single circular concrete pile of 0.25 m diameter constructed to undergo plastic deformations. The pile was cast in an under-reinforced configuration for that purpose. A 4-degree inclination multi-layered profile was employed with a super structure mass on top to study both inertial and kinematic forces affecting the response. A key objective is to study the inelastic demands in the reinforced concrete material.

9.3. Experimental Program

Using the laminar box (Figure 9-1) at the Powell Laboratory Shake table located at the University of California, San Diego (Magenes 1989; Trautner *et al.* 2018), the response of a reinforced concrete pile subjected to liquefaction-induced lateral spreading is explored. The laminar container composed of 43 stacked steel frames (previously 28 frames, Ashford and

Jakrapiyanun 2001) with 16 cold steel rollers supporting each frame allowing for lateral movement and designed to give minimal boundary effects, simulates a 1D shear beam. The box was 3.90 m long, 2.90 m high and 1.80 m wide (inner dimensions) and was inclined at 4° to the horizontal. This inclination corresponds to an infinite slope of about 7º in the field upon accounting for the laminate weight and water table corrections following the procedure of Taboada (1995). As noted by (Law and Lam 2001), this laminar box configuration essentially simulates a periodic boundary condition. The container was lined with an Ethylene Propylene Diene Monomer (EPDM) rubber liner which was placed to hold soil and water inside the laminar container.

9.4. Soil Properties

The 3 layered soil profile (2.90 m high) shown on Figure 9-2 was constructed using Ottawa F-65 sand (Bastidas 2016) with the following grain size characteristics: D_{60} = 0.24 mm, fines content F_c = 0.25%, and uniformity coefficient C_u = 1.56. Soil was poorly graded (Figure 9-3). The soil profile was constructed with a base dense layer (1.50 m), middle loose liquefiable layer (0.70 m) and a top dry layer (0.70 m). Water table was 0.70 m below the ground surface at the pile location (box centerline). Each layer had a target density, and this was achieved by monitoring the dry weight of sand used to occupy the volume of each layer. Quality control using sand cone tests verified the estimated densities.

The 1.50 m bottom layer was constructed by wet compaction. The layer was built in 0.25 m lifts compacting each layer using a plate compactor. Estimated soil relative density is 82 % and saturated density was about 2025 kg/m^3 (Dry density before saturation was 1695 kg/m^3). The layer was saturated from the bottom upwards after completion. Thereafter, the 0.70 m middle loose layer was pluviated through soil meshes at a constant rate falling from a uniform height passing through water before settling. This ensures a relatively uniform deposit with the mesh helping to break

down clumped soil particles to release any trapped air. The soil passed through about 20 cm of water before depositing. Estimated soil relative density for this layer is 53 % and saturated density was about 1950 kg/m^3 (Dry density before saturation was 1590 kg/m^3). Finally, the 0.70 m top layer referred to as crust was compacted to achieve an estimated soil relative density of 84 % and bulk density was about 1730 kg/m^3 (Dry density before saturation was 1700 kg/m^3).

9.5. Pile Properties

A reinforced concrete pile (Figure 9-4) of 0.25 m (10 in) diameter and a 25 mm cover was employed, constructed of regular strength concrete with 6 grade 60 #3 US longitudinal reinforcement and #3 spiral reinforcement spaced at 20 cm. The #3 bar corresponds to a 9.5 mm rebar diameter. The pile was cast with a base pedestal to enable connection to the box base. A preliminary static pushover test was performed on the pile before adding the sand to obtain the bending stiffness and base fixity rotational stiffness values. Pile connection was characterized to have a base rotational spring of 1500 kN-m/rad (emulating embedment in an assumed underlying firm soil stratum). Unconfined compression strength of the concrete was tested at 28 days and found to be about 16 MPa. Monotonic moment-curvature (fiber element modeling using OpenSees) is shown in Figure 9-5 identifying the concrete cracking limit and first yield curvatures. The pile was 3 m long and was casted to include a top concrete block of mass of 0.60 tons. An additional top mass was added to the concrete block to bring the total top mass to 1.84 tons was placed with its center at 1.00 m above the ground surface (Figure 9-2).

9.6. Instrumentation

The model was heavily instrumented (Figure 9-2). Sensors were placed in arrays with dense 20 cm spacing to document the soil profile response during shaking. A total of 160 sensors were installed with data collection rate of 256 samples per second.

Pore pressure sensors were deployed in the soil midway between the pile and container boundaries, as well as on both sides on the pile (upslope and downslope). Pressure transducers were installed on both sides of the pile to measure initial static soil pressure during filling and the dynamic pressures during shaking. High sampling accelerometers were deployed in the upslope soil array with the ability to record at 25,000 samples per second. With this high sampling rate, the data can be employed to track shear wave velocity changes (between any two adjacent accelerometers) during the shaking events. Strain gauges were installed on the reinforcement bars before concrete casting. Those gauges were densely deployed along the pile reinforcement before concrete casting. Strain data is used to back-calculate bending moment during shaking. Displacement transducers were mounted on the laminar box exterior wall to measure lateral displacements, and on the soil surface to measure horizontal and vertical displacements. The pile was also instrumented with transducers to measure pile head displacements above the ground surface.

9.7. Analysis Protocol

Focus is placed on system response mainly discussing excess pore-water pressure, displacements and pile bending moments. Thus, representative time histories were chosen to identify that response along with the peak bending moment. Bending moment was calculated based on strain gauge readings placed on the pile reinforcement. Bending moment is an indication of pressures acting on the pile. As the box was mildly inclined at 4°, the soil box started moving downslope when the shaking begun. Liquefaction of the saturated layer was observed during the test. Both soil box and pile head exhibited permanent displacements. The pile was seen to excessively deform and eventually fall on the soil. Cracking and settlement of the crust layer was also observed. A large gap formed between the pile and the upslope ground.

9.8. Soil Response

Input motion (Figure 9-6) for the experiment was in the form of sinusoidal acceleration with a 2 Hz frequency and amplitude of 0.15 g. Motion was gradually increased in 8 cycles to reach the target peak amplitude, to remain constant for 14 cycles, then ramped down in another 8 cycles.

Liquefaction occurred early in the shaking phase as evident from the reduction in acceleration at shallower depths (Figure 9-7, Figure 9-8) and the recorded excess pore pressure ratio r_u (Figure 9-9, Figure 9-10), where $r_u = u_e/\sigma_{vo}'$ in which u_e = excess pore pressure and σ_{vo}' = initial effective vertical stress. Accelerations (Figure 9-7, Figure 9-8) in the base layer show no reduction in values while the loose layer depicts a de-amplification trend. The asymmetric acceleration response is evidence of downslope movement of the soil layer with the spikes observed in the loose layer denoting the dilative tendency of the soil (Zeghal and Elgamal 1994).

Maximum positive accelerations do not coincide in time along the profile height. Rather, a time lag is noted as the wave propagates upwards through the soil.

Excess pore pressure ratios (Figure 9-9, Figure 9-10) show rapid liquefaction in the loose layer as it remained liquefied throughout the shaking event. Downslope records display more dilative response in the liquefied layer as seen from the transient fluctuations. Transducers in the base layer show the layer approaching liquefaction with the upslope records recording higher pore pressure values and significant dilative response. That, in addition to the monotonic peak in the upslope records then sudden drop, is evidence of large relative deformations between the pile and soil (Tokimatsu and Suzuki 2004). This summit response corresponds to the pile behavior exhibiting excessive movement as it fell on the downslope soil, confirming the large displacements between the pile and soil at this region.

Peaks in acceleration are observed to coincide with dips in excess pore pressures. These peaks and dips in acceleration cause the loose soil to exhibit phase transformation behavior as the sand transitions from contractive to dilative and vice versa (Wilson *et al*. 2000).

Excess pore water pressures were measured along the pile length and their ratios are shown in Figure 9-11 and Figure 9-12. It can be observed that: (i) Values fluctuate in the pile vicinity than further away from the pile, (ii) higher dilative tendency is seen near the pile than far from it due to soil moving away from the pile and being affected by its presence, (iii) higher dips in the downslope excess pore pressure than in the upslope due to soil moving away from the pile, (iv) change in rate of pore-pressure buildup in the upslope pile reading in the base layer due to pile failure and sudden movement (extension) away from the upslope soil.

Figure 9-13 shows lateral displacement profiles of the laminar container at selected time instants during the shaking event. From these displaced configurations, it can be noted that deformation was minimal within the crust layer above the water table. In the underlying saturated soil, the middle loose layer follows a curved (parabolic) trend. The underlying dense layer starts to accumulate deformations later than the loose layer as a result of the longer duration towards liquefaction. Figure 9-14 presents the displacements profiles for the first 6 seconds where the low deformations are observed for the base layer coinciding with the low excess pore pressures developed. Most of the deformations are displayed by the loose layer. Shear strain profiles shown in Figure 9-15 confirm that the highest strains are at the lower part of the loose layer and the upper part of the base dense layer for the first 6 seconds. Very low strains exist in the base stratum with virtually zero strains in the crust as it moves as a rigid body on top of the liquefied soil. Additional shear strain profiles till the end of shaking are presented in Figure 9-16 showing the increase in shear strain and displacement accumulation at the loose-dense interface with more strains

accumulating in the dense layer specifically at the base where the highest strains were recorded. Figure 9-17 illustrates the final deformed box configuration.

Soil box top frame displacement shows the same trend as the soil surface deformations (Figure 9-18). Generally, displacements accumulate with a milder slope until the instant of pile failure. Loss of pile resistance seems to affect the rate of accumulation as it continues to build up at a much steeper slope. Soil settles during shaking and accumulates 55 mm of settlement.

9.9. Pile Response

Figure 9-18 shows the pile head displacement compared to the soil and box deformations. Pile head started displacing with shaking and is observed to incur a change in the rate of increase around the 6-8 seconds. The change happens around the onset of pile failure and affects soil deformations as well. Measurements from the strain gauges embedded in the pile show plastic demands in the localized region below the loose-dense layer interface. During shaking, the reinforced concrete pile underwent permanent plastic deformation (Figure 9-19).

Strains placed on the longitudinal reinforcement exceed the material yield strain. Time histories of curvature (Figure 9-19) confirm that the yield curvature (thin horizontal line) is achieved at 1.90 m below soil surface. In general, high curvatures were recorded between 1.30 m and the pile base. Yield curvatures were achieved early on during shaking although peak values were recorded just before the 8 second time frame and the pile was observed to break afterwards.

Bending moment histories were interpolated from the curvatures based on a cyclic material model employed using Opensees. Profiles for bending moment, shear and subgrade reaction are generated for 3 specific time instances. These time instances are identified on Figure 9-18 and Figure 9-19. Profiles for the first time instant (Figure 9-20) denote maximum inertial force acting downslope as identified by the top mass acceleration (Figure 9-18) at 6.215 seconds. Second set

of profiles (Figure 9-21) are for the inertial force acting upslope opposite to the slope movement at 6.98 seconds. Last set (Figure 9-22) is for zero inertial forces at 7.875 seconds. All profiles are chosen for a region were maximum curvatures were achieved right before pile breakage.

Pile response profiles in terms of bending moment and shear along with the soil subgrade reaction are shown in Figure 9-20 for maximum inertial force acting downslope. Negative shear, means upslope direction, negative subgrade means upslope direction as well. Bending moment profile for the case of inertial force with no soil is presented to aid in the analysis. The soil profile is reducing the inertial response as evident from the reduced bending moments, constant shear in the upper 2 layers, with decrease in the base layer. Subgrade reaction shows soil resistance to the pile movement in the base layer. Figure 9-21 presents the second time instant with the inertial force acting upslope. Reversal in bending moments and shear force profiles suggest that the soil is not only resisting the pile moving upslope but applying high pressures. Subgrade reaction profile confirms that, showing the loose layer applying downslope pressures on the pile. The last profile at zero inertial force (Figure 9-22) shows kinematic pressures acting on the pile specifically at the crust level.

Analysis of all 3 profiles together with the previously presented data suggests the out-of-phase response of the inertial and kinematic forces. Furthermore, it is clearly shown that the yielding location of the pile and the spread of the inelastic demand below the loose-dense interface. An estimate of the plastic hinge length can be obtained from integrating curvature profiles greater than the yield value. Plastic hinge length was found to be 0.80 m, approximately 3 pile diameters, starting at 1.70 m depth (approximately 1 Diameter (D) below loose-dense interface), ending at 2.50 m depth (approximately 4 D below interface). Maximum curvature was recorded at 1.90m depth, 2 D below interface.

Pile failure was indicated by the sudden drop in curvatures at approximately 8 seconds of shaking. Curvature drop was noted in all sensors located in the plastic hinge region and below it. Failure can also be observed by the sudden increase in pile head displacements in Figure 9-18. The leap in pile head deformation (loss of its resistance) also affected the soil and box, with Figure 9-13 showing a large increase in deformed profiles after failure. Maximum box profile displacement was 10 cm approximately after 8s then increased to 42 cm (14 s) right after pile failure. This is evidence that the pile foundation provided support to the soil layer and absence of pile resistance will cause excessive movement. Pile head acceleration (Figure 9-18) also show de-amplification upon failure.

The location of the maximum bending moment (1.90 m) just below the loose-dense layer corresponds to both kinematic and inertial maximum response according to previous studies (Randolph 1981, Tokimatsu *et al.* 2005, Lombardi *et al.* 2010). The inertial component in bending moment is calculated to be 16 kN-m at the pile maximum moment location (1.90 m) higher than the recorded values suggesting soil resistance to the acting inertial load.

The behavior of the reinforced concrete pile is largely affected by the lateral pressures (Figure 9-23) and the displacement response as exerted by the stiffer upper crust layer. The values reported are from direct measurement by the total soil pressure transducers. Although the instrumentation recorded values as high as 160 kPa in the crust layer, this false high value is most likely a result of impact and momentum effects. During shaking and till the failure instant, it was observed that pile head displacements were much larger than the surrounding soil and the pile top struck the crust layer each cycle. The high relative pile velocity during the impact increased the recorded pressure reading. This can be confirmed by comparing the pile head and soil surface acceleration records (Figure 9-7, Figure 9-18).

Total pressure values recorded in the loose layer were very small in the range of 6 kPa before liquefaction and decreasing after. Pressures from the base layer are seen to be much larger than those of the loose layer, in the range of 60 kPa. In general, pressures along the pile height were 180° out of phase and peaks in the upper layer total pressure records correspond to their drops in the base layer.

9.10. Post Test Physical Observations

Extensive care was taken after shaking as to not disturb the model before careful inspection and documentation were conducted. Cracking of the soil surface was observed in the pile vicinity on both sides (Figure 9-24). The final pile position was resting on the downslope soil due to its failure, thus a gap was formed on the upslope side. The gap was measured to be 0.32 m deep.

Physical observations of the pile specimen after disassembly support the strain and curvature readings recorded. Cracks in the pile (Figure 9-25 - Figure 9-27) were observed along the majority of the pile starting from the middle of the top layer till the center of the base layer on the upslope face. A total of 13 cracks were noted, with a length of 43 cm from edge to edge and a 15.5 cm spacing. At the base of pile where it interfaces with a pedestal for base fixity and failure ultimately occurred. Spalling was observed with rebar exposure on the tension (upslope) side and crushing on compression (downslope) side.

9.11. Discussion

Among the important observations from this test are:

- Liquefaction of the loose layer was associated with clear reduction in accelerations within the upper zone of the liquefied layer and throughout the overlying ground (up to the ground surface).

- At shallower depths, acceleration behavior after 8 sec has less frequency than from start till 5 seconds (high frequency is propagating from the base upwards). Between 6 to 8 seconds as the character of response is changing, asymmetric behavior and large acceleration spikes show dilation and large strains (also evident in excess pore pressures).
- In general, loose sand excess pore pressures show more pronounced dilation after pile breakage.
- Gradual excess pore pressure build-up is observed in the dense layer, high dilative tendencies occur near the onset of pile breakage as it exhibits high relative displacements along with the soil. Large drops, evidence of dilative response is typical for excess pore pressures in dense sand.
- After 6 seconds, excess pore pressures start to pick up at the base layer, as after pile breakage, it is easier for soil to accumulate shear and build up pore pressures.
- Excess pore pressures in the base layer (1.87 m depth), show high dilative tendencies up to 10 seconds, as the pile moves upslope, the downslope transducers records a dip. After 10 seconds (pile breaks and falls on downslope soil), downslope dips decrease as the relative movement decreases (Downslope negatives are suction as pile moves upslope, upslope negatives are due to dilation as pile moves downslope).
- Deformed shape changes after 6 seconds as the base layer liquefies and starts accumulating deformation, a double parabolic (curved) deformed shape is noted.
- Displacement shape shows crust moving manily as a rigid body, with a parabolic shape in the loose layer and a second parabola in the dense as it loses strength. Such a parabolic deformed shape has been previously observed by other researchers (Elgamal et al. 1996;

Okamura et al. 2001; Dobry and Abdoun 2001; Abdoun et al. 2005; Goh and O'Rourke 2008; Thevanayagam et al. 2009; Dobry et al. 2010).

- The increase in the displacements specifically for the base layer can be attributed to breakage of pile. Deformation of the dense sand became clearer.
- Downslope shear strain accumulation in the liquefiable stratum was of the order of 0.50 % per cycle or more, reaching accumulated shear strains of 35% in the loose liquefied stratum.
- Soil surface displacement history was similar to the box but at lower values. This is an expected response as we move further from the pile, the displacement increases.
- Inertia is driving the high curvatures along the entire profile.
- Kinematic and Inertial forces are out-of-phase, curvature peaks coincide with the inertial force acting downslope.
- After pile failure, recorded reduction in top acceleration of mass is a direct result of pile loss of stiffness (reducing accelerations propagating upwards).
- There is a difference between dense and very dense sand profiles and very stiff clay when existing below loose liquefied layers, as liquefaction of the loose layer will result in weakening of the dense sand under it.
- Pile yielded and was getting weaker starting around 4 seconds, through 8 seconds when it broke (with curvature history at 2.90 m, staying constant till 8sec). Failure occurred at 8 seconds approximately, followed by curvature reduction along height. Upper layer was still feeling the effect of inertial mass till 10 seconds as evident by the negative curvatures.
- Settlement was increasing until 6 seconds then was steady and started to pick up after the pile broke.

9.12. Conclusions

A 3-layer soil stratum (Figure 9-2), at a 4-degree inclined configuration and a 0.25 m reinforced concrete pile was investigated using a 1-g shaking table experiment. The pile was subjected to local plastic demands, particularly where interfaces between soils of different stiffness exist. This popular configuration has been adopted widely in centrifuge tests; however, this investigation takes advantage of the large scale, reinforced concrete material, and inertial loading to study the inelastic behavior. The main outcomes are:

1. In the liquefiable layer, accumulated lateral strains are not uniform, and are highest near its base (interface with dense layer).

2. In the underlying dense layer, lateral strains are highest near its top at the interface with the overlying loose liquefied layer.

3. a) The underlying dense layer is affected by liquefaction of the loose layer above. As the base layer was not constructed to be adequately dense, it was subjected to high pore pressures from the overlying layer and affected by the pile failure.

b) Excess pore pressures migrate into the dense sand stratum, weakening its upper zone, allowing for a lower contrast between the stiffness of the upper liquefied and the lower denser soil formations.

4. At the interface between the saturated loose and underlying dense strata, plastic region is distributed over a large extent of its length (3D). In this test, peak curvature and moment occurred 2D below the interface between the loose and dense strata.

5. Inertia is driving the high curvatures along the entire profile. Kinematic and Inertial forces are out-of-phase, curvature peaks coincide with the inertial force acting downslope.

6. Total pressures are 180° out of phase between the upper crust and lower base layer. This suggests that the base layer resisted the pressures exerted by the upper crust. Acceleration records confirm this observation.

7. Pile foundation provides support to the soil layer and absence of pile resistance will cause excessive movement as observed after pile failure during shaking when deformation rate increased greatly post failure.

8. Excess pore-water pressures around the pile in a dense stratum decreases greatly with increase in soil-pile relative displacement. This phenomenon results in an increase in subgrade reaction due to this dilative response. In looser soils, pore pressures did not decrease appreciably, producing a softening behavior.

9.13. Acknowledgements

Chapter 9, in full, is currently being prepared for submission for publication of the material as it may appear in the following journal publication (The dissertation author was the primary investigator and author of this paper):

Ebeido, A. and Elgamal, A., "Response of Reinforced Concrete Pile in Multi-layer Lateral Spreading Liquefaction Shake Table Test".

Chapter 9, in part, is a reprint of material as it appears in the following conference publication (The dissertation author was the primary investigator and author of this paper):

Ebeido, A., Zayed, M., Kim, K., Wilson, P., and Elgamal, A., (2018). Large Scale Geotechnical Shake Table Testing at the University of California San Diego. Proc. of the 2nd GeoMEast International Congress and Exhibition on Sustainable Civil Infrastructures. Cairo, Egypt. 24-28 November.

Figure 9-1. Pictures of 1-g shake table test model

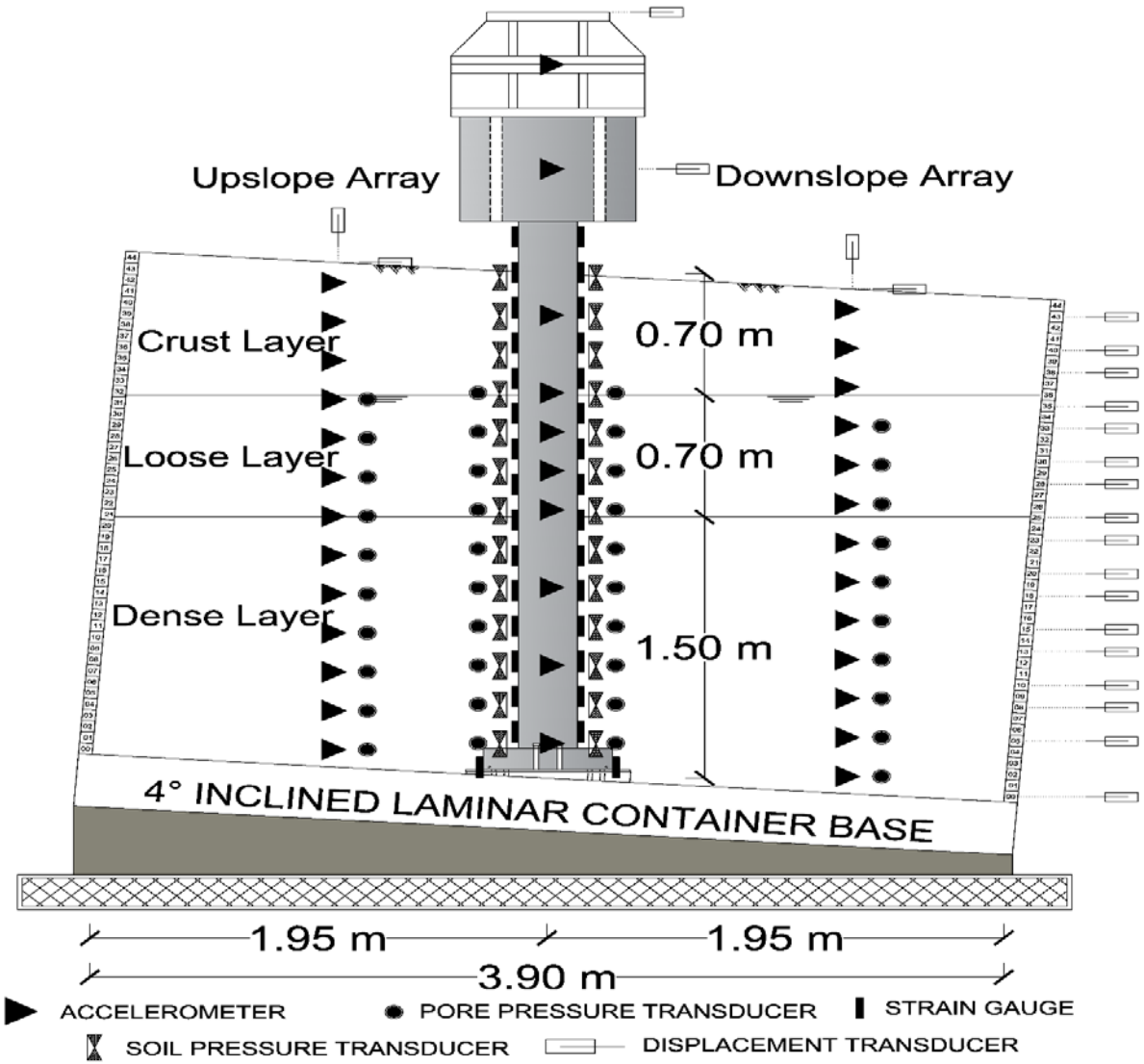

Figure 9-2. Schematic Layout of the test model

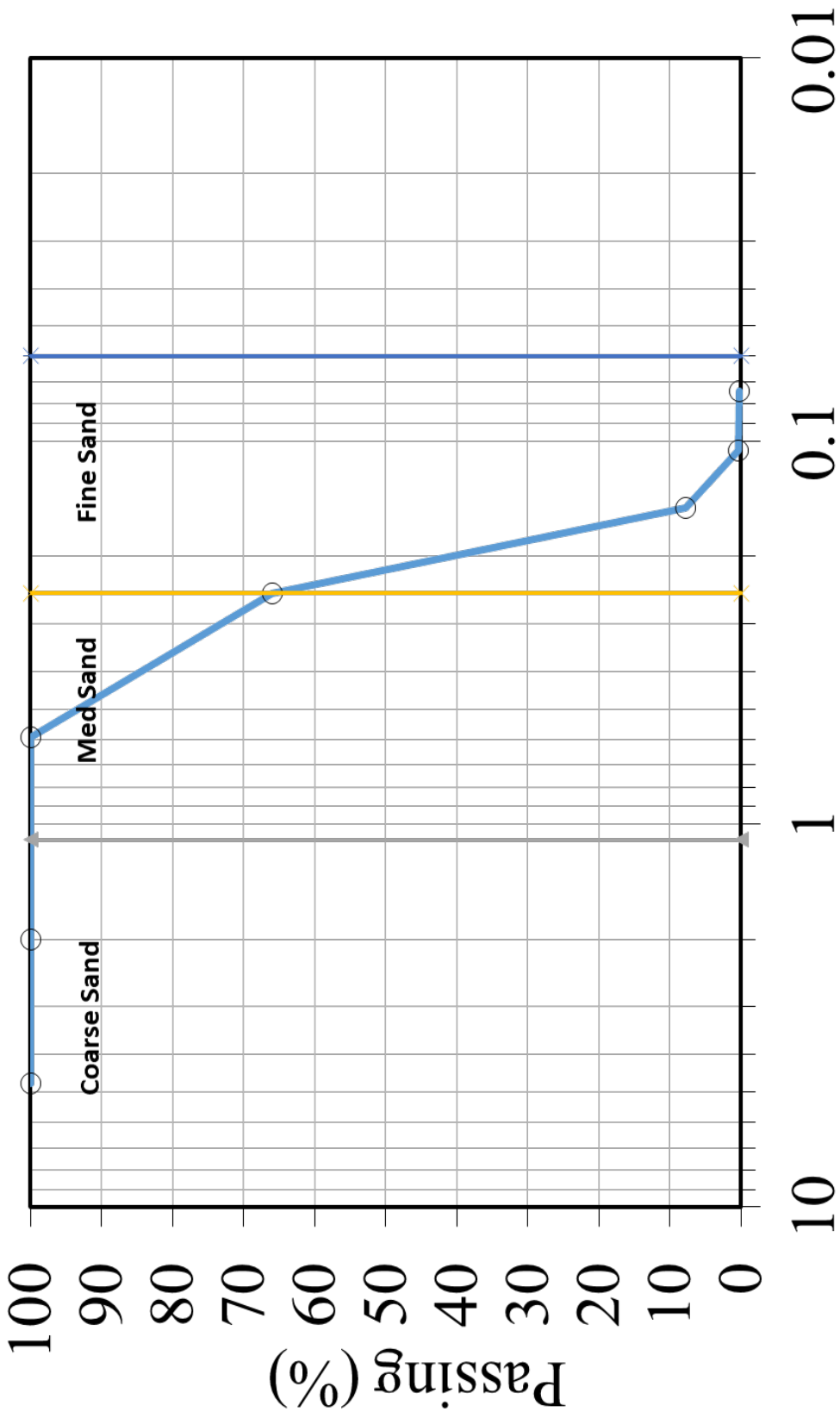

Figure 9-3. Grain size distribution for Ottawa F-65 sand employed in testing

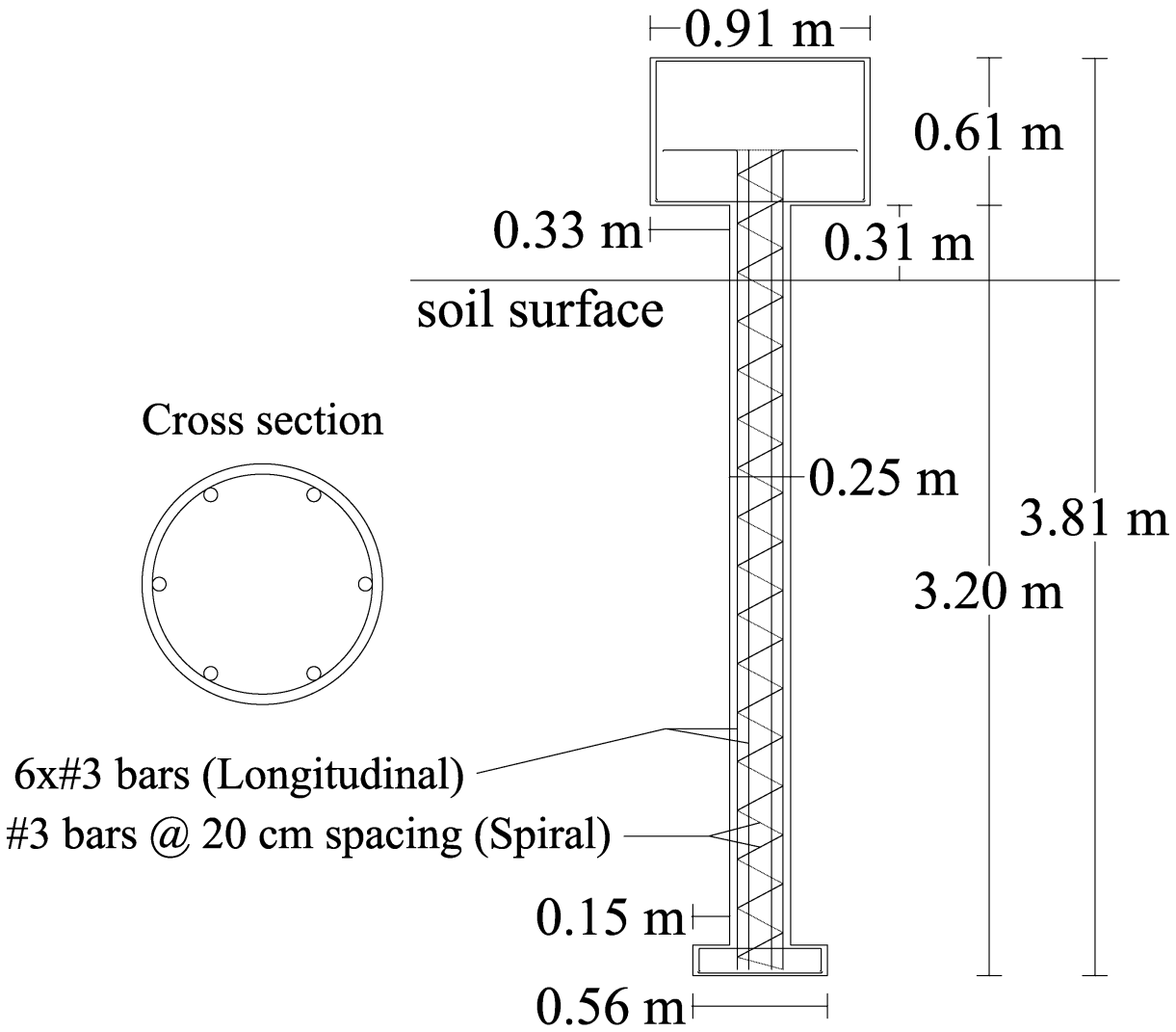

Figure 9-4. Reinforced concrete pile details

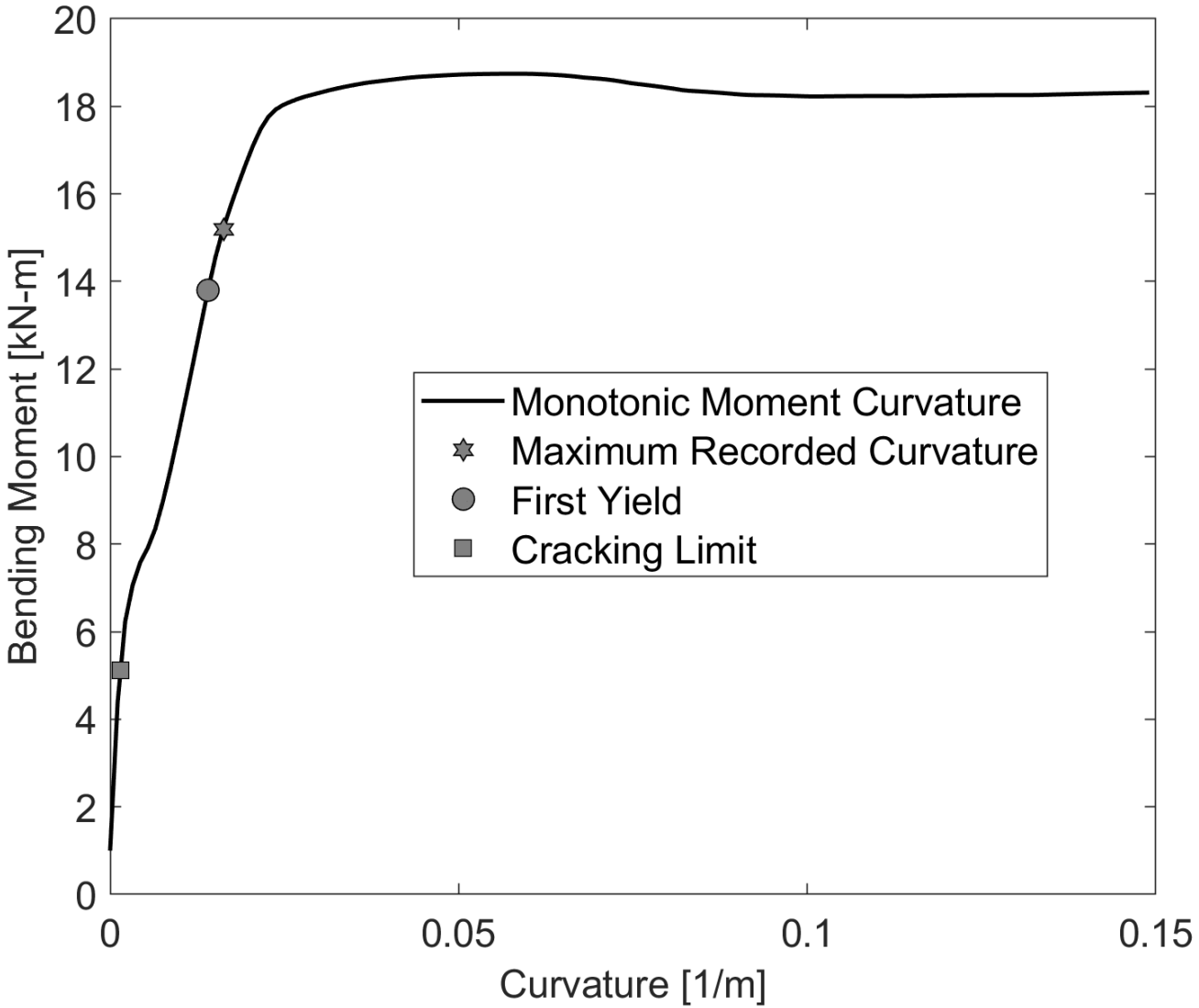

Figure 9-5. Monotonic moment-curvature for concrete pile

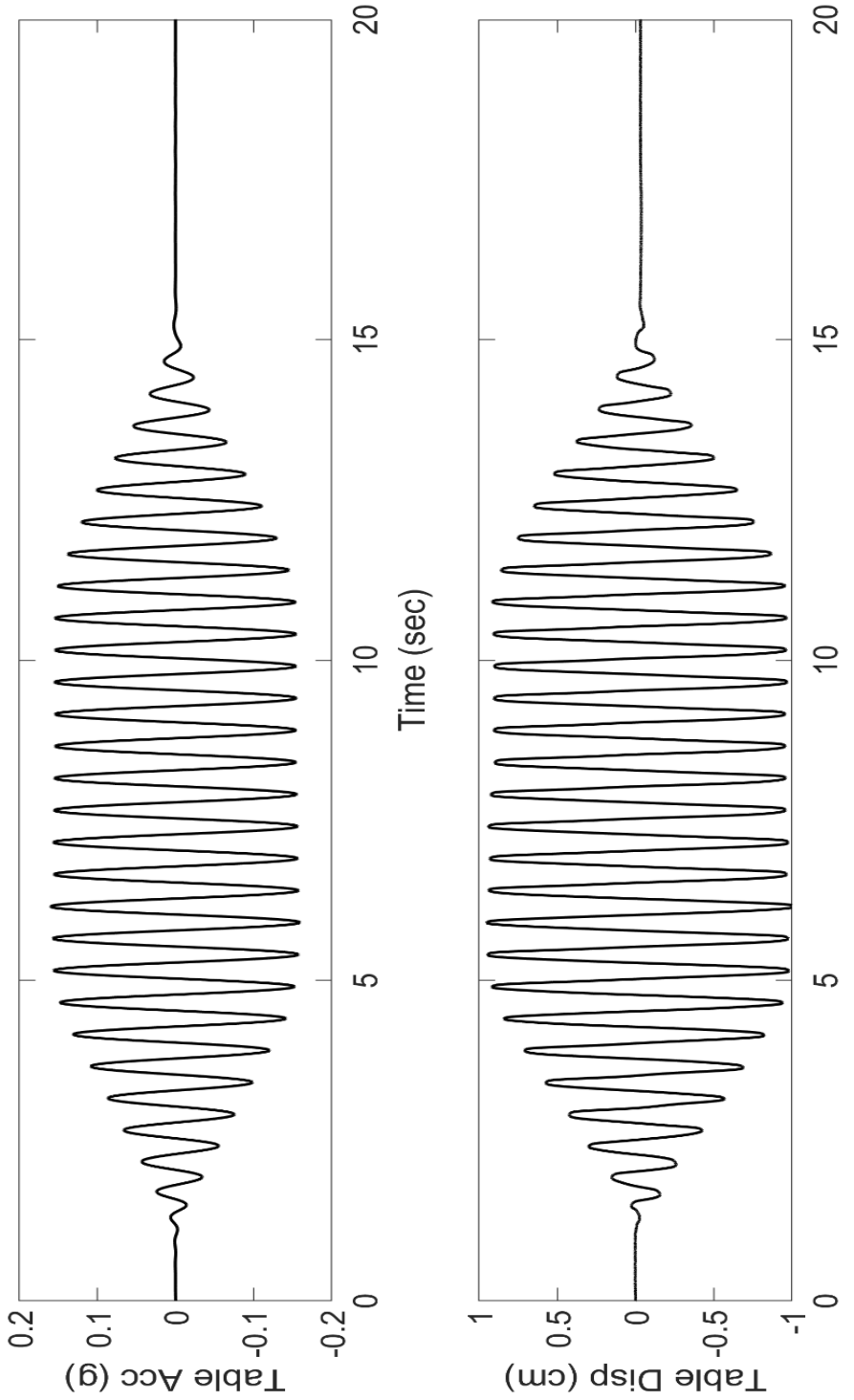

Figure 9-6. Input motion from shake table (acceleration and displacement)

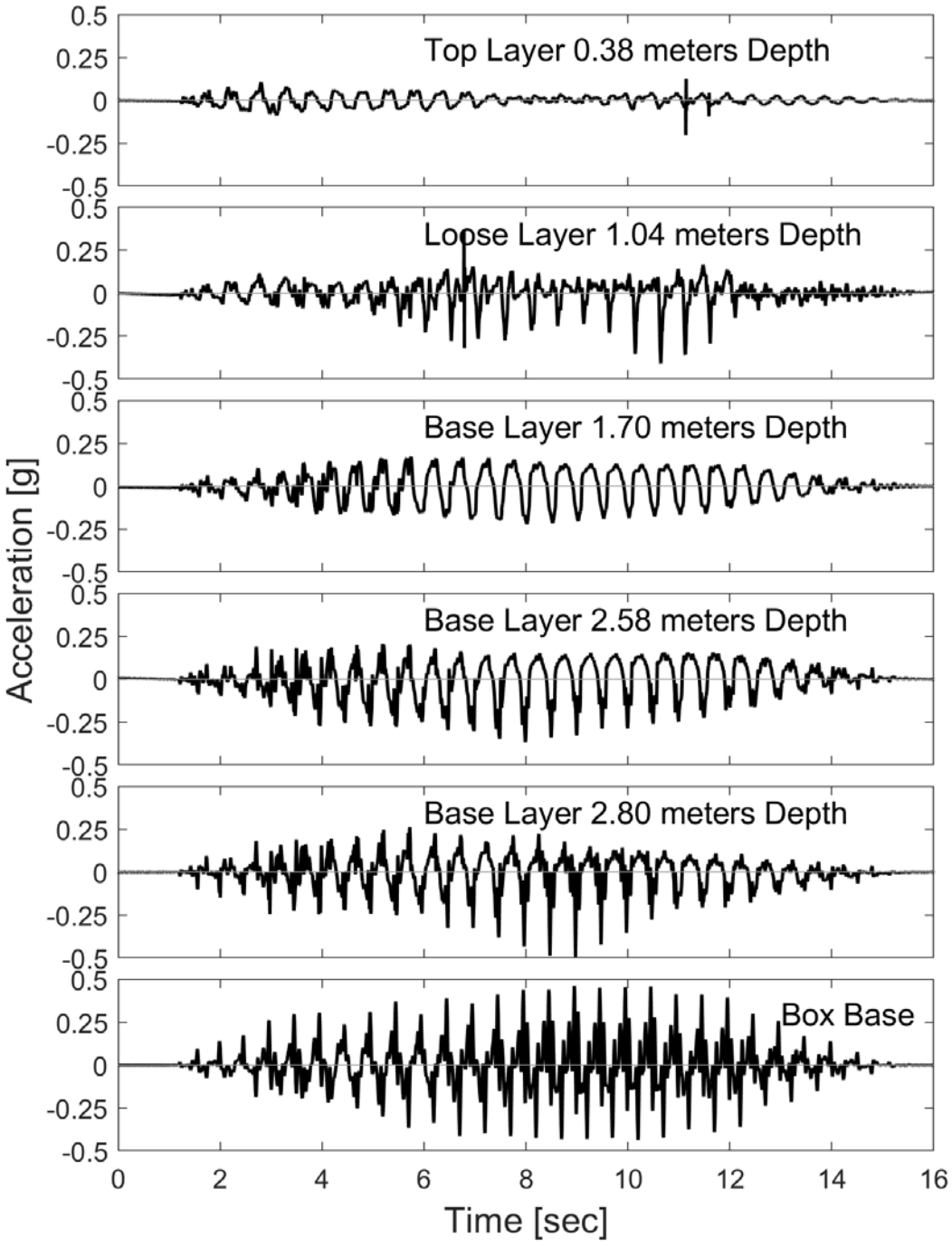

Figure 9-7. Soil acceleration selected time histories at the downslope array

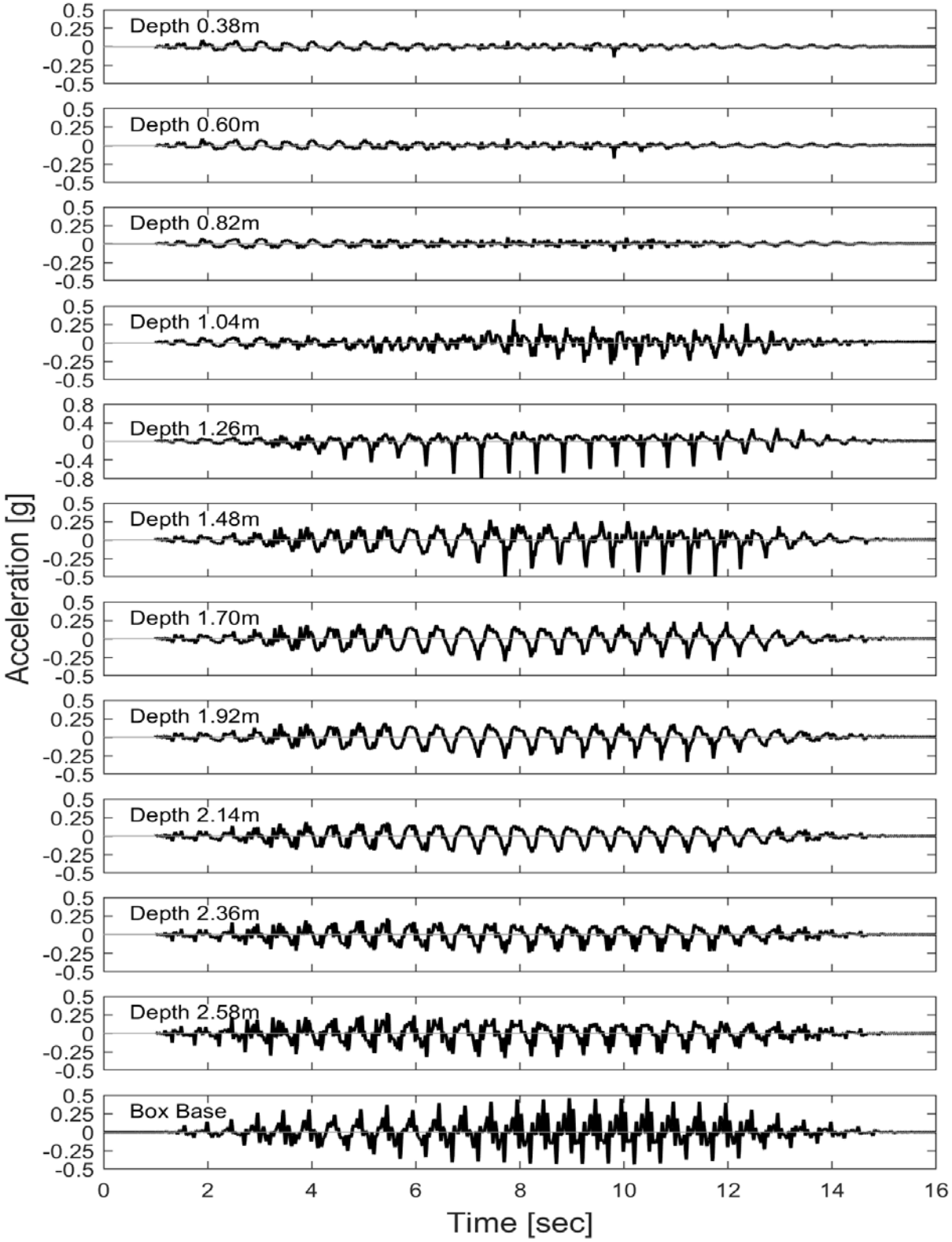

Figure 9-8. Soil acceleration time histories along model height at the upslope array

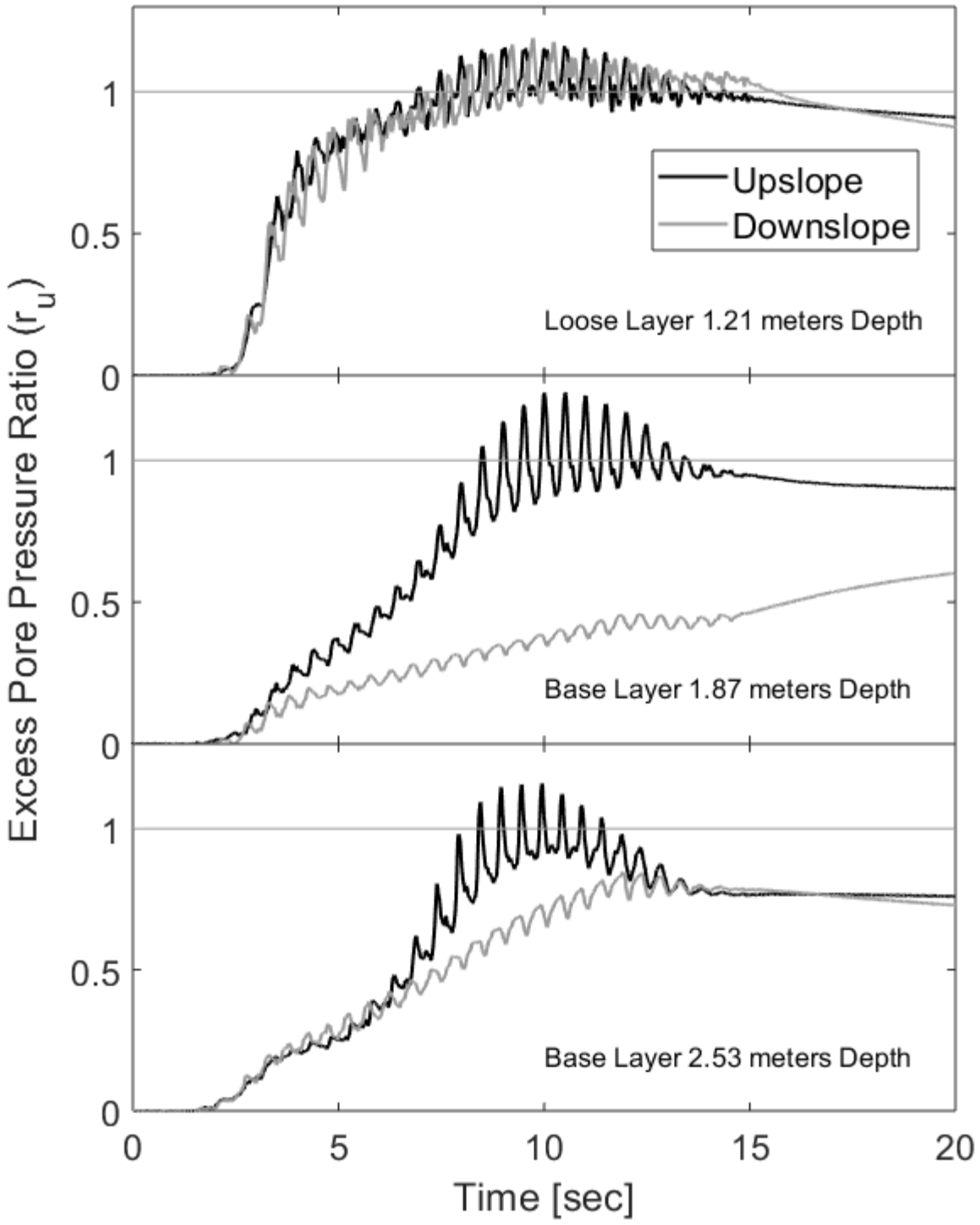

Figure 9-9. Excess pore water pressure time histories in the upslope and downslope soil at select locations

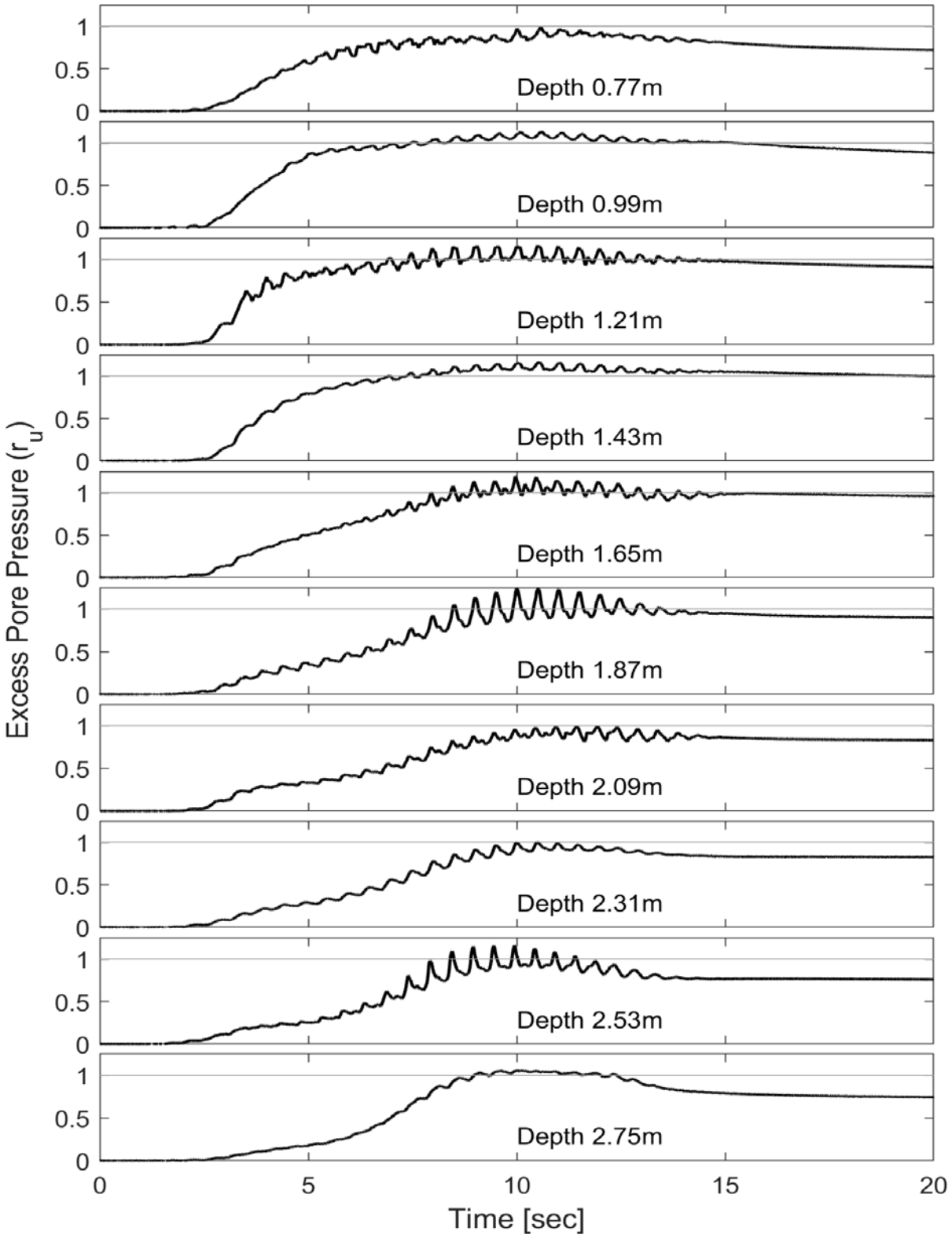

Figure 9-10. Excess pore pressure ratio time histories along model height in the upslope array

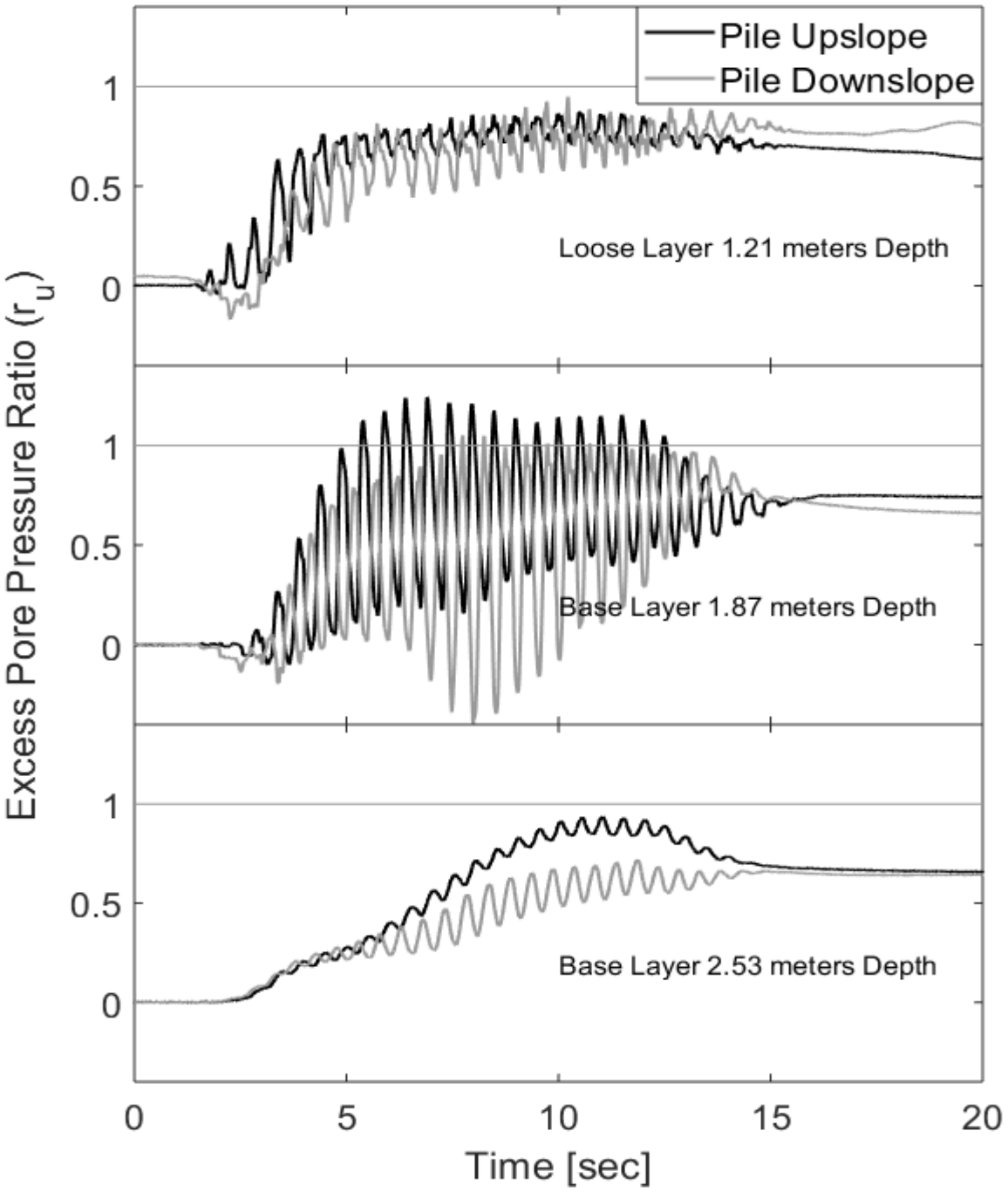

Figure 9-11. Excess pore water pressures recorded in the pile vicinity

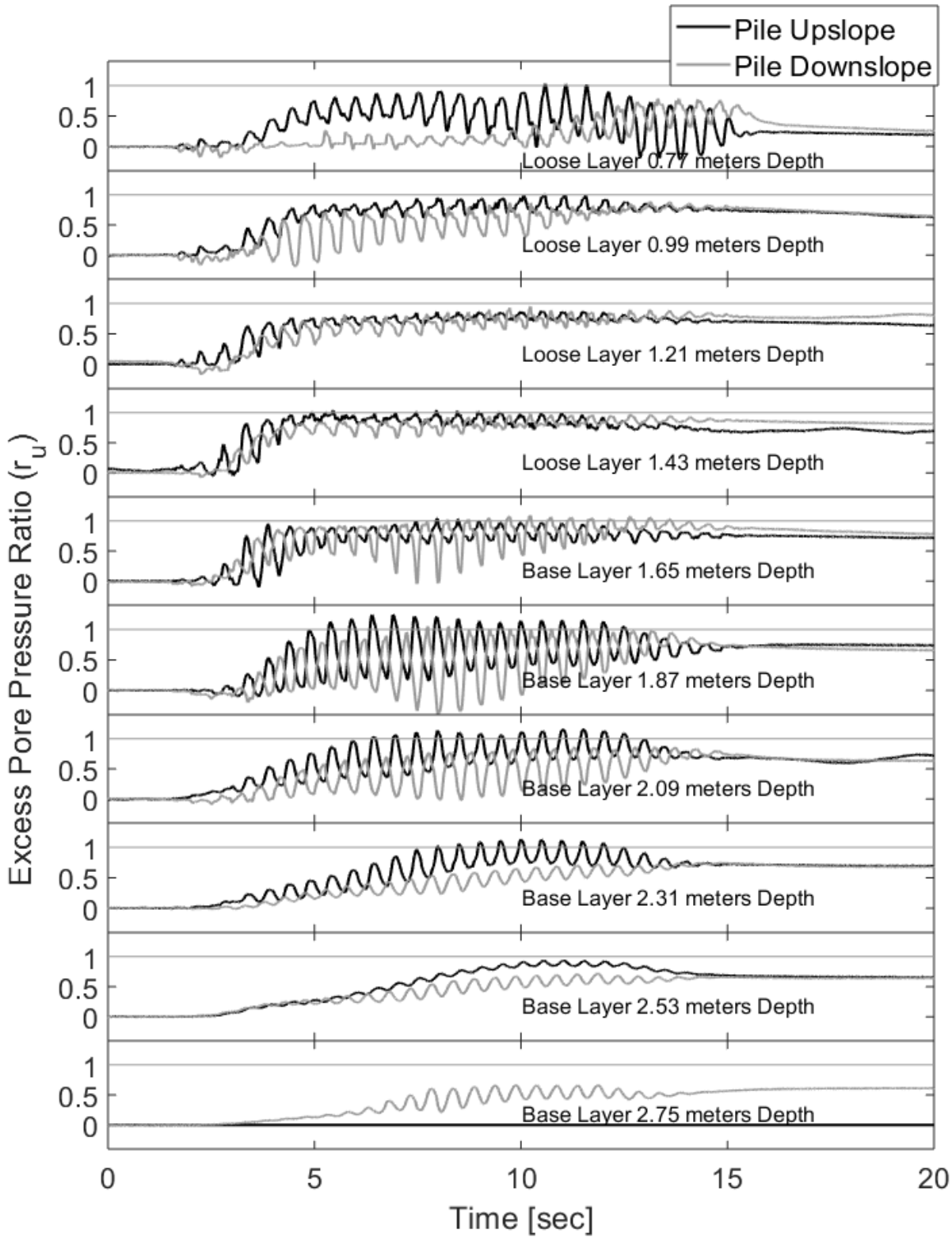

Figure 9-12. Excess pore water pressures time histories along model height on both sides of the pile

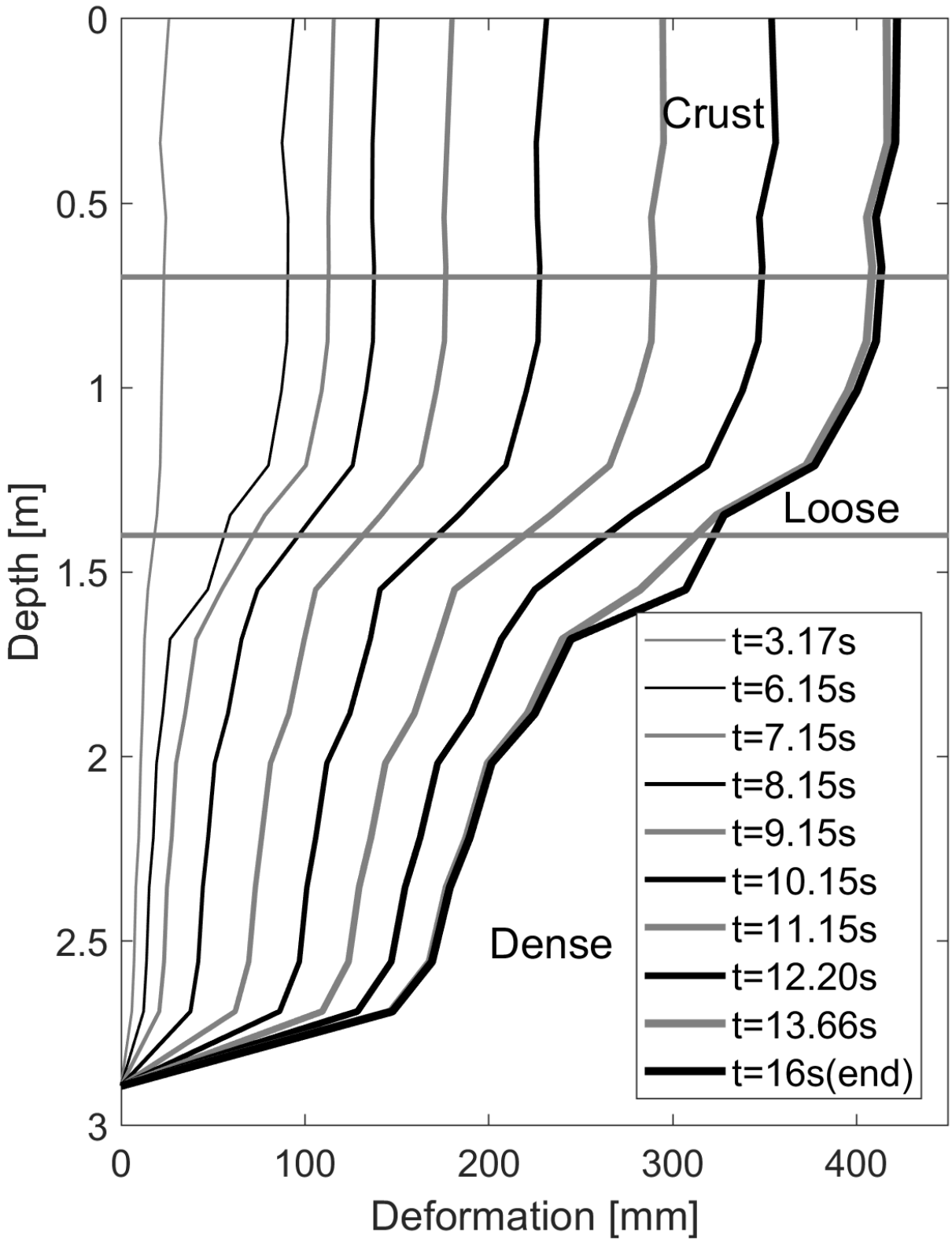

Figure 9-13. Soil box displacement profiles throughout the shaking

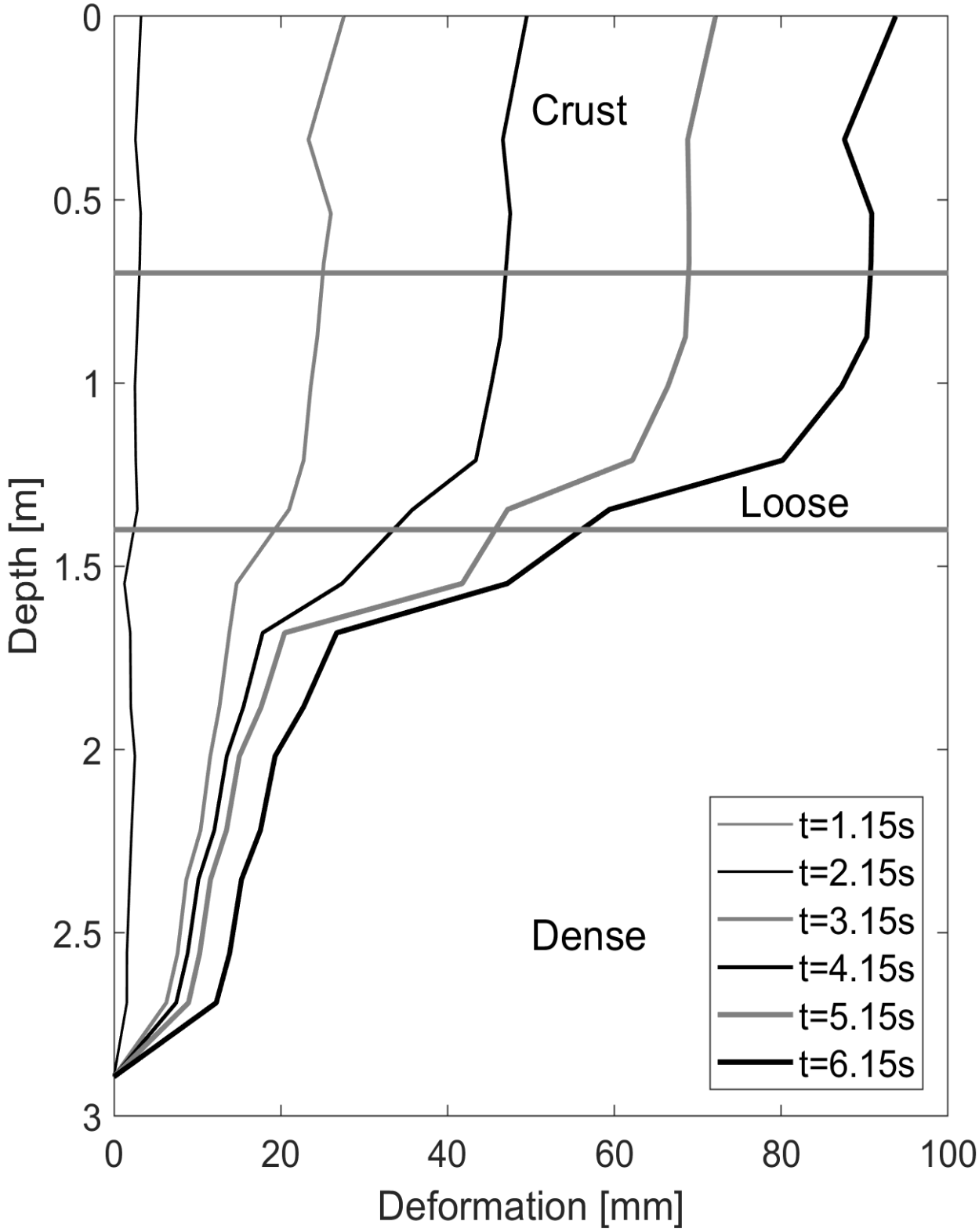

Figure 9-14. Soil box displacement profiles for the first 6 seconds of shaking

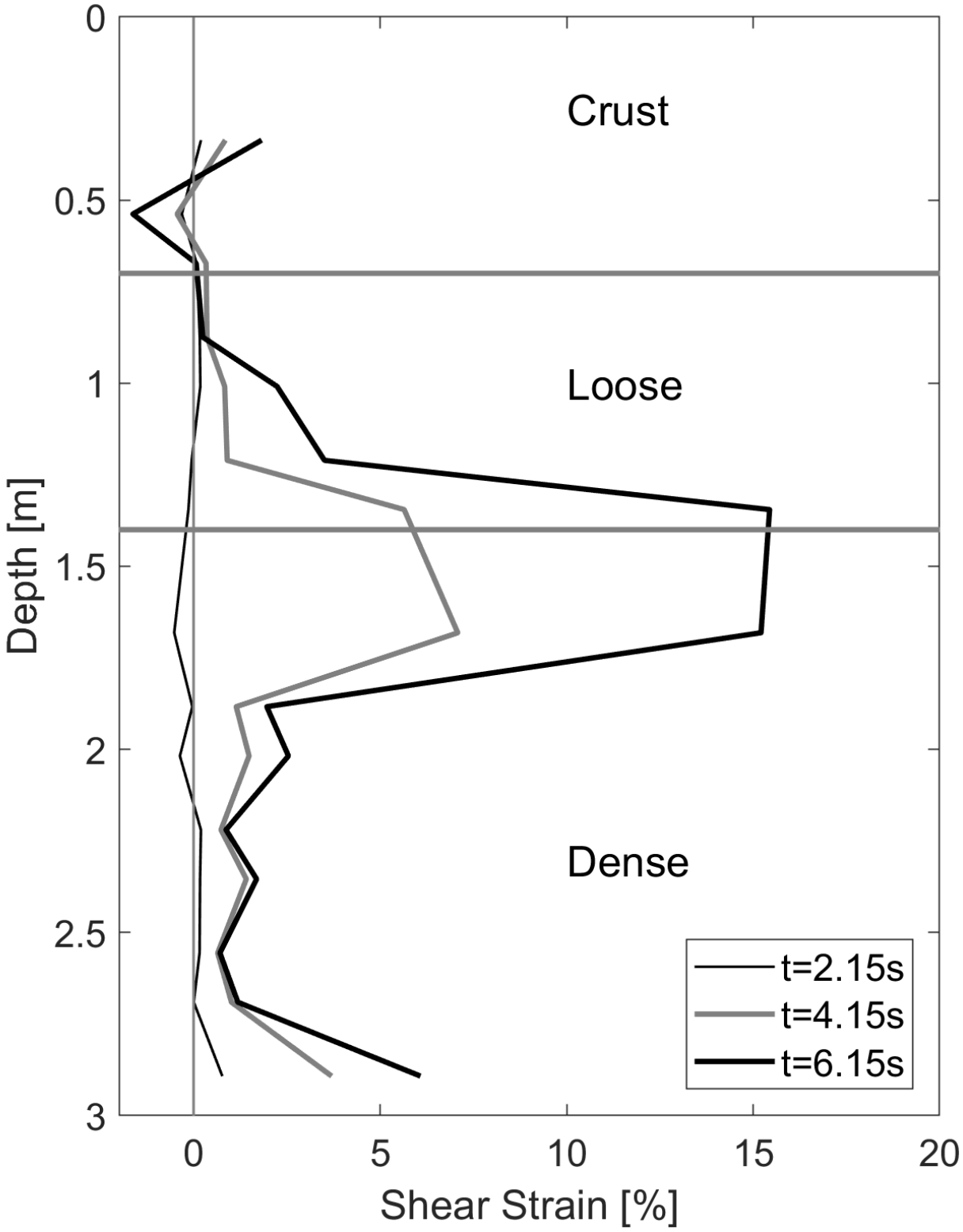

Figure 9-15. Soil box shear strain profiles for the first 6 seconds of shaking

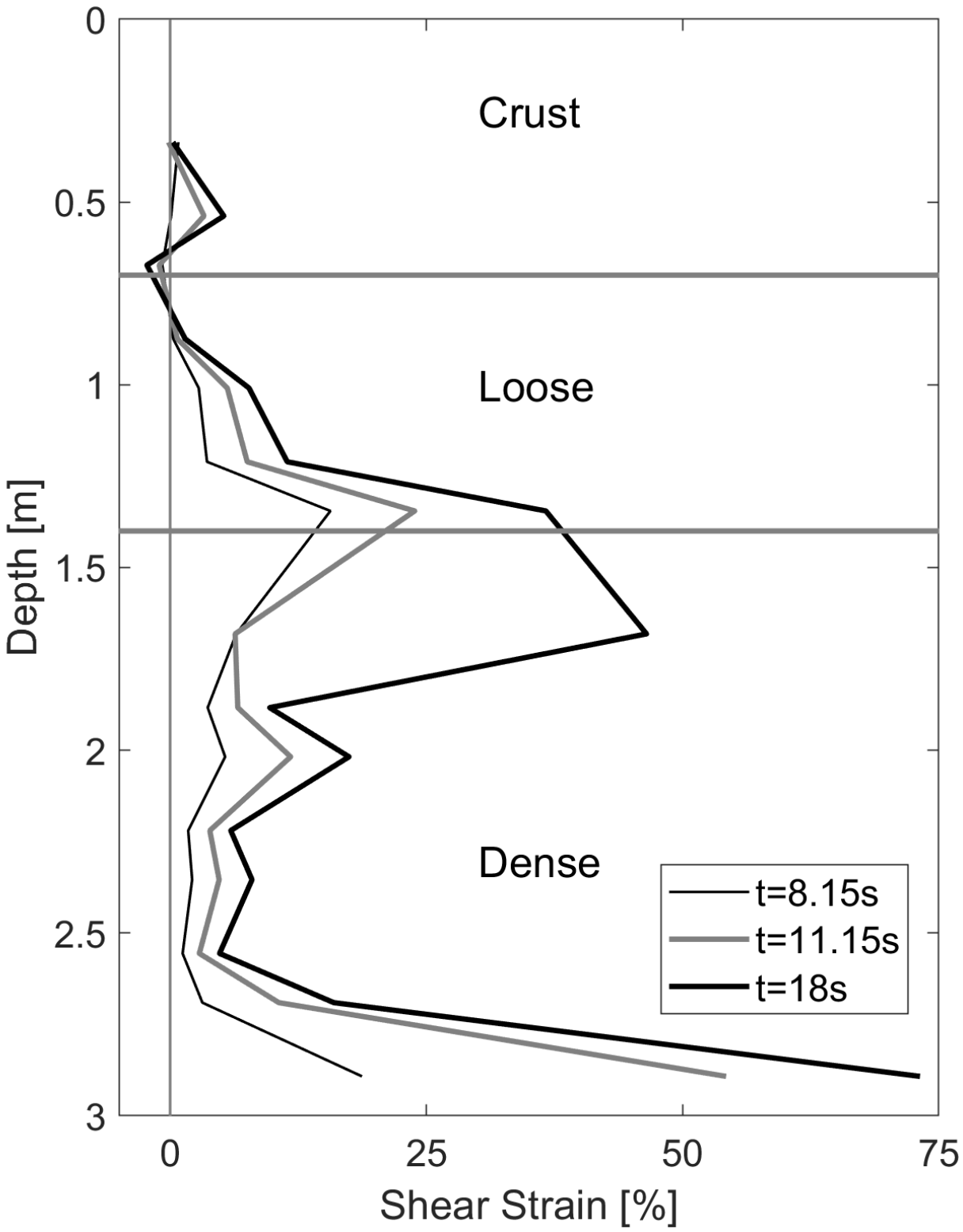

Figure 9-16. Soil box shear strain profiles throughout the shaking

Figure 9-17. Deformed laminar box configuration after shaking

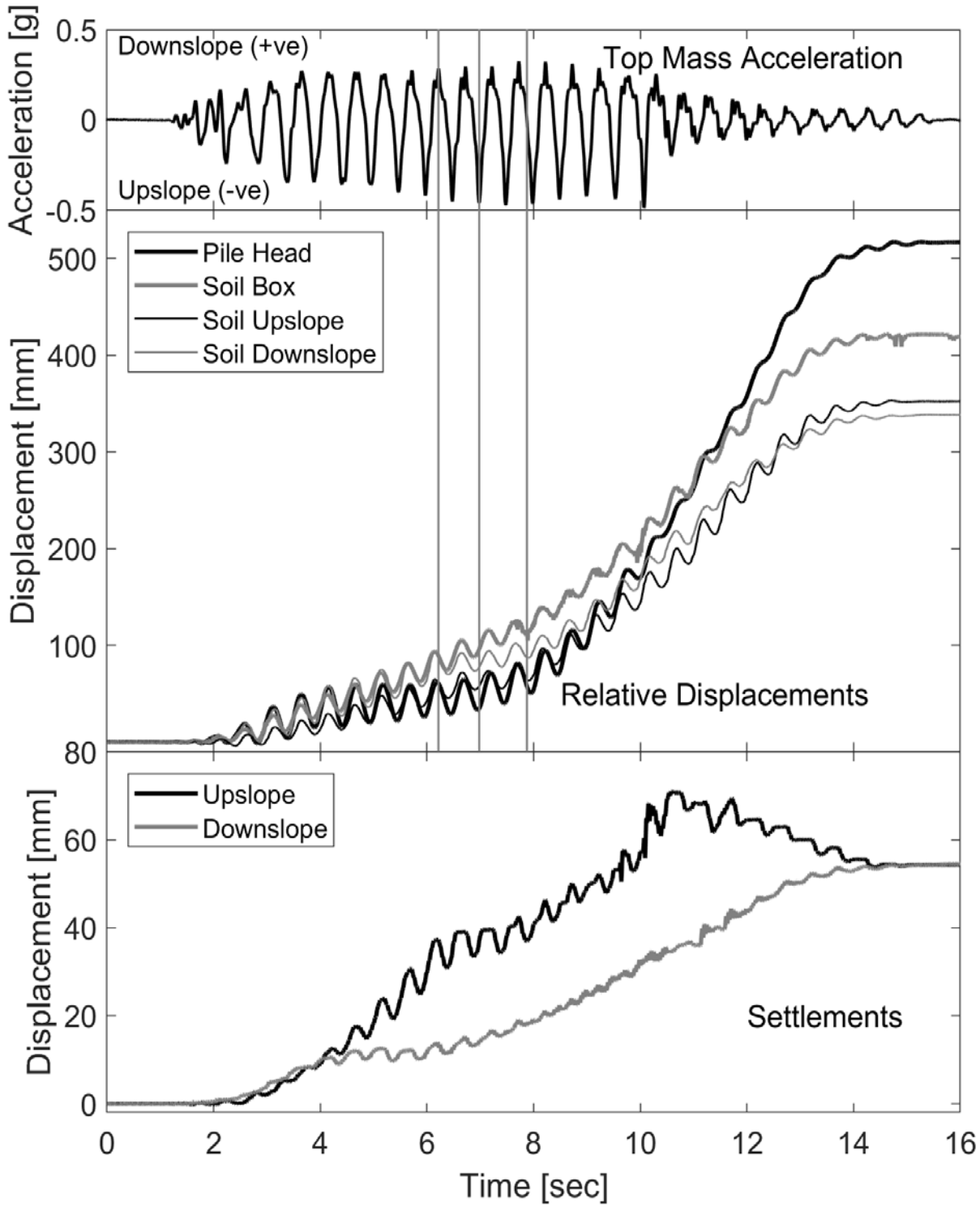

Figure 9-18. Pile head accelerations, pile and soil displacements and soil settlement time histories

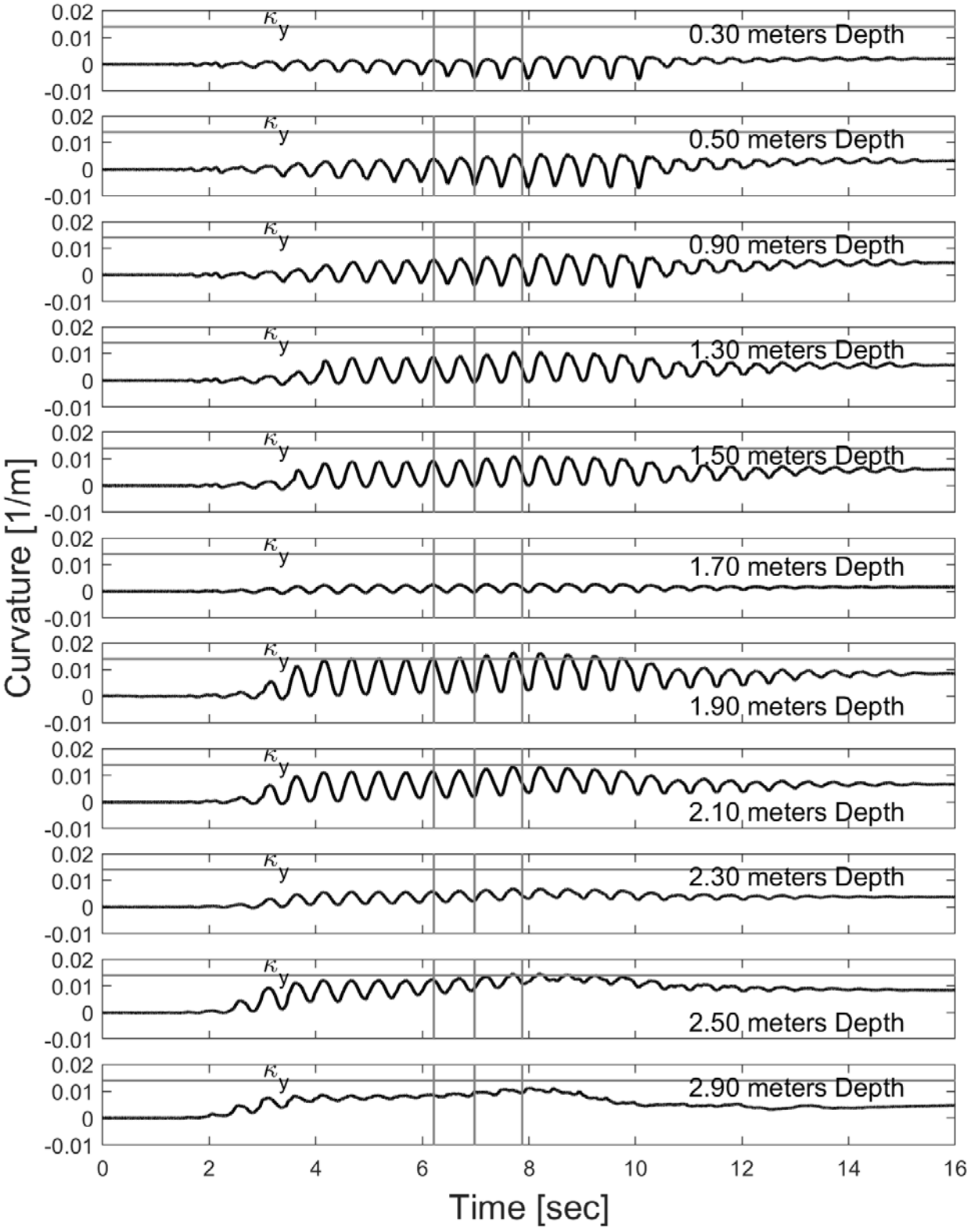

Figure 9-19. Curvature time histories along the pile profile

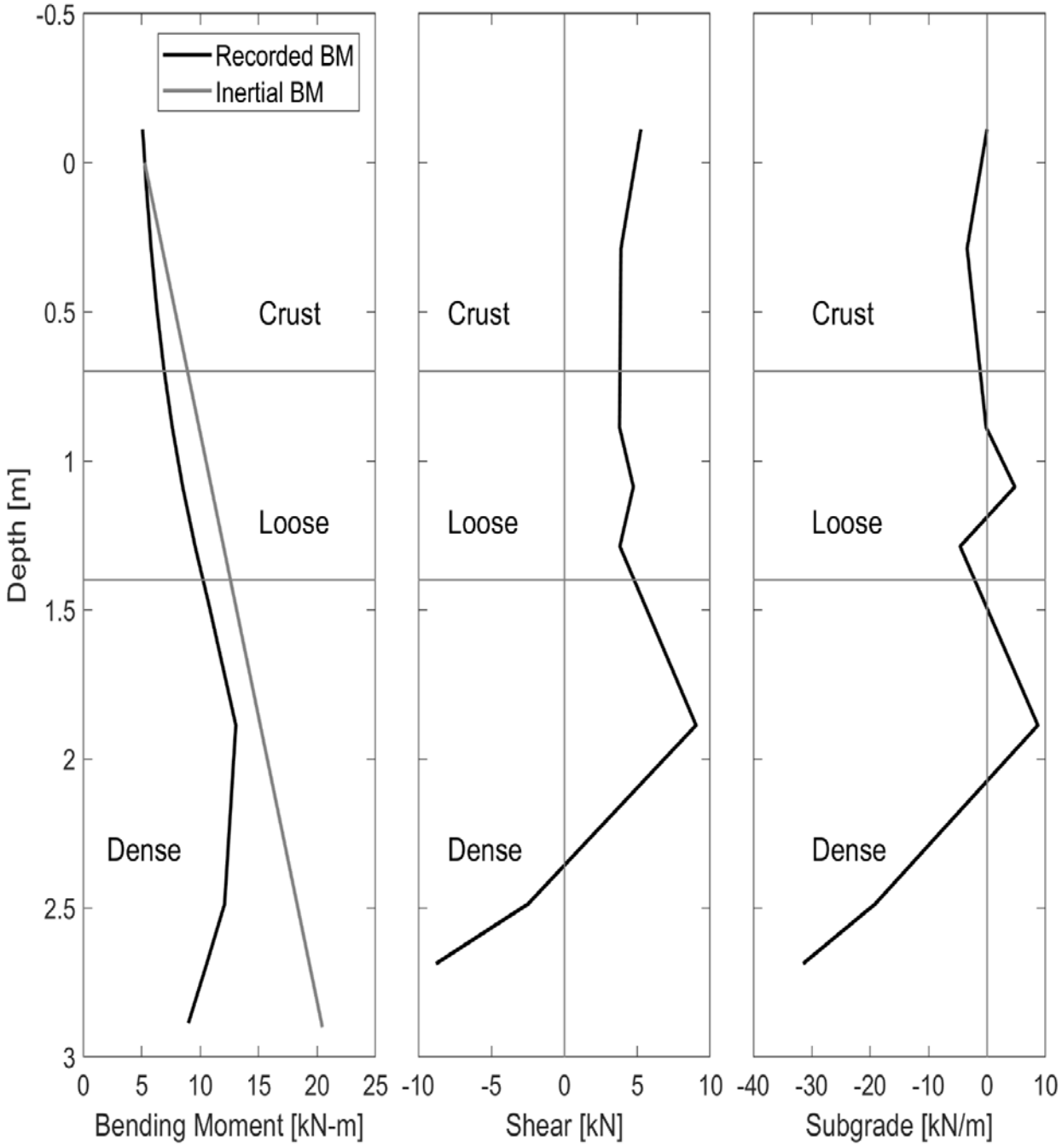

Figure 9-20. Pile response profiles at maximum inertia in the downslope direction (6.215 sec)

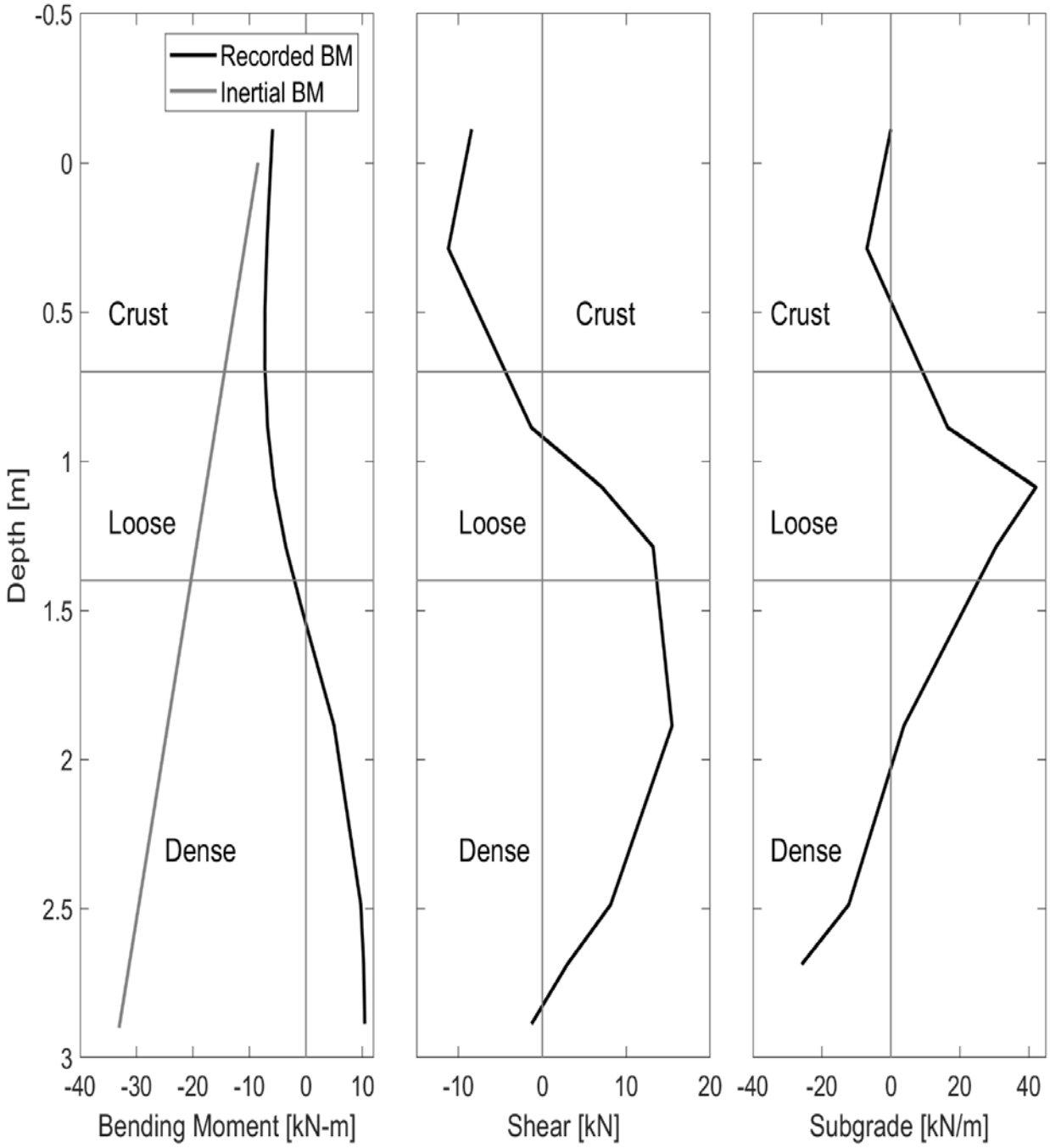

Figure 9-21. Pile response profiles at maximum inertia in the upslope direction (6.98 sec)

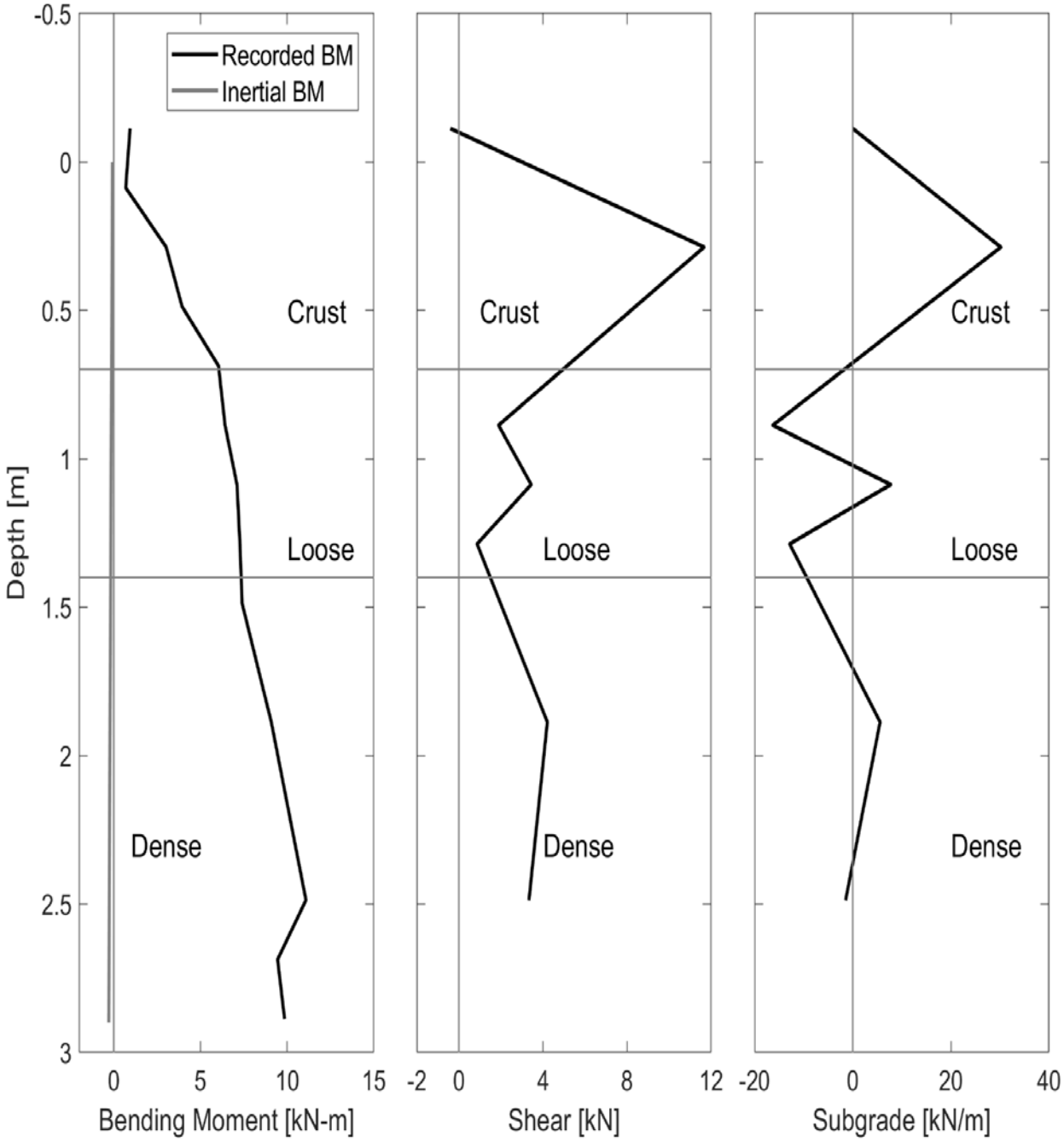

Figure 9-22. Pile response profiles at zero inertial force from the top mass (7.875 sec)

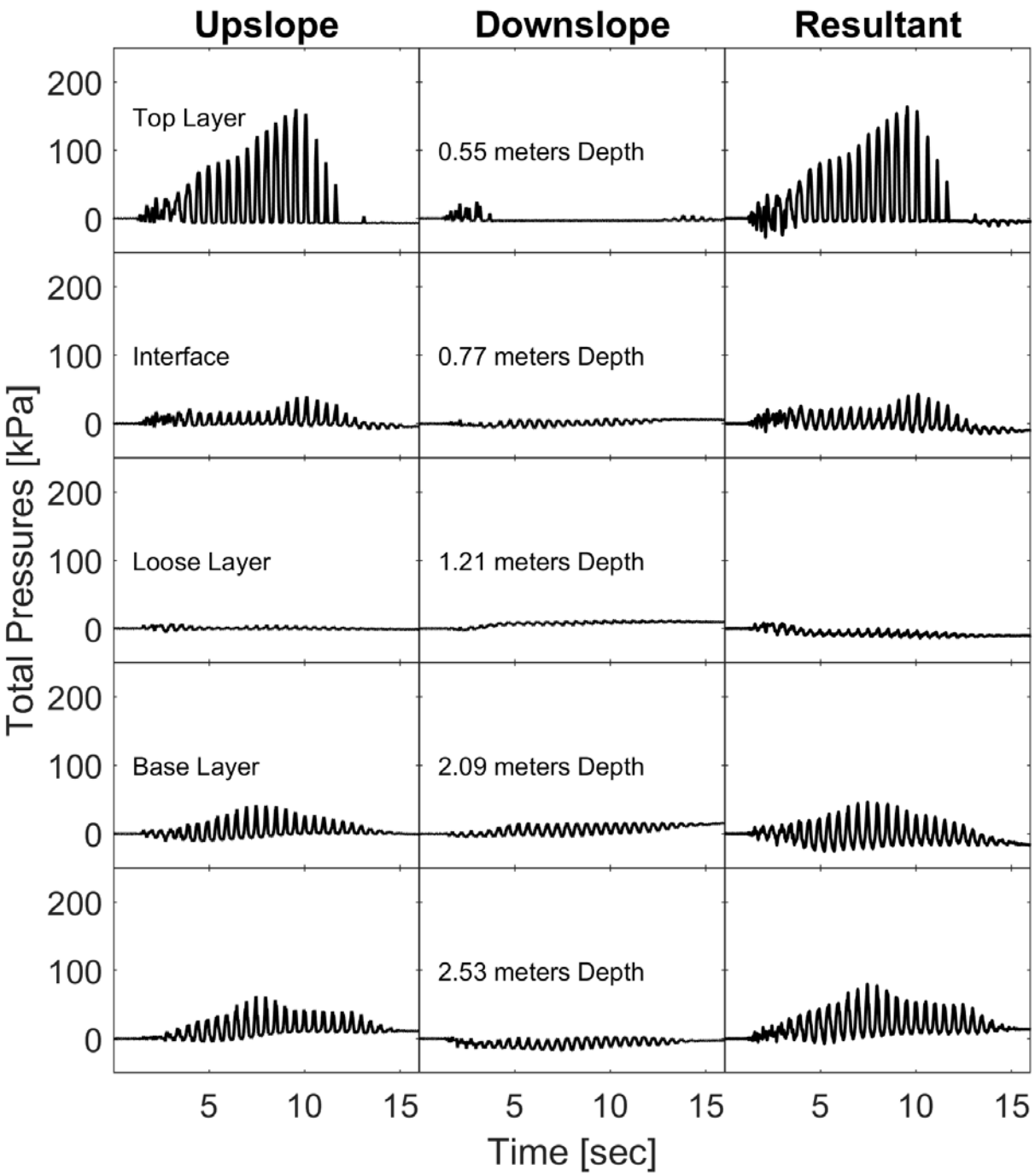

Figure 9-23. Total pressure time histories showing upslope, downslope and resultant

Figure 9-24. Final permanent deformation of the pile head supported by downslope soil

Figure 9-25. Observed breakage of the concrete pile at the base and cracking along the height

Figure 9-26. Pile breakage at the base

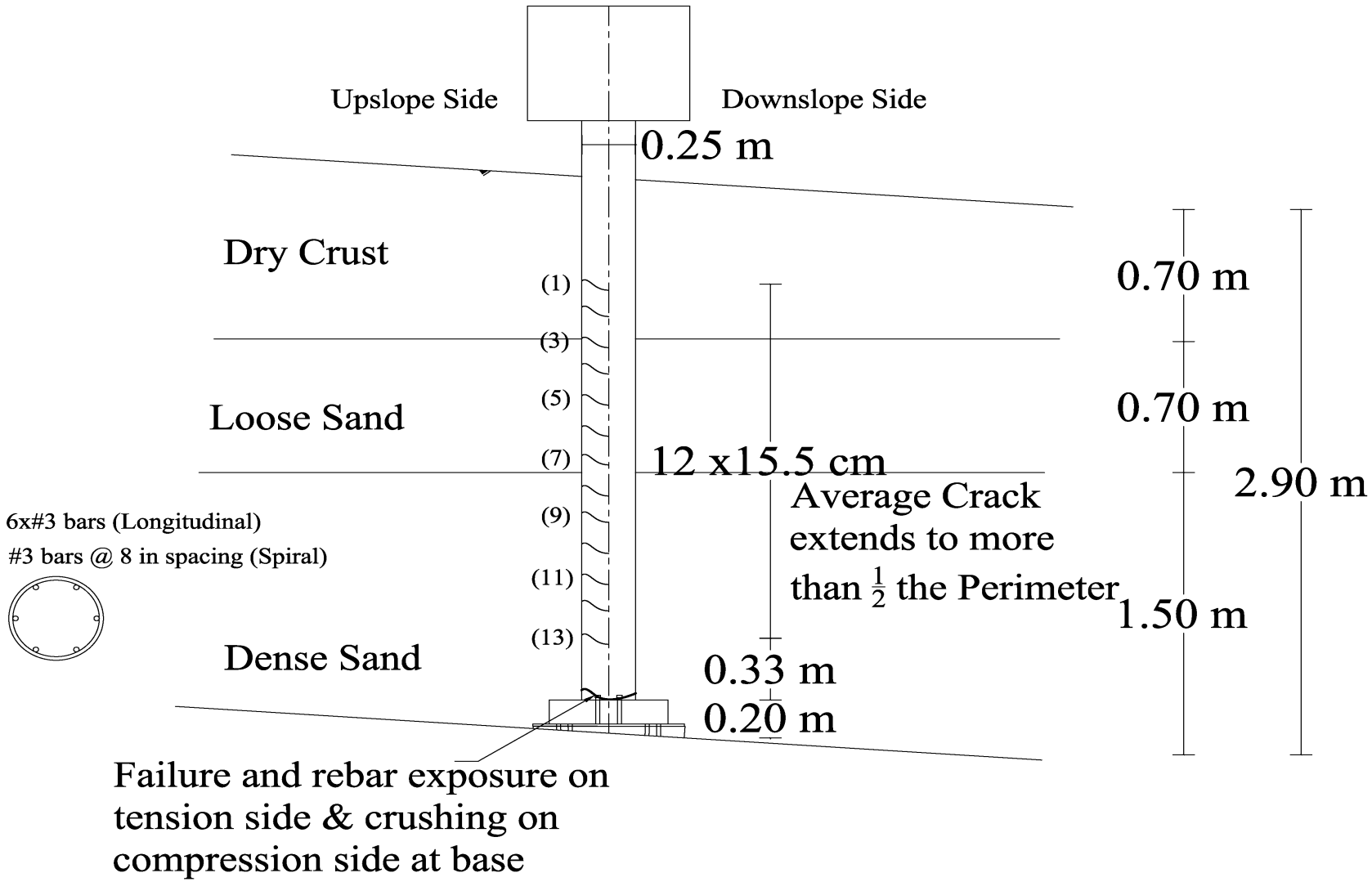

Figure 9-27. Layout of pile crack development during shaking

Chapter 10 Effect of Pile Head Restraint on the Soil-Pile Response in Large Shake Table Testing

10.1. Abstract

A large-scale laminar container shaking table experiment was conducted to investigate a restraint single pile response, due to the mechanism of liquefaction-induced lateral spreading. The pile was fixed at the base and pinned at the top placed in a 3 layered 5 m soil profile. Soil profile is characterized and discussed. Recorded data sets from this experiment are analyzed to document and track the evolution of lateral loading on the deployed single pile. The entire system response is evaluated. Ground and pile lateral displacement as well as excess pore pressures are discussed. In this test, the effect of the pile head restraint is investigated as it correlates to the pile lateral loads and observations from the recorded soil pressures and calculated bending moment. The restraint is seen to affect the box permeant displacement. As the soil liquefies, further shear strength reduction might permit the soil to more easily flow around the piles. As such, lateral ground deformation that continues to accumulate during the shaking process may not always result in significantly larger lateral pile loads.

10.2. Introduction

Damage of pile supported structures in laterally spreading liquefiable soils has been observed after many major earthquakes (Yoshida and Hamada 1990; Hamada and O'Rourke 1992; Tokimatsu and Asaka 1998; Mylonakis *et al.* 2006; Bhattacharya *et al.* 2011). Thus, the complex loading mechanism and pile foundation design in such soil remains a subject of research interest (Lombardi and Bhattacharya 2014; Finn 2015).

Case histories and physical modelling have been a crucial tool in fully investigating the effects of lateral spreading on pile foundation. Experiments on deep foundation has been

conducted in both centrifuge (Wilson *et al.* 2000; Abdoun *et al.* 2003; Gonzalez *et al.* 2009) and large scale (Suzuki *et al.* 2004; He *et al.* 2006; Towhata *et al.* 2006). With centrifuge testing emerging as a vital and cost-effective tool to study the problem (Dobry and Abdoun 2001), large scale testing although expensive and time consuming are still an important tool to complement the centrifuge and further investigate the material and mechanisms that cannot be modelled in smaller scales (Ubilla *et al.* 2011; Ebeido *et al.* 2018).

Design codes (JRA 1996; JRA 2002; EN 1998-5 Eurocode 8) advise engineers to consider both the kinematic loading exerted by the soil lateral pressures and the inertial forces due to the superstructure accelerations. These codes focus on the bending moment as the primary failure response with various aspects of bending failure mechanisms studied by (Dobry and Abdoun 1998; Wilson *et al.* 2000; Ramos *et al.* 2000; Cubrinovski and Ishihara 2004; Brandenberg *et al.* 2005; Tokimatsu and Suzuki 2005). This study builds on earlier work by investigating the aspect of pile restraint effect on its response and system behavior.

In the following sections, the experiment program is outlined. Recorded response time histories such as bending moments, displacements, and excess pore water pressures are discussed. Data from this test program are employed to document and elucidate the observed salient response characteristics. Finally, conclusions are drawn, and recommendations are presented.

10.3. Experimental Program

Figure 10-1 shows a picture of the laminar box set up mounted on the shake table at the Englekirk Structural Engineering Research Center at the University of California, San Diego. The container was inclined at 4° to the horizontal by means of an outside reinforced concrete ramp. The laminar box is composed of 31 stacked steel frames. The frames are lined with stainless steel plates to reduce their friction with their supporting roller bearings. A total number of 18 bearings

were placed between each 2 frames and rollers were painted by a smooth epoxy paint to further reduce the friction loses. This allows for optimum lateral movement and give minimal boundary effects. The entire box-ramp system was post tensioned to the shake table to ensure a very stiff connection. The response of a steel pipe pile restraint at the top was explored against liquefaction induced lateral spreading. Figure 10-2 presents a plan picture taken by a drone to show the pile restraint. Figure 10-3 and Figure 10-4 present the schematic model layout of the experiment and its plan view. Inner box dimensions are 6.75 m long, 4.90 m high and 3.0 m wide. As noted by (Law and Lam 2001), this laminar box configuration essentially simulates a periodic boundary condition. The container was lined with an Ethylene Propylene Diene Monomer (EPDM) rubber liner placed to hold soil and water inside the laminar container.

10.4. Soil Properties

The soil profile of 4.90 m height shown on Figure 10-3 was constructed in 3 layers using Ottawa F-65 sand (Bastidas 2016) with the following grain size characteristics: D_{60} = 0.24 mm, fines content F_c = 0.25%, and uniformity coefficient C_u = 1.56. The employed soil was poorly graded in the medium to fine range. Sand Profile (Table 10-1) was constructed with a base dense layer (1.70 m), middle loose liquefiable layer (1.50 m) and a top dry layer (1.70 m). Water table was 1.70 m below the ground surface at the pile location (box centerline). Each layer had a target density, and this was achieved by monitoring the dry weight of sand used to occupy the volume of each layer. Quality control using sand cone tests verified the estimated densities. CPTs were performed at 4 different locations before shaking at the locations shown on Figure 10-4.

The base layer of 1.70 m was constructed by wet compaction. The layer was built in 0.25 m lifts, each densified using a plate compactor. After completion, the base layer was saturated from the bottom up by means of previously installed perforated PVC tubes. This base stratum was

intended to be a stiff rigid layer and to ensure that, the layer was shaken by a series of white noise motions to further densify the sand and achieve the targeted 100% relative density. Saturated density was about 2200 kg/m^3 (Dry density = 1780 kg/m^3). Secondly, the 1.50 m middle loose layer was constructed by sand pluviation through soil meshes then passing through water. The falling rate and height were maintained to achieve a uniformly deposited layer. Estimated relative density is 55 % and saturated density is 2100 kg/m^3. Finally, the top layer (crust) of 1.70 m height was built dry with some compaction to achieve a soil relative density of 85 % and a bulk density of 1817 kg/m^3 (Dry density of 1730 kg/m^3).

After building the soil model and before shaking, in an effort to fully characterize the soil model, CPTs were performed at 4 different location in the soil box shown on Figure 10-4. Locations were chosen midway between the pile and box boundaries to minimize their effects on the test. A limited access Ramset was used to perform the test. Performing such testing allows for field like site characterizations and possible comparisons with case histories. Figure 10-5 shows the results obtained from one of the tests conducted at the Downslope Array. Water table readings agree with the target water level during model construction. Test results confirm the presence of 3 layers, each with a different stiffness. Tip resistance (q_c) and friction ratio (R_f) give a trend of increase in the top crust layer followed by a decrease at the interface with the middle loose layer. Readings through the middle stratum show a lower constant strength throughout the layer then values increase as the cone approached the dense bottom layer. Correlated values for SPT (N_{60}) and shear wave velocity are also presented and follow the presented trend. It is observed that the region of stiffness change at both loose layer interfaces are approximately 0.70 m affecting the heights of all 3 layers.

10.5. Pile Properties

A steel pipe pile (Figure 10-6) of 0.273 m outer diameter and 9.27 mm thickness was employed in the tested configuration. Pile steel grade was A53B with properties summarized in Table 10-2. The pile was welded to a 5 cm thick steel plate and bolted to the box base. A 4° inclined wedge was employed below the pile to counteract the inclination and enable the pile to stand vertically. A preliminary static pushover test was performed on the piles before adding the sand to obtain the bending stiffness and base fixity rotational stiffness values. Pile connection was characterized to have a base rotational spring of 1750 kN-m/rad and an assumed underlying firm soil stratum. Monotonic moment-curvature shown in Figure 10-7 is computed using a fiber section OpenSees model and gives a yield bending moment of about 200 kN-m. The pile is considered stiff and elastic as recorded bending moments did not approach the yield value. The pile head movement was restraint by means of steel cable connected to the very top of the pile (1.30 m above soil surface) and fixed to 2 steel columns much stiffer than the pile (Figure 10-1).

10.6. Instrumentation

The model included various top of the line instrumentation arrays (Figure 10-3). Sensors were placed closely at 20 cm spacing to collect comprehensive profile response data during shaking. Over 200 sensors were installed with data collection rate of 256 samples per second. Instrumentation was installed along both sides of the pile and outside of the box, and in the soil between the pile and box boundary as shown in Figure 10-3. Sensors installed were the same used in the smaller size test.

Pore pressure sensors were deployed on both sides of the pile and in the free soil, midway between the pile and container boundary (upslope and downslope) with an additional array in the free field on the pile side perpendicular to the shaking direction. Total pressure transducers were

installed on both sides of the pile and used to measure the initial static soil pressure during filling and the dynamic pressures during shaking. Accelerometers were placed alongside the pore pressure transducers and on the laminar box exterior boundary. High sampling rate accelerometers were used with the ability to record at 25,000 samples per second. With this high sampling rate, the data can be employed to track shear wave velocity changes during seismic events (Zayed 2020). Strain gauges were installed on the steel pile. Strain data is used to back-calculate bending moment during shaking. Displacement transducers were mounted on the laminar box exterior wall every other laminate to measure lateral displacements, and on the soil surface to measure horizontal and vertical displacements. Locations of vertical pots is shown in Figure 10-4. The Pile was also instrumented with transducers to measure pile head displacements above the ground surface in several locations to capture the restraint effect. Figure 10-6 presents a picture of the instrumented pile and free field. Additionally, a ShapeTape Array was installed in the upslope free field to track the soil profile movement with its location illustrated in Figure 10-4. The ShapeTape does not read dynamic readings but provides a valuable final soil profile to compare with the laminar box deformation profile.

10.7. Analysis Protocol

Focus is placed on system response mainly in terms of excess pore water pressure, ground deformation, and pile behavior. Bending moment in the piles was calculated based on the measured strain using the traditional Euler-Bernoulli beam theory (Wilson *et al.* 2000) and is an indicator of the acting pressure profile. Lateral soil pressures and soil reaction are also presented. Thus, representative time histories and profiles were chosen to identify the pile and soil response and highlight peak values and observations. The restraint pile is seen to halt the box movement and affect the system overall response. Results presented in this chapter are selected to clarify the

observations and verify the conclusions. The full data report including other shaking events performed on this model is presented in SSRP 19-01 (Ebeido *et al.* 2019).

10.8. Soil Response

Acceleration time histories are presented through the soil profile in Figure 10-8. Input motion was 16 seconds in the form of sinusoidal acceleration with a 2 Hz frequency and amplitude of 0.15 g. Input acceleration was increased gradually over a 6 second period (12 cycles) to reach the target amplitude then remained constant for 6 seconds (12 cycles). Finally, it was gradually decreased in 4 seconds (8 cycles).

Liquefaction occurred 6 seconds during shaking as evident from the reduction in acceleration at shallower depths (Figure 10-8) and the recorded excess pore pressure ratio r_u (Figure 10-11), where $r_u = u_e/\sigma_{vo}'$ in which u_e = excess pore pressure and σ_{vo}' = initial effective vertical stress.

Accelerations (Figure 10-8 and Figure 10-9) were uniform during the first 6 seconds throughout the entire profile showing the same gradual increase as the shaking was ramped up. At the onset of liquefaction, acceleration records in the loose and crust layers show a sudden de-amplification. The very dense base layer shows no reduction in values and agrees with the input motion. The asymmetric acceleration response in the loose stratum is evidence of downslope movement of the soil layer with observed spikes evident of the dilative tendency of the soil (Zeghal and Elgamal 1994). Although the crust layer exhibits the acceleration reduction, it does not show the asymmetric response. Thus, indicative of acceleration de-amplification from the strength reduction in the liquefiable layer but no movement of the crust. Hence, the crust is floating on the liquefiable stratum and following its movement.

A clear 180° phase shift is observed between the dense and loose layers. Crust accelerations coincide with the loose layer ones. It can be deducted that soil movement of the loose and crust strata are in an opposite direction to the base layer.

Excess pore pressure ratios (Figure 10-11 and Figure 10-12) complements the acceleration records and show the liquefaction of the loose layer and the continued liquefied state throughout the shaking. Downslope records away from the pile (near field) do not display any noticeable oscillations, and the absence of transient drops indicate no dilation presence in the near filed. This could be evidence of high system stiffness as the soil stratum moves together. Transducers in the base layer show no evidence of liquefaction as the excess pore pressure ratios remained well below liquefaction values. Sensors placed on the pile recorded transient drops before and after liquefaction which suggest the relative movement between the pile and surrounding soil. Upslope sand is seen to dilate more than the downslope which is a sign of soil flowing around the pile. Transducers on the pile in the base layer also records some dilative response.

Peaks in acceleration are observed to coincide with dips in excess pore pressures. These peaks and dips in acceleration cause the loose soil to exhibit phase transformation behavior as the sand transitions from contractive to dilative and vice versa (Wilson *et al*. 2000).

Figure 10-13 shows lateral displacement profiles of the laminar container and ShapeTape deformation profile and their respective shear strains. The box profiles are plotted every 2 seconds to track the evolution of container movement downslope. The ShapeTape does not record dynamic displacements so the end of shaking profile is presented. From these displaced configurations, it can be noted that deformation was minimal within the crust layer above the water table and it was even in the upslope direction relative to the top of the loose layer. In the loose saturated soil, displacements follow a “S” shape trend. The supporting shear strain profile shows highest strain

values in the center of the loose layer with much lower values near the interface with the top and bottom strata. The underlying dense did not accumulate any deformations. End of shaking results from the ShapeTape agrees well with the box displaced configuration. Soil surface and box top total deformation was approximately 7 cm and much lower than expected due to the presence of a restraint pile.

Soil settlement was recorded by means of vertical pots during shaking and presented in Figure 10-14. Records from both the upslope and downslope array are shown as the soil accumulates 2.00 and 1.50 cm of settlement respectively. The difference in values is small and over 7.70 m of distance between the 2 locations, differential settlement is minor and results in a slope correction of 0.04° which keeps the 4° inclination intact after shaking.

10.9. Pile Response

Pile head and box top displacements, pile bending moments and shear forces time histories are presented in Figure 10-15. Bending moments were calculated from strain gauges as the pile remained elastic. Shear forces were back calculated from bending moments. The vertical line denotes the maximum attained bending moment (at 11.25 s) in the pile and is shown on time histories for ease of analysis. Pile head and soil surface started displacing with shaking and is observed to reach their maximum values after 11 seconds of shaking. Both time histories are compatible and reach the same maximum 7 cm displacement. They are observed to reach their maximum values at the same time the pile head restraint was fully mobilized as evident from the shear force also shown on Figure 10-15. The force in the restraint accumulated as the pile displaced and reached a maximum of 13 kN, after that the pile was immobilized. The restraint not only halted the pile movement but forced displacement compatibility on the pile and the entire soil profile. It was able to restrain the entire box configuration.

Bending moments (Figure 10-15) are shown at the maximum negative and positive locations respectively (1 and 4 m) and follow the same trend of displacements and shear reaching maximum values of -21 and 68 kN-m (below the yield value). Shear force time histories are presented at the pile base and the maximum shear location corresponding to the zero-bending moment (2.20 m depth). The maximum shear located in the loose layer reached its peak value, 45 kN much earlier in shaking than the restraint at 7 seconds.

Figure 10-16 shows pile response profiles at both the maximum instance (11.25 s) and the end of shaking. Bending moment profiles exhibit the expected shape of the response with the negative peak occurring just above the crust-loose interface and the positive peak just below the loose-dense line. The maximum moment profile peak value is 1 pile diameter below the interface with it being sustained for approximately 3D before decreasing as previously observed by Lam *et al.* (2009) and in the earlier chapters. The residual bending moment is approximately 66% of the peak value.

Shear force profiles show high values occurring in the liquefiable layer, which is expected as the pile tries to resist the soil flow and restrain the soil profile. The high forces are being developed along the entire thickness of the loose layer. End of shaking values suggest pile movement towards the downslope soil as the sand is moving towards the direction of passive pressures.

Axial forces (Figure 10-16) were calculated based on the pile cross section properties and the average strain recorded on both sides of the pile. Observations from axial profiles are i) developed tension at the top of the pile is caused by the restraint pulling on the pile, ii) settlement of the loose and crust layer induced compressive forces that were able to counteract the restraint

pull, and iii) the displaced pile configuration resulting from the soil lateral deformation caused tension to develop near the bottom of the loose layer and the underlying dense stratum.

The calculated pile deformed shape is presented along with the box profile in Figure 10-17. The pile calculated profile was verified by the measured head displacement. Observations of differential movement between pile and soil in both the loose and dense layers support the dilative tendencies exhibited by the pore pressures (Figure 10-11). The pile was pushing on the soil in the dense layer and vice versa in the other strata.

The general behavior of any pile in a lateral spreading configuration is largely dictated by the lateral pressures (Figure 10-18, Figure 10-19), displacement response as exerted by the stiffer upper crust layer and the resistance of the base dense layer. The values reported are from direct measurement from total soil pressure transducers. Instrumentation recorded values as high as 150 kPa at 1.20 m depth exerted by the crust layer from the upslope movement of the soil towards the pile, while the downslope soil moved away resulting in a decrease of 25 kPa from the initial static pressure. The recorded upslope pressure of 175 kPa is much higher than the soil passive pressure and is almost double. Total pressures just beneath the crust interface at 2.0 m depth although lower than the crust but are still high in the range of 100 kPa (in the range of passive pressure). This depth is just below the interface was still affected by the upper crust. The downslope record at this location shows to no change.

The loose layer exerted minimal negligible pressures on the pile from the upslope side with no available date at the downslope location. Dense layer transducers recorded a decrease in the upslope pressures and an increase in the downslope ones. It is important to note that the bottom layer pressures are out of phase with the loose and crust one. Therefore, as the crust pushes, the downslope layer resists and the reduction in total pressures on the upslope dense side is only from

loss of initial static values resulting from the pile moving away. Estimated profiles presented in , although having missing data but illustrate the mechanism of the crust pushing as the downslope resists.

To compensate for the missing total pressure data, Figure 10-20 presents the soil subgrade reaction calculated from strain profiles. The subgrade reaction was then converted to total resulting pressures to compare. The soil is observed to exert pressure on the pile till 2 m depth (1.5D below the interface) then a uniform reduction along the liquefiable layer with the dense layer resisting the pile movement. The general trend agrees with the total pressure observations.

10.10. Post Test Physical Observations

Care was taken to document any physical observations before and during demolition. Figure 10-21 presents the box configuration after shaking. The pile was still being held back by the restraint as shown on Figure 10-22. Soil was heaving upslope the pile with some cracking and a downslope gap was observed.

10.11. *P-y* Lateral Analysis

In order to accurately model the tested configuration is a simple *p-y* analysis. Parameters such as the base rotational spring (1750 kN-m/rad) previously discussed and the restraint force need to be accounted. The force-displacement relationship of the restraint is shown in Figure 10-23. The pile head constraint relation (Figure 10-23) is discretized by a monotonic envelope shown in Figure 10-24 to be used in the numerical analysis.

Following the *p-y* curves proposed in Chapters 5 and 6 and presented in Figure 10-25, a lateral analysis is undertaken. Figure 10-26 presents a sample of the actual soil spring models used in the analysis showing the modified softer crust springs (Chapter 6), liquefied springs (Chapter 5) and dense sand springs according the API (2010) based on 34° friction angle correlated from

the relative density. In this analysis, no transition or reduction factors were used between layers. Recorded box deformation profiles (Figure 10-13) are applied to the lateral model. Results of the *p-y* model compared to the experimental recordings in terms of bending moments (at maximum location, 4 m depth) and pile head displacement against box top deformations are shown in Figure 10-27. The numerical model shows agreement with the experimental response specifically in terms of initial slope and maximum value for the bending moment plot. The computed pile head displacement is lower than the experimentally observed due to the pushover over loading instead of the dynamic excitation. Figure 10-28 presents comparison profiles for the bending moment and shear force at the maximum instant. The profiles show good agreement specifically in terms of maximum values and their locations.

10.12. Extension of the lateral *p-y* Model

The developed *p-y* lateral model is extended by applying increased box deformations using the same displaced shape up to about 1.00 meters at the top. Results of the extended model is presented in Figure 10-29 showing increased bending moment and pile head displacement till approximately 0.40 m of box top deformation then remaining constant afterwards. Figure 10-30 presents the box top displacement against the time step of the pushover analysis and Figure 10-31 illustrated the forces applied by soil springs at different depths also against the time step. Collectively from the figures, it is observed that the bending moment and pile head displacement plateau occurs at time step 700. At the same time step, the liquefied layer springs are applying almost minimal forces on the pile and the crust springs reach their peak, thus no additional forces are applied on the pile after.

10.13. Parametric Study

A small study was conducted to test the effect of the pile head condition on the maximum bending moment value and the pile head displacement. The experimental case with the cable restraint (modelled as a spring) was compared to two cases with a fixed pile head and a free pile head. Results are displayed for pile head displacement and maximum bending moment at 4 m depth in Figure 10-32. The removal of the restraint caused an additional 30% increase in the maximum bending moment from 170 kN-m to 223 kN-m and approximately 8 times increase in pile displacement at maximum imposed soil displacement (Top box displacement is approximately 1 m). The fixed pile head case resulted in zero pile head displacement and a much lower maximum bending moment (20 % of restraint case). Although the fixed head case shows a negative bending moment at the pile head of similar value to the maximum positive bending moment recorded at 4 m depth (37 kN-m). Results from this parametric study highlight how important the pile head condition is in the foundation performance against lateral spreading. Correct modeling of the pile head is important for accurate outcome.

10.14. Summary and Conclusions

A 3-layer soil stratum (Figure 10-3), at a 4-degree inclined configuration and a 0.273 m diameter elastic steel pipe pile was investigated using a 1-g shaking table experiment. The pile was restrained at the top above the soil surface. Peak bending moments are seen to occur near the interface between layers. This unique test takes advantage of the large scale and studies the restraining effect on the pile and the entire soil system. The main observations and conclusions are:

1. In the liquefiable layer, accumulated lateral strains are not uniform, and are highest in its lower half (Figure 10-13). The crust layer slides on the loose layer with no accumulated strains and the very dense base layer did not deform.

2. The laminar box deformed configuration agrees well with the inner soil profiles as evident from the ShapeTape Array.

3. Based on the observations of the free pile head experiment in Chapter 11, the entire soil system is affected by pile restraint. The constraint affected both pile and soil deformations. Displacement compatibility of the pile, box and surrounding soil is observed and is the effect of the restraint.

4. In analyses of pile slope restraining effects (e.g. MTD 20-15 2017), it is clear that pile head condition will play a significant role in dictating the outcomes.

4. The high restraint stiffness induced a rigid body effect, making soil layers move together, this removed any near field oscillations from pore pressure transducer recording.

5. The restraint affecting the entire system is proof that the pile affects the entire soil in the box and vice versa. This suggests that the soil tributary area affecting the pile is much larger than its diameter.

6. At the end of shaking, total pressures from the liquefiable and dense base soils disappear. Only the crust pressures remain.

7. The CPT profile suggests regions in the loose layer affected by the presence of upper and lower denser layers. In this experiment, the change in soil properties is not abrupt at layer interfaces but occurs gradually over a distance of 0.50 m.

8. For this experiment, applying approximately 2.4 times the passive pressure values when applying upslope crust loads.

9. Friction causes some axial tension and compression loads during bending. The deformed pile configuration exerts tensile forces on the bottom pile portion. Overall, there are no clear indication that down drag forces are playing any noticeable role.

10. The developed *p-y* curve lateral model shows good agreement with the experimental results and can be used for further studies and analysis.

10.15. Acknowledgements

Chapter 10, in full, is currently being prepared for submission for publication of the material as it may appear in the following journal publication (The dissertation author was the primary investigator and author of this paper):

Ebeido, A. and Elgamal, A., "Restraint Single Pile Response in Large Scale Laterally Spreading Experiment".

Table 10-1. Soil Profile Properties

Property	Base Dense Layer	Middle Loose Layer	Top Dry Crust
Water/soil condition	Fully saturated	Fully saturated	Relatively dry
Thickness (m)	1.70	1.50	1.70
γ_{bulk} (kg/m^3)	2200	2100	1817
γ_{dry} (kg/m^3)	1780	1610	1730
Relative density (%)	100	55	85

Table 10-2. Steel Pipe Pile Properties

Steel Grade	A53B
Pipe Pile Outer Diameter (m)	0.273
Wall Thickness (mm)	9.271
Elastic Modulus (kPa)	2.0×10^8
Yield Strength (kPa)	3.6×10^5

Figure 10-1. Picture of experiment setup

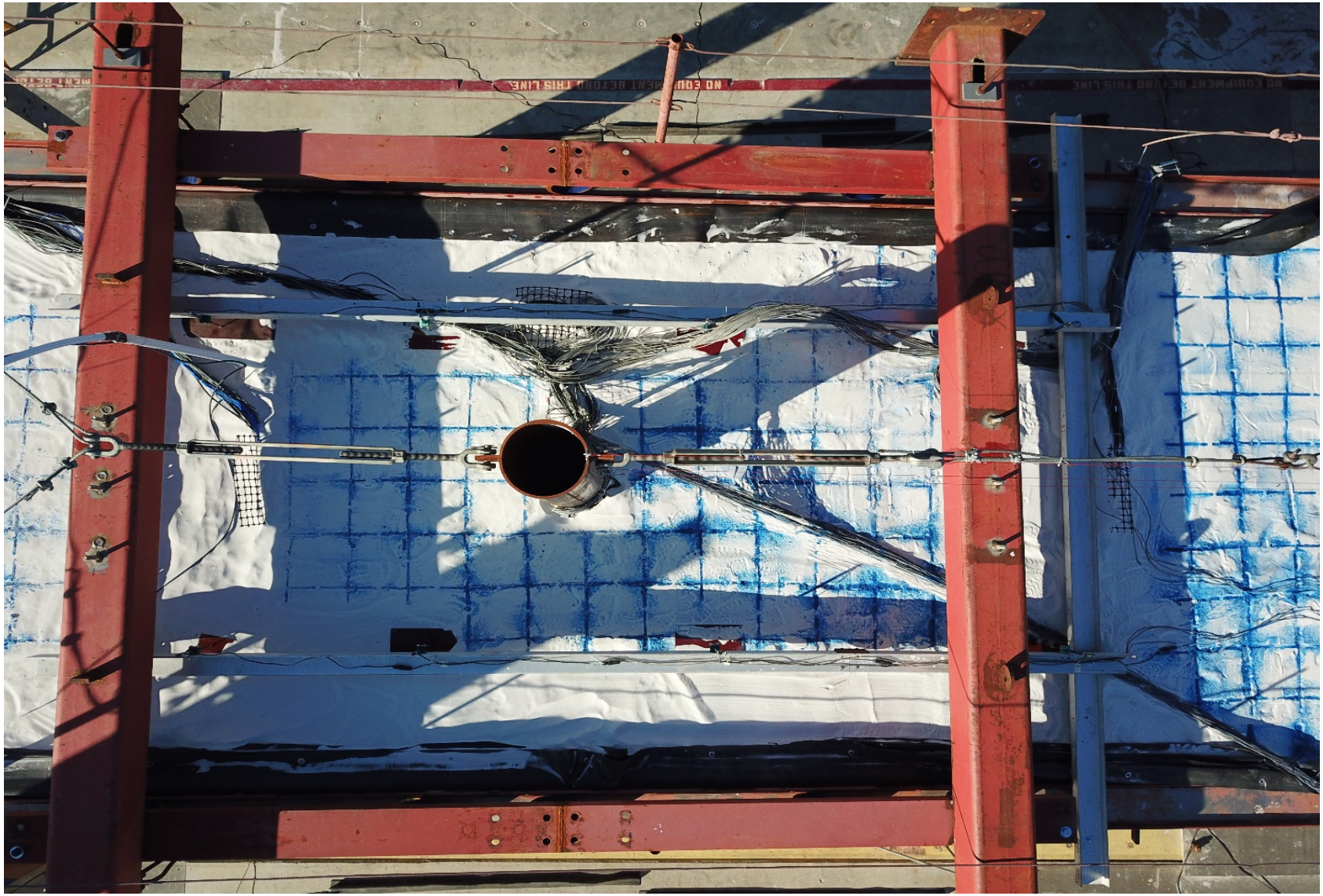

Figure 10-2. Picture of the restrained pile from the top (Drone shot)

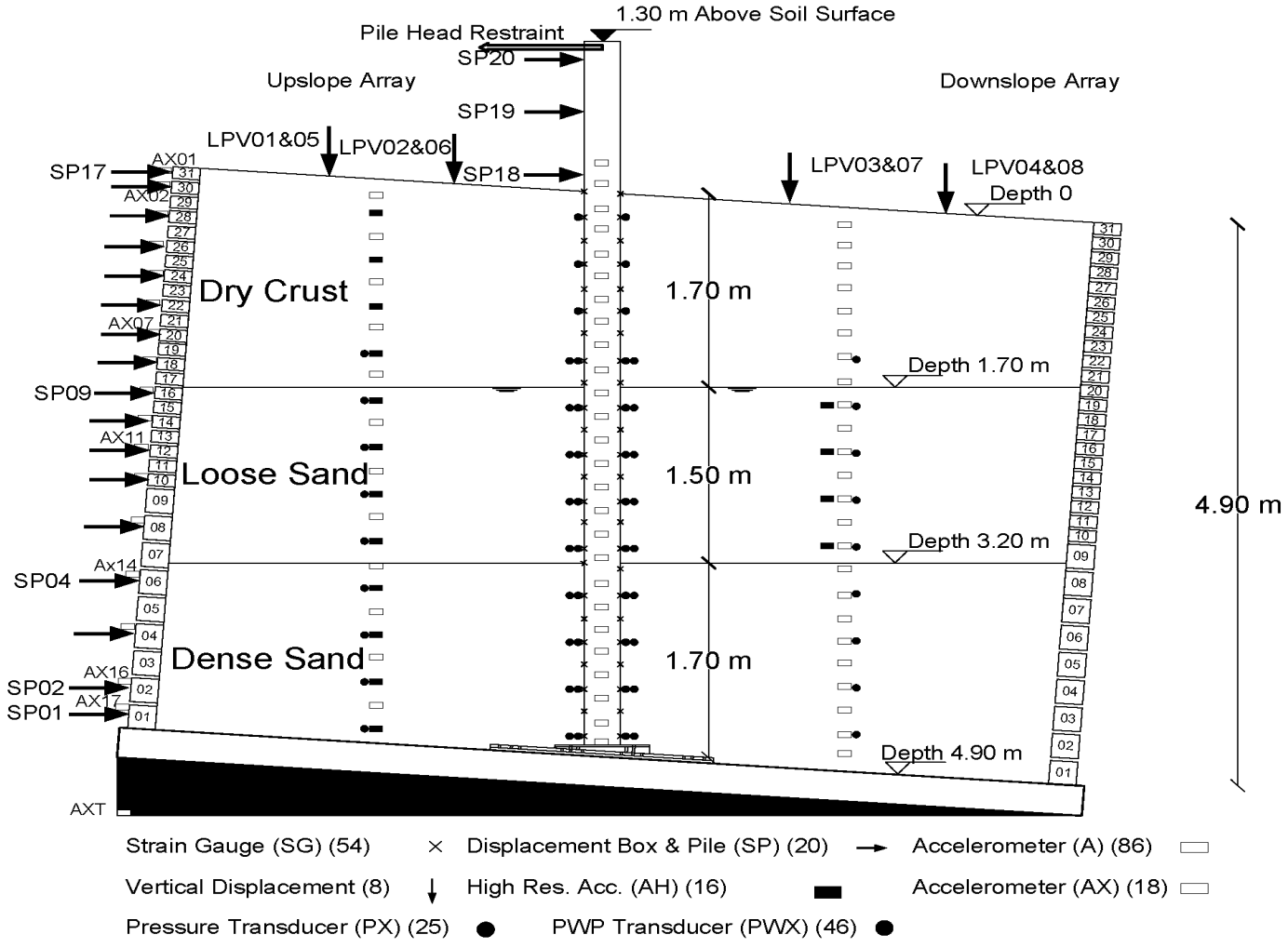

Figure 10-3. Experimental Layout

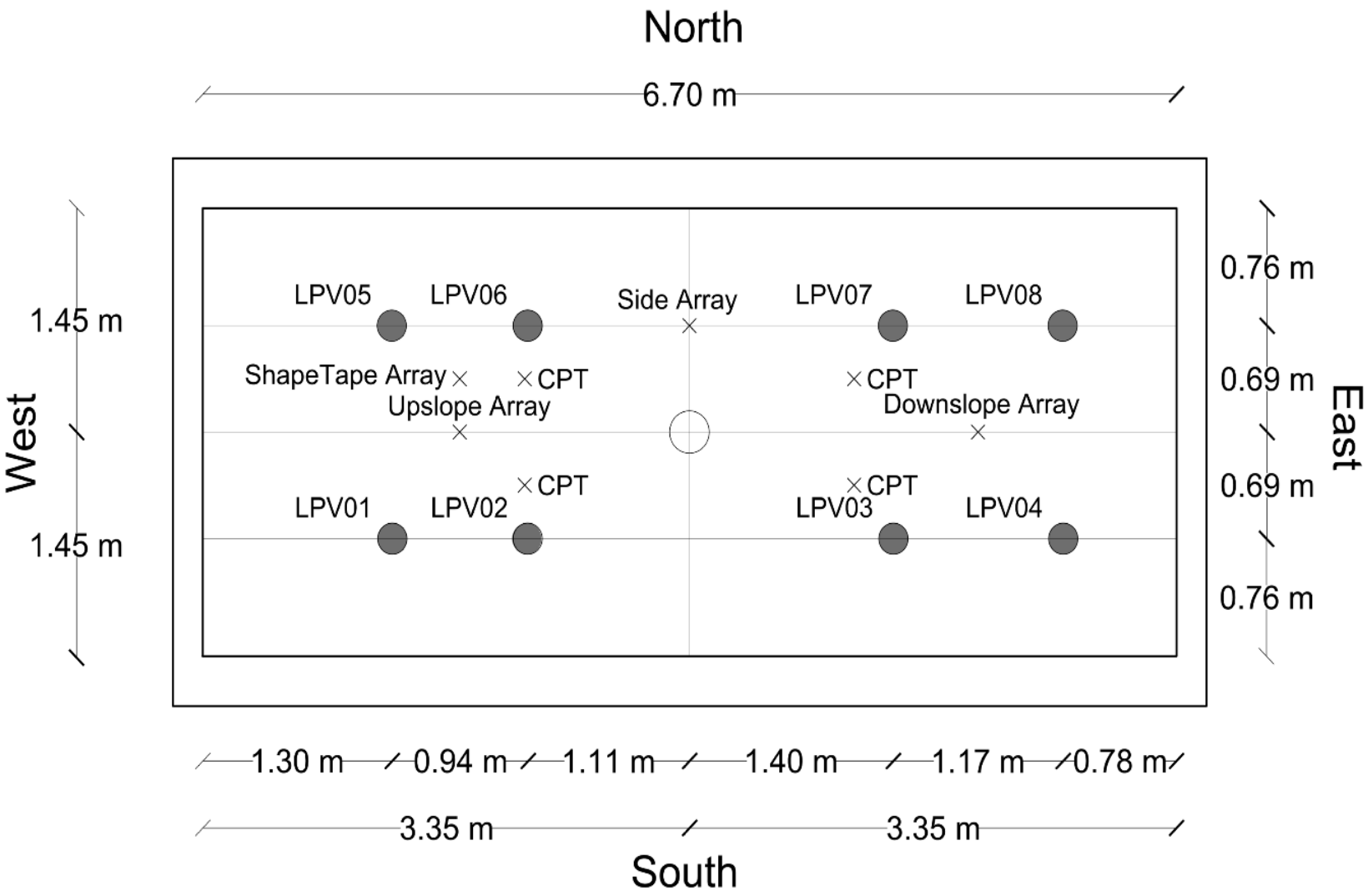

Figure 10-4. Experimental plan view

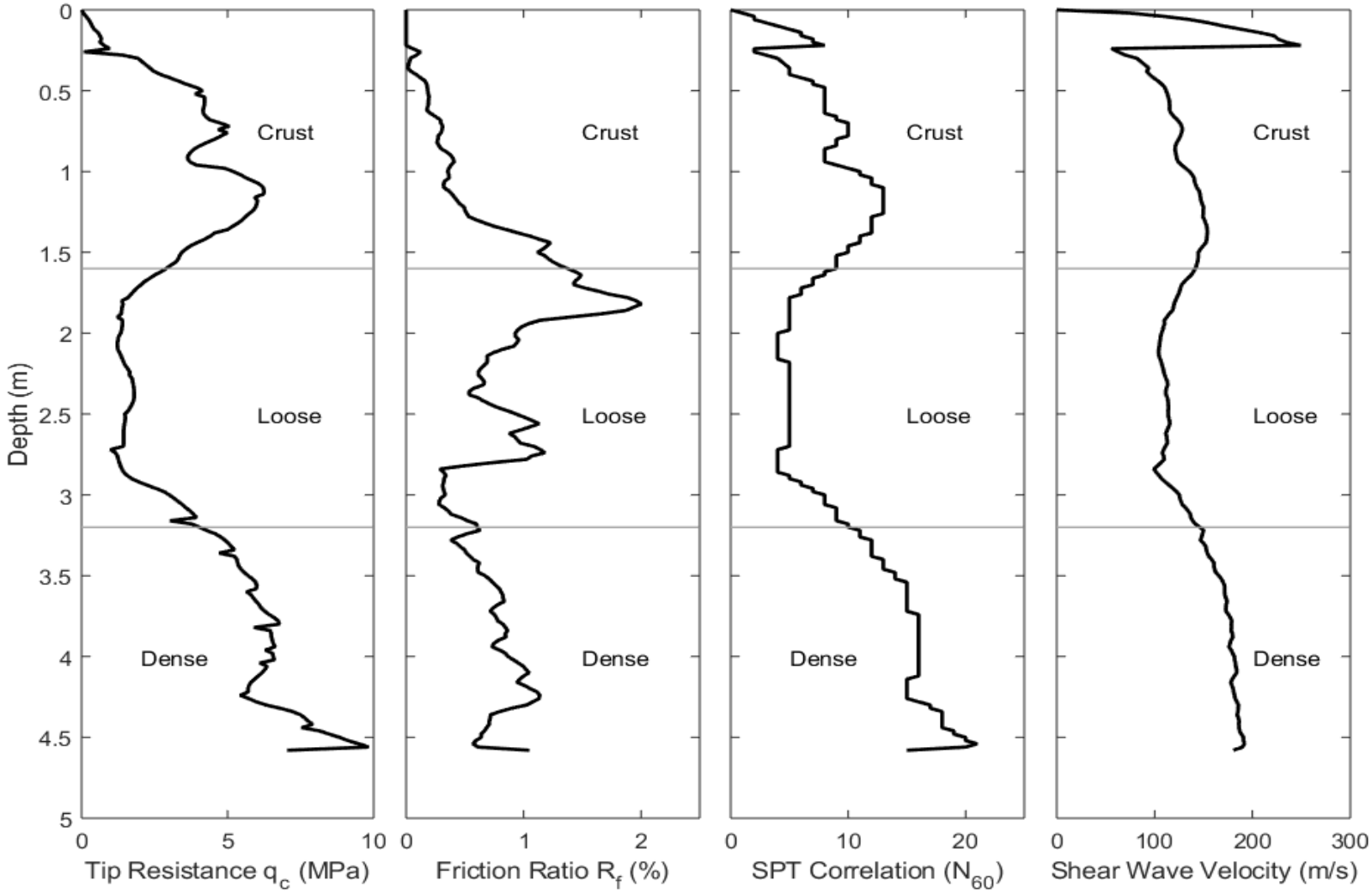

Figure 10-5. CPT investigation performed on downslope location shown in Figure 10-4

Figure 10-6. Picture of instrumented pile and free field before box filling

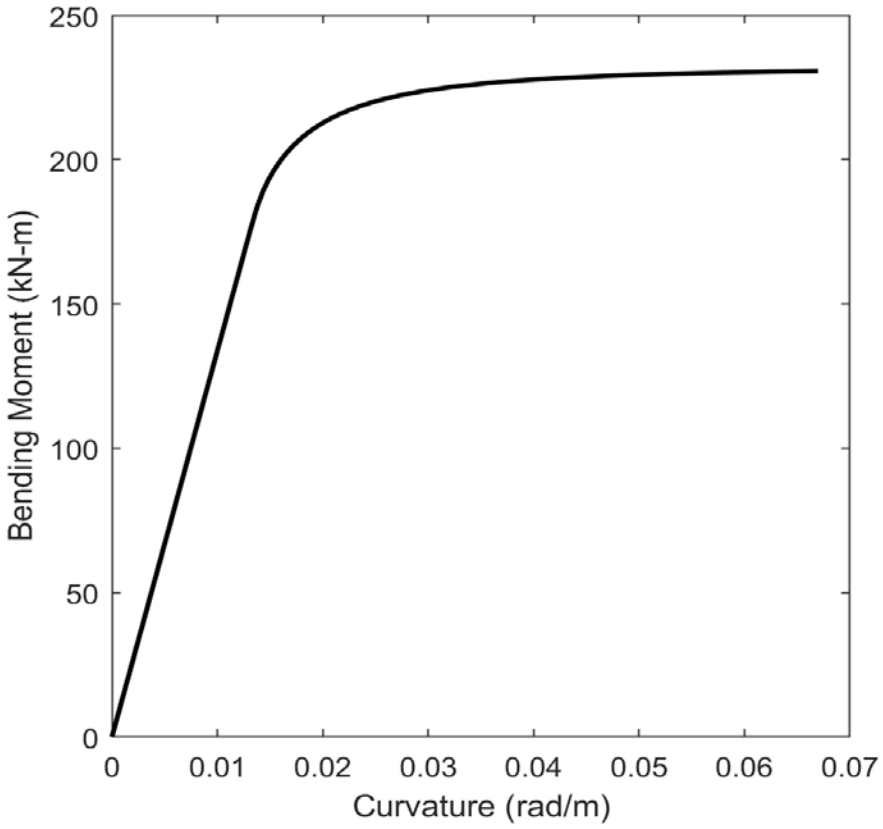

Figure 10-7. Moment Curvature diagram for steel pile

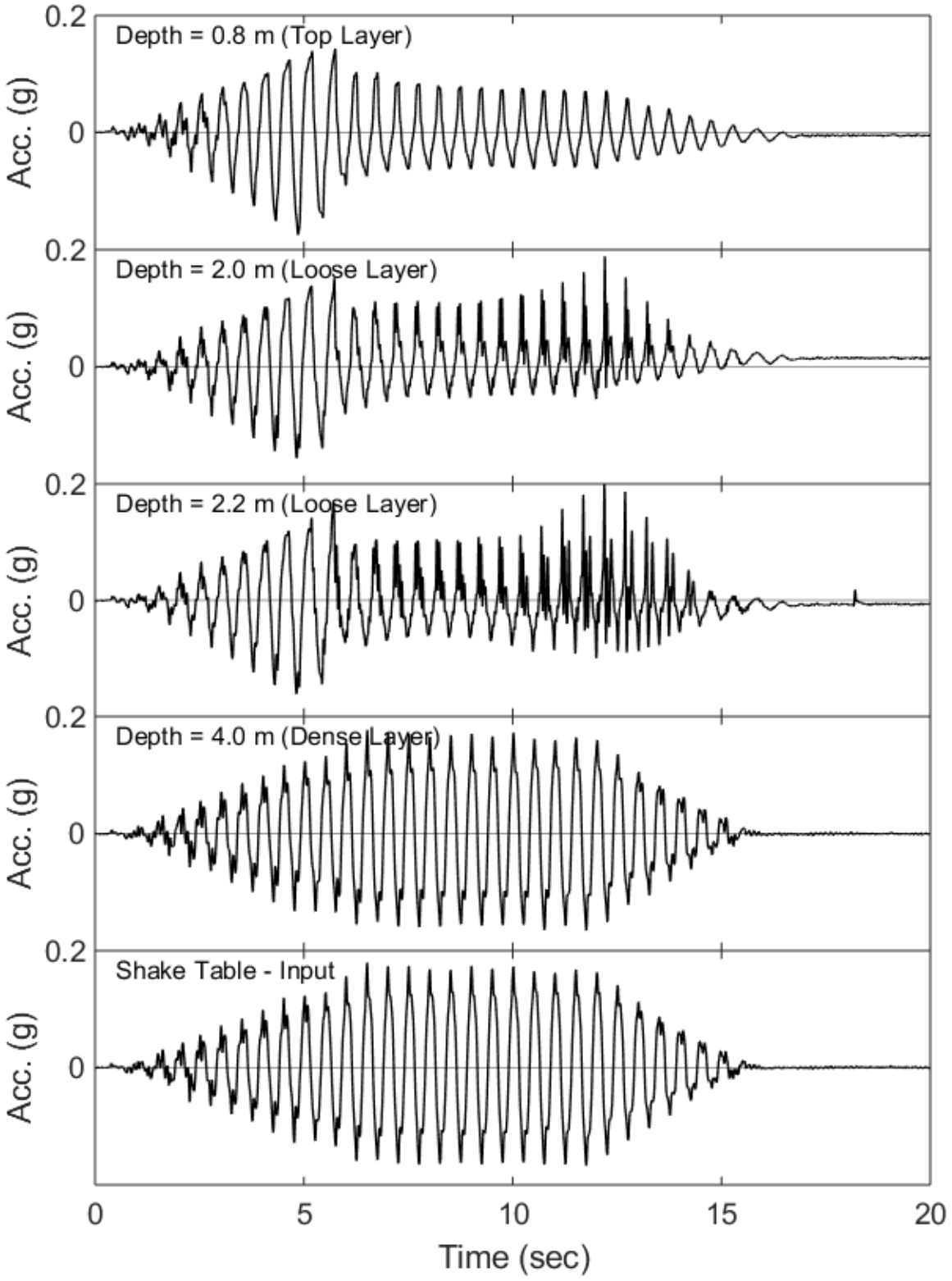

Figure 10-8. Acceleration time histories along the downslope array

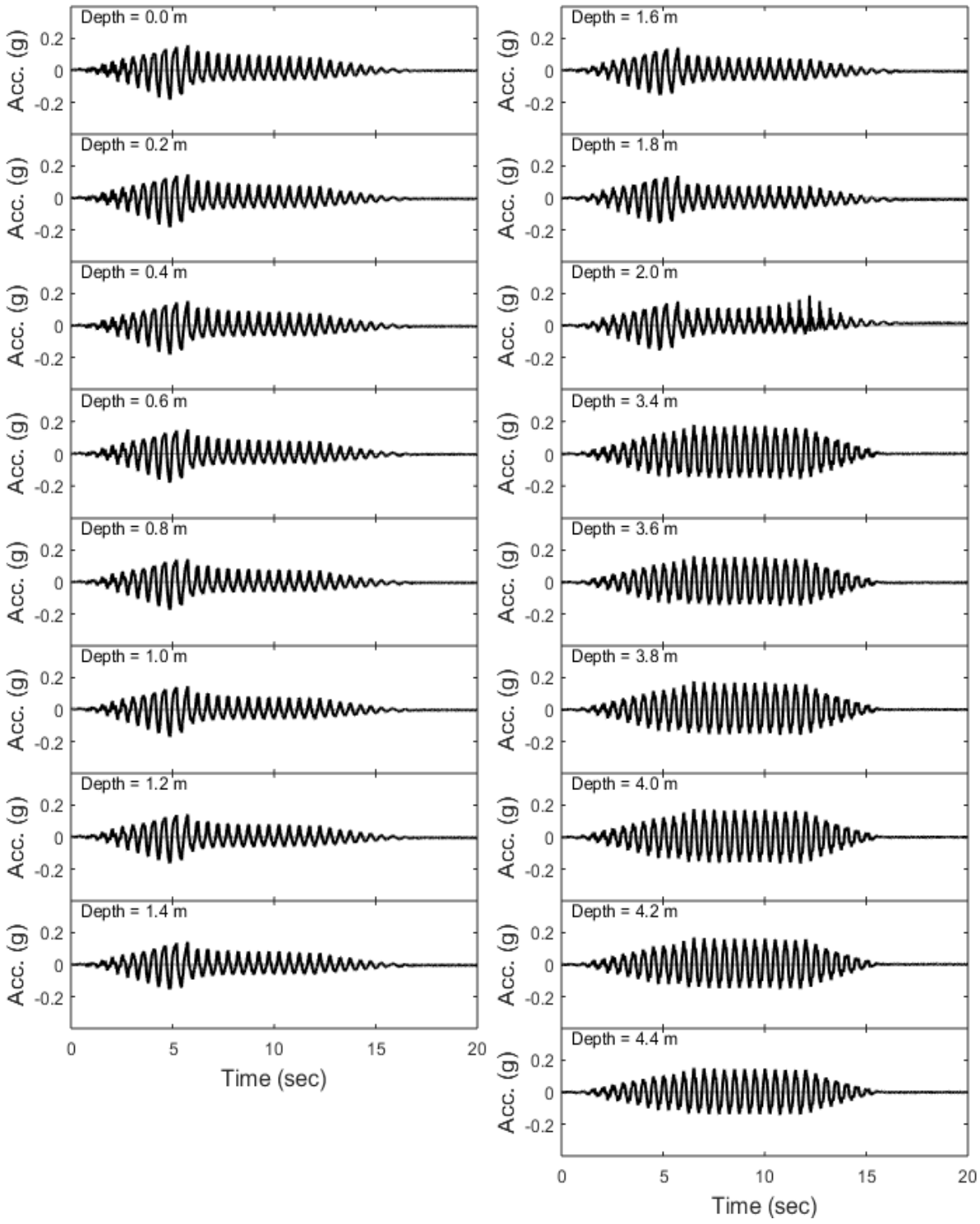

Figure 10-9. Detailed acceleration time histories along the downslope array

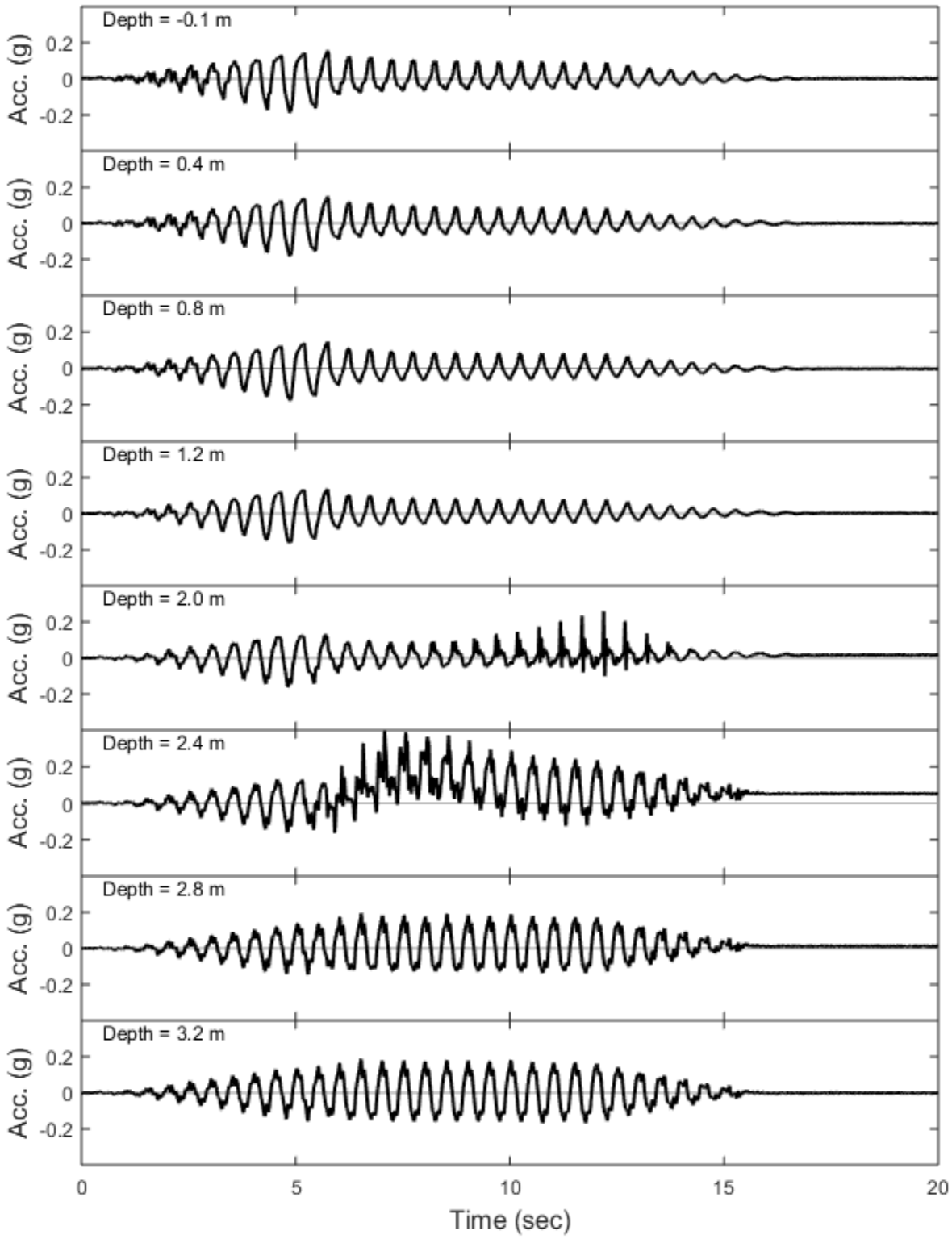

Figure 10-10. Acceleration time histories along the upslope array (Depth is calculated from the ground surface at box center)

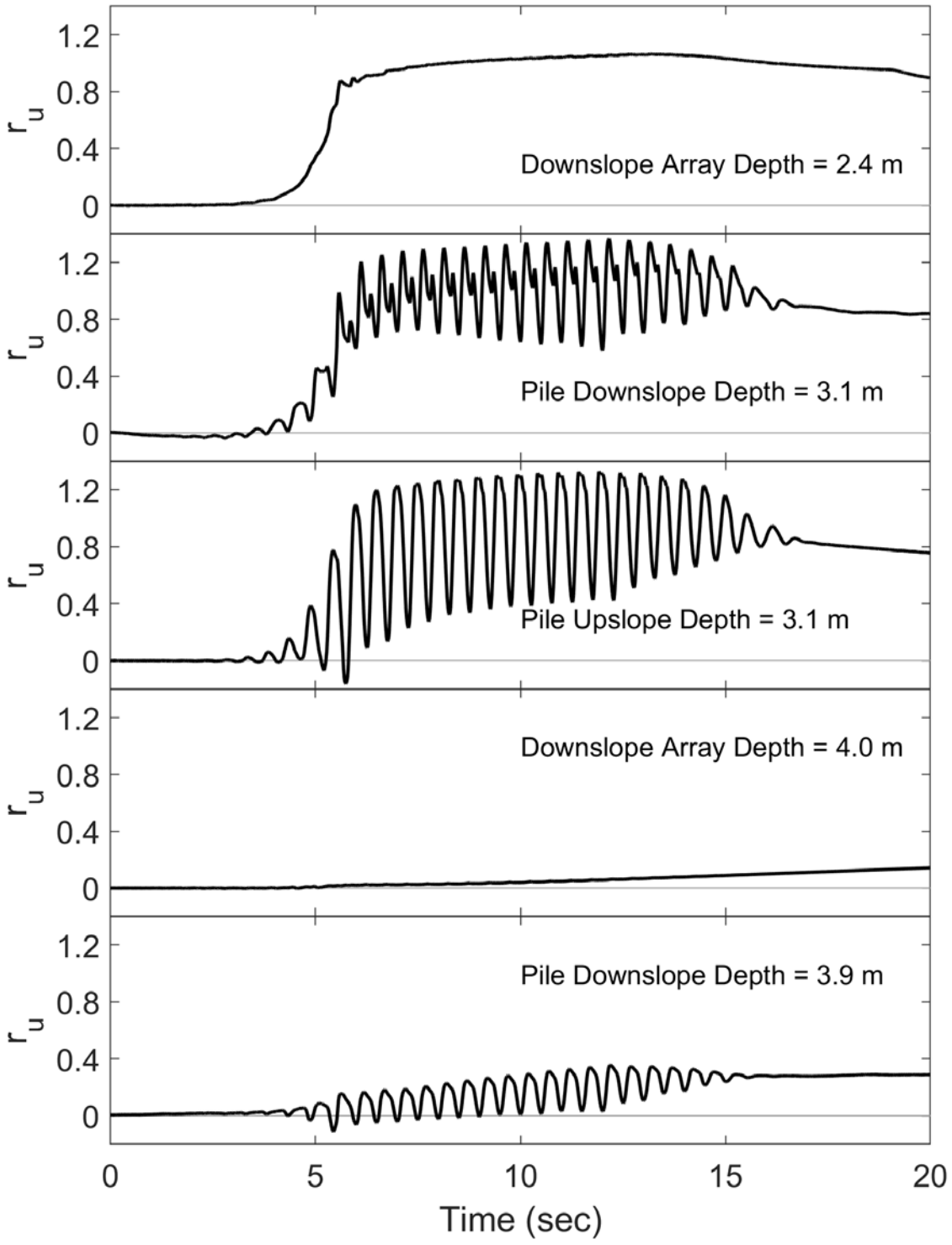

Figure 10-11. Excess pore-water pressure time histories in several locations

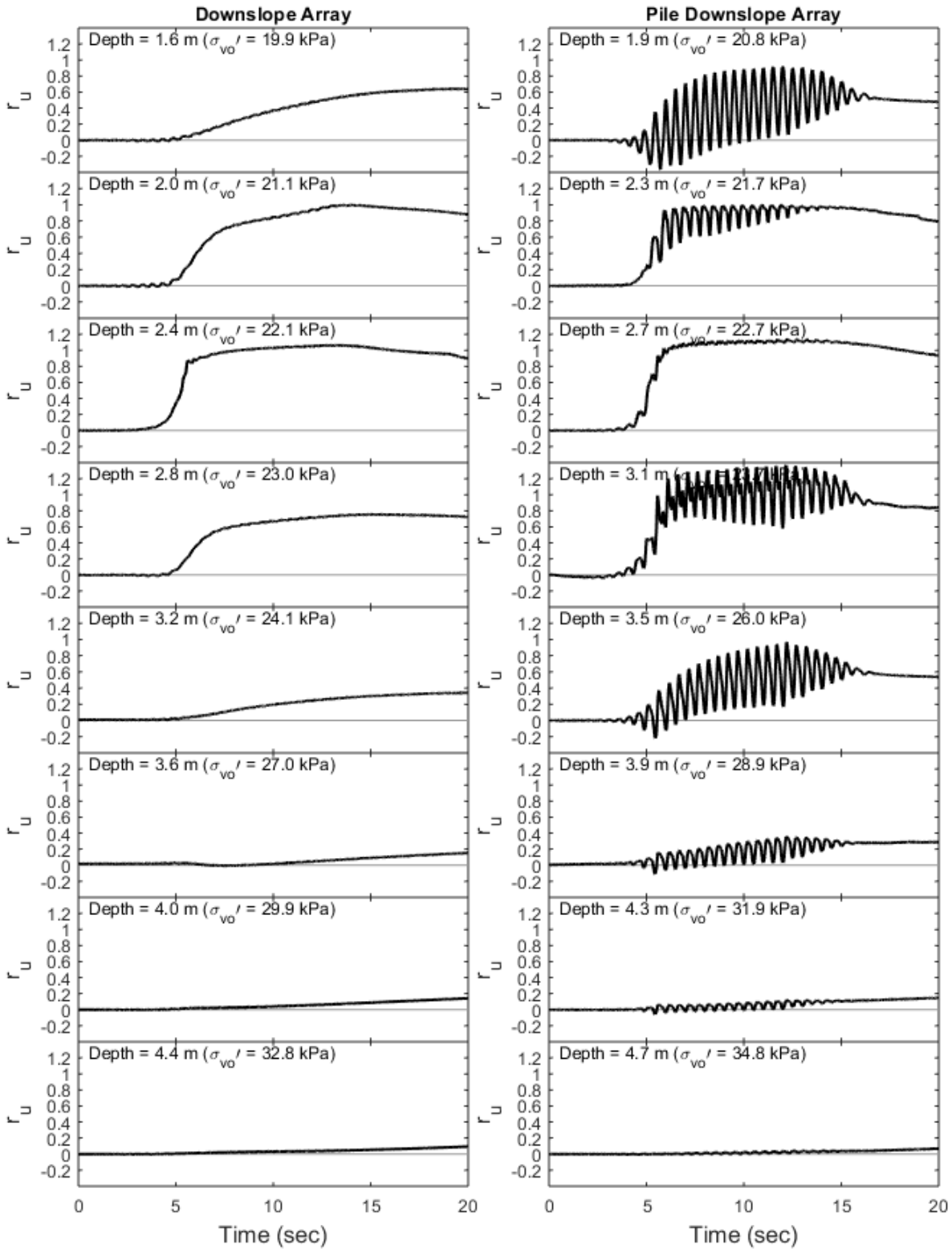

Figure 10-12. Detailed excess pore pressure time histories along the depth of the downslope and pile downslope array

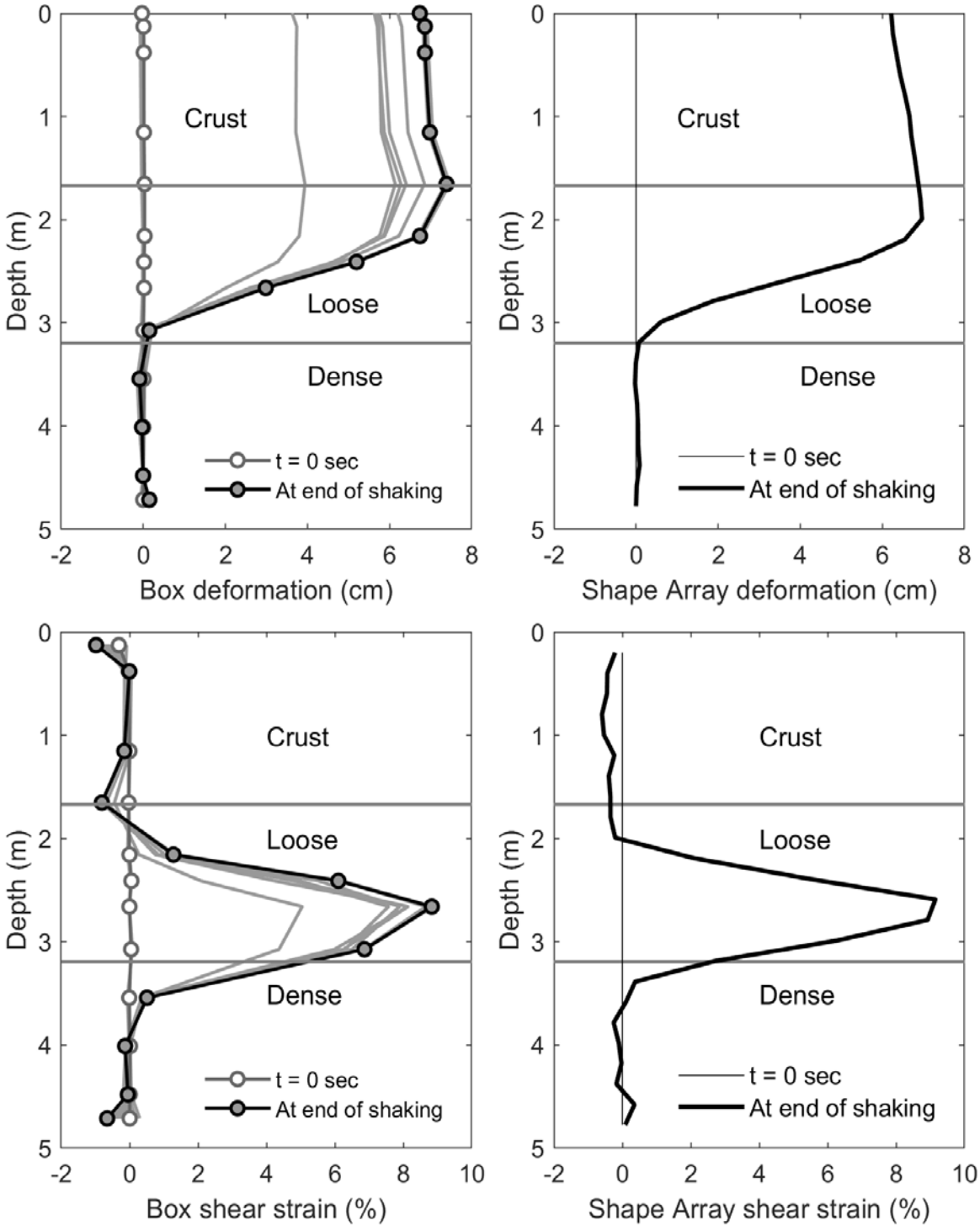

Figure 10-13. Soil box and shape array deformation and shear strain profiles (Box deformation plotted every 2 second interval)

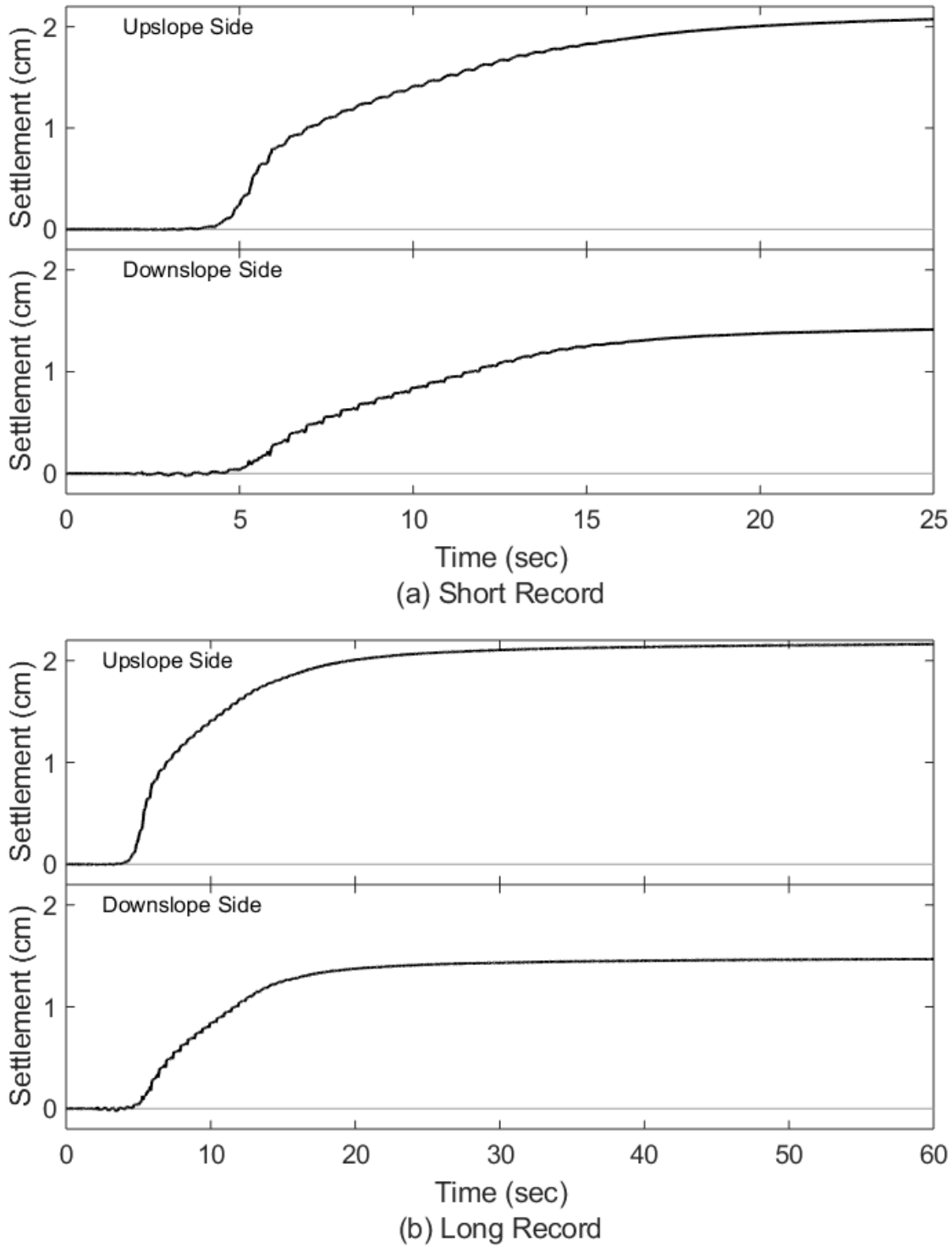

Figure 10-14. Soil surface settlement time histories

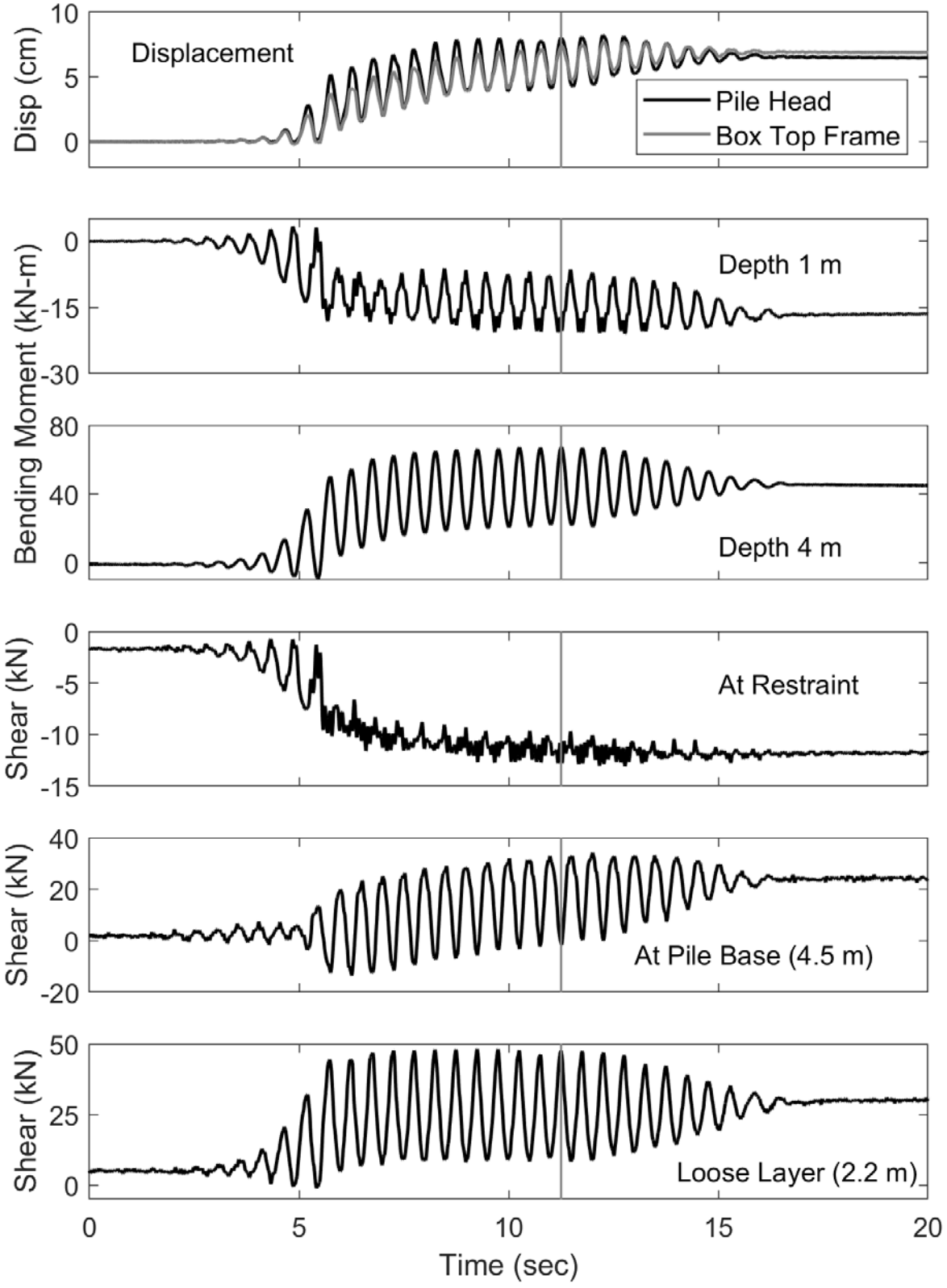

Figure 10-15. Pile response time histories at select locations

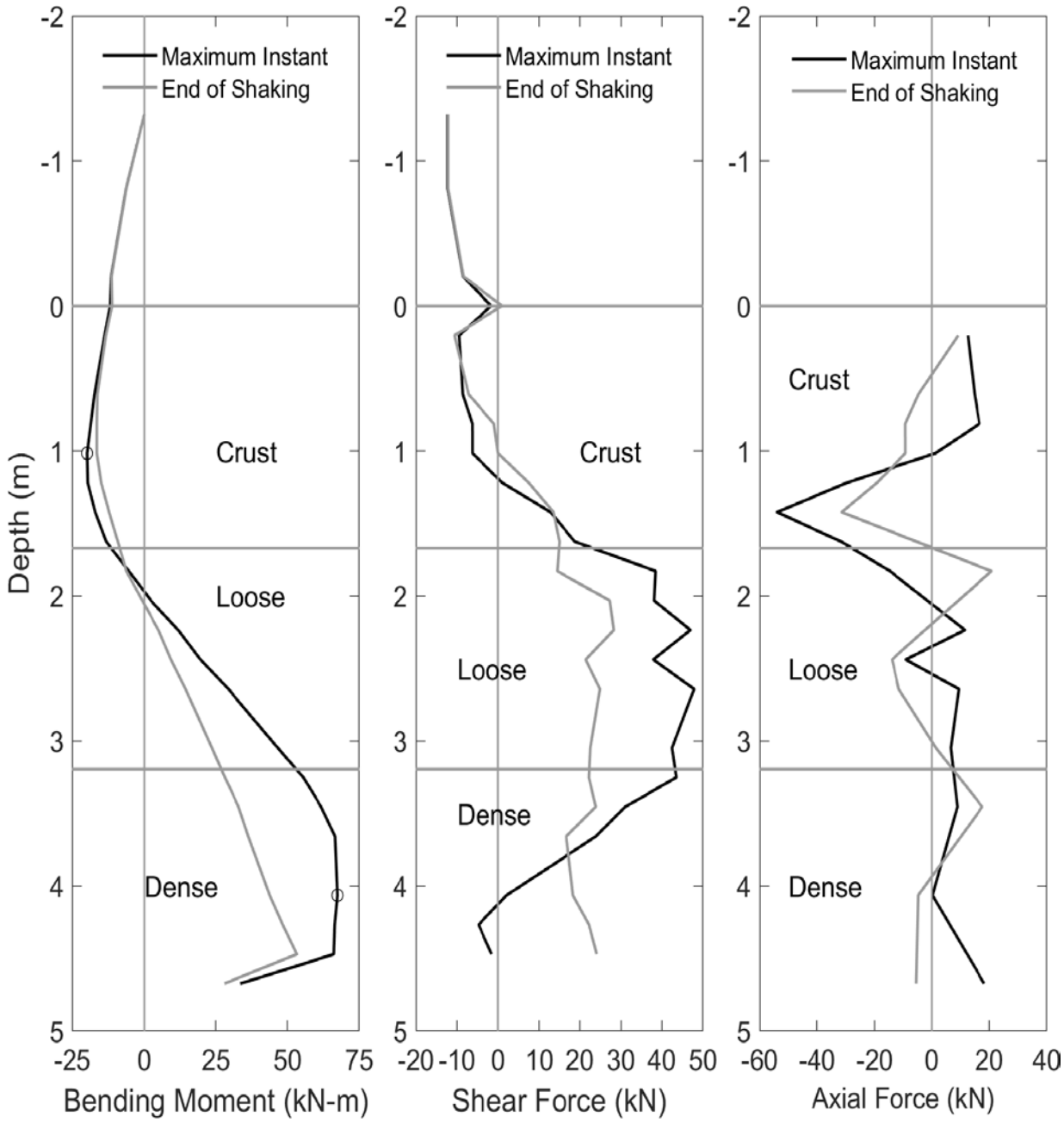

Figure 10-16. Pile response time histories at maximum instant (11.25 s) and end of shaking

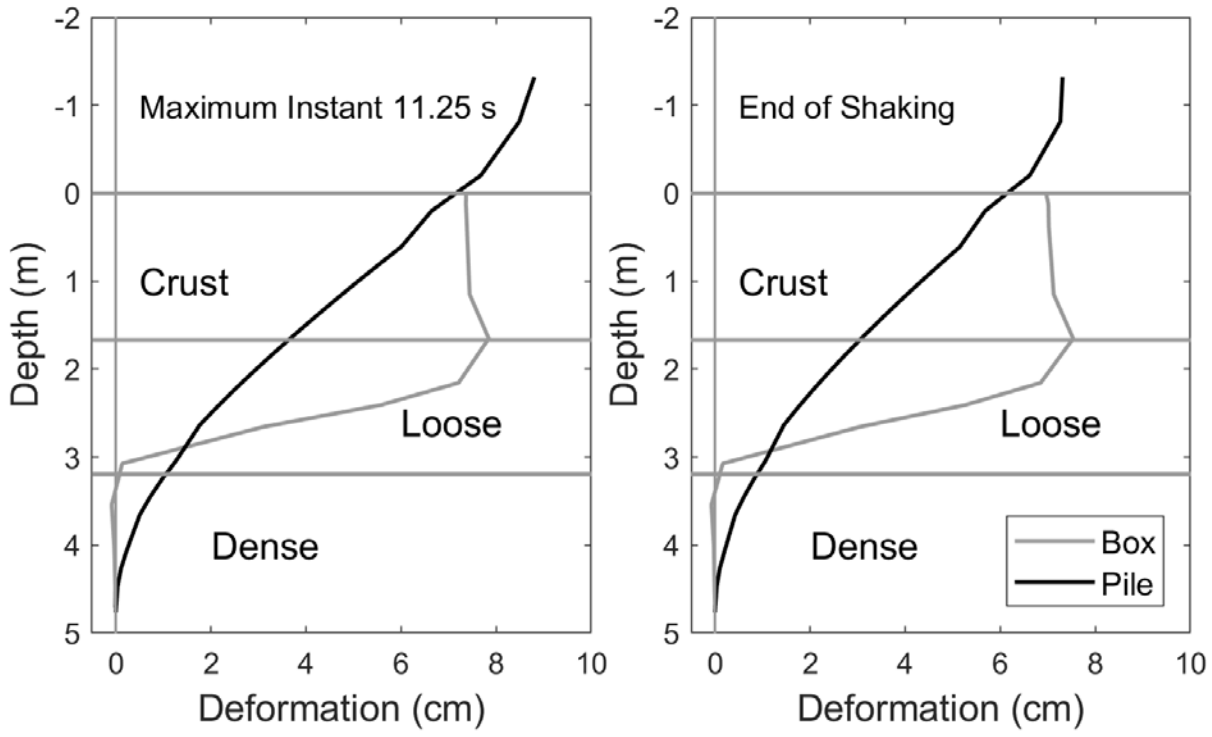

Figure 10-17. Pile and box deformation profiles at maximum instant and end of shaking

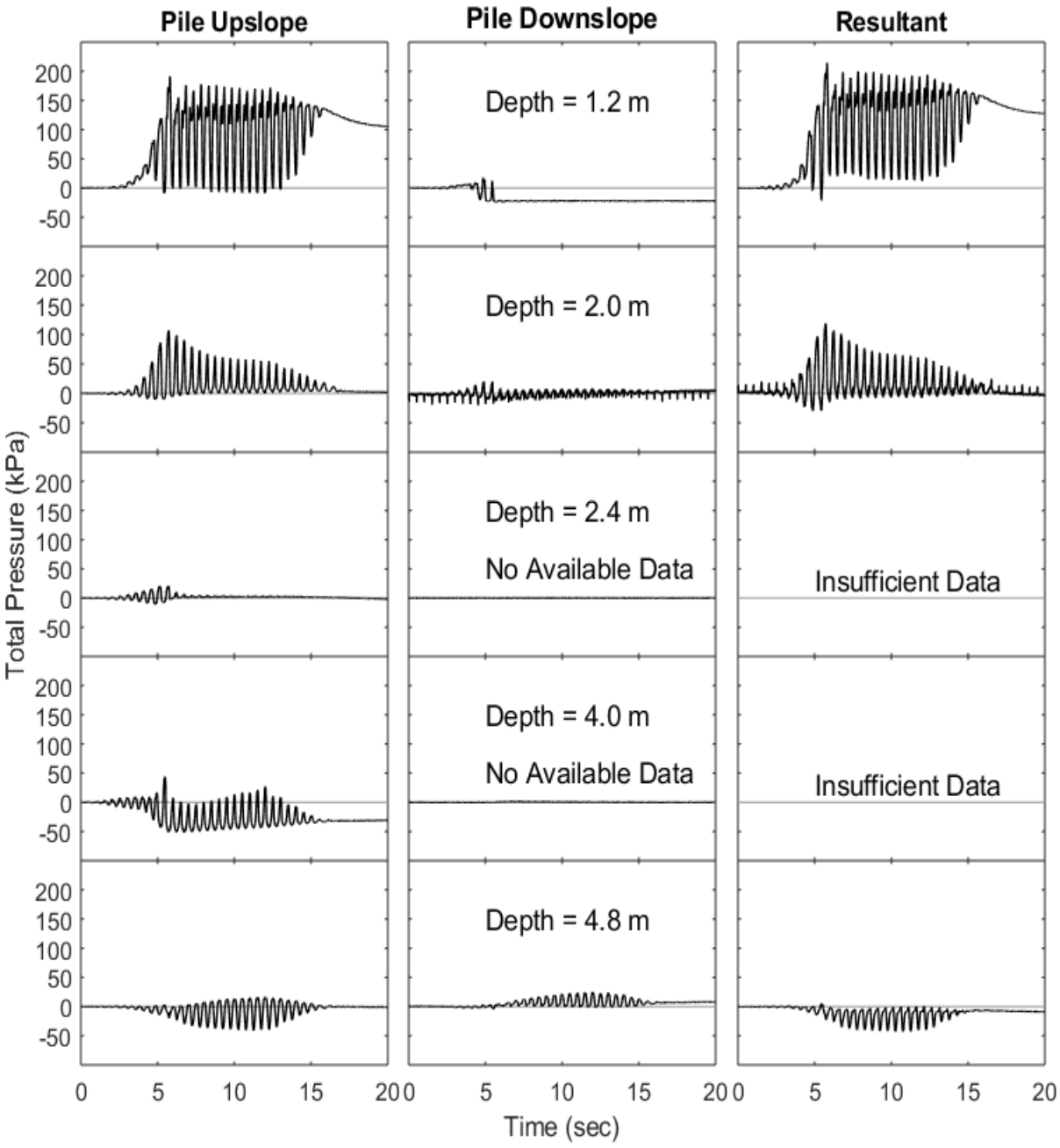

Figure 10-18. Total soil pressure time histories on both sides of the pile

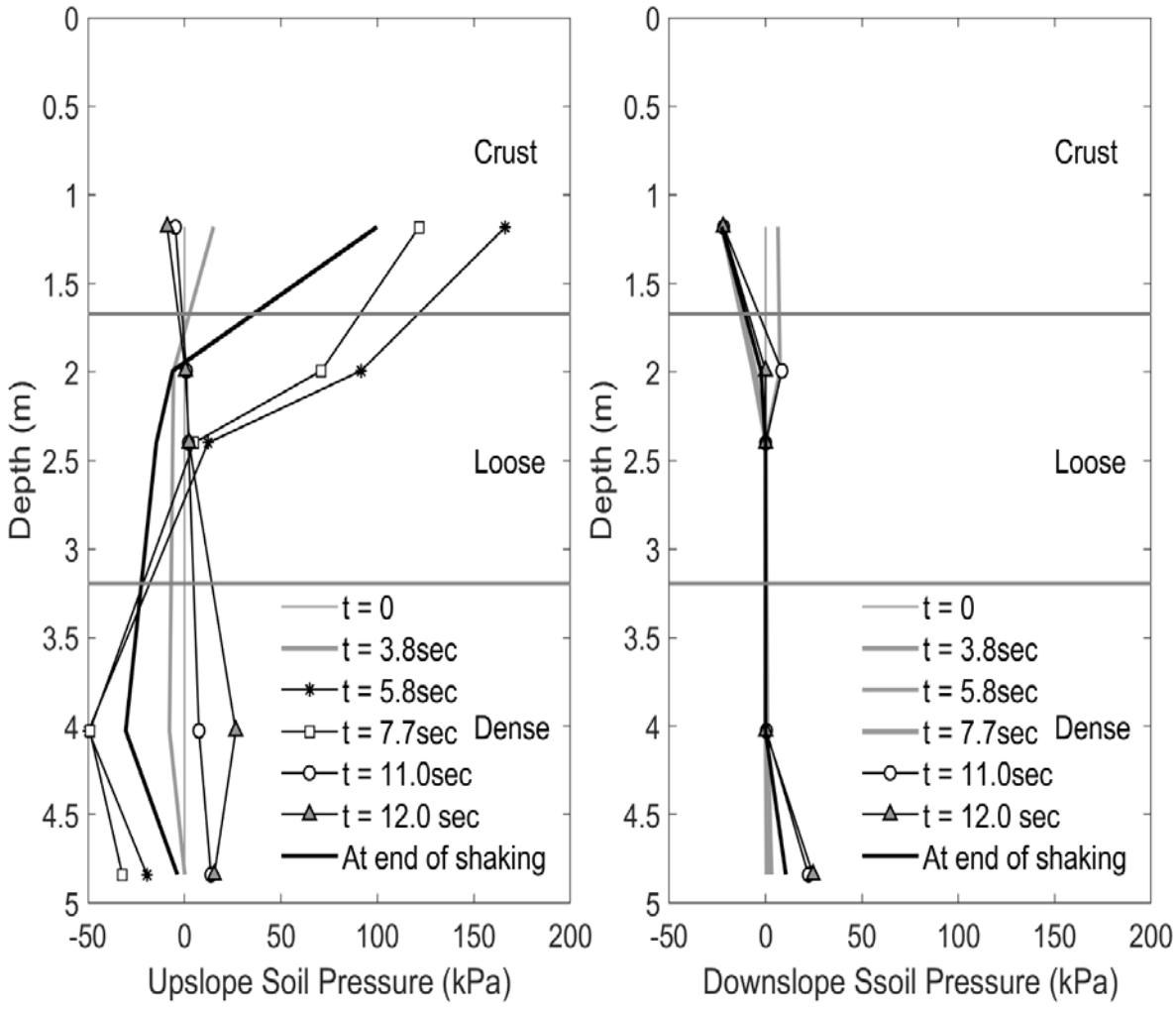

Figure 10-19. Total soil pressure profiles acting on the pile

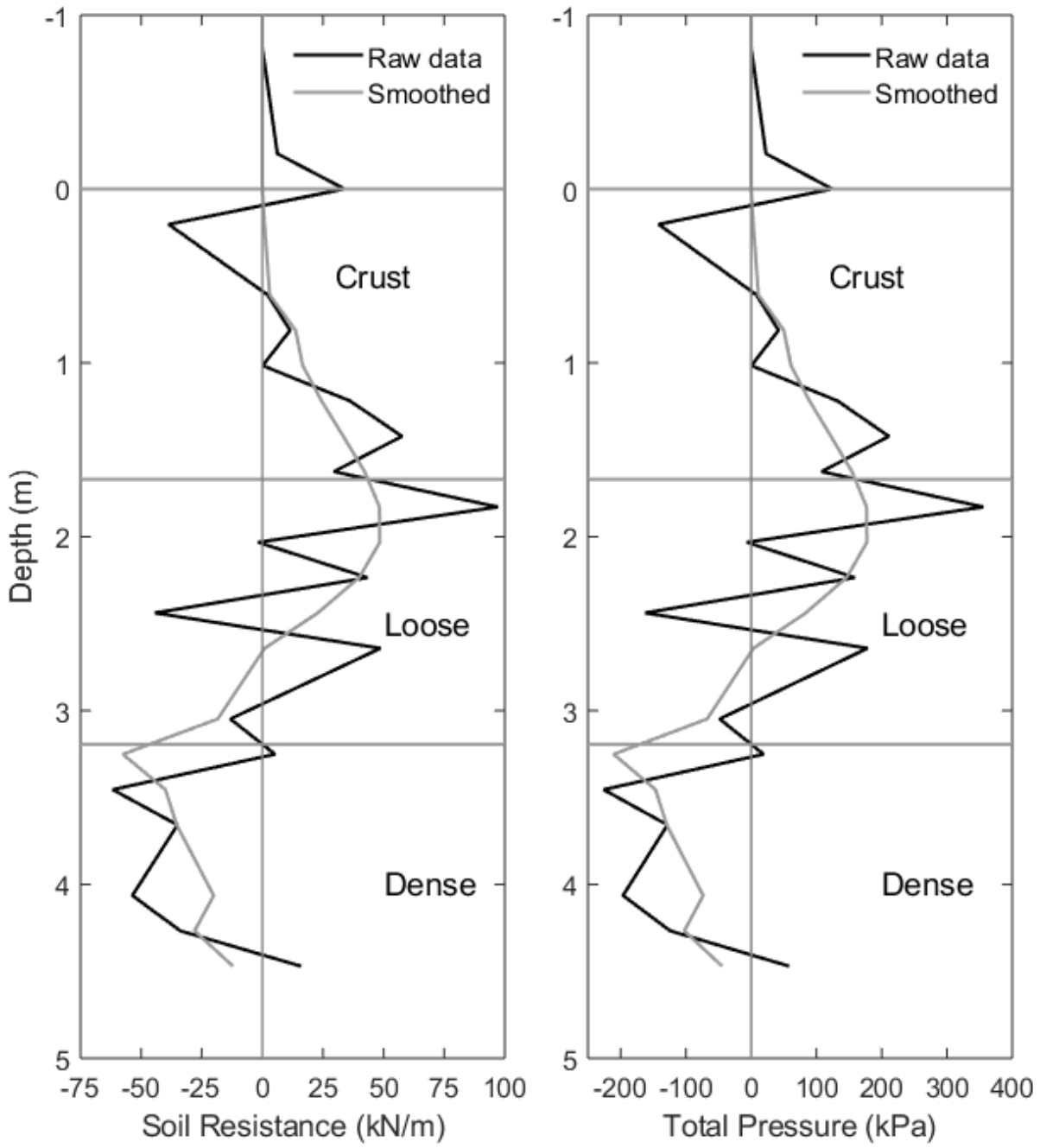

Figure 10-20. Soil resistance and total pressure profiles back calculated from strains at the maximum instance (11.25 s)

Figure 10-21. Picture of deformed laminar box configuration after shaking

Figure 10-22. Soil surface condition after shaking

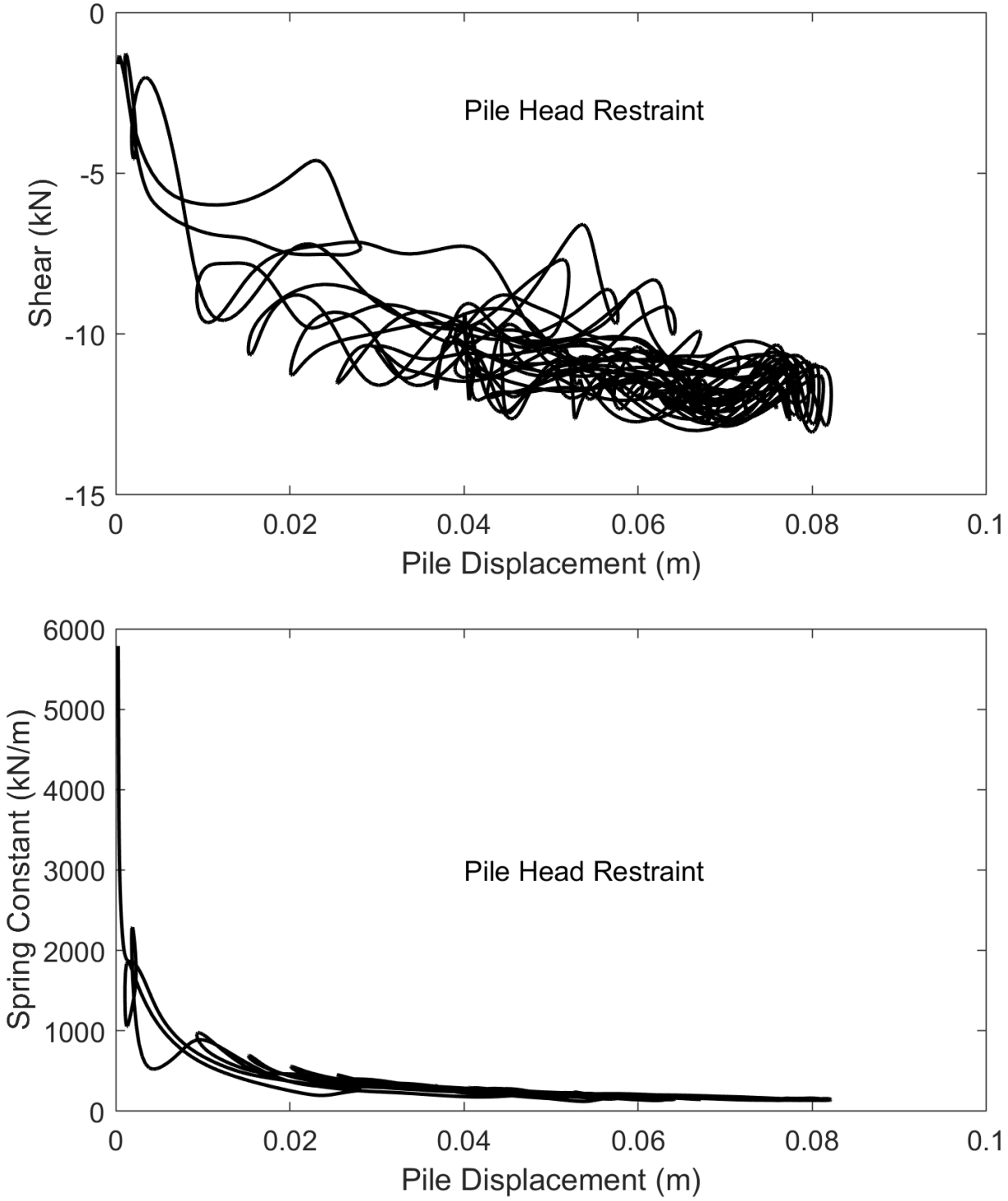

Figure 10-23. Pile head restraint response (Secant spring constant)

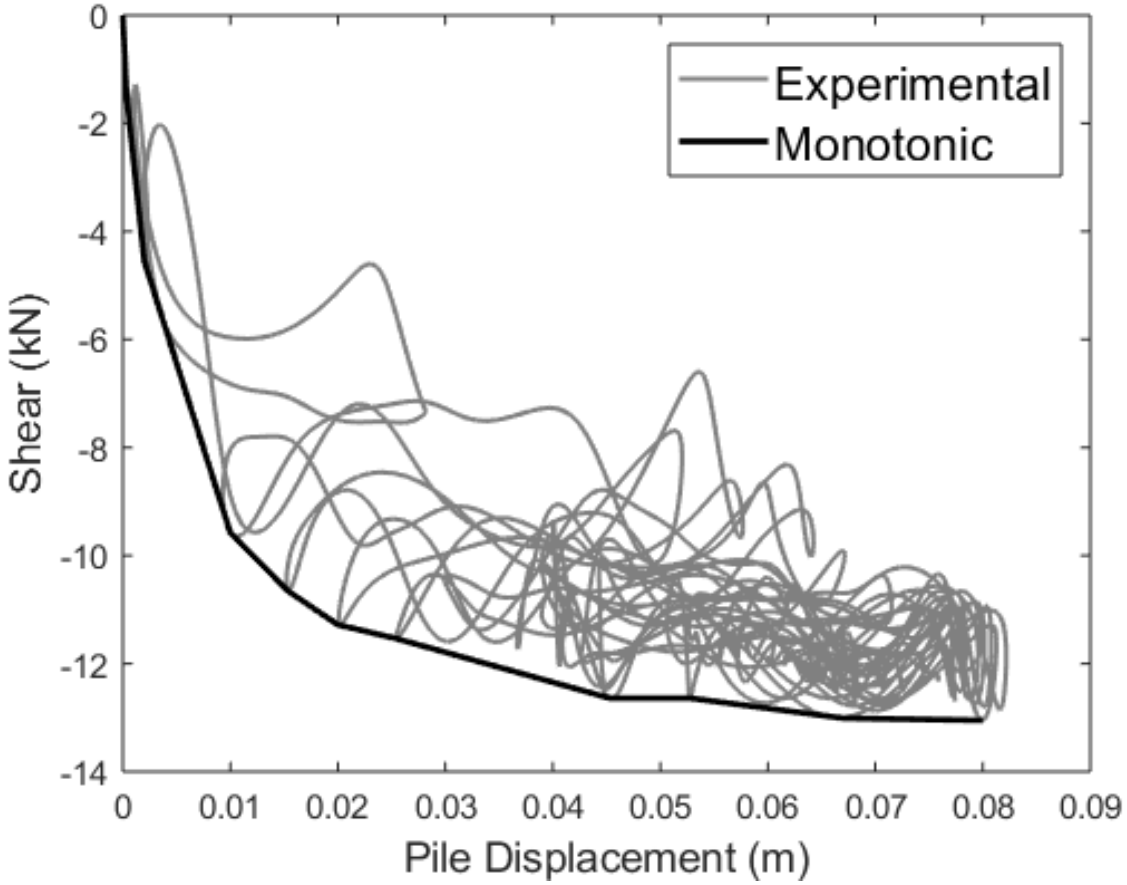

Figure 10-24. Pile head restraint envelope used in the *p-y* lateral model

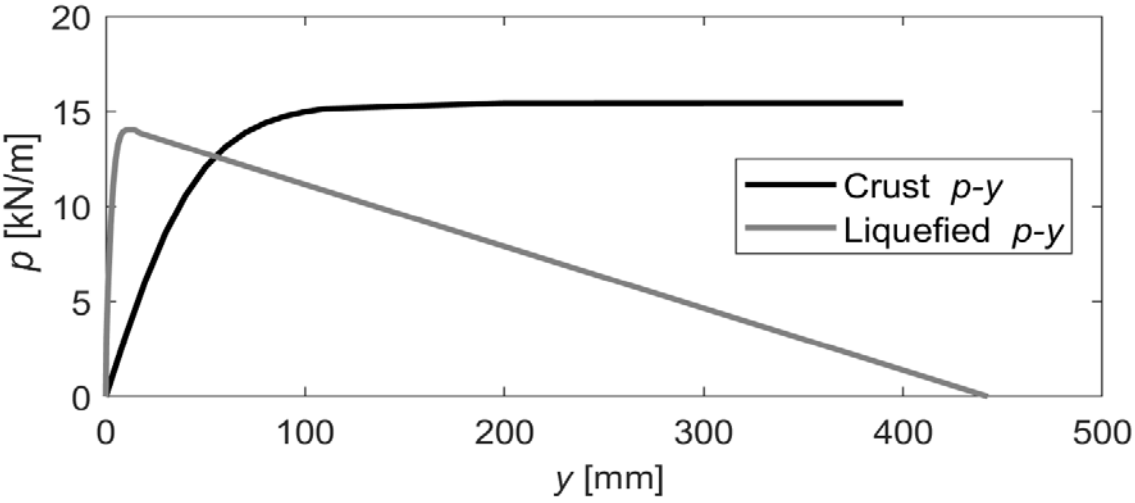

Figure 10-25. *p-y* curve models used in lateral analysis

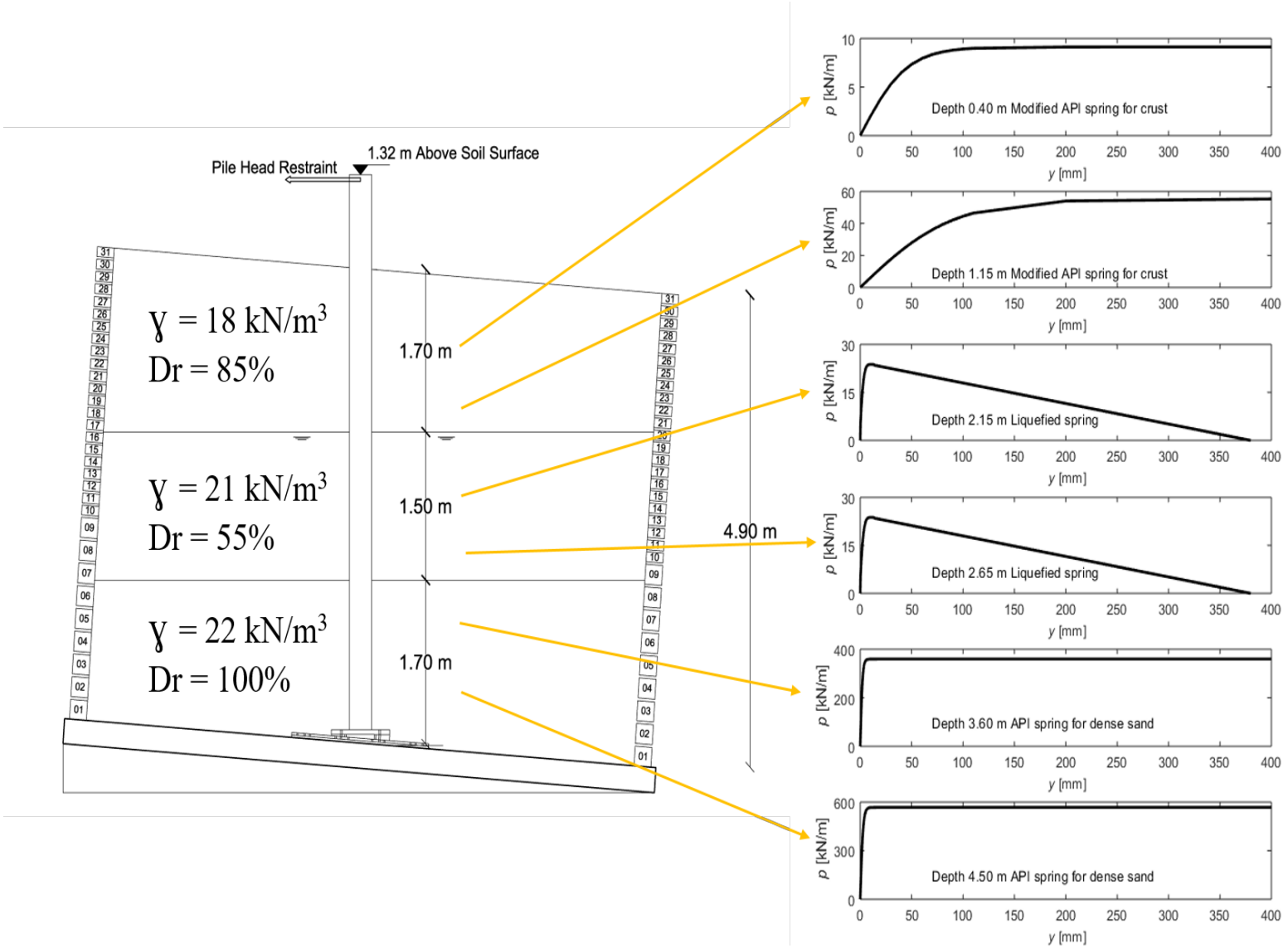

Figure 10-26. Example of the applied *p-y* curves in the pile lateral analysis

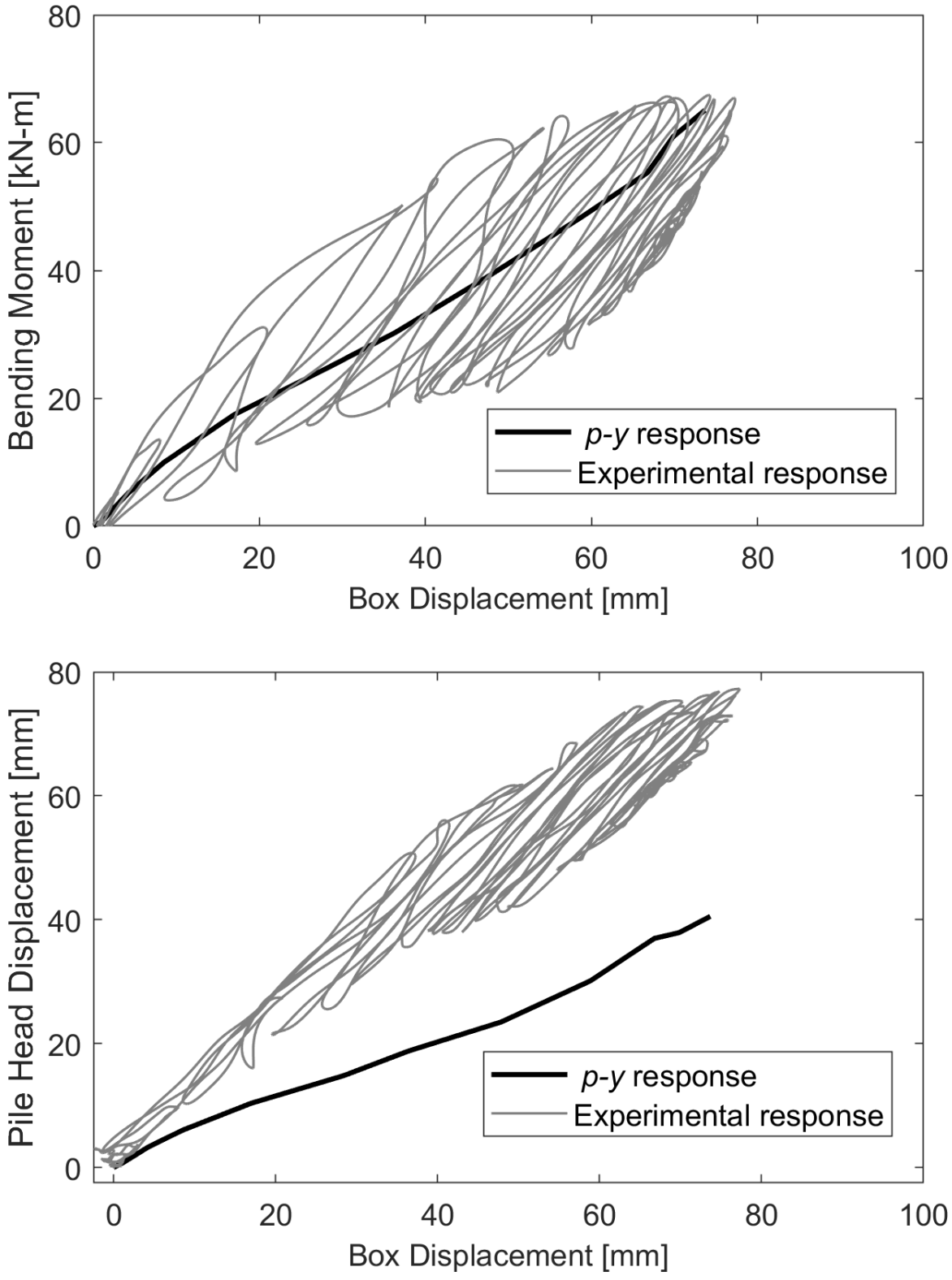

Figure 10-27. Comparison of experimental and *p-y* response (Bending moment plotted at maximum location, 4 m depth)

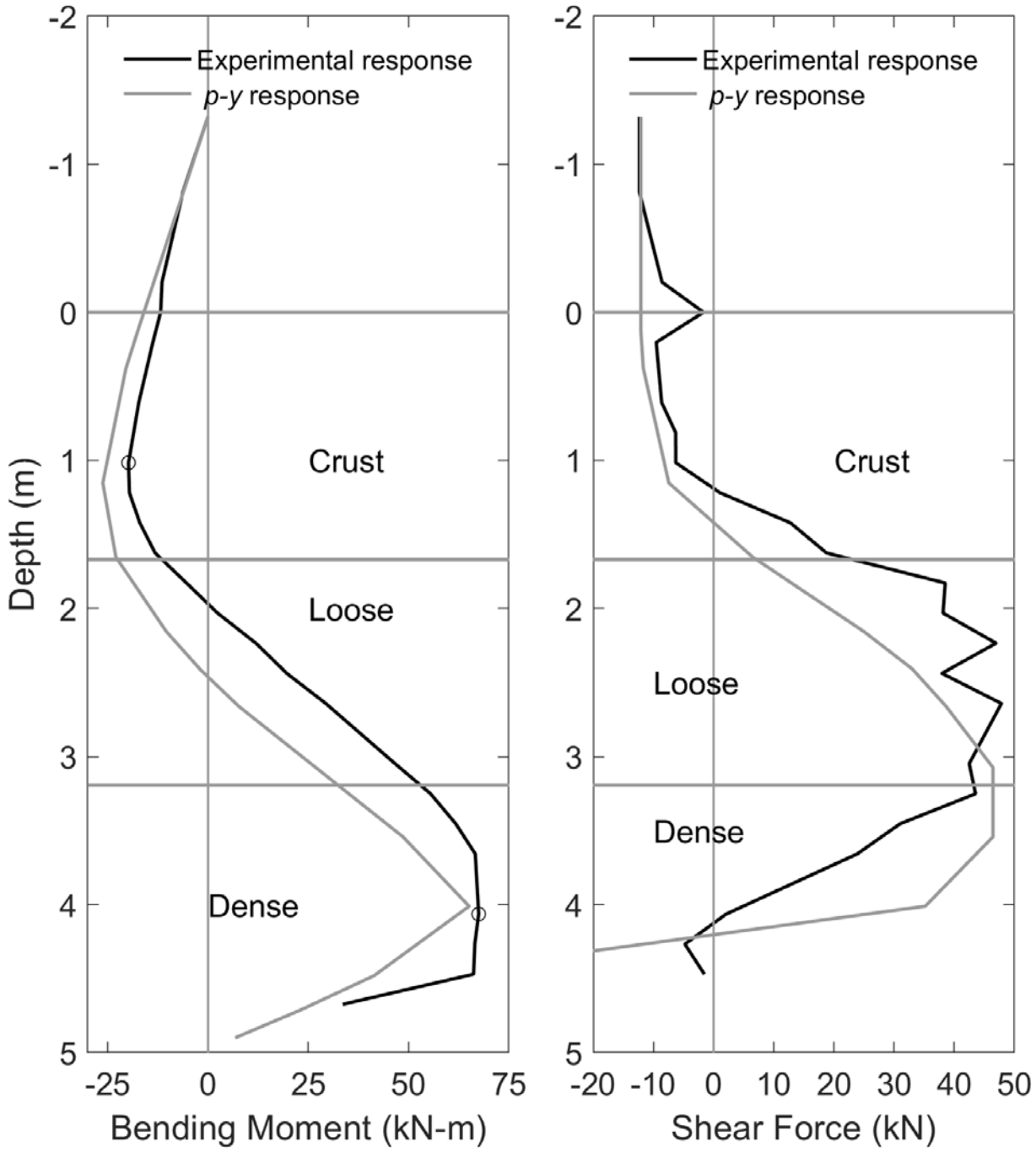

Figure 10-28. Profile comparison of experimental and *p-y* response

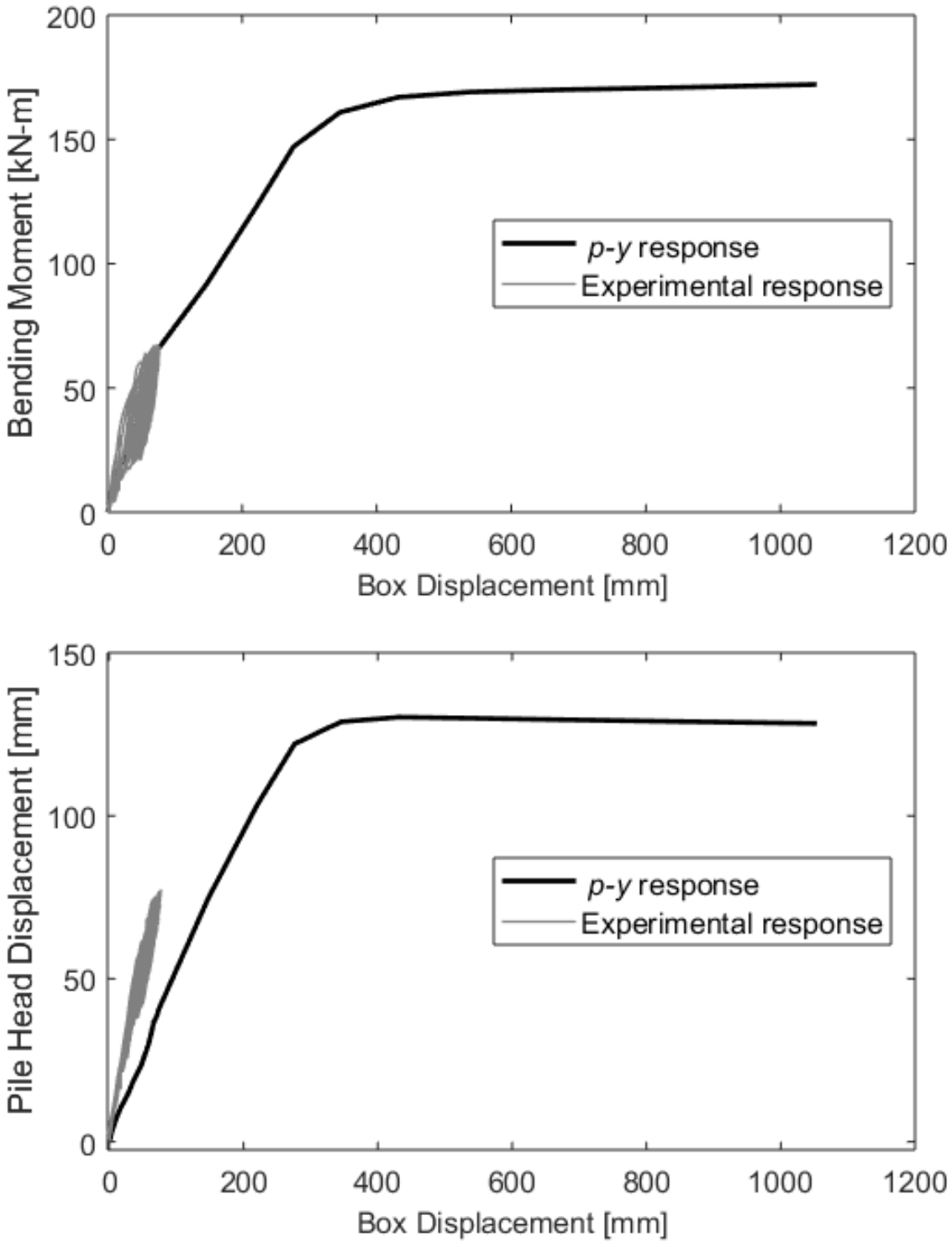

Figure 10-29. Extension of the *p-y* response for large ground deformation (curvature approximately 0.013 for bending moment = 170 kN-m)

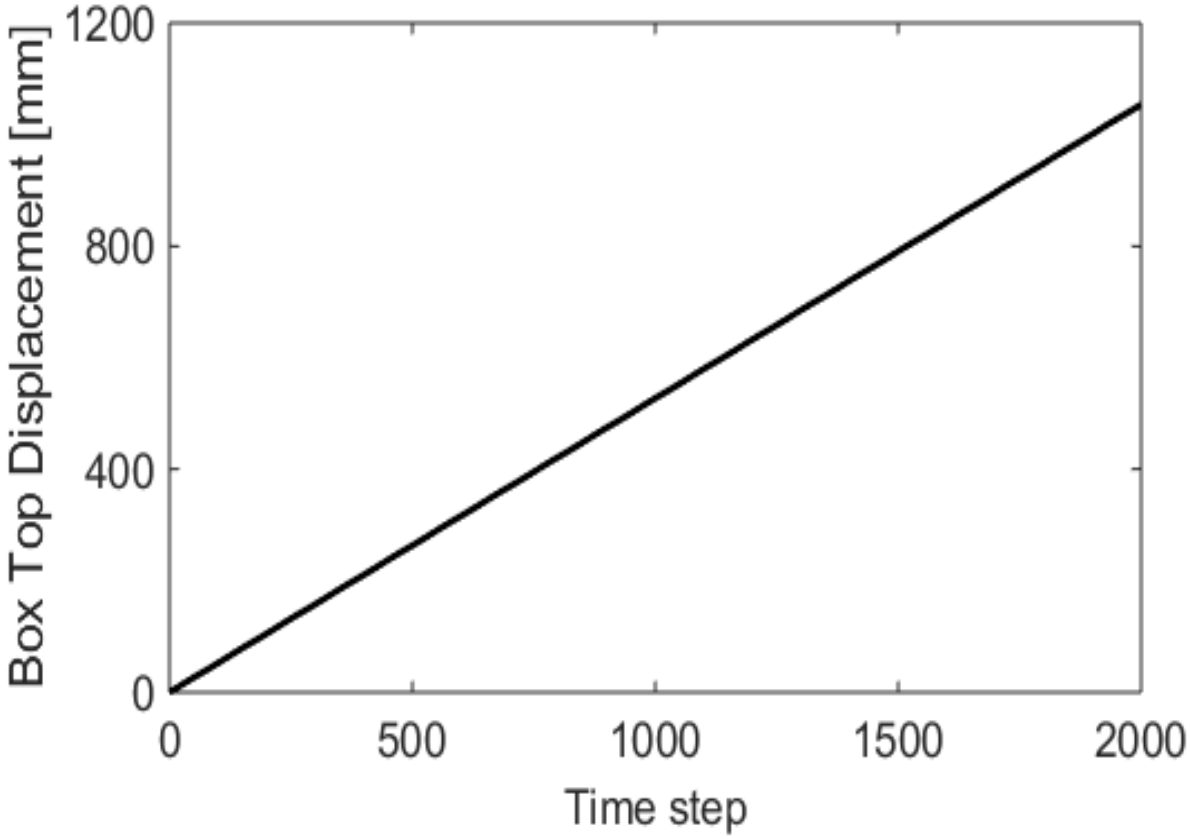

Figure 10-30. Box displacement time history applied in the *p-y* lateral analysis

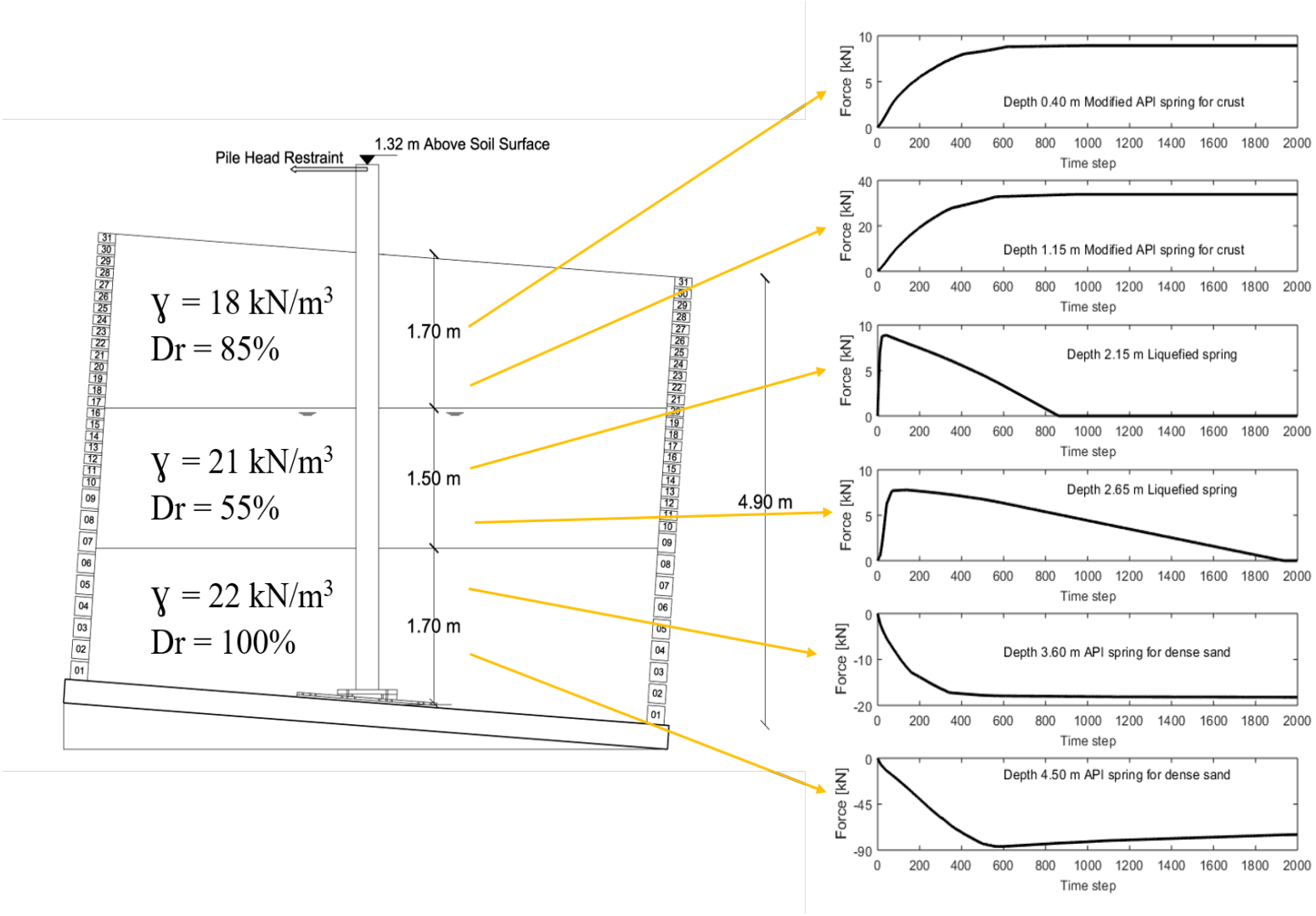

Figure 10-31. Resulting force time histories applied on the pile from the *p-y* lateral analysis

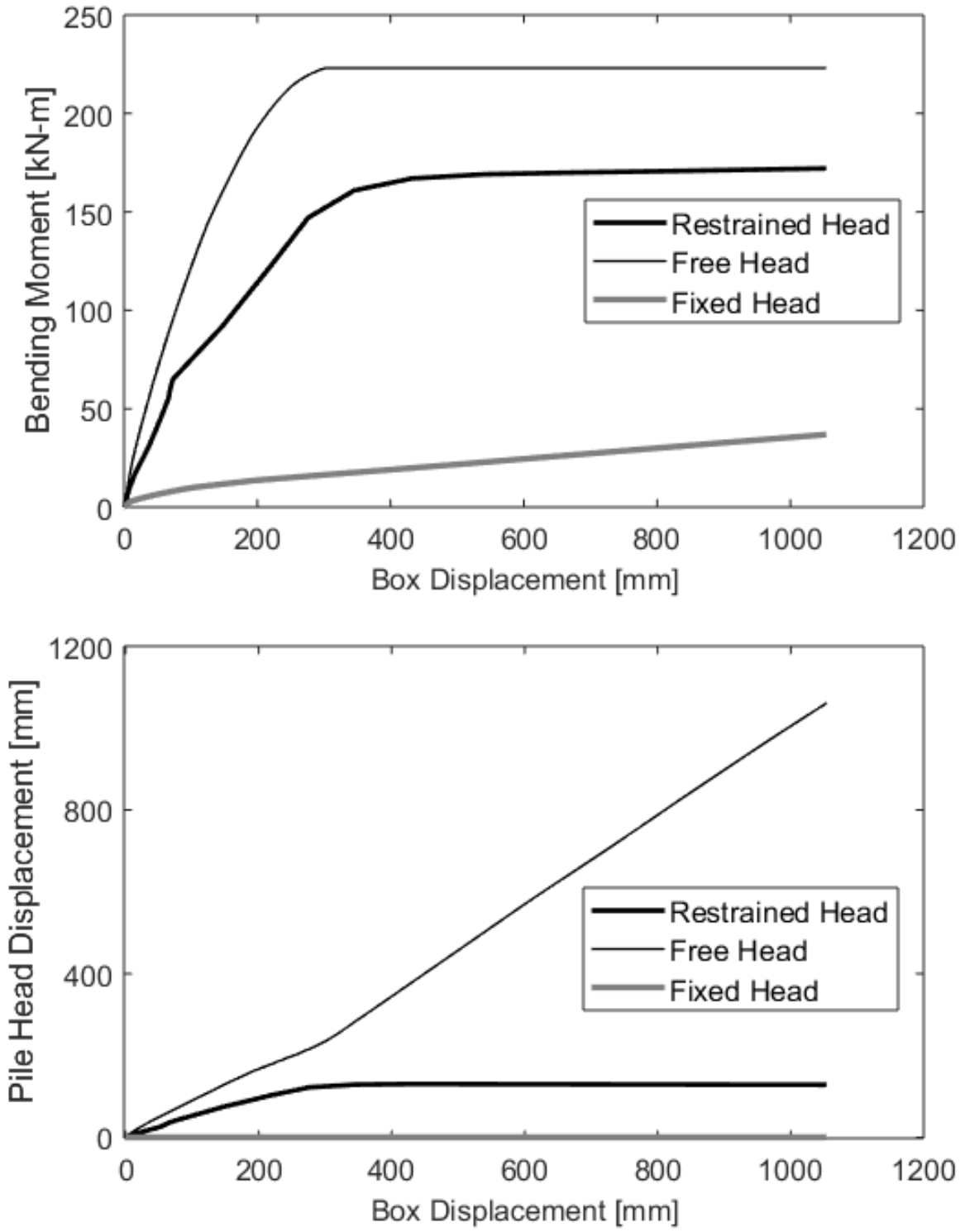

Figure 10-32. Comparison of *p-y* response results for different pile head conditions (Bending moment plotted at maximum location, 4 m depth)

Chapter 11 Prestressed Concrete Pile During Liquefaction-Induced Lateral Spreading

11.1. Abstract

A large-scale laminar container shaking table experiment was conducted to investigate a prestressed concrete single pile response, due to the mechanism of liquefaction-induced lateral spreading. The pile was fixed at the base and free at the top embedded in a 3 layered 4.90 m soil profile. Soil layering and properties are characterized and discussed. Recorded data sets from this experiment are analyzed to document and track the evolution of lateral loading on the deployed single pile. The entire system response is evaluated. Ground and pile lateral displacement as well as excess pore pressures are discussed. In this unique test, pile response is investigated as it correlates to the pile lateral loads and observations from the recorded soil pressures and calculated bending moment. The axial response is examined as a result of the liquefaction induced-lateral spreading mechanism. The pile response during and after shaking is vital for calibration of lateral *p-y* models pertaining to lateral spreading cases.

11.2. Introduction

Lateral spreading due to earthquake excitation presents a complex loading situation on piles and pile group systems (Boulanger and Tokimatsu 2005; Finn 2015). The underlying soil-pile interaction mechanisms take place as the soil undergoes significant change in its dynamic properties.

Case history investigations document a wide range of damage to structures and underlying pile foundations during liquefaction and lateral spreading (Hamada 1992; Hamada and O'Rourke 1992; Ishihara 1997; Tokimatsu and Asaka 1998; Berrill *et al.* 2001). The observed damage and deformations were analyzed in order to improve our understanding of the involved response

mechanisms (Ishihara and Cubrinovski 1998; Ishihara and Cubrinovski 2004; Koyamada *et al.* 2006). Field examinations have provided valuable insights that continue to refine the scope of necessary research (Ishihara and Cubrinovski 2004; Koyamada *et al.* 2006).

Pile foundations are affected by both inertial and kinematic forces; however, liquefaction of soil causes an increase in kinematic effects more than inertial effects (Tokimatsu *et al.* 2005). Martin and Chen (2005) discuss pile response based on two case histories and their investigation show that the relative stiffness between the pile and soil are important in predicting the failure modes of pile and soil. When the pile stiffness is high compared to the soil, forces acting on pile do not increase implying that soil flows around the pile. Softer pile with respect to the soil, lowers the lateral load acting on the pile as pile deflects.

Experiments play an important role as the observed quantitative response remains scarce. As such, investigations through physical modeling are a valuable resource. Centrifuge experiments were conducted to study liquefaction, lateral spreading and their effect on piles (Abdoun 1997; Haigh 2002; Bhattacharya *et al.* 2004; Brandenberg *et al.* 2004; Kagawa *et al.* 2004, Towhata *et al.* 2006; Motamed *et al.* 2008; Motamed and Towhata 2010). Brandenberg *et al.* (2005) show that direction of lateral loads from the varying soil layers depends on the incremental and total relative displacement between the pile and soil as well as the primary contribution of the pile stiffness to the lateral loading. Brandenberg *et al.* (2007) continue discussing the load transfer mechanisms of the crust and the softening of the load transfer mechanism related to the passive mode of failure and large zone of influence and interaction. Other centrifuge tests (Abdoun and Dobry 2002, Abdoun *et al.* 2003, and Dobry *et al.* 2003) showed that the largest pile bending moment was at the boundary between the liquefied and non-liquefied layers.

In addition to the above, large scale one-g shake table experiments were performed (Tokida *et al.* 1993; Hamada, 2000; Meneses *et al.* 2002; Tokimatsu and Suzuki 2004; Cubrinovski *et al.* 2006; Motamed *et al.* 2013 and Chang and Hutchinson 2013). Suzuki *et al.* (2006) document stiffer piles having larger relative cyclic displacement but smaller permanent counterpaerts as compatred to flexible piles. All these studies have provided insight and increased our understanding of the pile response mechanisms during liquefaction and lateral spreading. However, this challenging area remains a subject of research interest (Finn, 2015), with further efforts needed towards more accurate quantification of the outcomes.

Following in the footsteps of earlier studies, this study investigates lateral spreading effects on pile foundations. The experiment was configured after the mildly inclined ground configuration used in previous centrifuge studies (Taboada *et al.* 1996; Abdoun *et al.* 2003). Testing included a 5 m long single pile, with an upper dry soil stratum. As indicated by Ubilla *et al.* (2011), such one-g tests are needed as a complement to centrifuge studies where challenges remain in fully deciphering all consequences of the associated scaling laws. Additionally, this experiment was conducted on a reinforced concrete pile which is not straightforward to simulate in centrifuge experimentation.

In the following sections, the experimentation program is outlined. Recorded response time histories such as bending moments, displacements, and excess pore water pressures are discussed. Data from this test program are employed to discuss the salient response characteristics. Finally, conclusions are drawn, and recommendations are presented.

11.3. Experimental Program

Figure 11-1 shows a picture of the laminar box set up mounted on the shake table at the Englekirk Structural Engineering Research Center at the University of California, San Diego. The

container was inclined at 4° to the horizontal by means of an outside reinforced concrete ramp. The laminar box is composed of 31 stacked steel frames. The frames are lined with stainless steel plates to reduce their friction with their supporting roller bearings. A total number of 18 bearings were placed between each 2 frames and rollers were painted by a smooth epoxy paint to further reduce the friction loses. This allows for optimum lateral movement and gives minimal boundary effects. The entire box-ramp system was post-tensioned to the shake table platform to ensure a very stiff connection. The response of a prestressed concrete pile with a free head at the top was explored against liquefaction induced lateral spreading. Figure 11-2 illustrates the schematic experimental layout. Figure 11-3 and Figure 11-4 present the square pile cross section with its details. Inner box dimensions are 6.75 m long, 4.90 m high and 3.0 m wide. As noted by (Law and Lam 2001), this laminar box configuration essentially simulates a periodic boundary condition. The container was lined with an Ethylene Propylene Diene Monomer (EPDM) rubber liner placed to hold soil and water inside the laminar container. Deployed instrumentation are presented in Figure 11-5 and Figure 11-6. The full data report including other shaking events performed on this model is presented in SSRP 19-01 (Ebeido *et al.* 2019).

11.4. Soil Properties

The soil profile of 4.90 m height shown on Figure 11-2 was constructed in 3 layers using Ottawa F-65 sand (Bastidas 2016) with the following grain size characteristics: D_{60} = 0.24 mm, fines content F_c = 0.25%, and uniformity coefficient C_u = 1.56. The employed soil was poorly graded in the medium to fine range. Sand Profile was constructed with a base dense layer (2.00 m), middle loose liquefiable layer (1.76 m) and a top dry layer (1.10 m). Water table was 1.10 m below the ground surface at the pile location (box centerline). Each layer had a target density, and this was achieved by monitoring the dry weight of sand used to occupy the volume of each layer.

Quality control using sand cone tests verified the estimated densities. CPTs were performed at 4 different locations before shaking at the upslope and downslope arrays.

The base layer of 2.00 m was constructed by wet compaction. The layer was built in 0.25 m lifts, each densified using a plate compactor. After completion, the base layer was saturated from the bottom up by means of previously installed perforated PVC tubes. This base stratum was intended to be a stiff rigid layer and to ensure that, the layer was shaken by a series of white noise motions to further densify the sand and achieve the targeted 100% relative density. Saturated density was about 2200 kg/m^3 (Dry density = 1780 kg/m^3). Secondly, the 1.76 m middle loose layer was constructed by sand pluviation through soil meshes then passing through water. The falling rate and height were maintained to achieve a uniformly deposited layer. Estimated relative density is 55 % and saturated density is 2100 kg/m^3. Finally, the top layer (crust) of 1.10 m height was built dry with some compaction to achieve a soil relative density of 85 % and a bulk density of 1817 kg/m^3 (Dry density of 1730 kg/m^3).

After building the soil model and before shaking, in an effort to fully characterize the soil model, CPTs were performed at 4 different location in the soil box at the upslope and downslope arrays. Locations were chosen midway between the pile and box boundaries to minimize their effects on the test. A limited access Ramset was used to perform the test. Performing such testing allows for field like site characterizations and possible comparisons with case histories. Figure 11-7, Figure 11-8 and Figure 11-9 show the results obtained from one of the tests conducted at the 2 different arrays (upslope and downslope). Water table readings agree with the target water level during model construction. Test results confirm the presence of 3 layers, each with a different stiffness. Tip resistance and sleeve friction show a trend of increase in the top crust layer followed by a decrease at the interface with the middle loose layer. Readings through the middle stratum

show a lower constant strength throughout the layer then values increase as the cone approached the dense bottom layer. Correlated values for SPT and shear wave velocity are also presented and follow the presented trend. It is observed that the region of stiffness change at both loose layer interfaces are approximately 0.70 m affecting the heights of all 3 layers.

Additional shear wave velocity testing using high sampling accelerometer arrays and a vibration source was conducted. Figure 11-10 presents the shear wave velocity results of the pre-shaking characterization. Shear wave velocities for the different layers are observed to be about 150 and 100 for the dense and loose layers respectively and 150 to 200 m/s for the crust.

11.5. Pile Properties

A reinforced concrete pile (Figure 11-3, Figure 11-4) of 0.3 m (12 in) square cross section, 50 mm cover and a 19 mm chamfer on its corners was employed constructed from regular strength concrete with 6 grade 60 #6 US longitudinal reinforcement and W11 spiral reinforcement spaced at 50 mm. The #6 bar corresponds to a 19 mm rebar diameter. The pile was casted with a base pedestal to enable connection to the box base. A preliminary static pushover test was performed on the pile before adding the sand to obtain the bending stiffness and base fixity rotational stiffness values. Pile connection was characterized to have a base rotational spring of 1750 kN-m/rad. The pile was prestressed at 444 kN (100 kips) force. Figure 11-4 presents the section properties with parameters in Table 11-1 and Table 11-2 used for pile modelling.

Unconfined compression strength of the concrete was tested at 28 days and found to be 41.4 MPa. Monotonic moment-curvature is shown in Figure 11-4c. The pile was 5.5 m long and was casted to include a steel plate at the base connected with studs to enable anchoring to the base.

11.6. Instrumentation

The model included various top of the line instrumentation arrays (Figure 11-5). Sensors were placed closely at 20 cm spacing to collect comprehensive profile response data during shaking. Over 400 sensors were installed with data collection rate of 256 samples per second. Instrumentation was installed along both sides of the pile and outside of the box, and in the soil between the pile and box boundary as shown in Figure 11-5. Sensors installed were the same used in the smaller size test.

Pore pressure sensors were deployed on both sides of the pile and in the free soil, midway between the pile and container boundary (upslope and downslope) with an additional array in the free field on the pile side perpendicular to the shaking direction. Total pressure transducers were installed on both sides of the pile and used to measure the initial static soil pressure during filling and the dynamic pressures during shaking. Accelerometers were placed alongside the pore pressure transducers and on the laminar box exterior boundary. High sampling rate accelerometers were used with the ability to record at 25,000 samples per second. With this high sampling rate, the data can be employed to track shear wave velocity changes during seismic events (Zayed 2020). Strain gauges were installed on the steel pile. Strain data is used to back-calculate bending moment during shaking. Displacement transducers were mounted on the laminar box exterior wall every other laminate to measure lateral displacements, and on the soil surface to measure horizontal and vertical displacements. Locations of vertical pots is shown in Figure 11-6. The Pile was also instrumented with transducers to measure pile head displacements above the ground surface in several locations to capture the free head movement. Figure 11-6 presents a picture of the instrumented pile and free field. Additionally, a ShapeTape Array was installed in the upslope free field to track the soil profile movement with its location illustrated in Figure 11-6. The ShapeTape

does not read dynamic readings but provides a valuable final soil profile to compare with the laminar box deformation profile.

11.7. Analysis Protocol

Focus is placed on system response mainly in terms of excess pore water pressure, ground deformation, and pile behavior. Bending moment in the piles was calculated based on the measured strain using the traditional Euler-Bernoulli beam theory (Wilson *et al.* 2000) and is an indicator of the acting pressure profile. Lateral soil pressures are also presented. Thus, representative time histories and profiles were chosen to identify the pile and soil response and highlight peak values and observations.

11.8. Soil Response

Input motion (Figure 11-11) for the experiment was in the form of sinusoidal acceleration with a 2 Hz frequency and amplitude of 0.25 g. Motion was gradually increased in 10 cycles to reach the target amplitude to remain constant for 16 cycles then ramped down in another 10 cycles.

Liquefaction occurred early in the shaking phase as evident from the reduction in acceleration at shallower depths (Figure 11-12, Figure 11-13) and the recorded excess pore pressure ratio r_u (Figure 11-14, Figure 11-15, Figure 11-16), where $r_u = u_e/\sigma_{vo}'$ in which u_e = excess pore pressure and σ_{vo}' = initial effective vertical stress. Accelerations (Figure 11-12, Figure 11-13) in the base layer show no reduction in values while the loose layer records de-amplification. Asymmetric acceleration response is evidence of downslope movement of the soil layer with the spikes observed in the loose layer evident of the dilative tendency of the soil (Zeghal and Elgamal 1994).

Maximum positive accelerations do not coincide with instances where they occur within the 3 layers (base, loose and crust). An acceleration lag is noted as the wave propagates upwards through the soil.

Excess pore pressure ratios (Figure 11-14) show the rapid liquefaction of the loose layer and it remained liquefied throughout the shaking. Transducers in the base layer show the layer experiencing some strength loss but no liquefaction occurring. Excess pore pressure ratios on the pile are shown for 2 locations, upslope and downslope (Figure 11-15, Figure 11-16). Significant dilative tendencies are noted in both locations in the loose layer and upper portion of the lower dense layer. Liquefaction occurred more rapidly on the downslope side of the pile, with the higher dilative response in the upper non-liquefied portion of the dense layer. This suggests the downslope soil trying to move away from the pile.

Peaks in acceleration are observed to coincide with dips in excess pore pressures. These peaks and dips in acceleration are resulting from the loose soil exhibiting phase transformation behavior as the sand transitions from contractive to dilative and vice versa (Wilson *et al*. 2000).

Figure 11-17, Figure 11-18 and Figure 11-19 show lateral displacement profiles of the laminar container at selected time instants during the shaking event. From these displaced configurations, it can be noted that deformation was minimal within the crust layer above the water table. In the underlying saturated soil, the middle loose layer follows a parabolic trend. Most of the deformations are experienced by the loose layer. Shear strain profiles shown in Figure 11-19 confirms that the highest strains are at the lower part of the loose layer. Very low strains exist in the base stratum with negligible strains in the crust as it moves as a rigid body on top of the liquefied soil. Soil settles during shaking and accumulates approximately 40 mm of settlement (Figure 11-20).

11.9. Pile Response

Strains gauges placed on the longitudinal reinforcement (rebars) show values that exceed the material yield strain (Figure 11-21). Recorded curvature time histories match the expected response of a cantilever beam. In general, high curvatures were recorded between 3.00 m and the pile base (4.90 m). Axial strains also show similar behavior to the curvature and axial strain histories are shown in Figure 11-22.

Bending moment histories were interpolated from the curvatures based on a monotonic material model employed using OpenSees (Figure 11-4). Profiles for bending moment, and axial force are shown for the peak bending moment instant and end of shaking (Figure 11-23). A tensile axial force of about 200 kN is observed at the base of the pile (Axial diagram was plotted with the -444 kN prestressing force as a baseline) and a bending moment peak of 108 kN-m is noted. Figure 11-24 shows the compatibility of strain gauge reading placed on the rebar with those placed on the concrete surface as both end of shaking profiles are in agreement.

The behavior of the reinforced concrete pile is largely dictated by the lateral pressures (Figure 11-25 - Figure 11-28) and the displacement response as exerted by the stiffer upper crust layer. The values reported are from direct measurement from total soil pressure transducers. The instrumentation recorded values as high as 160 kPa at the base of the crust layer, about twice the plane strain passive pressure. Total pressure values recorded in the loose layer were very small in the range of 6 kPa before liquefaction and decreasing after. Downslope pressures from the base layer resisting the pile movement are seen to be much larger than the loose layer, in the range of 350 kPa. In general, pressures along the pile height were 180° out of phase and peaks in the upper layer total pressure records correspond to their drops in the base layer. Total pressure profiles show

the crust layer exerting pressures on the pile while the base dense layer is trying to resist the pile movement. Minimal pressures are applied by the liquefied layer.

11.10. Post Test Physical Observations

Figure 11-29 shows a picture of the deformed laminar box. Extensive care was taken after shaking as to not disturb the model before careful inspection and documentation were conducted. Cracking of the soil surface was observed in the pile vicinity on the upslope side presented in Figure 11-30 and Figure 11-31. The figures show soil heave on the upslope side with cracking and a downslope gap.

Physical observations of the pile specimen after disassembly support the strain and curvature readings recorded. Cracks in the pile (Figure 11-32 and Figure 11-33) were observed along the pile starting from the base till slightly above the loose layer interface. A total of 9 cracks were noted, only on the upslope face. Cracking is concentrated in the dense layer were the maximum bending moment was recorded.

11.11. *P-y* Lateral Analysis

In order to accurately model the tested configuration is a simple *p-y* analysis. Parameters such as the base rotational spring (1750 kN-m/rad) need to be considred. Following the *p-y* curves proposed in Chapters 5, 6 and 10, a lateral analysis is undertaken. In this analysis, no transition or reduction factors were used between layers. Recorded box deformation profiles (Figure 11-19) are applied to the lateral model. Results of the *p-y* model compared to the experimental recordings in terms of bending moments (at maximum location, 3.70 m depth) and pile head displacement against box top deformations are shown in Figure 11-34. The *p-y* model shows agreement with the experimental response specifically in terms of initial displacement slope and maximum value for the bending moment plot. The computed pile head displacement is lower than the experimentally

observed due to the pushover over loading instead of the dynamic excitation. Figure 11-35 presents comparison profiles for the bending moment between the *p-y* model and the experimental (rebar and concrete gauges) results. The profiles show good agreement specifically in terms of maximum values and their locations.

Figure 11-36 presents the imposed displacement at the soil surface against the applied time step. This figure can be used in correlation with Figure 11-37 to track the imposed displacement at any time step against the forces applied by the soil springs on the embedded pile. It can be observed that crust soil springs are still developing forces with the accumulated displacement. The upper portion on the liquefied layer peaked and the response is softening while the bottom portion is still increasing. On the other hand, the dense layer is applying forces in the opposite direction.

11.12. Conclusions

A 3-layer soil stratum, at a 4-degree inclined configuration and a 0.30 m prestressed reinforced concrete pile was investigated using a 1-g shaking table experiment. The pile was subjected to local plastic demands, particularly where interfaces between soil stiffnesses exist. This popular configuration has been adopted widely in centrifuge tests; however, this investigation takes advantage of the scale, concrete material and uniquely employed prestressed concrete material to study the inelastic behavior. The main result outcomes are:

1. In the liquefiable layer, accumulated lateral strains are not uniform, and are highest near its base (interface with dense layer).

2. In the underlying dense layer, lateral strains are highest near its top at the interface with the overlying loose liquefied layer.

3. a) The underlying dense layer is affected by the liquefaction of the loose layer above.

b) Excess pore pressures migrate into the dense sand stratum, weakening its upper zone, allowing for a lower contrast between the stiffness of the upper liquefied and the lower denser soil formations.

4. At the interface between the saturated loose and underlying dense strata, plastic region is distributed over a large extent of its length, about 3D. In this test, peak curvature and moment occurred 2D below the interface between the loose and dense strata.

5. Total pressures are 180° out of phase between the upper crust and lower base layer. This suggests that the base layer resists the pressures exerted by the upper crust. Acceleration records confirm the observation.

6. Crust pressures exerted are about twice the plane strain passive pressures for static loading.

7. The developed *p-y* model is in good agreement with the experimental results recorded.

11.13. Acknowledgements

Chapter 11, in full, is currently being prepared for submission for publication of the material as it may appear in the following journal publication (The dissertation author was the primary investigator and author of this paper):

Ebeido, A. and Elgamal, A., "Prestressed Concrete Pile Response in Large Scale Laterally Spreading Experiment".

Table 11-1. OpenSees Constitutive model parameters for concrete used in fiber section (Concrete01 material)

Concrete material properties	Core Concrete	Cover Concrete
Compressive strength, f'_c [MPa}	-56.4	-41.4
Strain at compressive strength, ε_c	-0.00357	-0.002
Crushing strength, f_{cu} [MPa}	-47.9	0
Strain at crushing strength, ε_{cu}	-0.0506	-0.004

Table 11-2. OpenSees constitutive model parameters for steel used in fiber section (Steel02 material)

Steel Material Properties		Rebar Steel (Grade 60)	Strand Steel (Grade 270)
Yield strength, *fy* [MPa]		455	1860
Elastic modulus, E [MPa]		$2x10^5$	$2x10^5$
Prestressing stress, σ_{Init} [MPa]		0	1131
Strain hardening ratio, b		0	0
Parameters to control transition from elastic to plastic	R0	18	18
	cR1	0.925	0.925
	cR2	0.15	0.15
Isotropic hardening parameters	a1	0.007	0.007
	a2	1	1
	a3	0.007	0.007
	a4	1	1

Figure 11-1. Picture of experimental setup

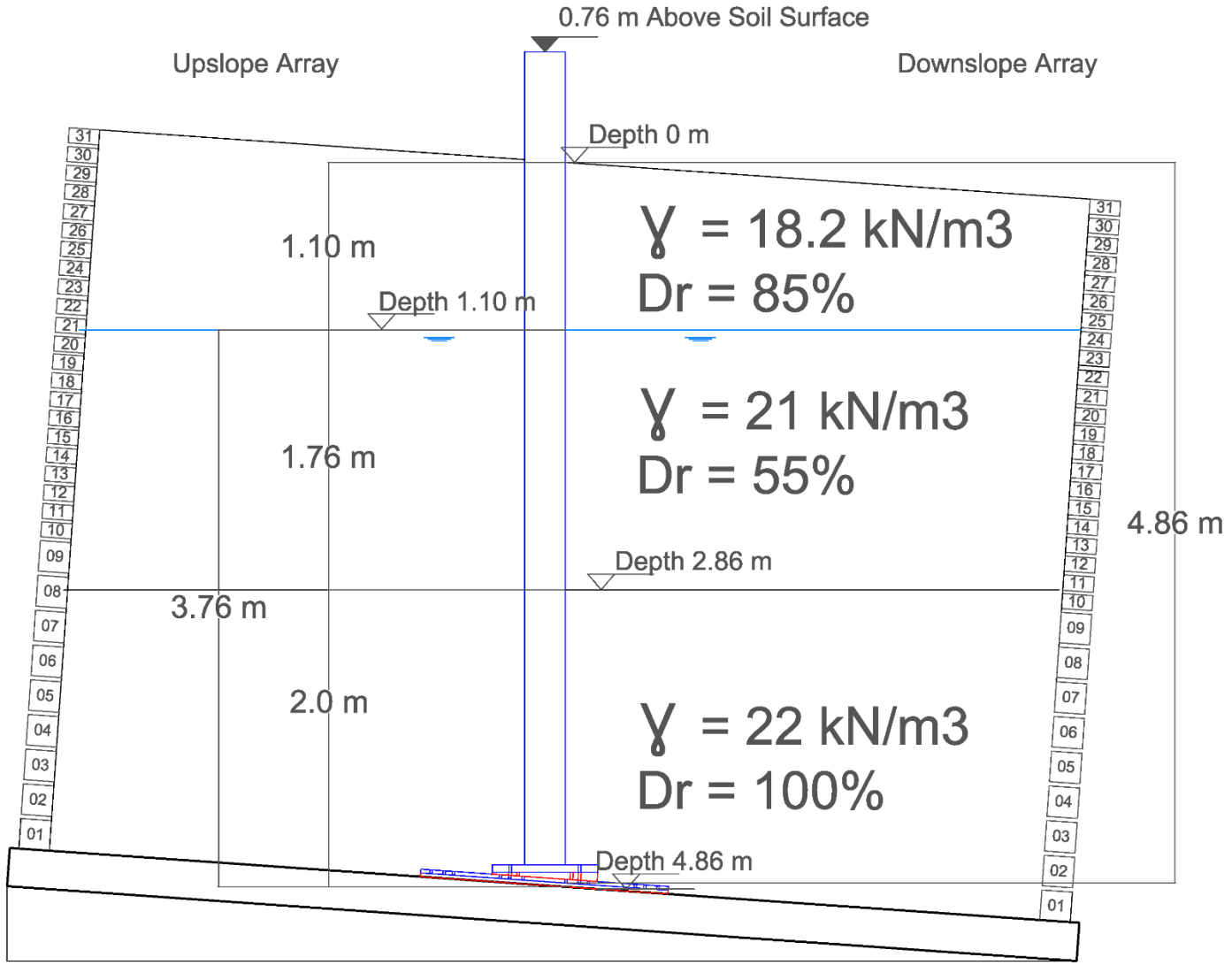

Figure 11-2. Experimental layout

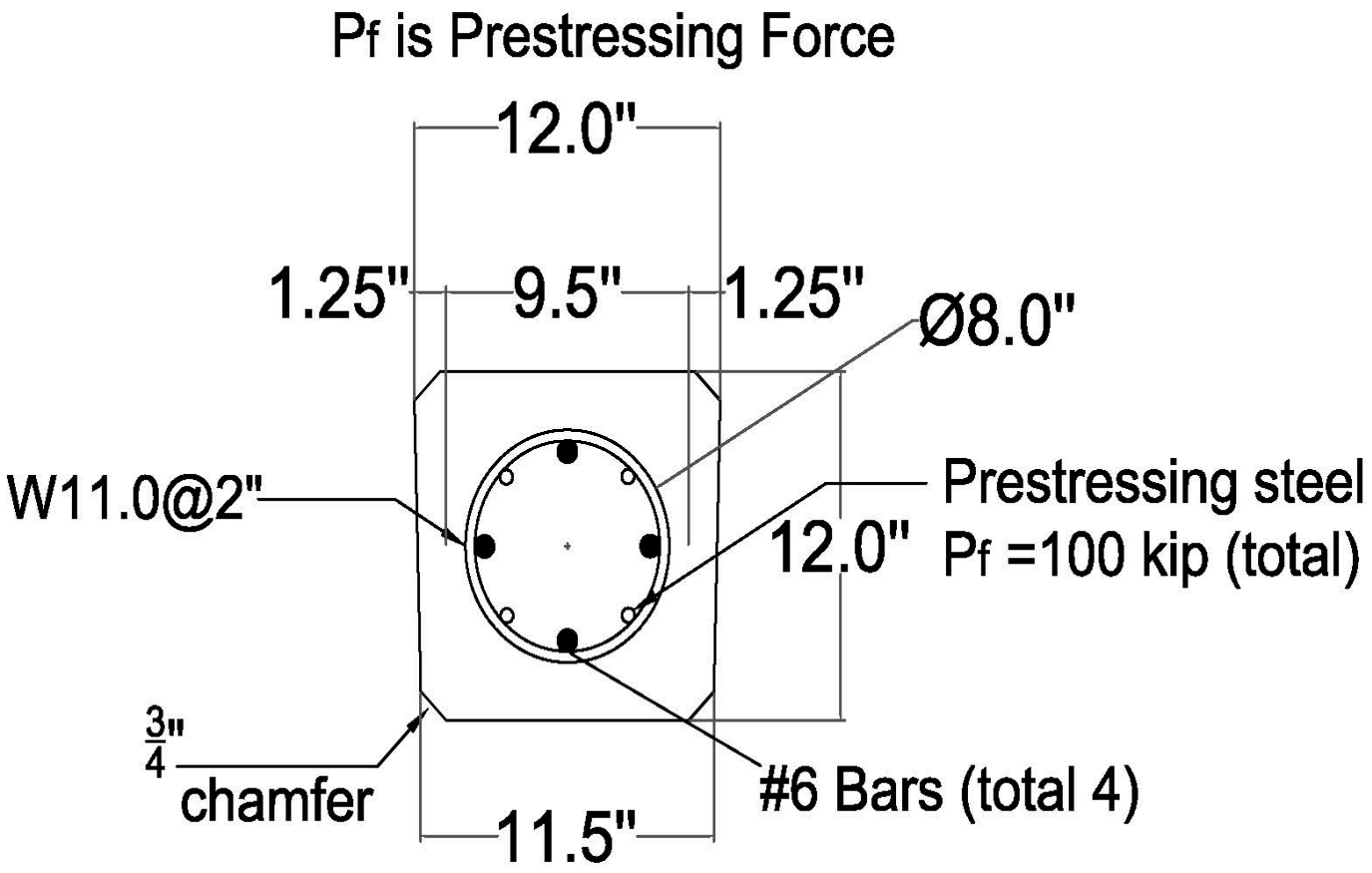

Figure 11-3. Pile cross section

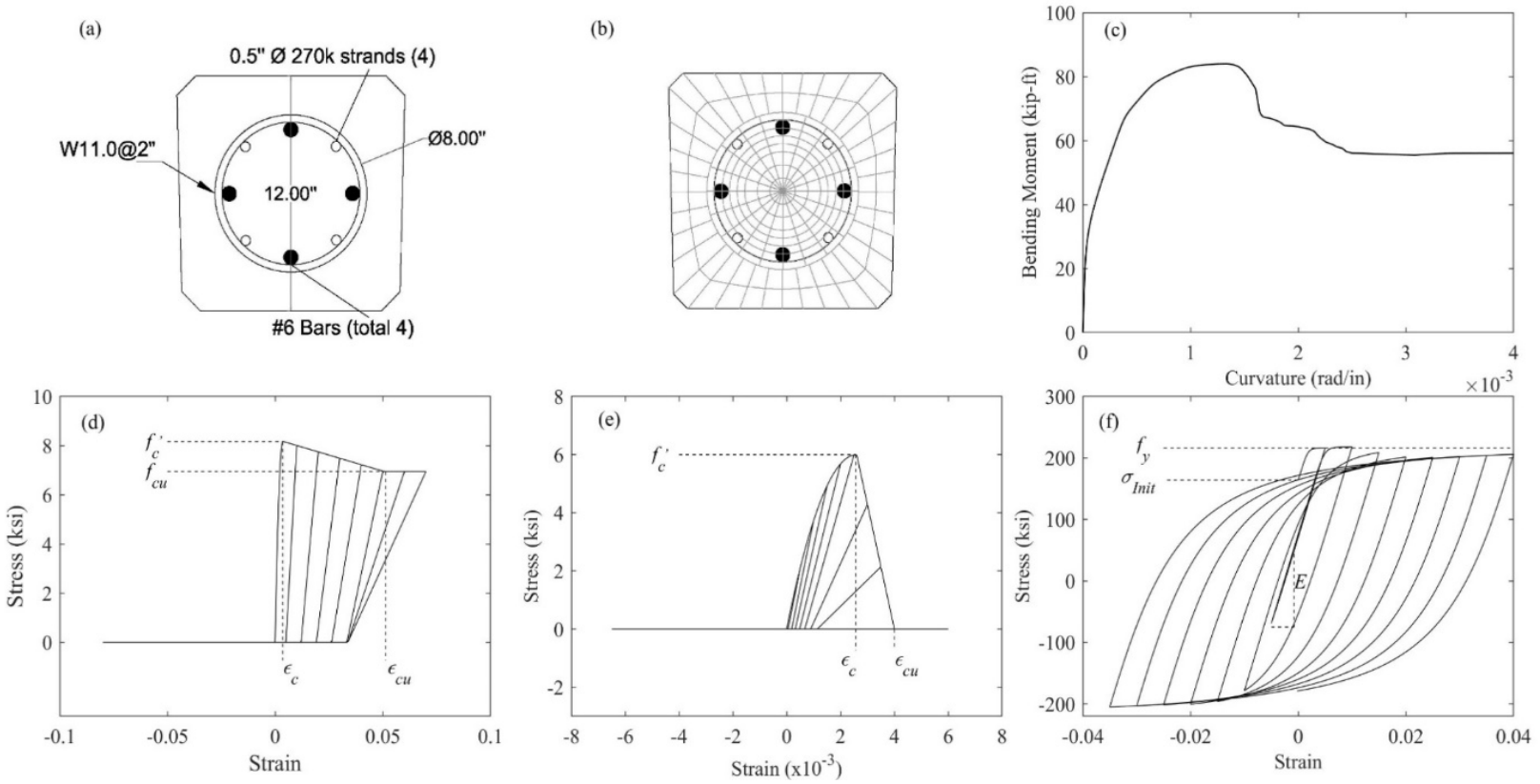

Figure 11-4. Prestressed reinforced concrete pile modeling using fiber section beam-column element with uniaxial material constitutive models: (a) pile geometry section; (b) fiber discretization of pile cross section; (c) Moment-curvature response of prestressed reinforced concrete pile cross section, (d) and (e) Core and cover Concrete01 Kent-Scott-Park model with degraded linear unloading/reloading stiffness; (f) Steel02 Giuffre-Menegotto- Pinto model with isotropic strain hardening and an axial initial stress (negative represents compressive axial force; positive represents tensile axial force).

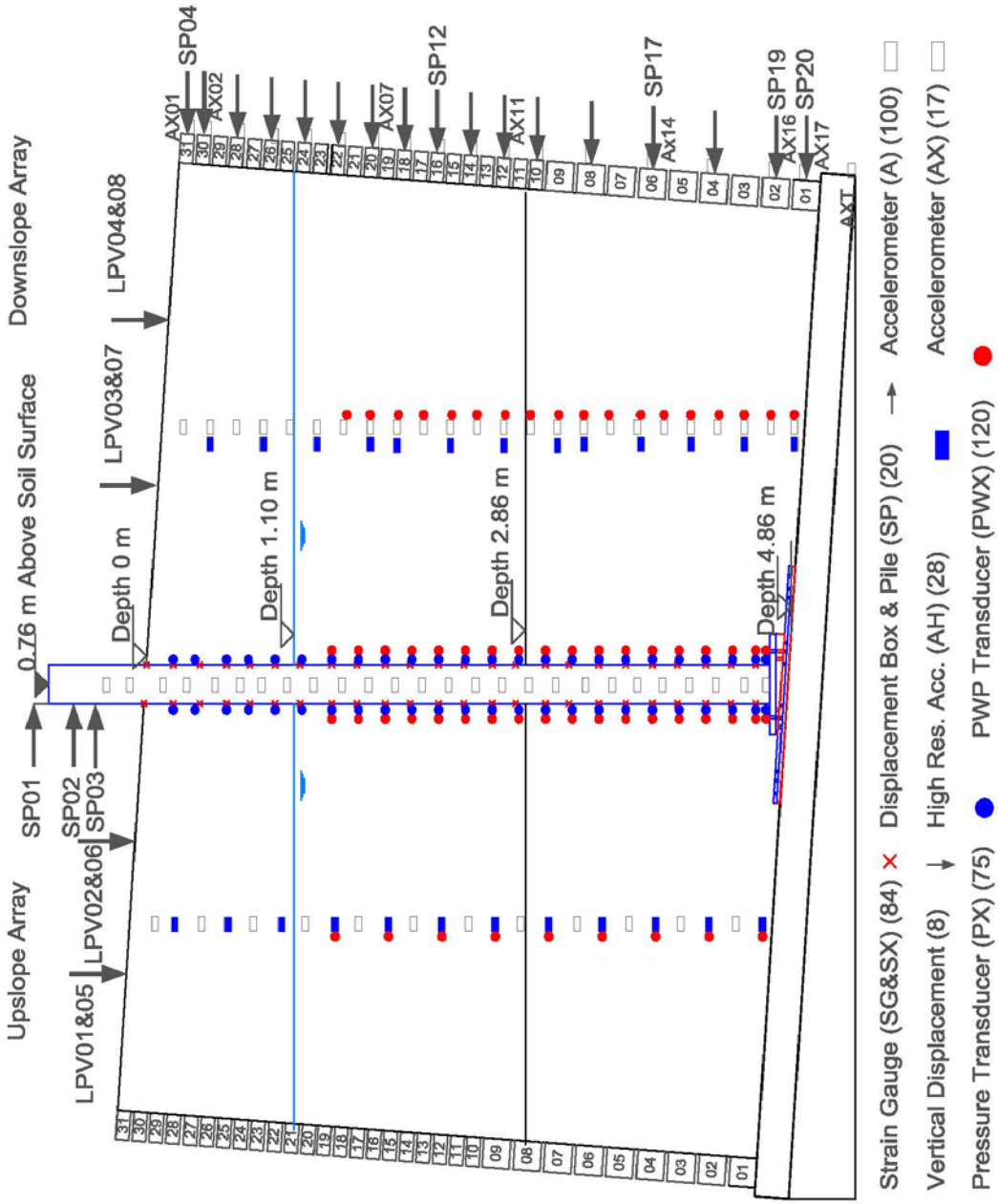

Figure 11-5. Instrumentation layout

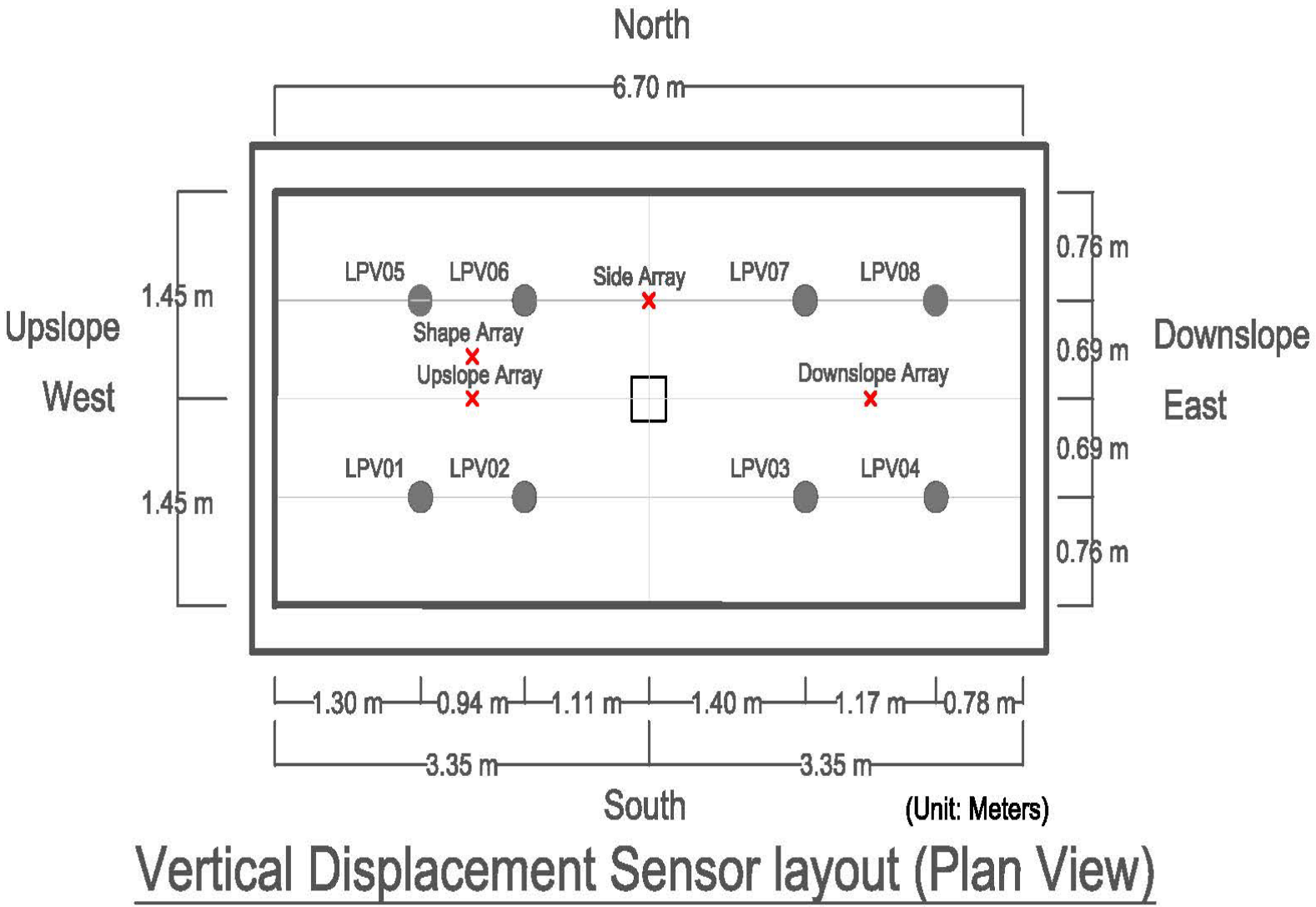

Figure 11-6. Experimental setup pan view

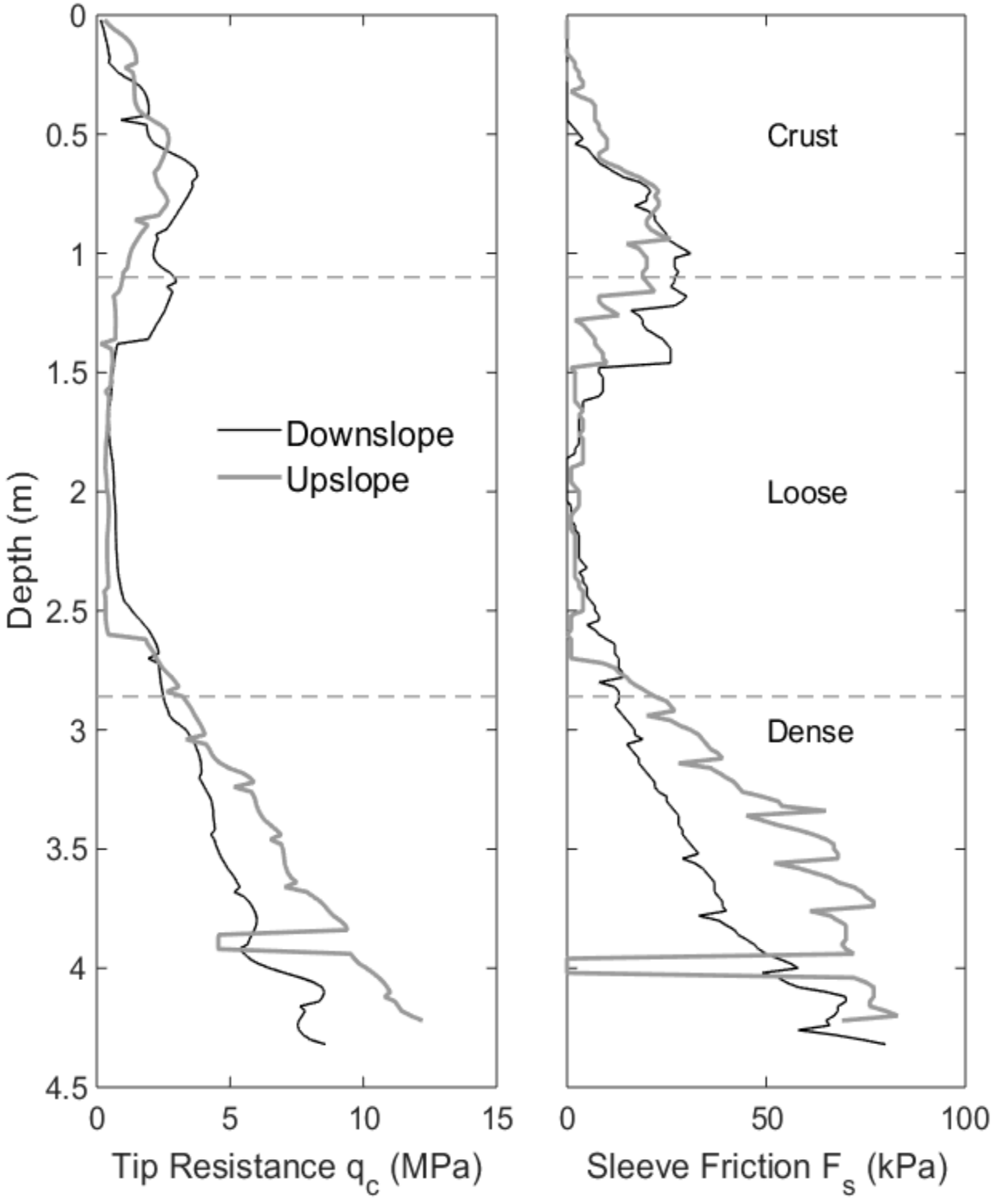

Figure 11-7. CPT profiling for the experiment

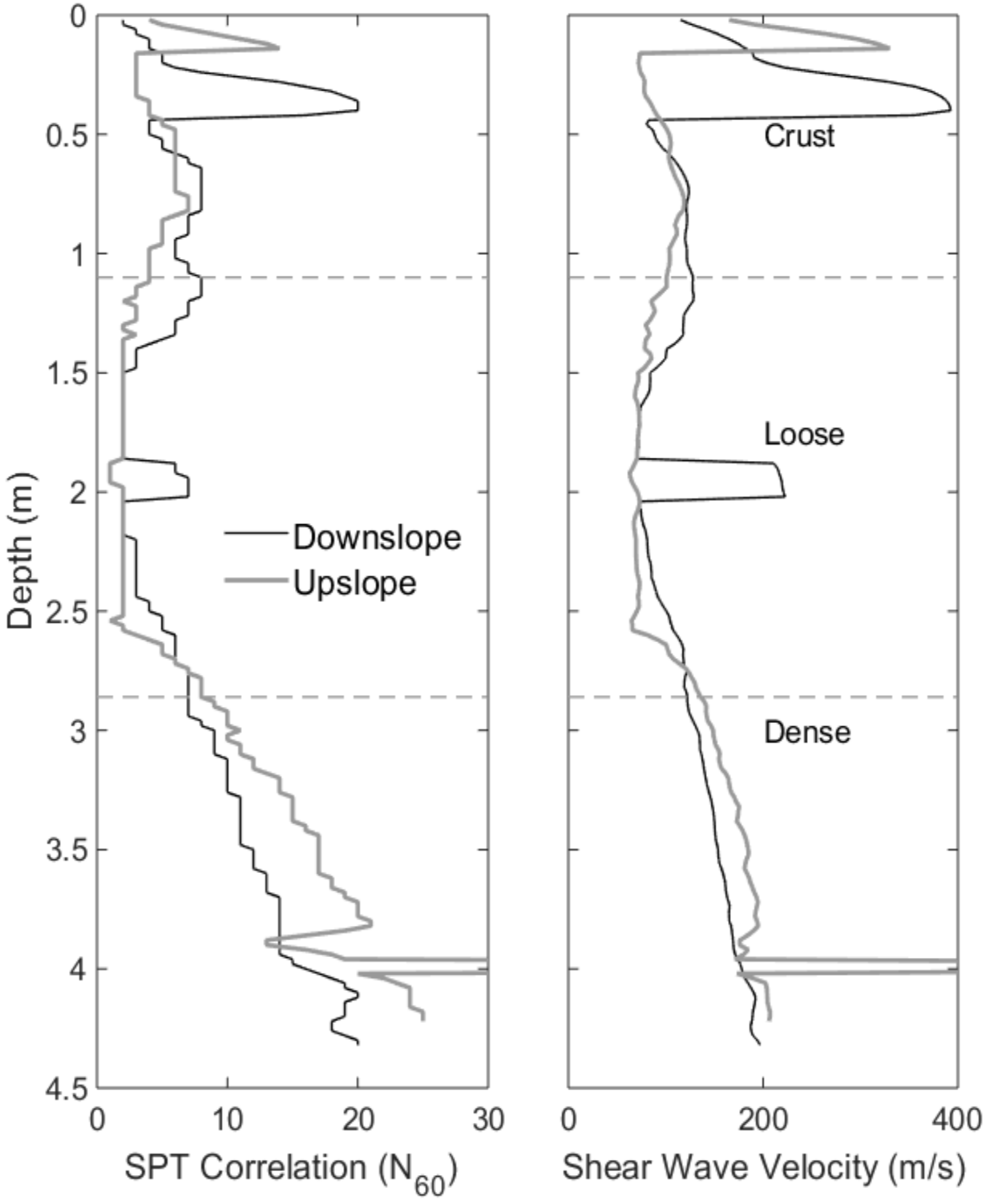

Figure 11-8. Calculated SPT and shear wave velocity profiles from CPT

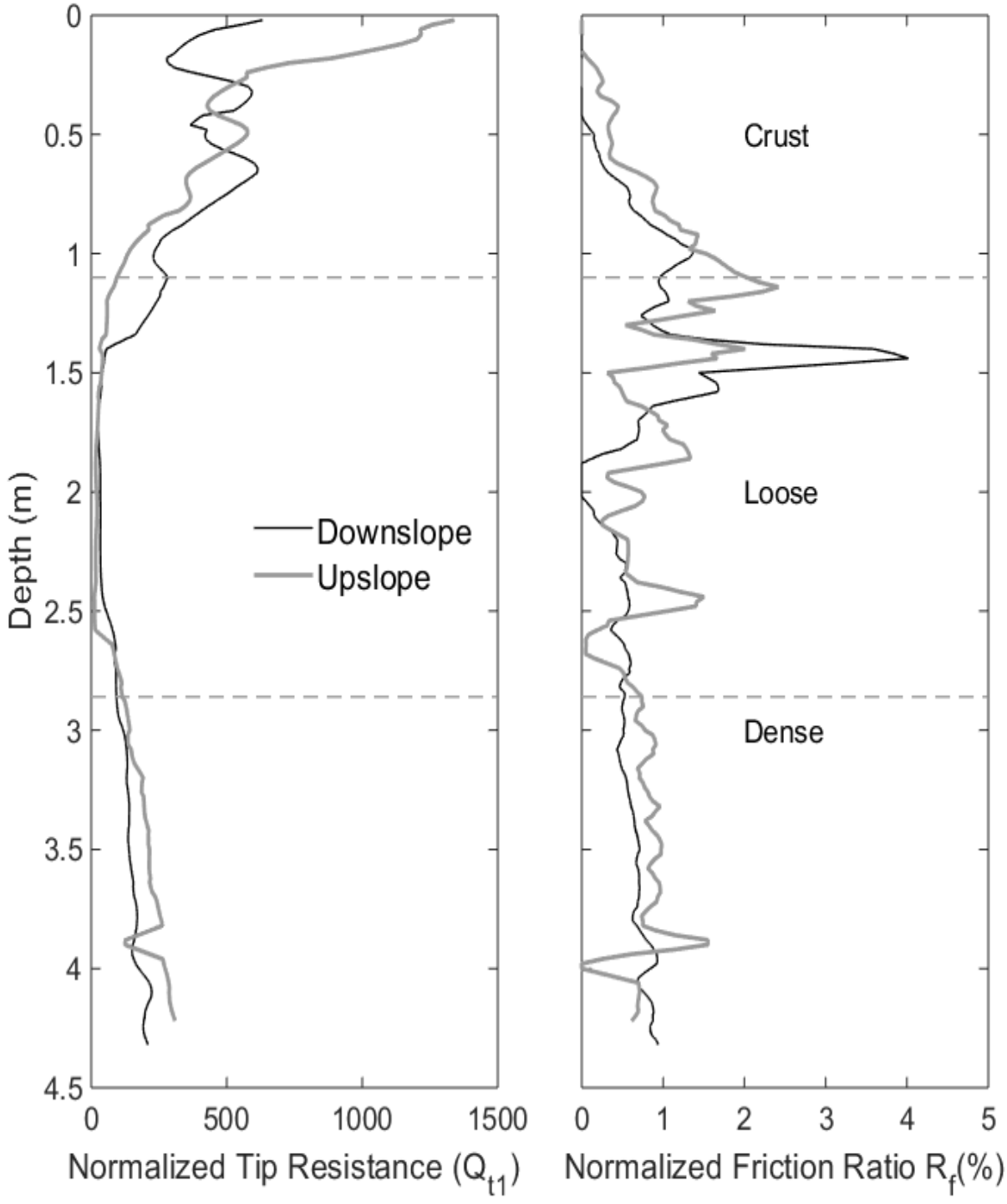

Figure 11-9. Normalized CPT results

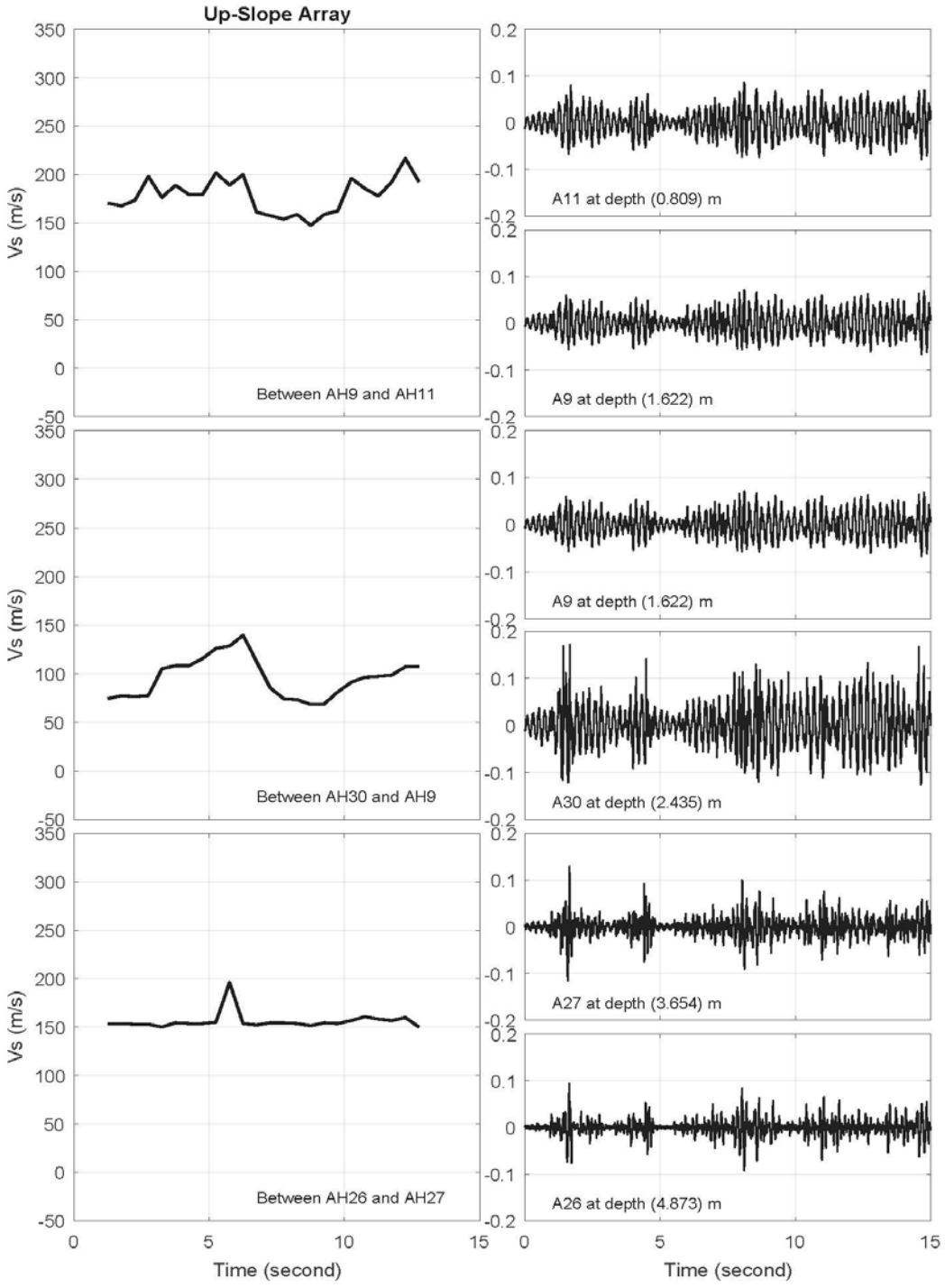

Figure 11-10. Initial shear wave velocity characterization

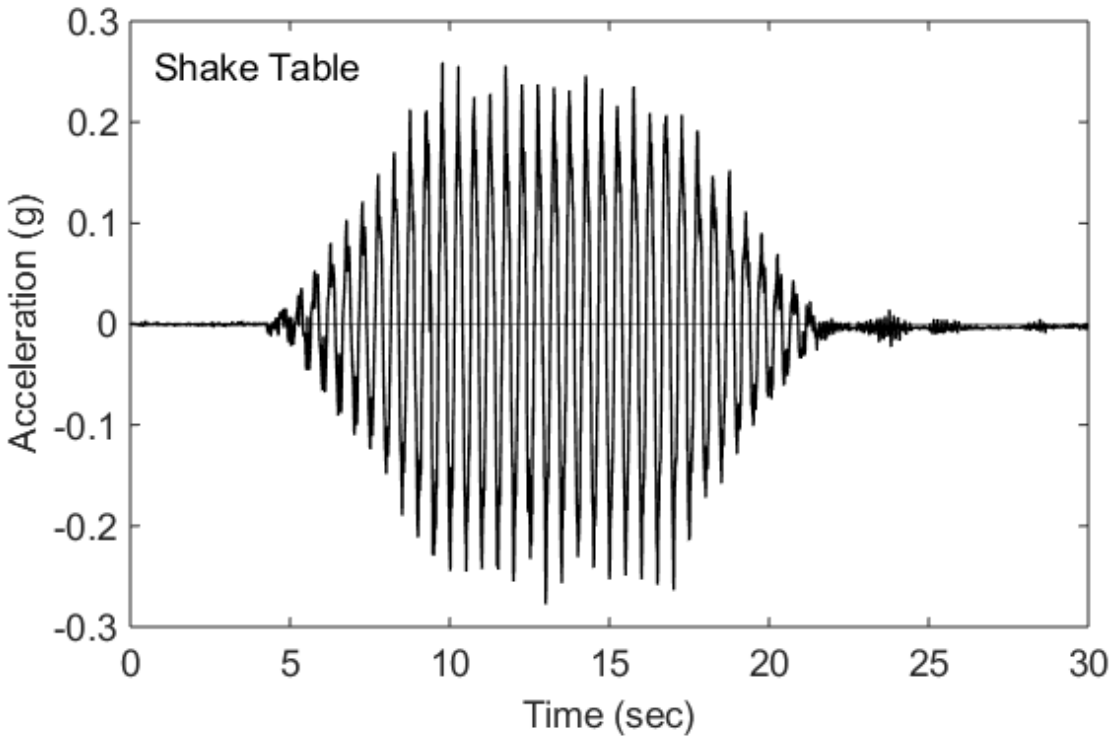

Figure 11-11. Input acceleration

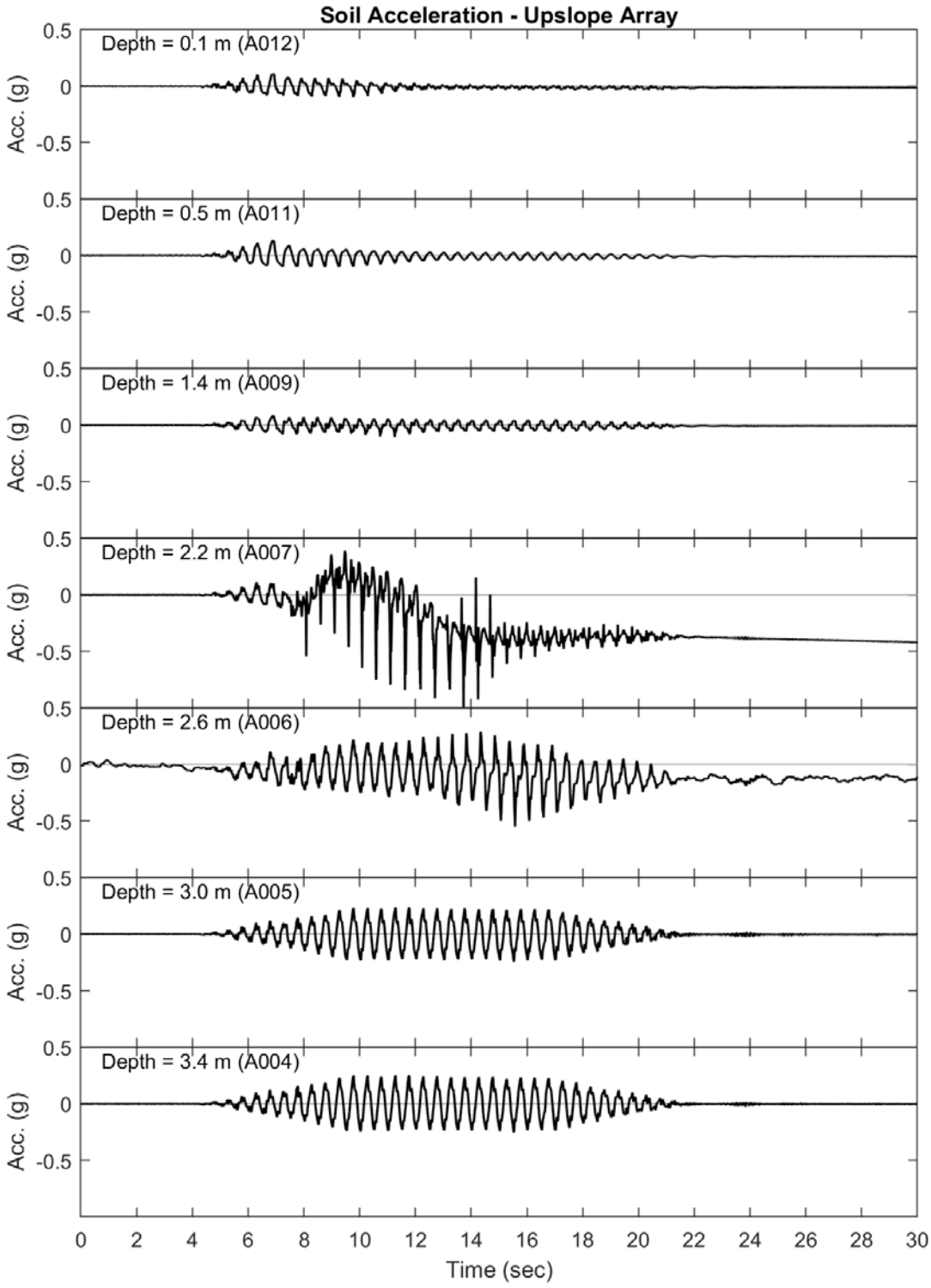

Figure 11-12. Upslope acceleration array attenuation

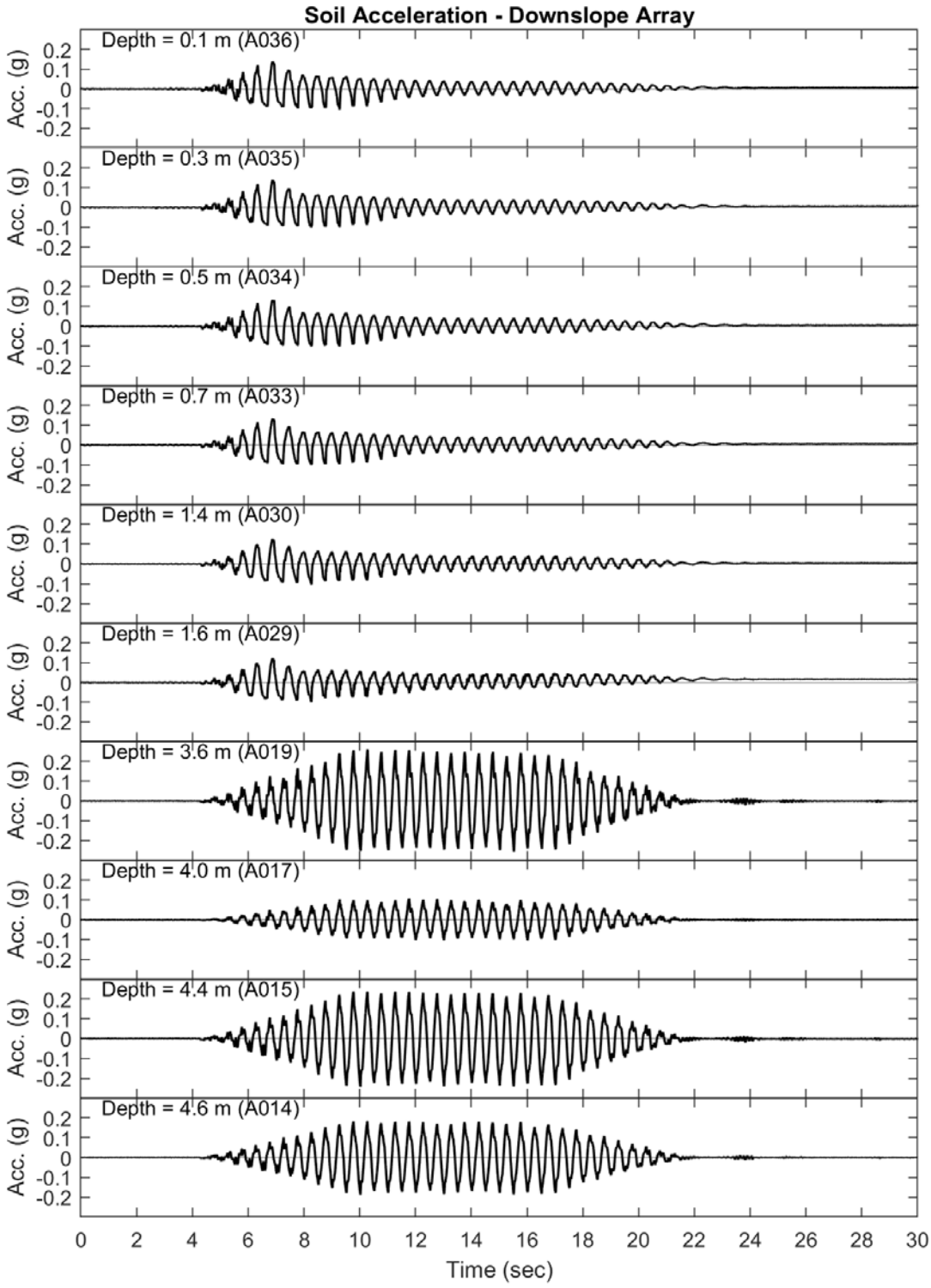

Figure 11-13. Downslope acceleration array attenuation

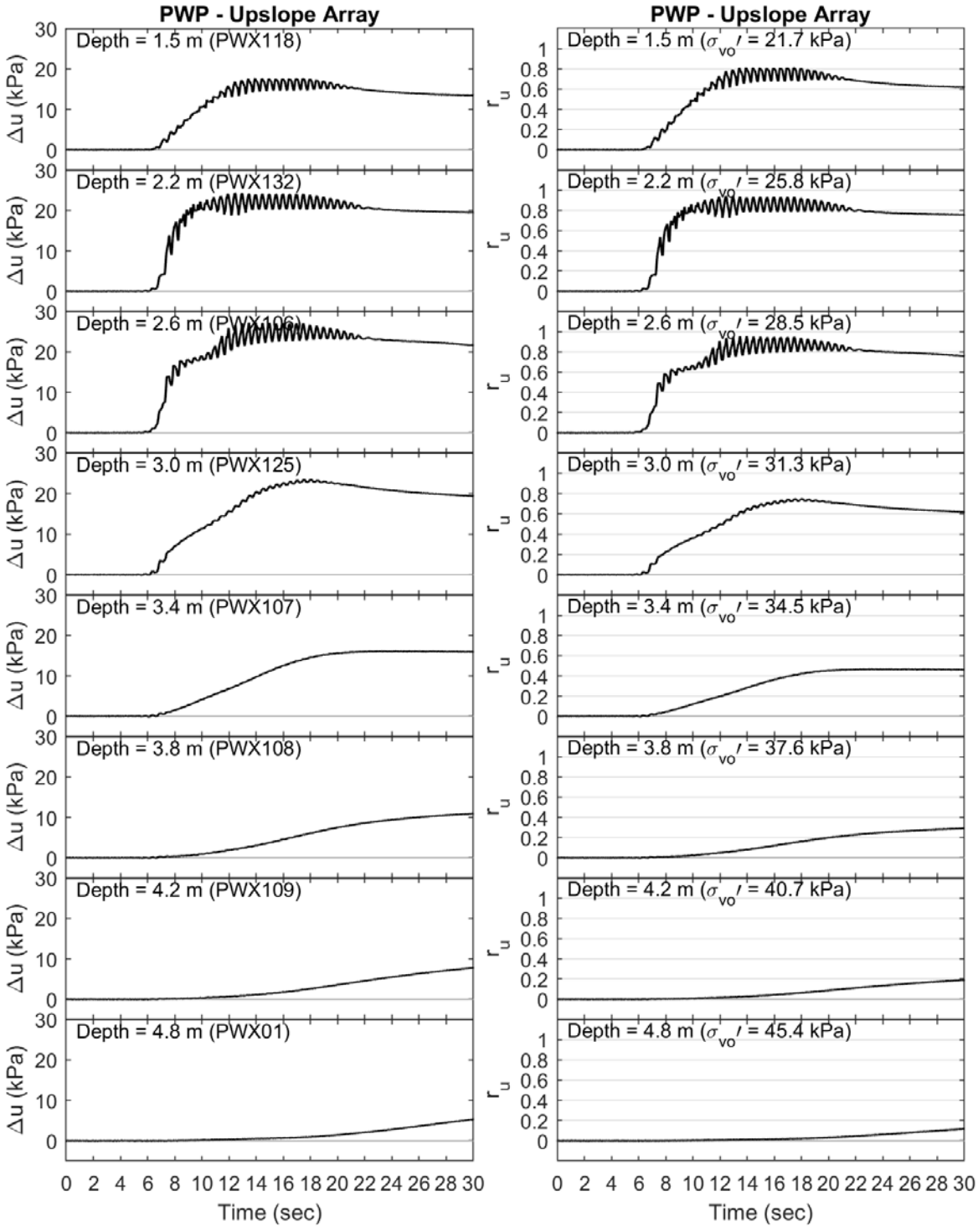

Figure 11-14. Excess pore pressure histories in the upslope array

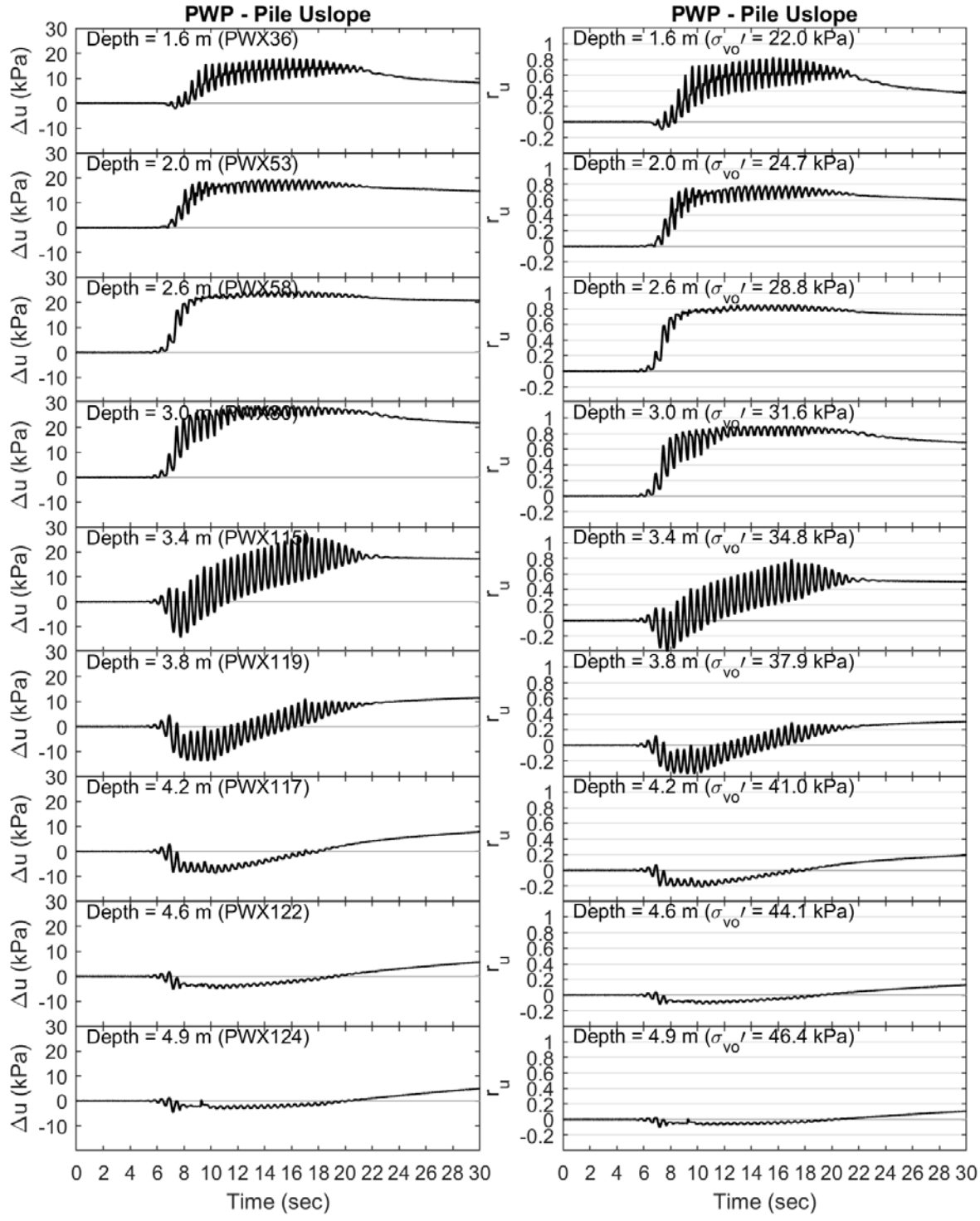

Figure 11-15. Excess pore pressure histories in the Pile vicinity upslope

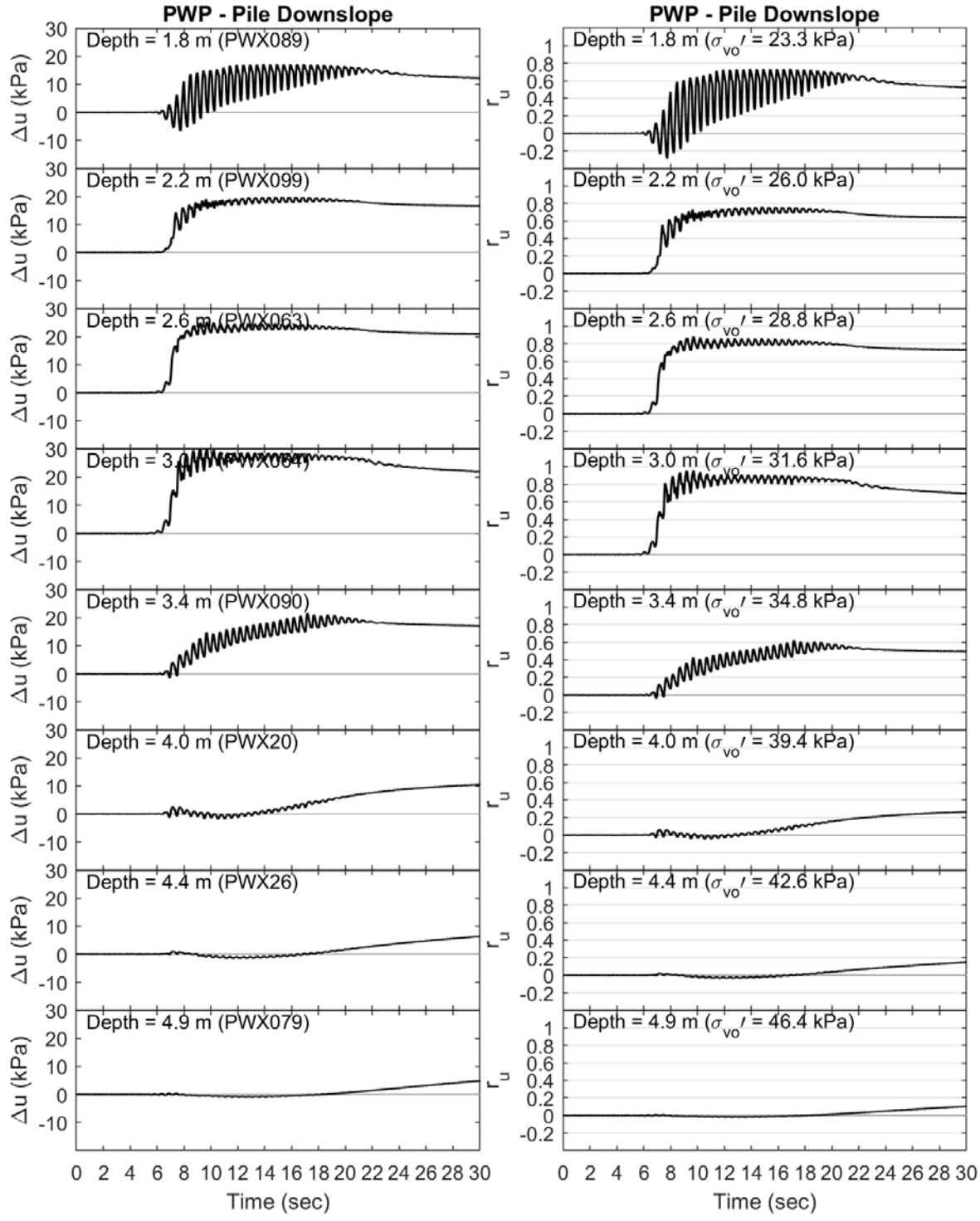

Figure 11-16. Excess pore pressure histories in the Pile vicinity downslope

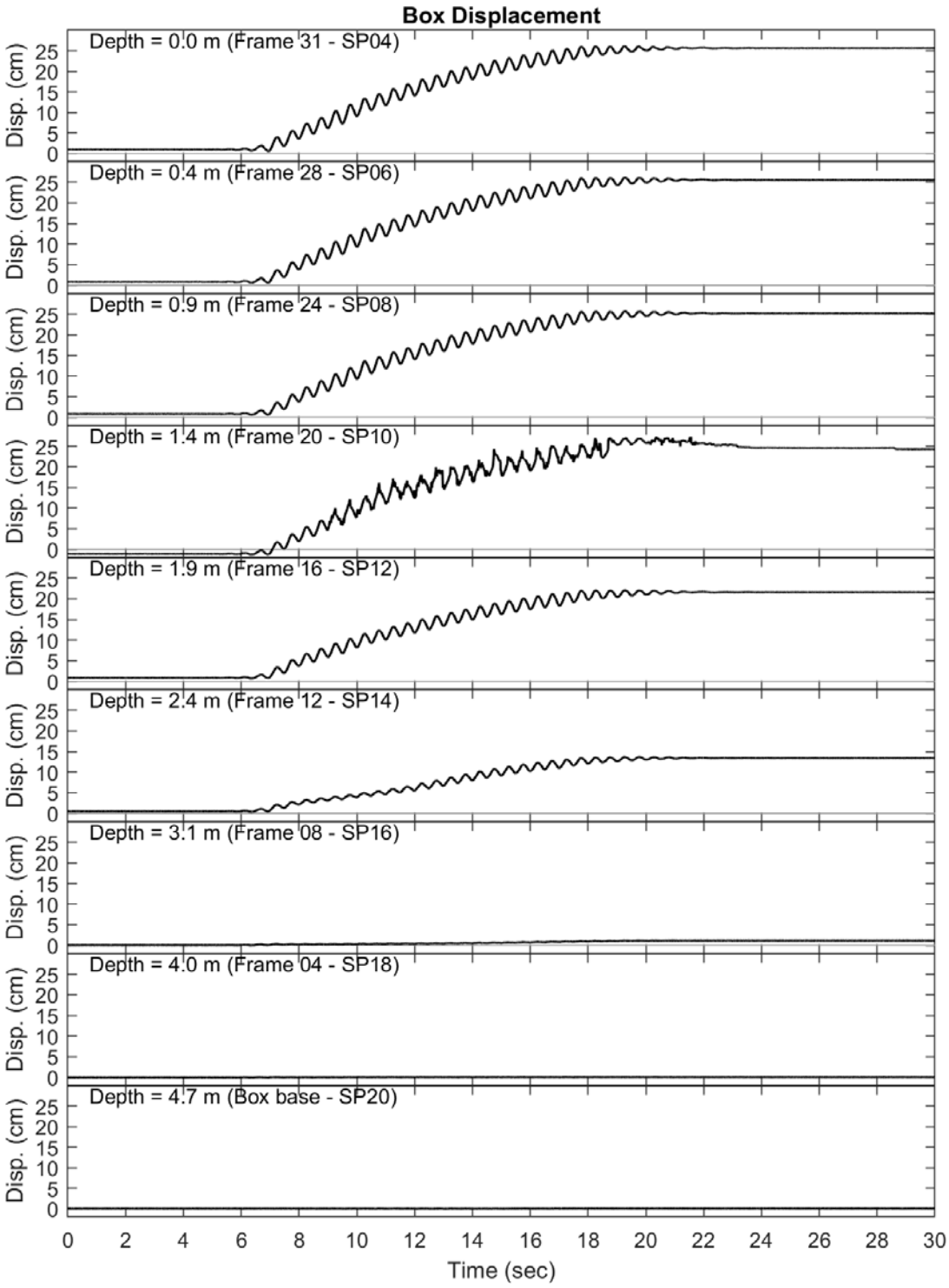

Figure 11-17. Box displacement time histories

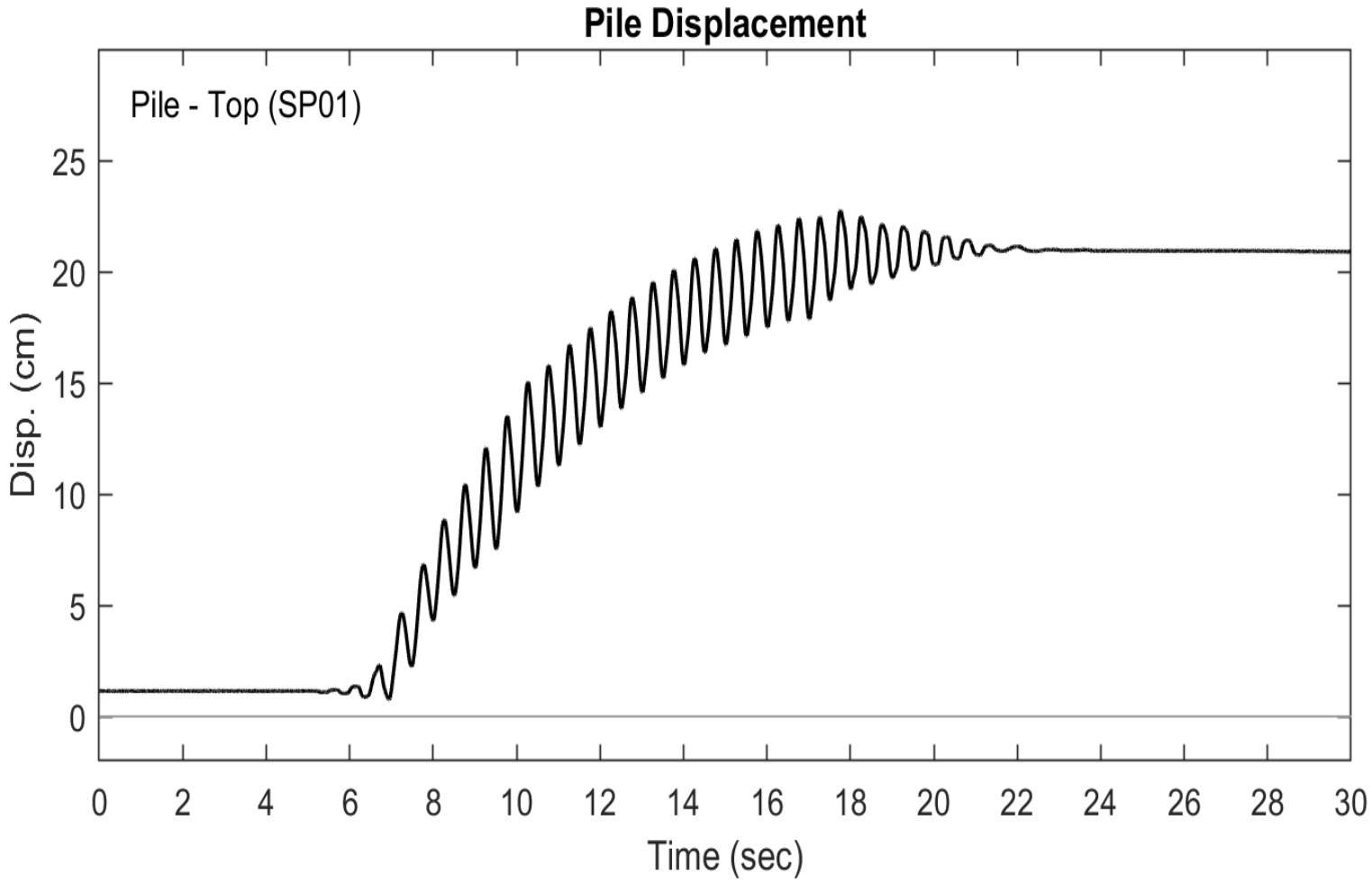

Figure 11-18. Pile head displacement time histories

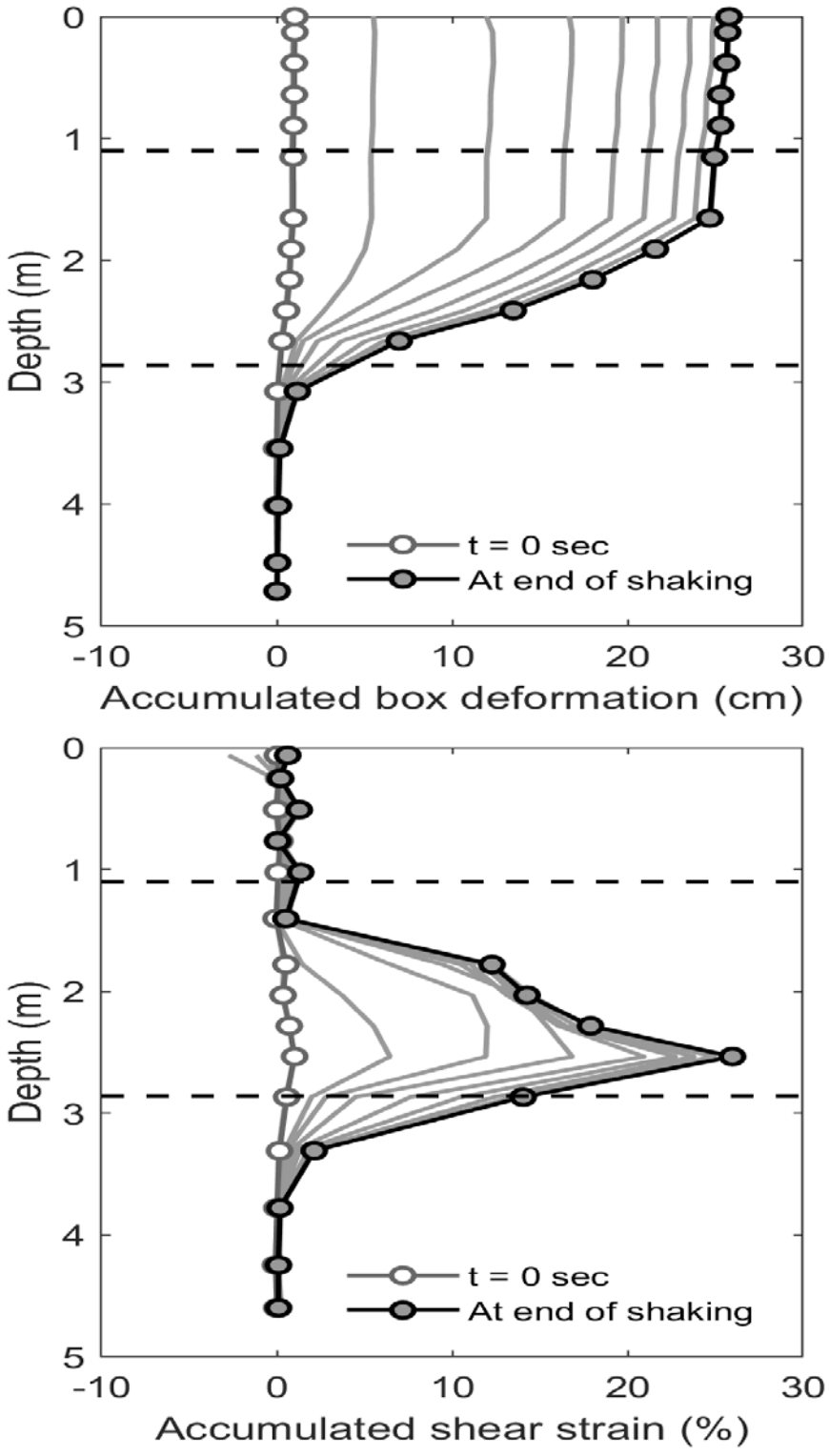

Figure 11-19. Box displacement and shear strain profiles (every 2 seconds of shaking)

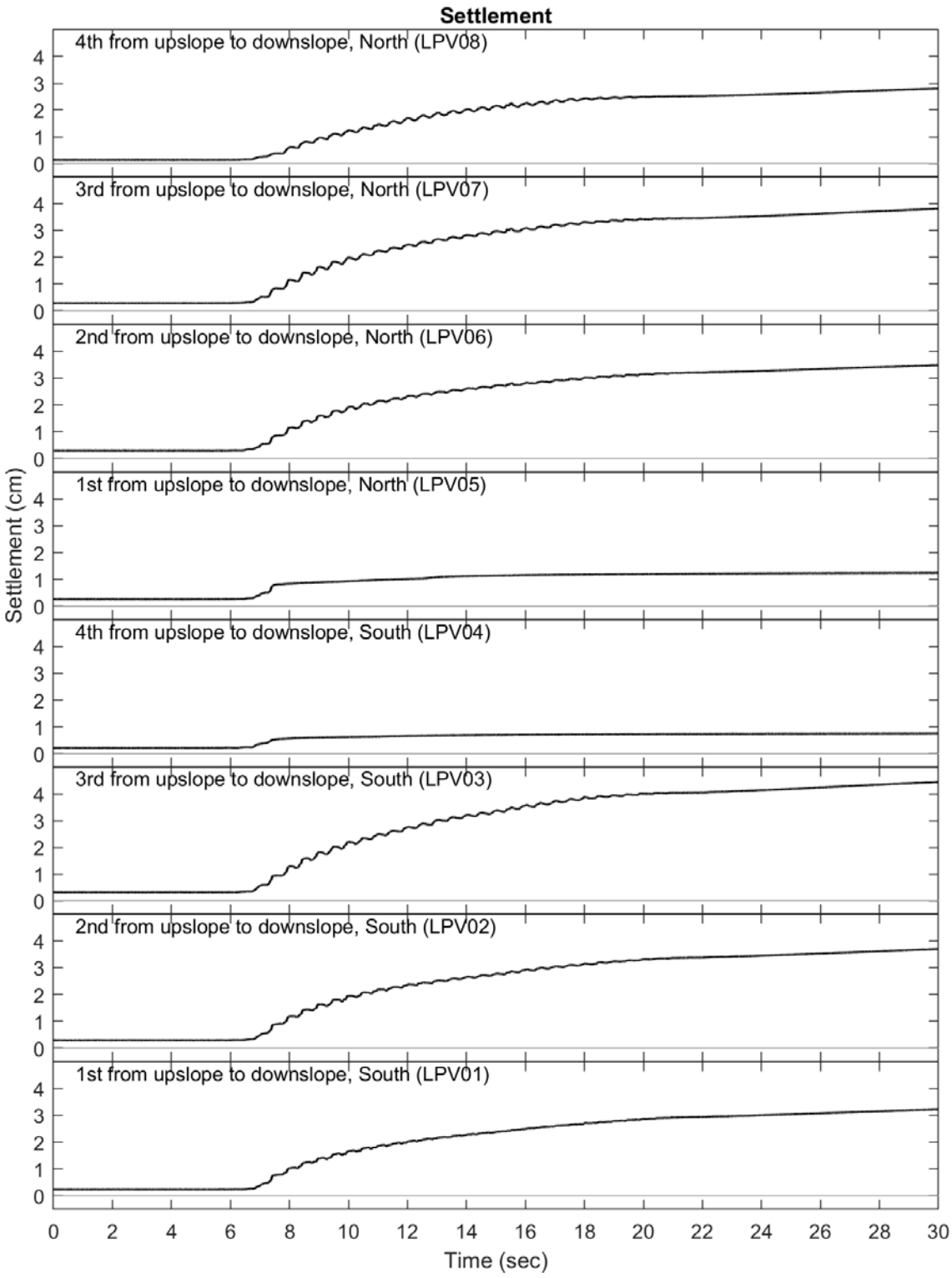

Figure 11-20. Surface settlement time histories

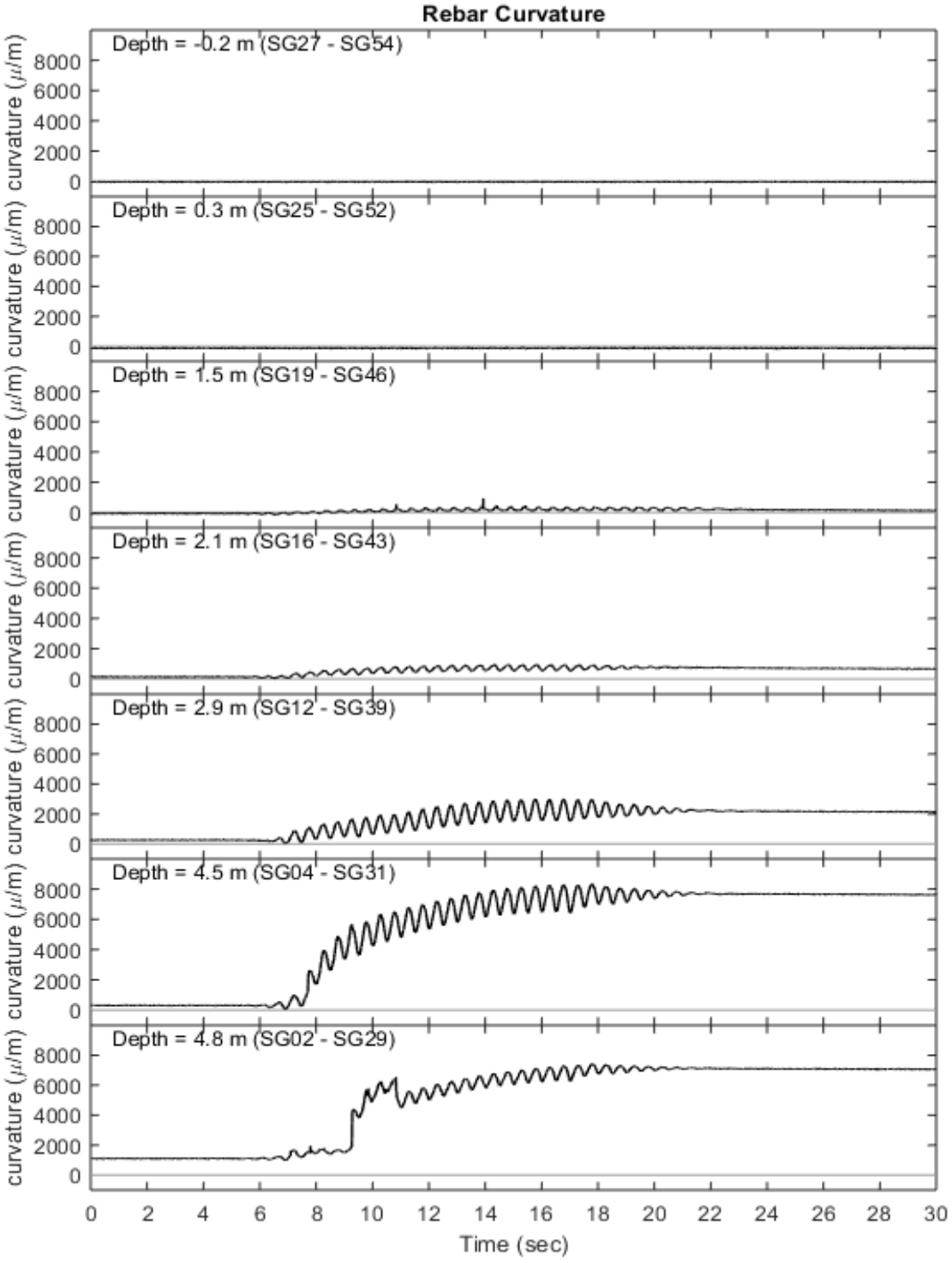

Figure 11-21. Pile curvature histories

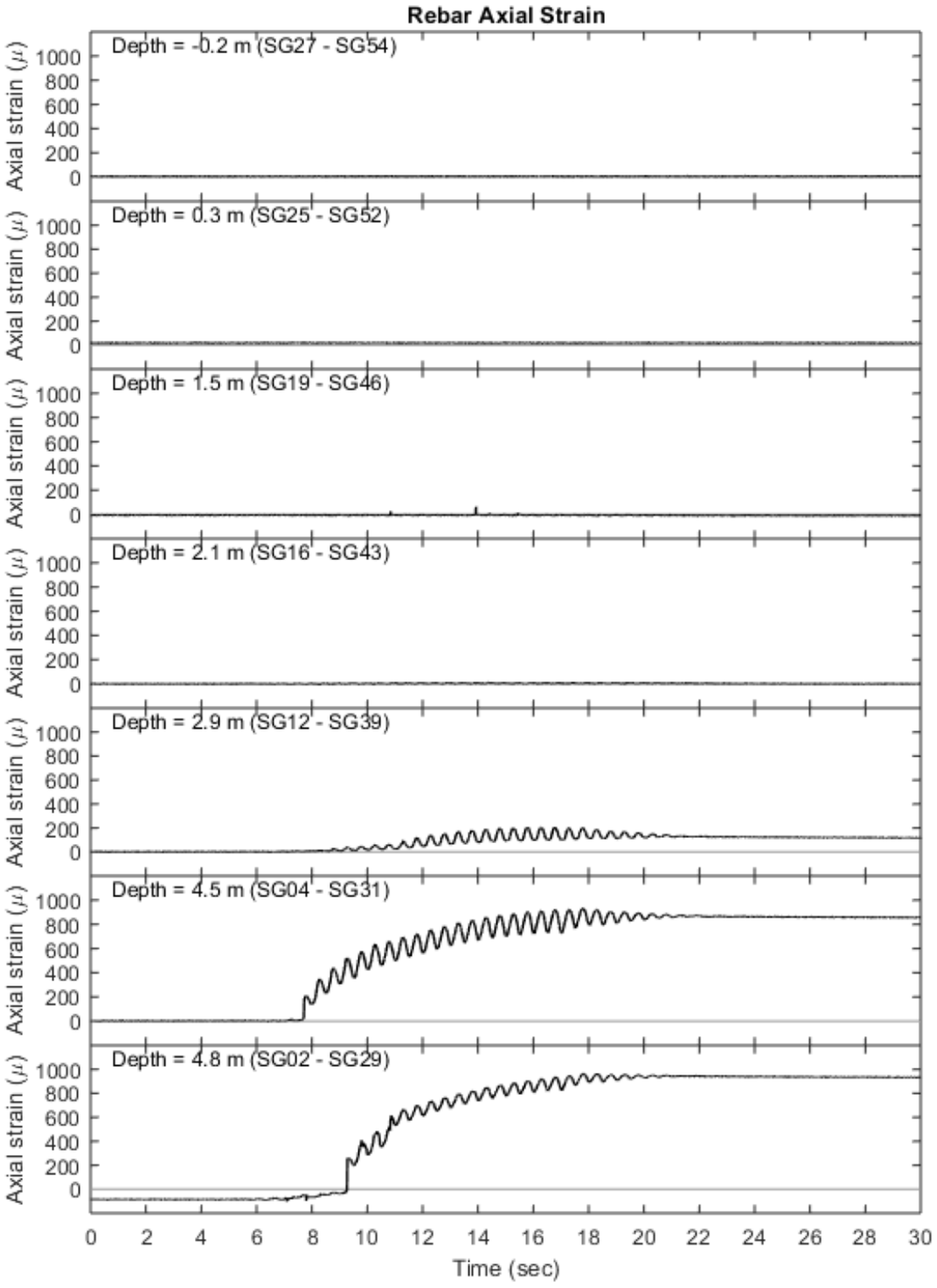

Figure 11-22. Pile axial strains histories

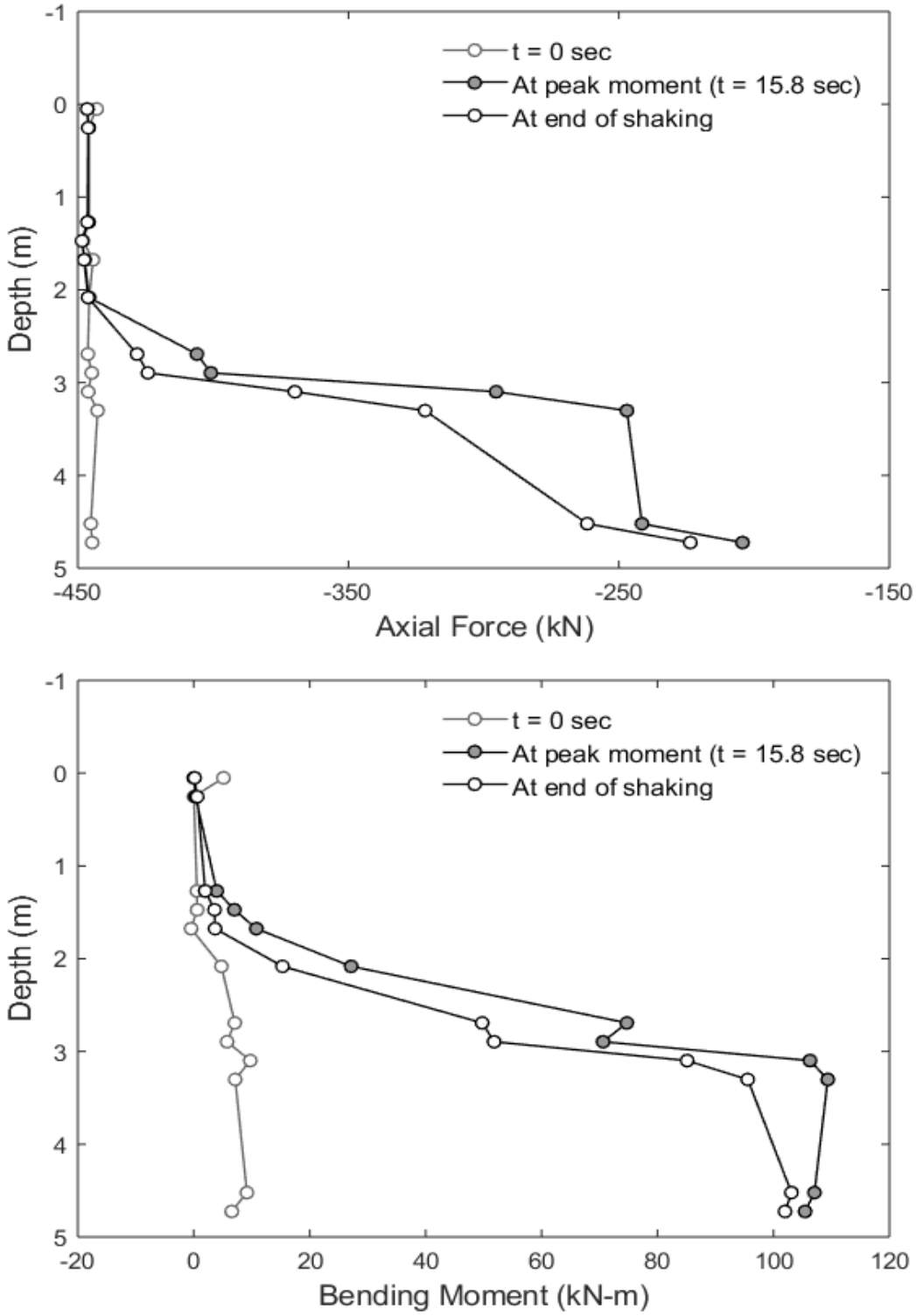

Figure 11-23. Pile axial and bending moment profiles

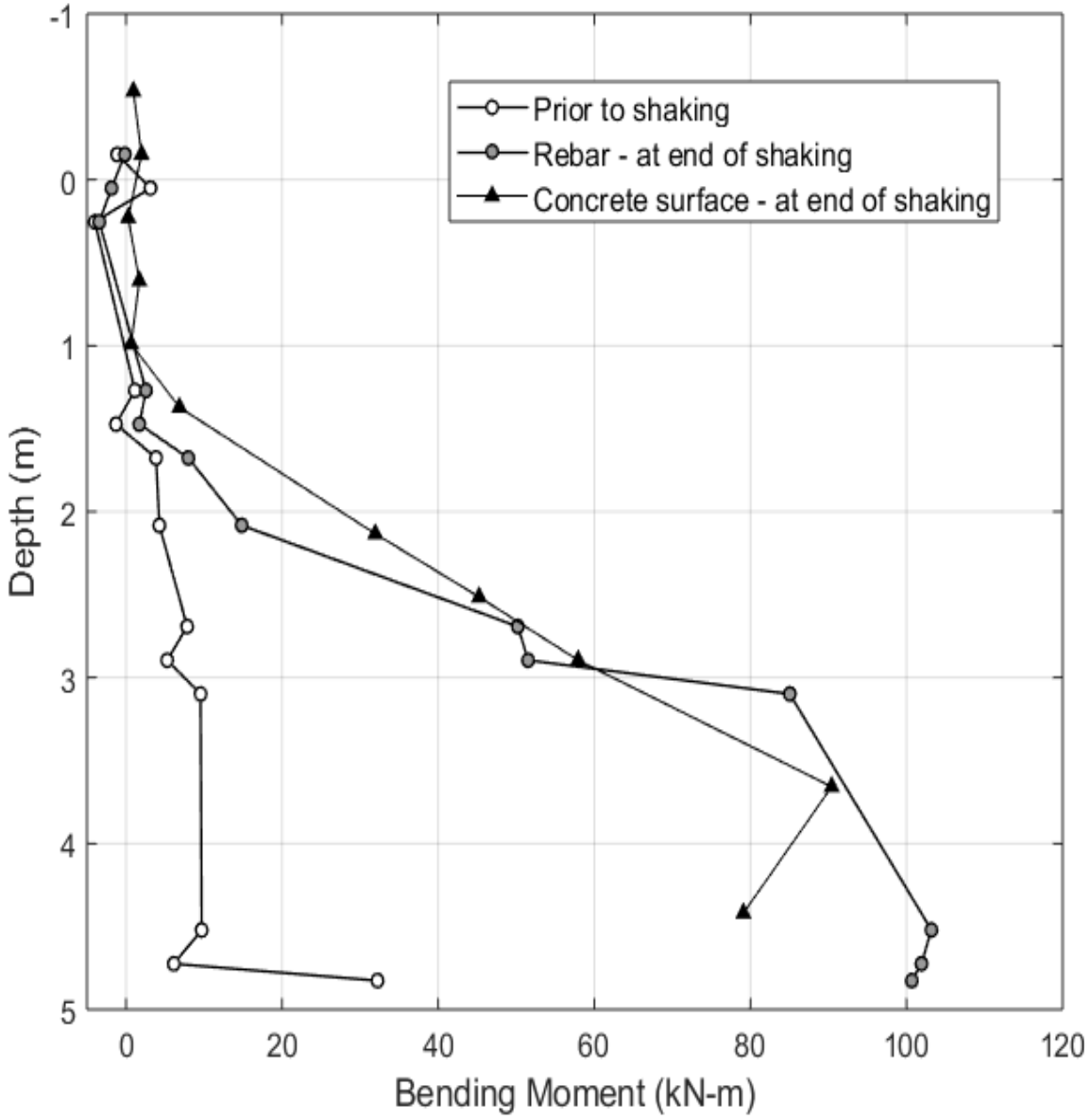

Figure 11-24. Bending moment profile from rebar and concrete gauges

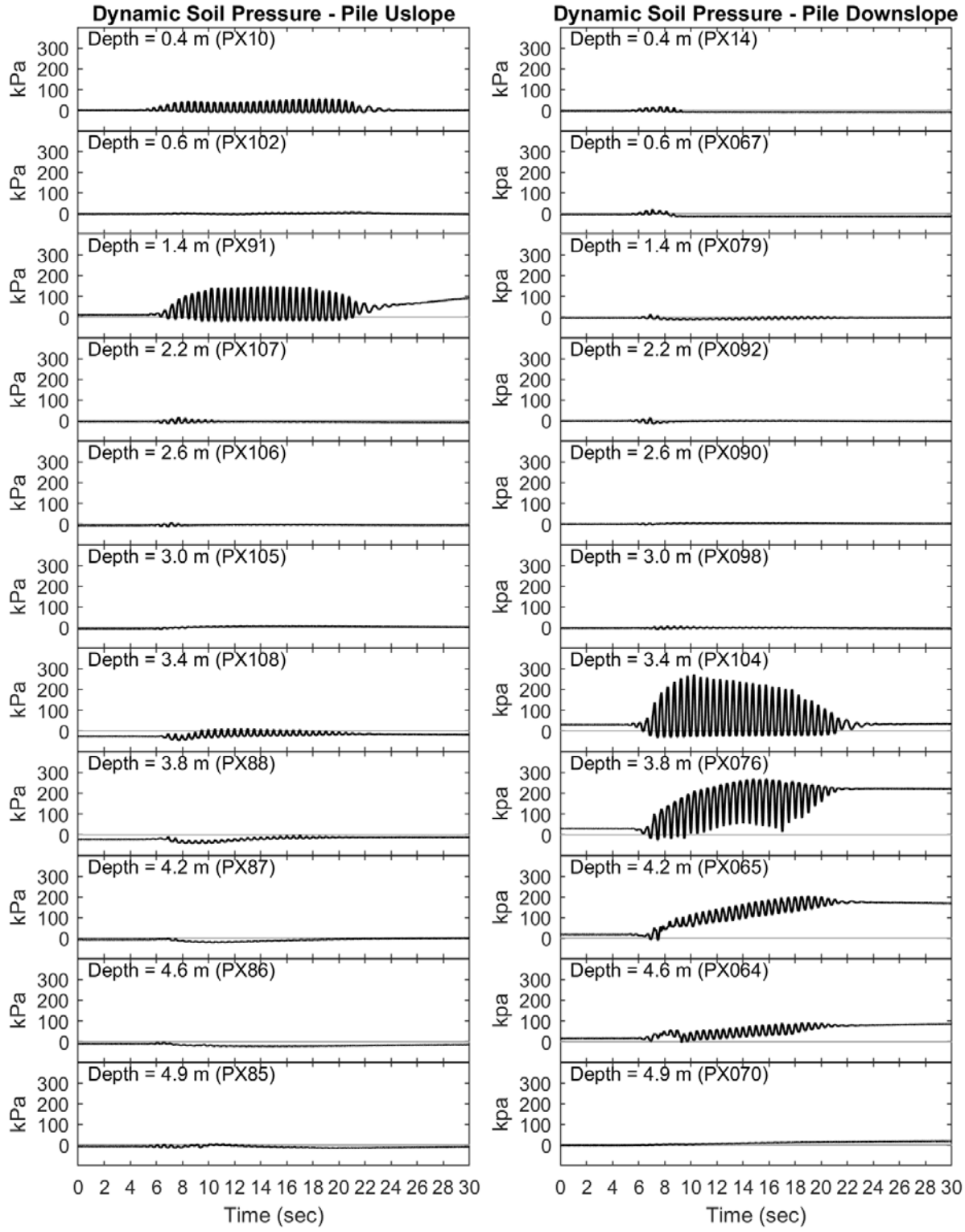

Figure 11-25. Total soil pressure histories

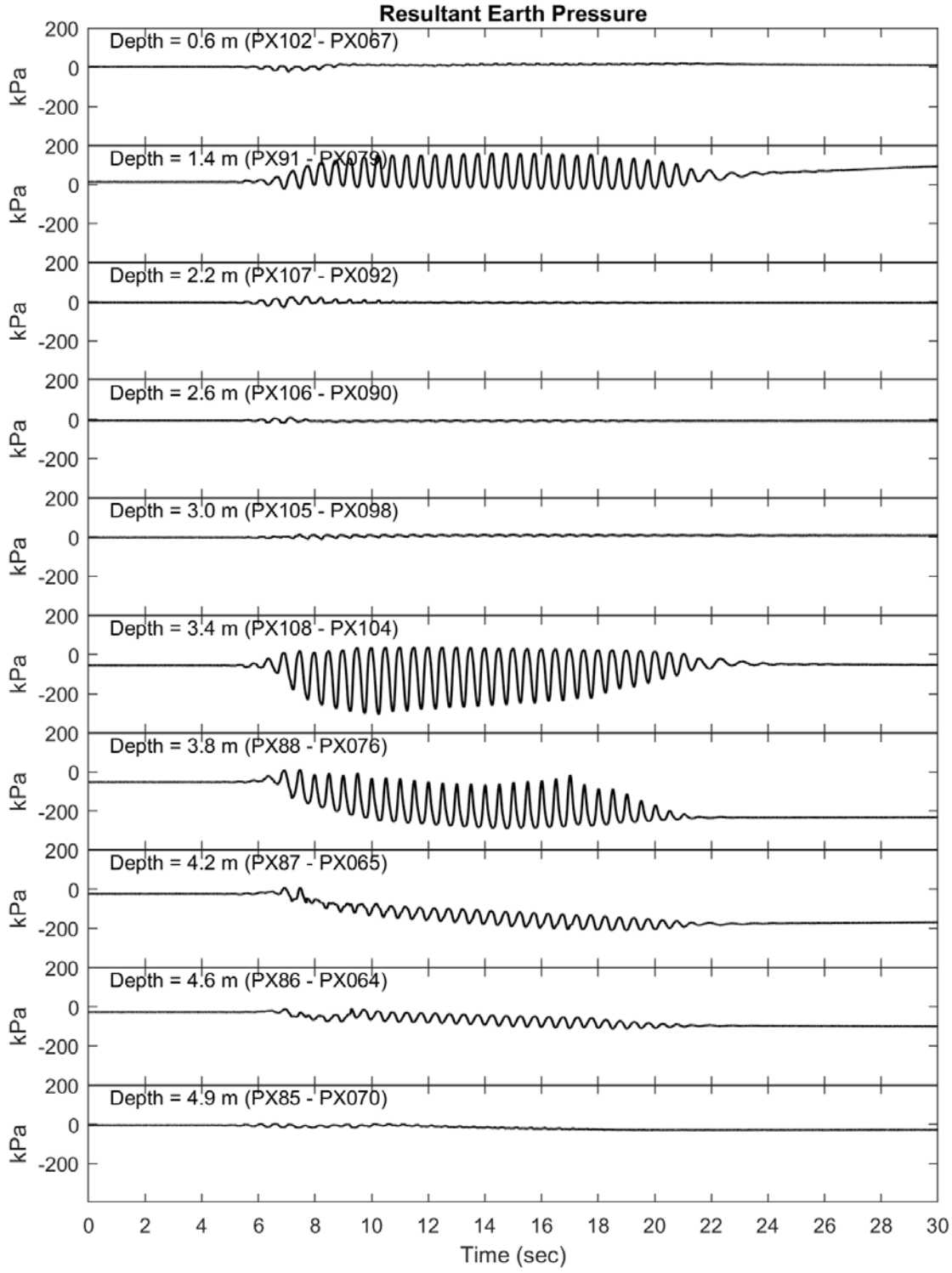

Figure 11-26. Resultant soil pressure histories

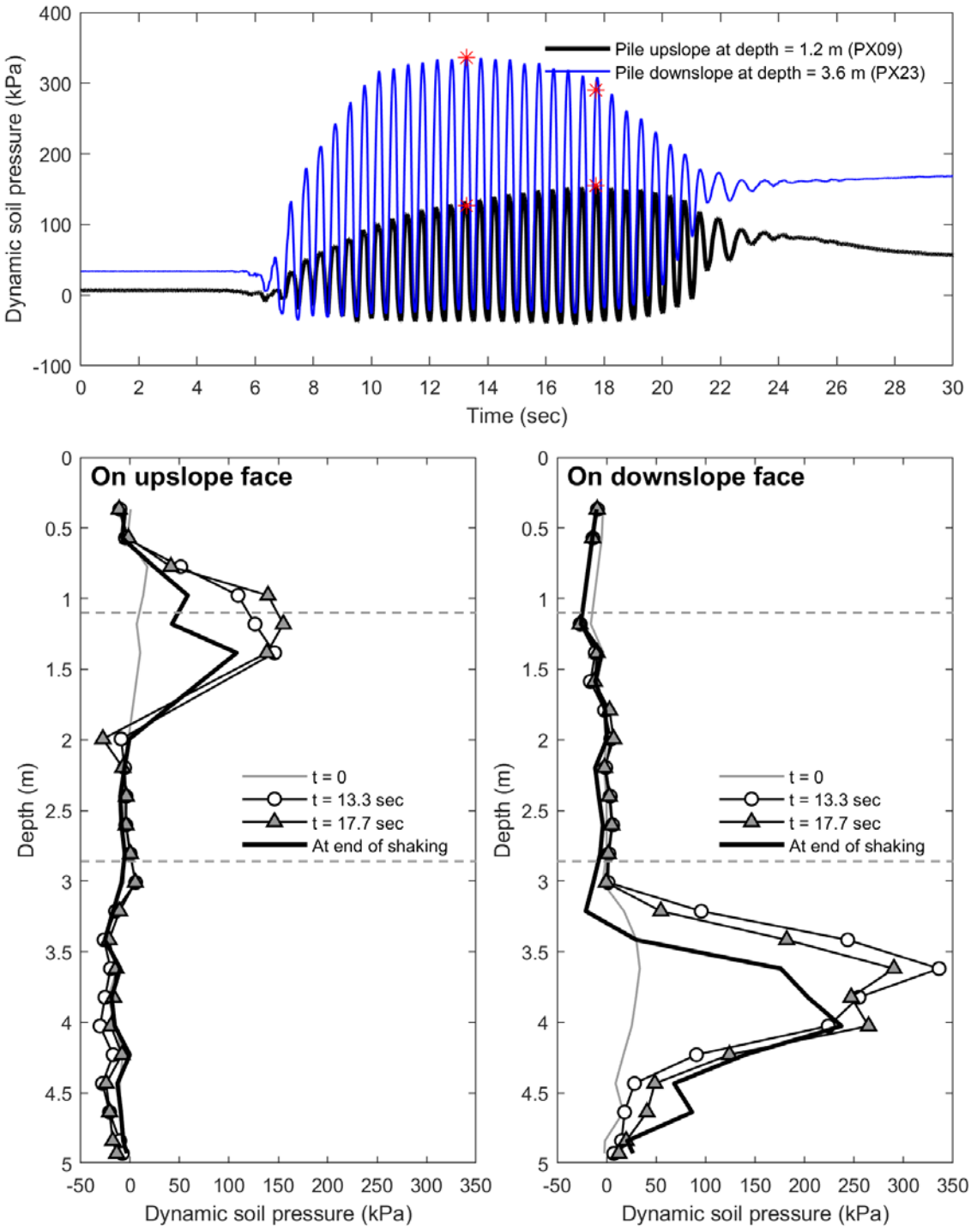

Figure 11-27. Total soil pressure profiles

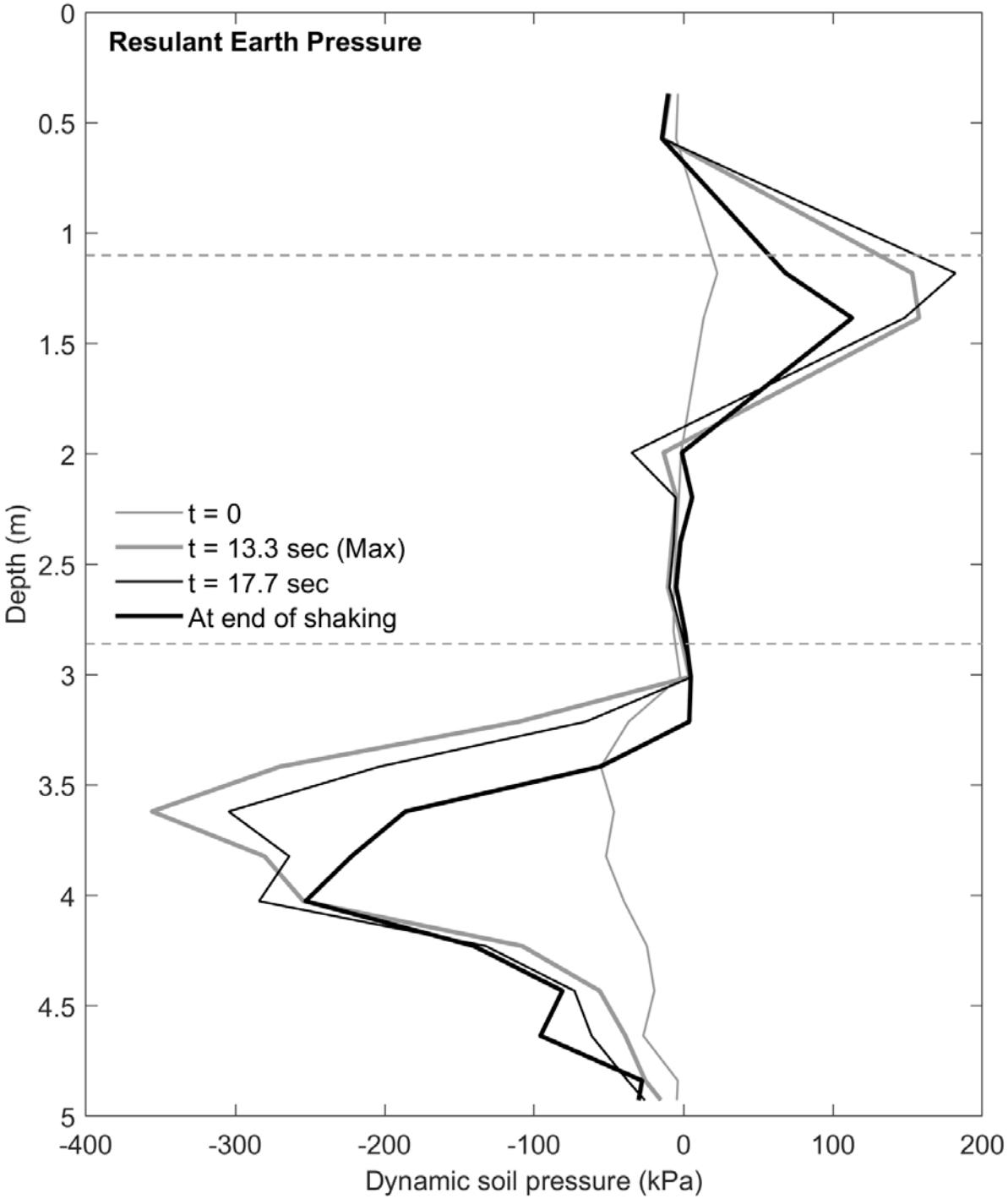

Figure 11-28. Resultant soil pressure profile acting on the pile

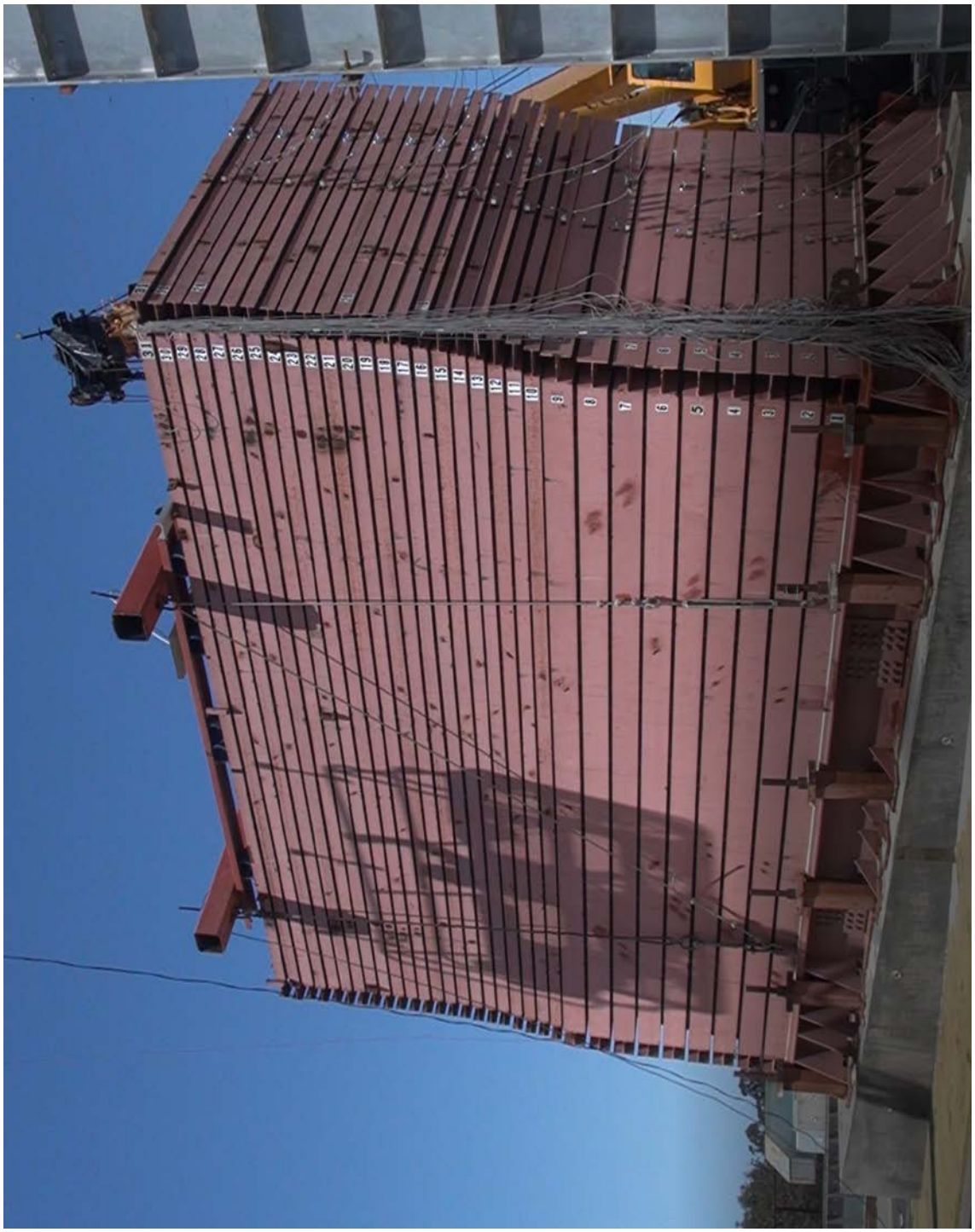

Figure 11-29. Picture of deformed laminar box after shaking

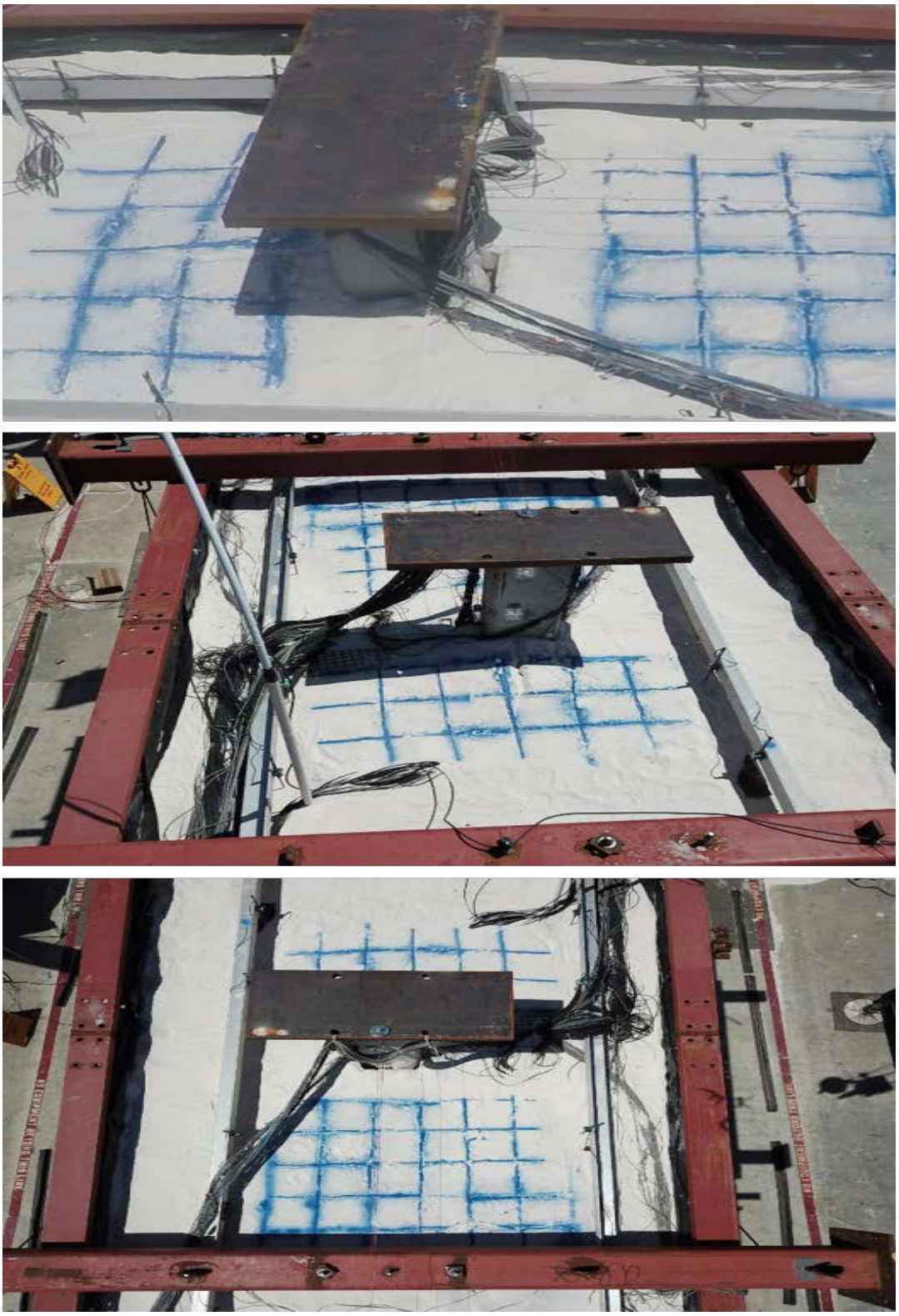

Figure 11-30. Soil surface view after shaking (showing upslope heave and downslope gap)

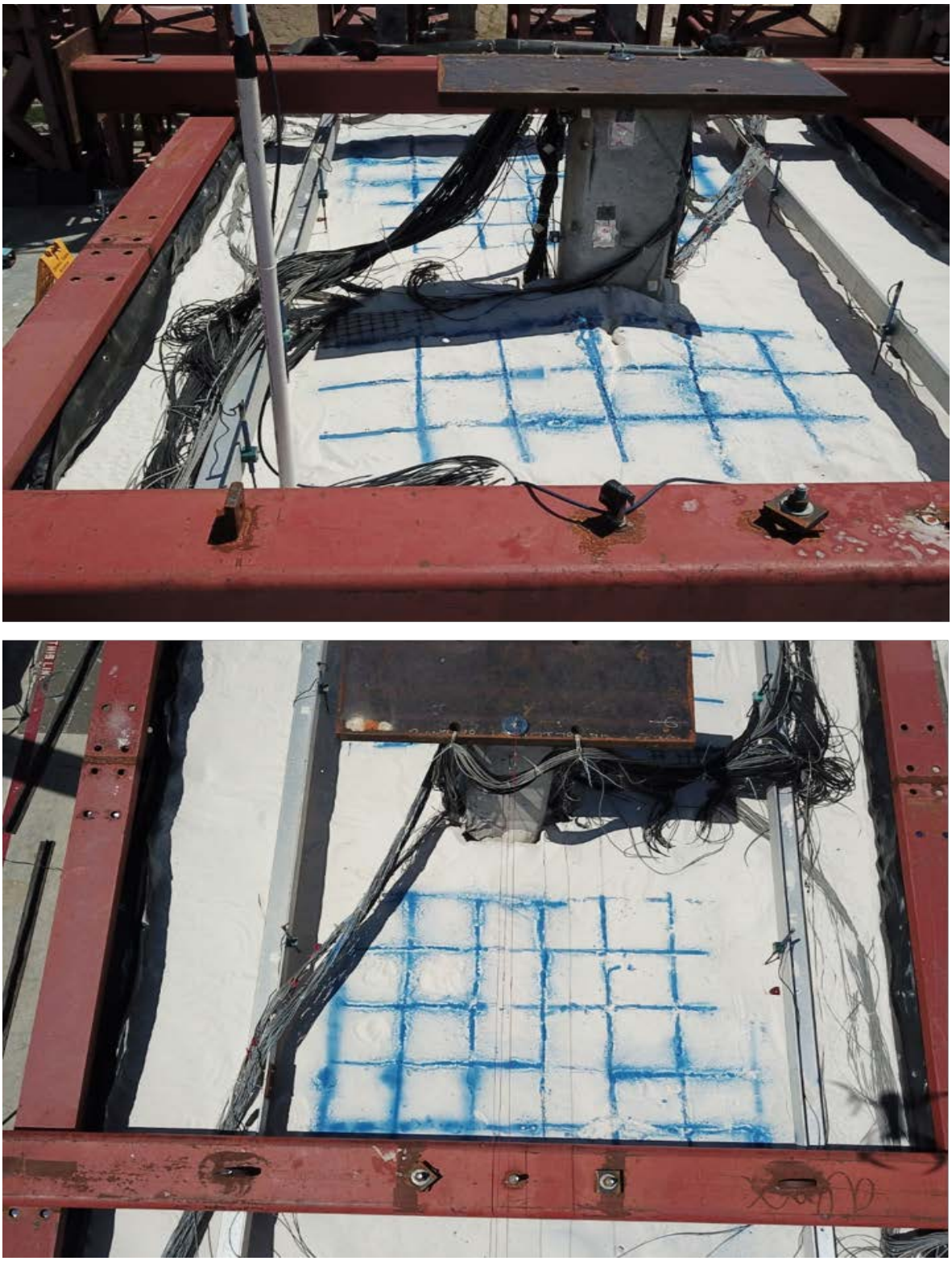

Figure 11-31. Zoomed in soil surface view after shaking (showing upslope heave and downslope gap)

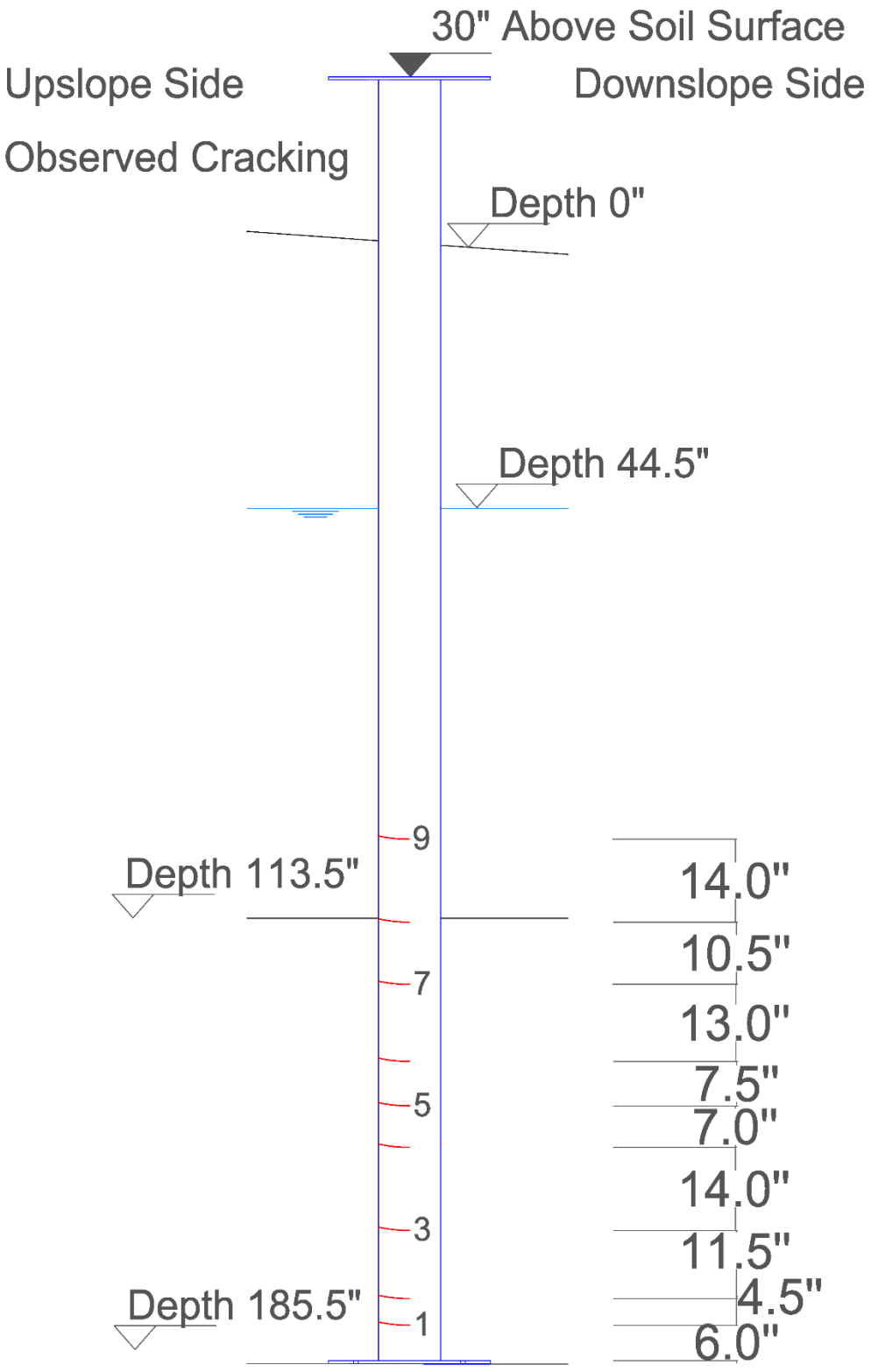

Figure 11-32. Observed cracking layout on the pile after excavation

Figure 11-33. Picture of pile cracking

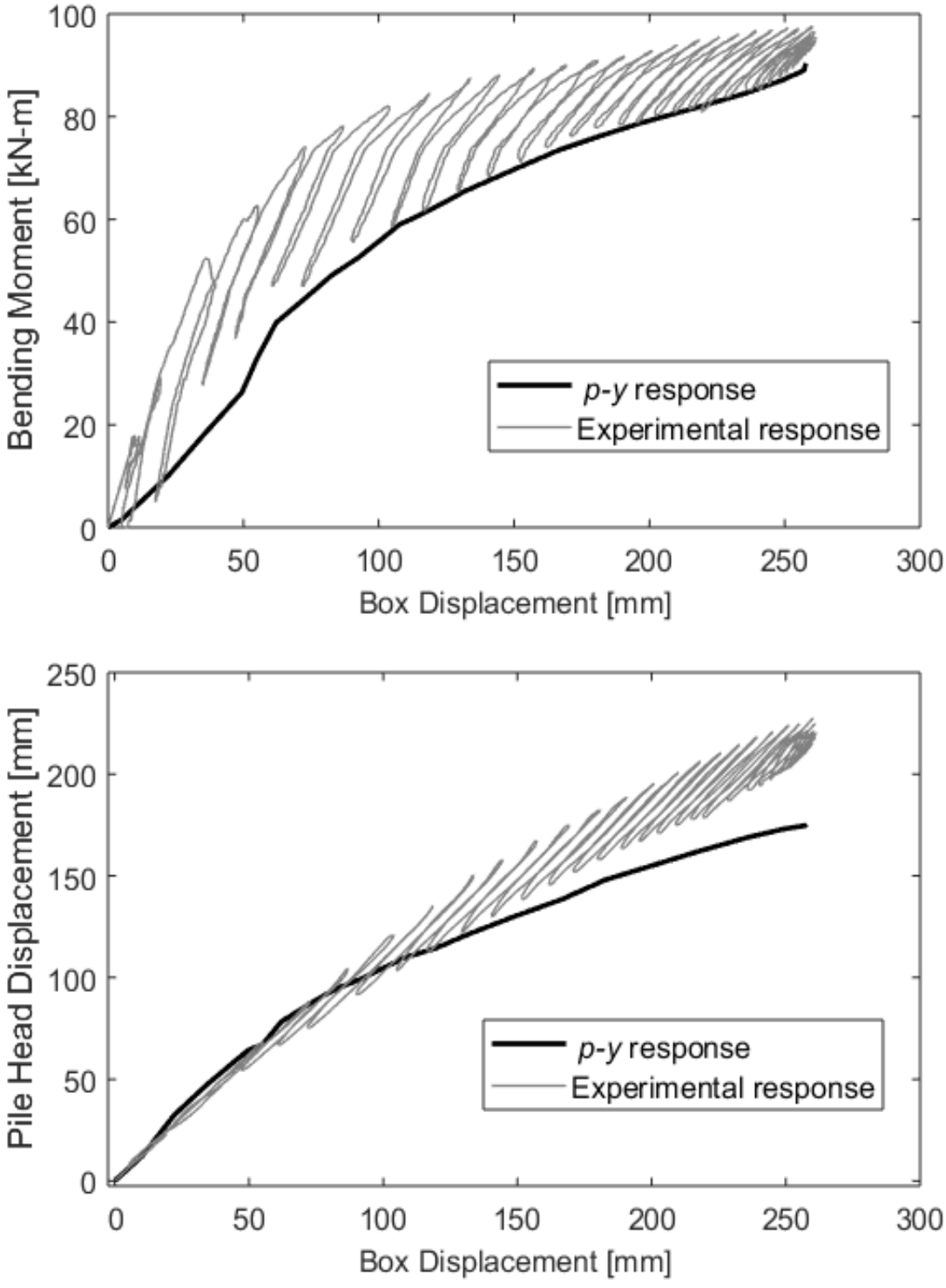

Figure 11-34. Comparison of experimental and *p-y* response (Bending moment plotted at maximum location, 3.70 m depth)

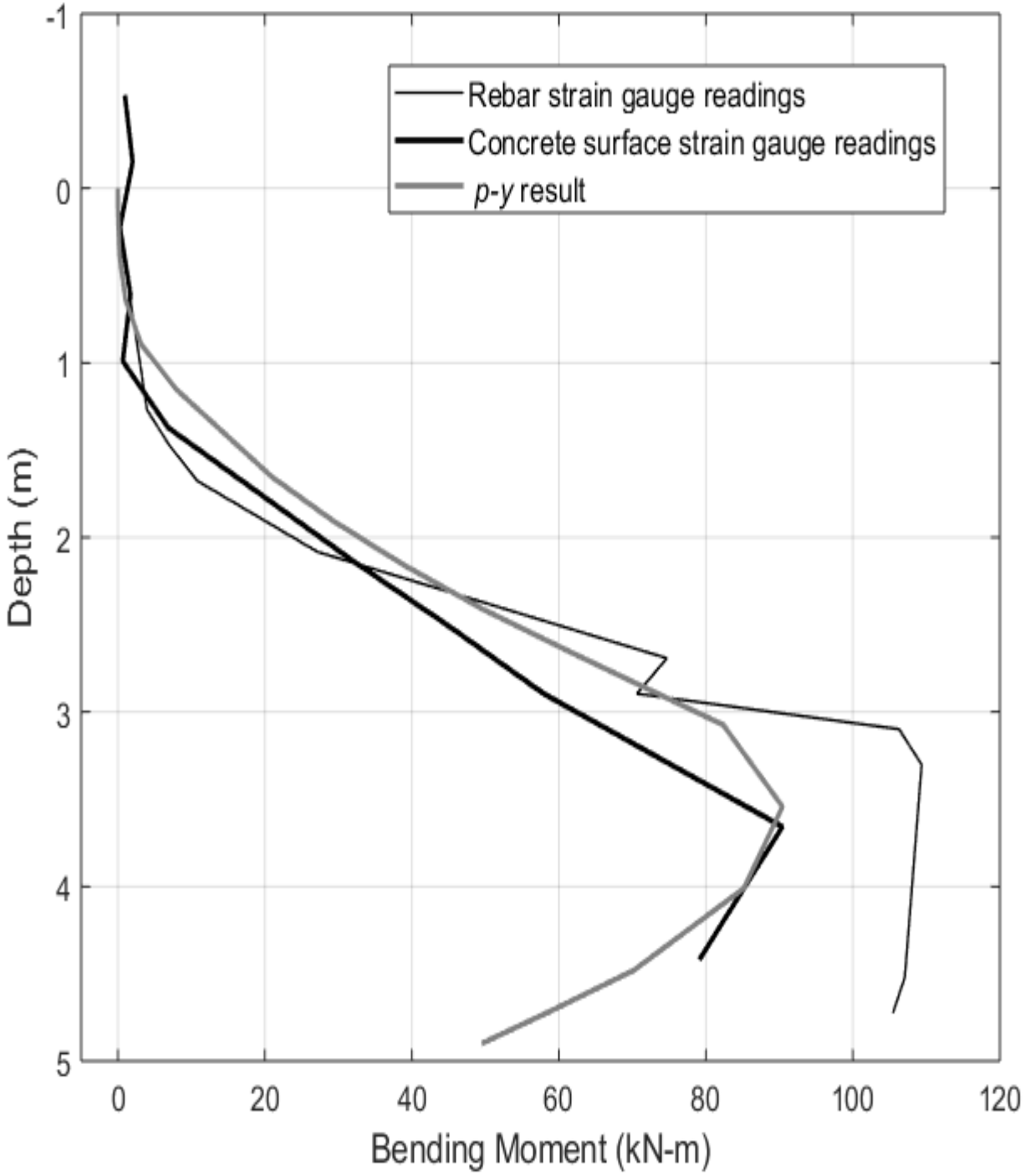

Figure 11-35. Profile comparison of experimental and *p-y* response

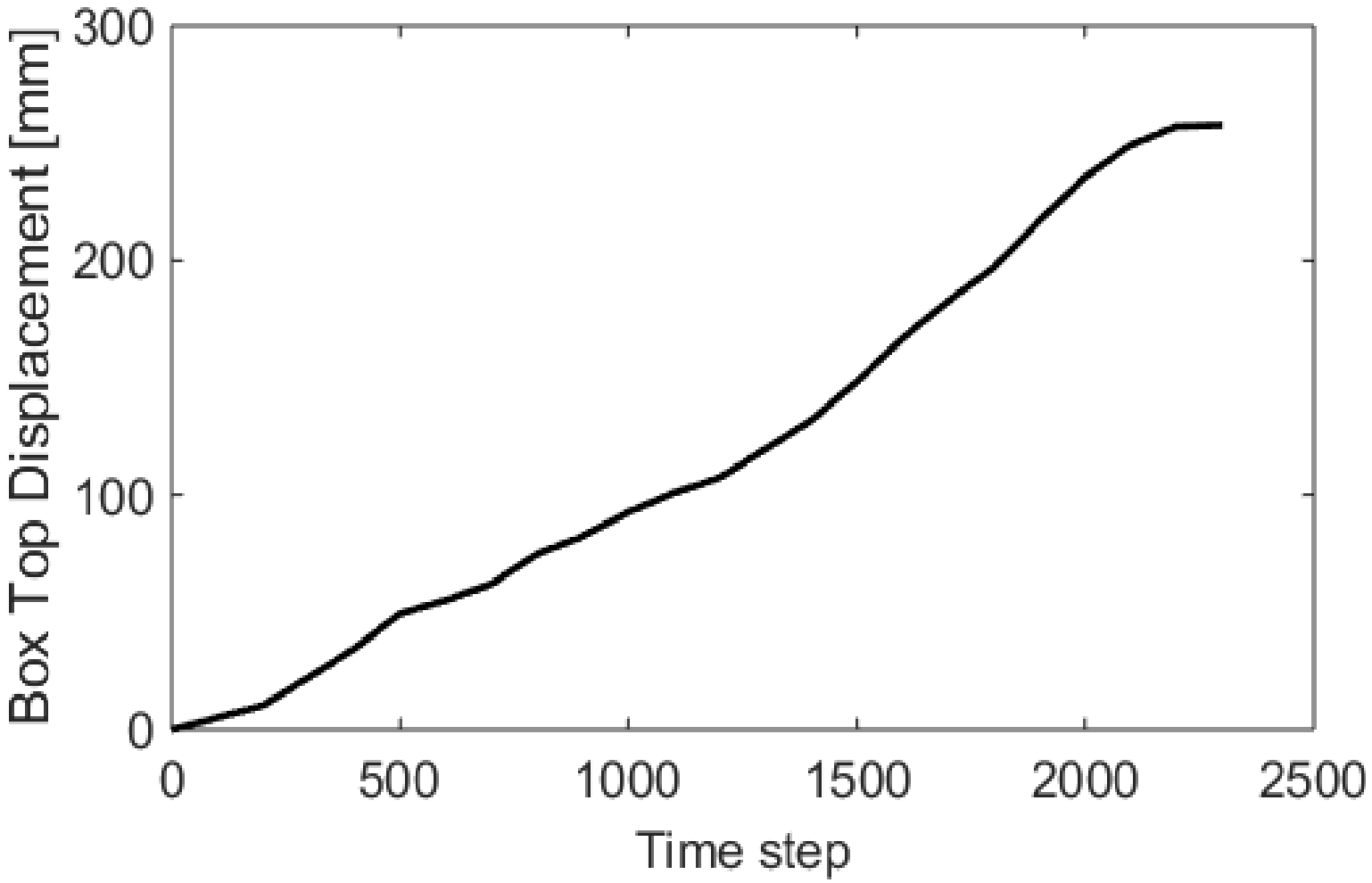

Figure 11-36. Box displacement time history applied in the *p-y* lateral analysis

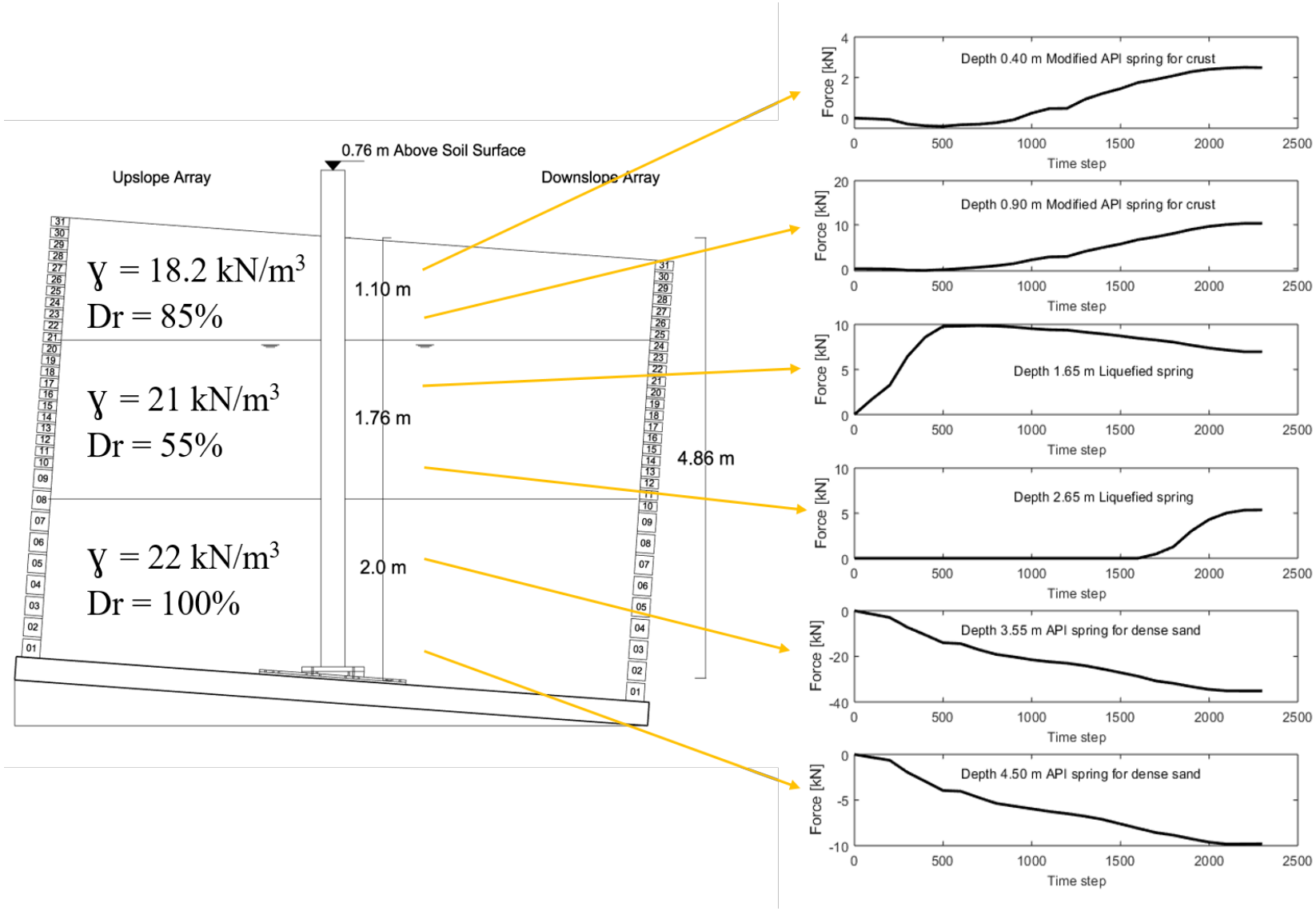

Figure 11-37. Resulting force time histories applied on the pile from the *p-y* lateral analysis

Chapter 12 Summary and Conclusions

12.1. Summary

Liquefaction of saturated cohesionless soil and the potentially induced lateral spreading are major causes of damage to embedded foundations and supported structures during earthquakes. Effects of liquefaction and lateral spreading on pile supported structures such as bridges, buildings and port facilities has been documented and studied via case histories over the past 50 years. A large number of cases describing damage and failure of pile foundations and/or their supported superstructure have been reported. As such, effects of liquefaction induced-lateral spreading have been studied by simplified procedures, advanced numerical models, a large number of centrifuge tests, a few large scale 1-g shake table experiments, and a number of full-scale field blast induced tests. All these studies have increased our understanding and provided insights about the underlying response mechanism. Yet, the complex loading scenario presented by lateral spreading during earthquake excitation is still a subject of much research interest due to the combination of cyclic and permanent deformations, inertial and kinematic effects, and the rapidly changing soil properties. Recently, performance-based design in geotechnical engineering has been receiving a great deal of attention, and many design codes are initiating the application of its concepts. As a result, estimation of deformation and extent of lateral load are becoming more important.

Some sections of this study addressed the implementation of the MTD 20-15 (2017) simplified method for design and analysis of pile foundations under liquefaction and lateral spreading. The outcomes are presented within the scope of a comparative study contrasting UCSD implementation results to those of an earlier investigation. The presented results are rather different with significant influence on the final displacement demands on the bridge. Challenges in implementing the simplified method are discussed with recommended modifications to the

methodology. In addition, ambiguities and limitations of the method are identified and recommendations and conclusions are drawn.

To improve the understanding of behavior of pile foundations during lateral spreading, a unique set of large scale one-g shake-table experimental data was analyzed. Within this scope, seven experiments were conducted to augment data from an additional earlier four test series from Japan. The ground models in the experiments were instrumented with pore pressure sensors and accelerometers as well as displacement transducers. The piles were instrumented with strain gauges and total pressure transducers along the depth, and displacement transducers at the top. Piles in different configurations were tested to examine the various response mechanisms. In this series of experiments, single piles and pile groups were tested, steel and concrete piles were employed, and different soil stratifications were constructed. These unique sets of data document pile responses of different stiffness, 2 different ground inclinations, inertial and kinematic interactions, and the effect of restraining the pile at the top. Sinusoidal accelerations with amplitude in the range of 0.15-0.5 g and frequency of 2 Hz were applied at the base of the experimental models.

In all models, liquefaction and permanent lateral soil deformation occurred. Maximum lateral soil displacement of as much as 1.0 m, about 3 pile diameters, was observed. Therefore, maximum lateral loads on the piles were induced (for the soil configuration and the imparted ground motion). Maximum bending moments and the corresponding lateral loads were noted quite early during shaking. The soil continued to accumulate deformations during shaking while the embedded piles experienced a softening response as rebounding occurred. Total pressures exerted on the piles have been quantified along with the soil subgrade reaction to document the evolution of soil pressures on the piles and the soil response. After the initial peak response, lateral load

might decrease with further shear strength reduction and deformation in the liquefied stratum as soil continues to flow around the piles.

Based on the pile bending moments, subgrade reactions and deflections from the experiments and the observed soil-pile interaction mechanism, a *p-y* curve model is proposed and calibrated to estimate pile bending moments and deflections due to the liquefaction induced-lateral spreading mechanism. This *p-y* curve is calibrated and verified for the liquefied layer response allowing for softening response. Another curve is calibrated for the crust simulating the softer load transfer mechanism for non-liquefied soils on top of liquefiable ones. The model allows for the higher soil displacements needed to fully mobilize peak crust pressures. The computed response matches well with the observed experimental counterpart.

12.2. Conclusions

12.2.1 Simplified Analysis Approach

The simplified method is widely used to estimate lateral displacement demand and the resulting pile foundation behavior and response. Table 12-1 gives a few suggestions for changes to be implemented in the application of this procedure. In light of the challenges and discrepancies discussed in the previous sections, some recommended modifications are presented below in order to potentially achieve more accurate results.

- Vary imposed displacement profile from abutment to far-end of sliding zone (Figure 12-1). Due to the change in soil profile, pile lengths and cross sections at each bent, the displacement profile needs to reflect that, imposing an appropriate displacement profile at each bent location.
- Local slope failures should be considered in the overall profile. Analysis should account

for the stability of smaller slopes that might be included in the overall failure wedge and their effect on the overall displacement profile.

- Schematic of the lateral imposed displacement profile might be defined to more closely mimic experimental observations. This profile might start from the upper crust through the liquefiable layer and into the underlying layer as affected by the liquefaction process. The smear zone of the underlying layer might need to be included depending on the soil type (Figure 12-2).
- For cases that include more than 1 bent in the analysis, one might conduct a separate analysis for each bent depending on the underlying soil configuration. Thereupon, the shear resistance of all bents can be combined. That is instead of creating a super-pile out of different bents.
- Such a multi-bent analysis will optimize the calculation of the rotational stiffness of the pile head and also allow for including the connectivity effect of the bridge deck. This connectivity is vital for the pile head stiffness and specifically important in cases where each bent has only 1 row of piles.
- Each pile should be modelled as accurately as possible. Most piles have different cross-sections with depth. Pipe piles maybe be empty, filled with sand, filled with concrete or contain rebar. The variation of the pile cross-section will affect the locations of maximum moment and shear force.
- The current procedure might underestimate residual strength of the liquefied soil and thus over predict the soil displacement (which is subject to significant uncertainty). Correlations using SPT or CPT need to be more carefully examined.

- Residual strength modeled by soft clay *p-y* curves might not provide an adequate tool for lateral load analysis of liquefied soil. A different set of *p-y* curves might be a better representation particularly depicting the gradual loss of soil strength with cyclic loading (such as the one proposed in this study).
- Use of site-specific earthquake motions in conducting sliding block displacement analysis might be helpful. Conversely, an empirical relationship dependent on peak velocity and peak acceleration instead of Newmark's sliding block analysis that is only PGA dependent might be of value to consider.
- Modeling the entire canyon with both side slopes in slope stability models might be warranted, particularly for deep narrow-canyon configurations. In cases where canyons are narrow, failure surfaces from both sides are likely to interact.
- Employing a global bridge finite element model is the preferred approach with its ability to accurately model soil profile spatial variations, the bridge superstructure connectivity with details that contribute to global response. Finite elements also can provide detailed results of forces and displacements in each foundation element.

12.2.2 Experimental Investigation

In the one-g shake-table experiments, the loose saturated sand layer liquefied in the first few cycles of shaking and soil deformations started as shaking begun. Generally, pile bending moments and displacements gradually increased before the onset of liquefaction. Maximum soil pressure was exerted either before liquefaction or right after. Subsequently, the liquefied soil experienced further loss in stiffness and strength and the pile either partially or fully rebounded

back. Maximum bending moments occurred at the base of the piles for the 2 layered profiles and in the dense layer for the 3-layer profiles.

In the case of a non-liquefied crust overlying a liquefiable sand layer, the crust was found to experience a softer load transfer mechanism requiring higher displacement to fully mobilize the layer pressures. In some cases, crust pressures exceed that of the passive plane strain cinfguration. On the other hand, the liquefied stratum load peaks early at very small displacements and exhibits strain softening behavior thereafter.

The proposed *p-y* curve lateral model is calibrated against experimental data and is in good agreement with the employed experimental results. The liquefied model behavior is different from the existing soil springs in practice that do not incorporate the degraded response. The proposed *p-y* curve shape was substantiated by earlier finding reported by other researchers. One vital part of the softening response is the reduction in lateral force demands on piles. By the time the bottom load curves peak, the upper locations are at or near their residual stages. This more accurately captures the response and avoids the sustained increase of lateral load (with ground displacement) when using other models.

Pile axial response during liquefaction induced lateral spreading has received less attention over the past years with relatively less focus placed on its importance. From the conducted experimentation set, the axial response is briefly investigated. Although the crust settled, little compressive axial load was imposed on the pile as a result of the gap formation around the pile. Reduction in compressive or tensile strains/forces developing in the bottom dense layer (due to the inclined ground configuration) was observed. In general, the loose liquefiable stratum did not impose additional compressive forces after the shaking stopped.

A few main conclusions from the experimental program are:

1. Soil pressure on both sides of the pile affects the resultant pressures on the pile. Reduction in downslope side pressure contributed significantly to overall lateral pressure in the early part of the response, and eventually upslope side pressures became dominant including pressure from crust.
2. Liquefied layer pressures are directly related to pore pressures in the layer with minimal contributions from the effective pressures.
3. Observed pile bending moment decrease and soil softening response suggests that with continued shaking and further accumulated ground displacement, soil pressure on the pile is reduced.
4. Post-earthquake reconnaissance inspections might not account for the peak pile bending moment and displacement (as the pile might have rebounded to some extent after experiencing peak load).
5. Pile foundation provides support to the soil layer and absence of pile resistance will cause substantial movement as observed after pile failure during shaking when deformation rate increased greatly post failure.
6. The entire soil system is affected by pile restraint. The restraint affected both pile and soil deformations. Displacement compatibility of the pile, box and surrounding soil was observed and is the effect of the restraint.
7. The restraint affecting the entire system is proof that the pile affects the entire soil in the box and vice versa. This suggests that the soil tributary area affecting the pile is much larger than its diameter.

8. The CPT profile suggests regions in the loose layer are affected by the surrounding soil as the strength degrades over a certain length. This correlates with the observed high total pressures and soil resistance over the same length beneath the crust layer.
9. In the inclined soil configuration, friction causes some axial tension and compression loads along with bending (e.g., tensile forces on the bottom pile portion were observed).

12.3. Main Findings

For piles subjected to liquefaction-induced lateral spreading, the main experimental findings of particular interest to the simplified analysis method include:

1. In the liquefiable layer, accumulated lateral strains are not uniform, and are highest near its base. A parabolic shape of deformation was observed (Figure 12-2).

2. In the underlying dense layer, lateral strains are highest near its top at the interface with the overlying loose liquefied layer.

3. At the interface between the saturated loose and underlying dense strata, high pile moments are distributed over a large extent of its length, about 3 times the pile diameter. In the studied experiments, peak curvature and moment occurred well below the interface between the loose and dense strata, at about 2 times the pile diameter (note: pile diameter is used as a yardstick here, but the distance might not be related to pile diameter as a physical entity).

4. Excess pore pressures migrate into the dense sand stratum, helping to weaken its upper zone, allowing for a lower contrast between the stiffness of the upper liquefied and the lower denser soil formations.

5. The deformed shape changes if the underlying non-liquefiable layer was dense sand or stiff clay (i.e., soil that does not lose strength because of liquefaction of the upper loose stratum).

Increase in pore pressures in the dense sand will allow deformations to occur in the upper portion of it.

6. The downslope side of the bottom dense layer develops significant pressures as it resists the pile movement.

7. Pressures acting on the pile are a combination of the crust pushing and the liquefied soil attempting to flow around the pile. Crust pressures are a result of upslope side pushing and downslope soil moving away from the pile.

8. Total pressures from the crust layer can exceed that of the static passive Plane strain pressures.

9. Pile group effects reduced lateral pressures on individual piles in the model. In general, pile groups exert a significant pinning effect on the ground.

10. The effect of the superstructure restraint is crucial for pile response as it can limit pile movement. The restraining effect extends to the surrounding ground as overall soil deformations might become more limited.

11. The proposed *p-y* curves are recommended for use to better capture soil-pile interaction (based on the employed experimental data).

12.4. Recommendations for Future Studies

1. Additional shake-table experiments can be of value using large laminar boxes including pile groups of different configurations. Such investigations will further quantify pile pinning effects and lateral loading on the pile groups. The group interaction mechanism and shadowing effects are of importance to investigate in future studies.

2. Additional shake-table experiments can be of value for liquefaction mitigation, pile foundation lateral spreading countermeasures and retrofit strategies, to reduce the exerted lateral pressures and ground deformations.

3. Centrifuge experiments can provide valuable insights, particularly as related to different superstructure and canyon configurations (e.g., to further document the overall superstructure restraining effect).

4. Centrifuge tests on similar configurations to the large-scale experiments would also enable more detailed studies concerning scaling laws. This contributes to a better understanding of earlier centrifuge tests (permitting closer interpretations of centrifuge and large-scale experimentation outcomes).

5. Calibration of numerical soil models to capture the experimental response and extending the numerical studies to more configurations and full-scale modeling.

6. Improve on the proposed *p-y* curve models to account for other soil property variables. Liquefied *p-y* curve models might more accurately account for depth, overburden pressures, and permeability. Crust model should be verified against other available data and include different soil strengths. The presence of cohesive soils as the upper crust should be further studied.

7. Pile behavior in liquefiable steep slopes might be different from that in mild slopes. One-g shake-table experiments and numerical studies can be conducted to explore this variation.

8. Liquefiable soils at deeper depths should be more loosely evaluated, and effect on the ground slope deformations further evaluated.

Table 12-1. Suggested modifications to MTD 20-15

Item	Suggested Change
Global Model	Highly recommended to model entire bridge using finite elements with emphasis on layer variability and soil profiles difference (except for very long bridges, can be partially modelled)
Slope Stability	Use Spencer's Method
Global Failure	Check both local and global slope failures. Model the entire canyon on both sides to get interaction between slopes. Should model entire bridge (if located in a narrow canyon) for much significant provided superstructure resistance
p-y curves	Apply new curves proposed in this study
Design Displacement	Consider estimated based on equation by Martin and Qiu (1994), then modified by NCHRP (2008) along with the Bray and Travasarou (2007) equation. NCHRP (2008) includes PGV and site amplification factors.
Soil Movement Profiles	Different soil movement profile for each bent according to geometry
Loading Pile Models	Load multi-bent pile models according to their respective location within the global context

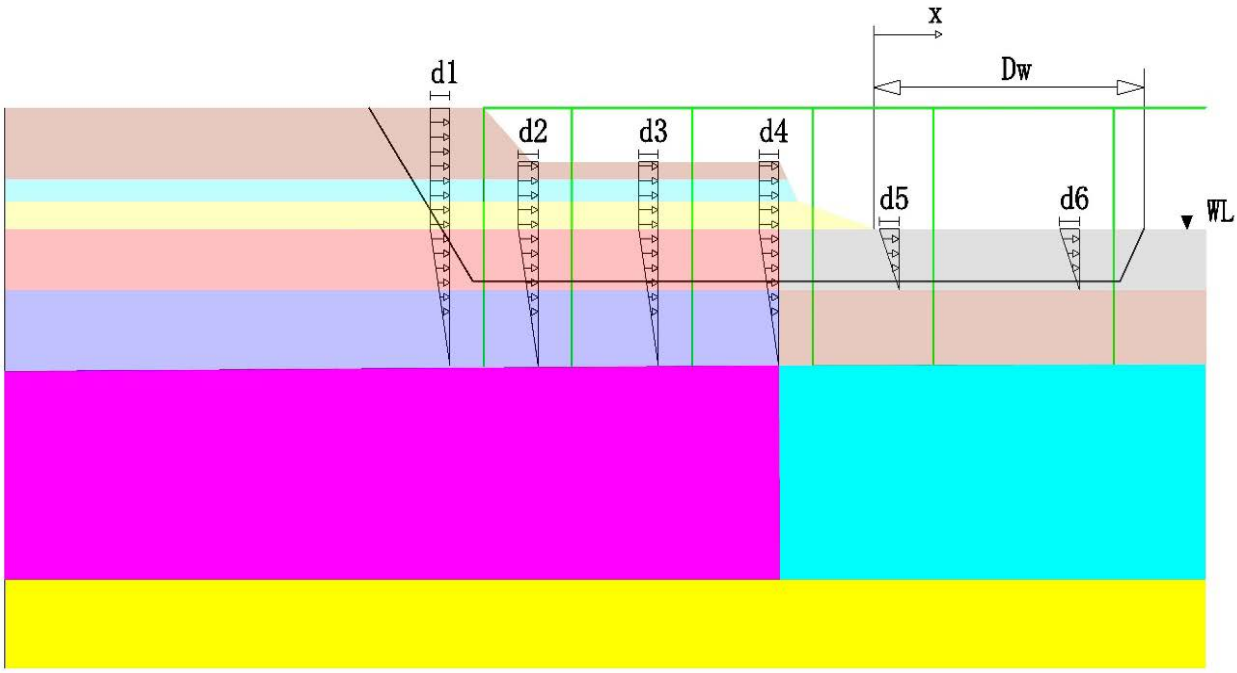

Figure 12-1. Modified soil movement profile for global bridge analysis

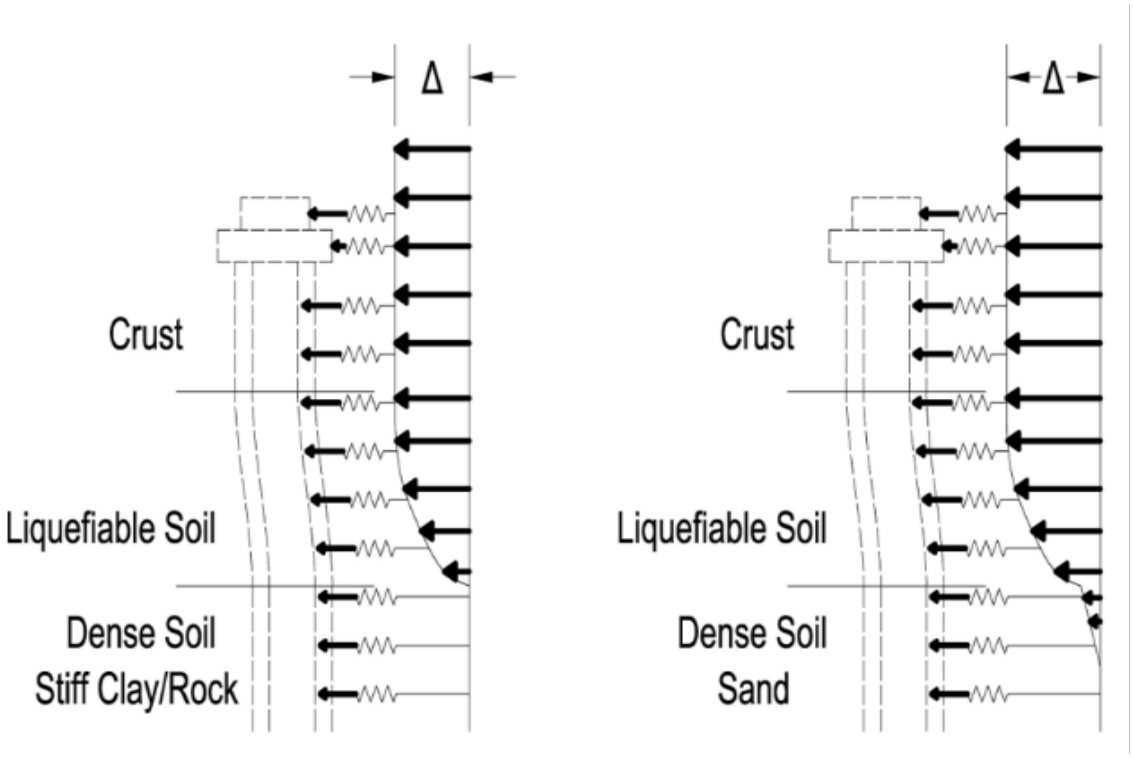

Figure 12-2. Proposed lateral soil imposed displacement profiles for different cases

References

Abdoun, T. and Elgamal, A.-W. (1995). "Prediction of seismically-induced lateral deformation during soil liquefaction," Proceedings of Eleventh African Regional Conference on Soil Mechanics and Foundation Engineering, Cairo, Egypt, Dec. 11-15.

Abdoun, T. (1997). "Modeling of seismically induced lateral spreading of multi-layered soil and its effect on pile foundations," Ph.D. Thesis, Rensselaer Polytechnic Institute, Troy, New York.

Abdoun, T. and Dobry, R. (2002). "Evaluation of pile foundation response to lateral spreading," Soil Dynamics and Earthquake Engineering 22(9-12), 1051-1058.

Abdoun, T., Dobry, R., O'Rourke, T. D. and Goh, S. H. (2003). "Pile response to lateral spreads: centrifuge modeling," Journal of Geotechnical and Geoenvironmental Engineering 129(10), 869-878.

Abdoun, T., Dobry, R., Zimmie, T. F., and Zeghal, M. (2005). Centrifuge research of countermeasures to protect pile foundations against liquefaction-induced lateral spreading. Journal of earthquake engineering, 9(spec01), 105-125.

AIJ. (2001). Architectural Institute of Japan. Recommendations for design of building foundations (in Japanese).

API. (2000). Recommended practice for planning, designing, and constructing fixed offshore platforms—working stress design.

American Petroleum Institute. (2010). Recommended Practice for Planning, Designing and Constructing Fixed Offshore Platforms - Working Stress Design, API RP 2A-WSD, 21st Edition, Errata and Supplement, 2010.

Arulanandan, K. and Scott, R. F. (1993). "VELACS: Verification of numerical procedures for the analysis of soil liquefaction problems," Conference proceedings, volume 1, Balkema, Davis, CA.

Ashford, S. A., Rollins, K. M., Bradford, S. C., Weaver, T. J. and Baez, J. I. (2000). "Liquefaction mitigation using stone columns around deep foundations: Full-scale test results." Soil Mechanics 2000, Transportation Research Record No. 1736, TRB, Washington D.C., 110-118.

Ashford, S., and Jakrapiyanun, W. (2001). Design and verification of the UCSD laminar container (SSRP-2001/07). University of California San Diego. Submitted to NEES-2 Workshop by National Science Foundation.

Ashford, S. A. and Rollins, K.M. (2002). "TILT: The Treasure Island liquefaction test final report," Report Number SSRP 2001/17, Dept. of Structural Engineering., Univ. of California, San Diego, San Diego, 509 p.

Ashford, S. A., Rollins, K. M. and Dusty Lane, J. (2004). "Blast-induced liquefaction for full-scale foundation testing," Journal of Geotechnical and Geoenvironmental Engineering, 130(8), Aug, 798-806.

Ashford, S. A., Boulanger, R. W., and Brandenberg, S. J. (2011). "Recommended design practice for pile foundations in laterally spreading ground," Pacific Earthquake Engineering Research Center Report No. 2011/04, Berkeley, CA, USA

ATC and MCEER. (2001). "Recommended LRFD guidelines for the seismic design of highway bridges," Part I: Specifications and Part II: Commentary and Appendices.

Bartlett, S. F. and Youd, T. L. (1992). "Case histories of lateral spreads caused by the 1964 Alaska earthquake," Ch.2 of Case Studies of Liquefaction and Lifeline Performance During Past Earthquakes, 2, United States Case Studies, 2-1 - 2-127.

Bastidas, A. M. P. (2016). Ottawa F-65 Sand Characterization. PhD Thesis. Department of Civil and Environmental Engineering. University of California Davis, Davis, CA.

Berrill, J.B., Christensen, S.A., Keenan, R.J., Okada, W. and Pettinga, J.K. (1997) Lateral-Spreading Loads on a Piled Bridge Foundation, Seismic Behavior of Ground and Geotechnical Structures (ed. S. E. Pinto), pp. 176–183. Rotterdam: Balkema.

Berrill, J. B., Christensen, S.A.,Keenan, R. P., Okada, W., and Pettinga, J. R. (2001) "Case study of lateral spreading forces on a piled foundation," Geotechnique 51, 501-517.

Bhattacharya, S. (2003). "Pile instability during earthquake liquefaction," PhD thesis, University of Cambridge, Cambridge, U.K.

Bhattacharya, S., Madabhushi, S. and Bolton, M. (2004). "An alternative mechanism of pile failure in liquefiable deposits during earthquakes," Geotechnique 54(3), 203-213.

Bhattacharya, S., Adhikari, S. and Alexander, N. A. (2009). Simplified method for unified buckling and dynamic analysis of pile supported structures in seismically liquefiable soils. Soil Dynamics and Earthquake Engineering; 29:1220–1235. DOI:10.1016/jsoildyn.2009.01.006.

Bhattacharya, S., Hyodo, M., Goda, K., Tazoh, T. and Taylor, CA. (2011). Liquefaction of soil in the Tokyo Bay area from the 2011 Tohoku (Japan) earthquake. Soil Dynamics and Earthquake Engineering, 31:1618–1628. DOI:10.1016/j. soildyn.2011.06.006

Bhattacharya, S., Tokimatsu, K., Goda, K., Sarkar, R., Shadlou, M., and Rouholamin, M. (2014). Collapse of Showa Bridge during 1964 Niigata earthquake: A quantitative reappraisal on the failure mechanisms. Soil Dynamics and Earthquake Engineering, 65, 55-71.

Boulanger, R.W., Kutter, B.L., Brandenberg, S.J., Singh, P. and Chang, D. (2003) Pile foundations in liquefied and laterally spreading ground during earthquakes: centrifuge experiments and analyses. Report No. UCD/CGM-03/01, Center for Geotechnical Modeling, University of California, Davis, CA. 2003.

Boulanger, R. W. and Tokimatsu, K. eds. (2005). “Proceedings of a Workshop on Seismic Performance and Simulation of Pile Foundations in Liquefied and Laterally Spreading Ground,” University of California, Davis, California, United States, ASCE.

Boulanger, R. W., Chang, D., Gulerce, U., Brandenberg, S. J., and Kutter, B. L. (2006). Evaluating pile pinning effects on abutments over liquefied ground. In Seismic Performance and Simulation of Pile Foundations in Liquefied and Laterally Spreading Ground (pp. 306-318).

Brandenberg, S. J., Boulanger, R. W., Kutter, B. L.,Wilson, D. W. and Chang, D. (2004). “Load transfer between pile groups and laterally spreading ground during earthquakes,” Proc., 13th World Conf. on Earthquake Eng., Vancouver, B.C., Canada.

Brandenberg, S. J., Boulanger, R. W., Kutter, B. L., and Chang, D. (2005). “Behavior of pile foundations in laterally spreading ground during centrifuge tests,” Journal of Geotechnical and Geoenvironmental Engineering, 131(11), 1378-1391.

Brandenberg, S. J., Boulanger, R. W., Kutter, B. L., and Chang, D. (2007a). “Liquefaction-Induced Softening of Load Transfer between Pile Groups and Laterally Spreading Crusts,” Journal of Geotechnical and Geoenvironmental Engineering, 133(1), 91-103.

Brandenberg, S.J., Boulanger, R.W., Kutter, B.L. and Chang, D. (2007b). Static pushover analyses of pile groups in liquefied and laterally spreading ground in centrifuge tests. Journal of Geotechnical and Geoenvironmental Engineering; 133(9):1055–1066.

Bray, J., and Ledezma, C. (2007). Evaluating seismic displacements and damage for pile foundations undergoing liquefaction-induced lateral spreading. In Proceedings, 4th International Conference on Earthquake Geotechnical Engineering, paper No. 1460.

Bray, J.D., and Travasarou, T. (2007). “Simplified procedure for estimating earthquake-induced deviatoric slope displacements.” J. Geotech. Geoenviron. Eng., 133(4): 381-392.

Caltrans, (2016). Personal Communications.

Caltrans, (2017). Bridge Memo to Designer (MTD) 20-15: Lateral Spreading Analysis for New and Existing Bridges. California Department of Transportation, Sacramento, CA 95816

Clough, G. W., Martin, J. R. and Chameau, J. L. (1994). "The geotechnical aspects," Practical lessons from the Loma Prieta Earthquake, National Research Council, National Academy Press, Washington, D.C., 29-63.

Chang, B. J. and Hutchinson, T. C. (2013). “Experimental investigation of plastic demands in piles embedded in multi-layered liquefiable soils,” Soil Dynamics and Earthquake Engineering 49, 146-156.

Cubrinovski, M., Ishihara, K. and Furukawazono, K. (1999). Analysis of Full-Scale Tests on Piles in Deposits Subjected to Liquefaction. Lisbon, Portugal, 2nd Int. Conf. on Earthquake Geotechnical Engineering.

Cubrinovski, M. and Ishihara, K. (2004). Simplified method for analysis of piles undergoing lateral spreading in liquefied soils. Soils and Foundations; 44(5):119–133.

Cubrinovski, M., Kokusho, T. and Ishihara, K. (2006). “Interpretation from large-scale shake table tests on piles undergoing lateral spreading in liquefied soils,” Soil Dynamics and Earthquake Engineering 26, 275-286.

Cubrinovski, M., Bradley, B., Wotherspoon, L., Green, R., Bray, J., Wood, C., Pender, M., Allen, J., Bradshaw, A., Rix, G. and Taylor, M. (2011). Geotechnical aspects of the 22 February 2011 Christchurch earthquake.

Dobry, R., Taboada, V., Liu, L. (1995). Centrifuge modelling of liquefaction effects during earthquakes. Proc. 1st Intl. Conf. On Earthquake Geotechnical Engineering, IS-Tokyo, 14-16.

Dobry, R., and Abdoun, T. (1998). Post-triggering response of liquefied sand in the free field and near foundations. Proc. Of Geotechnical Earthquake Engineering and Soil Dynamics III. Geotechnical special publication no. 75, Dakoulas P, Yegian M, Holtz RD (eds.). ASCE: Seattle, Washington, August 3–6; 2: 270–300.

Dobry, R. and Abdoun, T. (2001) Recent studies on seismic centrifuge modeling of liquefaction and its effect on deep foundation. Proc 4th Int Conf Recent Adv Geotech Earthquake Engng Soil Dynamics (ed. S. Prakash), San Diego CA.

Dobry, R., Abdoun, T., O'Rourke, T. D. and Goh, S. H. (2003). “Single piles in lateral spreads: Field bending moment evaluation,” Journal of Geotechnical and Geoenvironmental Engineering, 129(10) 879-889.

Dobry, R., Thevanayagam, S., Medina, C., Bethapudi, R., Elgamal, A., Bennett, V., and Mercado, V. M. (2010). Mechanics of lateral spreading observed in a full-scale shake test. Journal of geotechnical and geoenvironmental engineering, 137(2), 115-129.

Doi, M. and Hamada, M. (1992). "A summary of Case Studies on liquefaction-Induced Ground Displacements," Proceedings from the Fourth Japan-U.S. Workshop on Earthquake Resistant Design of Lifeline Facilities and Countermeasures for Soil Liquefaction, Vol. 1, Technical Report NCEER-92-0019, pp. 115-129

Dungca, J.R., Kuwano, J., Saruwatari, T., Izawa, J., Suzuki, H. and Tokimatsu, K. (2004) Shaking table tests on the lateral response of a pile buried in liquefied sand. Proc 11th Int Conf Soil Dynamics Earthquake Engng Berkeley, CA 2, 471–477.

Earthquake Engineering Research Institute (EERI). www.eeri.org

Ebeido, A., Elgamal, A. and Zayed, M., (2018a). “Pile response during liquefaction-induced lateral spreading: 1-g shake table tests with different ground inclination”. Proc. 9th international conference on Physical Modelling in Geotechnics. City, University of London. 17-20 July.

Ebeido, A., Zayed, M., Kim, K., Wilson, P., and Elgamal, A. (2018b). Large Scale Geotechnical Shake Table Testing at the University of California San Diego. In International Congress and Exhibition" Sustainable Civil Infrastructures: Innovative Infrastructure Geotechnology" (pp. 101-113). Springer, Cham.

Ebeido, A., Elgamal, A., Tokimatus, K., and Abe, A. (2019a). “Pile and pile-group response to liquefaction induced lateral spreading in four large scale shake-table experiments”. Journal of Geotechnical and Geoenvironmental Engineering.

Ebeido, A., Zayed, M., Kim, K., Elgamal, A., (2019b). “Large Scale liquefaction-induced lateral spreading: 1-g Shake Table Testing at the University of California San Diego”. Proc. of the 8th International Conference on Case Histories in Geotechnical Engineering. Philadelphia, Pennsylvania. 24-27 March.

Ebeido, A., Almutairi, A., Lu, J., Qiu, Z., and Elgamal, A. (2019c). Pile Foundation Response in Laterally Spreading Ground (SSRP-2019/01). University of California San Diego. Submitted to California Department of Transportation.

Elgamal, A., Zeghal, M., Taboada, V., and Dobry, R. (1996). Analysis of site liquefaction and lateral spreading using centrifuge testing records. Soils and Foundations, 36(2), 111-121.

EN 1998-1: Eurocode 8: Design of structures for earthquake resistance—Part 1: General rules, seismic actions and rules for buildings. CEN: Brussels, Belgium. 2004

EN 1998−5. (2004). Eurocode 8: Design of Structures for Earthquake Resistance Part 5: Foundations, Retaining Structures and Geotechnical Aspects (English). Comité Européen de Normalisation (CEN), Brussels.

Faris, A.T., Seed, R. B., Kayen, R. E., and Wu, J. (2006). A Semi-Empirical Model for the Estimation of Maximum Horizontal Displacement Due to Liquefaction-Induced Lateral Spreading, 8th National Conference on Earthquake Engineering, San Francisco, CA.

Federal Highway Administration (FHWA). www.fhwa.dot.gov, Aftermath of The Kobe Earthquake

Finn, W.D.L and Fujita, N. (2002). "Piles in liquefiable soils: Seismic analysis and design issues," Soil Dynamics and Earthquake Engineering, 22, 731-742.

Finn, W.L. (2005). A study of piles during earthquakes: issues of design and analysis. Bulletin of Earthquake Engineering; 3(2):141–234.

Finn, W. L. (2015). “1st Ishihara Lecture: An overview of the behavior of pile foundations in liquefiable and non-liquefiable soils during earthquake excitation,” Soil Dynamics and Earthquake Engineering 68, 69-77.

Franke, K. W. and Rollins, K. M. (2013). “Simplified Hybrid p-y Spring Model for Liquefied Soils,” Journal of Geotechnical and Geoenvironmental Engineering, ASCE, Vol. 139, No. 4, pp. 564-576.

Fujii, Y., Isemoto, N., Satou, K., Kaneko, O., Funahara, H. Arai, T. and Tokimatsu, K. (1998). "Investigation and analysis of a pile foundation damaged by liquefaction during the 1995 Hyogoken-Nambu earthquake," Soils and Foundations, Special Issue, Sept., 179-192.

GEER (2010a). Geo-engineering reconnaissance of the 2010 Maule, Chile earth- quake." Report No. GEER-022, Version 2, May 25, 2010, Geo-Engineering Extreme Events Reconnaissance.

GEER (2010b). Preliminary report on seismological and geotechnical engineering aspects of the april 4 2010 mw 7.2 El Mayor-Cucapah (Mexico) earthquake." Report No. GEER-023, Version 1, June 15, 2010, Geo-Engineering Extreme Events Reconnaissance.

Geschwindner, L. F. (2011). Unified design of steel structures. Wiley Global Education.

Goh, S. and O’Rourke, T. (1999). Limit state model for soil–pile interaction during lateral spread. Proc. of 7th US Japan workshop on earthquake resistant design of lifeline facilities and countermeasures against soil liquefaction. Seattle, WA.

Goh, S. H., and O'Rourke, T. D. (2008). Soil-pile interaction during liquefaction-induced lateral spread. Journal of Earthquake and Tsunami, 2(01), 53-85.

Gonzalez, L., Abdoun, T. and Dobry, R. (2005). "Effect of soil permeability on centrifuge modeling of pile response to lateral spreading," Proceedings of Workshop on Simulation and Seismic Performance of Pile Foundations in Liquefied and Laterally Spreading Ground, March 16-19, 2005, University of California at Davis, Davis, California 95616, USA.

González, L., Abdoun, T., and Dobry, R. (2009). Effect of soil permeability on centrifuge modeling of pile response to lateral spreading. Journal of Geotechnical and Geoenvironmental Engineering, 135(1), 62-73.

Haigh, S. K. (2002). “Effects of liquefaction on pile foundations in sloping ground,” PhD Dissertation, Cambridge University.

Haigh, S. K. and Madabhushi, S. P. G. (2002). "Centrifuge modelling of lateral spreading past pile foundations," Proceedings of International Conference on Physical Modelling in Geotechnics, St John's, Newfoundland, Canada, July 2002.

Hall, J. R. and Scott, R. F. (1995). "Evaluation of bridge damage in the 1990 Luzon and 1991 Costa Rica earthquakes," Southern California Earthquake Center, Task H-6 Report to Caltrans and the City and County of Los Angeles, on the Characteristics of Earthquake Ground Motion for Seismic Design.

Hamada, M. (1991). "Damage to piles by liquefaction-induced ground displacements," Proceedings of the 3rd U.S. Conference Lifeline Earthquake Eng., ASCE, Los Angeles, 1172-1181.

Hamada, M. (1992) “Large ground deformations and theri effects on lifelines: 1964 Niigata earthquake,” Technical Report NCEER-92-0001, eds. M. Hamada and T.D. O’Rourke, (National Center for Earthquake Engineering Research, Buffalo,NY), 3-1-3-123.

Hamada, M., Ohtomo, K. Sato, H. and Iwatate, T. (1992). "Experimental study of effects of liquefaction-induced ground displacement on in-ground structures," Proc. 4th Japan-US Workshop on Earthquake Resistant Design of Lifeline Facilities and Countermeasures for Soil Liquefaction, Technical Report NCEER-92-0001. NCEER, Buffalo, N.Y, Vol. 1, 481-492.

Hamada, M. and O'Rourke, T. eds. (1992) “Case studies of liquefaction and lifeline performance during past earthquakes,”Japanese Case Studies Technical Report NCEER-92-0001, Vol. 1., National Center for Earthquake Engineering Research, Buffalo,NY.

Hamada, M., Wakamatsu, K. and Ando, T. (1996). "Liquefaction-induced ground deformation and its caused damage during the 1995 Hyogoken-Nanbu earthquake," Proc., 6th Japan-U.S. Workshop on earthquake resistant design of lifeline facilities and countermeasures against soil liquefaction, Tech. Rep. NCEER-96-0012, M. Hamada and T. D. O'Rourke (eds.), September 11, 137-152.

Hamada, M. (2000). "Performance of foundations against liquefaction-induced permanent ground displacement," Proceedings of the 12th World Conference on Earthquake Engineering, Auckland, New Zealand, Paper No. 1754.

Hanshin Highway Authority (1996). Investigation on the seismic damage of bridge foundations in the reclaimed land.

He, L. (2005). Liquefaction-induced lateral spreading and its effects on pile foundations. Ph.D Dissertation, University of California, San Diego.

He, L., Elgamal, A., Abdoun, T., Abe, A., Dobry, R., Meneses, J., Sato, M., and Tokimatsu, K. (2006) Lateral load piles due to liquefactioninduced lateral spreading during 1g shake table experiments on. Proc. 8th U.S. Nat. Conf. Earthquake Enng, San Francisco, CA, Paper No. 881.

He, L., Elgamal, A., Abdoun, T., Abe, A., Dobry, R., Hamada, M., Meneses, J., Sato, M., Shantz, T., and Tokimatsu, K. (2009). Liquefaction-Induced Lateral Load on Pile in a Medium Dr Sand Layer, Journal of Earthquake Engineering, 13:7, 916-938.

He, L., Ramirez, J., Lu, J., Tang, L., Elgamal, A., and Tokimatsu, K. (2017). Lateral spreading near deep foundations and influence of soil permeability. Canadian Geotechnical Journal, 54(6), 846-861.

Hetényi M. (1946). Beams on Elastic Foundation. Theory with Applications in the Fields of Civil and Mechanical Engineering. The University of Michigan Press: Ann Arbor.

Hwang, J.I., Kim, C.Y., Chung, C.K. and Kim, M.M. (2004). Behavior of a Single Pile Subjected to Flow of Liquefied Soil in an Infinite Slope. Proc 11th Int Conf Soil Dynamics Earthquake Engng, Berkeley, CA 2, 573–580.

Idriss, I.M. and Boulanger, R.W. (2008). “Soil Liquefaction During Earthquakes,” Monograph MNO-12. Earthquake Engineering Research Institute (EERI), Oakland, California.

Idriss, I.M. and Abrahamson, N. A. (2000). "Geotechnical aspects of the earthquake ground motions recorded during the 1999 Chi-Chi earthquake," Proceedings of International Workshop on Annual Commemoration of Chi-Chi Earthquake, National Center for Research on Earthquake Engineering, Taipei, Taiwan, China, September 18-20, 2000, 9-22.

Ishihara, K. (1997) “Terzaghi Oration: Geotechnical aspects of the 1995 Kobe earthquake,” ICSMFE Proceedings, Hamburg.

Ishihara, K. and Cubrinovski, M. (1998a). Soil-Pile Interaction In Liquefied Deposits Undergoing Lateral Spreading. Croatia, XI Danube-European Conference.

Ishihara, K. and Cubrinovski, M. (1998b). Performance of Large-diameter Piles Subjected to Lateral Spreading of Liquefied Deposits. Taipei, Taiwan, Thirteenth Southeast Asian Geotechnical Conferene.

Ishihara, K. (2003) Liquefaction-induced lateral flow and its effects on foundation piles. Invited Lecture Proc 5th Nat Conf Earthquake Engng, Istanbul, Turkey.

Ishihara, K. and Cubrinovski, M. (2004). Case Studies of Pile Foundations Underoing Lateral Spreading in Liquefied Deposits. New York, NY, Fifth International Conference on Case Histories in Geotechnical Engineering.

JRA. (1996). Japanese Road Association: specification for highway bridges, Part V: seismic design.

JRA. (2002). "Specifications for highway bridges," Japan Road Association, Preliminary English Version, Prepared by Public Works Research Institute (PWRI) and Civil Engineering Research Laboratory (CRL), Japan, November 2002.

Kagawa, T., Sato, M., Minowa, C., Abe, A., and Tazoh, T. (2004). “Centrifuge simulations of large-scale shaking table tests: Case studies,” Journal of Geotechnical and Geoenvironmental Engineering 130(7), 663-672.

Knappett, J.A. and Madabhushi, S. P. G. (2009). Influence of axial load on lateral pile response in liquefiable soil. Part I: physical modelling. Geotechnique; 59(7):571–581. DOI:10.1680/geo.8.-009.3749.

Koyamada, K., Miyamoto, Y. and Tokimatsu, K. (2006). Field investigation and analysis study of damaged pile foundation during the 2003 Tokachi-Oki earthquake. ASCE, pp. 97-108.

Kramer, S.L. (1996). Geotechnical earthquake engineering, Prentice Hall, Upper Saddle River, NJ.

Kramer, S. and Wang, C.H. (2015). Empirical Model for Estimation of the Residual Strength of Liquefied Soil, Journal of Geotechnical and Geoenvironmental Engineering.

Krinitzsky, E.L. and Hynes, M. E. (2002). "The Bhuj, India, earthquake: Lessons learned for earthquake safety of dams on alluvium," Engineering Geology, 66(3-4), 163-196.

Kutter, B. L. (1984). "Earthquake deformation of centrifuge model banks," Journal of the Geotechnical Engineering Division, ASCE, 110(12), Dec. 1984, 1697-1714.

Lam, I., Arduino, P., and Mackenzie-Helnwein, P. (2009). OPENSEES soil-pile interaction study under lateral spread loading. In Contemporary Topics in In Situ Testing, Analysis, and Reliability of Foundations (pp. 206-213).

Law, H. K. and Lam, I. P. (2001). "Application of periodic boundary for large pile group," Journal of Geotechnical and Geoenvironmental Engineering 889-892.

Liu, L. and Dobry, R. (1995). "Effect of liquefaction on lateral response of piles by centrifuge model tests," Report submitted to NCEER.

Lombardi, D., Durante, M. G., Dash, S. R., & Bhattacharya, S. (2010). Fixity of piles in liquefiable soils. Fifth International Conference on Recent Advances in Geotechnical Earthquake Engineering and Soil Dynamics. May 24-29

Lombardi, D., and Bhattacharya, S. (2014). Modal analysis of pile-supported structures during seismic liquefaction. Earthquake Engineering & Structural Dynamics, 43(1), 119-138.

Long, J. H., 1984. "The Behavior of Vertical Piles in Cohesive Soil Subjected to Repetitive Horizontal Loading," Ph.D. dissertation, The University of Texas, Austin, Texas, p 332.

Magenes, G. (1989). Design, analysis and calibration of the UCSD shake table: University of California, San Diego, Department of Applied Mechanics/Engineering Sciences.

Martin, G. R., Marsh, M. L., Anderson, D. G., Mayes, R. L. and Power, M. S. (2002). "Recommended design approach for liquefaction induced lateral spreading," Proceedings of 3rd national seismic conference and workshop on bridges and highways, Portland, April 28-May 1, 2002.

Martin, G, and Chen, C. (2005). "Response of piles due to lateral slope movement". Computers and Structures. 83:588-98

Matlock, H. (1970). "Correlations of design of laterally loaded piles in soft clay." Proc. Offshore Technology Conference, Houston, TX, Vol. 1, No. 1204, pp. 577-594.

Matsui, T. and Oda, K. (1996). "Foundation damage of structures," Soils and Foundations, Special Issue on Geotechnical Aspects of the January 17, 1995 Hyogoken-Nambu Earthquake, January, January 189-200.

Mazzoni, S., McKenna, F., and Fenves, G.L. (2006). Open System for Earthquake Engineering Simulation User Manual, Pacific Earthquake Engineering Research Center, University of California, Berkeley. (http://opensees.berkel-ey.edu/OpenSees/manuals/usermanual/).

McGann, C. H., and Arduino, P. (2014). "Numerical Assessment of Three-Dimensional Foundation Pinning Effects during Lateral Spreading at the Mataquito River Bridge." J. Geotech. Geoenviron. Eng., ASCE. 140(8).

Meneses, J., Hamada, M., Kurita, M. and Elgamal, A. (2002). “Soil-pile interaction under liquefied sand flow in 1g shake table tests,” Proc., Int. Conf. on Advances and New Challenges in Earthquake Engineering Research, Harbin and Hong Kong, China.

Meymand, Philip James. (1998). "Shaking table scale model tests of nonlinear soil-pile superstructure interaction in soft clay," Ph.D. Dissertation, University of California, Berkeley, California.

Miwa, S., Ikeda, T. and Sato, T. (2006). “Damage process of pile foundation in liquefied ground during strong ground motion” Proc., 11th Int. Conf. on Soil Dynamics and Earthquake Engineering (ICSDEE), Issues 2–4, Part II, 325–336.

Mizuno, H., Iiba, M. and Hirade, T. (1996). "Pile damage during the 1995 Hyogoken-Nanbu earthquake in Japan," Proc. 11th World Conf. Earthquake Eng., Acapulco, Paper No. 977.

Mizuno, H. (1987) Pile damage during earthquakes in Japan (1923–1983). Proceedings ASCE session on dynamic response of pile foundations, Atlantic City, NJ, Vol. 1, pp. 53–77.

Moehle, J. P. and Eberhard, M. O. (2000). Bridge Engineering Handbook, CRC Press.

Mokwa, R.L. and Duncan, J.M. (2000a). "Experimental evaluation of lateral-load resistance of pile caps." J. Geotech. Geoenviron. Eng., ASCE. 127(2). 185-192.

Mokwa, R.L. and Duncan, J.M. (2000b). “Investigation of the Resistance of Pile Caps and Integral Abutments to Lateral Loading”, Final Contract Report, February, Virginia Transportation Research Council, Charlottesville, VA

Motamed, R., Sesov, V. and Towhata, I. (2008). “Shaking model tests on behavior of group piles undergoing lateral flow of liquefied subsoil,” The 14 th World Conference on Earthquake Engineering, Beijing, China.

Motamed, R., and Towhata, I. (2009). “Shaking table model tests on pile groups behind quay walls subjected to lateral spreading”. Journal of Geotechnical and Geoenvironmental Engineering, 136(3), 477-489.

Motamed, R., Towhata, I., Honda, T., Yasuda, S., Tabata, K., and Nakazawa, H. (2009). Behavior of pile group behind a sheet pile quay wall subjected to liquefaction-induced large ground deformation observed in shaking test in E-Defense project. Soils and Foundations, 49(3): 459–476. doi:10.3208/sandf.49.459.

Motamed, R. and Towhata, I. (2010). “Shaking Table Model Tests on Pile Groups behind Quay Walls Subjected to Lateral Spreading,” Journal of Geotechnical and Geoenvironmental Engineering 136(3) 477-489.

Motamed, R., Towhata, I., Honda, T., Tabata, K., and Abe, A. (2013). “Pile group response to liquefaction-induced lateral spreading: E-Defense large shake table test,” Soil Dynamics and Earthquake Engineering 51 35-46.

Mylonakis, G., Syngros, C., Gazetas, G. and Tazoh, T. (2006). The role of soil in the collapse of 18 piers of Hanshin Expressway in the Kobe earthquake. Earthquake Engineering and Structural Dynamics; 35:547–575. DOI:10.1002/eqe.543

NCHRP-12-49. (1998). "Comprehensive specification for the seismic design of bridges."

NISEE. “National Information Services for Earthquake Engineering”

Orense, R., Ishihara, K., Yasuda, S., Morimoto, I., and Takagi, M. (2000). “Soil spring constants during lateral flow of liquefied ground”. Proc., 12th World Conference on Earthquake Engineering.

Okamura, M., Abdoun, T. H., Dobry, R., Sharp, M. K., and Taboada, V. M. (2001). Effects of sand permeability and weak aftershocks on earthquake-induced lateral spreading. Soils and Foundations, 41(6), 63-77.

Ramirez, J. M. (2009). “Influence of Soil Permeability on Liquefaction-Induced Lateral Pile Response.” M.S. thesis, Department of Structural Engineering, University of California, San Diego, CA.

Ramos, R. (1999). “Centrifuge study of bending response of pile foundation to a lateral spread including restraining effect of superstructure,” Ph.D. thesis, Rensselaer Polytechnic Institute, Troy, N.Y.

Ramos, R., Abdoun, T., and Dobry, R. (2000). Effects of lateral stiffness of superstructure on bending moments of pile foundation due to liquefaction induced lateral spreading. Proc. of the 12th World Conference on Earthquake Engineering, Auckland, New Zealand.

Randolph, M. F. (1981). The response of flexible piles to lateral loading. Geotechnique, 31(2), 247-259.

Reese, L. C., Cox, W. R. and Koop, F. D. (1974). "Analysis of laterally loaded piles in sand," Proc., 6th Offshore Technology Conf., Houston, Texas, (Paper No. 2080), 473-483.

Reese, L. C.; Cox, W. R.; and Koop, F. D., 1975. “Field Testing and Analysis of Laterally Loaded Piles in Stiff Clay,” Proceedings, 7th Offshore Technology Conference, pp. 671-690.

Reese, L. C., Wang, S. T., Isenhower, W. M., Arrelaga, J.A., and Hendrix, J. A. (2005). “LPILE Plus Version 5.0,” Ensoft, Inc. Austin, TX.

Rollins, K.M., Gerber, T.M., Dusty Lane, J. and Ashford, S.A. (2005). "Lateral resistance of a full-scale pile group in liquefied sand," Journal of Geotechnical and Geoenvironmental Engineering, 131(1), 115-125.

SCEC (2002). Recommended procedures for implementation of DMG SPECIAL PUBLICATION 117 GUIDELINES for analyzing and mitigating landslide hazards in California- Los Angeles Section Geotechnical Group (ASCE), Document, Southern California Earthquake Center, Los Angeles, CA.

Schiff, A. J. (1991). "Philippines earthquake reconnaissance report: Chapter 1, Geoscience and Geotechnical," Earthquake Spectra, Suppl. A to Vol. 7.

SEAOC. (1991). "Reflections on the October 17, 1989 Loma Prieta earthquake," Ad Hoc Earthquake Reconnaissance Committee, Sacramento, Structural Engineers Association of California, (SEAOC).

Seed, H.B. (1968). "Landslides during earthquakes due to soil liquefaction," Journal of Geotechnical Engineering Division, ASCE, 94(SM5), 1055-1123.

Seed, H.B. and Idriss, M.I. (1971) “Simplified procedure for evaluating soil liquefaction potential” Journal of the Soil Mechanics and Foundations Division, Vol. 97, No. SM9, pp. 1249-1273.

Seed, R.B. and Harder, L. (1990). SPT-based analysis of cyclic pore pressure generation and undrained residual strength. Proc. Of the H. Bolton Seed memorial symposium; 2:351−376.

Shantz, T. (2013) Guidelines on Foundation Loading and Deformation Due to Liquefaction Induced Lateral Spreading.

Singh, P., Subramanian, P. K., Boulanger, R. W. and Kutter, B. L. (2000). "Behavior of piles in laterally spreading ground during earthquakes - centrifuge data report for PDS01," UCD/CGMDR-00/05.

Stewart, D. P., Chen, Y. R., and Kutter, B. L. (1998). ‘‘Experience with the use of methylcellulose as a viscous pore fluid in centrifuge models,’’ Geotech. Testing J., 21(4), 365–369.

Suzuki, H., and Tokimatsu, K. (2003). Effect of pore water pressure response around pile on p-y relation during liquefaction. In Proc., 11th Int. Conf. on Soil Dynamics and Earthquake Engineering (Vol. 2, pp. 567-572). Stallion Press.

Susuki, H., Tokimatsu, K., Sato, M. and Abe, A. (2005) Factor affecting horizontal subgrade reaction of piles during soil liquefaction and lateral spreading. Proceedings of workshop GSP 145 (eds R. W. Boulanger and K. Tokimatsu), Davis, CA, Vol. 1, pp. 1–10.

Suzuki, H., Tokimatsu, K., Sato, M., and Abe, A. (2006). “Factor affecting horizontal subgrade reaction of piles during soil liquefaction and lateral spreading”. Seismic performance and simulation of pile foundations in liquefied and laterally spreading ground (pp. 1-10).

Suzuki, H., Tokimatsu, K., Sato, M., and Tabata, K. (2008). Soil-pile-structure interaction in liquefiable ground through multi-dimensional shaking table tests using e-defense facility. In Proceedings of the 14th World Conference on Earthquake Engineering, Beijing, China, 12–17 October.

Taboada, V. M. (1995). “Centrifuge modeling of earthquake-induced lateral spreading in sand using a laminar box,” PhD thesis, Civil Engineering Dept., Rensselaer Polytechnic Institute, Troy, N.Y.

Taboada, V. M., Abdoun, T. and Dobry, R. (1996). “Prediction of liquefaction-induced laeral spreading by dilatant sliding block model calibrated by centrifuge tests,” Eleventh World Conference on Earthquake Engineering Paper No. 375.

Tazoh, T., Ohtsuki, A., Fuchimoto, M., Nanjo, A., Yasuda, F., Fujii, Y., Nakahira, A. and Kuroda, C. (2000). "Analysis of the damage to the pile foundation of a highway bridge caused by soil liquefaction and its lateral spread due to the 1995 Great Hanshin earthquake," Proceedings of the 12th World Conference on Earthquake Engineering, Auckland, New Zealand, Paper No. 1978.

Thevanayagam, S., Kanagalingam, T., Reinhorn, A., Tharmendhira, R., Dobry, R., Pitman, M.,and El Shamy, U. (2009). Laminar box system for 1-g physical modeling of liquefaction and lateral spreading. Geotechnical Testing Journal, 32(5), 438-449.

Tokida, K., Iwasaki, H., Matsumoto, H. and Hamasa, T. (1993). "Liquefaction potential and drag force acting on piles in flowing soils," Soil Dynamic and Earthquake Engineering, Computational Mechanics, (South Hampton, England), 349-364.

Tokimatsu, K., Mizuno, H. and Kakurai, M. (1996). "Building damage associated with geotechnical problems.," Special issue of Soils and Foundations, Japanese Geotechnical Society, January, 219-234.

Tokimatsu, K. and Asaka, Y. (1998) “Effects of liquefaction-induced ground displacements on pile performance in the 1995 Hyogoken-Nambu earthquake,” Soil and Foundations Special Issue on Geotechnical Aspects of the January 17, 1995 Hyogoken-Nambu earthquake, 2, 163-178.

Tokimatsu, K., Suzuki, H., and Suzuki, Y. (2001). “Back-calculated py relation of liquefied soils from large shaking table tests”. Proc., 4th International Conferences on Recent Advances in Geotechnical Earthquake Engineering and Soil Dynamics. San Diego, CA.

Tokimatsu, K. and Suzuki, H. (2004). “Pore water pressure response around pile and its effects on p-y behavior during soil liquefaction,” Soils and Foundations 44(6), 101-110.

Tokimatsu, K., and Suzuki, H. (2005). Effect of inertial and kinematic interactions on seismic behaviour of pile foundations based on large shaking table tests. Proc. of the 2nd CUEE conference on urban earthquake engineering. Tokyo Institute of Technology (Japan).

Tokimatsu, K., Suzuki, H., and Sato, M. (2005). “Effects of inertial and kinematic interaction on seismic behavior of pile with embedded foundation”. Soil Dynamics and Earthquake Engineering, 25(7-10), 753-762.

Tokimatsu, K., Suzuki, H., Tabata, K., and Sato, M. (2007). Three-dimensional shaking table tests on soil-pile-structure models using E-Defense facility. In Proceedings of the 4th International

Conference on Earthquake Geotechnical Engineering, Thessaloniki, Greece, 25–28 June. Paper no. I529.

Towhata, I., Sesov, V., Motamed, R. and Gonzales, M. (2006). “Model tests on lateral earth pressure on large group pile exerted by horizontal displacement of liquefied sandy ground,” Proc. 8th U.S. National Conference on Earthquake Engineering, San Francisco, California.

Trautner, C., Zheng, Y., McCartney, J. S., and Hutchinson, T. (2018). An approach for shake table performance evaluation during repair and retrofit actions. Earthquake Engineering & Structural Dynamics, 47(1), 131-146. doi:10.1002/eqe.2942

Turner, B., Brandenberg, S. J., and Stewart. J. P. (2014). "Comparison of design procedures and observed performance of bridges subjected to lateral spreading." Proceedings of the 10th National Conference in Earthquake Engineering, Earthquake Engineering Research Institute, Anchorage, AK,.

Turner, B., Brandenberg, S. J., and Stewart. J. P. (2015). "Analysis of Drilled Shaft Settlement Caused by Liquefaction." Proc. IFCEE.

Turner, B., Brandenberg, S. J., and Stewart. J. P. (2016). "Case Study of Parallel Bridges Affected by Liquefaction and Lateral Spreading." J. Geotech. Geoenviron. Eng., ASCE. 142(7).

Ubilla, J. (2007) Physical modeling of the effects of natural hazards on soil–structure interaction. PhD thesis. Rensselaer Polytechnic Institute, Troy, NY.

Ubilla, J., Abdoun, T. and Dobry, R. (2011). “Centrifuge scaling laws of pile response to lateral spreading,” International Journal of Physical Modelling in Geotechnics.

United States Geological Survey (USGS). www.walrus.wr.usgs.gov, The Loma Prieta, California, Earthquake of October 17, 1989-Liquefaction

Verdugo, R. (2012). Comparing liquefaction phenomena observed during the 2010 Maule, Chile earthquake and 2011 Great East Japan earthquake. In Proceedings of international symposium on engineering lessons learned from the 2011 Great East Japan Earthquake, March 1-4.

Weaver, T. J., Ashford, S. A. and Rollins, K. M. (2005). "Response of 0.6 m cast-in-steel-shell pile in liquefied soil under lateral loading," Journal of Geotechnical and Geoenvironmental Engineering, 131(1), 94-102.

Wilson, D. W., Boulanger, R. W. and Kutter, B. L. (2000). “Observed seismic lateral resistance of liquefying sand” Journal of Geotechnical and Geoenvironmental Engineering 126(10) 898-906.

Wood, H. (1908). "Distribution of apparent intensity in San Francisco in the California earthquake of April 18, 1906," Rpt. of the State Earthquake Investigation Comm., Carnegie Inst. of Washington, Washington, D.C., 220-245.

Yan, L. (2006). Sensor data analysis and information extraction for structural health monitoring. PhD Thesis, University of California, San Diego.

Yasuda, S., and Berrill, J. (2000). Observations of the earthquake response of foundations in soil profiles containing saturated sands. In: 1st International conference on geotechnical and geological engineering, Melbourne, Australia. p. 1441–71.

Yoshida, N. and Hamada, M. (1991). Damage to foundation pile and deformation pattern of ground due to liquefaction-induced permanent ground deformations. Proceedings 3rd Japan-U.S. Workshop on Earthquake Resistant Design of Lifeline Facilities and Countermeasures for Soil Liquefaction, National Center for Earthquake Engineering Research, NCEER-91-0001: 147-156

Youd, T. L., Idriss, I. M., Andrus, R. D., Arango, I., Castro, G., Christian, J. T., Dobry, R., Finn, W., Harder, D. L. Jr., Hynes, M. E., Ishihara, K., Koester, J. P., Liao, S. S. C., Marcuson, W. F. III, Martin, G. R., Mitchell, J. K. Moriwaki, Y. Power, M. S., Robertson, P. K., Seed, R. B., and Stokoe, K. H. II. (2001). "Liquefaction Resistance of Soils: Summary Report from the 1996 NCEER and 1998 NCEER/NSF Workshops on Evaluation of Liquefaction Resistance of Soils," ASCE/SEI Journal of Geotechnical Geoenvironmental Engineering, 127(10).

Zayed, M. (2020). Large-Scale Seismic Response of Ground and Ground-Structure Interaction Systems. PhD Thesis. Department of Structural Engineering. University of California San Diego, La Jolla, CA

Zeghal, M. and Elgamal, A.-W. (1994). "Analysis of site liquefaction using earthquake records" Journal of Geotechnical Engineering 120(6), 996-1017.